Hashemite Kingdom of Jordan

Jordan Journal of Biological Sciences

An International Peer-Reviewed Scientific Journal

Financed by the Scientific Research and Innovation Support Fund

This title is indexed in Scopus

http://jjbs.hu.edu.jo/

المجلة الأردنية للعلوم الحياتية
Jordan Journal of Biological Sciences (JJBS)
http://jjbs.hu.edu.jo

Jordan Journal of Biological Sciences (JJBS) (ISSN: 1995–6673 (Print); 2307-7166 (Online)): An International Peer- Reviewed Open Access Research Journal financed by the Scientific Research and Innovation Support Fund, Ministry of Higher Education and Scientific Research, Jordan and published quarterly by the Deanship of Scientific Research , The Hashemite University, Jordan.

Submission Address
Professor Wedyan, Mohammed A.
The Hashemite Universit y
P.O. Box 330127, Zarqa, 13115, Jordan
Phone: +962-5-3903333 ext.4147
E-Mail: jjbs@hu.edu.jo

المجلة الاردنية للعلوم الحياتية
Jordan Journal of Biological Sciences (JJBS)
http://jjbs.hu.edu.jo

International Advisory Board (Arranged alphabetically)

Instructions to Authors

Scopes

Study areas include cell biology, genomics, microbiology, immunology, molecular biology, biochemistry, embryology, immunogenetics, cell and tissue culture, molecular ecology, genetic engineering and biological engineering, bioremediation and biodegradation, bioinformatics, biotechnology regulations, gene therapy, organismal biology, microbial and environmental biotechnology, marine sciences. The JJBS welcomes the submission of manuscript that meets the general criteria of significance and academic excellence. All articles published in JJBS are peer-reviewed. Papers will be published approximately one to two months after acceptance.

Type of Papers

The journal publishes high-quality original scientific papers, short communications, correspondence and case studies. Review articles are usually by invitation only. However, Review articles of current interest and high standard will be considered.

Submission of Manuscript

Manuscript, or the essence of their content, must be previously unpublished and should not be under simultaneous consideration by another journal. The authors should also declare if any similar work has been submitted to or published by another journal. They should also declare that it has not been submitted/ published elsewhere in the same form, in English or in any other language, without the written consent of the Publisher. The authors should also declare that the paper is the original work of the author(s) and not copied (in whole or in part) from any other work. All papers will be automatically checked for duplicate publication and plagiarism. If detected, appropriate action will be taken in accordance with International Ethical Guideline. By virtue of the submitted manuscript, the corresponding author acknowledges that all the co-authors have seen and approved the final version of the manuscript. The corresponding author should provide all co-authors with information regarding the manuscript, and obtain their approval before submitting any revisions. Electronic submission of manuscripts is strongly recommended, provided that the text, tables and figures are included in a single Microsoft Word file. Submit manuscript as e-mail attachment to the Editorial Office at: JJBS@hu.edu.jo. After submission, a manuscript number will be communicated to the corresponding author within 48 hours.

Peer-review Process

It is requested to submit, with the manuscript, the names, addresses and e-mail addresses of at least 4 potential reviewers. It is the sole right of the editor to decide whether or not the suggested reviewers to be used. The reviewers' comments will be sent to authors within 6-8 weeks after submission.
Manuscripts and figures for review will not be returned to authors whether the editorial decision is to accept, revise, or reject. All Case Reports and Short Communication must include at least one table and/ or one figure.

Preparation of Manuscript

The manuscript should be written in English with simple lay out. The text should be prepared in single column format. Bold face, italics, subscripts, superscripts etc. can be used. Pages should be numbered consecutively, beginning with the title page and continuing through the last page of typewritten material.

The text can be divided into numbered sections with brief headings. Starting from introduction with section 1. Subsections should be numbered (for example 2.1 (then 2.1.1, 2.1.2, 2.2, etc.), up to three levels. Manuscripts in general should be organized in the following manner:

Title Page

The title page should contain a brief title, correct first name, middle initial and family name of each author and name and address of the department(s) and institution(s) from where the research was carried out for each author. The title should be without any abbreviations and it should enlighten the contents of the paper. All affiliations should be provided with a lower-case superscript number just after the author's name and in front of the appropriate address.
The name of the corresponding author should be indicated along with telephone and fax numbers (with country and area code) along with full postal address and e-mail address.

Abstract

The abstract should be concise and informative. It should not exceed **350 words** in length for full manuscript and Review article and **150 words** in case of Case Report and/ or Short Communication. It should briefly describe the purpose of the work, techniques and methods used, major findings with important data and conclusions. No references should be cited in this part. Generally non-standard abbreviations should not be used, if necessary they should be clearly defined in the abstract, at first use.

Keywords

Immediately after the abstract, **about 4-8 keywords** should be given. Use of abbreviations should be avoided, only standard abbreviations, well known in the established area may be used, if appropriate. These keywords will be used for indexing.

Abbreviations

Non-standard abbreviations should be listed and full form of each abbreviation should be given in parentheses at first use in the text.

Introduction

Provide a factual background, clearly defined problem, proposed solution, a brief literature survey and the scope and justification of the work done.

Materials and Methods

Give adequate information to allow the experiment to be reproduced. Already published methods should be mentioned with references. Significant modifications of published methods and new methods should be described in detail. Capitalize trade names and include the manufacturer's name and address. Subheading should be used.

Results

Results should be clearly described in a concise manner. Results for different parameters should be described under subheadings or in separate paragraph. Results should be explained, but largely without referring to the literature. Table or figure numbers should be mentioned in parentheses for better understanding.

Discussion

The discussion should not repeat the results, but provide detailed interpretation of data. This should interpret the significance of the findings of the work. Citations should be given in support of the findings. The results and discussion part can also be described as separate, if appropriate. The Results and Discussion sections can include subheadings, and when appropriate, both sections can be combined

Conclusions

This should briefly state the major findings of the study.

Acknowledgment

A brief acknowledgment section may be given after the conclusion section just before the references. The acknowledgment of people who provided assistance in manuscript preparation, funding for research, etc. should be listed in this section.

Tables and Figures

Tables and figures should be presented as per their appearance in the text. It is suggested that the discussion about the tables and figures should appear in the text before the appearance of the respective tables and figures. No tables or figures should be given without discussion or reference inside the text.

Tables should be explanatory enough to be understandable without any text reference. Double spacing should be maintained throughout the table, including table headings and footnotes. Table headings should be placed above the table. Footnotes should be placed below the table with superscript lowercase letters. Each table should be on a separate page, numbered consecutively in Arabic numerals.

Each figure should have a caption. The caption should be concise and typed separately, not on the figure area. Figures should be self-explanatory. Information presented in the figure should not be repeated in the table. All symbols and abbreviations used in the illustrations should be defined clearly. Figure legends should be given below the figures.

References

References should be listed alphabetically at the end of the manuscript. Every reference referred in the text must be also present in the reference list and vice versa. In the text, a reference identified by means of an author's name should be followed by the year of publication in parentheses (e.g.(Brown,2009)). For two authors, both authors' names followed by the year of publication (e.g.(Nelson and Brown, 2007)). When there are more than two authors, only the first author's name followed by "*et al*." and the year of publication (e.g. (Abu-Elteen *et al*., 2010)). When two or more works of an author has been published during the same year, the reference should be identified by the letters "a", "b", "c", etc., placed after the year of publication. This should be followed both in the text and reference list. e.g., Hilly, (2002a, 2002b); Hilly, and Nelson, (2004). Articles in preparation or submitted for publication, unpublished observations, personal communications, etc. should not be included in the reference list but should only be mentioned in the article text (e.g., Shtyawy,A., University of Jordan, personal communication). Journal titles should be abbreviated according to the system adopted in Biological Abstract and Index Medicus, if not included in Biological Abstract or Index Medicus journal title should be given in full. The author is responsible for the sccuracy and completeness of the references and for their correct textual citation. Failure to do so may result in the paper being withdraw from the evaluation process. Example of correct reference form is given as follows:-

Reference to a journal publication:

Bloch BK. 2002. Econazole nitrate in the treatment of *Candida vaginitis*. *S Afr Med J.* , **58**:314-323.

Ogunseitan OA and Ndoye IL. 2006. Protein method for investigating mercuric reductase gene expression in aquatic environments. *Appl Environ Microbiol.*, **64**: 695-702.

Hilly MO, Adams MN and Nelson SC. 2009. Potential fly-ash utilization in agriculture. *Progress in Natural Sci.*, **19**: 1173-1186.

Reference to a book:

Brown WY and White SR.1985. **The Elements of Style**, third ed. MacMillan, New York.

Reference to a chapter in an edited book:

Mettam GR and Adams LB. 2010. How to prepare an electronic version of your article. In: Jones BS and Smith RZ (Eds.), **Introduction to the Electronic Age**. Kluwer Academic Publishers, Netherlands, pp. 281–304.

Conferences and Meetings:

Embabi NS. 1990. Environmental aspects of distribution of mangrove in the United Arab Emirates. Proceedings of the First ASWAS Conference. University of the United Arab Emirates. Al-Ain, United Arab Emirates.

Theses and Dissertations:

El-Labadi SN. 2002. Intestinal digenetic trematodes of some marine fishes from the Gulf of Aqaba. MSc dissertation, The Hashemite University, Zarqa, Jordan.

Nomenclature and Units

Internationally accepted rules and the international system of units (SI) should be used. If other units are mentioned, please give their equivalent in SI.

For biological nomenclature, the conventions of the *International Code of Botanical Nomenclature, the International Code of Nomenclature of Bacteria,* and the *International Code of Zoological Nomenclature* should be followed.

Scientific names of all biological creatures (crops, plants, insects, birds, mammals, etc.) should be mentioned in parentheses at first use of their English term.

Chemical nomenclature, as laid down in the *International Union of Pure and Applied Chemistry* and the official recommendations of the *IUPAC-IUB Combined Commission on Biochemical Nomenclature* should be followed. All biocides and other organic compounds must be identified by their Geneva names when first used in the text. Active ingredients of all formulations should be likewise identified.

Math formulae

All equations referred to in the text should be numbered serially at the right-hand side in parentheses. Meaning of all symbols should be given immediately after the equation at first use. Instead of root signs fractional powers should be used. Subscripts and superscripts should be presented clearly. Variables should be presented in italics. Greek letters and non-Roman symbols should be described in the margin at their first use.

To avoid any misunderstanding zero (0) and the letter O, and one (1) and the letter l should be clearly differentiated. For simple fractions use of the solidus (/) instead of a horizontal line is recommended. Levels of statistical significance such as: $^{*}P < 0.05$, $^{**}P < 0.01$ and $^{***}P < 0.001$ do not require any further explanation.

Copyright

Submission of a manuscript clearly indicates that: the study has not been published before or is not under consideration for publication elsewhere (except as an abstract or as part of a published lecture or academic thesis); its publication is permitted by all authors and after accepted for publication it will not be submitted for publication anywhere else, in English or in any other language, without the written approval of the copyright-holder. The journal may consider manuscripts that are translations of articles originally published in another language. In this case, the consent of the journal in which the article was originally published must be obtained and the fact that the article has already been published must be made clear on submission and stated in the abstract. It is compulsory for the authors to ensure that no material submitted as part of a manuscript infringes existing copyrights, or the rights of a third party.

Ethical Consent

All manuscripts reporting the results of experimental investigation involving human subjects should include a statement confirming that each subject or subject's guardian obtains an informed consent, after the approval of the experimental protocol by a local human ethics committee or IRB. When reporting experiments on animals, authors should indicate whether the institutional and national guide for the care and use of laboratory animals was followed.

Plagiarism

The JJBS hold no responsibility for plagiarism. If a published paper is found later to be extensively plagiarized and is found to be a duplicate or redundant publication, a note of retraction will be published, and copies of the correspondence will be sent to the authors' head of institute.

Galley Proofs

The Editorial Office will send proofs of the manuscript to the corresponding author as an e-mail attachment for final proof reading and it will be the responsibility of the corresponding author to return the galley proof materials appropriately corrected within the stipulated time. Authors will be asked to check any typographical or minor clerical errors in the manuscript at this stage. No other major alteration in the manuscript is allowed. After publication authors can freely access the full text of the article as well as can download and print the PDF file.

Publication Charges

There are no page charges for publication in Jordan Journal of Biological Sciences, except for color illustrations,

Reprints

Ten (10) reprints are provided to corresponding author free of charge within two weeks after the printed journal date. For orders of more reprints, a reprint order form and prices will be sent with article proofs, which should be returned directly to the Editor for processing.

Disclaimer

Articles, communication, or editorials published by JJBS represent the sole opinions of the authors. The publisher shoulders no responsibility or liability what so ever for the use or misuse of the information published by JJBS.

Indexing

JJBS is indexed and abstracted by:

DOAJ (Directory of Open Access Journals)	CABI
Google Scholar	EBSCO
Journal Seek	CAS (Chemical Abstract Service)
HINARI	ETH- Citations
Index Copernicus	Open J-Gat
NDL Japanese Periodicals Index	SCImago
SCIRUS	Clarivate Analytics (Zoological Abstract)
OAJSE	Scopus
ISC (Islamic World Science Citation Center)	AGORA (United Nation's FAO database)
Directory of Research Journal Indexing (DRJI)	SHERPA/RoMEO (UK)
Ulrich's	

المجلة الأردنية للعلوم الحياتية
Jordan Journal of Biological Sciences (JJBS)
ISSN 1995- 6673 (Print), 2307- 7166 (Online)
http://jjbs.hu.edu.jo

The Hashemite University

Deanship of Scientific Research

TRANSFER OF COPYRIGHT AGREEMENT

Journal publishers and authors share a common interest in the protection of copyright: authors principally because they want their creative works to be protected from plagiarism and other unlawful uses, publishers because they need to protect their work and investment in the production, marketing and distribution of the published version of the article. In order to do so effectively, publishers request a formal written transfer of copyright from the author(s) for each article published. Publishers and authors are also concerned that the integrity of the official record of publication of an article (once refereed and published) be maintained, and in order to protect that reference value and validation process, we ask that authors recognize that distribution (including through the Internet/WWW or other on-line means) of the authoritative version of the article as published is best administered by the Publisher.

To avoid any delay in the publication of your article, please read the terms of this agreement, sign in the space provided and return the complete form to us at the address below as quickly as possible.

Article entitled:----------

Corresponding author: ----------

To be published in the journal: Jordan Journal of Biological Sciences (JJBS)

I hereby assign to the Hashemite University the copyright in the manuscript identified above and any supplemental tables, illustrations or other information submitted therewith (the "article") in all forms and media (whether now known or hereafter developed), throughout the world, in all languages, for the full term of copyright and all extensions and renewals thereof, effective when and if the article is accepted for publication. This transfer includes the right to adapt the presentation of the article for use in conjunction with computer systems and programs, including reproduction or publication in machine-readable form and incorporation in electronic retrieval systems.
Authors retain or are hereby granted (without the need to obtain further permission) rights to use the article for traditional scholarship communications, for teaching, and for distribution within their institution.

☐ **I am the sole author of the manuscript**

☐ **I am signing on behalf of all co-authors of the manuscript**

☐ **The article is a 'work made for hire' and I am signing as an authorized representative of the employing company/institution**

Please mark one or more of the above boxes (as appropriate) and then sign and date the document in black ink.

Signed:_____ **Name printed:** _____
Title and Company (if employer representative) : _____
Date: _____

Data Protection: By submitting this form you are consenting that the personal information provided herein may be used by the Hashemite University and its affiliated institutions worldwide to contact you concerning the publishing of your article.

Please return the completed and signed original of this form by mail or fax, or a scanned copy of the signed original by e-mail, retaining a copy for your files, to:

Hashemite University
Jordan Journal of Biological Sciences
Zarqa 13115 Jordan
Fax: +962 5 3903338
Email: jjbs@hu.edu.jo

Editorial Preface

Jordan Journal of Biological Sciences (JJBS) is a refereed, quarterly international journal financed by the Scientific Research and Innovation Support Fund, Ministry of Higher Education and Scientific Research in cooperation with the Hashemite University, Jordan. JJBS celebrated its 12th commencement this past January, 2020. JJBS was founded in 2008 to create a peer-reviewed journal that publishes high-quality research articles, reviews and short communications on novel and innovative aspects of a wide variety of biological sciences such as cell biology, developmental biology, structural biology, microbiology, entomology, molecular biology, biochemistry, medical biotechnology, biodiversity, ecology, marine biology, plant and animal biology, plant and animal physiology, genomics and bioinformatics.

We have watched the growth and success of JJBS over the years. JJBS has published 14 volumes, 60 issues and 800 articles. JJBS has been indexed by SCOPUS, CABI's Full-Text Repository, EBSCO, Clarivate Analytics- Zoological Record and recently has been included in the UGC India approved journals. JJBS Cite Score has improved from 0.7 in 2019 to 1.4 in 2021 (Last updated on 6 March, 2022) and with Scimago Institution Ranking (SJR) 0.22 (Q3) in 2021.

A group of highly valuable scholars have agreed to serve on the editorial board and this places JJBS in a position of most authoritative on biological sciences. I am honored to have six eminent associate editors from various countries. I am also delighted with our group of international advisory board members coming from 15 countries worldwide for their continuous support of JJBS. With our editorial board's cumulative experience in various fields of biological sciences, this journal brings a substantial representation of biological sciences in different disciplines. Without the service and dedication of our editorial; associate editorial and international advisory board members, JJBS would have never existed.

In the coming year, we hope that JJBS will be indexed in Clarivate Analytics and MEDLINE (the U.S. National Library of Medicine database) and others. As you read throughout this volume of JJBS, I would like to remind you that the success of our journal depends on the number of quality articles submitted for review. Accordingly, I would like to request your participation and colleagues by submitting quality manuscripts for review. One of the great benefits we can provide to our prospective authors, regardless of acceptance of their manuscripts or not, is the feedback of our review process. JJBS provides authors with high quality, helpful reviews to improve their manuscripts.

Finally, JJBS would not have succeeded without the collaboration of authors and referees. Their work is greatly appreciated. Furthermore, my thanks are also extended to The Hashemite University and the Scientific Research and Innovation Support Fund, Ministry of Higher Education and Scientific Research for their continuous financial and administrative support to JJBS.

Professor Wedyan ,Mohammed A.
March, 2024

JJBS

Volume 18, Number 2, June 2025
ISSN 1995-6673

Jordan Journal of Biological Sciences

CONTENTS

Original Articles

197 - 209 Short-term and Long-term Adverse Effects of COVID-19 Vaccines and its Associated Factors: A Cross-sectional Study from Jordan
Abdel-Ellah Al-Shudifat, Mohammad Al-Tamimi,, Mohammad Alkhateeb, Rand Dawoud, Anas Alahmad, Amel Mryyian, Basil Al-Ramahi, Arwa Qaqish, Manal M Abbas

211 - 220 Comparative Analysis of Microbiological and Enzymatic Methods for Strengthening Sandy and Weathered Soils to Mitigate Degradation and Desertification
Meiirzhan Dauletkul, Zina Tungushbayeva, Asem Kydyrbaeva, Dina Kulzhanova, Zhanat Bukharbayeva

221 - 230 Application of Chitosan/Hydroquinone Nanaoemulsions for Management Root Rot Disease on Cucumber Plants in Plastic Houses
El-Sayed H. E. Ziedan and Abdel-Tawab H. Mossa

231 - 241 Modulation of Gut Microbiota in Salmonella Typhimurium-infected Sprague Dawley Rats by Treatment with *Pichia kudriavzevii* 2P10 in Combination with Prebiotic Mannan-Oligosaccharide
Rahayu Wulan, Rika Indri Astuti, Yaya Rukayadi, Sri Estuningsih, Anja Meryandini

243 - 252 Phytochemical and Bioactivity Variations in *Calobota saharae*: Flavonoid Extraction, Antioxidant, and Anti-inflammatory Assessment
Atef CHOUIKH, Anis BEN ALI , Aida BOUSBIA BRAHIM

253 - 263 Molecular Characterization of Water Rattan Palm (*Calamus angustifolius* Griff.) from Kampar River, Riau Province, Indonesia Using *matK and trnL-trnL-trnF* Intergenic Spacer
Hapiz Al Khairi, Dewi Indriyani Roslim , Aristyanti Devie Vitovang, Meisita Hariani, Herman, Wahyu Lestari1, Adiwirman, Aldy Riau Wansyah Hasibuan, Linda Novita, Siti Zulaeha, Irni Furnawanthi Hindaningrum

265 - 274 Evaluation of the Synergistic Cytotoxicity of Camptothecin with Silver Nanoparticles: Potential Anti-angiogenic, Anti-inflammatory, and Antioxidant Agents
Moath alqaraleh, Futoon Abedrabbu Al-Rawashde , Khaled M. Khleifat

275 – 280 Microbial Solutions for Environmental Cleanup: *Sphingomonas paucimobilis* Role in Removing Heavy Metals and Aromatic Hydrocarbons
Raghad Shubbar Jaafar

281 – 290 Preparation and Characterization of *Newbouldia laevis* (P.Beauv.) Seem. mediated Gold and Alloy Nanoparticles and Evaluation of Its Bactericidal Effect on Clinical Pathogens
Oluwakemi Abike Thonda , Fatimah Adenike Ajadi, Olanrewaju Oludotun Daramola, Aderiike Adewumi Grace, Oludare Temitope Osuntokun, Daniel Ayandiran Aina, Temitope Elizabeth Oyewole, Rukevwe Collins Etareri

291 – 299 Biological Active Metabolite Compounds for Antibacterial Agent From Extremophile Microalgae
Mohd Asyraf Kassim, Tan Kean Meng, Mohamad Hafizi Abu Bakar , Siti Nurfatimah Mohd Shahpudin, Chee-Yuan Gan , Nur Farah Atiqah binti Mohd Pazli, Rohazila Mohamad Hanafiah

301 – 313 Attenuation of Quorum Sensing, Virulence Factors, and Biofilm Formation in *Pseudomonas aeruginosa* by *Psidium guajava* Leaf Extract
Haitham Qaralleh

315 – 321 The Effect of *Memantine* and *Lactobacillus acidophilus* Supernatant on Apoptosis and Expression of Key Long non-coding RNAs in a Colon Cancer Cell Line
Paniz Erfanian Goli Zadeh Rauf Mohajer, Aras Rafiee , Soheila Zamanlui Benisi

323 – 333 Characterization and In-vitro Evaluation of Positively Charged Oligopeptide as Gene Delivery Vehicle Candidate on BHK-21 Cells
Damai Ria Setyawati, Sjaikhurrizal El Muttaqien, Irvan Faizal, Efrida Martius, Indira Putri Negari, Asep Saepudin, Stefi Mitra Wahyuningsih, Neni Nurainy, Mulyoto Pangestu, and Tarwadi

335 - 341 First Application of *FLORICAULA* second intron (FLint2) as a Phylogenetic Marker in Bananas (Musaceae)
Lia Hapsari , Apriyono Rahadiantoro, Didik Wahyudi, Sundari Sundari, Rodiyati Azrianingsih

343 – 355 Morphological Characterization and Taxonomic Assessment of *Micromeria* Bentham from Jordan: Key Species and Their Taxonomic Significance
Bilal Azmi Ayasrah , Sawsan Atallah Oran, and Khaldoun Al-Hadid

357 – 365 Exploring The Potential of *Momordica charantia* L. as a Natural Therapeutic Agent for Osteoarthritis: In-Silico Analysis of ADAMTS-5 and Binding Potential Assessment
Olabode Oluwadare Akintoye; Ayodeji Johnson Ajibare; Blessing Tolulope Owolabi Olayinka Alfred Taylor ; Kehinde Samuel Olaniyi

367 – 381 Antimicrobial Potential of Biosurfactants from Microbial Sources: A Bibliometric Analysis
Achmad Rifky Alfian, Novita Yustinadiar, Abdul Rahman Siregar, FurzaniPa'ee, Ekachai Taowkrue, Neng Tanty Sofyana, Wahyu Aristyaning Putri

JJBS

Volume 18, Number 2,June 2025
ISSN 1995-6673
Pages 197 – 209
https://doi.org/10.54319/jjbs/180201

Jordan Journal of Biological Sciences

Short-term and Long-term Adverse Effects of COVID-19 Vaccines and its Associated Factors: A Cross-sectional Study from Jordan

Abdel-Ellah Al-Shudifat[1], Mohammad Al-Tamimi[2,*], Mohammad Alkhateeb[3], Rand Dawoud[3], Anas Alahmad[3], Amel Mryyian[3], Basil Al-Ramahi[4], Arwa Qaqish[5,6], Manal M Abbas[7,8]

[1]Department of Internal and Family Medicine, Faculty of Medicine, The Hashemite University, Zarqa, Jordan; [2]Department of Microbiology, Pathology and Forensic Medicine, Faculty of Medicine, The Hashemite University, Zarqa, Jordan; [3]Faculty of Medicine, The Hashemite University, Zarqa, Jordan; [4]School of Medicine, The University of Jordan, Amman, Jordan; [5]Department of Biology and Biotechnology, Faculty of Science, The Hashemite University, Zarqa, Jordan; [6]Department of Cellular Therapy and Applied Genomics, King Hussein Cancer Center, Amman, Jordan; [7]Department of Medical Laboratory Sciences, Faculty of Allied Medical Sciences, Al-Ahliyya Amman University, Amman, Jordan; [8]Pharmacological and Diagnostic Research Lab, Al-Ahliyya Amman University, Amman, Jordan

Received: May 23, 2024; Revised: August 26, 2024; Accepted: October 12, 2024

Abstract

Background: The continual monitoring of COVID-19 vaccine safety is a complex process that requires further investigation. This study aims to investigate the occurrence of adverse effects reported by adult Jordanian individuals who have received a minimum of one dose of the locally available COVID-19 vaccines. Methods: Participants were recruited from multiple sources (hospitals, centers, laboratories, universities, and general community) to complete a validated questionnaire of three sections: socio-demographics, vaccination status and potential short-term (STSE) and long-term adverse effects (LTSE) of vaccinations. Results: A total of 1047 participants were enrolled in this study with a mean age of (33.44±15.72 years) and (52.8%) were female participants. The mean duration between the first dose and the time of filling the questionnaire was 507.46±131.87 days. Pfizer-BioNTech, Sinopharm, and AstraZeneca vaccines were most administered with two or more doses (94.8%). Of total participants, 58.5% reported at least one STSE with fatigue being the predominant (37.1%). All study subjects reported at least one LTSE, with fatigue (N=402, 38.4%) being the most frequently reported, followed by decreased concentration (N=343, 32.8%) and mood disturbances (N=333, 31.8%). Older age, male gender, smoking, chronic co-morbidities, multiple COVID-19 infections, and COVID-19 vaccine type and number of doses were significantly associated with many STSE and LTSE ($P<0.05$). Sinopharm vaccine recipients had a significantly higher frequency of most LTSE, whereas AstraZeneca vaccine recipients had a significantly higher frequency of most STSE. Conclusion: The frequency of COVID-19 vaccines LTSE was reported. Most reported adverse effects are mild confirming the risk-benefit value of COVID-19 vaccines.

Keywords*:* adverse effects, AstraZeneca, COVID-19 vaccines, long-term, Pfizer-BioNTech, Sinopharm

1. Introduction

After the flu of 1918, COVID-19 has been recognized as the fifth pandemic (Liu *et al*., 2020a). Since it was first discovered in Wuhan, China in October 2019, COVID-19 quickly spread worldwide (Liu *et al*., 2020a). As of July 2024, 775 million people have been infected with COVID-19 and over 6 million have died globally (WHO 2024). Since the genetic code of SARS-CoV-2 was revealed, global vaccine companies and scientists have started a race toward vaccine development that the entire world depends on (Haidere *et al*., 2021). The best method for limiting the pandemic is vaccination in conjunction with infection prevention (Haidere *et al*., 2021).

Several different potential vaccines have been developed for COVID-19, including inactivated or weakened virus vaccines, protein-based vaccines, viral vector vaccines and RNA and DNA vaccines (WHO 2023). By July 2021, 322 vaccines have been proposed, of which 99 were tested in clinical trials, 25 have reached phase III efficacy studies and 18 have received approval based on reported efficacies of their vaccines (Tregoning *et al*., 2021). The most utilized vaccines around the globe are Pfizer–BioNTech, Moderna, AstraZeneca–University of Oxford, Johnson & Johnson, Sputnik V, Sinovac Biotech, Sinopharm, Novavax and Bharat Biotech (Tregoning *et al*., 2021).

Many COVID-19 vaccines were approved and used in Jordan including Pfizer-BioNTech, AstraZeneca, Sinopharm and Sputnik V (Qaqish *et al*., 2022). As of 2023, more than 10 million doses of COVID-19 vaccines have been administered in Jordan with Pfizer-BioNTech and Sinopharm being the most commonly used vaccines

* Corresponding author. e-mail: mohammad.altamimi@hu.edu.jo

(MOH 2023a, MOH 2023b). In the Middle East region, different COVID-19 vaccines were available in different countries with Pfizer-BioNTech and Sinopharm being the most common (Bizri *et al*., 2023). Pfizer-BioNTech was widely used in Saudi Arabia, United Arab Emirates, Qatar and Kuwait while Sinopharm was commonly used in United Arab Emirates and Bahrain (Ganesan *et al*., 2022; Bizri *et al*., 2023).

Most vaccinations, compared to placebo, lower the percentage of participants having confirmed symptoms of COVID-19, and, for some, there is strong evidence that they lower severe or critical disease (Graña *et al*., 2022). In comparison to a placebo, Pfizer-BioNTech, Moderna, AstraZeneca, Sinopharm, and Bharat Biotech all showed lower incidences of symptomatic COVID-19 with vaccine effectiveness (VE): 97.84%, 93.20%, 70.23%, 78.10% and 77.80%, respectively. There is high-certainty evidence that Pfizer-BioNTech, Moderna, Janssen (Ad26.COV2.S) and Bharat Biotech vaccines largely reduced the incidence of critical or severe disease from COVID-19 with efficacies of: 95.70%, 98.20%, 76.30% and 93.40%, respectively (Graña *et al*., 2022).

Numerous studies reported the immediate or short-term adverse effects (STSE) of COVID-19 vaccinations. Data on the long-term or delayed effects of vaccinations are still lacking. The public and the scientific community must have access to these studies. Most significantly, safety data must be offered in a transparent and evidence-based approach (Dar-Odeh *et al*., 2022).

It is critical to continuously monitor COVID-19 vaccine adverse effects, and studies are now being conducted to monitor vaccination safety. So far, no vaccine can be labeled completely free of adverse effects, but most of these adverse effects are preventable or treatable (Spencer *et al*., 2017). Early adverse effects have been reported after all types of vaccines but are more likely to occur after the new-generation vaccines (Abu-Halaweh *et al*., 2021). The most common adverse effect reported shortly after the first two doses was pain at the injection site, followed by fatigue, headache and myalgia (Mulligan *et al*., 2020; Ganesan *et al*., 2022). About one in six recipients of the COVID-19 vaccine may complain of long-term adverse effects (LTSE) (Dar-Odeh *et al*., 2022). The most frequently reported LTSE was fatigue and its related symptoms. Among COVID-19 vaccines Pfizer-BioNTech was the least associated with LTSE (Dar-Odeh *et al*., 2022).

In this study, we aim to compare LTSE associated with COVID-19 vaccines and explore the potential effect of gender, age, co-morbidities and vaccine type or number of doses on the development of these adverse effects.

2. Methods

2.1. Study Design

A cross-sectional observational design was implemented in this study. The sample population consisted of adult Jordanian individuals who were eighteen years of age or older and had received at least one dose of any of the locally available COVID-19 vaccines, including Pfizer-BioNTech (Pfizer, United States of America and BioNTech, Germany, COMIRNATY®), Sinopharm (Sinopharm China National Biotec Group, China, BBIP-CorV), AstraZeneca (Oxford University, United Kingdom and AstraZeneca, United Kingdom/Sweden, ChAdOx1-S), Sputnik (Gamaleya Research Institute of Epidemiology and Microbiology, Russia, Gam-COVID-Vac), Moderna (Moderna, USA, Spikevax), and Johnson & Johnson (Janssen Pharmaceutical Company of Johnson & Johnson, USA, Janssen).

2.2. Data Collection

Data was collected through the use of an online survey administered via the Google Forms platform and disseminated to participants through various channels, including personal interviews, university lectures, patient encounters and social media platforms. The survey was accessible for four months, starting from July 28th to November 28th, 2022. The mean duration between the first dose and the time of filling the questionnaire was about (507.46 days ± 131.87 days). The final sample size of the study consisted of 1047 individuals. Participants were recruited from multiple sources, including university students from four public and private institutions, inpatients and outpatients from three public and private hospitals, visitors to private and public tertiary care centers and clinics, visitors to private and public diagnostic laboratories, family members and friends of participants, and members of the community at large. The study population was diverse, with representation from different geographic regions, age groups, genders, and socio-economic statuses, as well as individuals with varying degrees of health.

The online questionnaire, available exclusively in the Arabic language, consisted of 45 questions that were divided into three sections: socio-demographics, vaccination status, and potential STSE and LTSE of the vaccine. The socio-demographic section comprised questions regarding gender, age, height, weight, co-morbidities, smoking status, and history of COVID-19 infection. The vaccination status section included questions about the number of doses received, type of vaccine, timing of doses, and immediate adverse effects after vaccination. The adverse effects section was further divided into sub-sections about different organ systems, including the neurological, cardio-vascular, respiratory, gastrointestinal, reproductive, musculoskeletal, integumentary, endocrine systems, as well as systemic signs and symptoms. Each sub-section focused on specific symptoms related to the respective organ system. Participants responded to the questions with yes or no. Body mass index (BMI) was calculated using weight in kilograms divided by height in meters squared. Adverse effects that occurred within 7 days post vaccination were considered STSE, while adverse effects after 7 days of vaccination were considered LTSE.

The questionnaire items pertaining to the STSE and LTSE of COVID-19 vaccines were chosen following a comprehensive review of the scientific literature that encompassed case reports, cross-sectional studies, clinical trials, systematic reviews, and meta-analyses, as well as other relevant studies that have documented vaccine adverse effects (Alqassieh *et al*., 2021; Dar-Odeh *et al*., 2022; Bhandari *et al*., 2022; Bhattacharya *et al*., 2022; Dawoud *et al*., 2022; Ilonze and Guglin, 2022; Medeiros *et al*., 2022). Furthermore, we consulted official reports from local regulatory bodies, such as the Jordanian Ministry of

Health (MOH 2023a), the Jordan Food and Drug Administration (JFDA 2023), and the Jordanian Center for Disease Control (JCDC 2023), to identify any available data on reported vaccine adverse effects. The opinions of specialized healthcare professionals were also sought to incorporate adverse effects reported within the community. In addition, a pilot test of the survey was conducted on 5 participants, and necessary modifications were made to the questionnaire before it was made available to the study participants. Participants were provided with a clear explanation of the purpose of the study and a guarantee of confidentiality prior to their participation, for which they were required to provide virtual consent.

2.3. Ethical Approval

The study was granted ethical approval by the institutional review board (IRB) at the Hashemite University (Reference No.22/4/2021/2022). To protect the participants' privacy, no personal information was included in the survey. Participants were given the option to withdraw from the study at any time without the need to provide an explanation. The data collected was assigned codes based on the national identification numbers of the participants, serving as deidentifiers. The collected data was used solely for statistical analysis purposes.

2.4. Statistical Analysis

The statistical analysis was conducted with the use of SPSS software (Statistical Package for the Social Sciences version 24.0 Chicago, IL, USA). Categorical variables were presented as numbers and percentages, while continuous variables were expressed as mean ± standard deviation (SD). Moreover, continuous variables, such as age and BMI, were stratified into age groups of 20 years or categorized as underweight, normal weight, overweight, or obese for BMI. The differences in baseline characteristics between vaccine types and number of doses were evaluated using the Chi-squared test or Fisher's exact test, as appropriate. Similarly, the Chi-squared test was utilized to compare the frequency of adverse reactions among different vaccine types and doses, and bivariate Pearson correlation was applied to confirm the results of the Chi-squared test, when applicable. Statistical significance was established at $P < 0.05$. Adverse effects that occurred with a frequency of less than 5% were excluded from inferential statistical analysis. Moreover, multivariate analysis was performed using binary logistic regression.

3. Results

3.1. Participants (Demographics)

A total of 1047 participants who received at least one of the vaccines Pfizer-BioNTech, Sinopharm, AstraZeneca, Moderna, Johnson and Johnson, and Sputnik vaccines concluded the sample of the study, with Pfizer-BioNTech being the majority 617 (58.9%). The demographic distribution of the selected individuals is shown in Table 1. Participants were 494 (47.2%) males and 553 (52.8%) females. The mean age was 33.44 ± 15.72 years, with the majority of the participants ages range between 20–60 years (69.1%). Most participants were non-smokers (N = 703, 67.1%) and only 376 (35.9%) had chronic diseases with hypertension (16.3%) and diabetes (12.3%) being the most frequent chronic diseases respectively (Table 1). The average BMI was 25.6 ± 5.3.

Table 1. Demographic, clinical data and COVID-19 infection and vaccination details of the study population (N = 1047).

	Variable		Number (%)	
Age (Years)	0-20		188 (18.0)	
	21-40		475 (45.4)	
	41-60		248 (23.7)	
	Above 60		136 (13.0)	
Gender	Male		494 (47.2)	
	Female		553 (52.8)	
BMI	Underweight <18.5		47 (4.5)	
	Normal 18.5-24.9		407 (38.9)	
	Overweight 25-29.9		390 (37.2)	
	Obese ≥30		203 (19.4)	
Smoking	Yes		344 (32.9)	
	No		703 (67.1)	
Chronic diseases	Yes		376 (35.9)	
	Hypertension		171 (16.3)	
	Diabetes Mellitus		129 (12.3)	
	Cardiac diseases		70 (6.7)	
	Hyperlipidemia		66 (6.3)	
	Thyroid diseases		61 (5.8)	
	Asthma		57 (5.4)	
	Others (cancer, kidney, digestive, lung disease, etc)		94 (9.0)	
COVID-19 Infection	Yes		573 (54.7)	
	Confirmed by RT-PCR		432 (41.3)	
	One		374 (35.7)	
	Two		150 (14.3)	
	Three		36 (3.4)	
	Four		13 (1.2)	
	After vaccine		354 (33.8)	
	Before vaccine		219 (20.9)	
COVID-19 Vaccination	Yes		1047 (100)	
	One dose		54 (5.2)	
	Two doses		733 (70.0)	
	Three doses		244 (23.3)	
	Four doses		16 (1.5)	
Type of vaccine	First dose	Second dose	Third dose	Forth dose
Sinopharm	329 (31.4)	320 (30.6)	22 (2.1)	2 (0.2)
Pfizer	617 (58.9)	592 (56.5)	235 (22.4)	14 (1.3)
Johnson	1 (0.1)	0 (0.0)	1 (0.1)	0 (0)
Moderna	2 (0.2)	1 (0.1)	2 (0.2)	2 (0.2)
AstraZeneca	88 (8.4)	74 (7.1)	0 (0)	0 (0)
Sputnik V	10 (1.0)	6 (.6)	0 (0)	0 (0)
Duration/days	First dose	Second dose	Third dose	
0-100	1 (0.1)	10 (1.0)	9 (0.9)	
101-200	27 (2.6)	51 (4.9)	18 (1.7)	
201-300	59 (5.6)	61 (5.8)	58 (5.5)	
301-400	83 (7.9)	119 (11.4)	101 (9.6)	
401-500	252 (24.1)	290 (27.7)	19 (1.8)	
Above 500	599 (57.2)	432 (41.3)	16 (1.5)	

3.2. Participants (COVID-19 infection and vaccination)

Out of all participants, only 573 (54.7%) reported COVID-19 infection, 75% of these infections were confirmed by Reverse transcription polymerase chain reaction (RT-PCR). While the majority of these had only one infection (N = 374, 65.3%), others had two (N =150, 26.2%), three (N = 36, 6.3%), and even some had four (N = 13, 2.3%) infections (Table 1). Participants who reported COVID-19 infection before any dose of vaccination were 219 (38.2%), while who got infected after receiving at least one dose of the vaccine were 354 (61.8%). Regarding

vaccination, 94.8% of the participants received at least two doses of the vaccine.

3.3. Reported STSE after vaccine administration

As demonstrated in Table 2, a total of 613 (58.5%) participants reported at least one STSE post-vaccination. Fatigue (37.1%) was the predominant STSE, followed by myalgia, fever, redness and pain at the site of infection, headache, arthralgia, and palpitation respectively. The frequency of reported STSE was almost the same after each dose of vaccination (Figure 1A, B and C) with no participants receiving a booster dose (third dose) of AstraZeneca vaccine (Figure 1C and Table 1). However, participants who received AstraZeneca had significantly higher percentages of almost all STSE (Figure 1 and Table 3). Sinopharm-vaccinated participants were significantly the least to report STSE post-vaccination (Figure 1 and Table 3). Of notice is that the first and the second doses were of the same vaccine type for most participants while the third dose were of a different vaccine type.

The number of vaccines doses each participant received showed significant association with age, gender, BMI, chronic diseases and COVID-19 infections (Table 3). Furthermore, despite no significant association with STSE in general, there was a significant association with fatigue, myalgia, fever, and headache as the frequency of these adverse effects increased with the second dose compared to the first dose and then dropped slightly with the third dose (Figure 2 and Table 3).

3.4. Reported LTSE after vaccine administration

All participants reported at least one LTSE (N = 1047). The most frequent LTSE reported as shown in Table 2 was fatigue (38.4%), followed by decreased concentration levels and mood changes being the second and third most frequent adverse effects respectively. Moreover, out of 553 female participants, 138(24.7%) reported irregularities in the menstrual period. Jaundice (1.9%) and bloody urine (1.6%) were the least reported LTSE. Participants who received third dose of Sinopharm were significantly the most to report all LTSE except menstrual irregularities, urinary frequency, change in libido, and change in bowel habits that were not statistically significant (Figure 3C and Table 3).

Fatigue-associated symptoms (headache, myalgia, muscle weakness) as well as most LTSE demonstrated in Table 3 had statistically significant associations with the number of vaccine doses participants got. However, menstrual irregularities, urinary frequency, and change in libido were not statistically significant. Interestingly, some LTSE frequencies either significantly increased with the second dose and then dropped with the third dose (fatigue, headache, loss of concentration, mood changes, muscle weakness or pain, difficulty of breathing and palpitation), or there was a gradual decrease of the frequencies of other LTSE with increased number of doses (Figure 4).

Table 2. Frequency of short-term (STSE) and long-term adverse effects (LTSE) of COVID-19 vaccines reported by study participants (N = 1047).

	Variable	Number (%)
Short-term adverse effects (STSE)	Yes	613 (58.5)
	Fatigue	388 (37.1)
	Myalgia	299 (28.6)
	Fever	291 (27.8)
	Redness and pain at injection site	272 (26.0)
	Headache	240 (22.9)
	Arthralgia	175 (16.7)
	Palpitation	51 (4.9)
Pregnancy or abortion during vaccination	Yes	11 (1.1)
	Normal pregnancy	6 (0.6)
	Abortion	5 (0.5)
Long-term adverse effects (LTSE)	Yes at least one	1047 (100)
	Any diagnosis after vaccination	54 (5.2)
	Clotting	8 (0.8)
	Lung disease	5 (0.5)
	Joint disease	12 (1.1)
	Other disease	29 (2.8)
	Increase in previous diseases after vaccine	102 (9.7)
	Fatigue	402 (38.4)
	Loss of concentration	343 (32.8)
	Mood changes	333 (31.8)
	Muscle weakness or pain	287 (27.4)
	Headache	276 (26.4)
	Menstrual period changes (females only)	138 (24.7)
	Dizziness	237 (22.6)
	Numbness and paraesthesia	234 (22.3)
	Change in weight	219 (20.9)
	Increased weight	122 (11.7)
	Decreased weight	97 (97)
	Anemia symptoms	185 (17.7)
	Hotness or cold	177 (16.9)
	Feeling cold	96 (9.2)
	Feeling hot	81 (7.7)
	Difficulty of breathing	166 (15.9)
	Joints pain	158 (15.1)
	Chest pain	150 (14.3)
	Palpitation	147 (14.0)
	Abdominal distension	139 (13.3)
	Thirst	131 (12.5)
	Urinary frequency	119 (11.4)
	Changes in bowel habits	108 (10.3)
	Constipation	60 (5.7)
	Diarrhea	34 (3.2)
	Bloody stool	14 (1.3)
	Changes in libido (married)	37 (6.8)
	Skin rash	69 (6.6)
	Difficulty in erection (males only)	20 (3.8)
	Difficulty in speaking	32 (3.1)
	Coma or loss of consciousness	28 (2.7)
	Difficulty in conception (married)	28 (2.7)
	Pain or blood during intercourse (females only)	9 (2.0)
	Jaundice	20 (1.9)
	Bloody urine	17 (1.6)

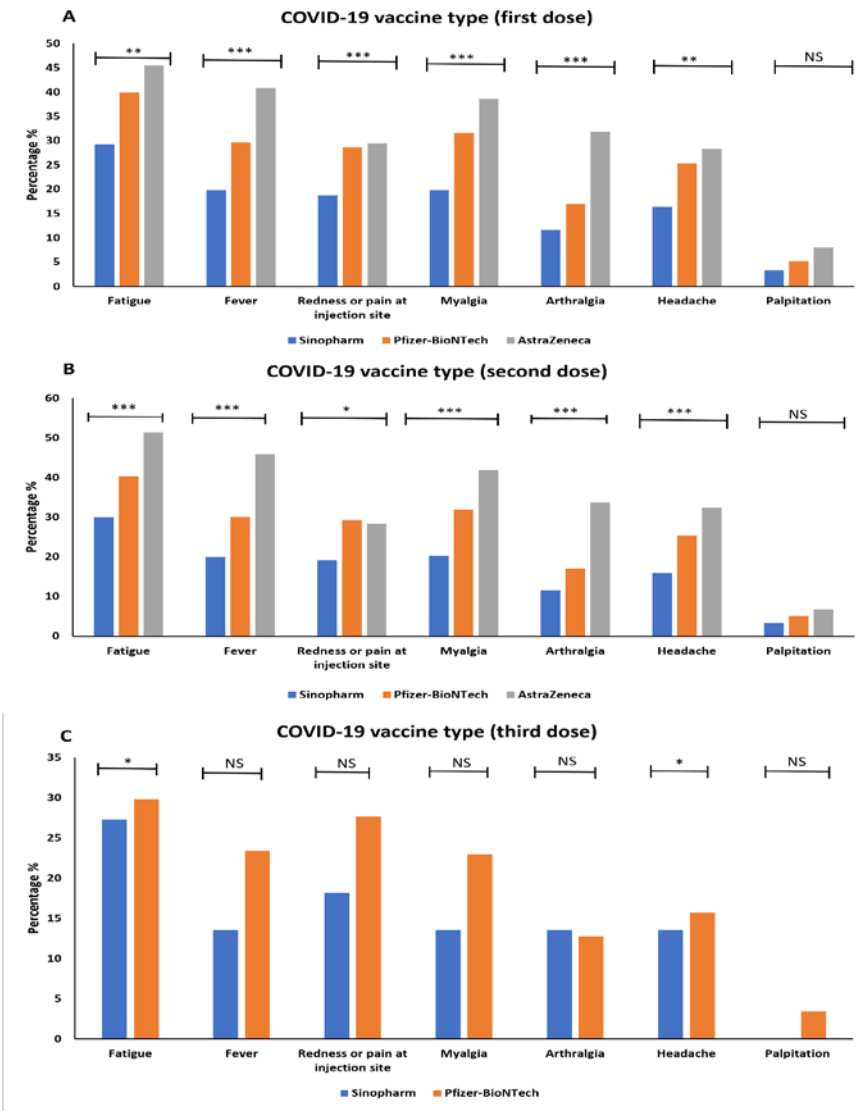

Figure 1. COVID-19 vaccine types and short-term adverse effects (STSE). The frequency of STSE according to COVID-19 vaccine type: first dose (A), second dose (B), and third dose (C). Adverse effects with a frequency less than 5% were not included. *Significance less than 0.05, **Significance less than 0.01, ***Significance less than 0.001, NS not significant

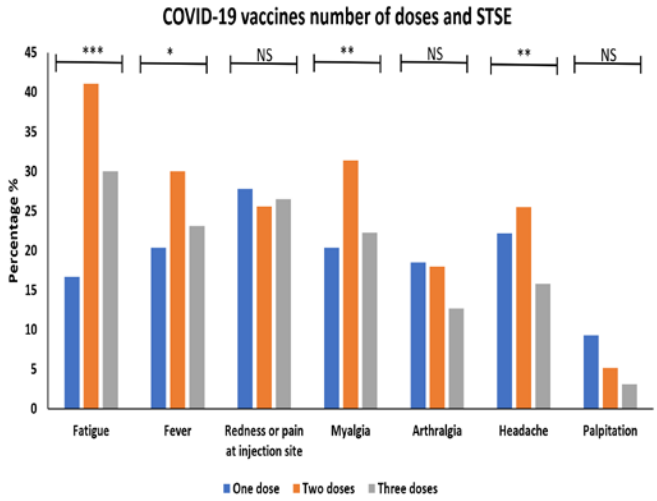

Figure 2. COVID-19 vaccines number of doses and STSE. The frequency of STSE according to COVID-19 vaccine number of doses. Adverse effects with a frequency less than 5% were not included. * Significance less than 0.05, ** Significance less than 0.01, *** Significance less than 0.001, NS not significant.

Table 3. Association of COVID-19 vaccination number of doses (one, two, or three doses) and type of vaccine (Pfizer-BioNTech, Sinopharm, and AstraZeneca) with demographics, COVID-19 infections and COVID-19 vaccination STSE and LTSE. Numbers are for P values estimated by cross tabulation with Chi-square test or Fisher-exact test. Adverse effects less than 5%, COVID-19 vaccines administered less than 5% (Johnson & Johnson, Moderna, and Sputnik), and the fourth dose administered for less than 5% were not included in the analysis.

	Number of vaccine doses	COVID-19 vaccination type (Pfizer-BioNTech, Sinopharm, and AstraZeneca)		
		First dose vaccine type	Second dose vaccine type	Third dose vaccine type
Age	0.000	0.000	0.000	0.000
Gender	0.000	0.258	0.309	0.000
BMI	0.000	0.009	0.001	0.000
Smoking	0.143	0.068	0.072	0.890
Chronic diseases	0.000	0.024	0.108	0.000
COVID-19 infection	0.000	0.129	0.002	0.000
Confirmed RT-PCR	0.001	0.150	0.057	0.005
Timing of infection	0.001	0.101	0.071	0.003
Short-term adverse effects	0.120	0.000	0.000	0.309
Fatigue (short-term)	0.000	0.005	0.000	0.027
Myalgia	0.008	0.000	0.000	0.053
Fever	0.046	0.000	0.000	0.053
Redness and pain at injection site	0.916	0.001	0.021	0.550
Headache (short-term)	0.006	0.004	0.003	0.014
Arthralgia	0.133	0.000	0.000	0.223
Palpitation (short-term)	0.122	0.282	0.341	0.397
Any diagnosis after vaccination	0.089	0.068	0.021	0.562
Increase in previous diseases	0.000	0.003	0.014	0.039
Fatigue (long-term)	0.000	0.288	0.108	0.000
Headache (long-term)	0.000	0.068	0.117	0.000
Loss of concentration	0.001	0.334	0.338	0.002
Mood changes	0.000	0.122	0.390	0.000
Muscle weakness or pain	0.001	0.155	0.392	0.004
Menstrual period changes	0.148	0.336	0.667	0.332
Dizziness	0.000	0.248	0.164	0.000
Numbness and paraesthesia	0.008	0.960	0.684	0.012
Change in weight	0.002	0.710	0.342	0.001
Anemia symptoms	0.000	0.278	0.017	0.000
Hotness or cold	0.000	0.158	0.532	0.000
Difficulty of breathing	0.000	0.134	0.254	0.000
Joints pain	0.028	0.254	0.462	0.017
Chest pain	0.000	0.723	0.166	0.000
Palpitation (long-term)	0.000	0.602	0.441	0.000
Abdominal distention	0.017	0.620	0.870	0.005
Thirst	0.001	0.315	0.030	0.033
Urinary frequency	0.072	0.875	0.911	0.060
Changes in bowel habits	0.004	0.108	0.052	0.086
Changes in libido	0.106	0.104	0.227	0.183
Skin rash	0.009	0.561	0.418	0.034

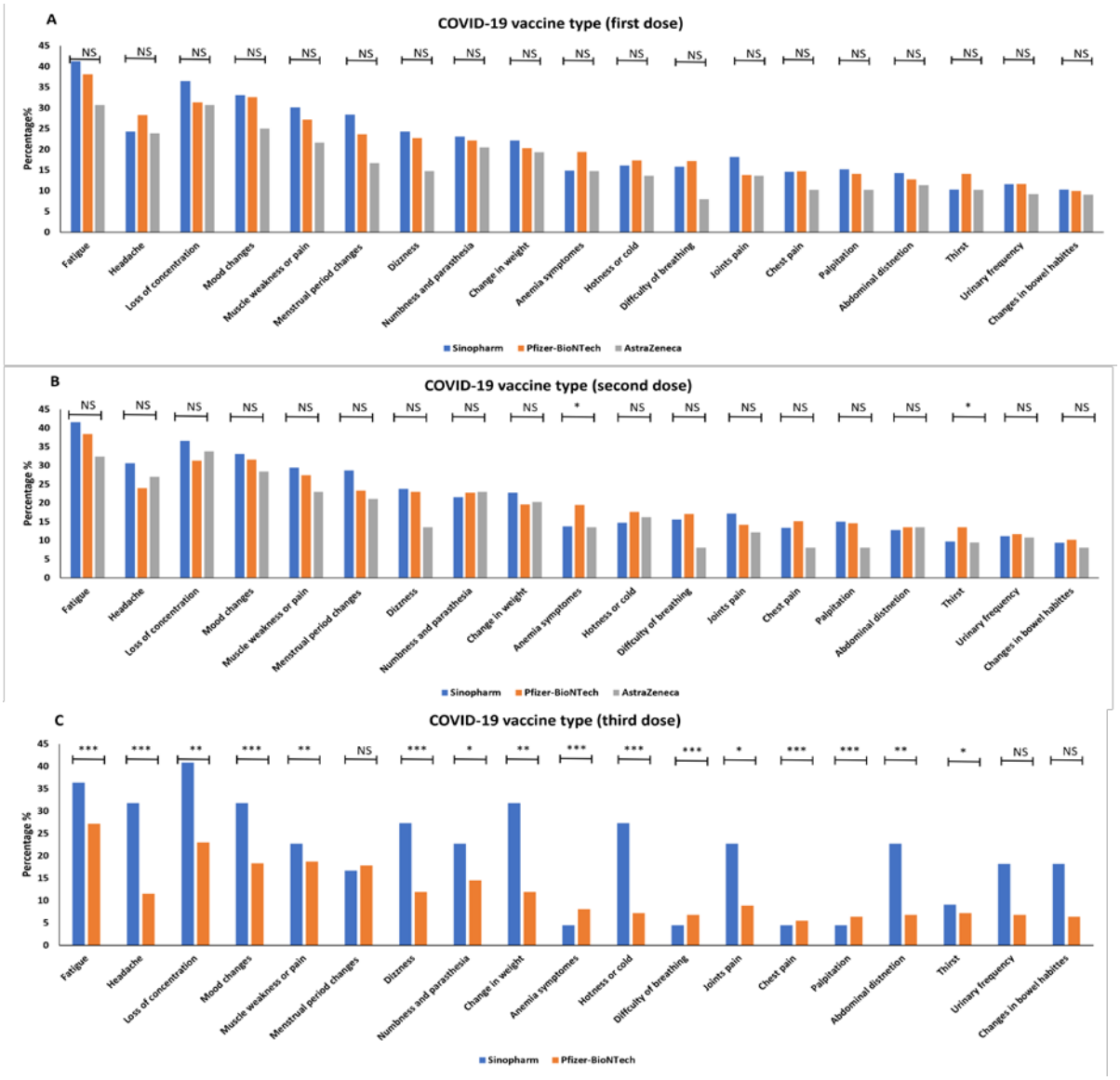

Figure 3. COVID-19 vaccine types and LTSE. (A) COVID-19 vaccine type first dose, (B) second dose, and (C) third dose). Adverse effects with a frequency less than 5% were not included. *Significance less than 0.05, **Significance less than 0.01, ***Significance less than 0.001, NS not significant.

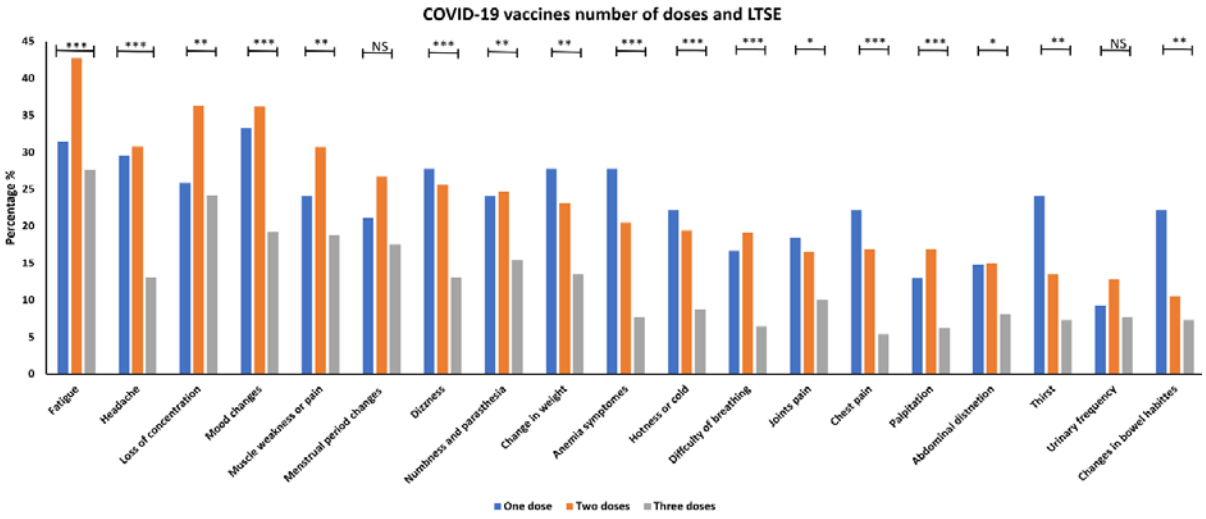

Figure 4. COVID-19 vaccines number of doses and LTSE. Adverse effects with a frequency less than 5% were not included. *Significance less than 0.05, **Significance less than 0.01, ***Significance less than 0.001, NS not significant.

3.5. Factors associated with LTSE

As demonstrated in Table 4, males have a statistically significant association with all of the reported LTSE, but not urinary frequency, which showed no significant association with gender (P > 0.05). Smokers reported more fatigue and urinary frequency in the long-term post-vaccination; however, smoking was not significantly associated with other LTSE. Fatigue had more statistically significant occurrence among males, older age smokers, individuals with chronic diseases, as well as those with multiple COVID-19 infections. Skin rash was not significantly associated with age, obesity, smokers, chronic diseases, or COVID-19 infection. However, skin rash was reported more among males (P = 0.002). Women who reported irregularities in menstrual cycle were associated with older age groups, obesity, chronic diseases as well the number of COVID-19 infections. On the other hand, Males reported more changes in libido.

Table 4. Association of age, gender, BMI, smoking, chronic diseases and COVID-19 infection with COVID-19 vaccine STSE and LTSE. Numbers are for P values estimated by cross tabulation with Chi-square test or Fisher-exact test. Adverse effects less than 5% were not included in the analysis.

	Age	Gender	BMI	Smoking	Chronic diseases	COVID-19 infection
Age	-	0.001	0.000	0.000	0.000	0.000
Gender	0.001	-	0.001	0.000	0.660	0.012
BMI	0.000	0.000	-	0.001	0.000	0.793
Smoking	0.000	0.000	0.001	-	0.301	0.434
Chronic diseases	0.000	0.660	0.000	0.301	-	0.137
COVID-19 Infection	0.000	0.023	0.403	0.101	0.050	-
Confirmed by RT-PCR	0.000	0.011	0.076	0.360	0.021	-
Timing of last infection related to vaccine	0.000	0.019	0.139	0.956	0.000	-
COVID-19 vaccination number of doses	0.000	0.000	0.000	0.143	0.000	0.000
First dose type of vaccine	0.000	0.263	0.009	0.068	0.024	0.129
Second dose type of vaccine	0.000	0.303	0.001	0.070	0.103	0.002
Thrid dose type of vaccine	0.000	0.000	0.000	0.897	0.000	0.000
Short-term adverse effects	0.000	0.000	0.000	0.378	0.008	0.000
Fatigue (short-term)	0.000	0.000	0.000	0.731	0.000	0.000
Myalgia	0.000	0.000	0.000	0.972	0.000	0.000
Fever	0.002	0.000	0.001	0.429	0.517	0.011
Redness and pain at injection site	0.132	0.003	0.044	0.013	0.259	0.005
Headache (short-term)	0.000	0.000	0.000	0.516	0.020	0.000
Arthralgia	0.121	0.000	0.246	0.537	0.237	0.000
Palpitation	0.205	0.000	0.004	0.941	0.838	0.000
Any diagnosis after vaccination	0.192	0.893	0.009	0.118	0.000	0.560
Increase in previous diseases	0.000	0.057	0.004	0.003	0.000	0.025
Fatigue (long-term)	0.000	0.000	0.149	0.031	0.000	0.005
Headache (long-term)	0.000	0.000	0.206	0.066	0.783	0.007
Loss of concentration	0.000	0.000	0.134	0.377	0.699	0.000
Mood changes	0.000	0.000	0.351	0.352	0.305	0.000
Muscle weakness or pain	0.000	0.000	0.401	0.256	0.000	0.000
Menstrual period changes	0.000	-	0.002	0.262	0.001	0.017
Dizziness	0.244	0.000	0.103	0.859	0.004	0.002
Numbness and paraesthesia	0.000	0.000	0.407	0.079	0.000	0.661
Change in weight	0.392	0.000	0.018	0.877	0.006	0.536
Anemia symptoms	0.017	0.000	0.000	0.318	0.441	0.070
Hotness or cold	0.611	0.000	0.052	0.280	0.008	0.072
Difficulty of breathing	0.467	0.000	0.064	0.239	0.000	0.000
Joints pain	0.000	0.004	0.000	0.095	0.000	0.028
Chest pain	0.181	0.000	0.178	0.068	0.000	0.214
Palpitation (long-term)	0.157	0.000	0.179	0.609	0.000	0.018
Abdominal distention	0.377	0.000	0.477	0.220	0.179	0.035
Thirst	1.000	0.003	0.385	0.324	0.033	0.193
Urinary frequency	0.889	0.315	0.365	0.040	0.244	0.011
Changes in bowel habits	0.031	0.015	0.061	0.447	0.000	0.004
Changes in libido	0.100	0.000	0.935	0.412	0.706	0.052
Skin rash	0.522	0.002	0.942	0.859	0.106	0.052

3.6. Multivariate analysis of factors associated with STSE and LTSE

Multivariate regression analysis, shown in Table 5, demonstrates the association between STSE and males, older ages, as well as participants who got infected with COVID-19. Regarding factors associated with LTSE once more, men exhibit statistically significant associations with joint discomfort and weariness. Moreover, males have statistically significant urine frequency (P = 0.038). Smokers are associated with more anemia-related symptoms (P = 0.034) and with muscle pain (P = 0.048). BMI and history of COVID-19 infection of the participants played a minor role, and most LTSE showed no statistically significant association as seen in Table 5. After immunization, individuals' experiences of being hot or chilly were statistically significantly correlated with the number of vaccine doses they had received (P = 0.009). Chronic tiredness, attention loss, and a sense of numbness in the limbs were the most reported symptoms and showed a statistically significant link among subjects who had

received the COVID-19 vaccination the earliest at the time of the interview. Moreover, more of the same people reported an increase in the severity of preexisting chronic illnesses.

Table 5. Multivariate regression analysis of the effect of age, gender, BMI, smoking, chronic diseases, COVID-19 infection and COVID-19 vaccine doses, type and duration on STSE and LTSE. Numbers are for P values estimated by binary logistic regression. Adverse effects less than 5% were not included in the analysis.

	Age	Gender	BMI	Smoking	Chronic diseases	COVID-19 infection	Vaccine doses	Vaccine type	Vaccine duration
Short-term adverse effects (any)	0.015	0.029	0.181	0.130	0.085	0.028	0.566	0.585	0.032
Fatigue (short-term)	0.005	0.278	0.233	0.665	0.158	0.024	0.889	0.954	0.493
Myalgia	0.089	0.202	0.113	0.182	0.250	0.080	0.532	0.780	0.719
Fever	0.094	0.131	0.117	0.116	0.021	0.130	0.540	0.983	0.198
Redness and pain	0.905	0.302	0.617	0.359	0.763	0.621	0.107	0.917	0.250
Headache (short-term)	0.241	0.123	0.331	0.340	0.060	0.132	0.500	0.766	0.716
Arthralgia	0.236	0.069	0.726	0.957	0.014	0.038	0.176	0.672	0.868
Palpitation (short-term)	0.096	0.999	0.130	0.999	0.065	0.824	0.370	0.296	0.316
Any diagnosis after vaccination	0.810	0.486	0.976	0.636	0.577	0.308	0.338	0.172	0.313
Increase in previous diseases	0.862	0.590	0.425	0.636	0.015	0.963	0.513	0.045	0.019
Fatigue (long-term)	0.846	0.028	0.397	0.409	0.022	0.987	0.475	0.182	0.035
Headache	0.899	0.087	0.812	0.444	0.644	0.306	0.564	0.114	0.264
Loss of concentration	0.764	0.950	0.332	0.785	0.768	0.708	0.340	0.233	0.049
Mood changes	0.550	0.232	0.245	0.546	0.485	0.780	0.599	0.928	0.554
Muscle weakness or pain	0.217	0.127	0.554	0.048	0.093	0.916	0.632	0.215	0.719
Menstrual period changes	0.178	0.999	0.156	0.999	0.296	0.235	0.729	0.065	0.388
Dizziness	0.769	0.258	0.824	0.832	0.103	0.527	0.407	0.498	0.113
Numbness and paraesthesia	0.435	0.062	0.300	0.645	0.045	0.127	0.499	0.705	0.025
Change in weight	0.611	0.049	0.080	0.477	0.796	0.580	0.003	0.002	0.839
Anemia symptoms	0.496	0.626	0.343	0.034	0.703	0.636	0.606	0.028	0.107
Hotness or cold	0.283	0.002	0.395	0.922	0.007	0.673	0.009	0.004	0.081
Difficulty of breathing	0.072	0.624	0.367	0.121	0.229	0.912	0.371	0.814	0.015
Joints pain	0.077	0.002	0.400	0.129	0.880	0.162	0.593	0.063	0.062
Chest pain	0.789	0.112	0.424	0.204	0.121	0.737	0.364	0.071	0.452
Palpitation	0.285	0.617	0.762	0.311	0.066	0.143	0.280	0.135	0.834
Abdominal distention	0.473	0.025	0.464	0.125	0.406	0.943	0.137	0.048	0.729
Thirst	0.136	0.283	0.665	0.847	0.654	0.933	0.699	0.242	0.359
Urinary frequency	0.378	0.038	0.916	0.559	0.774	0.960	0.718	0.094	0.751
Changes in bowel habits	0.317	0.133	0.030	0.751	0.302	0.338	0.260	0.447	0.621
Changes in libido	0.062	0.235	0.318	0.272	0.925	0.371	0.474	1.000	0.650
Skin rash	0.918	0.108	0.700	0.985	0.427	0.405	0.533	0.252	0.812

4. Discussion

The adverse reactions to vaccines in general are a globally well-documented issue that mandates appropriate reporting by many authorization and licensing agencies and bodies across the world (Spencer *et al.*, 2017; Dar-Odeh *et al*., 2022; Bhandari *et al*., 2022; JFDA 2023; WHO 2024). Numerous studies reported the STSE of COVID-19 vaccinations (Mulligan *et al*., 2020; Abu-Halaweh *et al*., 2021; Alqassieh *et al*., 2021; Dawoud *et al*., 2022; Ilonze and Guglin, 2022; Medeiros *et al*., 2022). Data on LTSE of COVID-19 vaccinations are limited due to the recent approval of these vaccines following the pandemic (Dar-Odeh *et al*., 2022). The introduction of new mRNA-based and other new technologies in COVID-19 vaccine development for the first time requires further attention and continuous mentoring of LTSE (Kadali *et al*., 2021). Furthermore, a lot of studies have investigated the adverse reactions to COVID-19 vaccines mainly Pfizer-BioNTech, AstraZeneca, and Moderna (Kadali *et al*., 2021; Menni *et al*., 2021; Riad *et al*., 2021). However, few studies evaluated the adverse effects of Sinopharm vaccine (Hatmal *et al*., 2021; Saeed *et al*., 2021). This study provides an epidemiological report for COVID-19 vaccines LTSE in Jordan and provides an analysis of factors contributing to the occurrence of these LTSE. The mean duration between the first vaccine dose and the time of the study was 507.46 ±131.87 days with more than 90% of participants passed one year.

The associations between age, gender, obesity, and smoking with chronic diseases overall or with certain chronic diseases reported in this study are very well-known as reported previously (Zhu *et al*., 2014) and observed by similar studies in Jordan (Khader *et al*., 2008). COVID-19 infection frequency, severity, hospitalization, and death rate proved to increase with age, male gender, obesity, chronic diseases, smoking, and other risk factors (Liu *et al*., 2020b). However, in this study, participants above 60 years of age with a significantly higher

frequency of obesity and chronic diseases had significantly lower rates of COVID-19 infections and recurrence. Also, males had lower rates of infection and recurrence. Mostly, this is related to the significantly higher frequency of booster doses (3rd dose) vaccination among these groups, consistent with other studies (Diesel *et al*., 2021) and emphasizing the protective effect of the third dose (McMenamin *et al*., 2022).

Approximately, 58.5% of the research population reported at least one STSE which is comparable to another study in Jordan (46.3%) (Abu-Halaweh *et al*., 2021) and other countries (60%) (Alhazmi *et al*., 2021). The most frequent STSE was fatigue (37.1%) followed by myalgia (28.6%), fever (27.8%), pain and redness at the injection site (26%), and headache (22.9%), in contrast to other studies where the pain at the injection site was the most frequently reported adverse effect (Abu-Halaweh *et al*., 2021; Zahid, 2021). The highest frequency of STSE reported in the AstraZeneca group followed by Pfizer-BioNTech, then Sinopharm is consistent with the findings of other studies (Alhazmi *et al*., 2021; Alqassieh *et al*., 2021; Dawoud *et al*., 2022). The frequency of adverse effects was similar after the first 2 doses of Pfizer-BioNTech and Sinopharm in contrast to AstraZeneca, which was higher after the second dose of the vaccine. This is not consistent with other studies that reported a higher frequency of adverse effects after the first dose compared to the second dose (Zahid, 2021). The third dose's STSE was lowest compared to the first 2 doses for both Pfizer-BioNTech or Sinopharm which is best justified by the long interval between the 2nd and the third doses. This could be due to the decreased cumulative effect of doses and the difference in the type of the vaccine in many people compared to the first 2 doses.

There is a statistically significant association between age and STSE with the least reported adverse effect frequencies being lowest in the above 60 age group and highest in below 20 age group. Fatigue was the most frequent STSE for below 60 age group while pain at the injection site was the most frequent for above 60 age group which correlates with findings from another study outside Jordan (Green *et al*., 2022). Females have reported more STSE than males consistent with another study's findings (Saeed *et al*., 2021). There was a statistically significant relationship between previous COVID-19 infection and STSE which contradicts the finding from another study outside Jordan that reported no significant difference (Lai *et al*., 2022). In this study, no systemic life-threatening STSE was reported, and the overall rate of the adverse effects was within the familiar range of these vaccines.

Few studies were done on the LTSE of COVID-19 vaccines, but this study provides a detailed analysis of LTSE in Jordan. 100% of study participants reported at least one LTSE, in contrast to another study done in 2021 in Saudi Arabia and Jordan, only 16.1% of participants reported at least one LTSE (Dar-Odeh *et al*., 2022). This can be explained by the time difference among studies as this study was done during 2022/2023, after a longer period after vaccine administration. A lot of LTSE becomes evident after a latent period and people usually take a long time to note a difference in their baseline. The most frequent LTSE was fatigue followed by loss of concentration and mood changes, while the least reported adverse effects were jaundice and bloody urine consistent with another study finding (Dar-Odeh *et al*., 2022). The frequencies of adverse effects were comparable for the first 2 doses but lower after the third dose, most likely due to longer duration between the second and third doses, the same trend as that of STSE. Patients receiving Sinopharm reported more frequencies for most of the LTSE effects than Pfizer-BioNTech after the third dose.

5.2% of participants received a diagnosis for a new disease after vaccination, most commonly being joint diseases. As consistent with other study findings, there was no statistically significant difference between males and females in this concern. In contrast, others reported more frequent arthritis in females (Chen *et al*., 2022; Chen and Chen, 2023). The highest percent of the newly diagnosed diseases was in the Pfizer-BioNTech vaccine group and the least in the AstraZeneca group. 9.7% of participants reported increasing in previous diseases severity including most chronic diseases, especially hypertension, diabetes mellitus (DM), cardiac diseases, and thyroid diseases. Other studies reported that the vaccine increases blood pressure in previously hypertensive patients and leads to poorer glycemic control in patients with DM, especially who take insulin and oral hypoglycemic agents (Angeli *et al*., 2022; Heald *et al*., 2021).

A statistically significant relationship between the rate of LTSE and gender is found to be more frequent in men. Fatigue was more reported in the elderly, smokers, and individuals with chronic diseases. This might be because these groups have little reserve in their bodies, making them more sensitive to notice changes related to their health status. Smokers reported more anemia-related symptoms. Smokers need higher basal hemoglobin levels compared to non-smokers. Hence, any reduction in hemoglobin makes them feel anemic even if they have near normal hemoglobin levels, known to be sufficient for smokers (Nordenberg *et al*., 1990).

The aim of this study is to determine the LTSE of available COVID-19 vaccines in Jordan, specifically Pfizer-BioNTech, Sinopharm, and AstraZeneca, comparing the frequencies of LTSE between them, analyzing the factors that affect the adverse effects and noticing the difference between LTSE and STSE trends. A few studies were conducted in Jordan about COVID-19 vaccine adverse effects and people's hesitancy toward vaccines, but all investigated STSE. Studies that analyzed LTSE are few in the world. These studies can decrease the hesitancy of people toward vaccination as a lot of rumors confuse the general opinion against vaccination benefits (Aloweidi *et al*., 2021). The best method to report most of the COVID-19 vaccine adverse effects, especially the serious ones, is to establish a public surveillance web portal in each country and increase people's awareness toward using. A good example of that lies in the United States, where a reporting system for vaccine adverse effects at a governmental level was issued just after the launching of vaccine campaign (Gee *et al*., 2021). In Jordan, there is a governmental reporting system, but most people are not aware of it which limits its utility, thus the hesitancy among Jordanians is still present (MOH 2023b).

The main limitation of this study is that it is an observational cross-sectional study that depends mainly on the Google Forms platform administrated via various methods including but not limited to personal interviews, social media platforms, and patient encounters. Although

this enabled us to reach the largest number of patients from different categories of people which gave a good distribution of social characteristics of the participants, it limited the ability to define precisely the adverse effects in patient words. The subjectivity of many adverse effects and the severity of each adverse effect are other limitations of the study. Many adverse effects can be affected by external factors like socioeconomic factors that were greatly disrupted during the pandemic. Other factors include the mood of the patients, individual tolerability and patient perspective about vaccines affected greatly by common rumors regarding safety issues. The unawareness of people in Jordan of the national adverse effects reporting system, which makes it not an effective system, limits the knowledge about infrequent adverse effects that may be serious. So, we recommend increasing people's awareness about this reporting system and using it to note every minor possible adverse effect and follow up with the patient to know the nature of all adverse effects in terms of reversibility and progression to avoid such limitations in future studies.

5. Conclusions

In conclusion, the results of this study suggest that a considerable subset of COVID-19 vaccine recipients may experience LTSE. At least one LTSE was reported by all study participants. Fatigue, decreased concentration, and mood disturbances were the most reported LTSE among the study population (>30.0%). COVID-19 vaccine type has been identified as a key factor with Sinopharm vaccine-recipients having the highest frequency of reported LTSE while AstraZeneca vaccine recipients had a significantly higher frequency of most STSE. A dose-dependent effect of vaccines was associated with increased frequency of some STSE and LTSE. Furthermore, male gender, old age, smoking, chronic co-morbidities, and multiple COVID-19 infections contributed significantly to reported LTSE. Reported LTSE are vaccine type- and dose-dependent; however, a direct causal link is difficult to establish since other contributing factors have been identified. The nature of the reported LTSE is generally mild and its significant effects on quality of life are unlikely. Attention and follow-up of individuals at higher risk of developing LTSE are warranted. Further studies are needed, employing multidisciplinary teams of various medical professionals to investigate post-vaccination symptoms in different populations, and establish future interventions and policies.

6. Author Contributions

Conceptualization, A.A-S., M.A-K., and M.A-T.; methodology, A.M and R.D.; validation, A.A-S., A.Q and M.A-T., and M.M.A.; formal analysis, M.A-T.; data curation, A.A-S., M.A-T., A.M., R.D., A.Q., M.M.A., B.A-R., A.A-A., and M.A-K. writing—original draft preparation, A.M., R.D., B.A-R., A.A-A., and M.A-K; writing—review and editing, A.A-S., M.A-T., A.M., R.D., A.Q., M.M.A., B.A-R., A.A-A., and M.A-K.; supervision, M.A-T.; project ad-ministration, M.A-T.; funding acquisition, A.A-S. All authors have read and agreed to the published version of the manuscript .

7. Funding

This research was funded by the Deanship of Scientific Research, the Hashemite University, Zarqa, Jordan.

8. Institutional Review Board Statement

The study was approved by the institutional review board (IRB) at the Hashemite University (Reference No.22/4/2021/2022). Informed Consent Statement: Informed consent was obtained from all subjects involved in the study.

Data Availability Statement

Data is available upon request.

Acknowledgments

We would like to thank Dr. Ola Soudah from the Department of Basic Medical Sciences, Faculty of Medicine, Yarmouk University, Irbid, Jordan for assistance with statistical analysis.

Conflict of Interests

The authors declare no conflict of interests.

References

Abu-Halaweh S, Alqassieh R, Suleiman A, Al-Sabbagh MQ, AbuHalaweh M, AlKhader D, Abu-Nejem R, Nabulsi R, Al-Tamimi M, Alwreikat M, Alnouti M, Suleiman B, Yousef M, Jarbeh ME, Al-Shudifat AE, Alqassieh A, Bsisu I. 2021. Qualitative Assessment of Early Adverse Effects of Pfizer–BioNTech and Sinopharm COVID-19 Vaccines by Telephone Interviews. *Vaccines (Basel).*, **9(9)**: 950. doi: 10.3390/vaccines9090950.

Alhazmi A, Alamer E, Daws D, Hakami M, Darraj M, Abdelwahab S, Maghfuri A, Algaissi A. 2021. Evaluation of side effects associated with COVID-19 vaccines in Saudi Arabia. *Vaccines (Basel).*, **9(6)**: 674**.** doi: 10.3390/vaccines9060674.

Aloweidi A, Bsisu I, Suleiman A, Abu-Halaweh S, Almustafa M, Aqel M, Amro A, Radwan N, Assaf D, Abdullah MZ, Albataineh M, Mahasneh A, Badaineh A, Obeidat H. 2021. Hesitancy towards covid-19 vaccines: An analytical cross–sectional study. *Int J Environ Res Public Health.*, **18(10)**: 5111**.** doi: 10.3390/ijerph18105111.

Alqassieh R, Suleiman A, Abu-Halaweh S, Santarisi A, Shatnawi O, Shdaifat L, Tarifi A, Al-Tamimi M, Al-Shudifat AE, Alsmadi H, Al Sharqawi A, Alnawaiseh H, Anasweh Y, Domaidah FA, Jaber HA, Al-Zarir MR, Bsisu I. 2021. Pfizer-biontech and sinopharm: A comparative study on post-vaccination antibody titers. *Vaccines (Basel).*, **9(11)**: 1223. doi: 10.3390/vaccines9111223**.**

Angeli F, Reboldi G, Trapasso M, Santilli G, Zappa M, Verdecchia P. 2022. Blood pressure increase following COVID-19 vaccination: a systematic overview and meta-analysis. *J Cardiovasc Dev Dis.*, **9(5)**: 150**.** doi: 10.3390/jcdd9050150.

Bhandari B, Rayamajhi G, Lamichhane P, Shenoy AK. 2022. Adverse Events following Immunization with COVID-19 Vaccines: A Narrative Review. *BioMed research international*., 2911333. doi: 10.1155/2022/2911333**.**

Ganesan S, Al Ketbi LMB, Al Kaabi N, Al Mansoori M, Al Maskari NN, Al Shamsi MS, Alderei AS, El Eissaee HN, Al Ketbi

RM, Al Shamsi NS, Saleh KM, Al Blooshi AF, Cantarutti FM, Warren K, Ahamed F, Zaher W. 2022. Vaccine Side Effects Following COVID-19 Vaccination Among the Residents of the UAE-An Observational Study. *Front Public Health*., **10**: 876336. doi: 10.3389/fpubh.2022.876336.

Bizri AR, Al Akoury N, Mhlanga T, Morales GDC, Haridy H, Hussey GD, Srivastava A. 2023. The COVID-19 experience in Africa and the Middle East. *Ann Med*., **55(1)**: 2222641. doi: 10.1080/07853890.2023.2222641.

Chen CC, Chen CJ. 2023. New-onset inflammatory arthritis after COVID-19 vaccination: A systematic review. *Int J Rheum Dis*., **26(2)**: 267-277. doi: 10.1111/1756-185X.14482.

Chen Y, Xu Z, Wang P, Li XM, Shuai ZW, Ye DQ, Pan HF. 2022. New-onset autoimmune phenomena post-COVID-19 vaccination. *Immunology*., **165(4)**: 386-401. doi: 10.1111/imm.13443.

Dar-Odeh N, Abu-Hammad O, Qasem F, Jambi S, Alhodhodi A, Othman A, Abu-Hammad A, Al-Shorman H, Ryalat S, Abu-Hammad S. 2022. Long-term adverse events of three COVID-19 vaccines as reported by vaccinated physicians and dentists, a study from Jordan and Saudi Arabia. *Hum Vaccin Immunother*., **18(1)**: 2039017. doi: 10.1080/21645515.2022.2039017.

Dawoud R, Haddad D, Shah V, Patel V, Abbas G, Guduru S, Dakka A, Kaushik V, Cheriyath P. 2022. COVID-19 Vaccine-Related Arthritis: A Descriptive Study of Case Reports on a Rare Complication. *Cureus*., **14(7)**: e26702. doi: 10.7759/cureus.26702.

Diesel J, Sterrett N, Dasgupta S, Kriss JL, Barry V, Vanden Esschert K, Whiteman A, Cadwell BL, Weller D, Qualters JR, Harris L, Bhatt A, Williams C, Fox LM, Meaney Delman D, Black CL, Barbour KE. 2021. COVID-19 vaccination coverage among adults—United States, December 14, 2020–May 22, 2021. *MMWR Morb Mortal Wkly Rep*., **70(25)**: 922-927. doi: 10.15585/mmwr.mm7025e1.

Gee J, Marquez P, Su J, Calvert GM, Liu R, Myers T, Nair N, Martin S, Clark T, Markowitz L, Lindsey N, Zhang B, Licata C, Jazwa A, Sotir M, Shimabukuro T. 2021. First month of COVID-19 vaccine safety monitoring—United States, December 14, 2020–January 13, 2021. *MMWR Morb Mortal Wkly Rep*., **70(8)**: 283-288. doi: 10.15585/mmwr.mm7008e3.

Graña C, Ghosn L, Evrenoglou T, Jarde A, Minozzi S, Bergman H, Buckley BS, Probyn K, Villanueva G, Henschke N, Bonnet H, Assi R, Menon S, Marti M, Devane D, Mallon P, Lelievre JD, Askie LM, Kredo T, Ferrand G, Davidson M, Riveros C, Tovey D, Meerpohl JJ, Grasselli G, Rada G, Hróbjartsson A, Ravaud P, Chaimani A, Boutron I. 2022. Efficacy and safety of COVID-19 vaccines. *Cochrane Database Syst Rev*., **12(12)**: CD015477. doi: 10.1002/14651858.CD015477.

Green MS, Peer V, Magid A, Hagani N, Anis E, Nitzan D. 2022. Gender differences in adverse events following the Pfizer-BioNTech COVID-19 vaccine. *Vaccines (Basel).*, **10(2)**: 233. doi: 10.3390/vaccines10020233.

Haidere MF, Ratan ZA, Nowroz S, Zaman SB, Jung YJ, Hosseinzadeh H, Cho JY. 2021. COVID-19 Vaccine: Critical Questions with Complicated Answers. *Biomol Ther (Seoul)*., **29(1)**: 1-10. doi: 10.4062/biomolther.2020.178.

Hatmal MM, Al-Hatamleh MAI, Olaimat AN, Hatmal M, Alhaj-Qasem DM, Olaimat TM, Mohamud R. 2021. Side effects and perceptions following COVID-19 vaccination in Jordan: a randomized, cross-sectional study implementing machine learning for predicting severity of side effects. *Vaccines (Basel)*., **9(6)**: 556. doi: 10.3390/vaccines9060556.

Heald AH, Rea R, Horne L, Metters A, Steele T, Leivesley K, Whyte MB, Stedman M, Ollier W. 2021. Analysis of continuous glucose tracking data in people with type 1 diabetes after COVID-19 vaccination reveals unexpected link between immune and metabolic response, augmented by adjunctive oral medication. *Int J Clin Pract*., **75(12)**: e14714. doi: 10.1111/ijcp.14714.

Ilonze OJ, Guglin ME. 2022. Myocarditis following COVID-19 vaccination in adolescents and adults: a cumulative experience of 2021. *Heart Fail Rev*., **27(6)**: 2033-2043. doi: 10.1007/s10741-022-10243-9.

JCDC. Jordan Center for Disease Control. 2023. https://www.cdc.gov/globalhealth/countries/jordan/default.htm. Accessed 17 February 2023.

JFDA. Jordan Food and Drug Administration. 2023. http://www.jfda.jo/Default.aspx. Accessed 17 February 2023.

MOH. Jordan Ministry of Health. 2023a. https://corona.moh.gov.jo/en. Accessed 17 February 2023.

MOH. Jordanian Ministry of Health. COVID-19 Vaccination Platform: MOH. 2023b https://vaccine.jo/cvms/. Accessed 13 March 2023.

Kadali RAK, Janagama R, Peruru S, Malayala SV. 2021. Side effects of BNT162b2 mRNA COVID-19 vaccine: A randomized, cross-sectional study with detailed self-reported symptoms from healthcare workers. *Int J Infect Dis*., **106**: 376-381. doi: 10.1016/j.ijid.2021.04.047.

Khader Y, Batieha A, Ajlouni H, El-Khateeb M, Ajlouni K. 2008. Obesity in Jordan: prevalence, associated factors, comorbidities, and change in prevalence over ten years. *Metab Syndr Relat Disord*., **6(2)**: 113-120. doi: 10.1089/met.2007.0030.

Lai FTT, Huang L, Peng K, Li X, Chui CSL, Wan EYF, Wong CKH, Chan EWY, Hung IFN, Wong ICK. 2022. Post-Covid-19-vaccination adverse events and healthcare utilization among individuals with or without previous SARS-CoV-2 infection. *J Intern Med*., **291(6)**: 864-869. doi: 10.1111/joim.13453.

Liu YC, Kuo RL, Shih SR. 2020a. COVID-19: The first documented coronavirus pandemic in history. *Biomed J*., **43(4)**: 328-333. doi: 10.1016/j.bj.2020.04.007.

Liu H, Chen S, Liu M, Nie H, Lu H. 2020b. Comorbid chronic diseases are strongly correlated with disease severity among COVID-19 patients: a systematic review and meta-analysis. *Aging Dis*., **11(3)**: 668-678. doi: 10.14336/AD.2020.0502.

McMenamin ME, Nealon J, Lin Y, Wong JY, Cheung JK, Lau EHY, Wu P, Leung GM, Cowling BJ. 2022. Vaccine effectiveness of one, two, and three doses of BNT162b2 and CoronaVac against COVID-19 in Hong Kong: a population-based observational study. *Lancet Infect Dis*., **22(10)**: 1435-1443. doi: 10.1016/S1473-3099(22)00345-0.

Medeiros KS, Costa APF, Sarmento ACA, Freitas CL, Gonçalves AK. 2022. Side effects of COVID-19 vaccines: a systematic review and meta-analysis protocol of randomised trials. *BMJ Open*., **12(2)**: e050278. doi: 10.1136/bmjopen-2021-050278.

Menni C, Klaser K, May A, Polidori L, Capdevila J, Louca P, Sudre CH, Nguyen LH, Drew DA, Merino J, Hu C, Selvachandran S, Antonelli M, Murray B, Canas LS, Molteni E, Graham MS, Modat M, Joshi AD, Mangino M, Hammers A, Goodman AL, Chan AT, Wolf J, Steves CJ, Valdes AM, Ourselin S, Spector TD. 2021. Vaccine side-effects and SARS-CoV-2 infection after vaccination in users of the COVID Symptom Study app in the UK: a prospective observational study. *Lancet Infect Dis*., **21(7)**: 939-949. doi: 10.1016/S1473-3099(21)00224-3.

Mulligan MJ, Lyke KE, Kitchin N, Absalon J, Gurtman A, Lockhart S, Neuzil K, Raabe V, Bailey R, Swanson KA, Li P, Koury K, Kalina W, Cooper D, Fontes-Garfias C, Shi PY, Türeci Ö, Tompkins KR, Walsh EE, Frenck R, Falsey AR, Dormitzer PR, Gruber WC, Şahin U, Jansen KU. 2020. Phase I/II study of

COVID-19 RNA vaccine BNT162b1 in adults. *Nature*., **586(7830)**: 589-593. doi: 10.1038/s41586-020-2639-4**.**

Nordenberg D, Yip R, Binkin NJ. 1990. The effect of cigarette smoking on hemoglobin levels and anemia screening. *JAMA*., **264(12)**: 1556-1559**.**

Qaqish A, Al-Omari M, Abbas MM, Ghazo M. 2022. Two years of COVID-19 pandemic in Jordan: A focus on epidemiology and vaccination. *J Glob Health*., **12**: 03063. doi: 10.7189/jogh.12.03063.

Riad A, Pokorná A, Attia S, Klugarová J, Koščík M, Klugar M. 2021. Prevalence of COVID-19 vaccine side effects among healthcare workers in the Czech Republic. *J Clin Med*., **10(7)**: 1428**.** doi: 10.3390/jcm10071428.

Saeed BQ, Al-Shahrabi R, Alhaj SS, Alkokhardi ZM, Adrees AO. 2021. Side effects and perceptions following Sinopharm COVID-19 vaccination. *Int J Infect Dis*., **111**: 219-226**.** doi: 10.1016/j.ijid.2021.08.013.

Spencer JP, Trondsen Pawlowski RH, Thomas S. 2017. Vaccine Adverse Events: Separating Myth from Reality. *Am Fam Physician*., **95(12)**: 786-794**.**

Tregoning JS, Flight KE, Higham SL, Wang Z, Pierce BF. 2021. Progress of the COVID-19 vaccine effort: viruses, vaccines and variants versus efficacy, effectiveness and escape. *Nat Rev Immunol*., **21(10)**: 626-636. doi: 10.1038/s41577-021-00592-1**.**

WHO. World health organizations. 2024. https://www.who.int/emergencies/diseases/novel-coronavirus-2019/situation-reports. Accessed 19 August 2024.

WHO. World health organizations. 2023. https://www.who.int/news-room/questions-and-answers/item/coronavirus-disease-(covid-19)-vaccines?gclid=Cj0KCQiA6LyfBhC3ARIsAG4gkF_jyBb7hk7I-UrPfbdEB16FqqoUjIc1lgSBgpcPI6SB7ICYJ5Aa4hgaAiigEALw_wcB&topicsurvey=v8kj13. Accessed 13 March 2023 **.**

Zahid MN. 2021. Unfolding the mild to moderate short-term side effects of four COVID-19 vaccines used in Bahrain: a cross-sectional study. *Vaccines (Basel)*., **9(11)**: 1369**.** doi: 10.3390/vaccines9111369.

Zhu Y, Armstrong JL, Tchkonia T, Kirkland JL. 2014. Cellular senescence and the senescent secretory phenotype in age-related chronic diseases. *Curr Opin Clin Nutr Metab Care*., **17(4)**: 324-328**.** doi: 10.1097/MCO.0000000000000065.

.

JJBS

Volume 18, Number 2, June 2025
ISSN 1995-6673
Pages 211 – 220
https://doi.org/10.54319/jjbs/180202

Jordan Journal of Biological Sciences

Comparative Analysis of Microbiological and Enzymatic Methods for Strengthening Sandy and Weathered Soils to Mitigate Degradation and Desertification

Meiirzhan Dauletkul[1], Zina Tungushbayeva[1], Asem Kydyrbaeva[2], Dina Kulzhanova[1], Zhanat Bukharbayeva[1,*]

[1]*Abai Kazakh National Pedagogical University, Department of Biology, 050010, 13 Dostyk Ave., Almaty, Republic of Kazakhstan;*
[2]*Asfendiyarov Kazakh National Medical University, Department of Molecular Biology and Medical Genetics, 050000, 94 Tole bi Str., Almaty, Republic of Kazakhstan.*

Received: July 30, 2024; Revised: October 3, 2024; Accepted: October 12, 2024

Abstract

Soil degradation and desertification represent significant environmental challenges, particularly in arid regions such as Kazakhstan. This research examines the potential of biological soil consolidation techniques to address these issues by enhancing soil strength. The objective of this study was to undertake a comparative analysis of two contemporary methods of calcium carbonate precipitation for the purpose of soil strengthening in sandy and weathered soils: microbially induced calcium carbonate precipitation and enzymatically induced calcium carbonate precipitation. Both methods are based on the precipitation of calcium carbonate, which is intended to enhance soil stability. The study was conducted on sandy soil samples collected from the vicinity of Aktau, Kazakhstan. The enzymatic precipitation method employed the use of urease, whereas the microbial approach involved the utilisation of *Sporosarcina Pasteurii* and bacterial isolates derived from the test site soil. Over the course of a 12-day experiment, the mechanical stability of the samples was assessed under vertical and horizontal loads. The findings demonstrate that both methods enhanced soil strength, with microbially induced calcium carbonate precipitation exhibiting greater efficacy, augmenting biocement stability by 2.5-3 times in comparison to the control, and enzymatically induced calcium carbonate precipitation yielding a 1.5-2 times improvement. The microbial method demonstrated a clear correlation between urease activity, calcium carbonate deposition, and mechanical resistance. The efficiency of soil-isolated bacterial strains was found to be comparable to that of the reference strain, indicating the potential for practical application. The results, validated in both laboratory and field conditions, indicate that these methods can be scaled for wider use in mitigating soil degradation and desertification.

Keywords: biological consolidation, biocement, calcium carbonate deposition, enzymatic deposition, microbially induced deposition.

1. Introduction

Soil degradation and desertification are significant environmental issues, especially in arid regions like Kazakhstan. Biological soil consolidation techniques, such as microbially induced calcium carbonate precipitation (MICP) and enzymatically induced calcium carbonate precipitation (EICP), have gained attention as sustainable solutions. MICP uses uratolytic bacteria to hydrolyze urea into ammonia and carbonate ions, which react with calcium ions to form calcium carbonate. These ions act as a binder for soil particles and serve as nucleation sites for calcium carbonate crystals. EICP, on the other hand, uses the enzyme urease without living organisms, catalyzing the same urea hydrolysis reaction to produce carbonate ions and calcium carbonate. However, EICP lacks the additional nucleation effect provided by bacterial cells in MICP. Both methods are environmentally friendly alternatives to chemical soil stabilization, but MICP generally achieves better results due to bacteria's role in enhancing calcium carbonate deposition. EICP is simpler to implement and may be more cost-effective in certain situations. This study aims to compare the effectiveness of MICP and EICP in consolidating sandy soils, particularly in desertification-prone regions, under laboratory and field conditions (Bulba et al., 2024).

The degradation of soil, driven by both economic activities and climate change, has accelerated the processes of desertification, particularly in arid regions. This has resulted in a notable decline in agricultural output, which directly endangers food security in Central Asia, including Kazakhstan. One of the most significant consequences of soil erosion is wind erosion, which not only reduces soil fertility but also has a considerable impact on biodiversity by destabilising local ecosystems. The loss of biodiversity, in conjunction with declining soil fertility, gives rise to a series of cascading effects, which serve to exacerbate the problem of desertification in these regions (Dagliya et al., 2022). The research conducted by Dagliya and colleagues

* Corresponding author. e-mail: zha.bukhar@gmail.com.

underscores the critical necessity for the implementation of soil stabilisation techniques to address the significant issue of large-scale desertification in Kazakhstan. The expansion of arable land has led to the deterioration of soil quality and a considerable reduction in biodiversity, necessitating the urgent development of effective solutions to combat this alarming phenomenon. This underscores the global significance of addressing soil degradation.

In response to this growing problem, researchers have been investigating a range of technological solutions with the aim of stabilising sandy soils. In their comprehensive review of innovative soil stabilisation methods, Mymrin et al. (2019) present a range of promising techniques. The researchers analysed the use of casein, a protein that serves as a natural binder, as well as chitosan derived from shrimp shells, a biopolymer known for its soil-binding properties. Furthermore, Mymrin et al. investigated the potential of using drainage system sediments to enhance soil structure. One of their most significant contributions was a method involving the use of slag, an industrial by-product of lime production, to strengthen sandy soils. This approach offers an economically viable solution through the repurposing of waste materials, thereby aligning with sustainable environmental practices. The work of Mymrin et al. contributes to the broader search for innovative, cost-effective solutions to improve soil stability in vulnerable regions like Kazakhstan.

In contrast, Bhurtel et al. (2024) adopted an alternative methodology, investigating the potential of biotechnological techniques for enhancing soil strength. The comparative study of biomedical soil stabilisation methods demonstrated the potential of bacteria and fungi in enhancing soil strength. The utilisation of microbial and fungal agents in soil stabilisation has garnered attention due to their intrinsic interactions with the soil environment, facilitating soil cohesion without the necessity for deleterious chemical additives. Bhurtel et al. emphasised the potential of stabilisation as a method that could complement or even replace traditional techniques, thereby creating a more sustainable and eco-friendly approach to improving soil strength. This is particularly pertinent in the context of addressing soil degradation in regions where soil disturbance from agricultural activities is a significant contributing factor to desertification.

A noteworthy method of enhancing soil density and mechanical resistance to erosion is through the precipitation of calcium carbonate. Chittoori et al. (2021) conducted an investigation into this process, with a particular focus on its capacity to bind soil particles and enhance soil resistance to mechanical displacement. This process, which is commonly referred to as "biocementation", entails the extraction of calcium from the soil in order to precipitate calcium carbonate, which serves as a natural binding agent. The precipitation of calcium carbonate has gained attention due to its ability to improve soil stability, offering an effective solution to the problem of desertification, particularly in sandy soils, which are highly susceptible to wind and water erosion. This research highlights the potential of biocementation as a promising strategy for soil stabilisation in arid regions such as Kazakhstan.

In recent years, there has been a notable shift in the focus of research towards biological solutions, particularly the utilisation of MICP and EICP. The efficacy of these methods has been explored by studies conducted by Cuccurullo et al. (2022), Zomorodian et al. (2023), and Kim and Youn (2016), with particular emphasis placed on their environmental benefits in comparison to traditional chemical stabilisers. MICP employs the use of urease-producing bacteria, such as *Sporosarcina Pasteurii*, to induce calcium carbonate precipitation, whereas EICP utilises urease enzymes to achieve a similar outcome. Both methods are praised for their non-toxic, environmentally friendly, and relatively straightforward implementation. Furthermore, the scalability of these methods renders them suitable for large-scale applications, such as the mitigation of dust storms and soil displacement, which are prevalent in desert regions. Nevertheless, it is essential to acknowledge that while both techniques have demonstrated efficacy in diverse geographical locations, further investigation is necessary to ascertain their cost-effectiveness and long-term environmental consequences.

Richardson et al. (2016) traced the early developments of MICP, noting that the first studies on microbial calcium deposition mechanisms emerged in the early 2000s. These pioneering studies established the foundations for the accelerated development of biological soil stabilisation techniques, which subsequently attracted significant scientific interest. The research demonstrated the potential of MICP for applications beyond soil stabilisation, such as crack sealing in building materials, thereby opening up further avenues for innovation in biocementation technologies.

Erdmann and Strieth (2022) expanded on the applications of enzymatic and microbial calcium carbonate deposition, noting that these methods are not limited to soil stabilisation but also play a crucial role in the development of sustainable building materials. The researchers demonstrated the potential of biocementation in the construction industry, particularly in the reinforcement of building facades and the enhancement of construction material density. This cross-disciplinary application highlights the versatility of biocementation technologies and their potential integration into broader sustainability initiatives.

In Kazakhstan, initiatives have already been launched to utilise these technologies for the stabilisation of soil. In their respective studies, Kurmanbaev et al. (2017) and Sembaev et al. (2019) have concentrated on the identification of microorganisms that can be employed for MICP, as well as the development of optimal methods for biocementation in Kazakhstan's distinctive environmental circumstances. Their work underscores the necessity of selecting the appropriate microbial strains and biocementation methods that are tailored to specific soil and climate conditions. This is of great consequence, as the process of biocementation is a complex, multi-component phenomenon that is influenced by a multitude of factors, including soil type, climate, and microbial activity. As Zhang et al. (2023) observed, the selection of MICP, EICP, or an alternative method is largely contingent upon the specific environmental conditions prevailing at the site in question. This renders the process a highly intricate engineering undertaking, necessitating meticulous evaluation of a multitude of variables.

While the results of MICP and EICP in laboratory settings have been promising, there is a dearth of large-scale studies that directly compare the effectiveness of

these methods under real-world conditions in Kazakhstan's arid regions. As Zhang et al. (2023) have observed, research into biocementation has, to date, been largely confined to small-scale studies or specific environmental conditions. This has resulted in a notable gap in the existing literature with regard to the performance of these methods in different regional settings. This research aims to address the aforementioned gap in the literature by providing a comparative analysis of calcium carbonate deposition methods in sandy soils, with specific consideration of the environmental conditions prevalent in Kazakhstan.

There is a paucity of research comparing the efficacy of MICP and EICP methods in the unique environmental conditions of Kazakhstan. While both methods show promise, a comprehensive analysis comparing their performance in sandy and weathered soils, especially in arid regions like Kazakhstan, is lacking. This study addresses this gap by assessing the degree of soil consolidation achieved using both microbiological and enzymatic methods, thereby optimising the technology for producing biocement samples resistant to environmental degradation.

Also, this study provides insights into optimizing soil stabilization in arid environments, with potential implications for large-scale efforts to combat desertification, reduce soil erosion, and enhance agricultural productivity. The use of indigenous bacterial strains offers an environmentally friendly and cost-effective alternative to traditional chemical stabilizers, making this research a potential model for other regions facing similar environmental challenges.

The study aims to assess the degree of consolidation of sandy soil during biocementation using the methods of microbiological and enzyme-induced deposition of calcium carbonate and optimise the technology for producing biocement samples that are resistant to external environmental factors.

2. Materials and methods

In the investigation of the physicochemical properties of sandy soils, standard laboratory methods were employed, including pH determination, total dissolved solids measurement, and X-ray fluorescence analysis for mineral composition.

Natural soils contain a wide variety of microorganisms, including strains capable of producing urease. In this regard, the study attempted to isolate isolates from sandy soils. The material for isolates isolation was 3 samples of sandy soils collected in the vicinity of Aktau, Mangistau region of Kazakhstan. Its physicochemical properties were investigated using standard laboratory methods. Three different sand samples were used, taken at three points 500 m apart.

The bacterial strain *Sporosarcina Pasteurii* was used as a reference strain. The original strain was stored at -80°C. For activation, the cells were thawed following cryopreservation, washed to eliminate the cryoprotective medium, and subsequently cultured in nutrient medium at 30°C for 24 hours. The isolation of natural bacterial isolates was carried out by washing the sand samples with a sterile 0.85% NaCl solution. The isolates were cultured in medium containing 3 g/L nutrient broth, 10 g/L NH_4Cl, 25.2 mM $NaHCO_3$; 3.7 g/L $CaCl_2$, 20 g/L urea. The plates were incubated at 30°C for 5 days. The method of sand biocementation is based on the ability of microorganisms to release urease, a urea-degrading agent, into the environment, which, in the course of further transformations, decomposes into ammonia and carbonic acid. Carbonic acid breaks down easily and can react with free calcium ions in the soil. The resulting calcium carbonate forms crystals that can bind soil particles together and fill in gaps.

Determination of urease-producing bacterial isolates was performed using a selective Kirstensen medium containing the indicator phenol red. A 40% urea solution in a ratio of 1:10 was added to the prepared medium during cooling (to 50°C). After that, the medium was poured into tubes in an inclined position and, after solidification, was used for the cultivation of microorganisms. Incubation was performed at 30°C for 20-24 hours after inoculation. The presence of urease activity was concluded by the presence of a characteristic pink-crimson colour of the medium. Isolates showing a positive reaction were cultured on selective media for 24 hours. Microorganisms were identified by protein profiling using MALDI-TOF Microflex mass spectrometry (Bruker, Germany). The obtained spectra were analysed by comparison with the MBT Compass library. The urease activity was determined by the potentiometric method, and the activity was expressed in mol/L. The measurement results of all indicators were averaged across the samples. The enzymatically induced precipitation of calcium carbonate was carried out by adding a solution containing 1 M urea, 0.76 M calcium chloride ($CaCl_2$) and the enzyme urease at a concentration of 3 g/l to a sand column. A solution containing 1 M urea, 0.76 M calcium chloride ($CaCl^2$) and a bacterial suspension with a cell concentration of 10^6/ml was used for microbially induced calcium carbonate precipitation.

The laboratory test of calcium carbonate deposition was carried out in a cylinder filled with sand, 15 cm high and 5 cm in diameter. The weight of the sand was 500 g. The bacterial suspension was inoculated on days 1 and 6 of the experiment. Every day for 12 days, 10 ml of substrate solutions containing 1 M urea and 0.76 M calcium chloride ($CaCl_2$) were added to the cylinder. At the end of the experiment, they were dried naturally at room temperature. As a control, a solution containing 1 M urea, and 0.76 M calcium chloride ($CaCl_2$), but no urease or bacteria was used. The content of calcium compounds in the samples was determined by X-ray semi-quantitative method. Compressive strength was determined in the laboratory using a hand press, using the vertical loading method. The study was carried out using the KP-9 compression device. The shear strength was determined by conducting shear tests under a horizontal load using a P10-C shear tester.

The field tests were carried out with the reproduction of the laboratory experiment scheme by laying out experimental plots of $1m^2$. The boundaries of the experimental plots were fenced with four metal plates 1 m long and 50 cm high, which prevented sand from moving and mixing within the plot. The solutions were applied by spraying onto the surface. The volume of the sprayed solution was 2 litres/m^2. Bacterial solutions were added on days 1 and 6, and substrates were added daily for 12 days. Compressive and shear strengths were determined in

samples taken from the experimental plots on day 12 of the experiment. The compressive strength was determined in surface layer samples taken from a depth of 10 cm using a hand press. The samples were delivered to the laboratory, where physical and mechanical tests were carried out. All measurements were made 3 times.

The shear strength of the soil is the most important indicator for determining the resistance of sandy soils to weathering. Therefore, the soil shear test was carried out directly in the field using the rotary shear method with a rotary impeller shear meter. The results of the measurements and calculations of the studied indicators are presented in the form of mean (±) standard deviation. The statistical significance of the differences was assessed using the parametric T-test. In instances where discrepancies were identified between the groups, p-values were calculated to ascertain the statistical significance. To illustrate, the comparison between the microbiological and enzymatic methods revealed that the compressive strength differences yielded a p-value of $p<0.05$, indicating statistically significant improvements in the MICP-treated samples in comparison to the control group. Additionally, confidence intervals for the compressive strength values were calculated. The MICP-treated samples exhibited 95% confidence intervals of 740.4 to 784.3 kPa, whereas the control had a CI of 240.2 to 258.4 kPa. Similarly, the EICP method yielded a compressive strength with a 95% confidence interval of 360.3 to 377.0 kPa.

3. Results

The first work characterised sand samples obtained from the sites where further studies were carried out. The samples were analysed for indicators relevant to the study. The physical, chemical, and mechanical characteristics of the soil samples employed in this study are presented in Table 1. These include pH, total dissolved solids, chloride (Cl) content, silicon dioxide (SiO_2), calcium oxide (CaO), and calcium carbonate ($CaCO_3$).

Table 1. Physical, chemical and mechanical characteristics of the soil under study

Indicator	Units of measurement	Value
pH		8.2±0.12
TDS	‰	455±5.7
Cl	‰	40±0.15
SiO_2	%	97±1.1
CaO	%	1.5±0.2
$CaCO_3$	%	1.5±0.2
ρ	mg/cm^3	1.5±0.05
Compressive strength	kPa	227±12.5
Shear strength	kPa	210±10

Source: compiled by the authors.

These parameters were of great importance to establish the baseline condition of the soil before the commencement of the biocementation process. For example, the compression and shear strength values (227 kPa and 210 kPa, respectively) served as a control reference for subsequent experiments.

Although the biochemical reactions contributing to soil strengthening have been outlined, it is essential to explain how these reactions specifically enhance soil structure. The precipitation of calcium carbonate plays a pivotal role in the binding of soil particles, forming crystals that fill voids and thereby enhance the overall strength of the soil matrix. This process of crystallisation increases the density of the soil and improves its resistance to mechanical stress. The precipitation of calcium carbonate acts as a cementing agent between particles, leading to increased compressive strength and improved stability under both vertical and horizontal loads. These processes contribute to the mitigation of soil degradation and desertification, particularly in sandy soils (Aliu et al., 2020; Kpoda et al., 2024).

Thirty cultures of microorganisms were inoculated from 3 sites, 11 of which showed urease activity based on changes in the colour of the medium. The colour of the medium in the negative control, which did not contain bacteria, was straw-coloured, while in the media containing urolithic bacteria and urea, the latter decomposed to form ammonia, which, when interacting with the indicator, gave a red-raspberry colour to the medium. The more pronounced the proteolytic activity of the bacteria was, the more intense the crimson colour of the medium was. The reaction equation is shown below:

$$CH_4N_2O + H_2O \leftrightarrow CH_2NO_2+, \quad (1)$$

$$CH_4NO_2 + NH_4 \rightarrow HCO_3 + NH_3. \quad (2)$$

Cultures that showed the most pronounced qualitative reaction (bright crimson colour of the medium) were marked and assigned numbers 1, 2, and 3, and the remaining cultures were also sequentially numbered. The measurement of urease activity showed that the cultures that gave the most pronounced qualitative reaction had the highest urease activity in the quantitative measurement (Figure 1). *Sporosarcina Pasteurii* was used as a control strain, the activity of which was the highest among the cultures studied, and one of the isolates (No. 2) had comparable activity. As a positive control, a urease solution with known activity was used, which was further used in the course of the study.

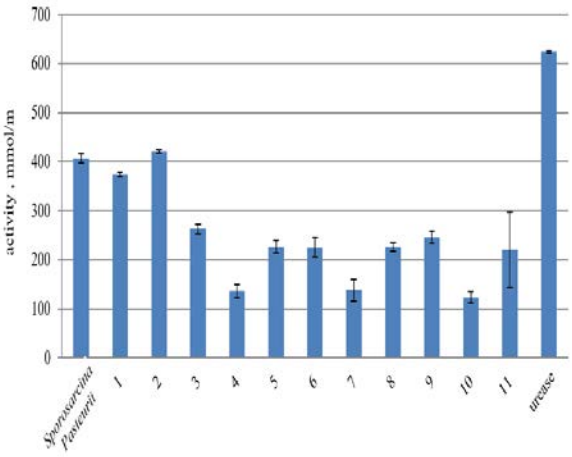

Figure 1. Urease activity in different bacterial isolates from soil samples
Source: compiled by the authors.

Isolates 1, 2, and 3 exhibited the highest urease activity, which is directly correlated with their capacity to induce calcium carbonate precipitation. It is noteworthy that

isolate 2 exhibited urease activity that was comparable to that of the control strain, *Sporosarcina Pasteurii*. This suggests that it has the potential to be an effective biocementation agent.

Despite the urease activity in the control sample being the highest, it did not result in the greatest calcium fixation. This suggests that factors other than urease activity play a role in calcium carbonate precipitation. The distribution and retention of calcium ions in the soil, environmental conditions such as temperature and moisture, and the presence of other nucleation sites or competing reactions within the soil matrix are all potential factors that may influence the process of calcium carbonate precipitation. Furthermore, the efficacy of precipitation may be contingent upon the interplay between microbial activity and soil attributes, including particle size and porosity.

However, the duration of the planned experiment was 12 days, and the urease measurement was performed on day 6 so that in real conditions the predicted enzyme activity could have increased while maintaining the bacterial production activity. Mass spectrometric analysis of proteins allowed us to determine the systematic affiliation of the three isolates. The determination was made to the genus, and the isolates obtained were identified as 1 – *Aeromonas sp*., 2 – *Bacsllus sp*., and 3 – *Staphilococcus sp*. Literature analysis confirms the presence of urease-producing capacity in many species of microorganisms belonging to these genera. However, no species-level analysis was carried out in this study. The addition of urea to the medium containing bacteria led to an increase in the pH of the medium, which creates optimal conditions for the growth of these microorganisms and contributes to the supersaturation of the solution with free calcium ions. When urea was added to the medium containing urease, reaction cascades occurred:

$$CO(NH_2)_2 + H_2O + \text{urease} \rightarrow NH_2COOH + NH_3, \quad (3)$$

$$NH_2COOH + H_2O \rightarrow NH_3 + H_2CO_3, \quad (4)$$

$$H_2CO_3 \rightarrow HCO_3^- + H^+ \quad (5)$$

$$2NH_3 + 2H_2O \rightarrow 2NH_4^+ + 2OH^-, \quad (6)$$

$$HCO_3^- + H^+ + 2OH^- \rightarrow CO_3^{2-} + 2H_2O, \quad (7)$$

$$CO_3^{2-} + Ca^{2+} \rightarrow CaCO_3. \quad (8)$$

Formulas 7 and 8 indicate the balance of CO_3^{2-} and HCO_3^-, H_2CO_3 – the balance of ions depends on the pH of the medium, with an increase in pH, dissociation to carbonate ions prevails and $CaCO_3$ precipitation occurs. When observing laboratory samples, this process looks like sample curing. After the laboratory experiment on cementation, the parameters of the biocement were studied. Among the laboratory parameters studied was the density, which was expected to increase in all experimental variants compared to the control. Figure 2 illustrates the density of the biocement samples obtained through microbial and enzymatic methods.

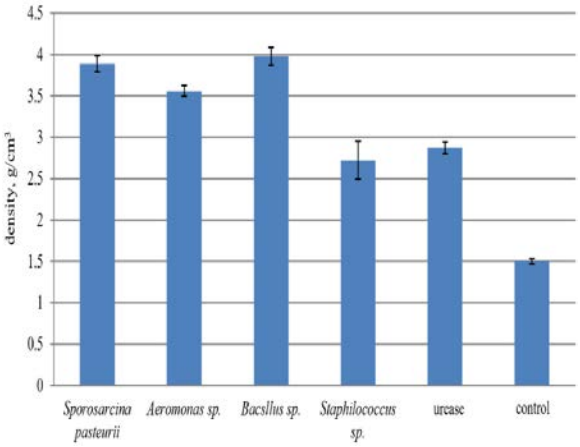

Figure 2. Density of biocement samples obtained by microbiological and enzymatic methods in the laboratory and the field

Source: compiled by the authors.

The density of soil in the control was 1.5g/cm^3. The diagram shows that the highest increase in density was observed in samples obtained using cultures of *Bacsllus sp*. isolate (3.98±0.1 g/cm^3), *Sporosarcina Pasteurii* (3.85±0.1 g/cm^3) and *Aeromonas sp*. Despite the high activity of native urease, the soil density was lower than in the above variants and amounted to 2.9±0.05 g/cm^3. When using an isolate of *Staphilococcus sp*., the density of the material obtained was 0.37 ± 0.05 g/cm^3. One of the most significant direct indicators of cementation efficiency is the calcium carbonate content of biocement. The study demonstrated a distribution pattern that was fully correlated with the ability to produce urease. The highest calcium carbonate content was observed in the medium containing *Bacsllus sp*. (7.2±0.4 mg/cm3), and the second highest calcium carbonate content was recorded in the sample obtained using culture of *Sporosarcina Pasteurii (6.6±0.*4 mg/cm^3), and the third highest – *Staphilococcus sp*. (6.1±0.7 mg/cm^3). The elevated urease activity of *Bacsllus sp*. facilitates accelerated urea hydrolysis, which in turn precipitates calcium carbonate at a faster rate. Furthermore, the robust cell walls and enhanced metabolic efficiency of *Bacsllus sp*. facilitate more efficacious calcium ion capture and crystal formation. The superior biocementation performance of this strain in comparison to other strains used in the study is likely attributable to its ability to thrive in the specific pH and temperature conditions of the soil (Suerbaev et al., 2009).

When using the *Aeromonas sp.* isolate, the content was 5.3±0.7mg/cm^3. The content of calcium carbonate in biocement obtained by the enzymatic method using urease solution was lower than in all variants of microbial deposition and amounted to 3.67±0.7 mg/cm^3, which is higher than in the control, but less effective than when using microorganisms. The concentration of calcium carbonate in the biocement samples is presented in Figure 3. As can be seen from these results, the urease concentration is not a decisive factor in the formation of calcium carbonate, as the urease activity in the control was the highest among the samples studied, which did not ensure maximum calcium fixation from the soil.

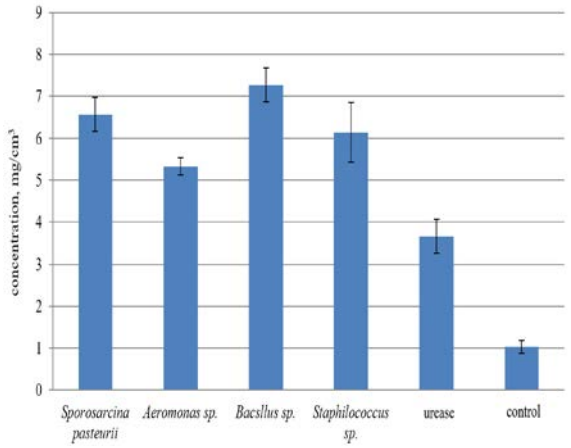

Figure 3. Calcium carbonate concentration in microbiologically and enzymatically produced biocement samples under laboratory and field conditions
Source: compiled by the authors.

As anticipated, microbial treatment resulted in elevated calcium carbonate content, with Bacillus sp. demonstrating the greatest yield (7.2 mg/cm³). The enzymatic method yielded a lower calcium carbonate content (3.67 mg/cm³), indicating that microbial methods are more efficacious in inducing calcium carbonate deposition.

The most important indicators are the mechanical properties of the samples obtained since the goal of the experiments is to produce biocement that is resistant to mechanical stress. To verify the reproducibility of the test results in the field, strength measurements were performed on both laboratory and field samples on a larger scale. This scaling makes it possible to move from laboratory conditions to field conditions, including exposure to natural weather and climate conditions, including large volumes of soil. The compressive and shear strengths of the biocement samples are shown in Figures 4 and 5 respectively. Figure 4 shows the compressive strength results. Several patterns can be observed from the chart above: firstly, in all variants of the experiment, the MICP technique showed the best results in increasing the strength characteristics of sandy soil.

In all the results of the experiment, there was a clear tendency for a more significant increase in strength indicators in the laboratory than in the field. It seems plausible to suggest that environmental factors, including temperature fluctuations, soil moisture content and wind conditions, may have contributed to the discrepancies observed between the laboratory and field results. In the field, the presence of natural elements such as precipitation and wind may have affected the consistency and distribution of calcium carbonate precipitation. For example, precipitation may have resulted in the dilution or washing away of some of the applied solutions, thereby reducing the concentration of active substances in the soil (Tonkha et al., 2024; Floqi et al., 2009). Furthermore, the fluctuations in temperature between day and night in the field may have resulted in a reduction in bacterial and enzymatic activity, consequently leading to a slower deposition rate of calcium carbonate. It can be reasonably deduced that the aforementioned factors resulted in a reduction in shear and compressive strength values in the field when compared to the more controlled conditions of the laboratory, where temperature and moisture were maintained at optimal levels for the biocementation process.

However, all the observed trends identified in the laboratory could be translated to open-field conditions with great accuracy. Under laboratory conditions, the biocement obtained using *Sporosarcina Pasteurii* culture had the best strength characteristics: the compressive strength of the soil was 762.7±28.3 kPa and the shear strength was 420.3±7.23 kPa compared to the control 249.3±9 kPa and 118.6±6.29 kPa, respectively. The characteristics of the soil treated with *Bacsllus sp.* culture were close – 765±10.69 kPa in compression and 394.67±8.29 kPa in shear.

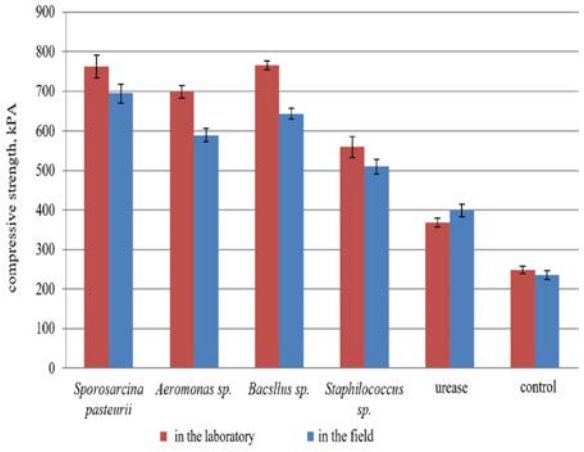

Figure 4. Compressive strength of microbiologically and enzymatically produced biocement samples under laboratory and field conditions
Source: compiled by the authors.

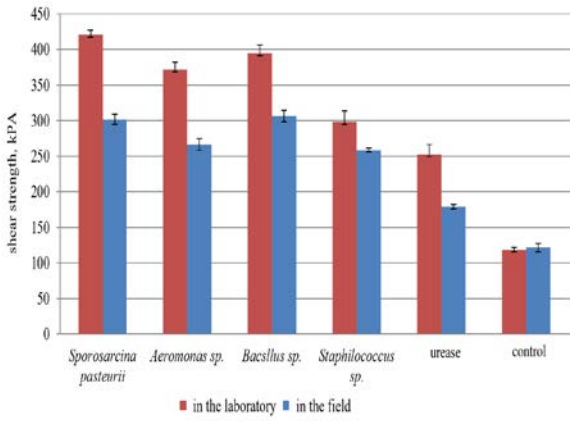

Figure 5. Shear strength of microbiologically and enzymatically produced biocement samples under laboratory and field conditions
Source: compiled by the authors.

The biocement samples obtained using the *Aeromonas sp.* culture withstood a pressure of 698±16.8 kPa in compression and 371.33±8.25 kPa in shear. The isolate of *Staphilococcus sp.* provided a sand strength of 559.3±26.1 kPa in compression and 298.33±5.68 kPa in lateral shear. Thus, the use of ureolytic bacteria cultures contributed to an increase in the strength of biocement by 2.5-3 times compared to the control. The use of the enzymatic method of calcium carbonate deposition, using a urea solution, increased the vertical compressive strength to 368.67±10.5 kPa and the lateral shear strength to 252.2±7.02 kPa. Thus, the strength indicators increased by 2 times compared to the control, but this method is inferior to the

microbiological method. Thus, the strength indicators increased by 2 times compared to the control, but this method is inferior to the microbiological method (Figure 5).

The study of samples obtained in the field showed a similar pattern of sample density distribution. It should be noted that all samples obtained in the laboratory using the same strains demonstrated a 10-20% higher efficiency in terms of increasing the strength of biocement. At the same time, the results of the evaluation of the mechanical properties of biocement obtained in different variants of microbiological precipitation of calcium carbonate were more homogeneous. This may be due to the peculiarities of the conditions that have a limiting effect on the growth and secretory activity of bacteria. The highest values of compression resistance were found in the sand sample treated with *Sporosarcina Pasteurii* culture – *603.67±24 kPa, close to the values of Bacillus sp.* – 643.3±13 *kPa*. This was followed by a sample of soil treated with *Aeromonas sp.* at 589.3±18.9 kPa and *Staphilococcus sp.* at 510±18.5 kPa. The compressive strength using the enzymatic method was 398.67±15.85 kPa, which is higher than in the control variant (235.33±11.93 kPa), but lower than in all microbiological samples (Figure 4). The most important for this study are the shear strength tests carried out in the field, as they characterise the ability of the soil to resist wind erosion to the greatest extent. The strength of the control sample was 121.63±6.29 kPa. The shear strength values after the microbiological treatment were as follows: soil samples obtained using *Bacsllus sp.* and *Sporosarcina Pasteurii had similar values – 6123306.17±11*.37 kPa and 301.83±7.08 kPa, respectively. Samples obtained from the areas treated with cultures of *Aeromonas sp.* and *Staphilococcus sp.* isolates were slightly lower – 266.17±10.98 kPa and 258.33±15.6 kPa, respectively. Enzymatic treatment provided a resistance of 179.17±14.21 kPa.

The results of the field tests for rotational shear resistance showed trends close to those in the laboratory. The maximum resistance at 50 cm is shown in Figure 6. The highest resistance was observed in the soil treated with a solution containing *Bacsllus sp.* – 299.5±12.97 kPa. The soil strengthened with the laboratory strain was practically not inferior in terms of rotational shear strength – 256.33±15.78 kPa, no significant differences in the indicators were observed. The strength of the sand treated with *Aeromonas sp.* was 51267311.66±31514.51 kPa and *Staphilococcus sp.* was 299.5±12.97 kPa. The strength of the soil in the urease-treated area was 162.5±6.61 kPa – the differences are significant in comparison with both the microbiological treatment and the control (97.16±9.25 kPa).

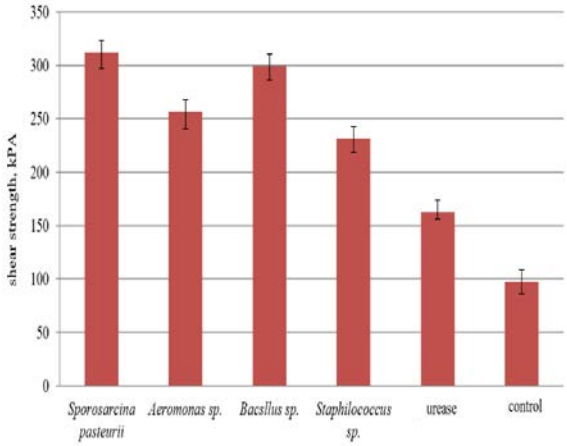

Figure 6. Strength of soil treated in different ways under rotational shear in the field
Source: compiled by the authors.

It is worth noting that the results of these tests show a lower resistance. One of the reasons may be that the resistance was studied in deeper layers, while the cementitious mortar was applied superficially, and samples were taken from more superficial layers for laboratory tests. As can be seen from the results of all the tests, both enzymatic and microbiological treatments proved to be effective in increasing the mechanical strength of sandy soils, both in the laboratory and in the field. However, the effectiveness of the bacteria is higher in all variants of the cultures used in the experiment – both the reference strain and local isolates. The laboratory determination of urease, calcium carbonate and all physical and mechanical strength parameters are directly correlated when using the microbial method of calcium precipitation.

4. Discussion

The main result of the work carried out to compare the microbiological and enzymatic methods of biocementation of sandy soil is the effectiveness of both methods in terms of strengthening soil strength. Increase of various physical and mechanical parameters of its stability under different types of mechanical load. These findings are consistent with numerous other studies, many of which have been reviewed in meta-analyses.

Iqbal et al. (2021) addressed the use of biocementation for strengthening building materials; the method is effective in terms of increasing strength, preventing and reducing cracking of materials, and increasing moisture resistance. Saif et al. (2022) and Ahenkorah et al (2021) analysed the results of enzyme-induced calcium deposition for soil strengthening. The authors point out that the results obtained in experiments on the precipitation of calcium carbonate with the addition of urease depend on many factors of the experiment. The study detected a difference in the effectiveness of the enzymatic method in different conditions – when treated in laboratory conditions, the shear strength of the soil was 252.2±7.02 kPa, and in field conditions – 179.16±14.21 kPa. This value is 35% lower than in the control. This difference is statistically significant, and a similar trend was also found in all variants of microbiological soil treatment. It is possible to assume that these changes are associated with the peculiarities of climatic conditions – temperature, moisture (precipitation can wash the solution into deeper layers).

This is determined by the relative volume of the applied solution that seeped into the soil depth, which requires larger volumes of active substances to achieve higher density. Researchers agree that the effectiveness of ureolytic reactions depends on many factors: method of enzyme application, concentration of urea, calcium ions and urease, urease activity, temperature of the applied solution, initial pH of the cementitious solution and soil pH, soil composition, curing time and chemical composition of pore water (Erdmann and Strieth, 2022; Ahenkorah et al., 2021).

Li et al. (2022) investigated the ability of soil to withstand vertical load under different microbial bioconcretion protocols. It is shown that there is a certain optimum temperature (25°C), solution concentration (2 mol/l), and concentration of dispersed particles above which the mechanical properties do not improve or deteriorate. Due to the many factors that can affect the result, a direct assessment of the mechanical properties of the soil is necessary to assess the effectiveness of the biocementation process. This study shows that the vertical compressive strength of the soil increases by 2-3 times compared to the control, and the shear strength increases by 2.5-4 times compared to the control when using MICP and by 1.5-2 times when using EICP. There is ample evidence of the effectiveness of both methods, with which the results of this study are consistent. Mo et al. (2021) cited the results of studies that show that the shear strength of the soil increased by up to 1080% (52-65 kPa) seven days after treatment. Another study showed that the use of bacterial calcium precipitation reduced calcium compression by up to 158%. Zamani and Montoya (2016), comparing MICP and EICP methods, found that the bacteria-catalysed process increased the unconfined compressive strength to 2.04 MPa, which is about five times higher than the soil strength after the enzymatic process of 0.43 MPa. Sun et al. (2018) studied the effect of a suspension of urease-producing Bacillus sp. bacterial cells and culture fluid containing the enzyme without bacterial cells on the ability to precipitate calcium. The results showed that the unconfined compressive strength of the sand treated with the cell suspension is 1.7 times higher than that of the sand treated with the urea-$CaCl_2$ liquid.

Konstantinou et al. (2021) demonstrated that high urease activity has no direct correlation with the quality of sand cementation; the lowest urease concentration (10 mmol/h/l) was more effective for larger particles. Microscopic analysis showed that at lower microbial urease activity, larger crystals are formed, which can fill the voids between the large sand particles. This may explain the obtained results when comparing the urease activity produced by the bacterial isolates with the reference solution. Even though the activity of the urease solution was the highest (624.3±2.51 mmol/l), the efficiency of calcium carbonate deposition and the increase in soil strength were the least significant compared to microbiological samples. Chen et al. (2022) conducted a large-scale study on the dynamics of calcium carbonate crystal formation in the process of biocementation. As such, MICP consists of many chemical and hydrodynamic processes. Bacterial cells play not only the role of crystal formation centres, which is well known but also provide the transport flow of substances in the soil system (Yang et al., 2022; Kuvatova et al., 2024). For this reason, microbial deposition is often more efficient than enzymatic deposition. Shirakawa et al. (2021), in a study of two types of ureolytic bacteria, concluded that the dynamics and growth pattern of calcium carbonate crystals may differ when they are used, but the mechanical properties of sand, such as compressive and shear strength, are directly related to the concentration of calcium carbonate. Similar data were obtained in the present study when comparing urease production and the concentration of calcium carbonate formed.

As for the study of individual bacterial species and the comparison of their calcium-fixing and urease activity, two species proved to be the best: reference *Sporosarcina Pasteurii* and *Bacillus sp.*, where statistically significant differences in the samples obtained with them were absent in all test variants. Many studies confirmed the high urease and calcium-fixing capacity of *Sporosarcina Pasteurii*, similar to that of the *Bacsllus* genus (Hammad et al., 2013; Jiang et al., 2016). However, the other two isolates used in the study, assigned to the genera *Aeromonas sp.* and *Staphilococcus sp.* also showed high rates of sandy soil bioconsolidation ability in this experiment. These microorganisms were isolated from the soil at the location of the experiment. In addition, 11 of the 30 samples tested contained microorganisms that tested positive for urease. This indicates the presence of urease-producing microorganisms in the soil. It has been shown that laboratory selection and cultivation can produce biomass of isolates that are successfully used for the bioconsolidation of sandy soil.

Gomez et al. (2019) studied the comparative effect of native microorganisms and culture *Sp. Pasteurii on the biocementation. As such, the precipitation of calcium carbonate crystals occurs even under the influence of natural soil microorganisms when a solution containing calcium and urea is added, but at a much slower rate than when a bacterial culture is added. It also changes the nature of crystal growth, which can be useful for some types of coarse-grained soils. Similar conclusions were reached by* Heveran et al. (2019) when studying strains with different urease activity, the authors propose to create strains aimed at a lower rate of enzyme release. *Isolation of urease-producing isolates from natural soils was also carried out in Kazakhstan.* Kurmanbaev et al. (2017) isolated 21 natural urease-producing strains, based on the results of quantitative measurement of urease, 4 strains were selected for MICP. Sembaev et al. (2019) described the isolation of a strain with a pronounced ability to biocementation.

Chen et al. (2021) review existing studies comparing different methods of biocementation (using exogenous, local bacteria and enzymes) and conclude that the effectiveness of the methods depends on many factors discussed above. In particular, the introduction of external bacterial strains can slow down the growth of the native bacterial biocoenosis, if present, and, if applied superficially, cause the formation of a dense crust that prevents further penetration of solutions and deeper cementation. In this study, to avoid such effects, gradual daily moistening with small amounts of the solution was used to ensure better penetration. All three methods described were compared, and the microbial method proved to be the most effective. Alotaibi et al. (2022)

compared the traditional method of soil strengthening with Portland cement with EICP and MICP methods, addressing efficiency, environmental friendliness and economic feasibility of application. The authors conclude that both biological methods are superior to the traditional ones in terms of environmental friendliness. Biocement produced by the EICP method is inferior in mechanical properties to microbial cement, but it has fewer metabolites and is, therefore, more environmentally friendly, and, most importantly for large-scale implementation, is much easier and more economical to produce (Chen et al., 2023; Dorvil et al., 2023).

There are few field studies on the effectiveness of sand biocementation in natural conditions. Meng et al. (2021) conducted similar studies using the MICP method in the Ulan Bukh Desert in China. The research has shown the formation of a dense crust 12.5 mm thick, which ensured the resistance of the mounds' soil to weathering. As a result, the soil strength was 459.9 kPa, while in the current study, the maximum vertical load strength was *603.67±24 kPa, and the minimum* was 510±18.5 kPa, which is a high value. Dagliya et al. (2022) conducted a study of MICP on sandy soil in India. A similar scheme of surface spraying of cementitious solutions was used. The study determined that the compressive strength and resistance to wind erosion appeared already from 5 days after the start of treatment and increased by 20 days. The thickness of the surface crust continued to increase, and the soil density increased by 85% compared to 0 days of the experiment. These statements coincide with the results of this study on the effectiveness of spray treatment in the field.

In general, the results obtained during the experiments are in good agreement with the literature data, and the developed protocols can be recommended for further testing and application for soil consolidation.

5. Conclusions

This study compared two contemporary calcium carbonate deposition techniques, namely MICP and EICP, to enhance the strength of sandy soils. Both methods demonstrated efficacy in improving soil stability under mechanical load, with MICP consistently exhibiting superior performance. In field tests, MICP achieved a maximum vertical load strength of 694.33 kPa, in comparison to 394 kPa for EICP, both of which surpassed the control's 235.33 kPa. Similarly, MICP yielded superior shear strength, reaching 301.83 kPa in comparison to EICP's 179.17 kPa and the control's 121 kPa.

It is noteworthy that the study demonstrated that indigenous bacterial strains can achieve biocementation results that are comparable to those of the reference strain, *Sporosarcina Pasteurii*. This highlights the potential for practical application of these strains. The findings highlight that MICP has an additional contribution beyond urease activity, namely the provision of enhanced soil consolidation due to bacterial interactions during the biocementation process.

Further research should concentrate on optimising the scalability and application methods of these technologies in order to enhance their practical implementation.

References

Ahenkorah I, Rahman M, Karim R, Beecham S. 2021. Enzyme induced calcium carbonate precipitation and its engineering application: A systematic review and meta-analysis. *Constr. Build. Mat.*, **308: 125000**. DOI: 10.1016/j.conbuildmat.2021.125000

Aliu H, Makolli S, Dizman S, Kadiri S, Hodolli G. 2020. Impact of environmental conditions on heavy metal concentration in honey samples. *J. Envir. Prot. Ecol.*, **21(1): 351–358**.

Alotaibi E, Arab MG, Abdallah M, Nassif N, Omar M. 2022. Life cycle assessment of biocemented sands using enzyme induced carbonate precipitation (EICP) for soil stabilization applications. *Scient. Rep.*, **12: 6032**. DOI: 10.1038/s41598-022-09723-7

Bhurtel A, Salifu E, Siddiqua S. 2024. Composite biomediated engineering approaches for improving problematic soils: Potentials and opportunities. *Scien. Total Envir.*, **914: 169808**. DOI: 10.1016/j.scitotenv.2023.169808

Bulba I, Drobitko A, Zadorozhnii Yu, Pismennyi O. 2024. Identification and monitoring of agricultural land contaminated by military operations. *Scient. Horiz.*, **27(7): 107–117**. DOI: 10.48077/scihor7.2024.107

Chen J, Liu B, Zhong M, Jing C, Guo B. 2022. Research status and development of microbial induced calcium carbonate mineralization technology. *PLoS ONE*, **17(7): e0271761**. DOI: 10.1371/journal.pone.0271761

Chen L, Song Y, Huang J, Lai C, Jiao H, Fang H, Zhu J, Song X. 2021. Critical review of solidification of sandy soil by microbially induced carbonate precipitation (MICP). *Crystals*, ***11(12)*: 1439**. DOI: 10.3390/cryst11121439

Chen YP, Li D, Zhang XC, Ma Q, Xu YQ, Luo ZS. 2023. Azacytidine-induced hypomethylation delays senescence and coloration in harvested strawberries by stimulating antioxidant enzymes and modulating abscisate metabolism to minimize anthocyanin overproduction. *Food Chem.*, **407: 135189**. DOI: 10.1016/j.foodchem.2022.135189

Chittoori BCS, Rahman T, Burbank M. 2021. Microbial-facilitated calcium carbonate precipitation as a shallow stabilization alternative for expansive soil treatment. *Geotechnics*, **1(2): 558–572**. DOI: 10.3390/geotechnics1020025

Cuccurullo A, Gallipoli D, Bruno AW, Augarde C, Hughes P, La Borderie C. 2022. Earth stabilisation via carbonate precipitation by plant-derived urease for building applications. *Geomech. Ener. Envir.*, **30: 100230**. DOI: 10.1016/j.gete.2020.100230

Dagliya M, Satyam N, Sharma M, Garg A. 2022. Experimental study on mitigating wind erosion of calcareous desert sand using spray method for microbially induced calcium carbonate precipitation. *J. Rock Mech. Geotech. Eng.*, **14(5): 1556–1567**. DOI: 10.1016/j.jrmge.2021.12.008

Dorvil W, Museau H, Salomon W, André D, Théodat J-M. 2023. Soil organic status in Saint-Raphael: Mechanisms, effects of agricultural practices and proxies. *Inter. J. Biol. Chem. Scien.*, **17(6): 2490–2511**. DOI: 10.4314/ijbcs.v17i6.28

Erdmann N, Strieth D. 2022. Influencing factors on ureolytic microbiologically induced calcium carbonate precipitation for biocementation. *World J. Microb. Biotech.*, **39: 61**. DOI: 10.1007/s11274-022-03499-8

Floqi T, Shumka S, Malollari I, Vezi D, Shabani L. 2009. Environment and sustainable development of the Prespa park. *J. Envir. Prot. Ecol.*, **10(1): 163–175**.

Gomez MG, Graddy CMR, DeJong JT, Nelson DC. 2019. Biogeochemical changes during bio-cementation mediated by stimulated and augmented ureolytic microorganisms. *Scient. Rep.*, **9: 11517**. DOI: 10.1038/s41598-019-47973-0

Hammad IA, Talkhan FN, Zoheir AE. 2013. Urease activity and induction of calcium carbonate precipitation by *Sporosarcina pasteurii* NCIMB 8841. *J. Appl. Scien. Res.,* **9(3): 1525–1533**. https://www.aensiweb.com/old/jasr/jasr/2013/1525-1533.pdf

Heveran CM, Liang L, Nagarajan A, Hubler MH, Gill R, Cameron JC, Cook SM, Srubar III WV. 2019. Engineered ureolytic microorganisms can tailor the morphology and nanomechanical properties of microbial-precipitated calcium carbonate. *Scien. Rep.*, **9: 14721**. DOI: 10.1038/s41598-019-51133-9

Iqbal DM, Wong LS, Kong SY. 2021. Bio-cementation in construction materials: A review. *Materials*, **14(9), 2175**. DOI: 10.3390/ma14092175

Jiang NJ, Yoshioka H, Yamamoto K, Soga K. 2016. Ureolytic activities of a urease-producing bacterium and purified urease enzyme in the anoxic condition: Implication for subseafloor sand production control by microbially induced carbonate precipitation (MICP). *Ecol. Eng*., **90: 96–104**. DOI: 10.1016/j.ecoleng.2016.01.073

Kim G, Youn H. 2016. Microbially induced calcite precipitation employing environmental isolates. *Materials*, **9(6): 468**. DOI: 10.3390/ma9060468

Konstantinou C, Wang Y, Biscontin G, Soga K. 2021. The role of bacterial urease activity on the uniformity of carbonate precipitation profiles of bio-treated coarse sand specimens. *Scient. Rep.*, **11: 6161**. DOI: 10.1038/s41598-021-85712-6

Kpoda DS, Tapsoba F, Cisse H, Ouedraogo S, Traore R, Traore I, Soubeiga AP, Nikiema M, Hien YE, Zongo C, Savadogo A. 2024. Isolation of antimicrobial-producing actinomycete strains from soil samples collected in the city of Ouagadougou, Burkina Faso. *Inter. J. Biol. Chem. Scien.*, **18(1): 206–223**. DOI: 10.4314/ijbcs.v18i1.17

Kurmanbaev AA, Nagmetova GJ, Bizhanova LJ. 2017. Identification of ureolytic bacteria promising for microbiological precipitation of calcite. *Actual Probl. Hum. Nat. Scien.*, **1–5**. https://cyberleninka.ru/article/n/vydelenie-ureoliticheskih-bakteriy-perspektivnyh-dlya-mikrobiologicheskogo-osazhdeniya-kaltsita

Kuvatova G, Anuarbekov K, Ryskulbekova L, Shekarban K, Mukhamadiyev N. 2024. Nutrient regime and balance of nutrients in soil under forage crops under application of different types of fertilizers (on the example of Kyzylorda region). *Scient. Horiz*., **27(8): 100–112**. DOI: 10.48077/scihor8.2024.100

Li J, Tian L, Xu Y, Tian Z, Zhang Z. 2022. Study on the solidification effect of dredger fill by microbial-induced calcium precipitation (MICP). *Materials*, **15(22): 7891**. DOI: 10.3390/ma15227891

Meng H, Gao Y, He J, Qi Y, Hang L. 2021. Microbially induced carbonate precipitation for wind erosion control of desert soil: Field-scale tests. *Geoderma*, **383: 114723**. DOI: 10.1016/j.geoderma.2020.114723

Mo Y, Yue S, Zhou Q, Liu X. 2021. Improvement and soil consistency of sand-clay mixtures treated with enzymatic-induced carbonate precipitation. *Materials*, **14(18): 5140**. DOI: 10.3390/ma14185140

Mymrin V, Aibuldinov EK, Alekseev K, Petukhov V, Avanci MA, Kholodov A, Taskin A, Catai RE, Iarozinski Neto A. 2019. Efficient road base material from Kazakhstan's natural loam strengthened by ground cooled ferrous slag activated by lime production waste. *J. Clean. Prod.*, **231: 1428–1436**. DOI: 10.1016/j.jclepro.2019.05.250

Richardson A, Coventry K, Pasley J. 2016. Microbiological deposition of calcite: Crack sealing applications. *Cement Applic.*, **1–4**. http://nrl.northumbria.ac.uk/id/eprint/28591/

Saif A, Cuccurullo A, Gallipoli D, Perlot C, Bruno AW. 2022. Advances in enzyme induced carbonate precipitation and application to soil improvement: A review. *Materials*, **15(3): 950**. DOI: 10.3390/ma15030950

Sembaev KD, Sembaeva J, Danlybaeva GA. 2019. Screening of ureolytic microorganisms promising for sand cementation. *Probl. Scien.*, **141(8)**. https://cyberleninka.ru/article/n/skrining-ureoliticheskih-mikroorganizmov-perspektivnyh-dlya-tsementatsii-peskov

Shirakawa MA, Kaminishikawahara KK, John VM, Kahn H, Futai MM. 2011. Sand bioconsolidation through the precipitation of calcium carbonate by two ureolytic bacteria. *Mat. Let.*, **65(11): 1730–1733**. DOI: 10.1016/j.matlet.2011.02.032

Suerbaev KA, Chepaikin EG, Kanapieva FM, Seitenova GZ. 2009. Carboxylation of organic compounds with metal alkyl carbonates (review). *Petrol. Chem.*, **49(4): 265–273**. DOI: 10.1134/S096554410904001X

Sun X, Miao L, Tong T, Wang C. 2018. Improvement of microbial-induced calcium carbonate precipitation technology for sand solidification. *J. Mat. Civil Eng*., **30(11)**. DOI: 10.1061/(ASCE)MT.1943-5533.0002507

Tonkha O, Pak O, Kozak V, Hryshchenko O, Pikovska O. 2024. Assessment of the influence of mineral fertilisers on the phosphate regime of meadow chernozem carbonate soil and yield of sunflower and winter wheat. *Plant Soil Scien.*, **15(1): 63–74**. DOI: 10.31548/plant1.2024.63

Yang Y, Li M, Tao X, Zhang S, He J, Zhu L, Wen K. 2022. The effect of nucleating agents on enzyme-induced carbonate precipitation and corresponding microscopic mechanisms. *Materials*, **15(17): 5814**. DOI: 10.3390/ma15175814

Zamani A, Montoya BM. 2016. Permeability reduction due to microbial induced calcite precipitation in sand. *Geo-Chicago*, **94–103**. DOI: 10.1061/9780784480120.011

Zhang K, Tang CS, Jiang NJ, Pan XH, Liu B, Wang YJ, Shi B. 2023. Microbial-induced carbonate precipitation (MICP) technology: A review on the fundamentals and engineering applications. *Envir. Earth Scien.*, **82: 229**. DOI: 10.1007/s12665-023-10899-y

Zomorodian SMA, Nikbakht S, Ghaffari H, O'Kelly BC. 2023. Enzymatic-induced calcite precipitation (EICP) method for improving hydraulic erosion resistance of surface sand layer: A laboratory investigation. *Sustainability*, ***15(6)*: 5567**. DOI: 10.3390/su15065567

JJBS

Volume 18, Number 2,June 2025
ISSN 1995-6673
Pages 221 – 230
https://doi.org/10.54319/jjbs/180203

Jordan Journal of Biological Sciences

Application of Chitosan/Hydroquinone Nanaoemulsions for Management Root Rot Disease on Cucumber Plants in Plastic Houses

El-Sayed H. E. Ziedan[1,*] and Abdel-Tawab H. Mossa[2]

[1]Plant Pathology Department and [2]Pesticide Chemistry Department, National Research Centre NRC), 33 El Bohouth Street (former El Tahrir St.)، P.O. 12622, Dokki, Giza, Egypt.

Received: May 9, 2024; Revised: September 10, 2024; Accepted: October 15, 2024

Abstract

Root rot is an epidemic fungal disease in cucumber caused by soil borne fungi of *Fusarium* spp., significantly reducing numbers of plants, vegetative growth and fruit yield during growing in plastic houses. Several nanoemulsions of chitosan alone and chitosan loaded with hydroquinone, sorbic acid, or propionic acid were prepared, characterized and *tested in vitro* against mycelial linear growth, condial sporulation and pathogenic potential of the fungal isolates, i.e. *Fusarium oxysporum* (MG018778) and *Fusarium solani* (MG018781) on cucumber. These nanoemulsions were also evaluated in greenhouse as soil drench for their effect on root rot incidence in cucumber plants, vegetative growth and fruit yield. Results *in vitro* indicated that nanaoemulsion of chitosan/hydroquinone was more effective than the other tested nanaoemulsions, with high efficacy against morphological characters tested of fungal isolates. Moreover, application of the chitosan/hydroquinone nanoemulsion, with 122.8 nm drop size, by the rate 0. 5 % as soil drench on transplanting's before cultivation and in combination with soil drench 30 days after plants cultivation in plastic house*s* was significantly suppressive root rot incidence on cucumber plants, increased survival plant, plant height, fresh weight and fruits yield of cucumber plants. Therefore, the nanoemulsion of chitosan/hydroquinone is an effective eco-friendly agent alternative fungicide for controlling root rot on cucumber cultivation.

Keywords: Cucumber, root rot, fungi, Fusarium, nanoemulsion, chitosan, hydroquinone.

1. Introduction

In order to provide fresh food for human consumption, industrial food, and medicine purposes, cucumber plants (*Cucumis sativus* L.) are among the most important economically fresh vegetables due to their rapid vegetative growth and extended fruiting period. They are widely distributed in open fields and under various soil and geographic conditions in protected houses (Essa *et al*., 2017). Cucumber is planted in open fields and protected houses with worldwide cultivation in 2,231,402 hectares, producing approximately 87.805 tons of fresh fruits (FOASTAT 2021). In Egypt, cucumber agriculture is expanding in newly reclaimed lands in open fields during the summer and in greenhouses throughout the autumn, winter, and summer seasons (Mossa *et al.,* 2021; Ziedan *et al.,* 2022; Ziedan, 2024a), and the global cultivation area reached, 19702 hectares which produced 433440.85 tons (FAOSTAT 2023).

Cucumber is one of the most important economic fresh vegetables due to its rapid growth and extended fruiting period. It is widely distributed in open fields and in various soil and geographic conditions in protected houses (Essa *et al.*, 2017).

Cucumber fruits have great economic and health benefits for humans due to their rich content of the high nutritional values. They are very important as fresh vegetables, medicinal plants, and weight loss remedy by reducing fat and including a high percentage of fibre. Cucumber fruit is rich in minerals, sugar, protein, thiamin, riboflavin, vitamin C, niacin; and they have antimicrobial properties and anticancer ones and many other bone disease remedies due to their content of secoisolariciresinol, lignans, lariciresinol, and pinoresinol (Pal *et al.,* 2020; Sambou *et al.,* 2023).

Many genera of soil-borne pathogenic fungi, *F. solani*, *F. oxysporum*, *Macrophomina phaseolina*, *Rhizoctonia solani*, *Sclerotium rolfsii*, and *Sclerotinia* spp. attack cucumber plants and cause wilt and root rot diseases (Elwakil *et al*., 2015; Farrag *et al*., 2013; Ziedan and Saad 2016; Ziedan *et al.,* 2022; Ziedan 2024 a). Synthetic fungicides were regularly used to treat fungal diseases and have a number of negative side effects, including environmental contamination, residues in edible plant portions, and resistant strains. For avoiding ricks of fungicides, alternatives of organic acids of sorbic and salicylic acids were used for controlling grapevine root rot (Ziedan *et al.,* 2020), polymer of chitosan and essential oils as the natural agents were used for management crown and anthracnose on banana fruits after harvest

* Corresponding author. e-mail: ziedanehe@yahoo.com.

(Hossain and Iqbal 2016; Zoeir *et al*., 2017; El-Zahaby *et al.*, 2018; Ziedan 2024 b). Chitosan and hydroquinone as a promising natural organic extraction are non-toxic, biodegradable, with direct harmful antifungal effect on growth, morphology and populations of plant pathogens, as well, enhancing systemic induce resistance in plant against invasion of root rot and wilt pathogens , in addition increasing productivity in cucumber (Elwakil 2003; Hanafi 2004), on fenugreekm (Ghule *el al.,* 2021), on chickpea (Hemeda 2006; Zian *et al.,* 2023). Chitosan directly significantly reduced mycelial growth, sporulation, spore germination and induce malformation, swellings and lysis of mycelial hyphal of *F. solani* the causal of root rot disease on fenugreek. It also enhances plant seed germination, increasing defense resistance enzymes, of chitinase, β-1, 3-glucanase (Ghule *el al.,* 2021). Chitosan and hydroquinone were controlling wilt disease of chickpea caused by fungi of *F. oxysporum* f. sp. *ciceris* and *Rhizoctonia solani* by enhancing the activation of enzymes related plant resistant, such as peroxidase, polyphenol oxidase and increase content of phenol and photosynthetic pigments (Zian *et al.,* 2023). As a result, the use of nanoparticles in managing plant diseases has become crucial to integrated pest management since various chemical, physical, and biological processes may be used to create eco-friendly agents (Mossa *et al*., 2021; Ziedan *et al.,* 2022). Nanoparticles are an efficient and convenient way to defend plants from diseases, such as bacteria, fungi, viruses, and nematodes, which are significant limiting factors in the production of food material (Khan *et al*., 2012). Recent studies have evaluated the effectiveness of nanoparticles and nano formulations in controlling fungi, and the results show that they are substantially more effective than conventional fungicides (Hossain and Iqbal 2016; Ziedan and Saad 2016; Mossa *et al.,* 2021; Ziedan *et al.,* 2022). In this manner, chitosan nanoemulsion were found to be more effective than chitosan, nanoemulsion of chitosan at 1.0% with droplet size (200 nm and 600 nm) respectively, its highly significances reduced mycelial growth of *Colletotrichum musae* (Berk. & Curt) Arx., the causal of anthracnose on banana fruits and *Colletotrichum gloeosporioides* (Penz.) Penz and Sacc., the causal of anthracnose on papaya and dragon fruits. In addition, *in vivo* was significantly suppressive incidence of anthracnose on fruits and maintaining their quality to 28 days under cold storage (Zahid *et al.,* 2012). Different application treatments of chitosan nanoparticles formulation were enhancing plant growth and yield components such as composite nano-size silver/chitosan nanoformulations are more efficient in combating a number of seed-borne fungi, of *Aspergillus flavus*, *Alternaria alterneta* and *R. solani* of chickpea (Kaur *et al.,* 2012). Cu-chitosan nanoparticles signifcantly enhanced growth of maize plants, chlorophyll content dry weight and enhanced defense responses against *Curvularia* leaf spot disease incidence by increasing enzymes activities of superoxide dismutase, peroxidase, polyphenol oxidase and phenylalanine ammonia-lyase (Choudhary *et al*., 2017).

Clay/chitosan nanocomposite at 20 µg mL -1 directly completely inhibited growth of *Penicillium digitatum* and incidence of green mold disease of orange cv. Valencia after harvest, inducted resistance of orange fruits and caused morphological alternations in mycelial hyphae of the fungal pathogen (Youssef and Hashim 2020). Chitosan nanoparticles (CNPs) as antifungal of *F. equiseti* was controlling tomato wilt and increased the efficacy of biocontrol agents (El-Morsy *et al.,* 2023). In addition, chitosan- potassium nanoparticles formulation increased plant vegetative growth, fruit yield and high and total soluble solids as well vitamin C, acidity, sugar strawberries fruits (Abd-Elrahman *et al*., 2023).

This investigation, aimed at preparation, characterization of antifungal nanoemulsions from safety organic material to suppress growth of fungi causing root rot disease on cucumber *in vitro* and their application *in vivo* for protecting cucumber plant during growth in plastic houses.

2. Materials and Methods

2.1. Chemicals and reagents

Chitosan (M.Wt. = 100.000-300.000), Polysorbate 80 (Tween 80), Sodium tripolyphosphate (TPP) and hydroquinone were obtained from VWR International 201, Rue Carnot F-94126 Fontenay/Bois, France, while systemic fungicide named Topsin M- 70% was provided from El-Deeb of Developmental Agriculture Company, Egypt.

2.2. Preparation of chitosan nanoemulsion

For preparation chitosan nanoemulsion, native chitosan and TPP were used for preparation an ionic gelation at room temperature. (Calvo *et al*., 1997; Rampino *et al.,* 2013; Waly *et al.,* 2015). Nanoparticles are created by inter- and intra-molecular linkages between amino groups of chitosan and charged phosphate groups of (TPP). Chitosan solution was prepared by swirling a 3 mg/ml chitosan into a 1% (v/v), pH 5, acetic acid solution. Afterward, 120 ml of TPP solution (0.5 mg/ml, w/v) was added under stirring to 100 ml of chitosan solution. Chitosan nanoparticles (NPs) were collected, cleaned by suspending in deionized water two to three times, centrifuged for 30 minutes at 10,000 rpm, then re-suspended in deionized water.

2.3. Preparation of hydroquinone-loaded chitosan nanoemulsion

Hydroquinone-loaded chitosan nanoemulsion according ionic cross-linking method (Rampino et al., 2013; Ding *et al.,* 2017). Chitosan (1000 mg) after dissolved in 100 ml of 1.0 % acetic acid was mixed with 1 mg/ml of hydroquinone then TPP solution (1 mg/mL) was dropped dropwise to chitosan suspension while being stirred (4000 rpm) for two hours. The resulting nanoparticles (NPs) were freeze-drying after being collected by centrifugation for 30 min then being re-suspended in deionized water.

2.4. Preparation organic acids and hydroquinone loaded chitosan nanoemulsion

Sorbic or propionic acids were loaded with chitosan nanoparticles according method described by (Ding et al., 2017). 1000 mg of chitosan was dissolved in 1.0 % acetic acid, pH 5) or 0.1%. of propionic acid, and sorbic acid. TPP was prepared in deionized water. Then, TPP solution was added drop wise into the chitosan solution at room temperature under magnetic stirring for 2 hrs; then

nanoparticles were obtained by after centrifugation at 13 000 rpm for 30 min at 4 °C then re-suspended in deionized water.

2.4.1. Nanoemulsion characterizations

Distribution of particle size of various nanoparticles was determined by dynamic light scattering PSS instrument (Santa Barbara, CA, USA) , at 23 °C with 632 nm helium-neon (HeNe) laser as the light source. The scattering angle was set to 90°.

2.4.2. Transmission electron microscopy (TEM)

Various prepared chitosan nanoemulsions were observed their dimentions size of nanoparticles by TEM (model JEM-1230, Jeol, Tokyo, Japan). The drops of chitosan nanoparticles only and its loaded either one of sorbic acid and propionic acid, and hydroquinone in deionized water, were diluted then transferred in grid of carbon-coated copper then dried at 27ºC then images were taken at 80 KV voltages at Centeral laboratory of scientific services in National Research Centre unit, Egypt.

2.5. Effect of nanoemulsion on fungi growth and pathological activity Fungal isolates tested

Two highly pathogenic isolates of fungi caused root rot on cucumber were identified according to morphological, cultural and molecular biology with accession numbers, i.e. *Fusarium oxysporum* (MG018778) and *Fusarium solani* (MG018781), in previous work (Attallah *et al*., 2019). These isolates were tested under stress of nanoemulsions of chitosan.

2.5.1. Mycelial linear growth

Different chitosan, nanoemulsion singly and in combinations with hydroquinone and organic acids of propionic and sorbic were tested on mycelial linear growth of fungi tested on PDA agar medium. Three Petri dishes plates (9 cm in diameter) were used as a replicates for each formulation, and tree plates free treatment were served as a control. Plates were incubated at 27±2 C for 7 days. The average diameters of mycelial linear growth of each plate was determined and calculated as the reduction % of fungal growth according to the following formulation (Duarte *et al*., 2014).

$$GI\ (\%) = [\ (Gc - Gt)/Gc] \times 100$$

Where: GI = Percentage of mycelial growth inhibition; Gc = linear mycelial in negative control; Gt = linear mycelial of the treatment

2.5.2. Conidia sporulation count

Conidiospores count was determined using haemacytometer slide. The average number of spores was calculated per cm² of fungal growth.

2.5.3. *Pathogenic potential of fungal isolates*

Mycelial colonies 10 days old of two fungal isolates tested as mentioned before being grown under stress of nanoparticles formulations were used for testing effect of nanoemulsion prepared on pathogenicity test of fungi using germinated seeds (Golden) of cucumber on wetted filter paper for two days then cultured on fungal mycelial growth. Ten germinated seeds were used of each plate; three plates were used as replicates for each treatment and ten plates without nanoparticles were served as a control. Plates were incubated at 27±2 C for 7 days. Root rot syndromes of developing cucumber seedlings were visually examined according to (Ziedan and Saad 2016).

2.5.4. Scanning electron microscopy (SEM) observations

For studying morphological changes of fungal isolates, pieces 4x4mm of each fungal isolates 5 days old growth, on potato dextrose agar medium (PDA) supplemented nanoemulsion of chitosan/hydroquinone 4000 ppm and fungi free stress (control). Each fungal isolate was fixed in buffer it in osmium tetroxide, dehydration in a graded ethanol series of ethanol solutions (25%, 50%, 75%, and two 100%) for 10 minutes, then coat with gold and view in scanning electron microscope quanta FEG250 field emission (Scan EM) at National Research Centre unit, Egypt.

2.6. Nanoemulsion for controlling root rot disease on cucumber

Different nanoemulsion of chitosan/hydroquinone at 0.5 and 1.0 % concentration as soil drench during transplanting's growth 2 days before cultivation in green house and /or soil drench by the rate 200 ml/plant, 30 days after cultivation of transplantings in open field (greenhouse). Treatments were distributed in randomized block design during growing season 2018/2019 in protective plastic green houses, Dokki, Agriculture Research Centre, Minsitry of Agriculture, Egypt as follows:

0- Control (plants free treatment)

Soil drench of transplanting's by chitosan/ hydroquinone nanoemulsion (0.5 %)

Soil drench of transplanting's by chitosan/ hydroquinone nanoemulsion (1.0%)

3-Soil drench of transplanting's and in field with chitosan/ hydroquinone nanoemulsion (0.5 %)

4- Soil drench of transplanting's and in field with chitosan/ hydroquinone nanoemulsion (1.0%)

5- Soil drench of transplanting's with (fungicide) Topsin M-70 (0.5%).

6-Soil drench of transplanting's and in field with (fungicide) Topsin M-70 (0.5%)

2.6.1. *Root rot assessment*

Root rot disease incidence on hundred cucumber plants, disease severity was determined according to (Downes and Ito 2001).

$$\text{Disease severity} = \Sigma\ (n \times r)/N \times 100$$

Where: n = number of plants in each numerical disease grade;r = number of the disease grade; N = total number of plants multiplied by the maximum numerical disease grade.

Disease severity was determined on the cucumber shoot by the linear scale (0-4) as grade of wilt syndromes on leaves, 3 months after cultivation according to (Carver et al., 1996) where:

0 = healthy plant
1 = intial sing of wilt on plant
2 = wilt more 25% of plant
3 = wilt more 50% of plant
4 = wilting more 75% to plant.

2.6.2. Morphological characters and yield components of cucumber plants

Plant height of cucumber plants, fresh weight of shoot, number of buds, and total number and yield of cucumber fruits (Kg) were calculated 5 months after cultivation.

2.7. Statistical analysis

Data were statistically analyzed using analysis of variance (ANOVA) comparing among means using least significant differences (L.S.D) *P*= 0.05 according to procedures outlined by (Snedecor and Cochran 1980).

3. Results

3.1. Preparation of nanoparticles of chitosan, hydroqinone and organic acids

Chitosan nanoemulsions and its loaded with each one of hydroquinone, sorbic acid and propionic acid were prepared based on chitosan high molecular weight, polysobate (tween- 80) and tripolyphosphate (TPP) by ionic gelation at room temperature as simple ionic cross-linking at 50% in distilled water. Stable nanoemulsions were suspended for assay droplet size and their distributions, as shown in (Fig. 1) nanoparticles of chitosan (214.5 nm), nanoparticles of chitosan/hydroquinone (228.8 nm), nanoparticles of chitosan/sorbic acid (224.2) and nanoparticles of chitosan/propionic acid (276.4).

Morphology and dimensions of chitosan nanoparticles were viewed by transmission electron microscopy (TEM) as shown in **(Fig. 2).** The droplets of nanoemulsion were spherical shape in a good dispersion. This visualization confirmed the distribution of droplet diameter sizes in the chitosan nanoemulsions**.**

Figure 1 . Particle size distribution of chitosan nanoparticles alone and those loaded with hydroquinone, sorbic acid, and propionic acid.

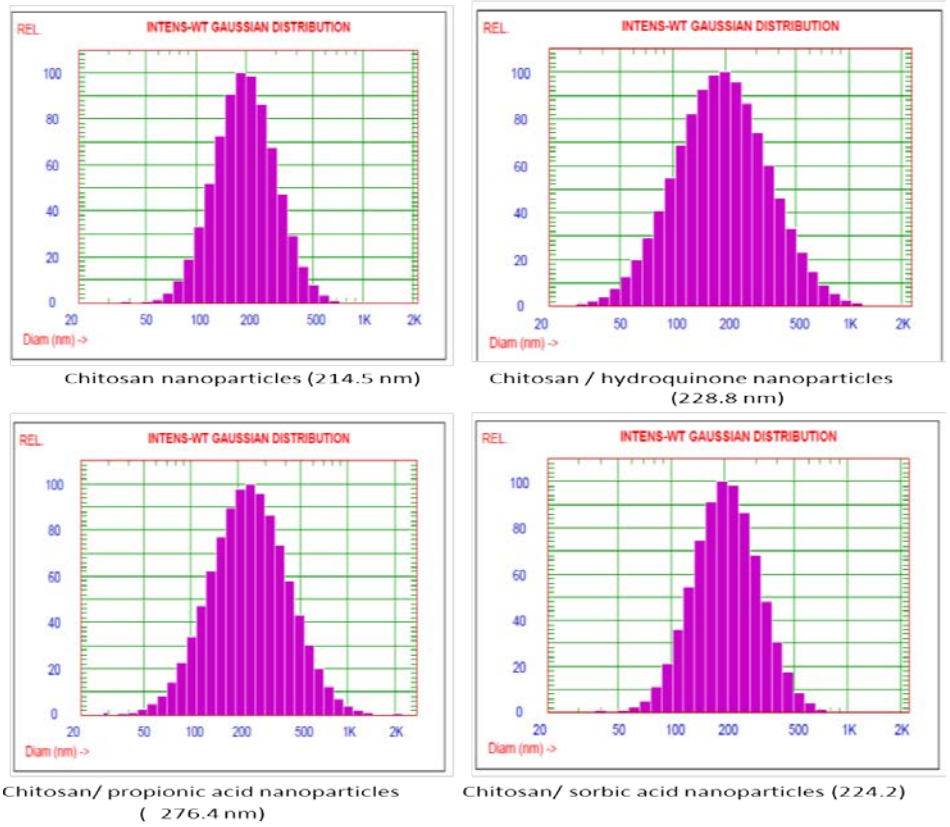

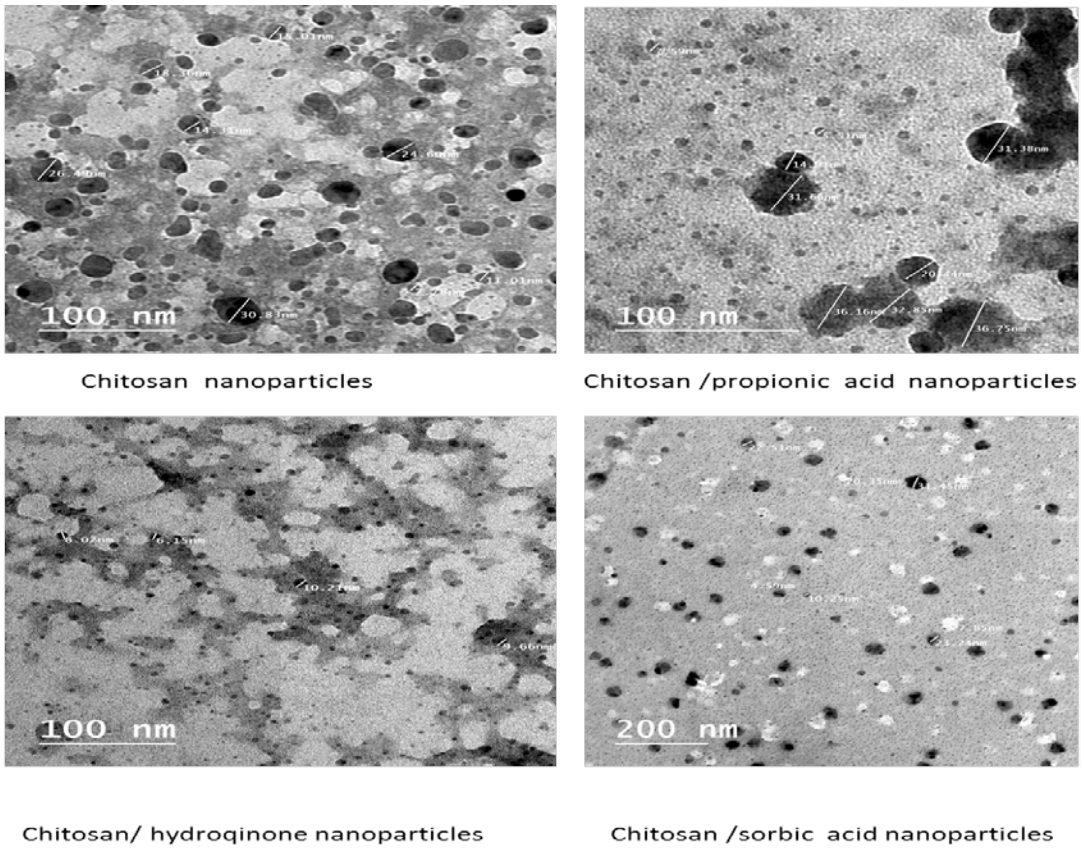

Figure 2 . TEM of exhibiting chitosan nanoparticles size

3.2. Effect of chitosan nanoemulsions on growth and pathogenic activity of fungi

Data in Table (1) indicated that testing 1000 and 2000 ppm of nanoemulsions of chitosan only or chitosan / propionic acid, chitosan / sorbic acid and chitosan / hydroquinone were reduced mycelial linear growth of the tested fungus of *Fusarium solani* and *F. oxysporum* than in untreated (fungi free nanoemulions test) which increased with higher concentrations. In this manner, the chitosan/hydroquinone nanoemulsion at 2000 ppm was the most effective against the mycelial linear of fungal growth which reduced *F. oxysporum* by 60% followed by chitosan / sorbic acid nanoemulsion (33%) then the chitosan alone nanoemulsion (34%), meanwhile the least effective was nanoemulsion of chitosan / propionic acid (24%). Meanwhile, nanoemulsion of chitosan significantly reduced mycelial growth of *Fusarium solani* by (41%), meanwhile nanoemulsions of chitosan/hydroquinone, chitosan / sorbic acid chitosan / propionic acid, which reduced mycelial linear growth by (33%).

In addition, data in Table (2) shows that all nanoemulsions significantly reduced conidia count production on both tested fungal isolates compared to the fungi free treatments (control). Nanoemulsion of chitosan/hydroquinone and chitosan nanoemulsion alone, respectively, were the best treatments that reduced conidia count production of *Fusarium solani* (81.3) and *F. oxysporum* (47.4%). In this respect, nanoemulsions of chitosan/sorbic acid and chitosan/propionic acid were the least effective in reducing the conidia count of *F. oxysporum* (28.4%) and *Fusarium solani* (62.5%) , respectively. Furthermore, as shown in Fig (3) , all chitosan nanoemulsions in this study reduced the rotting of the germinated seed of cucumber and mortality of developing cucumber seedlings than in the untreated (control). Nanoemulsion of chitosan/hydroquinone was the best treatment that reduced seed rotten and seedling death of cucumber caused by *Fusarium solani* followed by nanoemulsion of chitosan/ propionic acid, nanoemulsion of chitosan, respectively. Meanwhile, nanoemulsion of chitosan/sorbic acid showed the least effect.

Table 1 . Effect of chitosan nanoemulsions on growth of fungi pathogens

Treatment		% Reduction of mycelial linear growth	
Nanoemulsion	Con. ppm	*F. oxysporum*	*F. solani*
Control	000.0	00.0 g	00.0 e
Chitosan / propionic acid	1000	02.0 f	00.0 e
	2000	24.0 e	33.3 b
Chitosan / sorbic acid	1000	50.0 b	33.0 b
	2000	50.0 b	33.0 b
Chitosan /hydroquinone	1000	50.0 b	16.7 d
	2000	60.0 a	33.0 b
Chitosan	1000	24.0 e	25.1 c
	2000	34.0 d	41.3 a

The same letter in each colum are not significantly differences at $P \leq 0.05$.

Table 2. Effect of chitosan nanoemulsions on conidia count of fungal pathogens

Nanoemulsion (2000 ppm)	Conidia (x 10^5)/ cm^2			
	F. oxysporum		*F. solani*	
	count	% reduction	count	% reduction
Control	9.5 a	00.0	4.0 a	00.0
Chitosan / propionic acid	6.0 c	36.8	1.5 b	62.5
Chitosan / sorbic acid	6.8 b	28.4	1.3 c	67.5
Chitosan /hydroquinone	6.0 bc	36.8	0.5 e	87.5
Chitosan	5.0 d	47.4	0.8 d	81.3

The same letter in each colum are not significantly differences at $P \leq 0.05$.

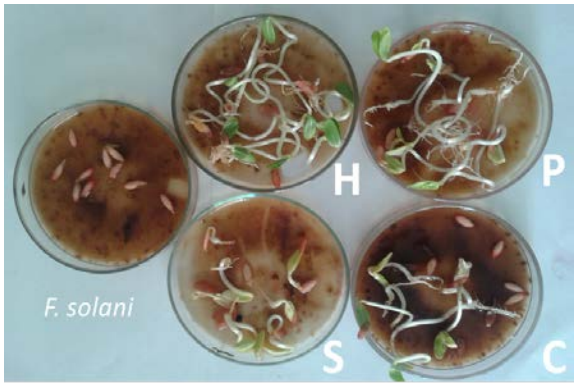

Fig ure 3. Effect of chitosan nanoemulsions on pathogenic activity of *F. solani* free treatment, H= chitosan/hydroquinone, P = chitosan/propionic acid, S = chitosan/sorbic acid and C = nano chitosan alone)

3.3. Application chitosan nanoemulsions on root rot disease incidence

Promising nanoemulsion of chitosan / hydroquinone as the a promising antifungal against pathogenic fungi of cucumber plants by the rate (0.5 and 1%) compared the systemic fungicide (Topsin-M-70) at (10g/L) were application were by suspended as the oil drench 2 days before cultivation the cucumber transplanting's or / and soil drenching 30 days after cultivation in greenhouse. Various applications of chitosan / hydroquinone nanoemulsion as in combination soil drench by 0.5% followed by 1.0% respectively significantly reduced root rot incidence, disease severity of cucumber plants and increased number of survival plants as well morphological characters and yield fruits of cucumber plants compared in untreated plants and the same treatments by fungicide (Tables 3 and 4), as shown in Table (3) and Fig (4). Applications of nanoemulsions of chitosan / hydroquinone by the rate (0. 5%) as soil drench of transplanting's alone or in combination with soil drench were the best treatments that reduced root rot incidence on cucumber plants 5 months after cultivation in greenhouse and recorded the highest survival % of cucumber plants, significantly enhancing morphological characters of cucumber plants than in the treatments by fungicide and in the control (no treatment), *i.e* shoot length, fresh weight of shoot, number of buds , number of cucumber fruits / plant and total yield of cucumber fruits, in Table (4) and Fig (4). In this respect, the significant of plant height of cucumber (230 cm) in combined treatment of transplanting and soil drench by (0.5%) of chitosan / hydroquinone nanoemulsion compared (110 cm) of plant height in untreated and fungicide application (120 cm). Moreover, the combined treatment of transplanting and soil drench after cultivation by nanoemulsion of chitosan / hydroquinone recorded, the highest values of the fresh weight of cucumber plant shoot (453.0 g /plant), yield components was (10) buds and yield was (9.2 kg of cucumber fruit / plant followed by the same the application by at (1.0 %) of nanoemulsion of chitosan / hydroquinone the fresh weight of shoot (226 g /plant), (6) buds and (5) kg of cucumber fruit / plant. Meanwhile, the lowest value was recorded with fungicide and plant free treatments (control) which recorded fresh weight/plant (74.8 and 40 g/plant), 1.6 and 1.0 kg/ fruit/plant respectively.

Table 3 . Effect of nanoemulsion of chitosan / hydroquinone on root rot disease incidence on cucumber plants under natural infestation in plastic houses

Soil drench			Survival plant %	Root rot incidence	
Materials	Con %	method		% Disease	D. severity
Nanoemulsion (chitosan/hydroquinone)	0.5	T	90 a*	40.0 c	1.0 d
		T + S	90 a	10.0 f	1.0 d
	1.0	T	85 b	35.0 e	1.8 c
		T + S	82.5 c	40.0 c	2.0 b
Topsin M-70%	0.5	T	75 e	46.0 b	2.0 b
		T + S	80 d	30.0 d	1.0 d
Control		0	65 f	70.0 a	3.7 a

T= transplanting's soil drench 2 days before cultivation

S = soil amendement 30 days after cultivation in greenhouse

The same letter in each colum are not significantly differences at $P \leq 0.05$.*

Table 4. Effect of nanoemulsion of chitosan / hydroquinone on morphological characters of cucumber plant grown under natural infestation by root rot causal pathogen in plastic houses

Soil drench			Morphological characters of cucumber plant				
Materials	Con	Method	length	bud/	fresh weight	fruit/plant	
	%		shoot (cm)	plant	shoot (g)	No.	Kg
Nanoemulsion (chitosan/hydroquinone)	0.5	T	200.0 c*	7	249.3 c	47 c	3.9 c
		T + S	230.0 a	10	453.0 a	110 a	9.2 a
	1.0	T	190.0 d	2	177.8 d	43 d	3.6 c
		T + S	220.0 b	6	266.4 b	60 b	5.0 b
Topsin M-70%	0.5	T	120.0 e	0	51.6 f	15 f	1.3 e
		T + S	120.0 e	0	74.8 e	20 e	1.6 d
Control		------	110.0 f	0	40.0 g	14 f	1.1 f

T= transplanting's soil drench 2 days before cultivation

S = soil drench 30 days after cultivation in greenhouse

* The same letter in each colum are not significantly differences at $P \leq 0.05$.

Figure 4 Application of nanoemulsion of chitosan /hydroquinone (left) and control (right) on root rot disease incidence and growth of cucumber plants

3.4. SEM observation chitosan/ hydroquinone nanoemulsion on morphology of mycelial growth of pathogenic fungi

The effect chitosan/ hydroquinone nanoemulsion (4000 ppm) on the morphological characteristics of the tested fungi i.e., *Fusarium oxysporum* and *Fusarium solani* were observed using Scanning electron microscopy (SEM). The mycelial growth of the fungal isolates was examined 5 days after treatment as shown in Fig (5); Malformation, reduced density of mycelial growth, branches of mycelial and conidia sporulation as well the absence of the conidiophores and swelling of mycelial cells were observed compared to the control (fungus free treatment). Also in Fig (5) absence the conidia and chlamydospores which clearly observation with *Fusarium solani* free treatment.

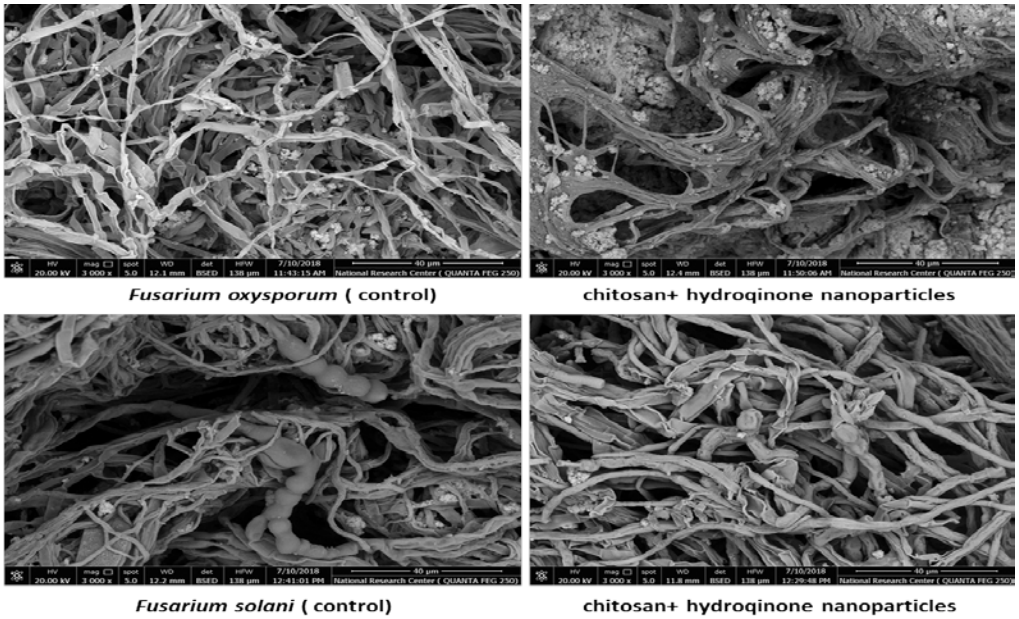

Figure 5 . SEM observation of nanoemulsion of chitosan/hydroquinone on fungal morphology

4. Discussion

Cucumber plants (*Cucumis sativus* L). plants are attaked by several soil and seed borne pathogenic fungi of *Fusarium* genera causing high losses of total plants, growth and productivity. (Farrag *et al.,* 2013 and Elwakil *et al.,* 2015; Ziedan and Saad 2026; Ziedan 2024 a).

To avoid human health problems when eating cucumber fruits, highly dangerous chemical pesticides are used in addition to the contamination of environmental elements with residues of these pesticides, which persist for long periods without decomposition (Ziedan 2024 b). The trend to use the safety organic natural materials and chemicals is quick to decompose and is efficient in resisting the form of nanoparticles in small quantities and has become important in order to produce healthy food free of pollutants (Mossa *et al.,* 2021; Ziedan *et al.,* 2022).

Chitosan nanoemulsion particles prepared by simple ionic cross-linking at room temperature and loaded with each one of hydroquinone, sorbic and propionic acids were spherical shape with droplets size distribution of stable nanoparticles were, 214.5, 228.8, 224.2 and 276.4 nm respectively; the same findings were reported by other studies which reported that droplets of nanoemulsion ranging between 20-200 nm (Diaz *et al.,* 2005; Wang *et al.,* 2009; Rampino *et al.* , 2013; Gokce *et al.* , 2014). Moreover, also the droplet sizes obtained were 82.6, 95.9, 131.9, and 117.4 nm, respectively of nanoemulsions of clove, black seed, lemon and orange essential oils (Mossa *et al.,* 2021)

In vitro, several nanoemulsions of chitosan as individual or it loaded with each one of hydroquinone, sorbic acid and propionic acid were evaluated on the common criteria of pathogenic fungal isolates, i.e. mycelial linear growth, condia sporulation production, and their pathological ability on germinated seeds and growing seedlings of cucumber. All nanoemulsions prepared in this study were significantly antifungal effect against *Fusarium* isolates causing root rot disease on cucumber in greenhouse, chitosan / hydroquinone at 2000 ppm was the most effective against mycelial linear growth of *F. oxysporum* by (60% followed by nanoemulsion of chitosan significantly reduced mycelial linear growth of *Fusarium solani* by (41%). In addition, nanoemulsions of chitosan was the best treatment reduced conidia count production of *Fusarium solani* by (81.3%), while nanoemulsions of chitosan/hydroquinone was the mot treatments reduced conidia count of *F. oxysporum* (47.4%). In addition, nanoemulsion of chitosan/hydroquinone highly reduced seed rot and seedling death of cucumber caused by *Fusarium solani* followed by nanoemulsion of chitosan/ propionic acid, nanoemulsion of chitosan respectively. Meanwhile, nanoemulsion of chitosan/sorbic acid had the lowest effect. These results are agreements with data reported that, chitosan nanoemulsion at the rate 1.0% with droplet size (200 nm), was suppress mycelial growth of *Colletotrichum musae* the causal of anthracnose disease on banana fruits and *Colletotrichum gloeosporioides* with droplet size (600 nm), the causal of anthracnose on papaya and dragon fruits (Zahid *et al.,* 2012).

Application of nanoemulsion of chitosan/hydroquinone by the rate (0.5%) as soil drench in plastic houses on the soil cucumber plant 2 days before cultivation followed by soil drench at 30 days after cultivation in greenhouses was highly reduced root rot incidence at 10% on cucumber plants and disease severity in addition, it highly significances increased plant shoot length, fresh weight of shoot and cucumber yield fruits compare the application with higher dose at (1.0%) and the systemic fungicide used Topsin - M70. These results are in agreements with results reported that, application of chitosan nanoemulsions *in vivo*, which significantly reduced incidence of anthracnose on fresh fruits of banana, papaya and maintaining their quality for 28 days in cold conditions. chitosan nanoemulsions could be used as a biofungicide for controlling anthracnose of fresh fruits in storage (Zahid *et al.,* 2012). Furthermore, composite of silver/chitosan nanoparticles was effective than single nanoparticles of silver or chitosan on various against fungi of seed borne plant pathogens on chickpea plants, i.e. *Aspergillus flavus, Alternaria alterneta, Rhizoctonia solani,* (Kaur *et al.,* 2012). Application of nanocomposite of clay/chitosan was completely application nanocomposite of clay/chitosan at 20 µg mL -1 was completely of was complete (100%) suppress green mold on orange cv. caused by fungal of *P. Penicillium digitatum*, illumination mycelial growth and sporulation of *Penicillium digitatum*, the pathogen, induce systemic resistant in orange fruits tissue and caused several malformations on the shape of mycelial hyphae (Youssef and Hashim 2020). In this respect, chitosan /hydroquinone as the main components of nanoemulsion formulation directly reduced fungal growth, sporulation and their germination, changed morphology of mycelial hyphae, reduced conidia spores and the propagules count of plant pathogens, and enhanced induce systemic resistance in plant against invasion of pathogens , by increasing defense resistance enzymes, of chitinase, β-1, 3-glucanase, peroxidase and polyphenol oxidase (Elwakil, 2003; Hanafi 2004; Choudhary *et al.,* 2017; Ghule *et al.,* 2021; Zian *et al.,* 2023).

Application nanoemulsion of chitosan / hydroquinone at (0.5%) as soil drench of transplanting's in combination with soil drench of plants in greenhouse significantly increased plant height, fresh weight of cucumber plant shoot, and fruit yield. In this manner, silver nanoparticles treatment during seed germination of spinach had positive effect on morphological and physiological parameters, water content, stomatal conductance, chlorophyll content, dry weight and leaf area of spinach plant grown free salt stress after seed germination and negatively effects under saline conditions (Bsoul *et al.,* 2023). In addition, chitosan nanoparticles was controlling wilt disease on tomato and enhanced antifungal of biocontrol agents (El-Morsy *et al.,* 2023). Furthermore, application of nano-sized chitosan loaded 1000 mg L−1 with nano K as spray and soil treatment of strawberries plants in sandy soil enhanced plant growth, increased fruit yield and maintained high of the marketable characters of strawberry fruits as well as increased the total soluble solids, vitamin C, acidity, sugar and anthocyanin (Abd-Elrahman *et al.,* 2023), chitosan nanoparticles was controlled wilt disease on tomato and enhanced antifungal of biocontrol agents (El-Morsy *et al.,* 2023).

5. Conclusions

In vitro, nanoemulsion of chitosan/hydroquinone was significantly reduced mycelial linear growth, condial spores production, pathogenic activity of the fungi of *Fusarium* spp. the causal of root rot disease of cucumber, Its application *in vivo* at (0.5%) was highly suppressive root rot incidence, disease severity and significantly enhancing the morphological characters of plant growth and fruit yield on cucumber plants in high quality. So, nanoemulsion of chitosan/hydroquinone as a promising alternative fungicides could be used as a biofungicide as eco-friendly agent, with cheap cost to control plant diseases and enhance quality and quantity.

Acknowledgment

The authors extend their appreciation to the National Research Centre, Egypt, for funding this work through research project No. (P11030135) during the period 2016–2019.

Author's contributions

EZ designed the research, conducted experiments, analyzed the data and submitted the manuscript for publication. AM prepared and characterized the nano formulation and contributed to writing and editing the manuscript.

References

Abd-Elrahman, S.H., Y.A. El-Gabry, F.A. Hashem, AF Ibrahim E.I. El-Hallous, Z.K. Abbas, D.E. Darwish, N.A. Al-Harbi, S.M. Al-Qahtani, N.M.Taha. 2023. Influence of nano-chitosan loaded with potassium on potassium fractionation in sandy soil and strawberry productivity and quality. *Agron* **13**: 1126.

Attallah, A.G., E.H. Ziedan, A.F. Sahab. 2019. Molecular characterization and pathogenicity of *Fusarium* species causing root rot disease of cucumber in greenhouse in Egypt. *Plant Arch* **19** : 1301-1307.

Bsoul, E.Y., S.A. Othman, A.A. Al-Ghzawi, M.I. Massadeh. 2023. Effect of silver nanoparticles on growth and physiological responses of spinach *(Spinacia oleracea* L.) under salt stress. *Jordan J Biol Sci* **16 (1) :** 1 – 6.

Calvo, P., C. Remunan-Lopez,, J.L. Vila-Jato, M.J. Alonso. .1997. Novel hydrophilic chitosan-polyethylene oxide nanoparticles as protein carriers. *Journal Appl Polym Sci* **63 (1)** :125-132.

Carver, C.E., D. Pitt, D.J. Rhodes. 1996. Aetiology and biological control of Fusarium wilt of Pinks (*Dianthus caryophyllus*) using *Trichoderma aureoviride*. *Plant Pathol* **45**: 618-630.

Choudhary, R.C., R.V. Kumaraswamy, S. Kumari, S.S. Sharma A. Pal, R. Raliya, P. Biswas, V. Saharan. 2017. Cu-chitosan nanoparticle boost defense responses and plant growth in maize (*Zea mays* L.). *Scientific Rep* 7: 9754

Diaz, S., S. Espinosa, E.A. Brignole. 2005. Citrus peel oil deterpenation with supercritical fluids optimal process and solvent cycle design. *The J Super Flui* **35** :49–61

Ding, R.L., F. Xie, Y. Hu, S.Z. Fu, J.B. Wu, J. Fan, W.F. He, Y. He, L.L.Yang, S. Lin, Q.L.Wen. 2017. Preparation of endostatin-loaded chitosan nanoparticles and evaluation of the antitumor effect of such nanoparticles on the Lewis lung cancer model. *Drug del* **24** :300-308.

Downes, F., K. Ito. 2001. **Compendium of Methods for The Microbiological Examination of Foods** Washington, D.C.. American Public Health Association (APHA).

Duarte, Y., O. Pino, B. Martínez. 2014. Effect of four essential oils on phytopathogenic fungi associated with spotted rains in rice. *Rev Prot Veg* **29 (1):**62–65.

El Zahaby, H.M., H.F. Maswada, E.H. Ziedan, H.A. Zoeir. 2018. Safe integrated control of postharvest rot diseases on banana fruit. *Plant Arch* **18 (2)**: 1345-1351

El-Morsy, E.S.M., Y.S. Elmalahy, M.M.A. Mousa. 2023. Biocontrol of *Fusarium equiseti* using chitosan nanoparticles combined with *Trichoderma longibrachiatum* and *Penicillium polonicum*. *Fungal Biol. Biot* **10**: 5.

Elwakil, M.A. 2003. Use of antioxidant hydroquinone in the control of seed-borne fungi of peanut with special reference to the production of good quality seed. *Pakistan J Plant Pathol* **2 (2)**: 75-79.

Elwakil, M.A., M.A. El-Metwally, A.Elsherbiny, K.N.M. Eisa 2015. Enhancing systemic acquired resistance in cucumber to control root rot and wilt diseases with reference to yield and quality. *Plant Pathol J* **14 (4)**: 223-233.

Essa, TA, A.H.M. El-Gamal, M.M.I. Afifi. 2017. Control of cucumber downy mildew by some plant growth promoting Rhizobacteria under greenhouse conditions. Middle East J Agric Res **6**: 395–408.

Farrag, E.S.H., M.H.A. Moharam, E.H.Ziedan. 2013. Effect of plant extracts on morphological and pathological potential of seed-borne fungi on cucumber seeds. *Inter J Agric Tech* **9 (1)** : 141- 149.

FOASTAT. 2021. **Food and Agriculture Organization of the United Nations**. Available online: https://www.fao.org/faostat/en/#search/Cucumbers %20 and %20 gherkins (accessed on 14 November 2021).

FAOSTAT. 2023. **Food and Agriculture Organization of the United Nations**, Rome, Italy. Retrieved January, 2023 on the world Wide Web: http://www. fao.org/faostat/en/#data/QC

Ghule, M.R., P.K. Ramteke, S.D. Ramteke, et al .2021. Impact of chitosan seed treatment of fenugreek for management of root rot disease caused by *Fusarium solani* under *in vitro* and *in vivo* conditions. *Biotech*. **11:** 290.

Gokce, Y., B. Cengiz, N. Yildiz, A. Calimli, Z. Aktas. 2014. Ultrasonication of chitosan nanoparticle suspension: Influence on particle size. Colloids and Surfaces A: *Physicochemical and Eng Aspects* **462**:75-81.

Hanafi,. AA. 2004. Effect of some antifungal compounds and Rizolex-Ton damping-off, root and pod rots diseases and pod yield of peanut. *Egypt J Appl Sci* **19** :52-61.

Hemeda, A.H. 2006. Induced resistance in chickpea against some seed-borne pathogenic fungi using the antioxidant, hydroquinone. *Egypt J Exp Biol (Bot)* **2**: 27 – 36 .

Hossain, M.S., A. Iqbal. 2016. Effect of shrimp chitosan coating on postharvest quality of banana (*Musa sapientum* L.) fruits. *Int. Food Res J* **23 (1)**: 277-283.

Kaur, P., R.Thakur, A.Choudhary. 2012. An in vitro study of the antifungal activity of silver/chitosan nanoformulations against important seed borne pathogens. *Inter J Sci & Tech Res* **1 (6) :** 83-86.

Khan, M.M.,M.R. Khan,F.A. Mohiddin. 2012. The relative performance of different inoculation methods with *Alternaria brassicae* and *A. brassicicola* on Indian mustard. *Plant Pathol J* **11**: 93-98.

Mossa, A.A., S.M.M. Mohafrash, E.H.E. Ziedan, I.S. Abdelsalam , A.F. Sahab. 2021. Development of eco- friendly nanoemulsions of some natural oils and evaluating of its efficiency against postharvest fruit rot fungi of cucumber. *Indusl Crops Prod* **159:**113049–113051

Pal, A., R. Adhikary, T. Shankar, A.K. Sahu, S. Maitra 2020. Cultivation of Cucumber in Greenhouse. In book: **Protected Cultivation and Smart Agriculture,** Smart Agriculture; Sagar Maitra, Djgats (ed), New Delhi Publishers: New Delhi, India, pp. 139–145. doi:10.30954/NDP-PCSA.2020.14.

Rampino, A., M. Borgogna, P. Blasi, B. Bellich, A. Cesàro A. 2013. Chitosan nanoparticles: preparation, size evolution and stability. *Inter J Pharma* **455 (1-2):** 219-228.

Sambou, A., N.W.Samb, N. Ayessou. 2023. Nutritional values of green and white cucumber (*Cucumis sativus* L.) and African horned cucumber (*Cucumis metuliferus* E.) J Hort and Post Res **6 (3):** 221-234

Snedecor, G.W., W.G. Cochran 1980. **Statistical Methods.** 7th Edn. Iowa State Univ. Press, Ames

Waly, A.I., A.F. Sahab, M.M. Marie, W.M. Elzoeerey, R. Abo Elela. 2015. Preparation of quaternized chitosan nanoparticle and its antimicrobial activity on polyester, cotton and polyester/cotton blend treated fabrics . *American-EurJ. Sust Agric* **9 (5) :** 52-59.

Wang, L., J. Dong, J. Chen, J. Eastoe, X. Li . 2009. Design and optimization of a new self-nanoemulsifying drug delivery system. *J Coll Interf Sci* **330 (2**) :443–448.

Youssef, K., A.F. Hashim .2020. Inhibitory Effect of Clay/Chitosan Nanocomposite against *Penicillium digitatum* on Citrus and Its Possible Mode of Action. *Jordan J Biol Sci* **13 (3**): 349 – 355.

Zahid, N., A. Ali, S. Manickam, Y. Siddiqui, M. Maqbool. 2012. Potential of chitosan-loaded nanoemulsions to control different *Colletotrichum* spp. and maintain quality of tropical fruits during cold storage. *J Appl Micr* **13**: 925–939, doi:10.1111/j.1365-2672.2012.05398.x

Zian, A.H., S.A. El-Blasy, H.M. El-Gendy, S.A. El-Sayed. 2023. Plant defense activation and down-regulation root rot and wilt in chickpea diseases by some abiotic substances. *In E3S Web of Conferences* 462, p. 02014). EDP Sciences.

Ziedan, E.H. 2024a. Distribution of epidemic diseases of cucumber under protective plastic houses in Egypt. *Analele Univ Orad Fasci Biol* **1:** 15-23

Ziedan, E.H., M.S. Saad .2016. Efficacy of nanoparticles on seed borne fungi and their pathological potential of cucumber . *Inter J Pharma Tech Res* **9 (10)** :16-24.

Ziedan, E.H.E. 2024 b. Application of essential oils and their volatile components as a green bio-fumigations pesticides eco-friendly on controlling various plant diseases. A review. *AFRIMED AJ –Al Awamia* **142:** 33-72.

Ziedan, E.H.E., M.M. Saad, A.A. El-Kafrawy, A.F. Sahab, A.T. Mossa. 2022. Evaluation of essential oils nanoemulsions formulations on *Botrytis cinerea* growth, pathology and gray mould incidence on cucumber fruits. *Bull Nati Rese Cent* 46:88.

Zoeir, H.A., H.M. El Zahaby, E.H. Ziedan, H.F. Maswada. 2017. Efficacy of antifungal activity of essential oils, salts and antioxidants acids on pathogenic fungi and their application methods for controlling postharvest diseases on banana fruits. *African J Micr Res* **11 (29)** : 1162-1170.

JJBS

Volume 18, Number 2,June 2025
ISSN 1995-6673
Pages 231 – 241
https://doi.org/10.54319/jjbs/180204

Jordan Journal of Biological Sciences

Modulation of Gut Microbiota in *Salmonella* Typhimurium-infected Sprague Dawley Rats by Treatment with *Pichia kudriavzevii* 2P10 in Combination with Prebiotic Mannan-Oligosaccharide

Rahayu Wulan[1], Rika Indri Astuti[2,3,*], Yaya Rukayadi[4], Sri Estuningsih[5], Anja Meryandini[2,3]

[1]*Doctoral Program of Microbiology, Department of Biology, Faculty of Mathematics and Natural Sciences, IPB University, Agathis Street, IPB Dramaga Campus, Bogor 16680, West Java, Indonesia;* [2]*Department of Biology, Faculty of Mathematics and Natural Sciences, IPB University, Agathis Street, IPB Dramaga Campus, Bogor 16680, West Java, Indonesia;* [3]*Biotechnology Center, IPB University, Kamper Street, IPB Dramaga Campus, Bogor 16680, Indonesia, West Java, Indonesia;* [4]*Department of Food Science, Faculty of Food Science and Technology, Universiti Putra Malaysia, 43400, Serdang, Selangor, Malaysia;* [5]*Department of Reproductive Pathology Clinic, Faculty of Veterinary Medicine, IPB University, IPB Dramaga Campus, Bogor 16680, West Java, Indonesia*

Received: April 19, 2024; Revised: October 7, 2024; Accepted: October 17, 2024

Abstract

Gut microbiota is significantly influenced by diet, including probiotics and prebiotics, and can be disrupted through infection with the foodborne pathogenic bacteria *Salmonella* Typhimurium. The effects of dietary probiotics yeast on modulating gut microbiota have not been widely explored. Therefore, this study aimed to investigate the effects of administering *Pichia kudriavzevii* 2P10 (PRO), mannan-oligosaccharide (MOS), and their combination (PMOS) on male Sprague Dawley (SD) rats, followed by injecting *S.* Typhimurium (ST) ATCC 14028 to induce non-typhoidal infection. The composition of rats' cecum microbiota was analyzed through next-generation sequencing analysis, and histological changes were observed using Hematoxylin-Eosin (HE) staining. The results showed that rats treated with *P. kudriavzevii* 2P10 and infected with *S.* Typhimurium (PRO.ST) had gut microbiota community structure closest to CONTROL, without the occurrence of dysbiosis. Firmicutes levels increased after the administration of *P. kudriavzevii* 2P10, MOS, and PMOS. Moreover, *P. kudriavzevii* 2P10 treatment increased Bacteroidetes, followed by a decrease in Firmicutes/Bacteroidetes ratio in gut microbiota. This phenomenon affected the production of short-chain fatty acids (SCFAs) propionate to impair ST. In conclusion, this study suggested that all treatments could modulate gut microbiota to prevent dysbiosis severity and damage to the histological structure of the cecum after ST infection, with *P. kudriavzevii* 2P10 showing the optimal efficacy.

Keywords: gut microbiota, *Pichia kudrivazevii*, probiotics yeast, *Salmonella* Typhimurium, prebiotics, mannan-oligosaccharide

1. Introduction

A stable and balanced gut microbiota is essential in health maintenance, providing various advantages, such as increasing the immune system against pathogens (Hasan and Yang, 2019; Ji *et al.*, 2020). The diversity and abundance of microbiota in the digestive tract are significantly influenced by diet, health status, lifestyle, microbial infection, age, genetics, and use of drugs or antibiotics (Rinninella *et al.*, 2019). Among the infections that can cause dysbiosis is a non-typhoidal *Salmonella* (NTS), namely *Salmonella enterica* serovar Typhimurium or *Salmonella* Typhimurium (ST), a food poisoning bacterium responsible for diarrheal infections, particularly in children (Kirk *et al.*, 2017). Among bacterial pathogens, ST is the primary cause of foodborne diseases that lead to hospitalizations and deaths globally. This infection causes acute inflammatory diarrhea capable of progressing to invasive systemic disease in susceptible patients (Anderson and Kendall, 2017).

Several studies showed that a healthy diet was mainly practiced by consuming probiotics and prebiotics to modulate gut microbiota, avoiding digestive tract infections (Hasan and Yang, 2019; Ji *et al.*, 2020). Furthermore, consuming probiotics has a good effect on the digestive tract in inhibiting the growth of pathogenic bacteria and has many healthy effects, such as increasing blood protein content (Adriani *et al.*, 2021). These probiotics are live microorganisms capable of conferring health benefits on the host when administered in sufficient amounts (Hill *et al.*, 2014). Compared to bacteria-based, there are probiotics yeast such as *Saccharomyces cerevisiae* var. *boulardii* (*S. boulardii)*, which have been explored for their effectiveness in treating various gastrointestinal disorders. This yeast plays a significant role in maintaining normal gut microbiota and inhibiting the pathogenicity of diarrheal. Numerous studies reported

* Corresponding author. e-mail: rikaindriastuti@apps.ipb.ac.id

S. boulardii as a biotherapeutic agent due to its antibacterial, antioxidant, anti-inflammatory, antiviral, anticarcinogenic, and immunomodulatory properties (Czerucka, Piche and Rampal, 2007; Abid *et al.*, 2022). Among the most often used genera of probiotic yeasts in Indonesia are *Saccharomyces, Pichia*, and *Candida*, which are widely applied in poultry and human health (Astuti *et al.*, 2023). A previous study isolated *P. kudriavzevii* 2P10, a probiotics yeast from the cocoa fermentation process, which showed antioxidant abilities and co-aggregates with ST (Wulan *et al.*, 2021).

Prebiotics are substrates selectively used by microbial hosts that are capable of conferring a significant health benefit (Gibson *et al.*, 2017). Mannan-oligosaccharide (MOS) is among prebiotics that is widely used to improve and maintain the structure of gut microbiota, facilitating the body's resistance to pathogens (Wang *et al.*, 2018). Furthermore, MOS prebiotics are used to treat pathogenic bacterial infections that have type 1 fimbriae, such as ST. The mannose structure in MOS constituent can impede the attachment of type 1 fimbriae to the intestinal epithelial wall, preventing ST infection (Zeiner, Dwyer and Clegg, 2012).

Based on the background above, this study aimed to evaluate the potential of yeast *P. kudriavzevii* 2P10 as probiotics and MOS prebiotics, with their combination in modulating gut microbiota *in vivo*. ST-infected-Sprague Dawley (SD) rats were used in in vivo study to elaborate on the potential of *P. kudriavzevii* 2P10 and MOS in interfering with gut microbiota, potentially lowering ST infection.

2. Material and Methods

2.1. Culture and Cultivation

In this study, *P. kudriavzevii* 2P10 was used as yeast probiotics, which had been characterized in previous investigations (Wulan *et al.*, 2021). Initially, a microbial growth curve was created to determine the harvest period for probiotic yeast and the pathogenic bacteria ST. *P. kudriavzevii* 2P10 was grown for 48 hours at 28 °C in a liquid yeast extract peptone dextrose (YPD) medium. Subsequently, *P. kudriavzevii* 2P10 cells were counted every 3 hours based on the total yeast count method on YPD agar media and incubated for 48 hours at 28°C (Rahmadhani *et al*., 2022). For the growth curve, ST was grown in a Mueller-Hinton (MH) liquid medium for 48 hours at 37 °C, while ST cells were counted every 2 hours based on the total plate count (TPC) method on *Salmonella Shigella* Agar (SSA) medium incubated for 24 hours at 37 °C. *Salmonella* will form transparent colonies with a black dot in the middle

For cultivation, *P. kudriavzevii* 2P10 was cultured in YPD liquid medium for 15 hours at 28 ºC aerobically, while ST ATCC 14028 was cultured with Mueller-Hinton (MH) liquid medium for 18 hours at 37 ºC aerobically. Each culture was harvested separately by washing and resuspending in PBS twice through centrifugation at 4000 rpm for 15 minutes, followed by dissolution in PBS to obtain a cell number of 10^8 CFU/mL.

2.2. Animals and Treatments

The methods used in this study were authorized by the Animal Ethics Committee of the Faculty of Veterinary Medicine, Bogor Agricultural University, Indonesia, No. 46/KEH/SKE/XI/2021. The experiment was carried out using male SD (10 weeks old) rats purchased from iRATco Veterinary Laboratory Services, Bogor, Indonesia. A total of 2 rats were placed in cage in a temperature-controlled room, with the experimental design shown in Figure 1. Before treatment, rats were acclimatized for 2 weeks and given Ciprofloxacin (10 mg/kg) treatment to eradicate ST in gut. The treatments conducted included CONTROL, *P. kudriavzevii* 2P10 (PRO), PMOS, as well as MOS without and with ST ATCC14028. The diet was supplemented with 5% MOS (Bio-Mos, Alltech, USA) and 1 mL 10^8 CFU/ mL *P. kudriavzevii* 2P10 for 15 days. Subsequently, rats were infected by 1×1 mL 10^8 CFU/ mL ST ATCC 14028 and allowed 3 days for an infection response, with water provided ad libitum.

The group without ST (CONTROL, PRO, PMOS, and MOS) infection was sacrificed on the 16th day, while those with ST (CONTROL.ST, PRO.ST, PMOS.ST, and MOS.ST) infection was carried out the 20th day (3 days after infection) by euthanasia ketamine-xylazine. From the contents of the cecum, bacterial DNA was extracted and used for 16S rRNA gene amplicon sequencing.

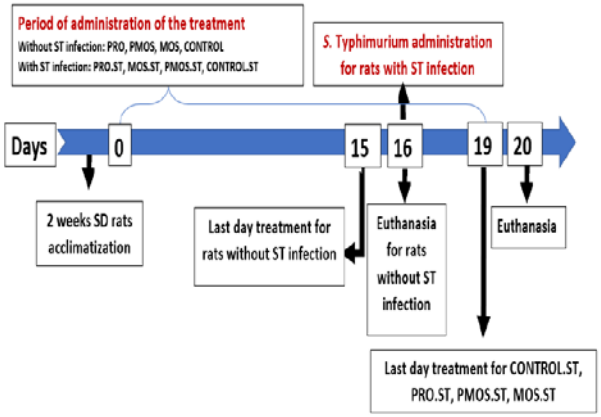

Figure 1. Chronological experimental design showing the treatments in the study. PRO: 1 mL (10^8 CFU/mL) of probiotics yeast *P. kudriavzevii* 2P10, MOS: mannan-oligosaccharide 5% in fed, PMOS: the combination of PRO and MOS, ST: Infection of 1 × 1 mL *S.* Typhimurium 10^8 CFU/mL.

2.3. Bacterial DNA extraction and 16S rRNA gene amplicon sequencing

The total genome DNA from cecum content samples was extracted using CTAB/SDS method (Sambrook and Russell, 2001). Subsequently, PCR reactions were conducted using Phusion® High-Fidelity PCR Master Mix (New England Biolabs), with the genomic DNA as a template. Amplification of the hypervariable region V3-V4 of bacterial 16S rRNA gene was performed using specific primers 341F 5′-TTTCTGTTGGTGCTGATATTGCCCTACGGGNGGCWGCAG-3′ and 806R 5′-ACTTGCCTGTCGCTCTATCTTCGGACTACHVGGGTWTCTAAT-3′ (Takahashi *et al.*, 2014; Matsuo *et al.*, 2021), where the underlined sequence served as an index or adapter.

PCR products quantification and qualification were performed by mixing the same volume of 1X loading buffer (contained SYB green) and operating electrophoresis on 2% agarose gel for detection. The mixture was purified with a Qiagen Gel Extraction Kit

(Qiagen, Germany). NEBNext® Ultra DNA Library Pre Kit for Illumina was generated for the sequencing library, which was assessed using the Agilent Bioanalyzer 2100 instrument and the Qubit@ 2.0 Fluorometer (Thermo Scientific). Subsequently, the library was sequenced using an Illumina NovaSeq platform, producing 250 bp paired-end reads.

2.4. Data analysis

The sequencing results were subjected to paired-end reads assembly and quality control, which included data splitting, sequence assembly, filtration, and chimera removal. Pairing-end reads were trimmed by removing the primer sequence and barcode, followed by sample distribution based on distinct barcodes for data splitting. In sequence assembly, paired-end reads were collected using FLASH V1.2.7, and the splicing sequences were called raw tags. Data filtration was carried out by quality filtering the raw tags, with specific settings applied to obtain high-quality clean tags following QIIME (V1.7.0) quality-controlled method (Caporaso *et al.* 2010). UCHIME Algorithm was used to determine chimera sequences by comparing the tags with the reference database (Gold database) to remove chimeras and obtain effective tags.

Sequence analysis was carried out using UPARSE software, where sequences with 97% or more similarity were assigned to the same OTU. Additional annotations were checked on representative sequences from each OTU. For each representative sequence, the Green Gene Database (http://greengenes.lbl.gov/cgi-bin/nph-index.cgi) (DeSantis *et al.*, 2006) was used based on the RDP 3 classifier 2.2 algorithm to annotate taxonomic information.

Alpha diversity was applied to assess the complexity of sample species diversity using six indices, including observed species, Chao1, Shannon, Simpson, and ACE. QIIME (Version 1.7.0) was used for calculation, while R (Version 2.15.3) was applied to visualize all indices. Meanwhile, beta diversity analysis was used to evaluate the variations in species complexity in the sample using QIIME software (version 1.7.0) to calculate unweighted UNIFRAC beta diversity.

2.5. Histological Analysis of the Cecum

Histological evaluation of the cecum was performed by fixing the fragments of 10% formalin for 24 hours, followed by dehydration and embedding in paraffin. Specifically, the 5-µm paraffin cecum sections were prepared and stained with hematoxylin as well as eosin. Histological micrographs were captured using an OptiLab Advance viewer and an Olympus CX23 Microscope device (Tokyo, JAPAN).

3. Results

3.1. P. kudriavzevii 2P10, Salmonella Typhimurium ATCC 14028, and Mannan-Oligosaccharide

Figure 2 shows the morphology of *Pichia kudriavzevii* 2P10, ST ATCC 14028, and MOS used in this study. The probiotic yeast *P. kudriavzevii* 2P10 forms round, white colonies on YPD agar media, with microscope observation showing oval cells and reproduces through budding. The pathogenic bacteria used to infect rats in this study was ST ATCC 14028, which appears black in SSA media, as shown in Figure 2C. The prebiotic used is the commercial prebiotic Bio-Mos Alltech, which has a dark brown color in powder form, as presented in Figure 2D.

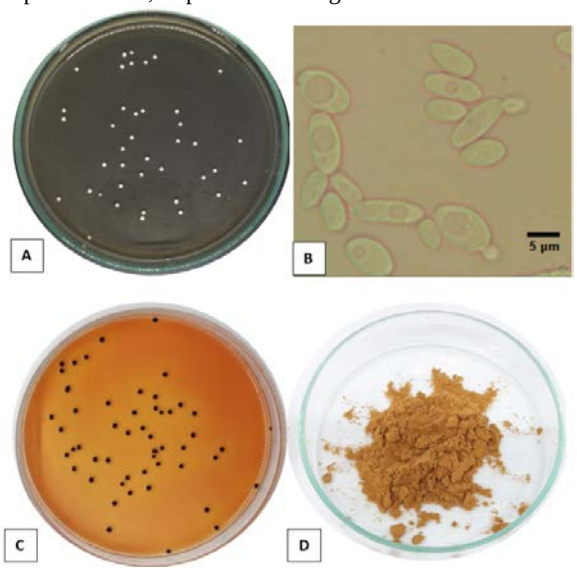

Figure 2. The morphology of: (A) Pure colony of probiotic yeast *Pichia kudriavzevii* 2P10 on yeast extract, peptone, and dextrose (YPD) agar medium at 28°C for 24 hours of incubation, (B) Probiotic yeast *Pichia kudriavzevii* 2P10 oval cells shape, (C) Black colony of *Salmonella* Tyhipimurium 2P10 *Salmonella Shigella Agar* (SSA) agar medium at 37°C for 24 hours of incubation, (D) Mannan-Oligosaccharide (Bio-Mos Alltech, USA)

3.2. The Growth Curve of P. kudriavzevii 2P10 and Salmonella Typhimurium ATCC 14028

Figure 3 shows the growth curve of both probiotics and prebiotics, with *P. kudriavzevii* 2P10 having a maximum cell number (N_{max}) at the 15th hour, reaching 9.33 log cell CFU/mL. Meanwhile, ST has a maximum cell number (N_{max}) at the 10th hour with a cell number of 12.62 log cell CFU/mL and tends to be stable at the 48th hour. The maximum growth rate (μ_{max}) of *P. kudriavzevii* 2P10 is 0.43 hour^{-1}, while μ_{max} value for ST is 0.43 hour^{-1}.

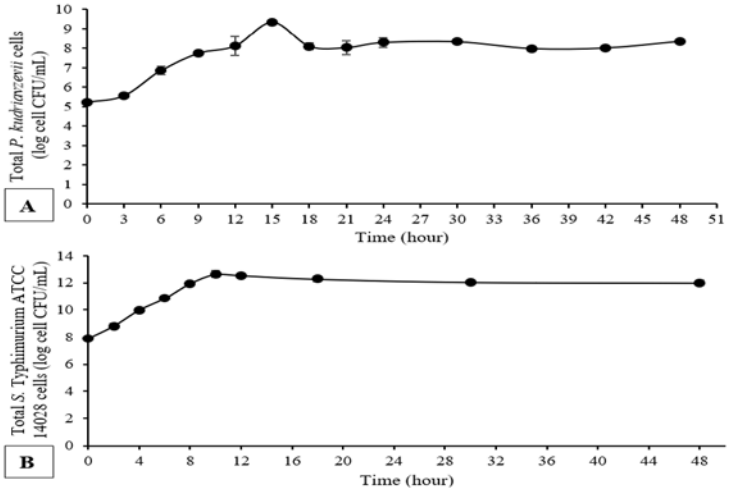

Microbes	N_{max} (log cell CFU/mL)	μ_{max} (hour^{-1})
P. kudriavzevii 2P10	9,33±0,0165	0,43±0,0746
S. Typhimurium ATCC 14028	12,62±0,2370	0,58±0,1039

Figure 3. Growth curve of (A) Probiotic yeast *Pichia kudriavzevii* 2P10 in liquid YPD medium at 28°C for 48 hours of incubation, (B) ST ATCC 14028 in liquid Mueller-Hinton medium at 37°C for 48 hours of incubation.

3.3. Gut Microbiota Analysis

3.3.1. Number of OTU in Rats' Gut Microbiota

The sequencing of 16S rRNA gene region V3-V4 in rats' cecum content across all treatments produced an average total tags of 102,245 and OTU of 1638. Moreover, OTU is a collection of V3-V4 16S rRNA sequences with more than 97% similarity. Based on the results, the most abundant OTU was found in the treatment with probiotic yeast (PRO) and PMOS, as shown in Table 1. The number of OTU in ST ATCC 14028-infected samples was decreased compared to those without infection in all treatments of PRO and MOS.

Table 1. Number of observed OTU (97% similarity) and alpha diversity indices of bacterial microbiota in cecum rats with and without **ST** infection

Sample name	Observed species (OTU)	Shannon	Simpson	Chao1	ACE
CONTROL	1657	6.89	0.957	1756	1799.331
CONTROL.ST	1630	6.91	0.965	1767	1855.420
PRO	1686	7.60	0.984	1789	1727.083
PRO.ST	1638	7.40	0.983	1656	1689.173
PMOS	1686	6.98	0.967	1822	1793.863
PMOS.ST	1642	7.16	0.975	1783	1661.841
MOS	1614	7.10	0.978	1710	1787.539
MOS.ST	1549	7.15	0.973	1642	1785.156

Note: CONTROL, control without ST infection (negative control); CONTROL.ST, control positive with ST infection; PRO, 1 mL of probiotics yeast *P. kudriavzevii* 2P10 10^8 CFU/mL; PRO.ST, 1 mL of probiotics yeast *P. kudriavzevii* 2P10 10^8 CFU/mL with ST infection; MOS, mannan-oligosaccharide 5% in fed; MOS.ST, mannan-oligosaccharide 5% in fed with ST infection; PMOS, the combination of PRO and MOS; PMOS.ST, the combination of PRO and MOS with ST infection; ST infection of 1 mL *Salmonella* Typhimurium ATCC 14028

3.3.2. Alpha Diversity of Rats' Gut Microbiota

The alpha diversity index of rats subjected to all treatments had higher Shannon and Simpson indices compared to those without treatment. The highest observed OTU (1686) was in rats fed with PRO without ST infection. The results were also confirmed by the highest Shannon and Simpson diversity index, with values of 7.60 and 0.984, as shown in Table 1. However, in the Chao1 diversity index, the highest was PMOS (1822), followed by PRO (1789) due to the influence of ST infection.

3.3.3. Beta Diversity Index in Rats' Gut Microbiota

Beta diversity was examined using principle component analysis (PCoA) graph and UPGMA cluster tree. Principle component analysis (PCoA) graph showed clustering patterns among microbiota community structures across treatments. Based on Figure 4, gut bacterial community structure of PRO.ST was similar to CONTROL on the same plot. Based on the results, rats fed with *P. kudriavzevii* 2P10 and infected with ST had normal gut microbiota without dysbiosis. However, ST infection in MOS-supplemented rats showed a similar community structure to infected CONTROL.ST. This showed that the administration of MOS without *P. kudriavzevii* 2P10 did not prevent dysbiosis. PRO and PMOS.ST treatments have similar gut microbiota community structures, while PMOS and MOS produced identical results.

Clusterization of the cecum bacterial communities based on the UPGMA cluster tree divided into three clusters. The first cluster was rat administrated with PRO, MOS, and PRO.ST, and the second cluster was rat administrated with PMOS, MOS.ST, CONTROL.ST, and PMOS.ST, and the last is control with no infection cluster (Figure 5).

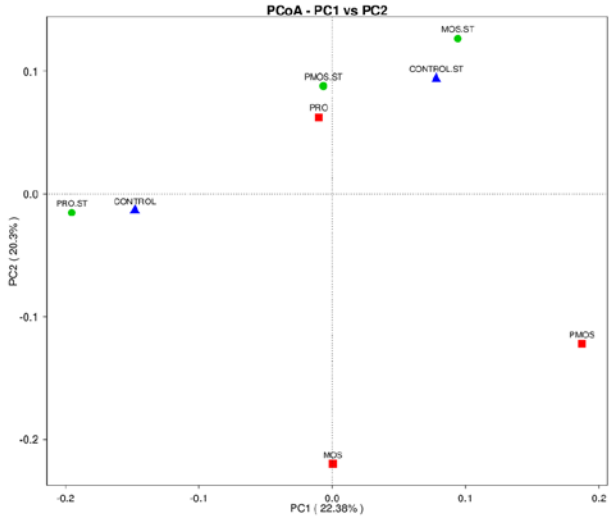

Figure 4. Principle component analysis (PCoA) based on unweighted UNIFRAC of gut microbial community of male SD rats in all treatments. Treatments: PRO (1 mL of *Pichia kudriavzevii* 2P10 10^8 CFU/mL), MOS (5% of Mannan-oligosaccharide), PMOS (PRO and MOS combination), ST (*Salmonella* Typhimurium infection 1×10^8 CFU/mL

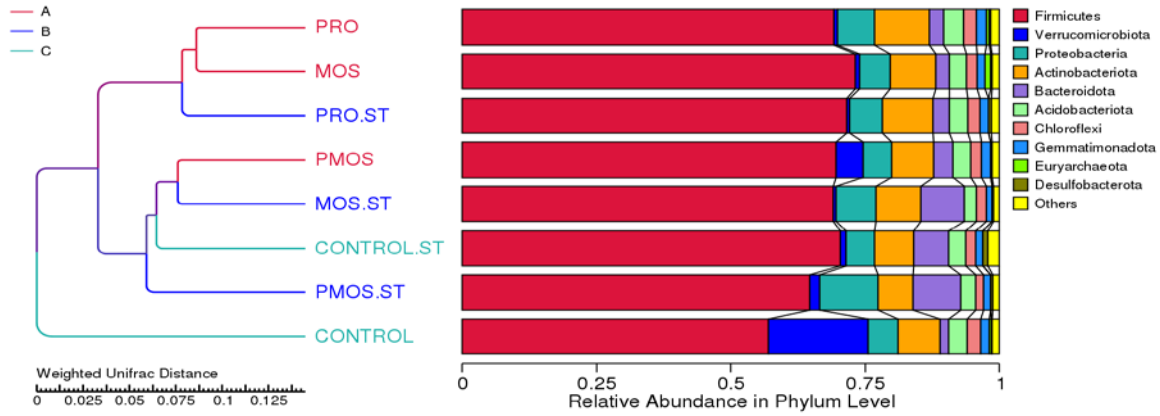

Figure 5. Clusters of bacterial communities in the caecum of rats treated with PRO (1 mL of *Pichia kudriavzevii* 2P10 10^8 CFU/mL), MOS (5% of Mannan-oligosaccharide), PMOS (PRO and MOS combination), ST (*Salmonella* Typhimurium infection 1×10^8 CFU/mL

3.3.4. Profile of Bacterial Gut Community at Filum Level

Firmicutes, Verrucomicrobiota, Proteobacteria, Actinobacteriota, Bacteriodota, Acidobacteriota, Chloroflexi, Gemmatimonadota, Euryarchaeota, and Desulfobacterota, formed the composition of the top 10 phyla in all treatments. According to Figure 6, Firmicutes dominated the phyla of bacterial microbiota with more than 65% relative abundance, compared to CONTROL at 57%. The highest relative abundance of Firmicutes was found in the MOS treatment (73.19%).

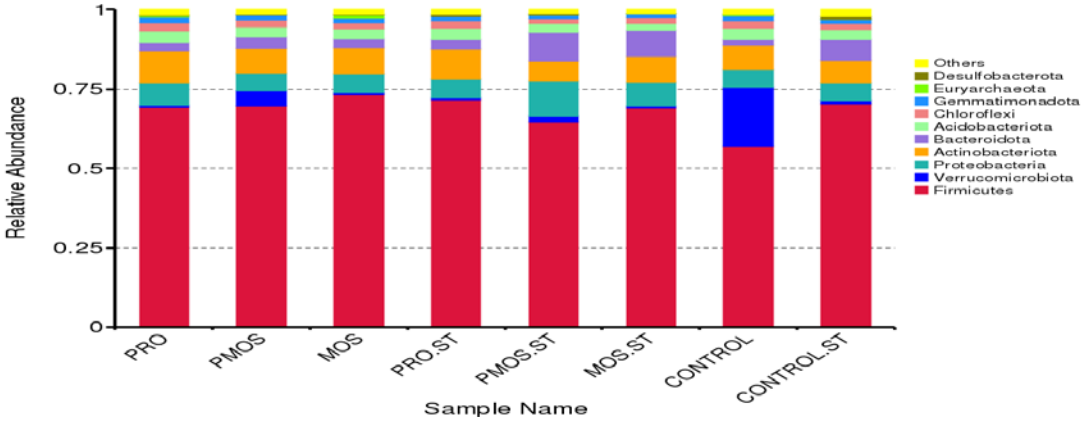

Figure 6. Profile of gut bacterial community at phylum levels following probiotic yeast and prebiotic treatments in Salmonella Typhimurium-infected and non-infected SD rats. The figure presents the relative abundance of OTU with more than 97% similarity. Treatments: PRO (Pichia kudriavzevii 2P10), MOS (Mannan-oligosaccharide), PMOS (PRO and MOS combination), ST (Salmonella Typhimurium infection).

3.3.5. Relative Abundance of Bacterial Gut Community at Family Level

Another phylum that is influential in gut microbiota is Bacteroidota (synonym: Bacteriodetes). Based on the results, all treatments without ST infection had a lower Firmicutes/Bacteroidetes ratio in the cecum compared to CONTROL, as shown in Table 2. Specifically, *P. kudriavzevii* 2P10, MOS, and PMOS showed potential to reduce the Firmicutes/Bacteroidetes ratio in gut microbiota. This showed that treatment with ST infection produced a lower Firmicutes/Bacteroidetes ratio than those ST.

Table 2. The relative abundance of cecum microbiota at the family level following treatment of *Pichia kudriavzevii* 2P10 (PRO), prebiotic mannan-oligosaccharide (MOS), probiotic yeast + prebiotic mannan-oligosaccharide (PMOS) in both ST ATCC 14028-infected and non-infected SD rats.

Relative abundance (%)	CONTROL	CONTROL.ST	PRO	PRO.ST	PMOS	PMOS.ST	MOS	MOS.ST
Firmicutes	0.488	0.633	0.590	0.623	0.613	0.556	0.645	0.617
Lachnospiraceae	0.213	0.234	0.365	0.296	0.242	0.165	0.353	0.227
Lactobacillaceae	0.100	0.315	0.080	0.161	0.238	0.264	0.076	0.231
Erysipelotrichaceae	0.023	0.016	0.047	0.054	0.074	0.049	0.083	0.086
Oscillospiraceae	0.072	0.018	0.029	0.038	0.027	0.034	0.032	0.018
Peptostreptococcaceae	0.046	0.040	0.057	0.048	0.026	0.033	0.053	0.028
Clostridiaceae	0.034	0.010	0.012	0.026	0.006	0.011	0.048	0.027
Verrucomicrobiota								
Akkermansiaceae	0.178	0.004	0.002	0.002	0.043	0.013	0.002	0.002
Bacteroidota	0.009	0.047	0.016	0.021	0.027	0.062	0.018	0.048
Muribaculaceae	0.008	0.004	0.011	0.020	0.025	0.046	0.015	0.037
Prevotellaceae	0.001	0.043	0.005	0.001	0.002	0.016	0.003	0.011
Proteobacteria								
Succinivibrionaceae	0.001	0.001	0.004	0.001	0.001	0.058	0.001	0.001
Others	0.324	0.315	0.390	0.354	0.317	0.320	0.335	0.334
F/B ratio*	36.37	10.81	26.84	23.57	19.33	7.22	28.32	8.55

Note: CONTROL, control without ST infection (negative control); CONTROL.ST, control positive with ST infection; PRO, 1 mL of probiotics yeast *P. kudriavzevii* 2P10 10^8 CFU/mL; PRO.ST, 1 mL of probiotics yeast *P. kudriavzevii* 2P10 10^8 CFU/mL with ST infection; MOS, mannan-oligosaccharide 5% in fed; MOS.ST, mannan-oligosaccharide 5% in fed with ST infection; PMOS, the combination of PRO and MOS; PMOS.ST, the combination of PRO and MOS with ST infection; ST. infection of 1 mL *Salmonella* Typhimurium ATCC 14028

*The Firmicutes/Bacteroidetes ratio

All treatments of PRO and MOS had a higher relative abundance of Firmicutes family members compared to CONTROL, as shown in Table 2. Lachnospiraceae had the highest abundance as observed in PRO (0.365) and MOS (0.353) among the top 10 families, followed by Lactobacillaceae. However, ST infection reduced the relative abundance of Lachnospiraceae in the treatment of PRO.ST, MOS.ST, and PMOS.T. The family with the second highest relative abundance was Lactobacillaceae, which was highest in CONTROL.ST (0.315), followed by PMOS (0.238), PMOS.ST (0.264), and MOS.ST (0.231). The reduction in the abundance of Lactobacillaceae could be attributed to treatment with ST infection. Regarding Clostridiaceae, the highest relative abundance was found in CONTROL (0.034) and MOS (0.042) in addition to Akkermansiaeceae. Moreover, Provotellaceae in CONTROL had the lowest value compared to other treatments.

In phylum Bacteriodota, the relative abundance in all treatments was higher than CONTROL, as shown in Table 2. Based on the results, ST infection also increased the abundance of Bacteriodota, with the highest being in observed PMOS.ST (0.062) and MOS.ST (0.048). In this study, the highest abundance of family members of phylum Bacteriodota were Muribaculaceae and Prevotellaceae.

3.4. Histopathology of Rats' Cecum

The confirmation of gut microbiota results was achieved through histological examination of rats' cecum. The histology results showed that the control-treated cecum, which was given standard feed and infected with ST ATCC 14028 (CONTROL.ST), had more severe cecal epithelial damage, as presented in Figure 7. This damage manifested as epithelial desquamation (ed) and a more tenuous structure of the villous epithelium of the cecum. Specifically, the histology of the cecum appeared normal in CONTROL treatment without ST infection, PRO, MOS, and PMOS.

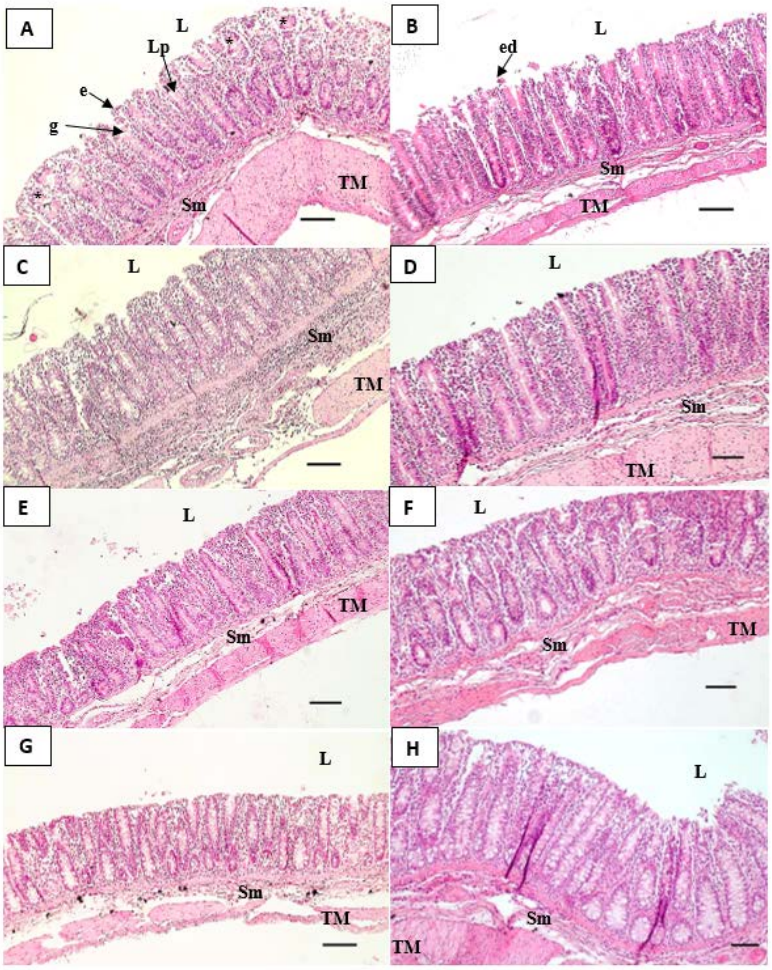

Figure 7. Photomicrographs of rat's cecum histology in all treatments with Hematoxylin-Eosin (HE) staining: A) CONTROL, B) epithelial desquamation in treatment CONTROL.ST= control with ST infection, C) PRO= Probiotic yeast *P. kudriavzevii* with no ST infection, D) PRO.ST= Probiotic yeast *P. kudriavzevii* with ST infection, E) MOS= 5% of prebiotic MOS with no ST infection, F)MOS.ST= 5% of prebiotic MOS with ST infection, G) PMOS= Combination of probiotics yeast and prebiotics with no ST infection, H) Combination of probiotics yeast and prebiotics with ST infection (PMOS.ST). After 4th days ST ATCC 14028 10^8 CFU/mL infection. L= cecal lumen; e= epithelial, ed= epithelial desquamation, g= goblet cell*; Lp= lamina propria; Sm= Submucosa; TM= Tunica Muscularis. Scale bar= 50 µm.

4. Discussion

Pichia sp. is a yeast from Ascomycota division isolated from fermented foods (Astuti *et al.*, 2023). As shown in Figure 2, *P. kudriavzevii* 2P10 used in this study is a yeast or single-cell fungi that reproduces through budding. This yeast is native to Indonesia from the cocoa fermentation process and has been characterized as a probiotic (Wulan *et al.*, 2021; Astuti *et al.*, 2023), due to the ability to survive at pH 3, 0.5% bile salts tolerance, withstand temperatures of 37°C and 41°C. Other characteristics include the non-hemolytic ability to auto-aggregate and co-aggregate with ST ATCC 14028, acting as an antioxidant (Wulan *et al.*, 2021). Generally, probiotic yeast at a dose of 10^8 CFU/mL is considered capable of modulating gut microbiota (Roobab *et al.*, 2020). A dose of ST ATCC 14028 1×10^8 CFU/mL through oral gavage is also effective in causing changes in beta diversity in broiler chickens consistently (Martins *et al.*, 2010; Sheets *et al.*, 2022). This infection is supported by the high growth rate in ST at μ_{max} 0.58 ± 0.1039 $hour^{-1}$ on the Mueller-Hinton medium (Figure 3).

ST is a major foodborne pathogen that causes diarrheal infections globally, particularly in children (Kirk *et al.*, 2017). Generally, rats are often used as biomedical models to explore the correlation between gut microbiota and gastrointestinal (GI) disease. Gut microbiota consists of bacteria, yeast, and viruses, with cecum of rats serving as the largest and most active fermentative digestive chamber. Specifically, cecum has the highest microbial community compared to the stomach and small intestine (Li *et al.*, 2017).

The top 10 gut microbiota in cecum of rats were Firmicutes, Verrucomicrobiota, Proteobacteria, Actinobacteriota, Bacteriodota, Acidobacteriota, Chloroflexi, and Gemmatimonadota, as shown in Figure 6. Firmicutes were found to be the most dominating phylum, with a relative abundance of over 65% (Li *et al.*, 2017; Sivixay *et al.*, 2021). Rat fed with *P. kudriavzevii* 2P10, MOS, and PMOS increased the abundance of Firmicutes, with MOS showing the best efficiency. Previous studies showed that the administration of a high-cholesterol diet with 1% MOS for 14 weeks increased the abundance of *Bacteroides ovatus*, a genus of Firmicutes known as mannan fermenter (Hoving *et al.*, 2018). Additionally, MOS reduced the colonization of *S.* enteritidis,

Salmonella, and *Escherichia coli* (Ghasemian and Jahanian, 2016; Azad *et al.*, 2020), serving as prebiotic commonly used in poultry to promote gut health and combat *Salmonella* infection (Micciche *et al.*, 2018). The administration of mannan-oligosaccharides has a dominant growth effect on firmicutes. The Firmicutes phylum plays a crucial role in maintaining health, and members of the Firmicutes phylum belong to commensal butyrate-producing bacteria (Lindstad *et al.,* 2021). Previous studies also reported that the most dominant phylum Firmicutes was found after the turkey was given Mannan-oligosaccharides (Corrigan *et al.*, 2012).

In this study, microbial diversity analysis was carried out by analyzing alpha and beta diversity to determine the influence of various treatments (Asriatno *et al.*, 2023). Alpha diversity indices, including the Simpson and Shannon indices, increased after administration of all treatments, with the highest value observed in *P. kudriavzevii* 2P10. This suggested that the diversity of gut microbiota could be affected by the administration of *P. kudriavzevii* 2P10, MOS, and PMOS. Significant improvements in gut microbiota richness are associated with positive health status, while decreases in species diversity are related to disease symptoms (Manor *et al.*, 2020; Bao *et al.*, 2022)**.** Based on the results, ST infection across all treatments caused a significant decrease in the Simpson and Shannon indices. Furthermore, this infection led to Salmonellosis, which caused a reduction in the diversity of gut microbiota. Several studies showed that Salmonellosis could lead to inflammatory bowel disease (IBD) and inflammation-induced dysbiosis (Bratburd *et al.*, 2018; Gillis *et al.*, 2018; Rinninella *et al.*, 2019; Bao *et al.*, 2022).

Based on beta-diversity analysis, the bacterial community cluster in rat cecum, PRO, MOS, and PRO.ST are in the same cluster, which is different from CONTROL.ST (Figure 3). The presence of PRO, MOS, and PRO.ST in the same cluster indicates the similarity of the bacterial community structure. ST infection in rats treated with probiotic yeast *Pichia kudriavzevii* 2P10 does not affect the structure of the cecum microbiota, so dysbiosis does not occur. Other studies have reported that probiotic yeast *Pichia kudriavzevii* Y33 has antibacterial properties against various pathogenic bacteria such as *Salmonella typhi, Escherichia coli, Shigella, Pseudomonas aeruginosa, Bacillus cereus, Staphylococcus aureus, Aeromonas hydrophila,* and *Listeria monocytogenes* (Lata *et al*., 2022). The mechanism of action of the probiotic yeast *S. boulardii* is by inhibiting the abundance of pathogenic bacteria, thereby increasing microbial diversity and restoring microbiota dysbiosis in mice (Gao *et al*., 2023).

Firmicutes and Bacteroidota (synonym Bacteroidetes) are the two main species that determine the homeostasis of gut microbiota, thereby serving as marker of health status. Bacteria from these species are the most common, representing 90% of gut microbiota (Rinninella *et al.*, 2019; Stojanov *et al.*, 2020). Phylum Firmicutes includes Gram-positive bacteria with 'firm' or rigid or semi-rigid cell walls, predominantly originating from the genera *Bacillus, Clostridium, Enterococcus, Lactobacillus,* and *Ruminococcus* (Seong *et al.*, 2018; Stojanov *et al.*, 2020). In PRO, PRO.ST, PMOS, PMOS.ST had a lower relative abundance of Firmicutes compared to CONTROL.ST. This is in line with previous yeast probiotic studies, that *Saccharomyces boluardii* also increased the relative abundance of Bacteroidetes and decreased Firmicutes and Proteobacteria. This condition is associated with improved metabolic health and reduced inflammation (Yu *et al.,* 2017).

In Bacteroidota, the relative abundance across all treatments was higher compared to CONTROL, as shown in Table 2. Specifically, ST infection increased the abundance of Bacteriodota in all treatments, with the highest being observed in PMOS.ST (0.062) and MOS.ST (0.048). Bacteroidetes is the largest phylum of Gram-negative bacteria that inhabit the digestive tract, consisting of approximately 7000 species of predominantly Gram-negative bacteria from the genera *Bacteroides, Alistipes, Parabacteroide*s, and *Prevotella*. Specific roles have been attributed to several Bacteroidetes genera play specific roles in the development of immune dysregulation, systemic diseases such as metabolic syndrome, and neurological disorders (Gibiino *et al.*, 2018). This study found two families in phylum Bacteriodota, namely Muribaculaceae and Prevotellaceae.

PRO, MOS, and PMOS treatments increased the abundance of phylum Bacteroidota compared to CONTROL after ST infection, with the highest observed PMOS.ST and MOS.ST. Previous studies reported that *Bacteroides* spp., in rats, mediated colonization resistance to ST by producing propionic short-chain fatty acids (SCFAs). Propionate directly inhibited the growth of pathogens in vitro by disrupting intracellular pH homeostasis, and increased intestinal propionate levels chemically to protect rats from ST infection (Jacobson *et al.*, 2018).

The results showed that the administration of *P. kudriavzevii* 2P10, MOS, and PMOS, including ST infection reduced Firmicutes/Bacteroidetes ratio in the cecum microbiota of rats compared to CONTROL. Moreover, this study is the first to report the effect of *P. kudriavzevii* 2P10 on gut microbiota in male SD rats. A previous investigation focusing on probiotic yeast *S. boulardii* in supernatant form reduced Firmicutes/Bacteroidetes ratio in 6-week-old male C57BL/6J rats (Gu *et al.*, 2022). *S. boulardii* also significantly improved the relative abundance of Bacteroidetes but decreased Firmicutes and Proteobacteria in adult BALB/c rats (Yu *et al.*, 2017). Furthermore, the administration in type 2 diabetic and obese rats (db/db) was associated with a significant increase in Bacteroidetes by approximately 37% and a 30% decrease in Firmicutes (Everard *et al.*, 2014).

The treatment with ST infection had a lower Firmicutes/Bacteroidetes ratio than those without infection due to a significant increase in the abundance of Bacteroidetes. This showed that a decrease in Firmicutes/Bacteroidetes ratio served as a marker of ST infection. Proteobacteria contribute to dysbiosis (Shin, Whon and Bae, 2015), showing a significant correlation between a decrease in Firmicutes and general microbial diversity in inflammatory bowel disease (IBD) (Morgan *et al.*, 2012).

At the family level, Lachnospiraceae and Lactobacillaceae were dominant in all treatments. Although the abundance of Lachospiraceae increased after the administration of *P. kudriavzevii* 2P10, MOS, and

PMOS, there was a significant decrease on the fourth day due to the effect of ST infection on rats. The family Lachnospiraceae is a phylogenetically and morphologically heterogeneous taxon of the class Clostridia, phylum Firmicutes. All members are anaerobic, fermentative, and chemoorganotrophic, some with hydrolyzing solid activities and fermenting carbohydrates (Stackebrandt, 2014). Furthermore, gut microbiota in the human cecum is formed by two anaerobic bacteria families, Lachnospiraceae and Ruminococcaceae (Lee *et al.*, 2018).

Carbohydrate metabolism by gut microbiota is an essential mechanism that provides the host with nutrition and energy. Butyrate and short-chain fatty acids (SCFAs) could be produced through the hydrolysis of starch and other sugars by Firmicutes families Lachnospiraceae, Lactobacillaceae, and Ruminococcaceae. Although Lachnospiraceae members are among the top producers of SCFAs, several taxa have been related to various intra- and extraintestinal diseases (Biddle *et al.*, 2013; Vacca *et al.*, 2020). Treatment of *P. kudriavzevii* 2P10, MOS, and PMOS reduced the abundance of Lactobacillaceae, which were not commonly found in the cecum as their main habitat is the ileum (Lee *et al.*, 2018).

The histological evaluation of the cecum structure confirmed dysbiosis in the gut microbiota. The results showed that the control cecum, which was fed standard food and infected with ST ATCC 14028 (CONTROL.ST), had more epithelial desquamation (ed) and tenuous cecum villous epithelial structure. The report of Setyawardani *et al.*, (2017) also showed that ST ATCC 14028 caused epithelial detachment in the ileum 10 days after infection. *Salmonella* Enteritidis P125109 infection caused mild erosion of the cecum mucosal epithelium in control treatments without probiotic administration. However, when probiotic *Lactobacillus rhamnosus* EM1107 was administered, there was no cecum epithelium erosion (Rolim *et al.*, 2021). In this study, control treatment without ST infection, PRO, MOS, and PMOS, cecum histology appeared normal. According to Gu *et al.*, (2022), there were no apparent pathological lesions in rats' colon tissue in a group of irritable bowel syndrome (IBS) model rats given the probiotic yeast *Saccharomyces boulardii* supernatant.

5. Conclusion

In conclusion, this study showed that ST infection could disrupt gut microbial community in SD rats. However, the treatments of *P. kudriavzevii* 2P10 and MOS modulated gut microbiota, potentially preventing the severity of dysbiosis after ST infection, which reduced Firmicutes/Bacteroidetes ratio. *P. kudriavzevii* 2P10 treatment in SD rats infected with ST provided Firmicutes/Bacteroidetes ratio similar to controls and other treatments without infection. The administration of *P. kudriavzevii* 2P10 also prevented damage to the histological structure of the cecum. The results showed that probiotic yeast *Pichia kudriavzevii* 2P10 treatment optimally modulated gut microbiota compared to MOS and PMOS.

Acknowledgments

The authors are grateful to the Ministry of Education, Culture, Research, and Technology, Indonesia, through a PMDSU scholarship to Prof. Anja Meryandini.

Funding Sources

This study was funded by the Ministry of Education, Culture, Research and Technology of the Republic of Indonesia through the 2018–2022 PMDSU scholarship**.**

Authors' contributions

R.W. contributed to the experimental design, study work, and writing of the manuscript preparation. R.I.A. contributed to the experimental design and revision of the manuscript before submission. Y.R. and S.E. contributed to the experimental design. A.M. contributed to the study plan and was responsible for the overall study and funding.

Declaration of Competing Interest

The authors declare no competing personal or financial interests regarding the publication of this study.

References

Abid R, Waseem H, Ali J, Ghazanfar S, Ali GM, Elasbali AM, Alharethi SH. 2022. Probiotic yeast *Saccharomyces*: back to nature to improve human health. *J Fungi*., **8(5)**:1–20.

Adriani L, Mushawwir A, Kumalasari C, Rosani U. 2021. Improving blood protein and albumin level using dried probiotic yogurt in broiler chicken. *Jordan J Biol Sci*., **14(5):** 1021–1024.

Anderson CJ, Kendall MM. 2017. *Salmonella enterica* serovar Typhimurium strategies for host adaptation. *Front Microbiol*., **8(1983)**:1–16.

Asriatno O, Nawangsih AA, Astuti RI, Wahyudi AT. 2023. *Streptomyces* – Alginate Beads Formula Promote Maize Plant. *Jordan J Biol Sci*.,**16(3):**537-546.

Astuti RI, Prastya ME, Wulan R, Anam K, Meryandini A. 2023. Current trends and future perspective of probiotic yeasts research in Indonesia. *FEMS Yeast Res*., **23**:1–13.

Azad MAK, Gao J, Ma J, Li T, Tan B, Huang X, Yin J. 2020. Opportunities of prebiotics for the intestinal health of monogastric animals. *Anim Nutr*., **6(4)**:379–388.

Bao H, Zhang H, Zhou Y, Zhu S, Pang M, Zhang X, Wang Y, Wang J, Olaniran A, Xiao Y, *et al.* 2022. Dysbiosis and intestinal inflammation caused by *Salmonella* Typhimurium in mice can be alleviated by preadministration of a lytic phage. *Microbiol Res*., **260(127020)**:1–9.

Biddle A, Stewart L, Blanchard J, Leschine S. 2013. Untangling the genetic basis of fibrolytic specialization by Lachnospiraceae and Ruminococcaceae in diverse gut communities. *Diversity*., **5(3)**:627–640.

Bratburd JR, Keller C, Vivas E, Gemperline E, Li L, Rey FE, Currie CR. 2018. Gut microbial and metabolic responses to *Salmonella enterica* serovar Typhimurium and *Candida albicans*. *MBio*., **9(6)**:1–14.

Caporaso JG, Kuczynski J, Stombaugh J, Bittinger K, Bushman FD, Costello EK, Fierer N, Pẽa AG, Goodrich JK, Gordon JI, *et al.* 2010. QIIME allows analysis of high-throughput community sequencing data. *Nat Methods*., **7(5)**:335–336.

Corrigan A, Horgan K, Clipson N, Murphy RA. 2012. Fffect of dietary prebiotic (mannan oligosaccharide) supplementation on the caecal bacterial community structure of turkeys. *Microb Ecol*., **64(3)**: 826–836.

Czerucka D, Piche T, Rampal P. 2007. Review article: Yeast as probiotics - *Saccharomyces boulardii*. *Aliment Pharmacol Ther*., **26(6)**:767–778.

DeSantis TZ, Hugenholtz P, Larsen N, Rojas M, Brodie EL, Keller K, Huber T, Dalevi D, Hu P, Andersen GL. 2006. Greengenes, a chimera-checked 16S rRNA gene database and workbench compatible with ARB. *Appl Environ Microbiol*., **72(7)**:5069–5072.

Everard A, Matamoros S, Geurts L, Delzenne NM, Cani PD. 2014. *Saccharomyces boulardii* administration changes gut microbiota and reduces hepatic steatosis, low-grade inflammation, and fat mass in obese and type 2 diabetic db/db mice. *MBio*., **5(3)**:1–9.

Ghasemian M, Jahanian R. 2016. Dietary mannan-oligosaccharides supplementation could affect performance, immunocompetence, serum lipid metabolites, intestinal bacterial populations, and ileal nutrient digestibility in aged laying hens. *Anim Feed Sci Technol*., **213**:81–89.

Gibiino G, Lopetuso LR, Scaldaferri F, Rizzatti G, Binda C, Gasbarrini A. 2018. Exploring Bacteroidetes: metabolic key points and immunological tricks of our gut commensals. *Dig Liver Dis*., **50(7)**:635–639.

Gibson GR, Hutkins R, Sanders ME, Prescott SL, Reimer RA, Salminen SJ, Scott K, Stanton C, Swanson KS, Cani PD, *et al.* 2017. Expert consensus document: The International Scientific Association for Probiotics and Prebiotics (ISAPP) consensus statement on the definition and scope of prebiotics. *Nat Rev Gastroenterol Hepatol*., **14(8)**:491–502.

Gillis CC, Hughes ER, Hooper L V, Santos RL, Correspondence SEW. 2018. Dysbiosis-associated change in host metabolism generates lactate to support *Salmonella* growth. *Cell Host Microbe*., **23**:54–64.

Gu Y, Wang C, Qin X, Zhou B, Liu X, Liu T, Xie R, Liu J, Wang B, Cao H. 2022. *Saccharomyces boulardii*, a yeast probiotic, inhibits gut motility through upregulating intestinal serotonin transporter and modulating gut microbiota. *Pharmacol Res*. **181(106291)**: 1-17.

Hasan N, Yang H. 2019. Factors affecting the composition of the gut microbiota, and its modulation. *PeerJ*., **7(8)**:1–31.

Hill C, Guarner F, Reid G, Gibson GR, Merenstein DJ, Pot B, Morelli L, Canani RB, Flint HJ, Salminen S, *et al.* 2014. Expert consensus document: The international scientific association for probiotics and prebiotics consensus statement on the scope and appropriate use of the term probiotic. *Nat Rev Gastroenterol Hepatol*., **11(8)**:506–514.

Hoving LR, Zande HJP Van Der, Pronk A, Guigas B, Dijk KW Van, Harmelen V Van. 2018. Dietary yeast-derived mannan oligosaccharides have immune-modulatory properties but do not improve high fat diet- induced obesity and glucose intolerance. *PLoS One*., **13(5)**:1–17.

Sambrook J, Russell DW. 2001. **Molecular Cloning : A Laboratory Manual**, third ed. Cold Spring Harbor Laboratory Press, New York.

Jacobson A, Lam L, Rajendram M, Tamburini F, Honeycutt J, Pham T, Van Treuren W, Pruss K, Stabler SR, Lugo K, *et al.* 2018. A gut commensal-produced metabolite mediates colonization resistance to *Salmonella* infection. *Cell Host Microbe*., **24(2)**:296–307.

Ji BW, Sheth RU, Dixit PD, Tchourine K, Vitkup D. 2020. Macroecological dynamics of gut microbiota. *Nat Microbiol*., **5(5)**:768–775.

Kirk MD, Angulo FJ, Havelaar AH, Black RE. 2017. Diarrhoeal disease in children due to contaminated food. *Bull World Health Organ*., **95(3)**:233–234.

Lata P, Kumari R, Sharma KB, Rangra S. 2022. In vitro evaluation of probiotic potential and enzymatic profiling of *Pichia kudriavzevii* Y33 isolated from traditional home-made mango pickle. *JEGB.*, **20(1)**: 1-10

Lee SM, Kim N, Park JH, Nam RH, Yoon K, Lee DH. 2018. Comparative analysis of ileal and cecal microbiota in aged rats. *J Cancer Prev*., **23(2)**:70–76.

Li D, Chen H, Mao B, Yang Q, Zhao J, Gu Z, Zhang H, Chen YQ, Chen W. 2017. Microbial biogeography and core microbiota of the rat digestive tract. *Sci Rep*., **8(1)**:1–16.

Lindstad LJ, Lo G, Leivers S, Lu Z, Michalak L, Pereira GV, Røhr ÅK, Martens EC, McKee LS, Louis P, Duncan SH, Westereng B, Pope PB, La Rosa SL. 2021. Human gut faecalibacterium prausnitzii deploys a highly efficient conserved system to cross-feed on β-mannan-derived oligosaccharides. *mBio.*, **12 (3)**: 1-18.

Manor O, Dai CL, Kornilov SA, Smith B, Price ND, Lovejoy JC, Gibbons SM, Magis AT. 2020. Health and disease markers correlate with gut microbiome composition across thousands of people. *Nat Commun.*, **11(1)**:1–12.

Martins FS, Dalmasso G, Arantes RME, Doye A, Lemichez E, Lagadec P, Imbert V, Peyron JF, Rampal P, Nicoli JR, *et al.* 2010. Interaction of *Saccharomyces boulardii* with *Salmonella enterica* serovar Typhimurium protects mice and modifies T84 cell response to the infection. *PLoS One*., **5(1)**:1–12.

Matsuo Y, Komiya S, Yasumizu Y, Yasuoka Y, Mizushima K, Takagi T, Kryukov K, Fukuda A, Morimoto Y, Naito Y, *et al.* 2021. Full-length 16S rRNA gene amplicon analysis of human gut microbiota using MinION™ nanopore sequencing confers species-level resolution. *BMC Microbiol*., **21(1)**:1–13.

Micciche AC, Foley SL, Pavlidis HO, McIntyre DR, Ricke SC. 2018. A review of prebiotics against *Salmonella* in poultry: Current and future potential for microbiome research applications. *Front Vet Sci*., **5(191)**:1–11.

Morgan XC, Tickle TL, Sokol H, Gevers D, Devaney KL, Ward D V., Reyes JA, Shah SA, LeLeiko N, Snapper SB, *et al.* 2012. Dysfunction of the intestinal microbiome in inflammatory bowel disease and treatment. *Genome Biol*., **13(9)**:1–18.

Rahmadhani N, Astuti RI, Meryandini A. 2022. Ethanol productivity of ethanol-tolerant mutant strain *Pichia kudriavzevii* R-T3 in monoculture and co-culture fermentation with *Saccharomyces cerevisiae*. *Hayati J Biosci*., **29(4)**:435–444.

Rinninella E, Raoul P, Cintoni M, Franceschi F, Miggiano GAD, Gasbarrini A, Mele MC. 2019. What is the healthy gut microbiota composition? A changing ecosystem across age, environment, diet, and diseases. *Microorganisms*., **7(14)**:1–22.

Rolim FRL, Oliveira CJB, de Freitas Neto OC, Dos Santos KMO, Guerra GCB, Rodrigues R V., de Assis POA, Araújo DF d. S, de Carvalho VAG, Lemos MLP, *et al.* 2021. Microbiological, immunological, and histological changes in the gut of *Salmonella* Enteritidis-challenged rats fed goat cheese containing *Lactobacillus rhamnosus* EM1107. *J Dairy Sci*., **104(1)**:179–197.

Roobab U, Batool Z, Manzoor MF, Shabbir MA, Khan MR, Aadil RM. 2020. Sources, formulations, advanced delivery and health benefits of probiotics. *Curr Opin Food Sci*., **32**:17–28.

Seong CN, Kang JW, Lee JH, Seo SY, Woo JJ, Park C, Bae KS, Kim MS. 2018. Taxonomic hierarchy of the phylum Firmicutes and novel Firmicutes species originated from various environments in Korea. *J Microbiol*., **56(1)**:1–10.

Setyawardani T, Rahayu WP, Palupi NS, Sumarmono. 2017. The potential of *Lactobacillus rhamnosus* and *Lactobacillus plantarum* isolated from goat's milk in inhibiting *Salmonella* Typhimurium ATCC 14028 infections in rats. *Int Food Res J*., **24(6)**:2625–2631.

Sheets TR, Wickware CL, Snyder AM, Weimer SL, Johnson TA. 2022. Ileal and cecal microbiota response to *Salmonella* Typhimurium challenge in conventional and slow-growing broilers. *Front Physiol*., **13(971255)**:1–13.

Shin NR, Whon TW, Bae JW. 2015. Proteobacteria: Microbial signature of dysbiosis in gut microbiota. *Trends Biotechnol*., **33(9)**:496–503.

Sivixay S, Bai G, Tsuruta T, Nishino N. 2021. Cecum microbiota in rats fed soy, milk, meat, fish, and egg proteins with prebiotic oligosaccharides. *AIMS Microbiol*., **7(1)**:1–12.

Stackebrandt E. 2014. **The Prokaryotes: Firmicutes and Tenericutes**, fourth ed. Springer-Verlag Berlin Heidelberg, New York.

Stojanov S, Berlec A, Štrukelj B. 2020. The influence of probiotics on the Firmicutes/Bacteroidetes ratio in the treatment of obesity and inflammatory bowel disease. *Microorganisms*., **8(11)**:1–16.

Takahashi S, Tomita J, Nishioka K, Hisada T, Nishijima M. 2014. Development of a prokaryotic universal primer for simultaneous analysis of bacteria and archaea using next-generation sequencing. *PLoS One*., **9(8)**:1–9.

Vacca M, Celano G, Calabrese FM, Portincasa P, Gobbetti M, De Angelis M. 2020. The controversial role of human gut Lachnospiraceae. *Microorganisms*., **8(573)**:1–25.

Wang H, Zhang X, Wang S, Li H, Lu Z, Shi J, Xu Z. 2018. Mannan-oligosaccharide modulates the obesity and gut micricrobiota in high-fat diet-fed mice. *Food Funct*., **9(7)**:3916–3929.

Wulan R, Astuti RI, Rukayadi Y, Meryandini A. 2021. Evaluation of indigenous *Pichia kudriavzevii* from cocoa fermentation for a probiotic candidate. *Biodiversitas*., **22(3)**:1317–1325.

Yu L, Zhao XK, Cheng ML, Yang GZ, Wang B, Liu HJ, Hu YX, Zhu LL, Zhang S, Xiao ZW, *et al.* 2017. *Saccharomyces boulardii* administration changes gut microbiota and attenuates D-Galactosamine-induced liver injury. *Sci Rep*., **7(1)**:1–7.

Zeiner S, Dwyer B, Clegg S. 2012. FimA, FimF, and FimH are necessary for assembly of type 1 fimbriae on *Salmonella enterica* serovar Typhimurium. *Infect Immun*., **80(9)**:3289–3296.

JJBS

Volume 18, Number 2,June 2025
ISSN 1995-6673
Pages 243 – 252
https://doi.org/10.54319/jjbs/180205

Jordan Journal of Biological Sciences

Phytochemical and Bioactivity Variations in *Calobota saharae*: Flavonoid Extraction, Antioxidant, and Anti-inflammatory Assessment

Atef CHOUIKH[1,2], Anis BEN ALI[1,3,*], Aida BOUSBIA BRAHIM[1,2]

[1]*Laboratory of Biology, Environment and Health. El Oued University, PO Box 789, 39000 Algeria;* [2]*Biology Department, Faculty of Life and Natural Science, El Oued University, PO Box 789, 39000 Algeria;* [3]*Cellular and MolecularBiology Department, Faculty of Life and Natural Science, El Oued University, PO Box 789, 39000 Algeria*

Received: April 19, 2024; Revised: October 7, 2024; Accepted: October 17, 2024

Abstract

This comprehensive study investigates the physiological growth stage-dependent variations in the chemical composition and bioactivity of extracts from *Calobota saharae* plants. The research explores the changes in carbohydrate, protein, and lipid content across different growth stages and correlates them with the qualitative phytochemical screening results. Flavonoid extracts were obtained and characterized using Fourier-Transform Infrared (FTIR) spectroscopy, highlighting spectral similarities and differences. Additionally, the antioxidant activity was assessed through DPPH free radical scavenging and erythrocyte hemolysis tests, revealing stage-specific efficacy. Furthermore, the anti-inflammatory potential of the extracts was evaluated, showing significant variations across growth stages. Correlation analysis was conducted to elucidate relationships between variables. Overall, this study provides insights into the dynamic chemical profile and bioactivity of *C. saharae* extracts throughout its growth stages, offering valuable implications for further research and potential applications in pharmaceutical and nutraceutical industries.

Keywords: Anti-inflammatory potential, Antioxidant activity, *Calobota saharae*, Flavonoid extracts, Physiological growth stages, Phytochemical screening.

1. Introduction

Plants play a pivotal role in traditional medicine and modern drug discovery due to their diverse range of bioactive compounds (Mustafa *et al*., 2017). Among these, the *Calobota saharae*, a species native to arid regions (Chouikh *et al*., 2018), has attracted considerable interest for its potential pharmacological applications. Understanding the chemical composition and bioactivity of *C. saharae* extracts across different physiological growth stages is essential for effectively utilizing its therapeutic potential effectively. This study aims to examine how variations in growth stages impact the chemical profile and bioactivity of *C. saharae* extracts.

The physiological growth stages of plants affect their metabolic activities, leading to fluctuations in nutrient content and secondary metabolite production (Li *et al*., 2020). Carbohydrates, proteins, and lipids serve as fundamental components of plant tissues (Ofoedum *et al*., 2024), while secondary metabolites such as flavonoids, alkaloids, saponins, and tannins contribute to their pharmacological properties (Kabera *et al*., 2014). By analyzing the variations in these constituents across growth stages, we gain insight into the dynamic nature of plant biochemistry and its implications for medicinal use.

Flavonoids, a class of polyphenolic compounds abundant in *C. saharae*, are well-known for their antioxidant, anti-inflammatory, and other health-promoting properties (Sun and Shahrajabian, 2023). Fourier-Transform Infrared (FTIR) spectroscopy provides a valuable method for characterizing the chemical structure of flavonoid extracts (Noh *et al*., 2017) and tracking spectral changes linked to different growth stages. Additionally, evaluating antioxidant activity through the DPPH free radical scavenging assay and erythrocyte hemolysis test offers key insights into the potential health benefits of *C. saharae* extracts.

Understanding the anti-inflammatory potential of C. saharae extracts is particularly important given the prevalence of inflammatory disorders. By assessing their effectiveness in inhibiting inflammation, we can evaluate their therapeutic relevance and pinpoint the optimal growth stages for extract preparation. Moreover, correlation analysis enables the exploration of relationships between chemical composition, bioactivity, and growth stages, providing insights into underlying mechanisms and guiding future research directions.

This study integrates plant physiology, chemistry, and pharmacology, offering a comprehensive understanding of the chemical composition and bioactivity of *C. saharae* extracts across different growth stages. These findings are vital for maximizing the therapeutic potential of this species and advancing drug discovery efforts in natural product-based medicine.

* Corresponding author. e-mail: benali-anis@univ-eloued.dz.

2. Materials and Methods

2.1. Plant material

The *C. saharae* plant was harvested at four distinct growth stages: in March, during the initial vegetative and flowering stages; in June, during the fruiting stage; and in September, at the second vegetative stage. These harvests were carried out in the Ghamra region of El Oued State, located at coordinates 33°32′0″N 6°47′0″E. After harvesting, the aerial parts of the plant were subjected to a controlled drying process under ambient temperatures, shielded from light and moisture. Once completely dried, the plant material was milled into a fine powder. This powder was then stored in glass containers, protected from light and heat, until further use.

2.2. Estimated nutritional value

In this experiment, each sample comprised 1 gram of plant material, which was combined with 5 mL of trichloroacetic acid (TCA) and subjected to mixing on a magnetic shaking device for 5 minutes. Subsequently, the mixture underwent centrifugal separation at 3000 revolutions per minute (rpm) for 10 minutes, yielding a supernatant for carbohydrate quantification. The resultant deposit 1 underwent an additional treatment with 2 mL of ether/chloroform (V/V) followed by a second centrifugal separation at 3000 rpm for 10 minutes. The second supernatant was collected to assess lipid content, while the second deposit was treated with 2.5 mL of a 0.1 M solution of sodium hydroxide (NaOH) to determine protein content (Chouikh *et al*., 2020).

2.2.1. Carbohydrate estimation

In this method, a solution containing 5% phenol and concentrated sulfurous acid was used, with absorbance measurements recorded at a wavelength of 490 nm. Glucose was utilized as the reference standard, and the carbohydrate content was reported in milligrams per gram of plant material (Chouikh *et al*., 2024b).

2.2.2. Protein estimation

The protein content of plant material was determined utilizing the Folin-Ciocalteu assay (Gurugubelli et al., 2023). This method involved the preparation of a reaction mixture containing Folin-Ciocalteau reagent (in V/V ratio), 0.1 M NaOH, 0.5% $CuSO_4$, and 0.1% $KNaC_4H_4.O_64H_2O$. Bovine Serum Albumin (BSA) was used as the reference standard for quantification. Absorbance measurements were conducted at 750 nm wavelength using a UV spectrophotometer. The obtained absorbance values were then correlated with known concentrations of BSA to determine the protein content in milligrams per gram of the plant material.

2.2.3. Lipid estimation

The analytical procedure employed Sulfophosphovanillinic reagent in conjunction with concentrated sulfurous acid (Chouikh *et al*., 2024a), with subsequent incubation of reaction tubes in a water bath set at 100 °C. Absorbance measurements were conducted at a wavelength of λ= 530 nm, with Soy serving as the reference standard. Lipid content results were quantified in milligrams per gram of plant material.

2.3. Qualitative phytochemical screening

A qualitative phytochemical analysis was carried out on *C. saharae* plant extracts at different growth stages to identify the presence of various secondary metabolites. Standardized procedures were followed, including detection of flavonoids and tannins using ferric chloride ($FeCl_3$) drops, anthocyanins with hydrochloric acid (HCl) and ammonia (NH_3), alkaloids with Wagner's reagent, and saponins through a shaking test for foam formation. Sterols and triterpenes were analyzed using a combination of acetic anhydride, chloroform, and sulfuric acid (Ben Ali *et a*l., 2024; Noudogbessi *et al*., 2013; Sharma *et al*., 2010).

2.4. The Flavonoid Extraction Procedure (Ethyl acetate phase)

Flavonoids were extracted from 20 grams of dried and ground plant material using ethyl acetate fractionation. The plant material was soaked in 100 mL of methanol for 24 hours in the dark at room temperature. After filtration, the solvent was evaporated using a rotary evaporator. The resulting extract was subjected to a second extraction stage (liquid-liquid phase separation) where it was mixed with equal volumes of hot distilled water (50°C) and ethyl acetate (V/V = 120 mL). The solution was shaken well and allowed to settle for approximately 2 hours. The mixture consisting of two aqueous and organic phases was separated. The aqueous phase was discarded, while the organic phase was dried in a rotary evaporator at 50°C. Thus, the flavonoid extract, the ethyl acetate phase, was obtained (Kanoun, 2011).

2.5. Fourier-Transform Infrared (FTIR) Characterization

The extracts were analyzed using Fourier-Transform Infrared (FTIR) spectroscopy with a Shimadzu-00463 spectrophotometer to characterize their molecular composition and structural features. The FTIR analysis was conducted with a high resolution of 4 cm^{-1} to ensure precise spectral details. To enhance the signal-to-noise ratio and obtain reliable spectral data, 64 coadded scans were accumulated. The examined spectral range spanned from 4000 to 650 cm^{-1}, encompassing the mid-infrared region where characteristic vibrational bands of various functional groups and molecular bonds are observed.

2.6. Estimation of antioxidant activity

2.6.1. Free radical DPPH scavenging activity

The assessment of the extracts' $DPPH^{\bullet}$ (2,2-diphenyl-1-picrylhydrazyl) scavenging activity followed the protocol outlined by (Chouikh and Alia, 2021). Briefly, varying concentrations of each extract (1 mL) were mixed with an equal volume of DPPH solution (10^{-4} mol) dissolved in methanol. Following a 15-minute incubation at room temperature, the absorbance was recorded at 517 nm. The inhibition activity was determined using the following formula (Faridi *et al*., 2023):

$$Inhibition(\%) = \left[\left(Absorbance_{Control} - Absorbance_{Sample}\right)/Absorbance_{Sample}\right] \times 100$$

The IC_{50} value, representing the concentration at which 50% of the free radicals were scavenged by the extract, was determined using linear regression analysis on the concentration-inhibition percentage curve. A lower IC_{50} value indicates a higher antioxidant capacity (Chouia *et al*., 2018).

2.6.2. Erythrocyte hemolysis test

This assay is utilized to evaluate the protective effects of plant extracts on erythrocyte blood cells against membrane damage induced by oxidative stress and free radicals. The assessment involves measuring the proportion of erythrocytes that have undergone lysis (Dolci and Panteghini, 2014).

To perform the assay, 40 µL of human erythrocytes are mixed with 2 mL of the plant extract and incubated for 5 minutes at 37 °C. Following this, 40 µL of hydrogen peroxide (30 mM), 40 µL of ferric chloride (80 mM), and 40 µL of ascorbic acid solution (50 mM) are added sequentially. After incubating for 1 hour at 37 °C, the mixture is centrifuged at 700 rpm for 10 minutes. The absorbance of the supernatant is then recorded at 540 nm (Ben Ali and Chouikh, 2024).

The percentage of hemolysis is determined using the following formula:

$$Hemolysis\% = \left(Absorbance_{Control}/Absorbance_{Sample}\right) \times 100$$

2.7. Estimation of anti-inflammatory activity

The albumin denaturation model was employed to assess the in vitro anti-inflammatory properties of Flavonoid extracts derived from *C. saharae*. Specifically, 1 ml of the extract at various concentrations was combined with 1 ml of human albumin (5%). Following a 15-minute incubation period at 27°C, the mixtures were subjected to further incubation in a water bath set to 70°C for 10 minutes. Subsequently, after cooling to room temperature, the absorbance of the solutions was measured at 660 nm. Diclofenac sodium served as the standard reference. The findings were quantified as milligrams of diclofenac sodium equivalent per milligram of extract to facilitate comparison (Ben Ali et al, 2023).

2.8. Statistical analysis

The results were analyzed using Microsoft Office Excel 2007. Mean values were calculated along with the standard error of the mean (SEM), denoted as ±, with a sample size of n = 3. To determine significant differences in the results, a one-way analysis of variance (ANOVA) was conducted at the significance levels of 0.001, 0.01, and 0.05.

3. Results

With the aim of understanding the effect of changing physiological conditions during the stages of plant growth on flavonoids, this study focused on tracking the chemical composition of the *C. saharae* plant in the laboratory throughout its various growth stages. The results are presented as follows:

3.1. Estimated nutritional value

3.1.1. Carbohydrate estimation

The carbohydrate content of the plant declines gradually as it matures physiologically. The highest carbohydrate content, estimated at 24.41±0.08 mg/g of plant material, occurs during the first vegetative stage. Subsequently, during the flowering stage, the carbohydrate content decreases to 21.23±0.05 mg/g of plant material, and further declines to 16.95±0.25 mg/g during the fruiting stage. The lowest carbohydrate content, 13.34±0.04 mg/g, is observed during the second vegetative stage. Statistical analysis reveals highly significant differences at a significance level of α=0.001 (Figure 1).

3.1.2. Protein estimation

During various stages of plant growth, significant variations in protein content were observed. The highest amount of protein was recorded during the flowering stage, with an estimated value of 12.10±0.14 mg/g of plant material. Conversely, the second vegetative stage exhibited the lowest protein content, with a value of 2.37±0.05 mg/g. The protein content during the first vegetative stage and fruiting stage was estimated at 8.57±0.31 mg/g and 10.53±0.09 mg/g, respectively. The results of the analysis of variance indicate significant differences in protein content across the stages of plant growth, with a significance level of α = 0.001.

3.1.3. Lipid estimation

The analysis revealed minor differences in fat content across the various stages of *C. saharae* growth. Specifically, during the first vegetative, flowering, and fruiting stages, the fat content was measured at 0.97±0.07, 0.77±0.01, and 0.88±0.04 mg/g of the plant sample, respectively. The lowest fat content was observed during the second vegetative stage, with a value of 0.12±0.01 mg/g of the plant sample. Statistical analysis demonstrated highly significant differences at a significance level of α = 0.001.

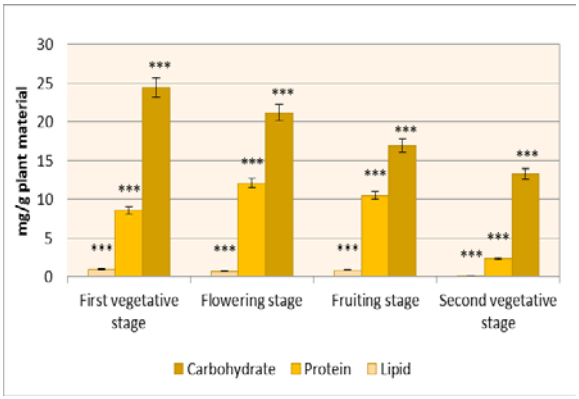

Figure 1: Nutritive values of *C. saharae* plant.

***: Statistically significant differences at the confidence level (α=0.001).

3.2. Qualitative phytochemical screening

Chemical detection of secondary metabolites was carried out based on the dry plant matter of the samples, and the results obtained are represented in Table (1).

Table 1. Phytochemical screening results of secondary metabolites.

Extract stage / Metabolites	*First vegetative*	*floral*	*Fruiting*	*Second vegetative*
flavonoids	+++	+++	+++	+++
Anthocyanin	-	-	-	-
Alkaloids	+++	+	++	++
Saponosides	+++	+++	+++	+++
Sterols and terpenes	-	+	-	+
Tannins	+++ Gallic	+++ Catechol	+++ Catechol	+++ Gallic

+++: The presence of the active ingredient in large quantities. ++: medium amount. +: a small amount. -: Absence of the active ingredient.

From the results obtained, it is clear that the *C. saharea* plant is rich in bioactive compounds, the most notable of which are flavonoids, alkaloids, saponins, and tannins. The abundance of these compounds varies depending on the physiological stage of the plant, while the absence of anthocyanin compounds was evident across all growth stages. Sterols and terpenes were absent during both the first and second vegetative stages but were present in the flowering and second vegetative stages.

3.3. Yield of flavonoid extract (ethyl acetate phase)

Flavonoid extracts were obtained from various physiological growth stages of *C. saharae* using the organic solvent ethyl acetate. The results, shown in Figure 2, indicate a significant impact of growth stage on extraction yield. The highest yield, 1.4%, was observed in the sample collected during the flowering stage, while the lowest yield, 0.74%, was noted in the extract from the first vegetative stage. Extracts from the fruiting and second vegetative stages exhibited similar yields, estimated at 1.18% and 1.3%, respectively.

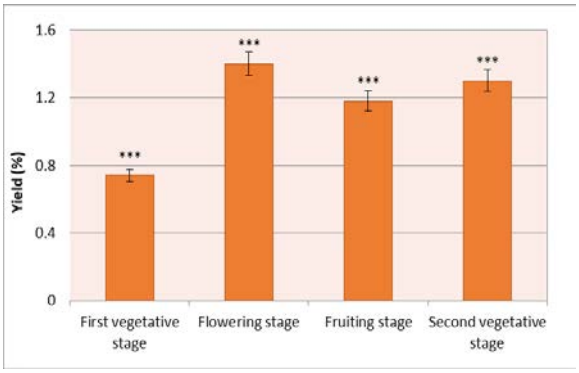

Figure 2: Yield results of flavonoid extracts for different growth stages of *C. saharae.*

***: Statistically significant differences at the confidence level (α=0.001).

3.4. Fourier-Transform Infrared (FTIR) Characterization

Flavonoid extracts from various physiological growth stages of C. saharae were analyzed spectroscopically. To facilitate spectral interpretation and monitor spectral changes, the spectrum was divided into two regions. The first region encompasses wavenumbers above 1600 cm^{-1}, typically featuring a limited number of peaks. Within this range, a broad absorption band was observed spanning 3700-3100 cm^{-1}, indicative of O-H bond presence. Additionally, two prominent absorption bands were noted between 2800 and 3000 cm^{-1}, corresponding to the C-H group, while spectral broadening at 1700-1750 cm^{-1} signifies the C=O functional group.

Conversely, the second spectral region, below 1600 cm^{-1}, is characterized by numerous peaks of varying intensities, many of which are challenging to identify. The bending observed in the 1200-1600 cm^{-1} range signifies the presence of aromatic rings in the studied extracts. The region from 1300-600 cm^{-1} is highly intricate and is known as the "fingerprint region," with the absorption observed in the spectral range of 700-900 cm^{-1} corresponding to the C-H functional group.

Analysis of the spectral curves revealed striking similarities among extracts from all physiological growth stages of the *C. saharae* plant, with only minor differences observed in transmittance intensity and the fingerprint region (Figure 3).

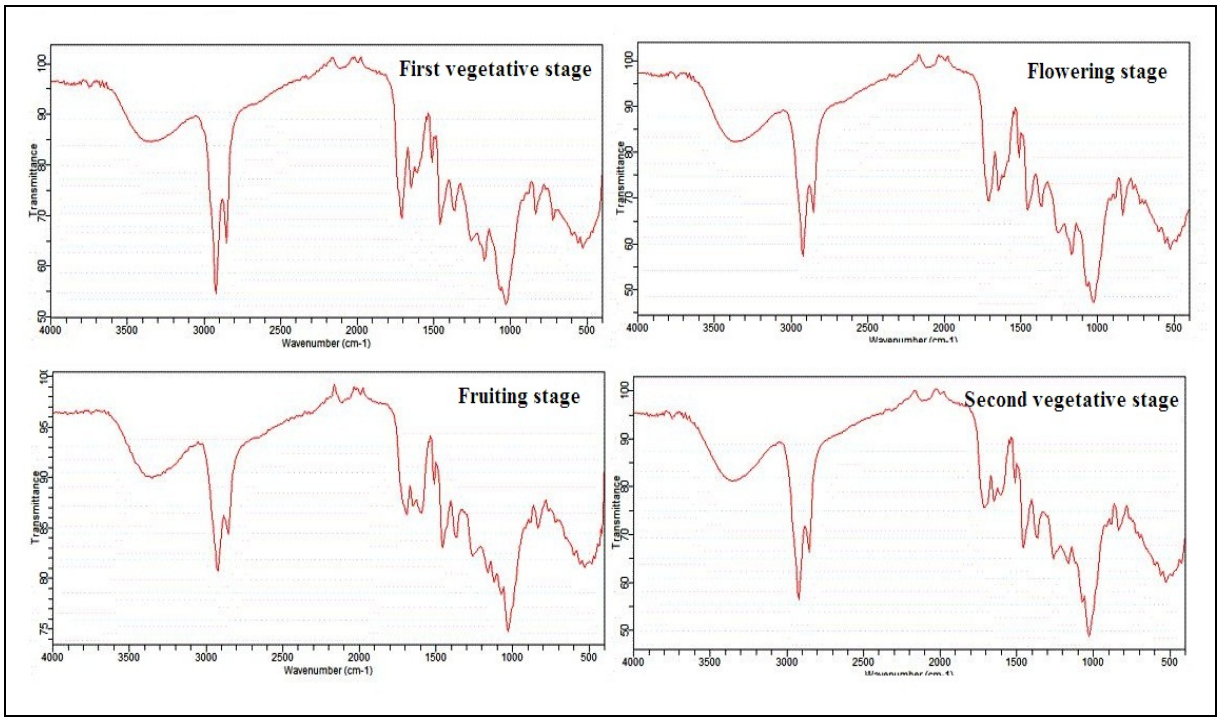

Figure 3: FTIR spectrum of extracts of different growth stages of *C. saharae*.

3.5. Estimation of antioxidant activity

3.5.1. Free radical DPPH scavenging activity

In the DPPH assay, noticeable discrepancies were observed in the IC_{50} values of *C. saharae* plant extracts. Statistical analysis using ANOVA revealed significant differences at a significance level of $\alpha = 0.001$. Notably, the extract obtained during the fruiting stage exhibited the highest efficacy in free radical scavenging, recording an IC_{50} value of 0.138±0.026 mg/mL. The IC_{50} values for the extracts obtained during the first and second vegetative stages, as well as the flowering stage, were recorded at 0.177 ± 0.031 mg/mL, 0.187 ± 0.036 mg/mL, and 0.213 ± 0.047 mg/mL, respectively (Figure 4).

Furthermore, the efficacy of these extracts was considerably lower compared to ascorbic acid, which demonstrated a significantly lower IC_{50} value of 0.005±0.001 mg/mL.

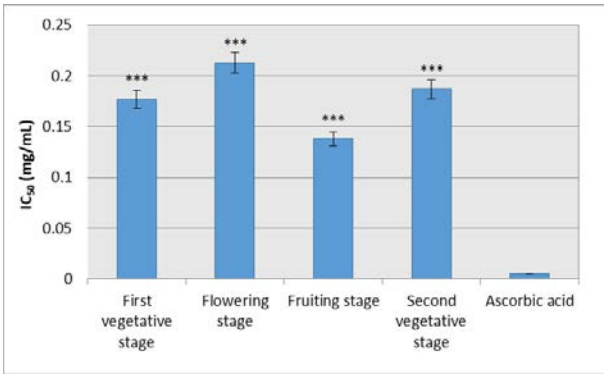

Figure 4. Value of IC_{50} of DPPH free radical scavenging test of extracts of different growth stages of *C. saharae* and Ascorbic acid.

***: Statistically significant differences at the confidence level (α=0.001) when compared to ascorbic acid.

3.5.2. Erythrocyte hemolysis test

The results indicate that the protective capacity of different plant extracts on red blood cells is relatively similar ($\alpha = 0.05$) at a concentration of 1 mg/mL. Table 2 shows that the first vegetative stage extract exhibited the lowest hemolysis rate, measured at 41.72±2.2%, followed by the second vegetative stage extract with a hemolysis rate of 48.96±1.9%, and then the fruiting stage extract with a hemolysis rate of 51.44±1.7%. Conversely, the flowering stage extract showed the highest hemolysis rate at 62.2±2.1%. These results indicate that the first vegetative stage extract demonstrates superior efficacy in protecting red blood cells compared to the other extracts studied.

However, it is worth noting that despite this efficacy, it remains relatively weak compared to ascorbic acid, which exhibited the lowest hemolysis rate of 17.09±1.6% under the same conditions. Therefore, while plant extracts show promise in protecting red blood cells, their effectiveness appears modest when compared to the potent effect of ascorbic acid.

Table 2. Percentage of Hemolysis (C: 1 mg/ml) of of extracts of of different growth stages of *C. saharae* and Ascorbic acid.

Extract stage	*First vegetative*	*floral*	*Fruiting*	*Second vegetative*	*Ascorbic acid*
Hemolysis (with C: 1 mg/ml)	41.72±2.2%***	62.2±2.1%***	51.44±1.7%***	48.96±1.9%***	17.09±1.6%***

***: Statistically significant differences at the confidence level (α=0.001) when compared to ascorbic acid.

3.6. Estimation of anti-inflammatory activity

Statistical analysis revealed significant differences in the anti-inflammatory efficacy of plant extracts across different growth stages, with a significance level of α = 0.001. The highest inhibitory capacity was observed during the flowering stage, estimated at 5.63±0.81 mg Diclofenac E/mg extract. Following this, the first vegetative stage exhibited a value of 4.15±0.87 mg Diclofenac E/mg extract. In comparison, both the fruiting and second vegetative stages showed similar inhibitory capacities, estimated at 3.45±0.32 and 3.96±0.58 mg Diclofenac E/mg extract, respectively. When comparing the effectiveness of these extracts to the reference compound Diclofenac, it can be concluded that their anti-inflammatory activity is significantly high (Figure 5).

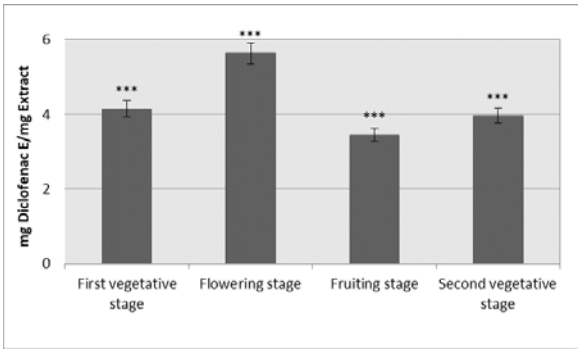

Figure 5. Estimation of anti-inflammatory activity of extracts of different growth stages of *C. saharae*.

***: Statistically significant differences at the confidence level (α=0.001).

3.7. Statistical study

To evaluate the strength and direction of the relationships between the studied variables, a correlation analysis was conducted using the Pearson Linear Correlation Coefficient test. This analysis produced correlation coefficient (R^2) values, which are presented in Table 3.

Table 3. Correlation coefficient (R^2) between the different variables studied.

Variable	Carbohydrate	Protein	Lipid	Yields	DPPH	Hemolysis	Anti-inflammatory
Carbohydrate	1						
Protein	0.627	1					
Lipid	0.685	0.883	1				
Yields	-0.606	0.001	-0.405	1			
DPPH	-0.234	0.122	0.438	-0.259	1		
Hemolysis	-0.812	-0.696	-0.929	0.708	-0.376	1	
Anti-inflammatory	0.428	0.428	0.027	0.394	-0.829	0.071	1

4. Discussion

Primary metabolic compounds such as carbohydrates, proteins, and fats play pivotal roles in the growth and development of organisms, particularly plants (Ofoedum *et al*., 2024). Their concentrations fluctuate across different physiological growth stages, as demonstrated in studies on *C. saharae* plants, revealing significant differences ($p < 0.001$) (Liu *et al*., 2022), as evidenced by the study on *C. saharae* plants, with significant differences observed ($p<0.001$). Conversely, (Ammar *et al*., 2004) observed that the protein content in leguminous shrubs is less susceptible to seasonal variations compared to other species.

Carbohydrates, as products of photosynthesis, are fundamental for synthesizing cellular compounds, providing energy, and aiding plant defense against pathogens (Bolton, 2009). The decline in carbohydrate content with plant maturation is influenced by factors such as maturity stage, utilized plant parts, and physiological condition. The initial vegetative stage typically exhibits the highest carbohydrate content due to increased development of young branches, which are crucial for the formation of structural components like semi-cellulose and pectin (Nour El-Din and Ahmed, 2004). Sugars also collaborate with proteins in glycoprotein formation, contributing to membrane stabilization and various cellular functions (Nguema-Ona *et al*., 2014).

This association elucidates the positive correlation ($R^2 = 0.617$) between carbohydrates and proteins. Conversely, the negative correlation ($R^2 = -0.606$) between carbohydrates and yield percentage is attributed to their structural relationship. Carbohydrates act as energy substrates for flavonoid biosynthesis; however, their content decreases as plants progress to allocate resources for organic compound synthesis (Cheynier *et al*., 2013), meeting the demands essential for growth and sustainability.

Crude protein serves as a key indicator of the nutritional quality of desert plants for ruminants (Nour El-Din and Ahmed, 2004), with legumes particularly valued for their rich protein and nutrient content (Semba *et al*., 2021). The protein levels in *C. saharae* plants fluctuate throughout their biological life cycle, influenced by factors

such as climate, harvest season, and physiological stage. Research indicates that protein content peaks during the early vegetative and flowering stages due to increased photosynthesis and nutrient absorption (Zhang *et al*., 2009). The flowering stage is characterized by heightened metabolic activity, typical of leguminous plants, which maximizes protein production. In the fruiting stages, protein is stored for seed development and enzyme activation, while declines in later vegetative stages may result from reduced biological activity or tissue aging (Ammar *et al*., 2004). Genetic, environmental, and soil factors contribute to the overall variation in protein content.

Fats serve as essential raw materials for synthesizing various compounds, including certain vitamins and hormones, and they act as solvents for fat-soluble vitamins (Ravisankar *et al*., 2015). In the *C. saharae* plant, fats are among the least abundant primary metabolites, with slight variations observed across different growth stages, likely reflecting their utilization in physiological functions such as cell membrane formation and energy storage in seeds. Fats can combine with sugars to form glycolipids, which are important for membrane function (Wiegandt, 2011). The correlation between fats and carbohydrates (R^2 = 0.685) suggests their interconnected metabolic roles, while the strong correlation between fats and proteins (R^2 = 0.883) highlights their structural and functional significance, particularly in cell membranes. During the second vegetative phase, fat content decreases significantly, likely due to lipid recycling during senescence an adaptive mechanism in response to environmental stress that aims to conserve resources for survival and subsequent vegetative cycles (Yang and Ohlrogge, 2009).

Chemical analysis of *C. saharae* plant samples revealed the synthesis of various secondary metabolites, including flavonoids, alkaloids, saponins, sterols, triterpenes, and tannins, while anthocyanins were absent. These findings align with previous studies utilizing aqueous extracts of the same plant (Guettaf *et al*., 2016). The presence of these compounds supports the plant's physiological growth, adaptation to environmental stresses, and overall resilience (Nour El-Din and Ahmed, 2004). Factors influencing the chemical diversity within a single plant include the plant part used, growth stage, genetic composition, environmental conditions, soil composition, and time of collection (Chouikh *et al*., 2015).

The fluctuation in the presence of these compounds throughout the plant's life cycle may reflect their vital functions and the plant's adaptive strategies in response to varying needs. Differences in localization and storage within the plant may also contribute to their appearance or absence at different stages (Nour El-Din and Ahmed, 2004). Moreover, variations in extraction methods or reagents used could influence the detection of certain compounds (Chatoui *et al*., 2016).

Flavonoid extracts from C. saharae plant samples were obtained using ethyl acetate, a commonly used solvent for flavonoid extraction (Boumaza and Boukaabache, 2015). The percentage yield of these extracts varied slightly across different physiological growth stages, despite consistent laboratory procedures. This fluctuation can be attributed to several factors, as flavonoid levels tend to increase in aerial parts during the development of new organs such as flowers, leaves, fruits, and seeds (Michalak, 2006). Additionally, the nature of chemical compounds plays a crucial role, with changes in the complexity and length of carbon chains affecting extraction efficiency (Chouikh *et al*., 2018). Furthermore, climatic conditions (Ksouri *et al*., 2008), lead to variations in environmental factors during plant growth stages, impacting flavonoid production. Lastly, the activity and condition of plants at different age levels during the study period can significantly influence flavonoid yields (Chouikh *et al*., 2018). These interconnected factors contribute to the observed fluctuations in flavonoid extraction yields from *C. saharae* plants across various growth stages.

The study revealed that the highest percentage yield was observed during the flowering stage, consistent with previous findings (Chouikh *et al*., 2018; Meriane *et al*., 2014). This increase in yield during flowering may be attributed to factors such as the relationship between flavonoids and pollinators as well as the coloration of flowers due to flavonoids (Chouikh *et al*., 2015; Ketaren Bunga Raya *et al*., 2015).

Conversely, the lowest percentage yield was observed during the first vegetative stage, which differs from some previous studies that reported the lowest yield during the fruiting stage (Chouia *et al*., 2018). This discrepancy may be attributed to the chemical nature of active compounds present in the plant during specific growth stages, the solubility characteristics of the solvent used, variations in harvesting periods and geographical regions, as well as differences in extraction methods and conditions (Abdelmadjide *et al*., 2020; Chouia *et al*., 2018; Feng *et al*., 2017).

Based on Fourier transform infrared (FTIR) spectroscopy, flavonoid extracts were found to contain hydroxyl (OH) groups and lacked aldehyde and methoxy functional groups, indicating that they are non-sugar, polyhydroxy flavonoids. These compounds, possibly belonging to the categories of flavonols, flavanones, or isoflavones (Meriane *et al*., 2014), possess hydroxyl groups and a phenolic ring, making them significant for biological purposes such as free radical inhibition, anti-inflammatory action against bacteria and viruses, and potential anti-cancer properties (Rahman *et al*., 2021)

In the DPPH assay, the results demonstrate a diminished free radical scavenging capacity of the investigated extracts compared to the reference compound, ascorbic acid, as observed in this study, corroborating the findings of (Bouchouka *et al*., 2012). This disparity may be explained by the limited presence of flavonoids in these extracts, which typically contain free radical scavenging entities. The literature suggests that strong antioxidant efficacy stems from an abundance of hydroxyl (OH) groups capable of interacting with free radicals (Chouikh *et al*., 2018).

The results further reveal that the extract obtained during the fruiting stage exhibits the most potent anti-DPPH activity. These findings align with those reported by Bouchouka et al. (2012) in their investigation of the raw methanolic extract from the same plant. This enhanced activity could be attributed to the accumulation of certain active constituents as reserves within the fruits (Chouikh *et al*., 2015), with compounds formed at this stage potentially possessing superior scavenging capabilities. Numerous researchers posit a substantial correlation between the

chemical structure of flavonoids and their free radical scavenging activity. Interestingly, the activity is notably diminished during the flowering stage, which contradicts the findings of Chouikh *et al.* (2018) and Meriana *et al*. (2014). This discrepancy may arise from variations in solvent type and its effectiveness in extracting active compounds, impacting their concentration in the extract or the nature of their chemical structures conducive to DPPH scavenging, such as the presence of hydroxyl groups, double bonds between carbon atoms, and heterogeneous oxo groups (Chouikh *et al*., 2018).

The protective effect of plant extracts against oxidative damage to red blood cells caused by two oxidizing agents, $FeCl_3$ and H_2O_2, was assessed. These radicals initiate lipid and protein oxidation reactions upon attacking red blood cells, leading to membrane damage, eventual cell lysis, and hemoglobin release (Abirami *et al*., 2014; Supriya *et al*., 2013). The observed capacity of the studied plant extracts to safeguard red blood cells can be elucidated through two hypotheses: firstly, flavonoids within the extracts may interact with free radicals, thereby neutralizing them (Nabavi *et al*., 2013). Alternatively, the flavonoids might interact with cellular membrane components, particularly lipids and proteins, shielding them from oxidative damage, as evidenced by the protective effects observed across all extracts (Chaudhuri et al., 2007). Moreover, a concentration-dependent increase in extract concentration correlates with greater red blood cell protection and decreased hemolysis, indicating a potential role of flavonoids in restoring and stabilizing oxidants through electron donation or proton modification (Ebrahimzadeh *et al*., 2014). Additionally, the observed inverse relationship (R^2= -0.929) between lipid degradation rate and flavonoid-lipid interactions, and the moderate relationship (R^2= -0.696) between protein degradation rate and flavonoid-protein interactions, further support the hypothesis of flavonoid-mediated protection against lipid peroxidation, thus reducing the degradation rate as flavonoid interaction with lipid and protein components increases (Khalili *et al*., 2014).

In contrast, the obtained results diverge from the findings of Chouikh *et al*. (2018) in their investigation of raw extracts derived from the same plant species, wherein the crude phenolic extract exhibited notable protective effects against red blood cell hemolysis. This discrepancy may stem from the distinct composition of compounds within the extracts. The crude extract contains phenols and tannins, which likely contributed to its protective efficacy by facilitating electron donation to H_2O_2, converting it into water (Ebrahimzadeh *et al*., 2014). Alternatively, the observed protection could be attributed to the abundance of compounds containing sugar radicals within the extract, which possess a strong membrane-blending capacity, a characteristic absent in the flavonoid extract under study. This was substantiated by the results of FTIR spectroscopy, which indicated the absence of aldehyde functional bonds.

The studied extracts exhibit promising anti-inflammatory activity, as evidenced by their ability to prevent protein denaturation by more than 20%, a hallmark of anti-inflammatory compounds (Williams *et al*., 2008). This activity is likely attributed to the presence of flavonoids containing numerous hydroxyl groups (OH), which facilitate the formation of hydrogen bonds with proteins, thus averting their denaturation.

Remarkably, the flowering stage extract demonstrated the highest inhibition capacity. This could be attributed to the elevated concentrations of non-saccharide flavonoids known for their potent anti-inflammatory properties. Alternatively, the unique nature of flavonoid compounds within this extract might enable interactions with proteins, notably albumin (Dufour *et al*., 2007). These findings align with those of Guettaf *et al*.(2016), underscoring the significant protein degradation inhibition capacity of the aqueous extract of *C. saharae*.

5. Conclusion

This study illuminates the intricate interplay between the physiological growth stages, chemical composition, and bioactivity of *C. saharae* extracts. Our investigation reveals pronounced fluctuations in nutrient content, secondary metabolite composition, and pharmacological efficacy throughout the plant's development. The decline in carbohydrate content with advancing growth stages underscores metabolic shifts, while the peak in protein content during the flowering stage signifies heightened biosynthetic activity. Flavonoid extracts, enriched with secondary metabolites, exhibit stage-specific variations in yield and composition, with the flowering stage yielding the highest flavonoid content. Analysis of FTIR spectra unveils structural insights into flavonoid extracts, crucial for quality assurance and standardization. Moreover, antioxidant assays demonstrate stage-dependent efficacy, with the fruiting stage displaying the highest radical scavenging capacity. The erythrocyte hemolysis test elucidates variable protective effects against oxidative stress across growth stages, hinting at potential health benefits. Additionally, the anti-inflammatory activity of *C. saharae* extracts underscores their therapeutic potential, with the flowering stage extract exhibiting the strongest inhibitory capacity. Correlation analysis elucidates intricate relationships between chemical constituents, bioactivity, and growth stages, offering insights into underlying mechanisms. Overall, our findings emphasize the significance of considering growth stage variability in pharmacological investigations and pave the way for harnessing the medicinal properties of *C. saharae* extracts for diverse therapeutic applications.

Conflict of interests

Authors declare that there is no conflict of interests.

Acknowledgement

The authors state that this study was conducted and funded by the Biology Department Laboratory at the Faculty of Natural and Life Sciences, El-Oued University, Algeria.

References

Abdelmadjide S, Mounir A, Atef C, Nadia Z and Néji B. 2020. Phytochemical study, antioxidant and antimicrobial activities of flavonoids and diethyl ether extracts from leaves and seeds of medicinal plant of Algerian flora: *Retama monosperma* (L.) Boiss. *Ponte Int Sci Res J*., **76(4)**.

Abirami A, Nagarani G and Siddhuraju P. 2014. In vitro antioxidant, anti-diabetic, cholinesterase and tyrosinase inhibitory potential of fresh juice from *Citrus hystrix* and *C. maxima* fruits. *Food Sci Hum Wellness.*, **3(1)**, 16-25. https://doi.org/10.1016/j.fshw.2014.02.001

Ammar H, López S, González J and Ranilla M. 2004. Seasonal variations in the chemical composition and in vitro digestibility of some Spanish leguminous shrub species. *Anim Feed Sci Technol*., **115(3-4)**, 327-340. https://doi.org/10.1016/j.anifeedsci.2004.03.003

Ben Ali A and Chouikh A. 2024. Bioactive Potential of Algerian *Citrullus colocynthis* Resin: Antioxidant & Anti-inflammatory Effects. *Not Sci Biol*. **16(3)**, 132-139. https://doi.org/0.15835/nsb16311782

Ben Ali A, Chouikh A and Haddad L. 2023. *Cyperus rotundus* tubers resin from Algeria: a promising source of natural antioxidants, anti-inflammatory, and photoprotective compounds. *Ovidius Univ Ann Chem*., **34(2)**, 132-139. https://doi.org/10.2478/auoc-2023-0017

Ben Ali A, Chouikh A and Haddad L. 2024. *Citrullus colocynthis* fruit resin and *Cyperus rotundus* tuber resin: Assessing their analgesic effects with hot plate and writhing tests. *Acta Period Technol*., **55(1)**, 1-12. https://doi.org/10.2298/APT2455001B

Bolton MD. 2009. Primary metabolism and plant defense—fuel for the fire. *Mol Plant Microbe Interact*., **22(5)**, 487-497. https://doi.org/10.1094/MPMI-22-5-0487

Bouchouka E, Djilani A and Bekkouche A. 2012. Antibacterial and antioxidant activities of three endemic plants from Algerian Sahara. *Acta Sci Pol Technol Aliment*., **11(1)**, 61-65.

Boumaza O and Boukaabache R. 2015. Recherche et détermination des métabolites secondaires de plantes issues de la famille des fabacées. 72.

Chatoui K, Talbaoui A, Aneb M, Bakri Y, Harhar H and Tabyaoui M. 2016. Phytochemical screening, antioxidant and antibacterial activity of *Lepidium sativum* seeds from Morocco. *J Mater Environ Sci*., **7(8)**, 2938-2946.

Chaudhuri S, Banerjee A, Basu K, Sengupta B and Sengupta PK. 2007. Interaction of flavonoids with red blood cell membrane lipids and proteins: antioxidant and antihemolytic effects. *Int J Biol Macromol.*, **41(1)**, 42-48. https://doi.org/10.1016/j.ijbiomac.2006.12.003

Cheynier V, Comte G, Davies KM, Lattanzio V and Martens S. 2013. Plant phenolics: recent advances on their biosynthesis, genetics, and ecophysiology. *Plant Physiol Biochem*., **72**, 1-20. https://doi.org/10.1016/j.plaphy.2013.05.009

Chouia A, Chouikh A, Alia F, Adjal EH, Chefrour A and Ait Kaki Y. 2018. Antibacterial activity and DPPH• radical scavenging of differents metabolites extracted from two plants: essential oil from (*Matricaria recutita* L.) and flavonoids from flowers and leaves of (*Hibiscus rosa-sinensis* L.). *An Univ Oradea Fasc Biol*., **25(1)**, 26-32

Chouikh A and Alia F.2021. Phytochemical properties, antibacterial and anti-free radical activities of the phenolic extracts of (Forssk) Webb. & Berthel. collected from Algeria Desert. *Ovidius Ovidius Univ Ann Chem*., **32(1)**, 33-39. https://doi.org/10.2478/auoc-2021-0005

Chouikh A, Alia F, Neffar S, Rebiai A, Adjal EH and Chefrour A. 2018. Evaluation of phenolic contents (quantitative and qualitative) and antioxidant activities in different physiological phases of *Genista saharae* COSS. & DUR. growing in the sahara of Algeria. *An Univ Oradea Fasc Biol*., **25(2)**.

Chouikh A, Ben Ali A, Bousbia Brahim A, Bekkouche A and Seghaier S. 2024. Phytochemical analysis and biological activities of *Matthiola livida* DC. extracts from Oued-Souf region: Insights into antioxidant and anti-inflammatory potential. *Acta Period Technol*., **55(1)**, 107-124. https://doi.org/10.2298/APT2455107C

Chouikh A, Ben Ali A, Bousbia Brahim A, Khezzani K and Bekkouche S. 2024. Comparative analysis of phytochemical composition and biological activities of sprouted and unsprouted *Chenopodium quinoa* willd. seeds: insights into nutritional value and functional properties. *Univ Cibiniensis Ser E: Food Technol*., **28(1)**, 55-64. https://doi.org/10.2478/aucft-2024-0005

Chouikh A, Chemsa AE, Aounallah C, Aounallah I and Fatma A. 2020. Phytochemical study, nutritive value, antioxidant and anti-inflammatory activities of phenolic extracts from desert plant *Calligonum comosum* L'Hér. *Alger J Biosci*., **1(02)**, 68-75. http://dx.doi.org/10.5281/zenodo.4395515

Chouikh A, Mayache B, Maazi Mohamed C, Hadef Y and Chefrour A. 2015. Chemical composition and antimicrobial activity of essential oils in Xerophytic plant *Cotula cinerea* Del (Asteraceae) during two stages of development: flowering and fruiting. *J Appl Pharm Sci*., **5(3)**, 029-034. https://doi.org/10.7324/JAPS.2015.50306

Dolci A and Panteghini M. 2014. Harmonization of automated hemolysis index assessment and use: Is it possible?. *Clin Chim Acta*., **432**, 38-43. https://doi.org/10.1016/j.cca.2013.10.012

Dufour C, Loonis M and Dangles O. 2007. Inhibition of the peroxidation of linoleic acid by the flavonoid quercetin within their complex with human serum albumin. *Free radic biol med*., **43(2)**, 241-252. https://doi.org/10.1016/j.freeradbiomed.2007.04.009

Ebrahimzadeh M, Nabavi S and Nabavi S. 2014. Antidepressant and antihemolytic activities of Vicia sojakii. *Eur Rev Med Pharmacol Sci*., **18(7)**, 971-974.

Ebrahimzadeh MA, Nabavi SM, Nabavi S, Eslami B, and Rahmani Z. 2010. Antioxidant and antihaemolytic activities of the leaves of Kefe cumin (*Laser trilobum* L) Umbelliferae. *Trop J Pharm Res*., **9(5)**. https://doi.org/10.4314/tjpr.v9i5.61053

Faridi UA, Zidan NS, Almutairi FM, Alalawy AI, Atteia HH, Al-Awthan YS and Sakran MI. 2023. The Antioxidative, Anticancer and Hepatoprotective of Quercetin Nanoparticles In-vitro and In-vivo. *Jordan J Biol Sci*., **16(1)**, 1117. https://doi.org/10.54319/jjbs/160114

Feng W, Hao Z and Li M. 2017. **Isolation and structure identification of flavonoids.** Flavonoids, from biosynthesis to human health/Ed. by Justino GC Intech Open, 17-43.

Guettaf S, Abidli N, Kariche S, Bellebcir L and Bouriche H. 2016. Phytochemical screening and antioxidant activity of aqueous extract of *Genista saharae* (Coss. & Dur.). *Der Pharm Lett.*, **8(1)**, 50-60.

Gurugubelli T, Poturaju YR and Imandi RS. 2023. Biochemical Profile of Five Species of Cultured Marine Microalgae. *Jordan J Biol Sci*., **16(3)**. https://doi.org/10.54319/jjbs/160312

Kabera JN, Semana E, Mussa AR and He X. 2014. Plant secondary metabolites: biosynthesis, classification, function and pharmacological properties. *J. Pharm. Pharmacol*. **2(7)**, 377-392.

Kanoun K. 2011. Contribution à l'étude phytochimique et activité antioxydante des extraits de *Myrtus communis* L.(Rayhane) de la région de Tlemcen (Honaine). Mémoire magister, Université Aboubekr Belkaid–Tlemcen.

Ketaren Bunga Raya KBR, Siti Hajar Ahmad SHA, Sanusi Fatin Farhana SFF, Munirah Mohammad MM, Nor Elliza Tajidin NET and Anwar Parvez AP. 2015. Changes in phytochemical contents in different parts of *Clinacanthus nutans* (Burm. f.) Lindau due to storage duration. *Post Harvest Technol*., **74(4),** 445-452. https://doi.org/10.1590/1678-4499.0469

Khalili M, Ebrahimzadeh MA and Safdari Y. 2014. Antihemolitička aktivnost trideset biljnih ekstrakata u mišjim eritrocitima. *Arhiv za Higijenu Rada i Toksikologiju*., **65(4)**, 399-405. https://doi.org/10.2478/10004-1254-65-2014-2513

Ksouri R, Megdiche W, Falleh H, Trabelsi N, Boulaaba M, Smaoui A and Abdelly C. 2008. Influence of biological, environmental and technical factors on phenolic content and antioxidant activities of Tunisian halophytes. *C R Biol*., **331(11)**, 865-873. https://doi.org/10.1016/j.crvi.2008.07.024

Li Y, Kong D, Fu Y, Sussman MR and Wu H. 2020. The effect of developmental and environmental factors on secondary metabolites in medicinal plants. *Plant Physiol Biochem*., **148**, 80-89. https://doi.org/10.1016/j.plaphy.2020.01.006

Liu A, Yuan K, Li Q, Liu S, Li Y, Tao M and Zhu W. 2022. Metabolomics and proteomics revealed the synthesis difference of aroma precursors in tobacco leaves at various growth stages. *Plant Physiol Biochem*., **192**, 308-319. https://doi.org/10.1016/j.plaphy.2022.10.016

Meriane D, Genta-Jouve G, Kaabeche M, Michel S and Boutefnouchet S. 2014. Rapid identification of antioxidant compounds of *Genista saharae* Coss. & Dur. by combination of DPPH scavenging assay and HPTLC-MS. *Molecules*., **19(4)**, 4369-4379. https://doi.org/10.3390/molecules19044369

Michalak A. 2006. Phenolic compounds and their antioxidant activity in plants growing under heavy metal stress. *Pol J Environ Stud*., ***15*(4)**.

Mustafa G, Arif R, Atta A, Sharif S and Jamil A. 2017. Bioactive compounds from medicinal plants and their importance in drug discovery in Pakistan. *Matrix Sci Pharma*., **1(1)**, 17-26.

Nabavi SF, Nabavi SM, Ebrahimzadeh MA, Eslami B and Jafari N. 2013. In vitro antioxidant and antihemolytic activities of hydroalcoholic extracts of *Allium scabriscapum* Boiss. & Ky. aerial parts and bulbs. *Int J Food Prop*., **16(4)**, 713-722. https://doi.org/10.1080/10942912.2011.565902

Nguema-Ona E, Vicré-Gibouin M, Gotté M, Plancot B, Lerouge P, Bardor M and Driouich A. 2014. Cell wall O-glycoproteins and N-glycoproteins: aspects of biosynthesis and function. *Front plant sci*., **5**, 108857. https://doi.org/10.3389/fpls.2014.00499

Noh CHC, Azmin NFM and Amid A. 2017. Principal component analysis application on flavonoids characterization. *Adv Sci Technol Eng Syst J*., ***2***, 435-440.

Noudogbessi J, Natta A, Tchobo F, Bogninou G, Bothon F, Bossou A and Sohounhloué D. 2013. Phytochemical screening of *Pentadesma butyracea* Sabine (Clusiaceae) acclimated in Benin by GC/MS. *Int Scholarly Res Notices*., **2013**.

Nour El-Din NM and Ahmed FA. 2004. Effect of seasonal variation on secondary metabolites and nutritive value of *Crotalaria aegyptiaca* Benth. *Egypt J Desert Res.*, **54(1)**, 121-139.

Ofoedum AF, Uyanwa NC, Chikelu EC, Iroagba LN, Ugwoezuonu JN, Anaeke EJ, Odeyemi TA, Okezie FP and Nwuka MU. 2024. Primary and Secondary Metabolites as Products of Microbial Metabolism: Uses and Application in Foods, Pharmaceutical and Allied Industries. A Review. *Eur J Appl Sci Eng Technol*., **2(2)**, 4-16. https://doi.org/10.59324/ejaset.2024.2(2).01

Rahman MM, Rahaman MS, Islam MR, Rahman F, Mithi FM, Alqahtani T and Hossain MS. 2021. Role of phenolic compounds in human disease: current knowledge and future prospects. *Molecules*., **27(1)**, 233. https://doi.org/10.3390/molecules27010233

Ravisankar P, Reddy AA, Nagalakshmi B, Koushik OS, Kumar BV and Anvith PS. 2015. The comprehensive review on fat soluble vitamins. *IOSR J Pharm*., **5(11)**, 12-28.

Semba RD, Ramsing R, Rahman N, Kraemer K and Bloem MW. 2021. Legumes as a sustainable source of protein in human diets. *Glob Food Sec*., **28**, 100520. https://doi.org/10.1016/j.gfs.2021.100520

Sharma S, Sharma U, Singh A, Sutar N and Singh PJ. 2010. Screening of Terminalia bellirica fruits extracts for its analgesic and antipyretic activities. *Jordan J Biol Sci*., **3(3)**, 121-124.

Sun W, & Shahrajabian MH. 2023. Therapeutic potential of phenolic compounds in medicinal plants—Natural health products for human health. *Molecules*., **28(4)**, 1845. https://doi.org/10.3390/molecules28041845

Supriya M, Nagamani J and Kumar JK. 2013. Cytoprotective and antimicrobial activities of stem extract of caesalpinia mimosoides. *Int J Pharm Biol Res*., **4(1)**, 18-25.

Wiegandt H. (2011). **Glycolipids**. Elsevier.

Williams L, O'connar A, Latore L, Dennis O, Ringer S, Whittaker J and Kraus W. 2008. The in vitro anti-denaturation effects induced by natural products and non-steroidal compounds in heat treated (immunogenic) bovine serum albumin is proposed as a screening assay for the detection of anti-inflammatory compounds, without the use of animals, in the early stages of the drug discovery process. *West Indian Med J*., **57(4)**.

Yang Z and Ohlrogge JB. 2009. Turnover of fatty acids during natural senescence of Arabidopsis, Brachypodium, and switchgrass and in Arabidopsis β-oxidation mutants. *Plant Physiol*., **150(4)**, 1981-1989. https://doi.org/10.1104/pp.109.140491

Zhang J, Subramanian S, Stacey G and Yu O. 2009. Flavones and flavonols play distinct critical roles during nodulation of *Medicago truncatula* by *Sinorhizobium meliloti*. *Plant J*., **57(1)**, 171-183. https://doi.org/10.1111/j.1365-313X.2008.03676.x

JJBS

Volume 18, Number 2,June 2025
ISSN 1995-6673
Pages 253 – 263
https://doi.org/10.54319/jjbs/180206

Jordan Journal of Biological Sciences

Molecular Characterization of Water Rattan Palm (*Calamus angustifolius* Griff.) from Kampar River, Riau Province, Indonesia Using *matK* and *trnL-trnL-trnF* Intergenic Spacer

Hapiz Al Khairi[1,2], Dewi Indriyani Roslim[1,*], Aristyanti Devie Vitovang[1], Meisita Hariani[1], Herman[1], Wahyu Lestari[1], Adiwirman[3], Aldy Riau Wansyah Hasibuan[1,2], Linda Novita[4], Siti Zulaeha[4], Irni Furnawanthi Hindaningrum[4]

[1] Department of Biology, Faculty of Mathematics and Natural Sciences, University of Riau, Binawidya Campus, Jl HR Soebrantas Km 12.5, Panam, Pekanbaru, Riau, Indonesia; [2] Department of Tropical Biology, Faculty of Biology, Universitas Gadjah Mada. Jl. Teknika Selatan, Sinduadi. Mlati, Sleman, 55281. Special Region of Yogyakarta, Indonesia; [3]Department of Agrotechnology, Faculty of Agriculture, University of Riau, Binawidya Campus, Jl HR Soebrantas Km 12.5, Panam, Pekanbaru, Riau, 28293, Indonesia; [4]Research Center for Applied Botany, National Research and Innovation Agency, Jl. Raya Jakarta-Bogor Km. 46, Cibinong, Bogor, Jawa Barat, 16911, Indonesia

Received: August 24, 2024; Revised: October 10, 2024; Accepted: October 22, 2024

Abstract

Calamus angustifolius Griff., commonly known as water rattan, is an important species found in the Kampar River region of Riau Province, Indonesia. *This rattan is* a valuable non-timber forest product (NTFP) playing a crucial role in rural economies, especially in Indonesia, which supplies about 80% of the global rattan market. This species thrives in watery habitats such as peat swamps and floodplain rivers, contributing to the structural complexity of tropical forests and supporting diverse wildlife. Understanding its molecular characterization and morphological analysis is crucial for its conservation and sustainable utilization. This study employed *matK* and *trnL-trnL-trnF intergenic spacer* DNA markers for molecular characterization. DNA sequences were analyzed using MEGA11. In this study, the obtained *matK* and *trnL-trnL-trnF IGS* sequences showed lengths 848 bp and 867 bp, respectively. There was no critical nucleotide based on *trnL-trnL-trnF IGS*, but three critical nucleotides were found based on *matK*. The study found significant genetic variation within the matK region, with unique nucleotide positions specific to *C. angustifolius*. However, the *trnL-trnF* region showed less variability, limiting its utility for species differentiation. The high frequency of A+T nucleotides in both markers indicates specific evolutionary patterns in this genus. This rattan is closely similar to *C. aruensis* and *Pigafetta elata* genetically. The *matK* gene proved to be a reliable DNA barcode, providing clear and distinct genetic profiles essential for species identification and genetic mapping. In contrast, the *trnL-trnL-trnF IGS* showed limited utility as a DNA barcode due to its low variability and poor resolution in distinguishing between individuals. This research underscores the need for genetic resource conservation to prevent the loss of valuable germplasm. These findings provide a foundation for conservation efforts and sustainable resource management of water rattan.

Keywords: *Calamus angustifolius*, water rattan, *matK*, *trnL-trnL-trnF intergenic spacer*, DNA barcode, molecular characterization, Riau, Indonesia.

1. Introduction

Due to high morphological similarities among species, the taxonomy of the rattan genus *Calamus* presents challenges for accurate species identification, often leading to ambiguity in classification. According to all available phylogenetic data, the rattan genus *Calamus* is the largest of all palm (Arecaceae) genera and is nested inside the subtribe Calaminae (Calameae: Calamoideae),. *Ceratolobus*, *Daemonorops*, *Pogonotium*, and *Retispatha* are the other four genera in the subtribe (Baker, 2015). Recent studies have highlighted the challenges in identifying species within the genus Calamus due to the complexity of morphological characteristics. One notable approach to overcome these challenges is the use of DNA barcoding (Kurian *et al*., 2020). The furniture business is the main application for rattan, a vine that grows in tropical woods (Myers, 2015). The role that non-timber forest products (NTFPs) play in rural communities' development, livelihoods, and efforts to reduce poverty has garnered increased attention in the last few decades (Suleiman *et al*., 2017). Similarly, *Calamus angustifolius* as one of the NTFPs is also utilized as a raw material in various industries.

Calamus angustifolius is a valuable source of rattan, which is used in the production of furniture, handicrafts, and other products. The rattan industry supports livelihoods in rural communities and contributes to local and national economies (Siebert, 2005). This plant also

[*] Corresponding author. e-mail: dewiindriyaniroslim@gmail.com.

contributes to the structural complexity of tropical forests, providing habitat and support for various organisms, including birds, insects, and other plants. Its climbing nature helps create vertical habitat layers, which are crucial for species that depend on understory and canopy environments.

The habitat of *C. angustifolius* consists of watery areas, such as peat swamps, river basins, and floodplain rivers in Indonesia. Numerous floodplain ecosystems in the province of Riau are home to genetically diverambse endemic plants and animals (Roslim *et al*., 2016) including habitat for *C. angustifolius*. This rattan grows in clumps and climbs on other plants. Uniquely, this type of rattan can be consumed because of its sweet taste and is also commonly referred to as "rotan getah manis." The shoot (umbut) of the young plant is often used by the Malay community in Riau to make a food preparation called "pangkek" (Ayu, 2018).

As the largest rattan-producing country, Indonesia has contributed approximately 80% of the world's rattan needs. There are several key points in presenting rattan as a commodity used in society, namely identifying its types and origins (Kaliky, 2018). Rattan has a very variable form, making it difficult to identify different species. Flowers and fruits serve as the morphological characters used for identification, but obtaining flowers from these plants is very difficult. Similarly, the similarity of fruits between species is strikingly close, making identification a time-consuming and challenging process.

One of the finest ways to research molecular taxonomy and identify and distinguish between species is through molecular analysis (Al-Rawashdeh, 2011). The shortcomings of morphological features may be overcome and species identification may be sped up with the use of DNA barcoding technique (Amandita *et al*., 2019). These techniques have proven highly effective with biochemical and morphological indicators for species identification and biodiversity assessment. This helps in the formulation of effective conservation strategies and the monitoring of endangered species (Antil *et al*., 2023; Mir *et al*., 2021; Odah, 2023). Unfortunately, there is no nucleotide-based validation of *C. angustifolius* in Genbank.

When it came to distinguishing between species, the varied combinations of the two loci were more effective than either locus individually (Ho *et al*., 2021). To generate DNA barcodes in plant systematics, cpDNA barcode sequences are suitable for application. Commonly used genes are *rbcL, matK, rpoB, rpoC1, ycf5(ccsA), trnH-psbA, trnL-F* (Chac and Thinh, 2023). On the other hand, the popular loci are *rbcL*, the *trnL-F intergenic spacer*, *matK, ndhF* and *atpB* (Awomukwu *et al*., 2015). The two DNA barcodes with the most variance, *matK* and *trnL-trnF IGS*, are thought to be able to identify plants into species and subspecies levels (Herman *et al*., 2023; Tanaka and Ito, 2020). In addition, the benefits of modern molecular markers like SNPs or *ITS* for future studies could point toward future research directions (Baldwin *et al*., 1995; Davey and Blaxter, 2010).

The *matK* gene encodes the maturaseK protein found in plant chloroplasts and has a length of approximately 1,500 base pairs in angiosperms (Kar and Goyal, 2015). It is located within the intron of the *trnK* gene. The *matK* gene functions in maturation, specifically splicing type II introns from RNA transcripts (Mustafa *et al*., 2018). Unlike *matK*, which encodes a protein, the *trnL-trnF IGS* is only a region covering the intron of the *trnL* gene and the spacer between the *trnL* and *trnF* genes and does not encode a functional gene (Borsch and Quandt, 2009; Shaw *et al*., 2007).

The CBOL plant working group proposed the use of *rbcL* and *matK* as a “core” universal plant barcoding regions (CBOL Plant Working Group, 2009). It is known that *matK* is more commonly used in molecular identification compared to the *rbcL* gene (Roslim, 2017). The proof of the usefulness of *matK* primer is when they are used in certain species or taxa (Amandita *et al*., 2019). There are already traces of proof of the success of using *matK* in solving taxonomic problems in palms or the Arecaceae family (Yao *et al*., 2023), but not yet in the *C. angustifolius* species. The formation of genetic collections is necessary for the conservation of genetic resources to prevent genetic erosion, resulting in the loss of valuable germplasm. Here, in this study, we described the molecular characteristics of water rattan palm (*Calamus angustifolius* Griff.) determined by *matK* and *trnL-trnL-trnF intergenic spacer*.

2. Materials and Methods

2.1. Material and procedure

Plant materials, water rattan palms, used in this study were collected and identified from three different locations in Riau Province. First, from Teratak Buluh Village (3 individuals, with 0°23'24.6"N 101°25'57.5"E coordinate of location), secondly from Langgam Village, Pelalawan (1 individual, with 0°16’27.2"N 101°42'30.0"E coordinate of location), and lastly from Kualu Village, Kubang (2 individuals, with 0°23'21.7"N 101°20'44.3"E coordinate of location) (Figure 1). DNA was extracted from the young leaf sample cut into small pieces and crushed by adding liquid nitrogen to the mortar, then the extraction process was carried out using the Genomic DNA Mini Kit Plant (Geneaid, New Taipei City, Taiwan) according to the manufacturer’s protocol. The extracted DNA was visualized and qualified by using electrophoresis (Mupid-exU), and it was stored at -20°C.

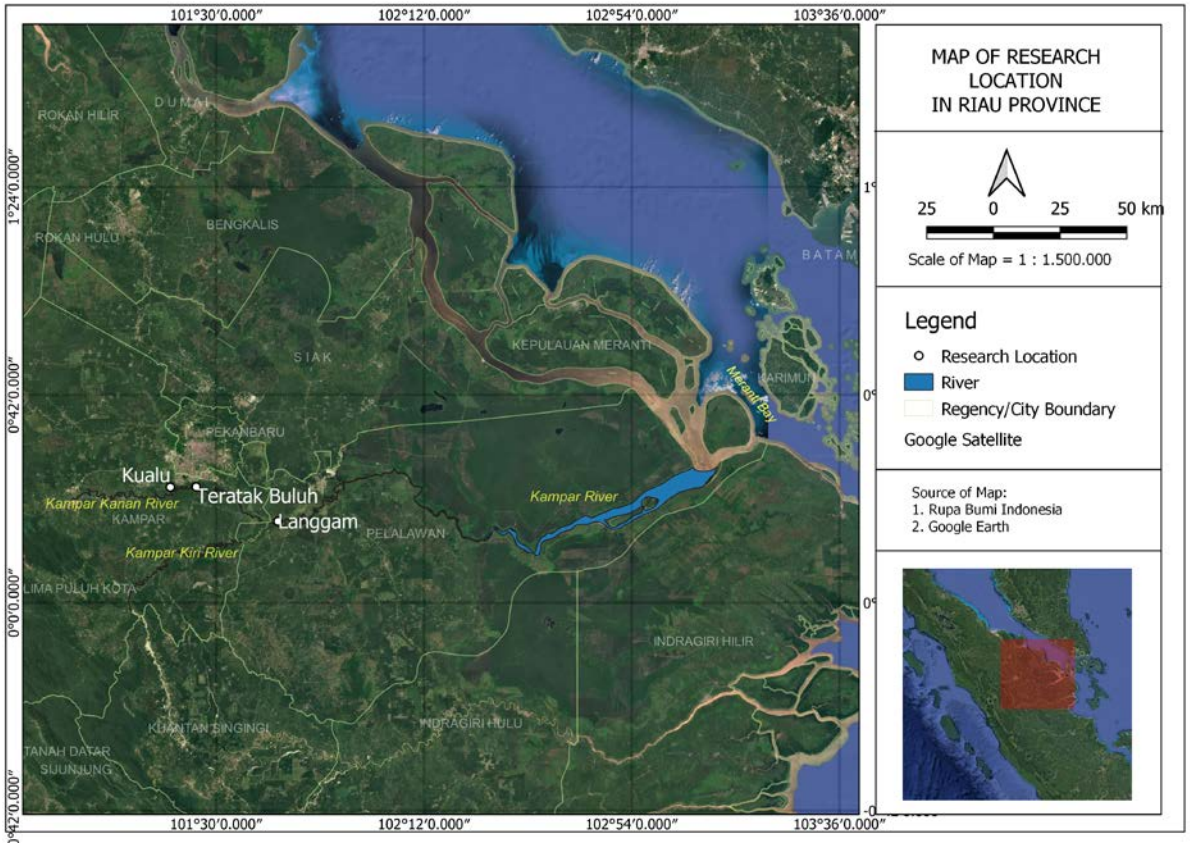

Figure 1. The map of water rattan palm sample used in this study (elaborated in Google Earth 2024).

Polymerase Chain Reaction (PCR) amplification was carried out in a total volume of 50 µl, containing final reaction compositions as follows: 1X PCR buffer, 0.2 mM dNTPs, 2.4 µM for each primer, and 2 U/µL DreamTaq DNA polymerase (*Thermo Scientific*). Two primer pairs were used for PCR amplification, matK-413f-1: 5'-TAA TTT ACR ATC AAT TCA TTC AAT ATT TCC-3' and matK-1227r-3: 5'-GAR GAT CCR CTR TRA TAA TGA AAA AGA TTT -3' for amplifying the *matK* region (Heckenhauer *et al*., 2016) and B49317_F2: 5'-CGA AAT CGG TAG ACG CTA CG-3' and A50272_R3: 5'-ATT TGA ACT GGT GAC ACG AG-3' for amplifying the *trnL-trnL-trnF IGS* (Taberlet *et al*., 1991).

The conditions for PCR amplification were as follows: 3 min at 95 ^{o}C, 35 cycles of 95^{o}C (45 s) denature, 49.2^{o}C for trnL- trnLtrnF IGS and 47.5 ^{o}C for matK (45 s) annealing, and 72 ^{o}C (90 s) extension, with a final extension cycle of 72 ^{o}C for 10 min (Herman *et al*., 2023). Amplicon of PCR was separated by electrophoresis in a 1% agarose gel added with 3 µl ethidium bromide, for 45 minutes at 50 Volts in 1x Tris-Borate-EDTA (TBE). The amplified products were resolved in 1% agarose gel using 1X TBE buffer, and then the PCR products were sequenced to PT. Genetika Science Indonesia as an intermediary, for further sequencing to be carried out at First Base Laboratories, Malaysia.

2.2. Data analysis

DNA sequence data analysis followed the procedure developed by Herman *et al*. (2023). DNA sequences forward and reverse primers were then aligned by using the BioEdit version 7.0.0 program (Hall, 1999). The BLASTn program on the https://blast.ncbi.nlm.nih.gov/ site was then used for both *matK* and *trnL-trnL-trnF IGS* to determine the similarity of the sequences studied to those in the GenBank database. Besides, the BOLD on the https://v3.boldsystems.org/ program is also used as an addition to similar sequence checks, specifically for *matK*. The top 10-12 accessions were used to determine nucleotide variations between the studied accessions. Management and analyzed DNA sequences were performed with MESQUITE (Maddison and Maddison, 2023). Multiple alignments were done using ClustalW (Thompson *et al*., 1994). Phylogenetic analysis were done by using the MEGA 11 (Tamura *et al*., 2021) using the different methods to perform three different phylogenetic trees, such as maximum likelihood (ML), neighbor joining (NJ), and maximum parsimony (MP). The trees were evaluated using methods like the bootstrap re-sampling method with 1000 replicates (Felsenstein, 1985) to assess its accuracy, assuring that the branches that frequently emerge are most likely to reflect the true evolutionary relationship.

3. Results

3.1. Species taxonomic description

Morphological features of Water Rattan Palm (*C. angustifolius*) are illustrated in Figure 2. Characteristic of this plant's morphology is habitating bushes, growing clusters, and climbing on other plants (Figure 2a). This rattan has a splintered, brown-green stem with a slightly rough stem surface (Figure 2b). The edible part of the stem is illustrated in Figure 2d. The leaves are green with a subulate leaf shape, the leaf ends are acuminate with a flat leaf edge (entire) and the leaves are placed in pairs and sitting leaves face to face. The top and bottom surfaces of

the leaves tend to have the same color, but on the bottom surface, some thorns are not so sharp. The rodent is round and has scratches on the skin of the fruit. When it is divided straight, it appears that there is an orange broth (Figure 2c). The old rod has a brown-colored thorn with a diameter of 20-25 mm and a street length of 30-35 cm, but it is arranged irregularly (Figure 2e). The fruit is green when it is young and will be yellowish when it is ripe. This rattan is also edible and has a delicate, clay flavor.

Figure 2. The morphology of rotan getah manis or water rattan palm (*Calamus angustifolius* Griff.) from Teratak Buluh, Kampar District, Riau Province, Indonesia. (a) Habitus, (b) fruit in bunches, (c) a fruit (upper) and a fruit sliced crosswise (lower), (d) edible rattan shoot, and (e) spiny stem. The red circle shows an edible rattan shoot.

3.2. Phylogenetic analysis for the gene matK

Eleven sequences were obtained (Table 1) and submitted to the GenBank Nucleotide database. All of the *matK* gene products size is about 848 bp of chloroplast plastid region for the *C. angustifolius* species, without any differences of nucleotides obtained. The sequence obtained was then searched into GenBank with BLASTn analysis (Table 2). The *matK* sequence of *C. angustifolius* has a 99% similarity with *C. jenkinsianus*, *C. tetradactylus*, *C. walkeri*, *C. henryanus*, *C. aruensis*, *C. castaneus*, and *C. caryotoides*, with the highest similarity score 99.53% for *C. jenkinsianus*. The sequence exhibited 98% similarity to *C. viminalis*, in addition to other plant species including *Pigafetta elata* and *Metroxylon warburgii*. The BOLD identification system also shows 99% similarity with *C. castaneus* and 98% with *C. viminalis* for plant species of *Calamus*.

Table 1. List of sequences obtained and submitted to Genbank from this study.

No	DNA Barcode	Sample Origin	Voucher	No. of Accession
1	*matK*	Teratak Buluh	DIR104	OQ174528
2			DIR105	OQ174529
3			DIR106	OQ174530
4		Langgam	DIR124	OQ942619
5	*trnL-trnL-trnF IGS*	Teratak Buluh	DIR113	OQ174515
6			DIR114	OQ174516
7			DIR115	OQ174517
8		Kualu	DIR122	OQ325046
9			DIR123	OQ325047
10		Langgam	DIR125	OQ942620
11			DIR031	MG836262

Table 2. BLASTn analysis based on the DNA sequence of the *matK*.

Species Name	Query Cover (%)	E-Value	Identity (%)	Accession
Calamus jenkinsianus	100	0.0	99.53	ON248739.1
Calamus tetradactylus	100	0.0	99.29	NC_079772.1
Calamus walker	100	0.0	99.29	ON248637.1
Calamus henryanus	100	0.0	99.29	NC_079715.1
Calamus aruensis	100	0.0	99.29	AM114551.1
Calamus castaneus	100	0.0	99.06	JX903669.1
Calamus caryotoides	100	0.0	99.06	NC_020365.1
Calamus viminalis	100	0.0	98.94	JQ435566.1
Pigafetta elata	100	0.0	98.59	AM114549.1
Metroxylon warburgii	100	0.0	98.36	NC_029959.1

According to all phylogenetic tree analyses (Figure 3), the specimen species *C. angustifolius* formed a group with its fellow species, even though the specimens were taken from different areas. Phylogenetic analysis indicates that *C. angustifolius* shares a close genetic relationship with *C. aruensis*, *P. elata*, *C. viminalis*, and *C. castaneus*, suggesting a shared evolutionary lineage within the Arecaceae family. Genetic distance analysis results (Table 3) in data that the average genetic distance between individuals of the species being studied is 0,000. The lowest genetic gap between species studied with access from the Genbank is 0.007, with two different species types: *C. aruensis* and *P. elata*, whereas the highest genetical distance value is obtained in species *M. warburgii* with a value of 0.873.

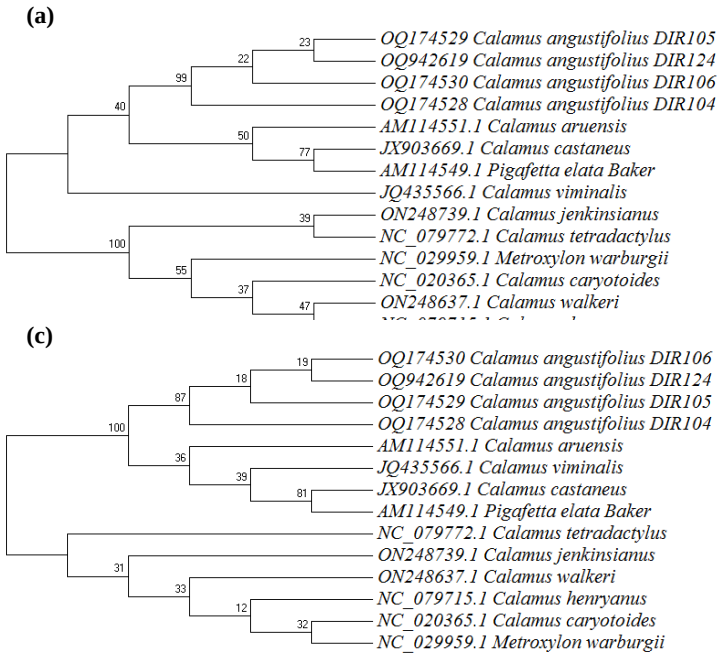

Figure 3. The Phylogenetics tree of *matK* sequences of all *Calamus angustifolius* accessions obtained from this study and related 10 accessions was inferred using the: (a) Maximum Likelihood method; (b) Maximum Parsimonial method; (c) Neighbour joining method. The bootstrap consensus tree was inferred from 1000 replicates.

Table 3. Genetic distance matrix based on the DNA sequence of the *matK* gene.

Species Name	1	2	3	4	5	6	7	8	9	10	11	12	13	14
1. *Calamus angustifolius* Teratak Buluh DIR104														
2. *Calamus angustifolius* Teratak Buluh DIR105	0.000													
3. *Calamus angustifolius* Teratak Buluh DIR106	0.000	0.000												
4. *Calamus angustifolius* Langgam DIR124	0.000	0.000	0.000											
5. *Calamus jenkinsianus*	0.860	0.860	0.860	0.860										
6. *Calamus tetradactylus*	0.856	0.856	0.856	0.856	0.005									
7. *Calamus walker*	0.856	0.856	0.856	0.856	0.005	0.002								
8. *Calamus henryanus*	0.856	0.856	0.856	0.856	0.005	0.002	0.000							
9. *Calamus aruensis*	0.007	0.007	0.007	0.007	0.856	0.853	0.852	0.852						
10. *Calamus castaneus*	0.010	0.010	0.010	0.010	0.870	0.866	0.865	0.865	0.005					
11. *Calamus caryotoides*	0.859	0.859	0.859	0.859	0.007	0.005	0.002	0.002	0.856	0.869				
12. *Calamus viminalis*	0.011	0.011	0.011	0.011	0.861	0.857	0.856	0.856	0.006	0.008	0.860			
13. Pigafetta *elata*	0.007	0.007	0.007	0.007	0.868	0.865	0.864	0.864	0.002	0.004	0.868	0.006		
14. *Metroxylon warburgii*	0.873	0.873	0.873	0.873	0.009	0.007	0.005	0.005	0.869	0.883	0.007	0.874	0.881	

An analysis of nucleotide variation in the *matK* gene showed that 542 nucleotides (59%) of the total aligned sequence were genetic variations. This number belongs to a large number and is a natural occurrence in the sequence of the *matK* gene. Three of these nucleotide variations are critical nucleotides that only the species *C. angustifolius* possesses. The critical nucleotide is the sequence number 46 (C on the water rattan and A on the other accessions), 439 (T on the water rattan, and G on other accessions), and 831 (T on the water rattan and A on the other accessions) (Table 4).

Table 4. Critical nucleotide in *matK* sequence of Water Rattan Palm (*Calamus angustifolius*) from Riau Province.

Accessions	Nucleotide number		
	46	439	831
Calamus angustifolius Teratak_Buluh_DIR104	C	T	T
Calamus angustifolius Teratak_Buluh_DIR105	.	.	.
Calamus angustifolius Teratak_Buluh_ DIR106	.	.	.
Calamus angustifolius Langgam_DIR124	.	.	.
Calamus jenkinsianus	A	G	A
Calamus tetradactylus	A	G	A
Calamus walkeri	A	G	A
Calamus henryanus	A	G	A
Calamus aruensis	A	C	C
Calamus castaneus	A	C	C
Calamus caryotoides	A	G	A
Calamus viminalis	A	C	C
Pigafetta elata	A	C	C
Metroxylon warburgii	A	G	A

The nucleotide substitution pattern was inferred using the maximum composite likelihood method, and the probability of substitution was estimated by Tamura *et al*. (Tamura *et al*., 2004) model. For purines, the transition/transversion rate ratio is k1 = 6.96, while for pyrimidines it is k2 = 7.556. R = 3.211 represents the overall transition/transversion bias. A = 32.88%, T/U = 34.21%, C = 16.62%, and G = 16.29% are the nucleotide frequencies (Table 5). The A+T frequency (67.09%) would be significantly higher than the C+G frequency (32.91%) if totaled. Nucleotides A have the highest frequencies compared to other nucleotides in codon 1 with a Frequency of 37.51%, whereas T in codons 2 and 3 with Frequencies of 39.30% and 29.83%, respectively. These evolutionary analyses were conducted in MEGA11 (Tamura *et al*., 2021).

Table 5. Nucleotide composition in *matK* sequence

Sp.	T(U)	C	A	G	Total	T-1	C-1	A-1	G-1	Pos #1	T-2	C-2	A-2	G-2	Pos #2	T-3	C-3	A-3	G-3	Pos #3
1	38.21	17.69	29.13	14.98	848	37.46	16.61	32.51	13.43	283	44.52	12.72	28.27	14.49	283	32.62	23.76	26.60	17.02	282
2	38.21	17.69	29.13	14.98	848	37.46	16.61	32.51	13.43	283	44.52	12.72	28.27	14.49	283	32.62	23.76	26.60	17.02	282
3	38.21	17.69	29.13	14.98	848	37.46	16.61	32.51	13.43	283	44.52	12.72	28.27	14.49	283	32.62	23.76	26.60	17.02	282
4	38.21	17.69	29.13	14.98	848	37.46	16.61	32.51	13.43	283	44.52	12.72	28.27	14.49	283	32.62	23.76	26.60	17.02	282
5	28.89	15.21	37.97	17.92	848	27.92	14.84	44.52	12.72	283	32.16	13.78	37.10	16.96	283	26.60	17.02	32.27	24.11	282
6	29.25	14.98	37.85	17.92	848	28.27	14.84	44.17	12.72	283	32.86	13.07	37.10	16.96	283	26.60	17.02	32.27	24.11	282
7	29.01	15.09	37.85	18.04	848	28.27	14.84	44.17	12.72	283	32.51	13.43	37.10	16.96	283	26.24	17.02	32.27	24.47	282
8	29.01	15.09	37.85	18.04	848	28.27	14.84	44.17	12.72	283	32.51	13.43	37.10	16.96	283	26.24	17.02	32.27	24.47	282
9	37.97	17.81	29.13	15.09	848	37.10	16.96	32.51	13.43	283	44.52	12.37	28.27	14.84	283	32.27	24.11	26.60	17.02	282
10	37.85	18.04	29.01	15.09	848	37.10	16.96	32.51	13.43	283	44.17	12.72	27.92	15.19	283	32.27	24.47	26.60	16.67	282
11	29.01	14.98	37.97	18.04	848	28.27	14.84	44.17	12.72	283	32.51	13.43	37.10	16.96	283	26.24	16.67	32.62	24.47	282
12	38.09	17.69	29.25	14.98	848	37.46	16.96	32.16	13.43	283	44.52	12.01	28.98	14.49	283	32.27	24.11	26.60	17.02	282
13	37.70	17.80	29.39	15.11	854	36.84	16.84	32.98	13.33	285	43.86	12.63	29.12	14.39	285	32.39	23.94	26.06	17.61	284
14	29.27	15.22	37.59	17.92	854	29.12	14.39	43.86	12.63	285	32.63	13.68	36.84	16.84	285	26.06	17.61	32.04	24.30	284
Avg.	34.21	16.62	32.88	16.29	848.9	33.46	15.91	37.52	13.11	283.3	39.31	12.96	32.12	15.61	283.3	29.83	21.00	29.00	20.17	282.3

Note: (1-4) *C. angustifolius* (5) *C. jenkinsianus,* (6) *C. tetradactylus,* (7) *C. walkeri,* (8) *C. henryanus,* (9) *C. aruensis,* (10) *C. castaneus,* (11) *C. caryotoides,* (12) *C. viminalis,* (13) *Pigafetta elata, and* (14) *Metroxylon warburgii.*

3.3. Phylogenetic analysis for the trnL-trnL-trnF Intergenic Spacer

Using the universal primer from Taberlet *et al.* (1991), we obtained PCR products for *C. angustifolius trnL-trnL-trnF IGS* about 867 bp. The sequence was searched against a database using BLAST search, which shows all the top 10 BLASTn accessions had a similarity of 99% to *C. angustifolius trnL-trnL-trnF IGS* sequence (Table 6). The highest score is 99.77% similarity with multiple plant species *M. warburgii*, *C. caryotoides*, and also *C. hollrungii* that was not even found on the top 10 BLASTn accessions with *matK*. The difference in BLASTn results is quite striking between *matK* and *trnL-trnL-trnF IGS*.

Table 6. BLASTn analysis based on the DNA sequence of the *trnL-trnL-trnF Intergenic Spacer*.

Species Name	Query Cover (%)	E-Value	Identity (%)	Accession
Metroxylon warburgii	100	0.0	99.77	NC_029959.1
Calamus caryotoides	100	0.0	99.77	NC_020365.1
Calamus hollrungii	100	0.0	99.77	AJ241279.1
Calamus jenkinsianus	100	0.0	99.66	NC_067841.1
Calamus tetradactylus	100	0.0	99.65	NC_079772.1
Salacca zalacca	100	0.0	99.31	NC_063109.1
Calamus henryanus	100	0.0	99.20	NC_079715.1
Eugeissona tristis	100	0.0	99.42	AJ241278.1
Salacca wallichiana	100	0.0	99.09	ON248811.1
Calamus walkeri	100	0.0	99.09	ON248637.1

Looking at the phylogenetic tree result of this sequence (Figure 4), it appears that *C. angustifolius* still cannot be differentiated from most of the different species. Furthermore, the genetic distance analysis based on the *trnL-trnL-trnF IGS* sequences (Table 7) revealed that the average genetic distance among individuals of the studied species is 0,000. But, surprisingly, this value (0,000) is also obtained between species *C. angustifolius* with eight out of 10 BLASTn access tops. These species include *C. jenkinsianus*, *C. caryotoides*, *C. hollrungii*, *C. tetradactylus*, *S. zalacca*, *C. henryanus*, *S. wallichiana*, and *C. walkeri*. While the other two accessions (*M. warburgii* and *E. tristis*) are still detected, there are genetic distances that are supposed to exist between different species. Effective DNA barcoding depends on the marker's capacity to distinguish between closely related species, but this is hampered by the low variability of *trnL-trnL-trnF IGS* markers.

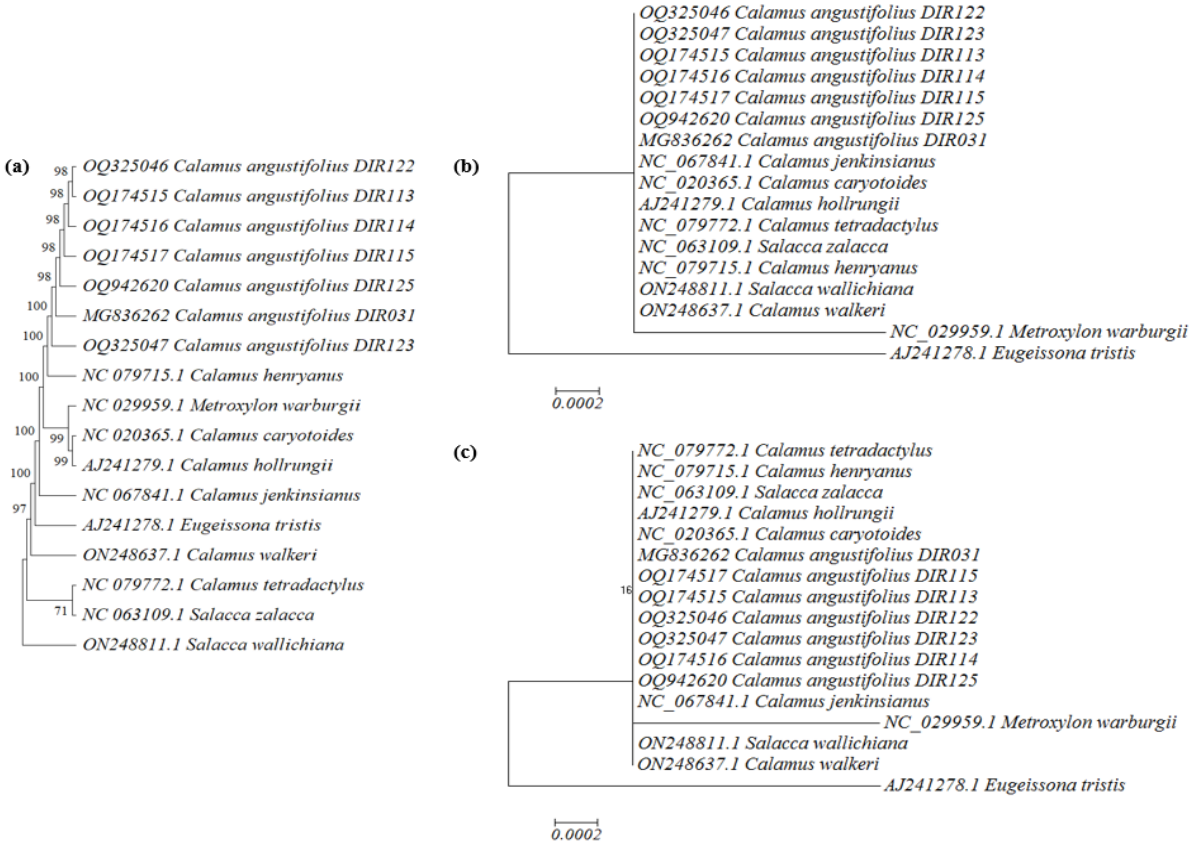

Figure 4. The Phylogenetics tree of *trnL-trnL-trnF Intergenic Spacer* sequences of all *Calamus angustifolius* accessions obtained from this study and related 10 accessions was inferred using the: (a) Maximum Parsimonial method; (b) Maximum Likelihood method; (c) Neighbour joining method. The bootstrap consensus tree was inferred from 1000 replicates.

Table 7. Genetic distance matrix based on the DNA sequence of the *trnL-trnL-trnF Intergenic Spacer.*

Species Name	1	2	3	4	5	6	7	8	9	10	11	12	13	14	15	16	17
Calamus angustifolius Kualu DIR122																	
Calamus angustifolius Kualu DIR123	0.000																
Calamus angustifolius Teratak Buluh DIR113	0.000	0.000															
Calamus angustifolius Teratak Buluh DIR114	0.000	0.000	0.000														
Calamus angustifolius Teratak Buluh DIR115	0.000	0.000	0.000	0.000													
Calamus angustifolius Langgam DIR125	0.000	0.000	0.000	0.000	0.000												
Calamus angustifolius Langgam DIR031	0.000	0.000	0.000	0.000	0.000	0.000											
Calamus jenkinsianus	0.000	0.000	0.000	0.000	0.000	0.000	0.000										
Metroxylon warburgii	0.001	0.001	0.001	0.001	0.001	0.001	0.001	0.001									
Calamus caryotoides	0.000	0.000	0.000	0.000	0.000	0.000	0.000	0.000	0.001								
Calamus hollrungii	0.000	0.000	0.000	0.000	0.000	0.000	0.000	0.000	0.001	0.000							
Calamus tetradactylus	0.000	0.000	0.000	0.000	0.000	0.000	0.000	0.000	0.001	0.000	0.000						
Salacca zalacca	0.000	0.000	0.000	0.000	0.000	0.000	0.000	0.000	0.001	0.000	0.000	0.000					
Calamus henryanus	0.000	0.000	0.000	0.000	0.000	0.000	0.000	0.000	0.001	0.000	0.000	0.000	0.000				
Eugeissona tristis	0.002	0.002	0.002	0.002	0.002	0.002	0.002	0.002	0.003	0.002	0.002	0.002	0.002	0.002			
Salacca wallichiana	0.000	0.000	0.000	0.000	0.000	0.000	0.000	0.000	0.001	0.000	0.000	0.000	0.000	0.000	0.002		
Calamus walker	0.000	0.000	0.000	0.000	0.000	0.000	0.000	0.000	0.001	0.000	0.000	0.000	0.000	0.000	0.002	0.000	

The nucleotide variations analyzed were also only 26 variations, and could not find any critical nucleotides at all. The frequencies of the nucleotides are 35.07% for A, 31.00% for T/U, 17.95% for C, and 15.98% for G (Table 8). For purines, the transition/transversion rate ratio is k1 = 0.947, while for pyrimidines it is k2 = 1.638. R = 0.577 is the total bias for transition and transversion. Matches *matK*, The A+T frequency (66.03%) would be significantly higher than the C+G frequency (33.95%) if totaled in *trnL-trnL-trnF IGS*. Nucleotides A have the highest frequencies compared to other nucleotides in codon 1, 2, and 3 with Frequencies of 35.18, 33.89%, and 36.09%, respectively. These results are also obtained in the same way as *matK*.

Table 8. Nucleotide composition in *trnL-trnL-trnF Intergenic Spacer* sequence.

Sp.	T(U)	C	A	G	Total	T-1	C-1	A-1	G-1	Pos #1	T-2	C-2	A-2	G-2	Pos #2	T-3	C-3	A-3	G-3	Pos #3
1	30.91	17.99	35.06	16.03	867	30.45	17.30	36.33	15.92	289	30.80	18.34	33.22	17.65	289	31.49	18.34	35.64	14.53	289
2	30.91	17.99	35.06	16.03	867	30.45	17.30	36.33	15.92	289	30.80	18.34	33.22	17.65	289	31.49	18.34	35.64	14.53	289
3	30.91	17.99	35.06	16.03	867	30.45	17.30	36.33	15.92	289	30.80	18.34	33.22	17.65	289	31.49	18.34	35.64	14.53	289
4	30.91	17.99	35.06	16.03	867	30.45	17.30	36.33	15.92	289	30.80	18.34	33.22	17.65	289	31.49	18.34	35.64	14.53	289
5	30.91	17.99	35.06	16.03	867	30.45	17.30	36.33	15.92	289	30.80	18.34	33.22	17.65	289	31.49	18.34	35.64	14.53	289
6	30.91	17.99	35.06	16.03	867	30.45	17.30	36.33	15.92	289	30.80	18.34	33.22	17.65	289	31.49	18.34	35.64	14.53	289
7	30.91	17.99	35.06	16.03	867	30.45	17.30	36.33	15.92	289	30.80	18.34	33.22	17.65	289	31.49	18.34	35.64	14.53	289
8	31.15	17.93	34.94	15.98	870	30.69	17.24	36.21	15.86	290	31.03	18.28	33.10	17.59	290	31.72	18.28	35.52	14.48	290
9	30.99	17.97	35.14	15.90	868	33.79	17.24	35.52	13.45	290	30.10	16.61	34.60	18.69	289	29.07	20.07	35.29	15.57	289
10	30.91	17.99	35.06	16.03	867	32.53	17.30	34.95	15.22	289	31.83	16.96	32.87	18.34	289	28.37	19.72	37.37	14.53	289
11	30.91	17.99	35.06	16.03	867	32.53	17.30	34.95	15.22	289	31.83	16.96	32.87	18.34	289	28.37	19.72	37.37	14.53	289
12	30.88	17.97	35.14	16.01	868	30.34	20.34	34.83	14.48	290	31.83	17.65	33.91	16.61	289	30.45	15.92	36.68	16.96	289
13	31.16	17.87	35.05	15.92	873	29.90	19.24	34.02	16.84	291	31.62	18.56	34.02	15.81	291	31.96	15.81	37.11	15.12	291
14	30.96	17.89	35.09	16.06	872	32.65	17.53	34.71	15.12	291	29.90	17.87	35.74	16.49	291	30.34	18.28	34.83	16.55	290
15	30.72	18.13	35.10	16.05	866	30.10	22.15	33.56	14.19	289	33.56	14.88	36.33	15.22	289	28.47	17.36	35.42	18.75	288
16	31.31	17.83	34.97	15.89	875	30.82	20.89	32.88	15.41	292	34.25	16.78	34.25	14.73	292	28.87	15.81	37.80	17.53	291
17	31.31	17.83	34.97	15.89	875	32.53	19.18	32.19	16.10	292	30.48	18.84	35.96	14.73	292	30.93	15.46	36.77	16.84	291
Avg.	30.98	17.96	35.06	16.00	869	31.12	18.21	35.18	15.49	290	31.30	17.75	33.90	17.06	290	30.53	17.93	36.10	15.45	289

4. Discussion

Phylogenetic tree analysis, supported by low genetic distance values based on the *matK* sequence, indicates that *C. angustifolius* from the Kampar River, Riau Province (Indonesia), is genetically very similar to *C. aruensis* and *P. elata*. Furthermore, it also shows a close genetic relationship with *M. warburgii* and *C. jenkinsianus*. Investigating the molecular phylogenetic relationships among taxa can lead scientists to make new discoveries (Ha *et al*., 2022).

If we compare based on their morphology, both *Calamus* species (*C. angustifolius* and *C. aruensis*) have

some very similar morphologies. The obvious difference is that the habitus of *C. aruensis* is a Robust, single- or rarely multi-stemmed rattan that can reach a height of 50 meters. The fruit is globose, cream-white in color, solitary, and has a short stalk. Broad in New Guinea, extending from the Bismarck Archipelago to the Raja Ampat Islands (Baker *et al*., 2024). On the other hand, *P. elata* is a plant that is Large, straight, single-trunked, and belongs to the Aracaceae family (areca nuts). This plant also goes by the name "wanga" in Sulawesi. Mature plants have a trunk diameter of up to 40 cm and a maximum height of 50 meters. When the fruit is young, it is greenish, and as it ages it turns greenish-yellow. Other than its sour flavor, this fruit is rarely eaten and can result in yellowing teeth (Syamsiah *et al*., 2018).

The close phylogenetic relationship indicates that these species might share genetic traits that contribute to their adaptability and resilience to environmental changes. This suggests that conservation strategies for these species can be coordinated. Conservation strategies can be optimized by managing the species within the same framework, which is especially important in regions where resources for conservation are limited. Understanding the genetic diversity and relationships among *Calamus* species can inform conservation strategies by identifying genetically distinct populations that may be prioritized for protection, thereby safeguarding valuable germplasm and promoting sustainable use. The sustainable management and harvesting of rattan, including *C. angustifolius*, are essential for forest conservation. Overharvesting or unsustainable practices can lead to habitat degradation, impacting biodiversity and ecosystem services.

The nucleotide composition in a DNA sequence has significant implications for the properties and functions of the genome of an organism. Some traits and genomic behavior are impacted by increased adenine (A) and thymine (T) compositions. There is an increased susceptibility to mutations because the A-T rich genome region tends to be less stable and more susceptible to denaturation under heat or chemical stress. These regions can denature more easily than G-C rich regions, which are more stable due to the stronger hydrogen bonds between guanine and cytosine pairs (Vinogradov and Anatskaya, 2017). While a higher A-T content is associated with certain genomic characteristics such as increased mutation rates, the implications for *C. angustifolius* require further investigation to determine any impact on its genome stability (Zhang *et al*., 2022).

The nucleotide composition can affect the architecture of the entire genome. A-T rich areas, for instance, are frequently more pliable and flexible, which may have an impact on the chromatin's high-level structure. This may have an impact on procedures like chromatin remodeling and the nucleus's arrangement of the genome (Vergara and Gutierrez, 2017; Zagirova *et al*., 2024). The A-T rich genome may also evolve differently from the G-C rich genomes due to variations in the rate of mutation and the pressure of selection. This has consequences for evolution. For instance, a rich area of A–T might experience a faster rate of mutation accumulation, leading to a higher level of genetic diversity there (Lynch *et al*., 2016).

The transition rate ratios for purines and pyrimidines are k1 and k2, respectively. In *matK* gene sequences, purins have a transition speed ratio of 6.96 (k1 = 6.96). This indicates that purines transversions (from A <-> G) are around 6.96 times less common than purines transitions. k2 = 7.556: Pyrimidines transition rate ratios are 7.556. In other words, transitions involving pyrimidines are around 7.556 times less common than those using pyrimidines (C <-> T). The entire magnitude of the transition bias towards transversion is expressed as R = 3.211. This number indicates the frequency of transitions over the whole DNA sequence in comparison to transversions in general.

On the other hand, k1 for purines in *trnL-trnL-trnF IGS* region has a ratio of transitions to transversions is 0.947. This suggests that transitions are less frequent than transversions among purines. While k2 for pyrimidines has a ratio of transitions to transversions is 1.638. This indicates that transitions are more frequent than transversions among pyrimidines. The value of overall transition/transversion bias is R = 0.577. The transition/transversion rate ratios (k1 and k2) indicate the frequency of nucleotide substitutions, with higher values suggesting a bias towards transitions (substitutions between purines or between pyrimidines) over transversions (substitutions between a purine and a pyrimidine). The overall bias (R) supports this preference, which is common in molecular evolution due to the less disruptive nature of transitions. A value less than 1 indicates a higher frequency of transversions than transitions in the entire sequence.

Higher nucleotide diversity in the *matK* region made it possible to distinguish across species more clearly and strengthened its usefulness as a marker in genetic research. In this study, *the trnL-trnL-trnF IGS* region demonstrated limited variability among *Calamus* species, restricting its effectiveness for species differentiation within this genus. This statement is supported by the genetic distance result generated by the *trnL-trnL-trnF IGS* sequence in *C. angustifolius* with the top 10 accessions of BLASTn not being able to discriminate or differentiate between the species. The species that are taxonomically different such as *S. zalacca* and *S. wallichiana*, cannot be distinguished (the value remains 0.000), let alone to species that belong to his genus. In addition, phylogenetic analysis continues to classify *C. angustifolius* among distantly related species. Individuals within the same species will be grouped into a single cluster on the phylogenetic tree, distinct from individuals belonging to other species. So, we decided that the *trnL-trnL-trnF IGS* sequence has no power to be used as a DNA barcode for the species *C. angustifolius*. Molecular markers such as single nucleotide polymorphisms (SNPs) and internal transcribed spacers (*ITS*) are increasingly used in plant identification because it has a greater resolution for genetic diversity studies (Schwartz *et al*., 2007) and offers promising avenues for future research on *Calamus* species.

Since purines and pyrimidines generally result in more persistent and subtle modifications to DNA structure, their high transition/transversion ratios suggest that transitions happen more frequently. Nucleotide transitions are repeatedly preferred over transversions in molecular evolution. The role of selection is often cited in explanations for this pattern of amino acid modifications because transitions have more conservative effects on proteins (Stoltzfus and Norris, 2016). Evolution and mutation processes frequently reveal a greater frequency of

transitions than transversions. Numerous reasons might be blamed for this bias, including chemical stability, DNA repair mechanisms, and natural selection's tendency to preserve the genome's stability (Lyons and Lauring, 2017). In summary, the statement describes an analysis of nucleotide variations and frequencies, highlighting that transitions and transversions have different rates depending on the nucleotide type, with an overall bias favoring transversions.

5. Conclusions

This study validated that the barcoding DNA technique using *matK* can better identify *Calamus* plant species, especially *C. angustifolius*. These findings underscore the value of the *matK* gene in genetic and taxonomic studies of *Calamus*, providing a foundation for future research aimed at conservation and sustainable management of water rattan populations. The *trnL-trnL-trnF intergenic spacer*, however, was less effective in this role. In the future, we also suggest the use of *matK* for analysis to solve taxonomic problems in the genus *Calamus*.

Acknowledgements

This research was fully sponsored by a grant from DIPA Universitas Riau year 2023 under "Unggulan Universitas Riau" with contract number 8345/UN19.5.1.3/AL.04/2023. Thanks to LPPM of Universitas Riau.

References

Al-Rawashdeh IM. 2011. Molecular taxonomy among *Mentha spicata*, *Mentha longifolia* and *Ziziphora tenuior* populations using the RAPD Technique. *Jordan J Biol Sci.*, **4(2)**: 63–70.

Amandita FY, Rembold K, Vornam B, Rahayu S, Siregar IZ, Kreft H and Finkeldey R. 2019. DNA barcoding of flowering plants in Sumatra, Indonesia. *Ecol Evol.*, **9(4)**: 1858–1868.

Antil S, Abraham JS, Sripoorna S, Maurya S, Dagar J, Makhija S, Bhagat P, Gupta R, Sood U and Toteja R. 2023. DNA barcoding, an effective tool for species identification: a review. *Mol Biol Rep.*, **50(1)**: 761–775.

Awomukwu DA, Nyananyo BL, Uka CJ, Spies P and Sizani BL. 2015. DNA barcoding, identification and validation of the genus *Phyllanthus* in Nigeria using plastid rbcL and matK genetic markers. *GJSFR-G.*, **15(1)**.

Ayu DF. 2018. **Ensiklopedia Produk Pangan Indonesia**, third ed. PT. Penerbit IPB Press, Bogor.

Baker WJ. 2015. A revised delimitation of the rattan genus *Calamus* (Arecaceae). *Phytotaxa.*, **197(2)**: 139–152.

Baker WJ, Barford AS, Cámara-Leret R, Dowe JL, Heatubun CD, Petoe P, Turner JH, Zona S, Dransfield J and Smith LT. 2024. **The Palms of New Guinea**. Royal Botanic Gardens, Kew, United Kingdom.

Baldwin BG, Sanderson MJ, Porter JM, Wojciechowski MF, Campbell CS and Donoghue ML. (1995). The ITS region of nuclear ribosomal DNA: A valuable source of evidence on angiosperm phylogeny. *Ann Missouri Bot Gard.*, **82(2)**: 247-277.

Borsch T and Quandt D. 2009. Mutational dynamics and phylogenetic utility of noncoding chloroplast DNA. *Plant Syst Evol.*, **282(3–4)**: 169–199.

CBOL Plant Working Group. 2009. A DNA barcode for land plants. *Proc Natl Acad Sci USA.*, **106**: 12794–12797.

Chac LD and Thinh BB. 2023. Species identification through dna barcoding and its applications: A review. *Biol Bull.*, **50(6)**: 1143–1156.

Davey JW and Blaxter ML. 2010. RADSeq: Next-generation population genetics. *Brief Funct Genomics*, **9(5-6)**: 416-423.

Felsenstein J. 1985. Confidence limits on phylogenies: an approach using the bootstrap. *Evolution.*, **39(4)**: 783–791.

Ha DC, Cao PB, Nguyen VD and Le CT. 2022. Molecular phylogeny and deep origins of the hybrid mokara dear heart (Orchidaceae). *Jordan J Biol Sci.*, **15(5)**: 805–811.

Hall TA. 1999. BioEdit: a user-friendly biological sequence alignment editor and analysis program for windows 95/98/NT. *Nucleid Acids.*, **41**: 95–98.

Heckenhauer J, Barfuss MHJ and Samuel R. 2016. Universal multiplexable matK primers for DNA barcoding of angiosperms. *Appl Plant Sci.*, **4(6)**.

Herman, Al-Khairi H, Wansyah AR, Asmania, Utami RI, Anzaelina DN, Oktaviano Z, Lestari W, Adiwirman, and Roslim DI. 2023. The Ability of matK and trnL-trnL-trnF intergenic spacer to discern certain species accessions of the Families Solanaceae and Fabaceae. *SABRAO J Breed Genet.*, **55(1)**: 97–106.

Ho VT, Tran TKP, Vu TTT and Widiarsih S. 2021. Comparison of matK and rbcL DNA barcodes for genetic classification of jewel orchid accessions in Vietnam. *J Genet Eng Biotechnol.*, **19(1)**.

Kaliky F. 2018. Identification of the types of rattan in the home industry in Waitatiri Village, Salahutu District, Central Maluku Regency. *Jurnal Agrohut.*, **9(1)**.

Kar P and Goyal AK. 2015. Maturase K gene in plant DNA barcoding and phylogenetics. In: Ali MA, Gabor G, Al-Hemaid F (Eds.). **Plant DNA Barcoding and Phylogenetics.** Lambert Academic Publishing, Germany. pp. 79-90.

Kurian A, Dev SA, Sreekumar VB and Muralidharan EM. 2020. The low copy nuclear region, RPB2 as a novel DNA barcode region for species identification in the rattan genus Calamus (Arecaceae). *Physiol Mol Biol Plants.*, **26(9)**: 1875–1887.

Lynch M, Ackerman MS, Gout J, Long H, Sung W, Thomas WK and Foster PL. 2016. Genetic drift, selection and the evolution of the mutation rate. *Nat Rev Genet.*, **17**: 704–714.

Lyons DM and Lauring AS. 2017. Evidence for the selective basis of transition-to-transversion substitution bias in two RNA viruses. *Mol Biol Evol.*, **34(12)**: 3205–3215.

Maddison WP and Maddison DR. 2023. **Mesquite: a modular system for evolutionary analysis**. Version 3.81. http://www.mesquiteproject.org.

Mir RA, Bhat KA, Rashid G, Ebinezer LB, Masi A, Rakwal R, Shah AA and Zargar SM. 2021. DNA barcoding: a way forward to obtain deep insights about the realistic diversity of living organisms. *Nucleus.*, **64(2)**: 157–165.

Mustafa KM, Ewadh MJ, Al-Shuhaib MBS and Hasan HG. 2018. The in silico predicton of the chloroplast maturase K gene polymorphism in several barley varieties. *Agriculture* (*Pol'nohospodarstvo*)., **64(1)**: 3–16.

Myers R. 2015. What the Indonesian rattan export ban means for domestic and international markets, forests, and the livelihoods of rattan collectors. *For Policy Econ.*, **50**: 210–219.

Odah MAA. 2023. Unlocking the genetic code: Exploring the potential of DNA barcoding for biodiversity assessment. *AIMS Mol Sci.*, **10(4)**: 263–294.

Roslim DI. 2017. Identification of pandan plant (*Benstonea* sp.) from Riau, Indonesia using three DNA barcodes. *SABRAO J Breed Genet.*, **49(4)**: 346–360.

Roslim DI, Khumairoh S and Herman. 2016. Confirmation of tuntun angin (*Elaeocarpus floribundus*) taxonomic status using matK and ITS sequences. *Biosaintifika.*, **8(3)**: 393.

Schwartz MK, Luikart G and Waples RS. 2007. Genetic monitoring as a promising tool for conservation and management. *Trends Ecol Evol.*, **22(1)**: 25-33.

Shaw J, Lickey EB, Schilling EE and Small RL. 2007. Comparison of whole chloroplast genome sequences to choose noncoding regions for phylogenetic studies in angiosperms: The Tortoise and the hare III. *Am J Bot.*, **94(3)**: 275–288.

Siebert, S. F. (2005). The abundance and distribution of rattan over an elevation gradient in Sulawesi, Indonesia. *For Ecol Manage.*, **210(1–3)**, 143–158.

Stoltzfus A and Norris RW. 2016. On the causes of evolutionary transition:transversion bias. *Mol Biol Evol.*, **33(3)**: 595–602.

Suleiman MS, Wasonga VO, Mbau JS, Suleiman A and Elhadi YA. 2017. Non-timber forest products and their contribution to households income around Falgore Game Reserve in Kano, Nigeria. *Ecol Process.*, **6(1)**.

Syamsiah, Hala Y, Hiola SF and Azis K. 2018. Local knowledge of wanga (*Pigafetta elata*) as materials of traditional house at South Sulawesi, Indonesia. In *AIP Conference Proceedings*, Vol. 2030, American Institute of Physics Inc.

Taberlet P, Gielly L, Pautou G and Bouvet J. 1991. Universal primers for amplification of three non-coding regions of chloroplast DNA. *Plant Mol Biol.*, **17(5)**: 1105–1109.

Tamura K, Nei M and Kumar S. 2004. Prospects for inferring very large phylogenies by using the neighbor-joining method. *Proc Natl Acad Sci USA.*, **101(30)**: 11030–11035.

Tamura K, Stecher G and Kumar S. 2021. MEGA11: Molecular Evolutionary Genetics Analysis Version 11. *Mol Biol Evol.*, **38(7)**: 3022–3027.

Tanaka S and Ito M. 2020. DNA barcoding for identification of agarwood source species using trnL-trnF and matK DNA sequences. *J Nat Med.*, **74(1)**: 42–50.

Thompson JD, Higgins DG and Gibson TJ. 1994. CLUSTAL W: improving the sensitivity of progressive multiple sequence alignment through sequence weighting, position-specific gap penalties and weight matrix choice. *Nucleic Acids Res.*, **22**: 4673–4680.

Vergara Z and Gutierrez C. 2017. Emerging roles of chromatin in the maintenance of genome organization and function in plants. *Genome Biol.*, **18(1)**.

Vinogradov AE and Anatskaya OV. 2017. DNA helix: the importance of being AT-rich. *Mamm Genome.*, **28(9–10)**: 455–464.

Yao G, Zhang YQ, Barrett C, Xue B, Bellot S, Baker WJ and Ge XJ. 2023. A plastid phylogenomic framework for the palm family (Arecaceae). *BMC Biol.*, **21(1)**.

Zagirova D, Kononkova A, Vaulin N and Khrameeva E. 2024. From compartments to loops: understanding the unique chromatin organization in neuronal cells. *Epigenetics Chromatin.*, **17(1)**.

Zhang Y, Wu L, Wang Z, Wang J, Roychoudhury S, Tomasik B, Wu G, Wang G, Rao X and Zhou R. 2022. Replication stress: A review of novel targets to enhance radiosensitivity-from bench to clinic. *Front Oncol.*, **12**.

JJBS

Volume 18, Number 2,June 2025
ISSN 1995-6673
Pages 265 – 274
https://doi.org/10.54319/jjbs/180207

Jordan Journal of Biological Sciences

Evaluation of the Synergistic Cytotoxicity of Camptothecin with Silver Nanoparticles: Potential Anti-angiogenic, Anti-inflammatory, and Antioxidant Agents

Moath alqaraleh [1,*], Futoon Abedrabbu Al-Rawashde [1], Khaled M. Khleifat [2],

[1] Department of Medical Laboratory Sciences, Faculty of Allied Medical Sciences, Al-Balqa Applied University, Al-Salt 19117, Jordan; [2] Department of Medical Laboratory Sciences, Faculty of Science, Mutah University, Al-Karak 61710, Jordan.

Received: September 9, 2024; Revised: October 13, 2024; Accepted: October 24, 2024

Abstract

Background: The high cytotoxicity of camptothecin is considered one of the greatest problems, aside from resistance within the course of cancer therapy. Conversely, silver nanoparticles (SNPs) provide great potential for increasing drug efficacy and reducing adverse effects. The purpose of the research was to explore the cytotoxic impact of camptothecin with SNPs on Various cancer cell lines and also to determine the level of several inflammatory, oxidative stress and angiogenesis biomarkers as possible targets influenced by these treatments.

Methods: The SNPs were produced by *Aspergillus flavus* and characterization was performed by scanning electron microscopy (SEM) and zetasizer. SNPs were tested separately and in combination with camptothecin against normal fibroblast cells and different cancer cell lines including A549, HT-29 MCF7 and PANC-1. In addition, several inflammatory, oxidative stress and angiogenesis biochemical markers were evaluated using Enzyme Linked Immuno Assay (ELISA).

Results: SNPs significantly increased the toxicity of camptothecin against A549, MCF7, and PANC-1 cells at 0.75 µg/ml, while having insignificant toxicity on normal fibroblast cells. In addition, SNPs caused a decrease in vascular endothelial growth factor (VEGF) production and changed the inflammatory marker and antioxidant enzyme profile; thus, it was evident that co-incubation of SNPs and camptothecin effectively interrupted the pathways important for cancer cell survivability.

Conclusion: Combined SNPs and camptothecin increase the potentiating effect of camptothecin cytotoxicity and affect several cancer-related processes such as oxidative stress, inflammation, and tumor vascularization. This approach offered a unique strategy against cancer treatment, particularly for cancers that do not respond to chemotherapeutic agents like pancreatic cancer. More research is required to establish this combination for its therapeutic application.

Keywords: inflammatory cytokines, antioxidant enzyme, angiogenesis, pancreatic cancer, Silver Nanoparticles (SNPs), Camptothecin.

1. Introduction

Cancer is now recognized as one of the most malign diseases of the twentieth century (Al-Rawashde *et al*., 2021, Hamlat *et al*., 2023). The number of cases of cancer in Jordan has increased, rising from 12.6 per 100,000 persons in 2005 to 17.2 per 100,000 in 2010, according to recent cancer statistics. With 11.3% of all new cases, cancer ranked as the second most frequent malignancy in both genders by 2012. In Jordan in 2013, malignancies of the colon, rectum, anus, and small intestine made up about 2% of all fatalities. The 5-year survival rate for individuals with cancer decreases dramatically with age, falling from 60.4% for those under 50 to 49.3% for those 70 years of age or over. As the illness worsens, survival rates similarly drop as follows: 72.1% for locally located cancer, 53.8% at regional stage, and 22.6% for distant metastases (Sharkas *et al*., 2017).

Natural phytochemicals provide effective alternatives in the treatment of cancers (Al-Rawashde *et al.*, 2023, Al-Rawashde *et al.*, 2022). Camptothecin, an alkaloid found in the bark of the *Camptotheca acuminata* plant, is a strong anticancer drug that causes apoptosis and DNA damage by blocking DNA topoisomerase I, which can increase DNA damage in the S-phase stage during the proliferation cycle, resulting in cell damage (Yakkala *et al.*, 2023, Kohorst and Kaufmann, 2023). However, clinical trials have not employed it because of its high toxicity, poor targeting, and solubility issues (Sun et al., 2021). Moreover, it has nonselective toxic effects that could affect all types of cells (healthy as well the malignant) and lead to undesired side effects. Furthermore, it could also influence the bone marrow cells, allowing them to become more susceptible to different diseases (Ghanbari-Movahed *et al*., 2021).

Therefore, combination therapy, which provides an alternative approach to treating cancer, has been given tremendous attention lately owing to its potential to decrease drug resistance in cancer cells by chemosensitizing tumor cells to chemotherapy drugs, as well as decreasing the doses of drugs and enhancing the selectivity (Abd El Latif *et al*., 2024, Wang *et al*., 2023), Moreover, a combination of biocompatible nanoparticles

* Corresponding author. e-mail: muath.garalleh@bau.edu.jo.

and anticancer drugs can overcome drug resistance development or impair it or, at least, lower the side effects to zero levels, reduce healthy cell damage and induce selective cytotoxicity only within cancer cells (Blagosklonny, 2023).

Furthermore, combinations of chemotherapeutic agents with silver nanoparticles (SNPs) have gained significant attention, since SNPs have emerged among several types of nanoparticles that possess antibacterial and anticancer capabilities. For example, when SNPs are taken by bacteria or living cells, they release and produce silver ions or reactive radical species, which causes essential cellular processes to be disrupted and ultimately leads to severe cellular damage and death. As a result, SNPs are now frequently found in food containers and antiseptic medical dressings (Talapko e*t al.*, 2020).

For that reason, this investigation aims to assess the cytotoxic effects of SNPs combined with camptothecin on healthy fibroblast cells and different cancer cell lines (A549, HT-29, MCF7, and PANC-1) and to evaluate the antiangiogenic, anti-inflammatory, and antioxidant effectiveness of these combinations.

2. Material and methods

2.1. Material

Ten percent of fetal bovine serum, one percent of penicillin/streptomycin solution, and Dulbecco Modified Eagle Medium containing L-glutamine were acquired from EuroClone (UK). Additionally, we acquired trypsin and Phosphate Buffer Saline (PBS) from EuroClone (UK). Promega (USA) supplied MTT reagents, Trypan blue stain, stop solution, and Dimethyl Sulfoxide (DMSO), while TPP (Zollstraße, Switzerland) supplied cell culture plates.

2.2. Biosynthesis of SNPs

Aspergillus flavus was selected to generate SNPs since it has been documented as a reliable source that creates silver particles with a small size (Gopa and Pullapukuri, 2023). In our previous work, the fungus was collected from the store buildings in Mutah University, Jordan. This was followed by identification analysis using a sequence similarity test and the accession number of MG973280.1 was acquired. Then, the *Aspergillus flavus* was used for the biogenesis of SNPs using XRD, ATR-FTIR, and UV-vis spectrum of absorption for characterization (Al-Soub *et al.*, 2022).

2.3. Morphology and Particle Size Analysis

JEM-2010 microscope (JEOL, Tokyo, Japan) were used for scanning electron microscope (SEM) images. SEM images were obtained at pressures of 0.07 and 0.05 mbar and an acceleration voltage of 0.16 kV. Dynamic light scattering by Malvern Analytical in Malvern, United Kingdom, was used to determine the size distribution of the silver particles in liquid solutions with the Zetasizer Nano ZSP (Al-Limoun *et al.*, 2020, Abu Hajleh *et al.*, 2023).

2.4. Cancer cell lines culture

Several human cancer cell lines were used including the lung cancer cell line (A549), the colorectal cancer cell line (HT-29), the breast cancer cell line (MCF7), and the pancreatic cancer cell line (PANC-1). A fibroblast cell line was also used for comparison purposes. The growing media for the cell lines have 15% fetal bovine serum, 100 µg/mL penicillin-streptomycin (Alqaraleh *et al.*, 2023, Al-Rawashde *et al.*, 2021, Alshaer *et al*., 2023). All the cell lines used in this study were identified and have no contamination according to the American Type Culture Collection (ATCC).

2.5. Colorimetric MTT assay

Microculture tetrazolium test using 3-(4,5-dimethylthiazol-2-yl)-2,5-diphenyltetrazolium bromide dye (MTT) to determine the cell viability. 5 * 10^3 of cultured A549, HT-29, MCF7, PANC-1, and A fibroblast cells were seeded in each well of the ninety-six well-plates (Al-Tawarah *et al.*, 2020). After 24 h, the cultured cells were exposed to camptothecin with 0. 75 to 200 µM to the cells and SNPs of 0. 75 to 200 µg/ mL. Further, cells were treated with a medium containing 0. 75 µg/ ml of SNPs and with camptothecin at (0. 75 to 200 µM) for 72 hours. Afterwards, 15 µL of the dye was added to each well in the plate, followed by incubation for Four hours. Consequently, 100 µL of organic solvent was added to each well. The cell viability was determined using Microplate Reader BiotechTM ELx800TM (Bio-Tek Instrument, USA) with absorbance at 590 /630 nm.

2.6. Angiogenesis, Inflammation and Antioxidant Assays

The PANC-1 cell line was seeded at 500,000 cells to each well, and the following day the cells were cultured with 0.75 µg/ mL of SNPs, and a combination of 0.75 µM of camptothecin followed by incubation for 72 hours at 37 °C. The markers' concentrations such as interleukin 1 beta (IL-1 beta), tumor necrosis factor-alpha (TNF alpha), Catalase (CAT), Glutathione peroxidase (GPX), matrix metalloprotease 9 (MMP9) and VEGF were determined by following the manufacturer's ELISA instructions.

2.7. Statistical analysis

The results were revealed as the average ± SD based on three to four separate experiments. ANOVA was used to evaluate the statistical differences between the treatment and control groups. Dunnett's post hoc test was then used for additional analysis using GraphPad Prism version 10. P-value <0.0001 (****), P-value <0.001 (***) and P-value <0.01 (**); all of these P-value were viewed as highly significant statistical differences, while p-values < 0.05 (*) were regarded as statistically significant.

3. Results

3.1. Morphology and Particle Size results

The charge, size, and polydispersity index (PDI) variations before and after lyophilization are depicted in Figure 1. The average size and average charge before lyophilization were 150.455 nm and -25 mV, respectively, with a standard variation of 10.415 nm and 2. The PDI was 0.27. However, following lyophilization, the size became 277.5 nm, the PDI was 0.29, and the average charge changed to -14 mV. The particles after lyophilization are made up of many smaller particles, all less than 0.3 µm, according to SEM images Figure 2.

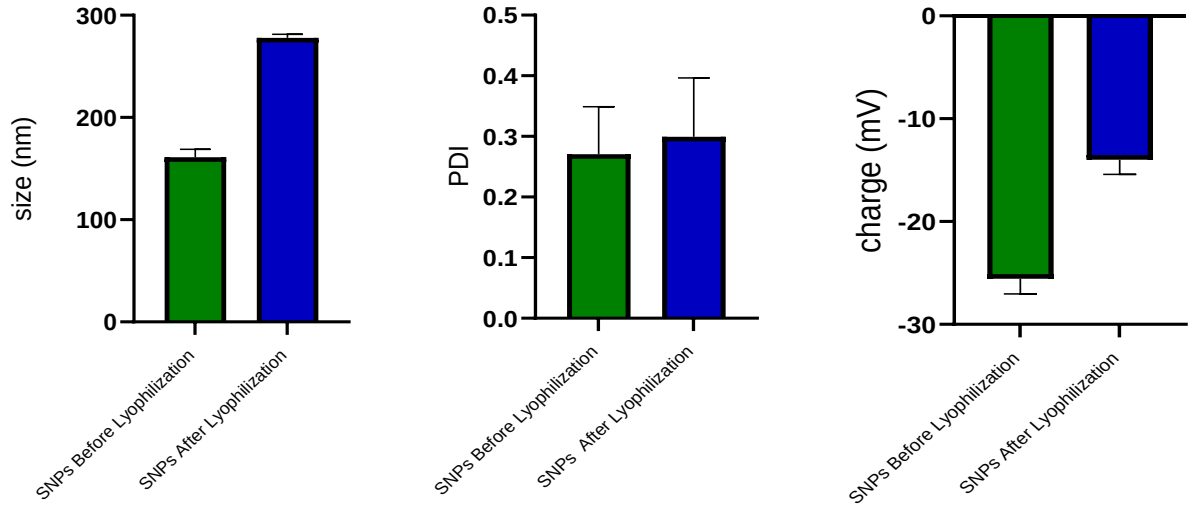

Figure 1. SNPs size, Zeta potential distribution, and polydispersity index were measured before and following lyophilization.

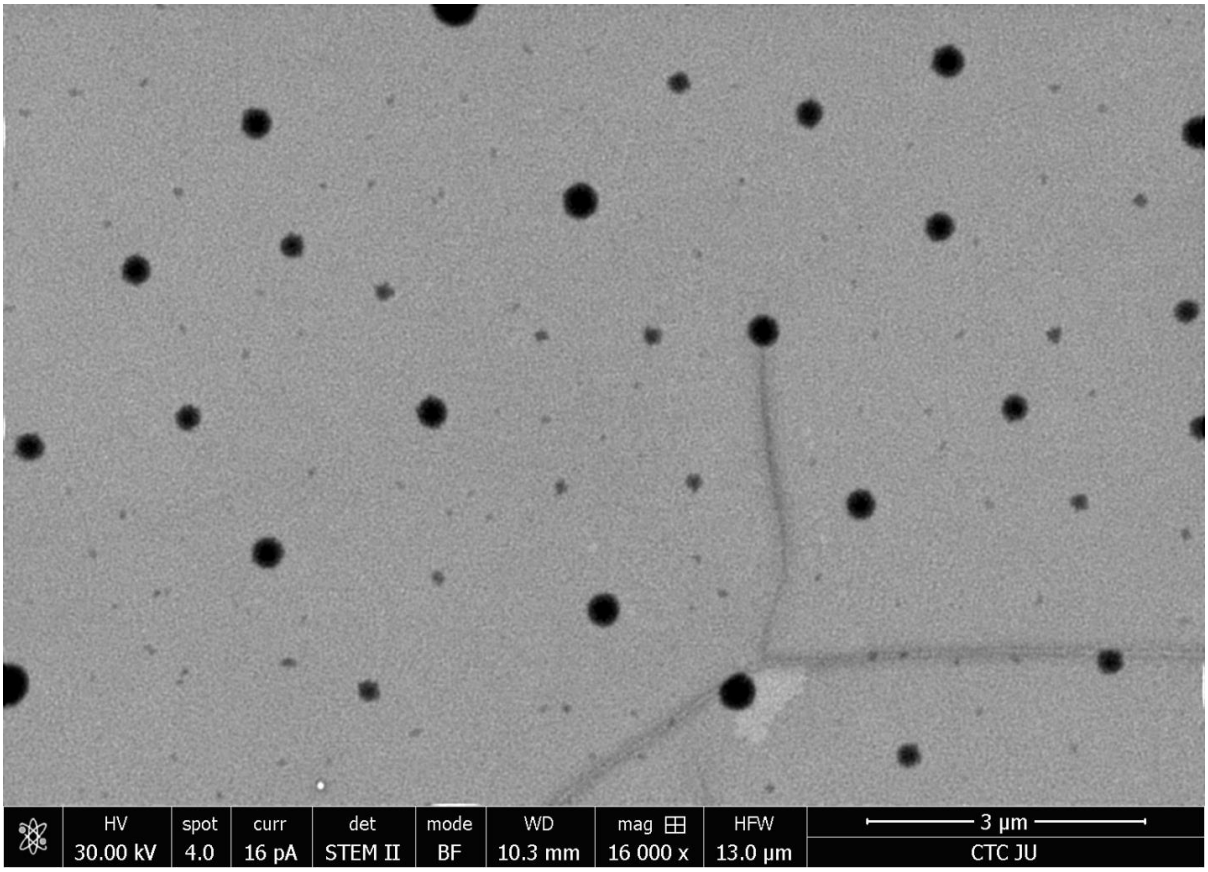

Figure 2. SEM image of SNPs produced by reacting 1.0 mM silver nitrate with *Aspergillus flavus*

3.2. Cytotoxicity results

The harmful impact of SNPs on the fibroblast cell line is displayed in Figure 3A to evaluate selective cytotoxicity. At concentrations from 1.5 to 200 µg/ ml, significant cell death was seen. A concentration of 0.75 µg/ ml of SNPs was chosen for additional cytotoxicity testing to reduce toxicity to the normal fibroblast cell line and increase cytotoxicity when combined with camptothecin against different cancer cell lines. The cytotoxicity of camptothecin both by itself and in conjunction with 0.75 µg/ml of SNPs is depicted in Figure 3B. The results show that when camptothecin and SNPs are used together, the combined effect is significantly less cytotoxic than when they are used independently.

The toxic influences of SNPs on the A549 cell line are illustrated in Figure 4A at concentrations from 0.75 to 200 µg/ ml. Notably, cell death is significantly observed at concentrations between 1.5 and 200 µg/ ml. The effects of camptothecin both by itself and in conjunction with 0.75 µg/ ml of SNPs are shown in Figure 4B. The findings show that when camptothecin and SNPs are combined, the cytotoxicity increases significantly in comparison to when camptothecin is used alone at 0.75 µm, 1.5 µm and 3 µm.

The HT-29 cell line is used to demonstrate the cytotoxicity of SNPs in Figure 5A, where doses from 1.5

to 200 µg/ ml led to substantial cell death. The cytotoxic effects of camptothecin both by itself and in combination with 0.75 µg/ml of SNPs are displayed in Figure 5B. The results show that, when compared to camptothecin alone, the addition of SNPs to camptothecin does not significantly increase cytotoxicity.

Comparably, Figure 6A shows how SNPs cytotoxicity affects the MCF7 cell line, with doses between 1.5 and 200 µg/ml causing notable cell loss. The cytotoxicity of camptothecin alone and in combination with 0.75 µg/ml of SNPs is displayed in Figure 6B. Compared to the cytotoxicity of camptothecin alone, Figure 6B shows a considerable increase in the cytotoxicity of camptothecin and SNPs combination, especially at doses between 1.5 µm and 0.75 µm.

Furthermore, Figure 7A demonstrates the toxic effects of SNPs on the PANC-1 cell line, with doses from 1.5 to 200 µg/ ml showing significant cell loss. The cytotoxicity of camptothecin, both by itself and in combination with 0.75 µg/ ml of SNPs on the PANC-1 cell line is illustrated in Figure 7B. When camptothecin is mixed with SNPs, the results show a significant increase in cytotoxicity compared to camptothecin alone, with effective cell death occurring at all concentrations that have been tested.

In conclusion, results indicate that the combination of silver particles and camptothecin is considered a viable combination for improving cancer treatment, particularly for pancreatic cancer; therefore, the PANC-1 cell line was used for subsequent investigations in this study.

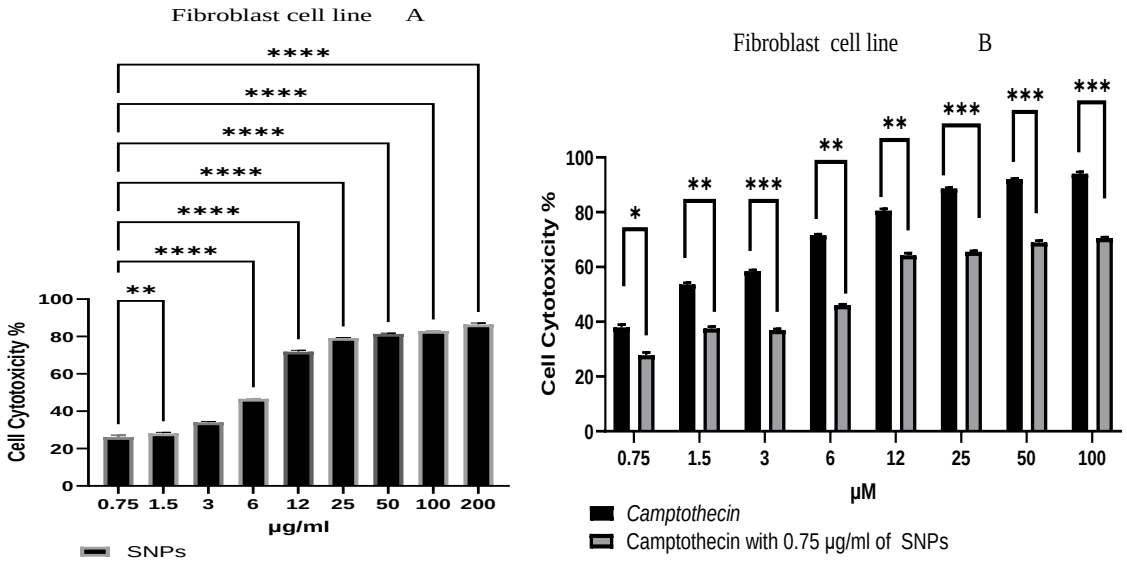

Figure 3. cytotoxicity effect of A- SNPs, B- Camptothecin and Camptothecin with 0.75 µg/ml of SNPs on fibroblast cell line. The averages of the three measurements ± standard deviation are used to describe the results (n = 3–4 independent repetitions).

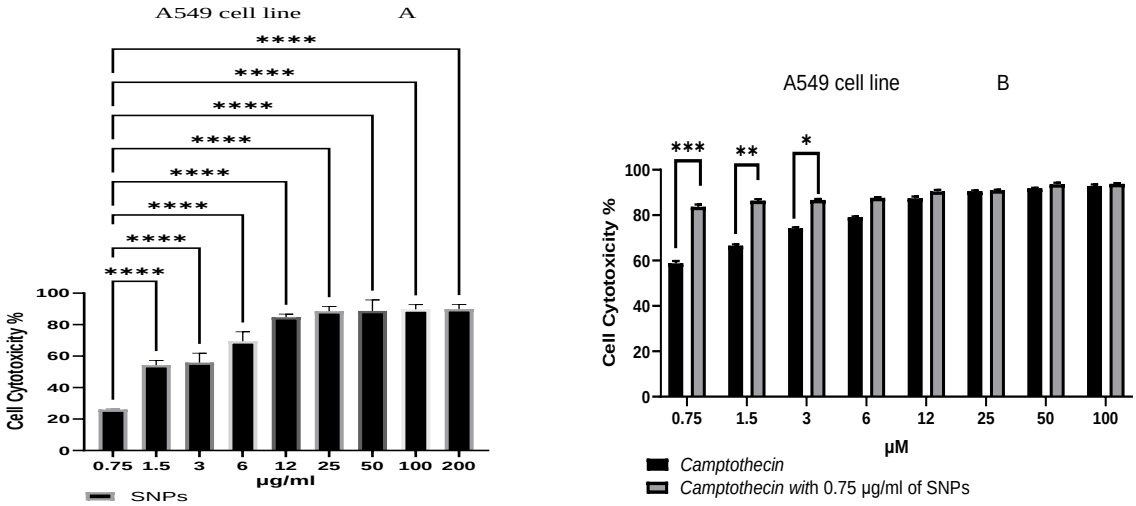

Figure 4. cytotoxicity effect of A- SNPs, B- Camptothecin and Camptothecin with 0.75 µg/ml of SNPs on A549 cell line. The averages of the three measurements ± standard deviation are used to describe the results (n = 3–4 independent repetitions.

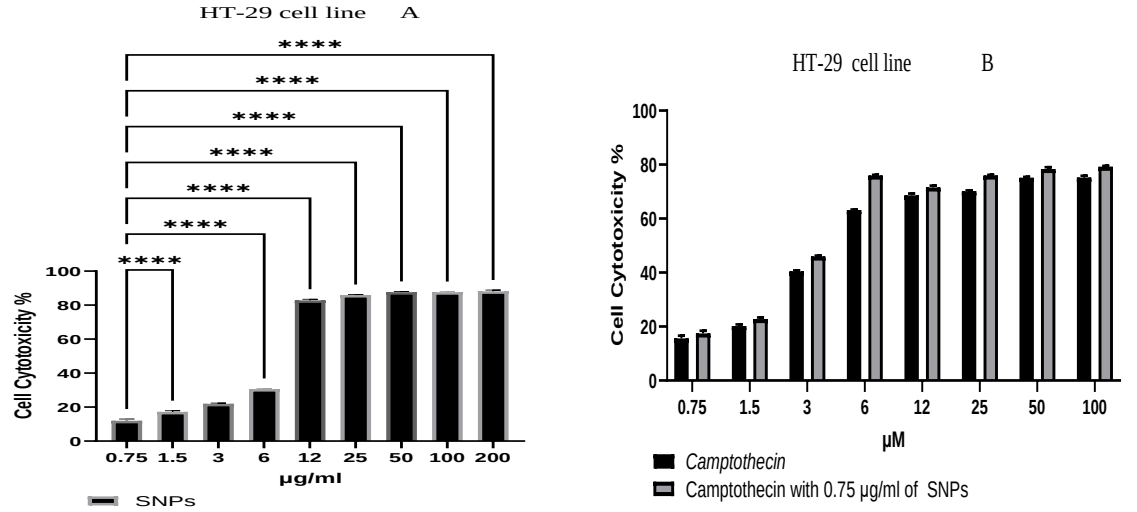

Figure 5. cytotoxicity effect of A- SNPs, B- Camptothecin and Camptothecin with 0.75 µg/ml of SNPs on HT-29 cell line. The averages of the three measurements ± standard deviation are used to describe the results (n = 3–4 independent repetitions).

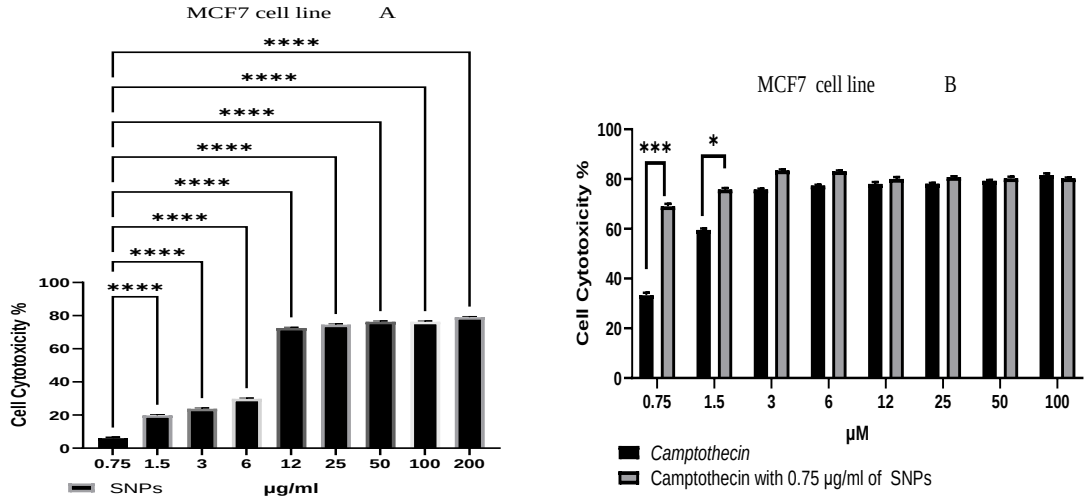

Figure 6. cytotoxicity effect of A- SNPs, B- Camptothecin and Camptothecin with 0.75 µg/ml of SNPs on MCF7 cell line. The averages of the three measurements ± standard deviation are used to describe the results (n = 3–4 independent repetitions).

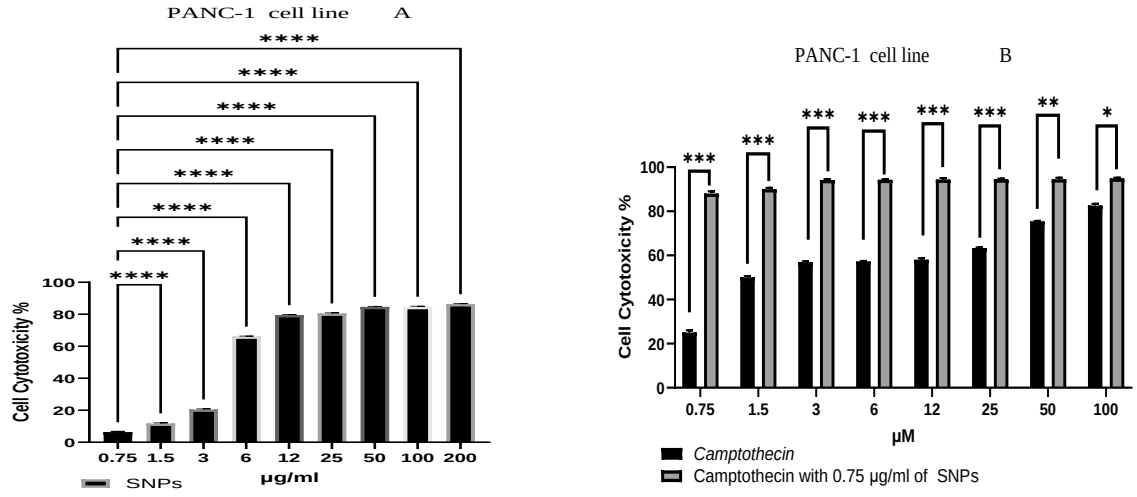

Figure 7. cytotoxicity effect of A- SNPs, B- Camptothecin and Camptothecin with 0.75 µg/ml of SNPs on PANC-1 cell line. The averages of the three measurements ± standard deviation are used to describe the results (n = 3–4 independent repetitions).

3.3. Angiogenesis, Inflammation and antioxidant results

VEGF contributes significantly to controlling angiogenesis, which is the generation of blood vessels for tumor development and spreading, something crucial to the tumor's survival and growth. MMP-9, on the other hand, is an enzyme that contributes to the breakdown of the extracellular matrix to assert tumor invasiveness and metastasis. Thus, MMP-9 facilitates the degradation of

structural barriers and invasion of cancer cells into tissues and surrounding stroma and their distal dissemination to distant organs. Both, VEGF and MMP-9, stimulate tumor growth, invasion, and metastasis(Alves *et al.*, 2023, Uslukaya *et al.*, 2023, Rashid and Bardaweel, 2023), and therefore both targets were investigated in this research. In the current study, the influence of the treatments on VEGF levels is seen in Figure 8A. The simultaneous administration of camptothecin along with SNPs, as well as camptothecin alone, significantly reduced VEGF levels in comparison to the control group. Notably, there was an even more significant reduction in VEGF levels when camptothecin and SNPs were combined. Moreover, the effect of the treatments on MMP9 levels is seen in Figure 8 B. MMP9 levels were much greater in the control group than in the treatment groups. In contrast to the control, MMP9 levels were significantly decreased by both SNPs and camptothecin alone. However, no significant difference between camptothecin and SNPs alone or in combination was observed. This suggests that the combination did not lower MMP9 levels any further than the individual treatments did.

Moreover, cytokines and antioxidants are involved in the progress of cancer, and both have antagonistic functions. TNF α and IL-1β the main pro-inflammatory cytokines support tumor growth through chronic inflammation which enhances cell growth. Some of these cytokines are known to phosphorylate both the NF-κB and the STAT3 pathways that increase tumor cell invasion and metastasis besides inhibiting anti-tumor immunity. On the other hand, antioxidant enzymes such as CAT and GPX have the responsibility of eliminating what is known as reactive oxygen species (ROS) generated during inflammation. It recognizes that the regulation of stress and the reactivity of the tumor microenvironment in terms of cytokine oppression, as well as the antioxidant stability of the cancer cell, determine the chemo-sensitivity and progress of cancer (Acevedo-León *et al.*, 2023, Bardelčíková *et al.*, 2023). Thus, TNF α, IL-1β, CAT and GPX were selected in this study.

The effect of both camptothecin and SNPs together and separately on TNFα expression levels is shown in Figure 8C. Comparing the silver particle-treated group to the control group, there was a significant rise in TNFα levels. Nevertheless, in comparison to the control, camptothecin individually did not significantly affect TNFα levels. Interestingly, when compared to the other treatment groups, the combination of camptothecin with SNPs led to a substantial decrease in TNFα levels. Furthermore, the effects of SNPs and camptothecin on IL-1β expression levels are shown in Figure 8D, both separately and in combination. IL-1β levels were notably greater in the silver particle-treated group relative to the control group. It is noteworthy that despite no significant difference between camptothecin alone compared to the control, the incorporation of silver particles into camptothecin considerably increased IL-1β levels relative to the control group and compared to camptothecin alone. The effect of different treatments on GPX levels is displayed in Figure 8E. When evaluated against the control group, the group treated with SNPs showed a substantial decrease in GPX levels. In the same direction, GPX levels significantly decreased in comparison to the control when camptothecin was used alone. Furthermore, in comparison to the control, there was also a decrease in GPX levels when camptothecin and SNPs were combined. Figure 8F shows the impact of various treatments on CAT levels. The group treated with SNPs exhibited no significant increase in CAT levels in comparison to the control group. Moreover, CAT levels did not alter significantly from the control in the groups treated with camptothecin alone or combined with SNPs. Furthermore, there was no notable difference in CAT levels between the combination therapy group and the camptothecin group, suggesting that the addition of SNPs to camptothecin did not further change CAT levels.

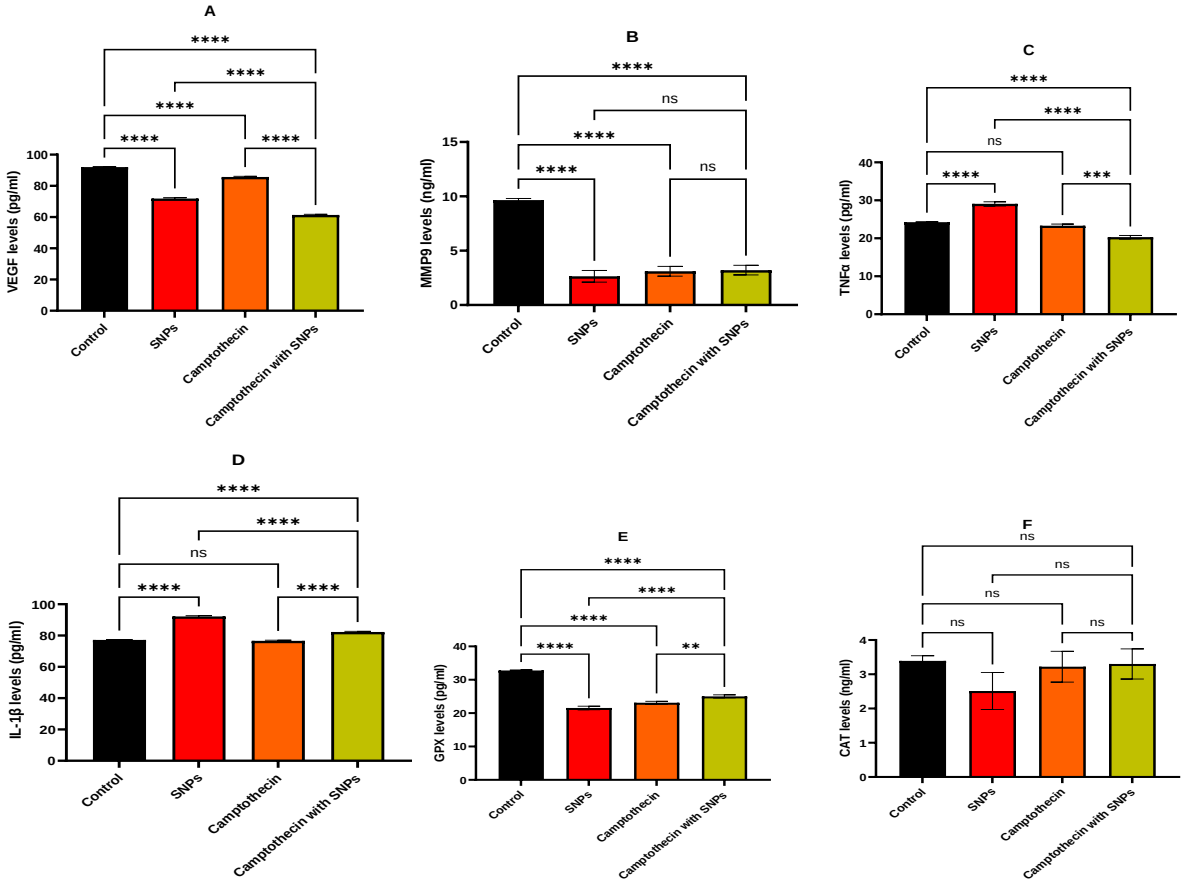

Figure 8. The expression level of A- VEGF, B- MMP 9, C- TNFα, D- IL1β, E- GPX and F- CAT, under the effect of 0.75 µg/ml of SNPs, 0.75 µM of Camptothecin and 0.75 µM of Camptothecin with 0.75 µg/ml of SNPs on PANC-1 cell line. The averages of the three measurements ± standard deviation are used to describe the results (n = 3–4 independent repetitions).

4. Discussion

Nanomedicine has become an important area of research with the advancement of nanotechnology, especially in the design of nanoscale materials for imaging and drug administration (Mir *et al*., 2017). Nanoparticles are extensively utilized as a therapeutic approach against different types of cancer due to their targeted delivery and enhanced therapeutic index (Crucho and Barros, 2017, Al-Qaraleh *et al*., 2024, Alahmad *et al.*, 2022). Because of their remarkable impair in vital cellular functions as well as their role in severe cellular damage or death, in particular, silver particles hold great promise for future developments in nanotechnology (Kalantari *et al.*, 2020). Aside from their exceptional thermal behavior and unusual visual qualities, they also display remarkable use in a wide range of healthcare, such as Antimicrobial dressings, wound treatment, and anticancer drugs (Dutt *et al.*, 2023, Jdayea and Neamah, 2024). In addition, SNPs are used in other biological applications, including diabetes, antiviral, and anti-inflammatory medicines (Konduri *et al*., 2024). Nevertheless, During the chemical production of nanoparticles, hazardous byproducts that might damage the environment are frequently produced (Khan *et al.*, 2021). Therefore, Biological synthesis is the best option to allay these worries since it uses inexpensive, easily handled, non-toxic, plentiful, and ecologically friendly microbes and plant materials (Gunti *et al.*, 2022, Lakshmeesha *et al.*, 2019).

In our previous study, we successfully characterized the biogenesis of SNPs using *Aspergillus flavus* through UV–vis absorption spectroscopy, ATR-FTIR, and XRD analyses (Al-Soub *et al*., 2022, Alqaraleh *et al*., 2023). Furthermore, in the present study, the SNPs were characterised using Zetasizer and SEM; the findings show that lyophilization has a substantial effect on the size, charge, and PDI. The SNPs had a PDI of 0.27, a surface charge of -25 mV, and an average size of 150.455 nm before lyophilization, indicating a reasonably homogeneous and stable nanoparticle dispersion appropriate for biological applications. The cause of the increase in particle size that results from lyophilization is the formation of aggregates through the nanoparticles, and this is known to occur especially when nanoparticles go through solvent elimination processes such as freezing and drying (Trenkenschuh and Friess, 2021, Eliyahu *et al.*, 2020). Furthermore, the reduction of the surface charge from -25 mV to -14 mV also supports this because the lower surface charges are associated with reduced electrostatic repulsive forces acting between particles and thus encourage the formation of aggregates (Shrestha *et al.*, 2020, Hedberg *et al*., 2012). Despite these changes in the size, charge and PDI, the SNPs remain within acceptable ranges for nanoparticulate formulations, indicating that none of their fundamental characteristics has been lost for possible therapeutic use (Abu Hajleh *et al.*, 2023, Al-Soub *et al*., 2022, Alqaraleh *et al*., 2023).

We also observed the cytotoxic activity of SNPs with and without camptothecin on several types of cancer cell lines such as A549, HT-29, MCF7 and PANC-1. For selective cytotoxicity of SNPs, a range of doses, from 0.75 to 200 µg/ml, were tested in this study. Fibroblast cells showed significant cell death at higher doses and insignificant toxicity at 0.75 µg/ml. To balance safety and efficacy, a concentration of 0.75 µg/ml of SNPs was chosen for further testing. This dose enhances the camptothecin cytotoxic effects from 0.75 to 200 µm, in PANC-1 cell lines, while achieving minimal toxicity to normal fibroblast cell lines. This indicates that the combination of silver particles and camptothecin is considered a viable combination for improving cancer treatment, particularly for pancreatic cancer, which is resistant to traditional chemotherapy (Mizrahi *et al*., 2020). The synergistic effect may be caused by the unique properties of SNPs, such as their capacity to boost camptothecin intracellular transport and effectiveness by raising its bioavailability or ease of absorption by cancer cells. Furthermore, it has been demonstrated that SNPs produce silver ions and ROS, which can impair essential biological processes including protein synthesis and DNA replication. Because of these modifications, cancer cells may become more cytotoxic, especially since camptothecin inhibits topoisomerase I and degrades DNA (Mikhailova, 2020, Alfei *et al.*, 2024, Patel *et al.*, 2024, Hamad *et al.*, 2020, Flores-López *et al.*, 2019, Choudhary *et al.*, 2022).

Additionally, the results of this study indicate that the combination of SNPs has a significant effect on several indicators associated with oxidative stress, inflammation, and angiogenesis in cancer cells. In particular, the combined administration of SNPs and camptothecin demonstrated a significant reduction in VEGF levels, that outweighed the effects of either treatment alone. This observation implies a synergistic impact in suppressing angiogenesis, a crucial process for tumor development and metastasis. Nevertheless, while either camptothecin or SNPs alone decreased MMP9 levels, which is an indicator of cancer invasion and metastasis, their cooperation did not intensify this decrease. This aligns with findings from several studies where SNPs alone and in combination with chemotherapy were shown to downregulate angiogenic factors (Zhan *et al*., 2024, Abdelfattah *et al*., 2022, Gurunathan *et al*., 2018). Moreover, Different inflammatory indicators were affected by the treatments. TNFα and IL1β levels were significantly elevated by SNPs alone, but not by camptothecin alone (Yuan and Gurunathan, 2017). Nevertheless, their combined effect was a considerable reduction in TNFα and IL1β, suggesting the possibility of an anti-inflammatory effect that might lower inflammation in cancer cells (Yuan and Gurunathan, 2017). Furthermore, when both treatments were administered at the same time, there was no further decrease in GPX and CAT levels as there was when they were administered separately, which dramatically reduced the levels of the enzymes. These results highlight the intricate ways in which SNPs and camptothecin interact to address inflammation, angiogenesis, and oxidative stress, and they point to possible therapeutic advantages in the management of cancer (Zhan *et al.*, 2024, Abdelfattah *et al*., 2022, Gurunathan *et al.*, 2018, Yuan and Gurunathan, 2017).

These results indicate that augmentation of proinflammatory cytokines may promote the growth of tumor, and that proinflammatory cytokines and ROS could be up-regulated by SNPs. SNPs, however, can induce cellular injury and may be linked to increased production of ROS that may surpass the production of proinflammatory cytokines. The present study has also revealed that even though combination treatments decrease the synthesis of pro-inflammatory cytokines, they do not enhance the levels of antioxidant enzymes that protect against ROS, amplifying the cytotoxic effect on cancer cells and which could account for the synergistic effect of the combination treatments for pancreatic cancer. Hence, this combination is a potentially effective approach in offering more selective and powerful methods of cancer therapy given that standard chemotherapy treatment is not as effective as required.

5. Conclusion

This study showed how camptothecin may be administered with SNPs to increase the effectiveness of cancer therapy. It was found that 0.75 µg/ml was the ideal dose of SNPs to reduce toxicity to normal cells and greatly increase camptothecin's anticancer effects, particularly in cell lines associated with pancreatic, lung, and breast cancer. The results of the research on selective cytotoxicity served as the foundation for these conclusions. It is quite probable that the SNPs' capacity to impede cellular functions and trigger oxidative stress is what gives them their synergistic effect on cancer cells. These results demonstrate how SNPs may be used as an adjuvant method in cancer treatment, reducing adverse effects and enhancing the therapeutic benefits of traditional chemotherapy. Furthermore, this work has some limitations, including the following: the study used only a small number of cancer cell lines, which may be inadequate to give the best picture of the cell's behavior. Furthermore, the action mechanism of camptothecin and the silver particles on cancer cells needs to be fully explored, especially regarding the use of different ratios of camptothecin to silver particles as well as testing the expression levels of a different biomarker, which involved invasion and metastasis process, under the influence of such a combination. Future research should focus on testing the combination across a larger variety of cancer cell lines and enhancing the selectivity and efficiency of the novel formulation in vivo since it may lead to significant improvements in clinical experiments.

Acknowledgment

We would like to acknowledge Al-Balqa Applied University for its support and collaboration.

References

Abd El Latif HM, El-Morsy AM, Ibrahim HM and Morsi DS. 2024. Synergistic antineoplastic and immunomodulatory effects of hesperidin in ehrlich ascites carcinoma tumor model treated with cisplatin. *Jordan J Biol Sci*.,**17(1)**.

Abdelfattah A, Aboutaleb AE, Abdel-Aal ABM, Abdellatif AA, Tawfeek HM and Abdel-Rahman SI. 2022. Design and

optimization of pegylated silver nanoparticles for efficient delivery of doxorubicin to cancer cells. *J Drug Deliv Sci Technol.*,**71**: 103347.

Abu Hajleh MN, Al-Limoun M, Al-Tarawneh A, Hijazin TJ, Alqaraleh M, Khleifat K, Al-Madanat OY, Qaisi YA, AlSarayreh A and Al-Samydai AJM. 2023. Synergistic effects of agnps and biochar: A potential combination for combating lung cancer and pathogenic bacteria. *Molecules*., **28(12)**: 4757.

Acevedo-León D, Gómez-Abril SÁ, Sanz-García P, Estañ-Capell N, Bañuls C and Sáez G. 2023. The role of oxidative stress, tumor and inflammatory markers in colorectal cancer patients: A one-year follow-up study. *Redox Biol*., **62**: 102662.

Al-Limoun M, Qaralleh HN, Khleifat KM, Al-Anber M, Al-Tarawneh A, Al-sharafa K, Kailani MH, Zaitoun MA, Matar SA and Al-soub TJCN. 2020. Culture media composition and reduction potential optimization of mycelia-free filtrate for the biosynthesis of silver nanoparticles using the fungus tritirachium oryzae w5h. *Curr. Nanosci.,* **16(5)**: 757-769.

Al-Qaraleh SY, Al-Zereini WA, Oran SA, Al-Madanat OY, Al-Qtaitat AI and Alahmad A. 2024. Enhanced anti-breast cancer activity of green synthesized selenium nanoparticles by pegylation: Induction of apoptosis and potential anticancer drug delivery system. *ANSN.*, **15(2)**: 025006.

Al-Rawashde FA, Al-Sanabra OM, Alqaraleh M, Jaradat AQ, Al-Wajeeh AS, Johan MF, Wan Taib WR, Ismail I and Al-Jamal HAN. 2023. Thymoquinone enhances apoptosis of k562 chronic myeloid leukemia cells through hypomethylation of shp-1 and inhibition of jak/stat signaling pathway. *APJCP.*, **16(6)**: 884.

Al-Rawashde FA, Al-Wajeeh AS, Vishkaei MN, Saad HKM, Johan MF, Taib WRW, Ismail I and Al-Jamal HAN. 2022. Thymoquinone inhibits jak/stat and pi3k/akt/mtor signaling pathways in mv4-11 and k562 myeloid leukemia cells. *Pharmaceuticals*., **15(9)**: 1123.

Al-Rawashde FA, Taib WRW, Ismail I, Johan MF, Al-Wajeeh AS and Al-Jamal HA. 2021. Thymoquinone induces downregulation of bcr-abl/jak/stat pathway and apoptosis in k562 leukemia cells**.** *APJCP***.,** **22(12)**: 3959.

Al-Soub A, Khleifat K, Al-Tarawneh A, Al-Limoun M, Alfarrayeh I, Al Sarayreh A, Al Qaisi Y, Qaralleh H, Alqaraleh M and Albashaireh A. 2022. Silver nanoparticles biosynthesis using an airborne fungal isolate, aspergillus flavus: Optimization, characterization and antibacterial activity. *Iran. J. Microbiol*., **14(4)**: 518.

Alahmad A, Al-Zereini WA, Hijazin TJ, Al-Madanat OY, Alghoraibi I, Al-Qaralleh O, Al-Qaraleh S, Feldhoff A, Walter J-G and Scheper T. 2022. Green synthesis of silver nanoparticles using hypericum perforatum l. Aqueous extract with the evaluation of its antibacterial activity against clinical and food pathogens. *Pharmaceutics*., **14(5)**: 1104.

Alfei S, Schito GC, Schito AM and Zuccari G. 2024. Reactive oxygen species (ros)-mediated antibacterial oxidative therapies: Available methods to generate ros and a novel option proposal. *Int. J. Mol. Sci..*, **25(13)**: 7182.

Alqaraleh M, Khleifat KM, Abu Hajleh MN, Farah HS and Ahmed KA-A. 2023. Fungal-mediated silver nanoparticle and biochar synergy against colorectal cancer cells and pathogenic bacteria. *Antibiotics*., **12(3)**: 597.

Alshaer W, Alqudah D, Daoud F, Obeidat RM, Sibai OA and Zakaraya ZZ. 2023. Telmisartan enhances the accumulation of doxorubicin as a combination therapy for the management of triple negative breast cancer. *Jordan J Biol Sci*., **16(3)**.

Alves B, Peixoto J, Macedo S, Pinheiro J, Carvalho B, Soares P, Lima J and Lima RT. 2023. High vegfa expression is associated with improved progression-free survival after bevacizumab treatment in recurrent glioblastoma. *Cancers*., **15(8)**: 2196.

Bardelčíková A, Šoltys J and Mojžiš J. 2023. Oxidative stress, inflammation and colorectal cancer: An overview. *Antioxidants*., **12(4)**: 901.

Blagosklonny MV. 2023. Selective protection of normal cells from chemotherapy, while killing drug-resistant cancer cells. *Oncotarget*., **14**: 193.

Choudhary A, Singh S, Ravichandiran V and methods. 2022. Toxicity, preparation methods and applications of silver nanoparticles: An update. *Toxicol. Mech. Methods.,* **32(9)**: 650-661.

Crucho CI and Barros MT. 2017. Polymeric nanoparticles: A study on the preparation variables and characterization methods. *Mat Sci Eng C.*, **80**: 771-784.

Dutt Y, Pandey RP, Dutt M, Gupta A, Vibhuti A, Raj VS, Chang C-M and Priyadarshini A. 2023. Silver nanoparticles phytofabricated through azadirachta indica: Anticancer, apoptotic, and wound-healing properties. *Antibiotics*., **12(1)**: 121.

Eliyahu S, Almeida A, Macedo MH, das Neves J, Sarmento B and Bianco-Peled H. 2020. The effect of freeze-drying on mucoadhesion and transport of acrylated chitosan nanoparticles. *Int. J. Pharm*., **573**: 118739.

Flores-López LZ, Espinoza-Gómez H and Somanathan R. 2019. Silver nanoparticles: Electron transfer, reactive oxygen species, oxidative stress, beneficial and toxicological effects. Mini review. *J Appl Toxicol*., **39(1)**: 16-26.

Ghanbari-Movahed M, Kaceli T, Mondal A, Farzaei MH and Bishayee A. 2021. Recent advances in improved anticancer efficacies of camptothecin nano-formulations: A systematic review. *Biomedicines*., **9(5)**: 480.

Gopa DR and Pullapukuri K. 2023. Green synthesis of silver nanoparticles from aspergillus flavus and their antibacterial performance. *CPPM.*, **18(5)**: 761-768.

Gunti L, Dass RS and Mahata PK, 2022. **Multifaceted role of phyto-assisted selenium nanoparticles (senps) in biomedical and human therapeutics. In: Selenium and nano-selenium in environmental stress management and crop quality improvement**. Springer., pp: 437-458.

Gurunathan S, Kang M-H, Qasim M and Kim J-H. 2018. Nanoparticle-mediated combination therapy: Two-in-one approach for cancer. *Int. J. Mol. Sci.,* **19(10)**: 3264.

Hamad A, Khashan KS and Hadi A. 2020. Silver nanoparticles and silver ions as potential antibacterial agents. *JIOP*., **30(12)**: 4811-4828.

Hamlat N, Alqaraleh M, Kasabri V, Mizher H, Hassani A, Afifi F, Al Alawi S, Ouafi S and Khwaldeh A. 2023. Dual amylase/glucosidase inhibition, antilipolytic and antiproliferative potential of the aerial parts of and on a obesity related-colorectal cancer cell line panel. *Curr. Issues Pharm*., **37(3)**: 131-137.

Hedberg J, Lundin M, Lowe T, Blomberg E, Wold S and Wallinder IO. 2012. Interactions between surfactants and silver nanoparticles of varying charge. *J. Colloid. Interface Sci..*, **369(1)**: 193-201.

Jdayea NA and Neamah SI. 2024. Copper nanoparticles and culture media elicit biomass, secondary metabolites, and antioxidant activity in the cell suspension culture of momordica charantia l. *Jordan J Biol Sci*., **17(2)**.

Kalantari K, Mostafavi E, Afifi AM, Izadiyan Z, Jahangirian H, Rafiee-Moghaddam R and Webster TJ. 2020. Wound dressings functionalized with silver nanoparticles: Promises and pitfalls. *Nanoscale*., **12(4)**: 2268-2291.

Khan M, Khan MSA, Borah KK, Goswami Y, Hakeem KR and Chakrabartty I. 2021. The potential exposure and hazards of metal-based nanoparticles on plants and environment, with special

emphasis on zno nps, tio2 nps, and agnps: A review. *Environ. Adv.*, **6**: 100128.

Kohorst MA and Kaufmann SH, 2023. **Drugs targeting DNA repair, cell cycle, and apoptosis. In: Cancer pharmacology: An illustrated manual of anticancer drugs**, second edition. Springer Publishing Company., pp: 193-216.

Konduri VV, Kalagatur NK, Gunti L, Mangamuri UK, Kalagadda VR, Poda S and Krishna SBN. 2024. Green synthesis of silver nanoparticles from hibiscus tiliaceus l. Leaves and their applications in dye degradation, antioxidant, antimicrobial, and anticancer activities. *S Afr J Bot* ., **168**: 476-487.

Lakshmeesha TR, Kalagatur NK, Mudili V, Mohan CD, Rangappa S, Prasad BD, Ashwini BS, Hashem A, Alqarawi AA and Malik JA. 2019. Biofabrication of zinc oxide nanoparticles with syzygium aromaticum flower buds extract and finding its novel application in controlling the growth and mycotoxins of fusarium graminearum. *Front. microbiol.*, **10**: 1244.

Mikhailova EO. 2020. Silver nanoparticles: Mechanism of action and probable bio-application. *J. Funct. Biomater*.., **11(4)**: 84.

Mir M, Ishtiaq S, Rabia S, Khatoon M, Zeb A, Khan GM, ur Rehman A and ud Din F. 2017. Nanotechnology: From in vivo imaging system to controlled drug delivery. *Nanoscale Res. Lett*.., **12**: 1-16.

Mizrahi JD, Surana R, Valle JW and Shroff RT. 2020. Pancreatic cancer. *The Lancet*., **395(10242)**: 2008-2020.

Patel KD, Keskin-Erdogan Z, Sawadkar P, Sharifulden NSAN, Shannon MR, Patel M, Silva LB, Patel R, Chau DY and Knowles JC. 2024. Oxidative stress modulating nanomaterials and their biochemical roles in nanomedicine. *Nanoscale Horiz*., **9(10),** 1630-1682.

Rashid ZA and Bardaweel SK. 2023. Novel matrix metalloproteinase-9 (mmp-9) inhibitors in cancer treatment. *Int. J. Mol. Sci*., **24(15)**: 12133.

Sharkas GF, Arqoub KH, Khader YS, Tarawneh MR, Nimri OF, Al-Zaghal MJ and Subih HS. 2017. Colorectal cancer in jordan: Survival rate and its related factors. *J. Oncol*.., **2017(1)**: 3180762.

Shrestha S, Wang B and Dutta P. 2020. Nanoparticle processing: Understanding and controlling aggregation. *Adv. Colloid Interface Sci*.., **279**: 102162.

Sun Y, Zhang N, Wang C, Bai X, Wei Y and Liu J. 2021. The biosynthesis of camptothecin derivatives by camptotheca acuminata seedlings. *Natural Product Research*., **35(14)**: 2403-2407.

Talapko J, Matijević T, Juzbašić M, Antolović-Požgain A and Škrlec I. 2020. Antibacterial activity of silver and its application in dentistry, cardiology and dermatology. *Microorganisms*., **8(9)**: 1400.

Trenkenschuh E and Friess W. 2021. Freeze-drying of nanoparticles: How to overcome colloidal instability by formulation and process optimization. *Eur J Pharm Biopharm*, **165**: 345-360.

Uslukaya O, YEĞİN Z, TAŞKESEN F and YILDIRIM İ. 2023. Elevated expression levels of cox-2, il-8 and vegf in colon adenocarcinoma. *CMB.*, **69(6)**.

Wang W, Zhang D, Jiang Z, Zhang X, Jiang Y and Luan Y. 2023. A nanodrug-enabled chemosensitization of cancer stem cells against tumor progression and metastasis. *Chem Eng J*., **477**: 147121.

Yakkala PA, Penumallu NR, Shafi S and Kamal A. 2023. Prospects of topoisomerase inhibitors as promising anti-cancer agents. *Pharmaceuticals*., **16(10)**: 1456.

Yuan Y-G and Gurunathan S. 2017. Combination of graphene oxide–silver nanoparticle nanocomposites and cisplatin enhances apoptosis and autophagy in human cervical cancer cells. Int J *Int J Nanomedicine*., 6537-6558.

Zhan H, Lv Y, Shen R, Li C, Li M and Li Y. 2024. Bimetallic gold/silver and bioactive camptothecin hybrid nanoparticles for eradication of cancer stem cells in a combination. *Mol. Pharm*., **21(3)**: 1450-1465.

JJBS

Volume 18, Number 2,June 2025
ISSN 1995-6673
Pages 275 – 280
https://doi.org/10.54319/jjbs/180208

Jordan Journal of Biological Sciences

Microbial Solutions for Environmental Cleanup: *Sphingomonas paucimobilis* Role in Removing Heavy Metals and Aromatic Hydrocarbons

Raghad Shubbar Jaafar*

Biological Development Department, Marine Science Center, University of Basrah, Basrah, Iraq.

Received: June 24, 2024; Revised: October 21, 2024; Accepted: November 7, 2024

Abstract

Bioremediation is considered a modern method for addressing pollution, with the objective of safeguarding the environment by eliminating heavy metals and aromatic hydrocarbon compounds from contaminated sites. Bacteria are heavily involved in these treatments because they are easily isolated, grow rapidly, and exhibit high adaptability to shifting environmental conditions. The main objective of this research was to isolate and identify *Sphingomonas paucimobilis* bacteria from soil contaminated with oil in southern Iraq. Additionally, the study aimed to evaluate their ability to remove heavy metals such as lead and cadmium as well as investigate their potential for degrading aromatic hydrocarbon compounds.

The results of the current study revealed the bacteria's ability to tolerate high levels of both lead and cadmium (200 and 50 ppm, respectively), as confirmed by the findings of the Minimum Inhibitory Concentration (MIC). The removal percentages for these metals were as follows: lead removal (58.78% and 27.95%) at concentrations of 25 and 50 ppm, and cadmium removal (48.21% and 22.37%) at concentrations of 25 and 50 ppm. The bacteria exhibited a high potential for effectively eliminating several aromatic hydrocarbon compounds, including naphthalene, 2-methylnaphthalene, pyrene, and benzo(b)fluoranthene + benzo(k)fluoranthene. The removal percentage was dependent on both concentration and incubation time, with higher removal observed at lower concentrations (2%) and longer incubation periods (28 days) (99.72%, 99.43%, 88.81%, 88.31%).

In conclusion, the present study provides important insights into the field of bioremediation by presenting *Sphingomonas paucimobilis* as a promising microbial agent capable of effectively addressing environmental pollution from heavy metals and aromatic hydrocarbons, thus underscoring its potential for real-world bioremediation applications.

Keyswords: -Bioremediation, environmental sustainability, pollution control, microbial, degradation

1. Introduction

The most prominent organic pollutants in the environment are those organic compounds contained in poly aromatic hydrocarbon compounds. The harmful effects of hydrocarbons on the environment result from multiple causes: 1. their toxicity and the damage/and or mutations they causes to the genetic components, as well as their carcinogenic nature; 2. their spreading in all environments and the difficulty of removing (Ghosal *et al.*, 2016); 3. their ability to congregate in various food chains, and thus is considered one of the substances that are dangerous to the general health of humans (Xue, 2005).

Several strategies have been developed to eliminate petroleum pollution, which has become a "global" environmental threat. Recently, Biodegradation is one of the most prominent of these strategies, which is based on the use of microorganisms as a tool to remove these pollutants. This is due to several reasons, the most prominent being environmentally friendly (Jaafar, 2019). Bacteria are currently considered the leading organism in the field of bioremediation (Jaafar, 2019). The entry of hydrocarbon pollutants into the environment has a negative impact on organisms in general, including bacteria. Truskewycz et al. (2019) stated that although soil contamination leads to a decrease in bacterial diversity, it increases their total activity. They attributed the reason for this to the adaptation of bacteria to such contaminated environment in addition to the enrichment of the indigenous soil microflora, which are capable of breaking down these pollutants occurring in the original soil. Therefore, the success of the hydrocarbon biodegradation process is subject to selecting the appropriate bacteria for specific hydrocarbons types and concentration, that the ability to biodegrade petroleum oil is associated with the concentration and composition of hydrocarbons (Xu *et al.*, 2018). The high levels of hydrocarbons lead to inhibiting the bacterial activity or even death the bacteria(Ma *et al.*, 2018), and the degradation ability varies with hydrocarbons types. The order of degradation is as follows: linear alkanes > branched alkanes > low molecular weight alkyl aromatics > monoaromatics > cyclic alkanes > polyaromatics > asphaltenes (Varjani &

* Corresponding author. e-mail: raghad.jaafar@uobasrah.edu.iq.

Upasani, 2017). Bacteria have proven effective ability in degradation of PAH (Fuchs *et al.*, 2011) .Previous studies have identified key bacteria that can act as eco-friendly agents in solving the problem of pollution caused by PAH compounds.

Sphingomonas paucimobilis is a notable bacterium known for its ability to degrade PAH compounds. Studies have demonstrated that this species can effectively break down a variety of PAHs, including naphthalene, phenanthrene, and pyrene. The bacterium initiates the degradation process using dioxygenase enzymes, which leads to the cleavage of aromatic rings and subsequent mineralization (Haritash & Kaushik, 2009). The *Pseudomonas* genus, particularly *Pseudomonas aeruginosa* and *Pseudomonas putida*, is extensively researched for its ability to degrade PAHs. These bacteria feature a versatile metabolic system that enables them to degrade a wide range of PAHs, such as pyrene, anthracene, and benzo[a]pyrene. The catabolic genes involved in PAH degradation in *Pseudomonas* are generally organized in clusters, which supports efficient degradation across diverse environmental conditions(Medić & Karadžić, 2022)

2. Materials And Methods

2.1. Collection of Samples

In January 2022, thirty soil samples were gathered from two distinct stations within Basrah's southern city, North Rumaila oil field. These samples, taken from a depth of up to 20 cm, were meticulously labeled and stored in plastic bags. To get the samples ready for more analysis, each one was dried in the air, ground with a porcelain pestle and mortar, and then sifted through a 2 mm sieve. The fine soil parts that resulted were gathered in different bags and kept in a dry spot for later analysis.

2.2. Isolating and determining the identity of bacteria

A scientific approach has been employed to isolate bacteria from soil samples, which involves adding varying concentrations of crude petroleum obtained from Al - Shua'aba Refinery (2% and 5%), to Mineral Salts Medium (MSM), with the composition: - KCl, K_2HPO_4, KH_2PO4, $FeSO_4.7H_2O$, NaCl, $MnSO_4.7H_2O$, $CaCl_2$, and distilled water. The pH of the medium is adjusted within a range of 7.0 - 7.8 to create optimal conditions for bacterial proliferation. 100 mL conical flask with a medium containing a specific concentration of crude oil and 1 gram of soil were prepared. The culture was then placed in a shaking incubator (120 rpm) at a temperature of 30°C for seven days. Nutrient agar from Hi Media (India) was employed to isolate *Sphingomonas paucimobilis.* The bacteria's identification involved morphological and biochemical assessments. Additionally, to improve precision in identification, the Vitek II automated device from Biomerieux (USA) was employed for bacterial identification (Jaafar, 2019).

2.3. Assays to assess tolerance to heavy metal exposure

2.3.1. Preparation of Heavy Metal Concentrations for Tolerance Assays.

In readiness for tolerance assessments on heavy metal concentrations, we created stock solutions (1000 mg/L) of Lead nitrate and Cadmium nitrate salts. These salts were dissolved in sterile deionized water to form the stock solutions. The working standard solutions were made by diluting 100 ml of the stock standard solution of the chosen ion to a final volume of one liter with distilled water, from which working concentrations of metal salts were prepared following the protocol detailed in the cited study (Jaafar, 2019), (Etorki *et al.*, 2014).

2.3.2. Assessment of Heavy Metal Tolerance

To determine the tolerance of the isolated bacteria to heavy metals, a test was conducted. The bacteria were grown in heavy metal-free nutrient broth (NB, Hi media) at 30°C for 24 hours. Afterward, 0.1ml from the bacterial culture was aseptically transferred onto nutrient agar plates containing various concentrations of Cd and Pb (25, 50, 100, 250, 500, 1000, 1500, 1800 and 2000 ppm). These plates were then incubated at 30°C for 24 hours. The lowest concentrations of Cd and Pb that inhibited bacterial growth were identified as the tolerance levels. To ensure accuracy, this procedure was repeated three times, including a control experiment without heavy metals. This testing method was adapted from a study conducted by Andrea *et al.* (2017).

2.3.3. Assessment of the Bacterium's Heavy Metal Removal Capacity

To examine the bacterium's capacity for heavy metal removal, the following steps were undertaken. First, the bacteria were cultured in 10 ml of NB broth at 30°C for one day. Then, 2 ml of the bacterial suspension was introduced into conical flask containing 100 ml NB broth with the concentration 25 and 50 pp of Pb and Cd. The mixture was then left to incubate at 30°C for 24 hours.

Following the incubation period, the culture was centrifuged at 3000 rpm for 20 minutes. The supernatant was then collected and subjected to analysis to determine the removal of Pb and Cd using a flame atomic absorption spectrophotometer (AAS 6300, Shimadzu, Japan). This process was repeated three times to ensure the accuracy and reliability of the results.

The following equation was utilized to compute the percentage of removal:

% elimination = (reduction in heavy metal concentration ÷ Initial heavy metal concentration) × 100 (Andrea *et al.*, 2017)

2.3.4. Assessing the bacterium's capacity for oil degradation

To evaluate the bacterium's ability to degrade oil, an experimental setup was utilized. A 50 mL Erlenmeyer flask containing Mineral Salt Medium (MSM) was prepared with crude oil concentrations of 2% and 5%. To this medium, 1 mL of an overnight bacterial culture was added. The flasks were then incubated in an orbital shaker set at 25°C for durations of 7 and 28 days, with a shaker speed of 120 rpm. After the incubation period, the remaining crude oil was quantified. The experiment was replicated to ensure the accuracy and reliability of the results (Jaafar, 2019).

2.3.5. Recovery of residual crude oil components

The method described by Emiliana (Pandolfo E., 2023) was employed to extract residual crude oil from the MSM medium. This extraction procedure involved the addition

of 50 ml of carbon tetrachloride (CCl4) solvent to the bacterial culture. CCl4 is a commonly utilized solvent for extracting hydrocarbons while concurrently inhibiting bacterial growth and activity. The addition was conducted under continuous agitation of the mixture. Subsequently, the culture was transferred to a separating funnel and allowed to undergo settling. The separation procedure involved employing a separation column with dimensions of 25 cm in length and 3 cm in diameter, as outlined by (Farid, 2006). This column was packed with 8 grams of silica gel and a small amount of glass wool. The residual oil, dissolved in 25 ml of benzene, was cautiously poured into the separation column. The aromatic fraction was collected in a 50 ml beaker. Similar extraction techniques were conducted for the control flasks. Gas chromatography was used to estimate the hydrocarbons present in the aromatic fraction, the suspension was then decanted, and the remaining oil underwent drying in an oven set at 40°C to eliminate the CCl4 solvent.

3. Results And Discussions

3.1. Bacterial Identification

The bacteria isolated were characterized based on their morphology and biochemical features. To optimize the identification process, an automated bacterial identification tool (Vitek II, C8300 Biomerieux USA) was utilized. The resulting outcome achieved a confidence level of 95%.

Table 1. The cellular morphology and biochemical properties of *S. paucimobilis*.

Phenotypic characteristic	
Appearance based on morphology.	Results
Configuration	Rode
Mobility	+
Color	Yellowish
Biochemical reactions	
Formation H_2S	-
Nitrite reduction	-
Urease	+
Oxidase	+
Simon citrate	+
Sugar(Glucose, Sucrose)	-

3.2. Pattern of metals resistance by bacteria

The minimum inhibitory concentration (MIC) denotes the smallest dosage of a substance needed to inhibit observable growth of a microorganism following an overnight period of incubation. MICs are predominantly employed in diagnostic settings to ascertain breakpoints for antimicrobial resistance and also serve as a research method for evaluating the in vitro efficacy of newly developed antimicrobial compounds (Chhetry *et al.*, 2022). The results of bacterial tolerance to heavy metals (Pb and Cd) are represented in the Table 2. Results indicated that cadmium (Cd) exhibited greater toxicity than lead (Pb), as reflected by their respective minimum inhibitory concentrations (MICs) ,(500 and 2000 ppm), respectively. Metals that demonstrated lower MIC values were found to be more toxic, whereas metals with higher MIC values were considered to be less toxic (Mishra & Mishra, 2018). Jaafar (2019) recorded high tolerance to the Pb than Cd by *S. paucimobilis* (Tangaromsuk *et al*., 2002) . This can be explained based on the concentrations present in the environment to which bacteria have adapted (Sodhi *et al.*, 2020a). Pollution stemming from a particular metal has the potential to boost the tolerance of bacterial communities towards that metal. Furthermore, a variety of physical and chemical factors play a substantial role in heightening bacteria's susceptibility to varying concentrations of metals (Campillo-Cora *et al.*, 2023), (Manikant Tripathi *et al*., 2024). The findings of the current study are also in line with those of previous research (Afzal *et al.*, 2017), (Jaafar, 2019), (Sodhi *et al.*, 2020b).

3.3. Removal of heavy metals by bacteria

In the bioremediation study, two different concentrations of Pb (25 and 50 ppm) and Cd (25 and 50 ppm) were applied under consistent conditions, including a temperature of 25°C, pH of 7, vibration at 120 rpm, and an incubation period of 24 hours. The results of the study demonstrated that the bacteria used in the experiment were capable of removing both Pb and Cd. The removal percentages for Pb were 27.95% and 58.78% for the respective concentrations, while for Cd, the removal percentages were 22.37% and 48.21% (Table 2). These results indicate that the removal process followed a diffusion pattern, as the removal percentage increased with higher metal concentrations. Dong *et al.* (2023) indicated high percentage of heavy metals removal by SRB bacteria as increase the concentration, increasing the concentration of metals ions facilitated the binding of these metals with functional group in bacterial cell wall. Results also indicated higher remediation ability of bacteria in relation to Pb than Cd. This may be due to various mechanisms employed by organisms to eliminate heavy metals, as well as the heavy metal's capability to cause oxidative damage, thereby diminishing the organisms' remediation potential (Oziegbe *et al.*, 2021).

Table 2. The minimum inhibitory concentration (MIC) (ppm), and the elimination of heavy metals (%)

Levels of heavy metal concentrations.	MIC (ppm)	Percentage (%) of removal during 24 hours.
Pb(50ppm)	2000	58.78
Pb(25ppm)		27.95
Cd(50ppm)	500	48.21
Cd(25ppm)		22.37

3.4. Bacterial aromatic hydrocarbons degradation study

The evaluation of degradation potentials exhibited by bacterial strains isolated from polluted sites is of utmost importance when it comes to designing and developing a durable bioremediation strategy (Azadi & Shojaei, 2020). Results of the present study indicated that the isolated bacteria identified as *S. Paucimobilis* was able to degrade *TPH* compound with the total removal capacity reach to (99.82% and 99.90%) for both concentrations (2% and 5%) during the incubation period of 7 days, while the removal capacity during the 28 days' incubation reach to (99.76% and 99.88%). Li *et al.* (2020) in their study indicated ability of *S. changbaiensis to degrade the TPH within the percentage* $39.2 \pm 1.9\%$ during 30 days of incubation. Srivastava & Kumar (2019) reported ability of

S. Paucimobilis to degrade PAH compound. Sphingomonas sp. has integrated a diverse set of metabolic pathways for aromatics into its system. These pathways include meta-cleavage of catechol, dihydroxylation, and subsequent meta-cleavage of aromatic rings mediated by dioxygenase and dehydrogenase enzymes, as well as ring cleavage via Baeyer-Villiger oxidation. These metabolic capabilities enable Sphingomonas sp. to efficiently break down and utilize a wide range of aromatic compounds (Zhou *et al.*, 2022).

Table 3. Total percentage (%) of PAH compound degradation by *S. Paucimobilis* in different concentration of crude oil and incubation period

24 h incubation period		28 incubation period	
Total percentage (%) of PAH compound degradation		Total percentage (%) of PAH compound degradation	
Concentration 2%	Concentration 5%	Concentration 2%	Concentration 5%
99.82%	99.90%	99.76%	99.88%

3.5. Special degradation ability of different aromatic compounds

Present results related to the degradation ability of *S. Paucimobilis* for the flowing compound (Naphthalene,2-methylnaphthalene, pyrene, and Benzo(b) fluoranthene+Benzo(k)fluoranthene during 24h incubation period were (99.80, 96.69, 71.13, and 56.11%) and (83.71, 87.89, 49.74, and 50.535%) for concentration 2% and 5% respectively (Fig.1, 2). Results related to the degradation the same compounds but during 28 days' incubation were as follow (99.72, 99.43, 88.81, and 88.31%) and (98.84, 16.32, 18.32, and 16.08%) for concentration 2% and 5% respectively (Fig.3, 4). The results demonstrated the strong capability of *S. Paucimobilis* to degrade the PAH compound, with a predicted concentration-dependent ability. At higher initial concentrations of mixed PAHs, it was found that increased toxicity levels and competitive inhibition occurred. Fu *et al.* (2014) indicated ability of Sphingomonas sp. to degrade phenanthrene, anthracene, fluoranthene and pyrene, with the degradation percentage reaching to (99 ± 0.4%, 67 ± 2%, 97 ± 3%, 72 ± 8%, and 6 ± 2%) each at the level 100 mg L^{-1} and benzo[a]pyrene at 10 mg L^{-1}, respectively. Li *et al.* (2023) predicated that S. *multivorum* was more efficient in degrading fluorine and phenanthrene with the efficiency of 74.6% and 76.4% in 10 days, respectively. Zhang *et al.* (2022) reported in their study The ability of *Sphingobium* sp. to degrade naphthalene reached 100%. Additionally, it demonstrated partial degradation of pyrene, chrysene, and indole within 6 hours, with degradation rates of 39.0%, 78.0%, and 55.3%, respectively. (Zhou *et al.*, 2016), demonstrated ability of six strain of sphingomonas to degrade fluorine with different removal percentage (87.2 ± 3.8 85.4 ± 4.5 74.9 ± 4.7 83.0 ± 5.4 68.7 ± 3.1 63.2 ± 1.9, N.G.). The Sphingomonas bacteria are classified as bacteria that reside in soil that has been polluted with hydrocarbon compounds. Their notable capacity to degrade numerous aromatic hydrocarbon compounds into smaller components can be attributed to their high proficiency in this process (Kertesz *et al.*, 2018). This susceptibility can be interpreted as follows: 1-The reason behind this capability can be attributed to the existence of a diverse collection of genes that code for ring-hydroxylating dioxygenases, enzymes that play a crucial role in the degradation of aromatic hydrocarbon compounds; 2-The occurrence of multiple insertion elements and transposons, in conjunction with the arrangement of degradative genes in various dispersed clusters, offers the possibility of forming more efficient combinations of existing genes. This, in turn, can lead to the development of novel degradation pathways with enhanced capabilities (Kertesz *et al.*, 2018).

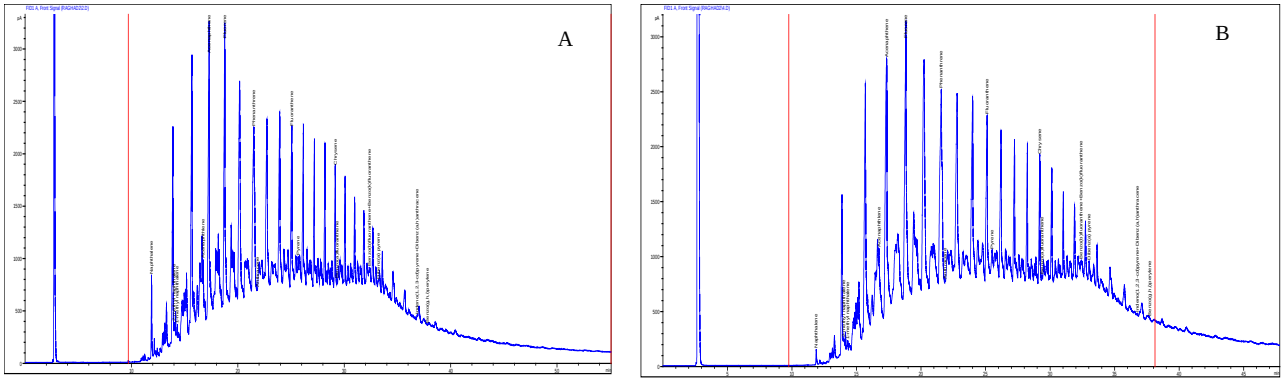

Figure1. Sample A consisted of Crude oil (Aromatic fraction, 5%) combined with *S. Paucimobilis*, whereas sample B contained Crude oil (Aromatic fraction 5%) without *S. Paucimobilis*. Both samples were subjected to a 24-hour incubation period.

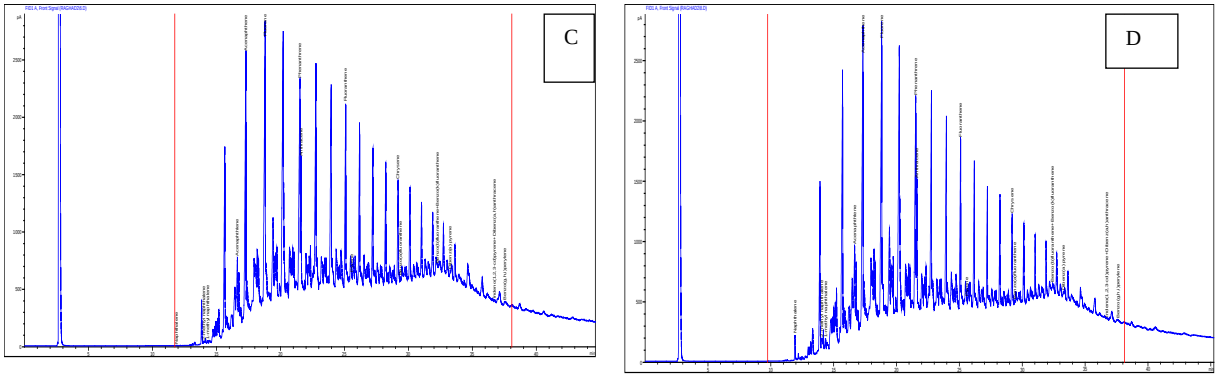

Figure2. Sample C contained Crude oil with an aromatic fraction of 2%, along with *S. Paucimobilis*, while sample D contained Crude oil with an aromatic fraction of 2% without *S. Paucimobilis*. Both samples underwent a 24-hour incubation period.

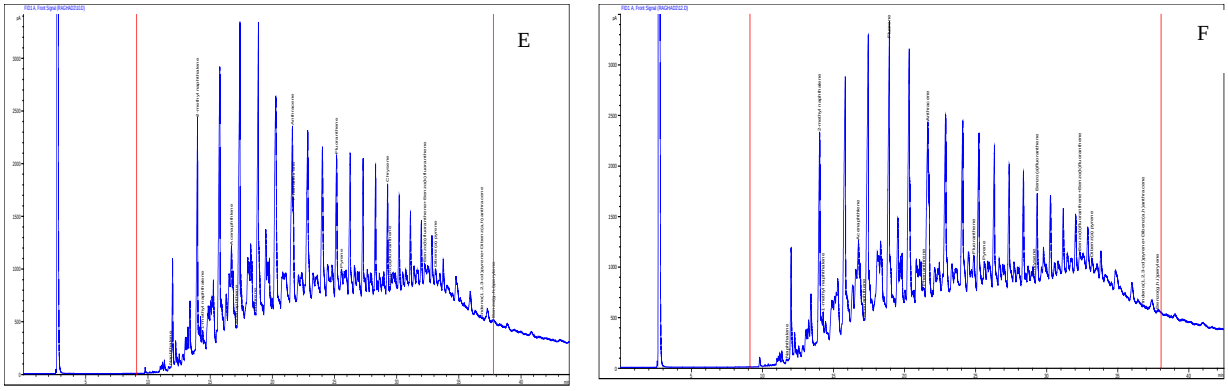

Figure3. E Crude oil (Aromatic fraction, 5%) with *S. Paucimobilis* and F: Crude oil (Aromatic fraction 5%) without *S. Paucimobilis.* 28 days' incubation period.

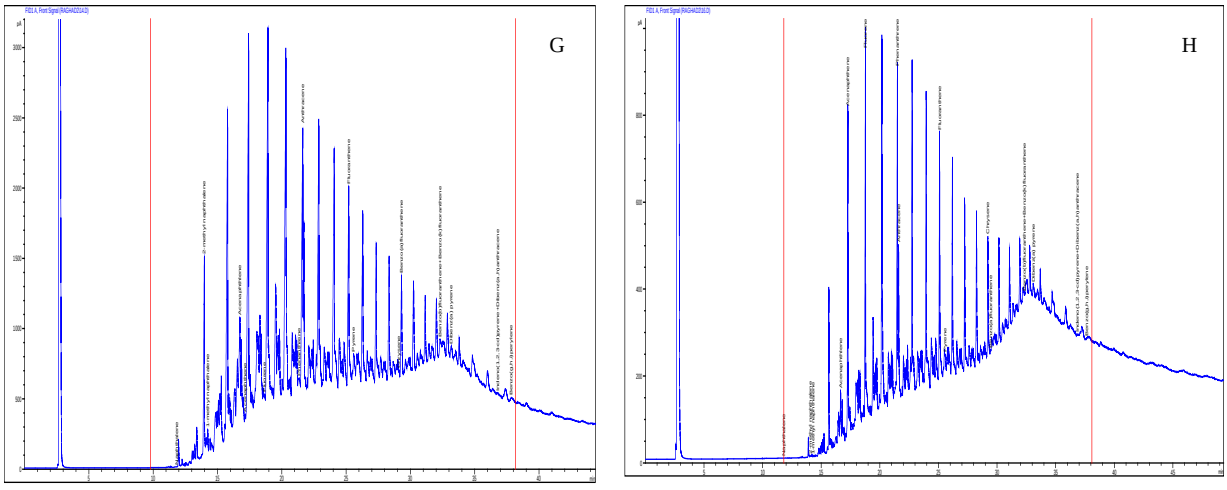

Figure4. E Crude oil (Aromatic fraction, 2%) with *S. Paucimobilis* and F: Crude oil (Aromatic fraction 2%) without *S. Paucimobilis.* 28 days' incubation period.

4. Conclusion

In conclusion, this research highlights the potential of Sphingomonas bacteria in bioremediation, especially for removing heavy metals and aromatic hydrocarbons from polluted environments. The bacteria exhibited strong tolerance to high levels of lead and cadmium, achieving significant removal rates. Additionally, Sphingomonas demonstrated the ability to degrade a variety of aromatic hydrocarbons, indicating its versatility in addressing different contaminants. These findings emphasize the value of using Sphingomonas as a sustainable solution for pollution cleanup. Further exploration and application of these bacteria could play a crucial role in enhancing bioremediation techniques and promoting environmental conservation.

5. Grant Details

The research was self-funded, as it was not conducted using any external support.

6. Conflicting Interests and Ethics

The authors assert that there are no conflicts of interest associated with the publication of this manuscript. Furthermore, they confirm strict adherence to ethical guidelines, encompassing plagiarism, informed consent, misconduct, data fabrication or falsification, double publication or submission, and redundancy.

7. Life Science Reporting

This research did not involve any experiments that posed a threat to life sciences.

References

Afzal, A.M., Rasool, M.H., et al., 2017. Assessment of heavy metal tolerance and biosorptive potential of Klebsiella variicola isolated from industrial effluents AMB Express 7, 184, 1–9.

Andrea, M., Huët, L., et al., 2017. Bioremediation of heavy metals from aquatic environment through microbial processes: A potential role for probiotics? J. Appl. Biol. Biotechnol. 5, 6, 14–23.

Azadi, D. & Shojaei, H., 2020. Biodegradation of polycyclic aromatic hydrocarbons, phenol and sodium sulfate by Nocardia species isolated and characterized from Iranian ecosystems Sci. Rep. 10, 1.

Campillo-Cora, C., González-Feijoo, R., et al., 2023. Do heavy metals affect bacterial communities more in small repeated applications or in a single large application? J. Environ. Manage. 325, 116494.

Chhetry, A.K., Dhakal, S., et al., 2022. Study of Antibacterial Activity of Root Bark, Leaves, and Pericarp Extracts of Diploknema butyracea and Evaluation of Prospective Antioxidant Activity J. Trop. Med. 2022, 12.

Dong, Y., Gao, Z., et al., 2023. Study on the Effectiveness of Sulfate Reducing Bacteria to Remove Heavy Metals (Fe, Mn, Cu, Cr) in Acid Mine Drainage Sustainability 15, 5486.

Etorki, A.M., El-Rais, M., et al., 2014. Removal of Some Heavy Metals from Wastewater by Using of Fava Beans Am. J. Anal. Chem. 05, 04, 225–234.

Farid, 2006. Effect of plant extracts on the microbial degradation of petroleum University of Basrah.

Fu, B., Li, Q.X., et al., 2014. Sphingobium sp. FB3 degrades a mixture of polycyclic aromatic hydrocarbons Int. Biodeterior. Biodegradation 87, 44–51.

Fuchs, G., Boll, M., et al., 2011. Microbial degradation of aromatic compounds — from one strategy to four Nat. Rev. Microbiol. 9, 803–816.

Ghosal, D., Ghosh, S., et al., 2016. Current state of knowledge in microbial degradation of polycyclic aromatic hydrocarbons (PAHs): A review Front. Microbiol. 7, AUG.

Haritash, A.K. & Kaushik, C.P., 2009. Biodegradation aspects of Polycyclic Aromatic Hydrocarbons (PAHs): A review J. Hazard. Mater. 169, 1, 1–15.

Jaafar, R.S., 2019. The potential role of sphingomonas paucimobilis in bioremediation of soils contaminated with hydrocarbon and heavy metal Malaysian J. Sci. 38, 3, 48–58.

Kertesz, M.A., Kawasaki, A., et al., 2018. Aerobic Hydrocarbon-Degrading Alphaproteobacteria: Sphingomonadales.

Li, D., Li, K., et al., 2023. Synergistic PAH biodegradation by a mixed bacterial consortium: based on a multi-substrate enrichment approach Environ. Sci. Pollut. Res. 30, 9, 24606–24616.

Li, Q., Huang, Y., et al., 2020. Application of alkyl polyglycosides for enhanced bioremediation of petroleum hydrocarbon-contaminated soil using Sphingomonas changbaiensis and Pseudomonas stutzeri Sci. Total Environ. 719, 137456.

Ma, Y., Li, X., et al., 2018. Remediation of hydrocarbon–heavy metal co-contaminated soil by electrokinetics combined with biostimulation Chem. Eng. J. 353, 410–418.

Manikant Tripathi , Sukriti Pathak 1, Ranjan Singh , Pankaj Singh Pradeep Kumar Singh , Awadhesh Kumar Shukla , Sadanand Maurya, S.K. and B.T., 2024. A Comprehensive Review of Lab-Scale Studies on Removing Hexavalent Chromium from Aqueous Solutions by Using Unmodified and Modified Waste Biomass as Adsorbents toxics Rev. 12, 657, 1–21.

Medić, A.B. & Karadžić, I.M., 2022. Pseudomonas in environmental bioremediation of hydrocarbons and phenolic compounds- key catabolic degradation enzymes and new analytical platforms for comprehensive investigation World J. Microbiol. Biotechnol. 38, 10, 165.

Mishra, A. & Mishra, K.P., 2018. Bacterial Response as Determinant of Oxidative Stress by Heavy Metals and Antibiotic J. Innov. Pharm. Biol. Sci. 2, 3, 229–239.

Oziegbe, O., Oluduro, A.O., et al., 2021. Assessment of heavy metal bioremediation potential of bacterial isolates from landfill soils Saudi J. Biol. Sci. 28, 7, 3948–3956.

Pandolfo E., A.B.C. and L.R., 2023. Recent Advances in Bacterial Degradation of Hydrocarbons water 15, 375.

Sodhi, K.K., Kumar, M., et al., 2020a. Multi-metal resistance and potential of Alcaligenes sp. MMA for the removal of heavy metals SN Appl. Sci. 2, 11.

Sodhi, K.K., Kumar, M., et al., 2020b. Multi-metal resistance and potential of Alcaligenes sp. MMA for the removal of heavy metals SN Appl. Sci. 2, 11, 1885.

Srivastava, S. & Kumar, M., 2019. Biodegradation of polycyclic aromatic hydrocarbons (PAHs): A sustainable approach In: Sustain. Green Technol. Environ. Manag. 111–139.

Tangaromsuk, J., Pokethitiyook, P., et al., 2002. Cadmium biosorption by Sphingomonas paucimobilis biomass Bioresour. Technol. 85, 1, 103–105.

Truskewycz, A., Gundry, T.D., et al., 2019. Petroleum Hydrocarbon Contamination in Terrestrial Ecosystems — Fate and Microbial Responses 1–20.

Varjani, S. & Upasani, V.N., 2017. A new look on factors affecting microbial degradation of petroleum hydrocarbon pollutants Int. Biodeterior. Biodegradation 120, 71–83.

Xu, X., Liu, W., et al., 2018. Petroleum Hydrocarbon-Degrading Bacteria for the Remediation of Oil Pollution Under Aerobic Conditions : A Perspective Analysis 9, December, 1–11.

Xue, W. and D.W., 2005. Metabolic activation of polycyclic and heterocyclic aromatic hydrocarbons and DNA damage: A review texiocology Appl. Pharmacol. 206, 1, 73–93.

Zhang, L., Liu, H., et al., 2022. Unveiling degradation mechanism of PAHs by a Sphingobium strain from a microbial consortium mLife 1, 3, 287–302.

Zhou, L., Li, H., et al., 2016. Sphingomonas from petroleum-contaminated soils in Shenfu, China and their PAHs degradation abilities Brazilian J. Microbiol. 47, 2, 271–278.

Zhou, M., Liu, Z., et al., 2022. *Sphingomonas* Relies on Chemotaxis to Degrade Polycyclic Aromatic Hydrocarbons and Maintain Dominance in Coking Sites Microorganisms 10, 6, 1109.

JJBS

Volume 18, Number 2,June 2025
ISSN 1995-6673
Pages 281 – 290
https://doi.org/10.54319/jjbs/180209

Jordan Journal of Biological Sciences

Preparation and Characterization of *Newbouldia laevis* (P.Beauv.) Seem. mediated Gold and Alloy Nanoparticles and Evaluation of Its Bactericidal Effect on Clinical Pathogens

Oluwakemi Abike Thonda[1,*], Fatimah Adenike Ajadi[2], Olanrewaju Oludotun Daramola[3], Aderiike Adewumi Grace[4], Oludare Temitope Osuntokun[5], Daniel Ayandiran Aina[1], Temitope Elizabeth Oyewole[1], Rukevwe Collins Etareri[1]

[1] Department of Microbiology, School of Science and Technology, Babcock University, Ilishan- Remo, Ogun State, Nigeria; [2]Department of Microbiology, Faculty of Sciences, Federal University of Health Sciences, Ila Orangun, P.M.B 204, Osun Nigeria; [3]Department of Physics, Lead City University, Ibadan, Nigeria; [4]Department of Basic Sciences, School of Science and Technology, Babcock University, Ogun State, Nigeria; [5]Department of Microbiology, Faculty of Science, Adekunle Ajasin University, Akungba Akoko. Ondo State Nigeria.

Received: July 5, 2024; Revised: September 25, 2024; Accepted: November 7, 2024

Abstract

Green synthesized nanoparticles using medicinal plants has become optimistic which can overcome the challenges of antimicrobial resistance while also providing additional benefits, such as cost-effectiveness and sustainability. The study, therefore, seeks to synthesize gold and alloy nanoparticles using *Newbouldia laevis* (P.Beauv.) Seem extracts and investigate their anti-bacterial property against multidrug pathogenic bacterial strains. The characterization of the nanoparticles synthesized was carried out using Ultra violet visible spectroscopy, fourier transform infrared spectroscopy, scanning and transmission electron microscope, energy dispersive analysis, and X-ray diffractive. The antibiotic susceptibility of the test organism and anti-bacterial effects of the synthesized nanoparticles were evaluated using disc diffusion and agar-well diffusion method, respectively. The absorbance peak results of the gold and alloy nanoparticles range between 228 - 530 nm, while the band gap of each is at 3.46 eV and 3.52 eV, respectively. The gold and alloy nanoparticles showed almost similar functional groups which ranged between 464.90 cm^{-1} and 3426.25 cm^{-1}. The shape of the synthesized nanoparticles was spherical, and the average particle size was 34.61 nm and 79.86 ± 32.11 nm, respectively. The gold and alloy nanoparticles inhibited the organisms at varying levels. The gold nanoparticles highest zone of inhibition was 23.5 mm against *Pseudomonas aeruginosa*, while alloy nanoparticle was 20 mm against *Staphylococcus aureus*. The synthesized gold and alloy nanoparticles using *Newbouldia laevis* extract showed increased sensitivity rate against the multidrug resistance organisms, which can be related to the presence of functional groups and bioactive compounds. This may be useful in various clinical applications, may reduce the resistance of these bacteria to antibiotics, and may be used as drug delivery systems.

Keywords: Alloy-*Newbouldia laevis*, Bactericidal effect, Green synthesis, Medicinal plant, *Newbouldia laevis*, *Newbouldia laevis*-nanoparticles.

1. Introduction

Since the use of plants to make herbal drugs combinations, it has greatly improved human health and their wellbeing, these plants have historically offered hope and life for new therapeutic substances. Ascorbic acid, phenols, citric acid, polyphenols, flavonoids, alkaloids, and terpenoids are the main classes of bioactive substances found and present in plants. (Timoszyk, 2018; Stozhko et al., 2019). Numerous substances under these categories of compounds possess antioxidant activities as well as the capacity to convert gold ions into metallic gold (Sathishkumar et al., 2018). It has been demonstrated that a variety of secondary metabolites present in plants, such as flavonoids, alkaloids, terpenoids, and tannins, have anti-microbial properties *in-vitro* and are abundant in plants (Singh et al., 2016). *Newbouldia laevis* (*N. laevis*) often refers to as the "Tree of Life" or boundary-tree, and is one of the magical plants (Byrappa et al., 2008). *N. laevis* is a growing plant with a height of approximately 7-8 (up to 15) meters. *N. laevis* is an average-sized angiosperm that is a member of the Bignoniaceae family. Searching for substances which possess antimicrobials and property in plants and plant parts are necessary because of their wide spread usage in treatments of variety of infections, infectious diseases and health-related problems. *Newbouldia laevis* is a plant that is frequently planted as an ornamental. Its leaves are glossy and dark-green in colour, enormous, spectacular purple-lilac blooms, and can be easily planted and replicated. Essentially, it is a symbolic or sacred tree that is planted effectively as a fence and frequently allowed to spread into a stockade. The stem, the fruits, and the leaves have been used as a

* Corresponding author. e-mail: thondao@babcock.edu.ng .

febrifuge for dressing of wound, and as a medicine for stomachaches (Iwu, 2000). It has been scientifically reported that *N. laevis* have medicinal value which ranged from anti-inflammatory to anti-oxidant, anti-microbial, anti-fungi, pain-killer and wound healing properties (Makarov et al., 2014; Omeje et al., 2020). To be precise, it has been claimed that combining stem bark with clay and red pepper can effectively treat many illnesses, such as bone lesions, and prevent pneumonia, fever, colds, and cough (Byrappa et al., 2008). In Africa, traditional medicine frequently used *N. laevis* to cure certain conditions like coughs and cold, toothaches, malaria, fever, stomachaches, STDs, constipation and breast cancer, eye problems and dysentry (Arbonnier, 2004; Ugwoke et al., 2024).

There are several names for *N. laevis*, often known as the boundry tree which is the common name, including Aduruku (Hausa), Ogirisi (Igbo), and Akoko (Yoruba). According to Usman and Osuji (2007), the bark is chewed and consumed in Nigeria to treat toothaches, diarrhea, and stomachaches. Swollen legs (Elephantiasis), syphilis, dysentry, rheumatism swellings, constipation, piles, and roundworms have all been successfully treated with the plant. According to Usman and Osuji (2007), boundry tree has also been reported to be helpful for chest discomfort, epilepsy, earaches, aching feet, and convulsions in youngsters. People have used the fruits, leaves, and stem as remedies for stomachaches, wounds, fevers, and other ailments (Obum-Nnadi, et al., 2020). Plants play important roles in our daily activities, right from the use of plants as food, such as vegetables, to their use as medicine for treating infections and in post-harvest storage of some agro commodities for security purposes. The plant is used to cure septic wounds and eye infections in parts of South Eastern and Midwestern Nigeria (Usman and Osuji, 2007). Obum-Nnadi et al. (2020) reported in their research findings the phytochemical and active compounds present in plants to be alkaloids and phenyl propanoids detected in the root, flavonoids, and tannins found in the leaf. Additionally, *N. laevis* is rich in diverse bioactive compounds, including tannins, terpenoids, and flavonoids, making it an ideal candidate for addressing the global issue of Antimicrobial Resistance (AMR). Furthermore, *N. laevis* has a wealth of different bioactive substances, such as flavonoids, terpenoids, and tannins, which makes it an excellent option for combating the global challenge of antimicrobial resistance (AMR).

Green synthesis that uses bacteria, fungus, plants, actinomycetes, algae, and other microorganisms, may be used as a cost-effective, environmentally benign, and a biocompatible method (Sathishkumar et al., 2018; Bachheti et al., 2020; Riaz et al., 2023). During green synthesis, several of phytochemical compounds, such as alkaloids, terpenoids, and phenolics assist in lowering and stabilizing metal ions (Khanna et al., 2019). A quite number of researchers have investigated the synthesis of metallic nanoparticles such as alloys, silver, and gold using various plant parts like leaves and barks. Thirumurugan et al. (2010) reported the synthesis of gold-nanoparticles using the *Azadirachta indica* plant, while Singh and Kochhar (2012) reported the production of gold nanoparticles using extracts from the leaves and bark of *Ficus carica*. Gold nanoparticles (AuNP) have been used as laboratory tracers in DNA finger-printing to find the presence of DNA in samples and immune-chemical experiments for protein interactions discovery. Additionally, they have been used to identify aminoglycoside drugs including gentamycin, neomycin, and streptomycin. In order to diagnose cancer and distinguish different bacterial groups, gold nanorods are essential for detecting cancer stem cells (Tomar *et al.*, 2013). The alloy nanoparticles' structural characteristics are different from those of their bulk counterparts. Bimetallic alloy nanoparticles, in particular, showed advantages above regular metallic nanoparticles (Mohl *et al*., 2011). According to Sánchez-López et al. (2020), metallic nanoparticles have demonstrated efficacy against a varieties of infections as well as selectivity for specific bacterial strains. Furthermore, to combat antibiotic resistance and boost the effectiveness of antibiotics, metallic nanoparticles have been used in combination with them (Allahverdiyev et al., 2011; Ghasemi and Jalal, 2016). Different nanoparticles suppress pathogens by different ways; for example, metallic NPs particularly have been revealed to penetrate cell walls of bacteria and form pores on the surface of the membranes, which results in creation of free radicals that damage the cell membrane (Acharya et al., 2023).

Plants generally have been reported and identified to be a huge source of novel drug compounds, which has contributed to human health and wellbeing. Plants such as *N. leavis* are rich in varieties of bioactive compounds such as tannins, terpenoids, flavonoids and many more. Scientific reports on the phytochemical constituent of the plants make it a better drug candidate. However, antimicrobial resistance (AMR) today is a major global problem that needs urgent attention as to find alternative therapy and research for novel drug candidate that can be used to tackle AMR. However, the goal of this study was to examine the characterization of *N. leavis* mediated gold and alloy nanoparticles and to determine their anti-microbial properties against pathogenic microorganisms of clinical importance.

2. Materials and Methods

2.1. Sample Collection and Organisms

Fresh *N. laevis* leaf sample were obtained from Ilishan-Remo Ogun State, Nigeria; they were identified by plant taxonomist and authenticated in the Department of Botany, University of Ibadan, Oyo State, Nigeria. The culture media used for culturing the isolates were MacConkey agar, Mannitol salt agar and nutrient agar (Himedia Laboratories Pvt. Ltd., Mumbai, India). The clinical isolates such as *Pseudomonas aeruginosa (P. aeruginosa*), *Escherichia coli* (*E. coli*), *Proteus vulgaris* (*P. vulgaris*), *Listeria monocytogenes* (*L. monocytogenes*), and *Staphylococcus aureus* (*S. aureus*) used as test organisms for gold and alloy nanoparticles were multidrug resistance pathogens and obtained from Microbiology Department, Babcock University, Ilishan, Ogun State, Nigeria.

2.2. Preparation of Newbouldia laevis extract

Aqueous extraction of the samples was prepared according to Aina *et al.*, 2018. Briefly, the plants were air dried at room temperature, and pulverized into fine powder. Five (5 grams) of the powdered samples was dispensed in 50 ml of distilled water and heated in the

water bath for twenty minutes. The solution was allowed to cool and filtered (Whatman filter paper No. 1); centrifugation was done at 4000 rpm for fifteen minutes. The supernatant was collected inside bottle and kept for further analysis and was used for the synthesis of the NP.

2.3. Preparation of 1 mM Gold and 1 mM Alloy

Approximately, 0.2589g of tetrachloroauric(III)acid trihydrate ($HAuCl_4 \cdot 3H_2O$) and silver nitrate ($AgNO_3$) (0.1699g) were dissolved in 1000ml of water to obtain 1 mM concentrations of gold and silver, respectively**.** The preparation of the alloy was done at 50:50 mixture ratio of silver and gold salts.

2.4. Preparation and Confirmation of organisms

The test organisms were collected and were resuscitated by sub-culturing on macConkey agar and nutrient agar. The organisms were inoculated by using four quadrant streaking method, followed by incubation at 37℃ for 18 hours. They were re-identified to confirm the identity using standard methods according to Thonda et al. (2020). The test organisms were standardized following 0.5 McFarland's standard ($x10^8$CFU/ml) using the spectrophotometer at 600 nm; the test organisms were then introduced into 2 ml of normal saline in a test tube to maintain bacterial activity by controlling the turbidity of the suspension. Each test tube was labelled according to the name of the organism.

2.5. Synthesis of Gold and Alloy nanoparticles

The biological synthesis of (gold and alloy) nanoparticles with *N. laevis* was done by introducing approximately 1 ml of the extract to each of the reaction vessels which contains forty milliliters (40 ml) of 1 mM gold and alloy solution respectively. Under static conditions, the reaction was carried out at room temperature (37 ℃ for 2 hours). The solutions were then put under sunlight for 30 minutes after thorough shaking to obtain visible colour change.

2.6. Characterization of N. laevis synthesized Gold and Alloy Nanoparticles

The UV-visible analysis of the NP was carried out using Shimadzu UV-visible (UV-1650PC) spectrophotometer with scan between 200 and 800 nm. The vibrational frequencies of the nanoparticles were determined through Fourier Transform Infrared Spectroscopy (FTIR) (model 84005 Shimadzu, Japan) transmission spectra by potassium bromide (KBr) as described by Liaqat *et al*. (2022). Fourier transform infrared spectroscopy analysis was carried out to identify the functional group present that assists in the synthesis of NP. The synthesized NP were further characterized using Scanning Electron Microscope (SEM) to determine the shape of the nanoparticles. Transmission Electron Microscope (TEM) was used for imaging and analytical characterization of the nanoparticles size and morphology and distribution of the NP, while Electron Diffractive X-ray analysis (EDX) analysis was conducted to identify the composition of elements of the synthesized nanoparticles present, and X-ray diffraction (XRD) analysis was carried out to analyze the crystalinity of the NP. The results were recorded (Varadavenkatesan et al., 2021; Oyewole et al., 2023).

2.7. Antibiotic Sensitivity Testing of the test organisms

The susceptibility testing of the test organisms was evaluated using Kirby - bauer disk diffusion methods (Thonda et al., 2021; Bale et al. 2022). The array of antibiotics and its concentration used were gentamycin (10 µg), augmentin (30 µg), ofloxacin (5 µg), ceftazidime (30 µg), cefixime (30 µg), ciprofloxacin (5 µg). nitrofurantoin (300 µg), and ceftriazone (30 µg). Briefly, the test organisms were standardized and inoculated by streaking onto Mueller Hinton agar plates; they were allowed to diffuse after the antibiotic disk was then placed gently on the plates. Incubation of the plates was done in an inverted position at 37 ℃ for 24 hours. The resultant zone diameter of inhibition was measured and recorded.

2.8. Antimicrobial activities assay of N. laevis gold and alloy synthesized nanoparticles

Determination of antimicrobial activities of the gold nanoparticles (AuNP-NL), and alloy nanoparticles (AlloyNP-NL), was carried out using agar well diffusion method. The NP gradient concentrations were prepared at various concentrations ranging from 10-100 µg/ml. Approximately, 750 ml of Mueller Hinton agar was prepared following the manufacturer's instruction; the media was dispensed into petri dishes and allowed to set. Each petri dish was labelled appropriately with gradient concentrations and control. Then, the test organisms were standardized following the McFarland standard; the standardized organisms were spread using a swab stick. A sterile cork borer (6 mm) was used to aseptically bore wells on each plate and appropriately labeled. A sterile micropipette was used to introduce approximately 0.1 ml each of the various concentrations of the synthesized AuNP-NL and AlloyNP-NL, including the control, into the bored holes. The incubation of plates were done at 37 ℃ for 24 hours (Oyewole et al., 2023). After incubation, the inhibition zone was examined and measured using a measuring ruler and the values were recorded in triplicates appropriately. These measurements were considered as the zone diameter of inhibition of the nanoparticles under investigation at different concentrations. Minimum inhibitory concentration and minimum bactericidal concentrations were determined using agar well diffusion method (Coyle 2005; Thonda et al., 2021).

3. Results and Discussion

Visual observation of the gold and alloy NP is depicted in Figure 2. Gold nanoparticles colour initially changed visually from colourless to light yellow and then changed to dark violet on addition of *N. laevis* extract as shown in figure 2a while alloy NP colour changed visually from colourless to dark purple on the addition of *N. laevis* extract, which acted as a reducing agent (Figure 2b). The colour changes that were obtained in the experiment indicated the formation of the respective nanoparticles. The colour variations observed in the solution indicated the presence of both gold and alloy NP, attributed to the activation of surface plasmon vibrations. The rapid consumption of reactants led to the generation of smaller nanoparticles. The absorbance peaks for the gold nanoparticles was observed at 301.25 nm at UV region and 530.72 nm at visible light region (Figure 3a). The formation of AuNP-NL was ascertained by the detection of

surface plasmon resonance (SPR) peak in UV–visible spectra analysis at 530nm resulting in the peak intensity which fall within limits (500 nm-600 nm). This maybe a result of surface plasmon resonance (SPR) features of gold nanoparticles. It has been reported that the colour variation in AuNP is thus due to the SPR features, which is dependent on the concentration, size, and shape of the NPs (He and Lu, 2018). The results of those findings are similar to the report of Dharman et al. (2023) who observed a dark yellow to dark greenish-yellow colour using cucurmin extract for the gold nanoparticles synthesis of with absorption peak at 530 nm which is a result of the excitation of the SPR (Dharman et al., 2023). The band gap was obtained at 3.46 eV as depicted in figure 3b. In figure 4a, the alloy nanoparticles (AlloyNP-NL) spectrum had peaks absorbance at 228.41 nm and 310.19 nm at the UV region and 529.57 nm at visible light region. The alloy NP band gap was obtained at 3.52 eV as shown in figure 4b. This is in line with the study of Fouda et al., (2022) who observed absorbance peak at 530 nm. Maliszewska et al. (2021) observed a single plasmon (SPR) band at 522 – 523 nm and reported that a single SPR peak appeareing at a λmax in the 520–540 nm region indicated the creation of tiny, spherical, and monodispersed AuNPs (Muddapur et al., 2022).

Figure 1: Visual observation of NP before and after exposure to sunlight (A) Gold nanoparticles before and after (B) Alloy nanoparticles before and after being synthesized with *Newbouldia laevis.*

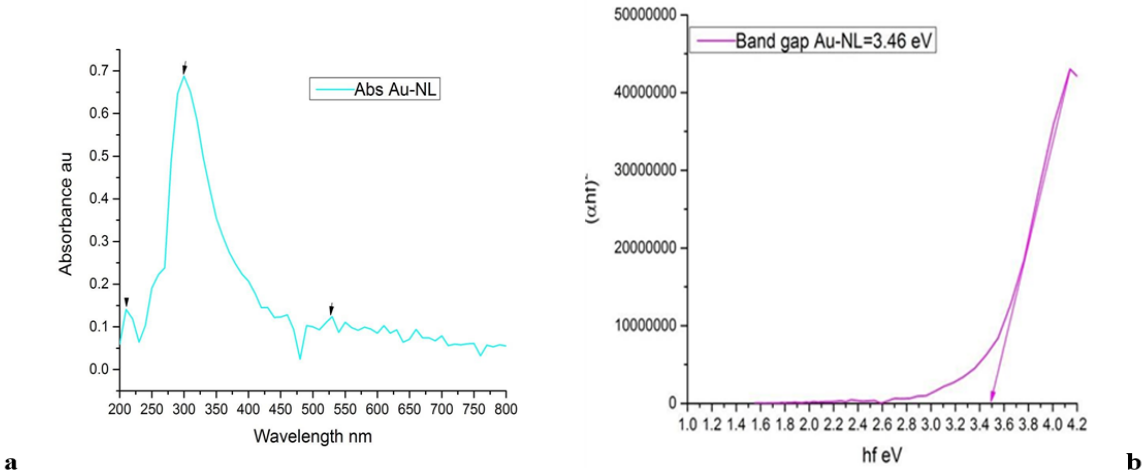

Figure 2: (a) UV-Vis Spectra of AuNp-NL showing the absorbance peak (b) Band gap of AuNp-NL showing at 3.46 eV

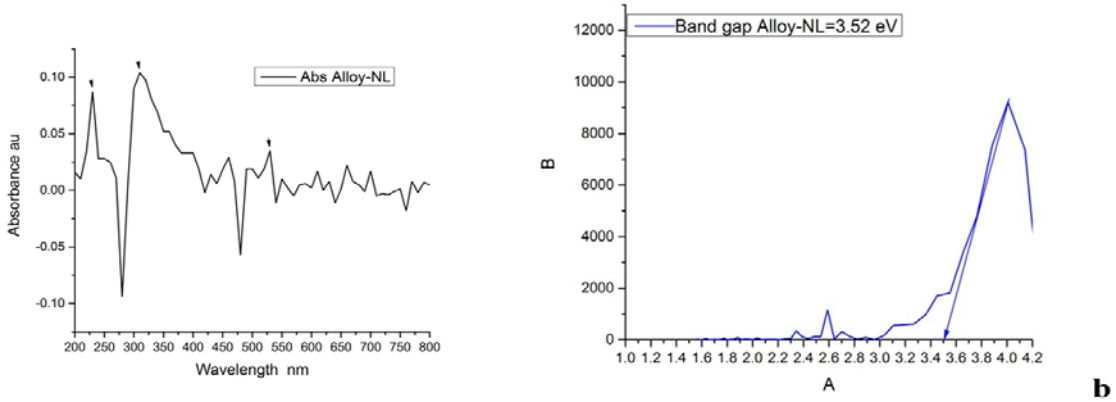

Figure 3: (a) UV-Vis Spectra of AlloyNp-NL showing the absorbance peak (b) Band gap of AlloyNps-NL showing at 3.52 eV

The FTIR analysis of the gold and alloy mediated nanoparticles *N. laevis* is depicted in Figure 5. The gold and alloy showed minimum absorbance peak at 464.90cm^{-1} and 470.96cm^{-1} respectively. However, the maximum absorbance peaks observed for gold nanoparticles was 3426.25cm^{-1} and 3419.33cm^{-1} for alloy nanoparticles in FTIR spectrum respectively. The gold NP showed 12 peak values while alloy nanoparticles showed 17 peak values (Figure 5). The extract's functional groups for the synthesized nanoparticles were identified using FTIR. Gold and the alloy nanoparticles investigated showed the same functional groups of Oxide of metal, Polysulfides (S-S stretch), -C-O-C- vibration, Secondary alcohol C-O stretch, gem-Dimethyl or ‘‘iso’’- (doublet), Methyl C-H asym./sym. Bend, CH stretching Vibration, methyne C-H stretch Symmetric CH_3 Stretch and –OH stretch. Whereas different functional groups detected in gold NPs are indicated at 659.62 cm^{-1} (aliphatic bromo compounds) and at 1626.25 cm^{-1} (C-Br stretch, Alkenyl C=C stretch). *N. leavis* has been reported to have some functional groups of compounds in which the peak ranges from 756.12cm^{-1} to 3448.84 cm^{-1}. The functional groups are: polychlorinated (C-Cl str.), nitramines (C-N vib.), secondary alcohol (C-O str.), tertiary alcohol (O-H Def.), secondary alcohol (O-H def.), alkanes (C-H def.), Nitrosamines (N=O str.), amino acid ($NH3^{+}$def.), ketones (C=O str.) and ketones (C=O overtone; C=O str.) (Omeje et al., 2020). Some functional groups such as secondary alcohol and alkanes were present in both *N. leavis* extract and the synthesized NP. Similarly, different functional groups were found for alloy at 907.98 cm^{-1} (Vinyl C-H out of plane bend) and at 1572.60 cm^{-1} (Secondary amine, >N-H bend) respectively. As a result of the presence of bioactive phytochemicals in the *N. laevis*, leaves extract such as alkaloids flavonoids, and tannins as revealed by Obum-Nnadi, et al. (2020) has the capacity to convert gold and alloy into NP and stabilize the products. A broad peak in the range of 3426 to 3419 cm^{-1} was identified as O-H vibrations and or N-H stretches associated with N-substitute amide in this study. Aina *et al*. (2018) also reported the same peak as O-H stretch. The peaks at 2426 cm^{-1} and 2360 cm^{-1} were attributed to atmospheric carbondioxide (CO_2) absorption, suggesting that the nanoparticles possess CO_2 absorption capabilities. Furthermore, the 1384 cm^{-1} peak was linked with C-H in plane bending of alkenes and aromatics. The presence of these characteristic peaks confirmed the successful encapsulation of certain biomolecules, such as proteins and carbohydrates from *N. laevis* on the synthesized nanoparticles.

The gold and alloy nanoparticles shapes (Figure 6) were characterized using SEM. The results revealed the spherical polydispersed shape of AuNP-NL and AlloyNP-NL. The TEM image used to analyze the size distribution and average particle size of the NP is shown in Figure 7. The sizes of the particle vary from 15 to 60 nm, with the majority of particles for AuNP-NL falling between 35 and 40 nm in size. The average particle size of AuNP-NL was 34.61 nm in size (Figure 7A), while the average particle size of the AlloyNP-NL and its standard deviation was 79.86 ± 32.11 nm (Figure 7B). The size of the gold NP is comparable to the study of Tao et al. (2019), which found that the nanoparticles were spherical in shape and highly crystalline in nature; AuNPs with particle sizes of 20–60 nm were prepared and thereby reduced $HAuCl_4$ using aqueous extract of *aloe-vera* leaves while the extract was being protected. AuNPs were also found to have good stability and to be less prone to oxidation and agglomeration. The size of the NPs reported in this study is in line with the report of Huang et al. (2019) who found that the average particle sizes of AuNPs produced using the *Dillenia indica* aqueous leave extract ranged from 5 to 50 nm, while those formed using *Garcinia mangostana* aqueous extracts peel and *Mentha longifolia* leaves were 32.9 ± 5.3 nm and 36.4 nm, respectively (Lee et al., 2016; Li et al., 2021). The secondary metabolites identified from plants varied between the plants and are utilized as stabilizing, capping, and reducing agents which may be responsible for the variance in particle sizes.

Element dispersive (EDS) analysis of AuNP-NL and AlloyNP-NL synthesized from *N. laevis* is depicted in Figure 8. Signals of Gold were found in AuNP-NL at 74.72 weight % along with other elements of C (4.50 wt. %) and O (20.68 wt. %) with composition percentage which showed the purity of the synthesized AuNP-NL (Figure 8a). However, the alloyNP-NL showed Au element in 75.56 wt. % along with other elements of C, Fe, O and Na with 5.34, 7.40, 13.37 and 3.30 wt. % respectively. It was noticed that Au content was in higher percentage in the AuNP-NL and AlloyNP-NL (Figure 8b). The signals from the other elements in the EDS could be the result of compounds that are partially or fully bound to the alloyNP and AuNPs. The corresponding XRD patterns of the NP are presented in Figure 8c and 8d. Gold nanoparticles and AlloyNP-NL exhibited the same five distinct peaks at 2θ. All five peaks attributed to crystallographic planes corresponded to standard Bragg reflections (110), (111), (121), (200) and (311) of the face center cubic (fcc) lattice plan according to JCPDS files. The crystalline form of the *N. laevis* nanoparticles is confirmed by the observation of distinctive Bragg diffraction peaks (Kratosova et al., 2013).

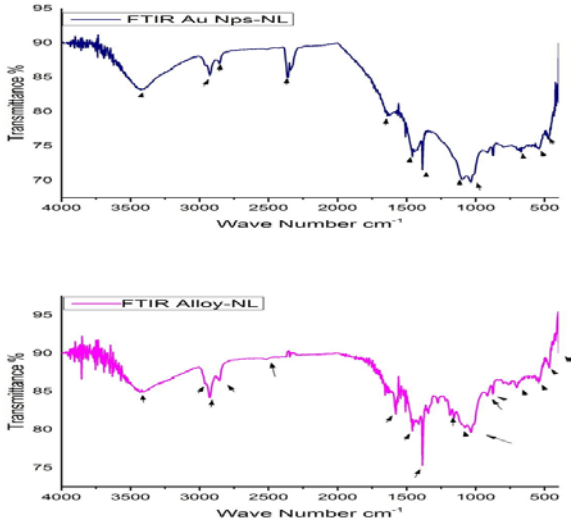

Figure 4: FTIR spectra for AuNP-NL and AlloyNP-NL synthesized nanoparticles

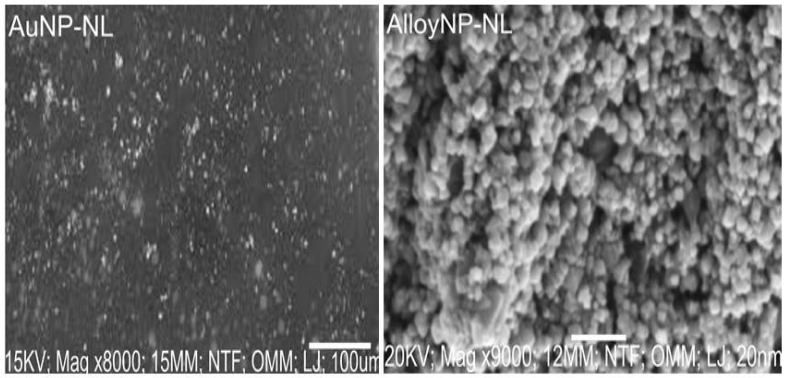

Figure 5: SEM Images of *N. laevis* mediated gold and alloy NP

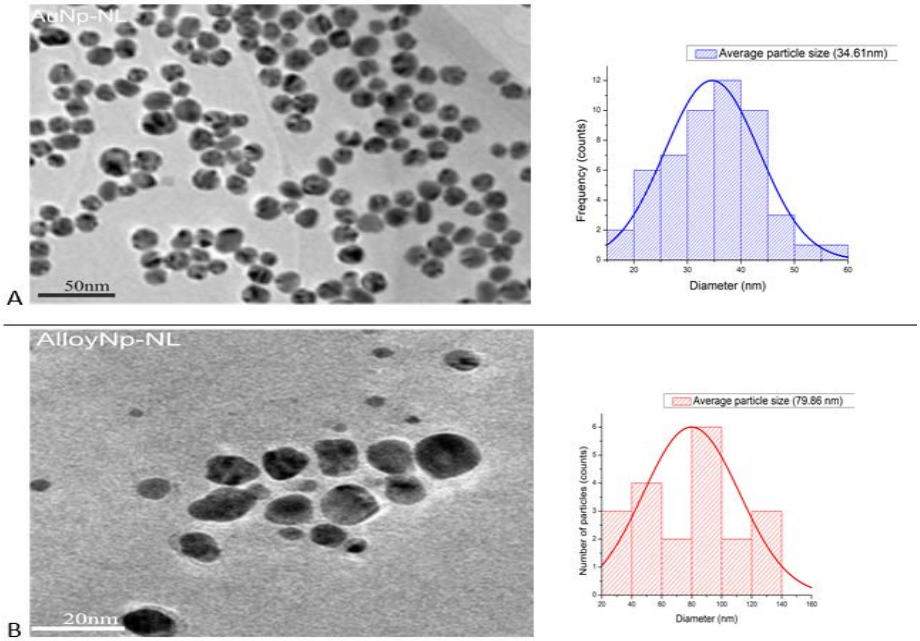

Figure 6: TEM Images and Histogram distribution of the Particles Size (A) AuNP-NL (B) AlloyNP-NL

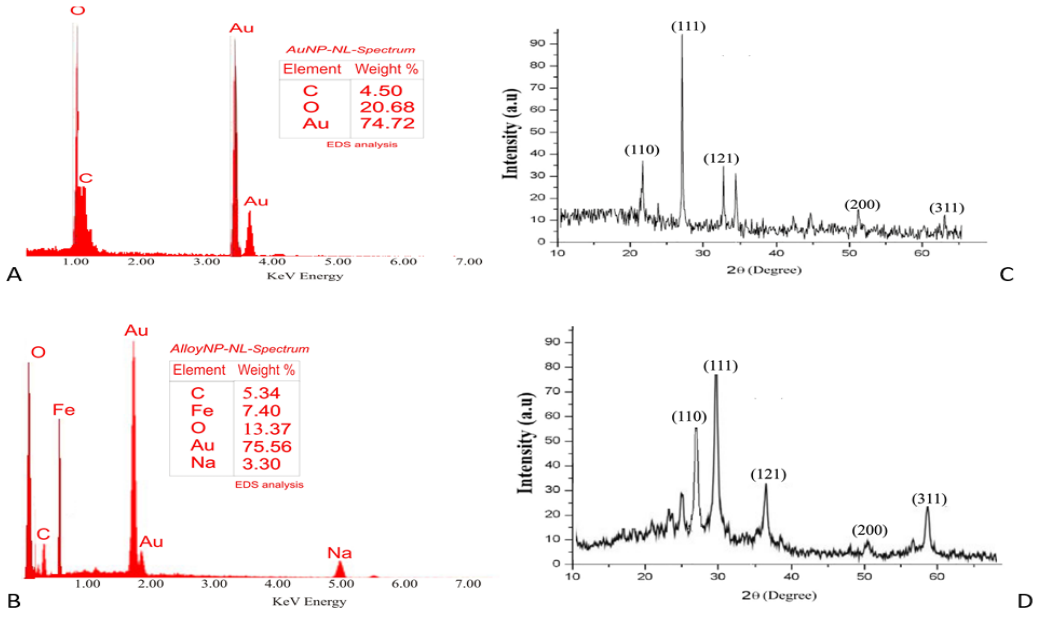

Figure 7: EDS analysis of AuNP-NL (A), AlloyNP-NL (B) and XRD spectra of AuNP-NL (C), AlloyNP-NL (D) synthesized from *N. laevis*

The evaluation of the antibiotic sensitivity test was carried out on the organisms (*P. aeruginosa*, *P. vulgaris*, *E. coli*, *L. monocytogenes* and *S. aureus*) as depicted in Figure 9. The zones of inhibition of each organisms were measured in millimetre (mm). The results showed that all the test organisms were 100% resistant to augmentin, ceftazidime, cefixime and ceftriaxone; they showed no inhibition zones against all tested bacterial strains, while the organisms showed 40% resistant to nitrofurantoin. However, they are 100% susceptible to gentamicin, ofloxacin and ciprofloxacin (Figure 9). The effectiveness of commercially used antibiotics varied across different bacterial strains, indicating the importance of choosing appropriate antibiotics based on bacterial susceptibility profiles to ensure effective treatment. Additionally, the data underscores the emergence of antibiotic resistance in certain bacterial strains, highlighting the reason for judicious antibiotic use and the development of possible alternative treatment strategies.

The evaluation of anti-bacterial activities of AuNP-NL, AlloyNP-NL, positive and negative control, was examined against test organisms namely *P. aeruginosa*, *P. vulgaris*, *E. coli*, *L. monocytogenes* and *S. aureus*. The zones of inhibition (mm) are represented in Tables 1 and 2 respectively. There was no inhibition zone (anti-bacterial activity) observed at concentrations of 10 µg/ml and 20 µg/ml (the lowest concentrations) as well as the negative control (water) for all tested organisms. The organisms were sensitive to ciprofloxacin antibiotics (positive control) as it showed inhibitory zones ranging from 15.5 mm and 26 mm. Zones of inhibition were observed at 40 µg/ml for all strains, except *P. vulgaris*, which showed no activity at 40 µg/ml (Table 1). The synthesized nanoparticles are concentration-dependent as there is a clear trend of increasing antibacterial activity with increase in concentration. The AuNP was more effective at higher concentration as compared to ciprofloxacin. All bacterial strains showed maximum zones of inhibition at the highest concentration tested (100 µg/ml). The higher the concentration is, the better is the activity of the synthesized nanoparticles. The anti-bacterial activity of the alloy nanoparticles against test organisms is presented in Table 2. The Alloy-NP exhibit significant antibacterial activities especially at higher concentrations as compared to the negative control as compared to the positive control which showed wide zones of inhibition against all the organisms. *P. aeruginosa* and *P. vulgaris* exhibited inhibition zones only at higher concentrations (60 µg/ml and above). *Staphylococcus aureus* showed an irregular inhibition pattern, but significant inhibition was at higher concentration. *E. coli* and *L. monocytogenes* showed a consistent increase in inhibition zones from 40 µg/ml. There was no activity for synthesized alloy nanoparticles at 10 µg/ml and 20 µg/ml; No inhibition zone against *P. aeruginosa* and *P. vulgaris* at 40 µg/ml as shown in Table 3. As the concentrations of alloy nanoparticles increased, the antibacterial activities also increased. These nanoparticles could be promising candidates for treating infections, particularly those caused by resistant strains. The Minimum Inhibitory Concentration (MIC) of AuNP-NL and AlloyNP-NL was determined at concentrations 100, 50, 25, 12.5, 6.25 and 3.12 mg/ml. The results showed that the organisms were inhibited at concentrations 100, 50.0 25.0 and 12.5. The MIC of the gold and alloy nanoparticles was 50 and 25 mg/ml respectively, which indicated that nanoparticles are effective at higher concentrations. The minimum bactericidal concentration of both alloy and gold NP was recorded at 25 mg/ml.

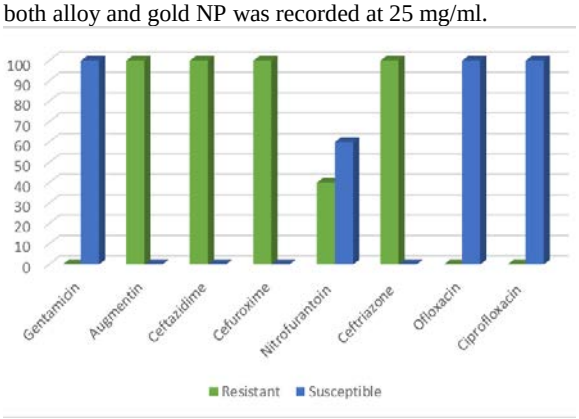

Figure 8: Antibiotic Susceptibility of the test organisms using disk diffusion method

Table 1: Antibacterial activity of synthesized AuNp-NL against test organisms using agar well diffusion method

Concentration	Ciprofloxacin (10µg)	Water	10	20	40	60	80	100
	Zones of inhibition (mm)							
Escherichia coli	15.5	0	0	0	8	10.5	12.5	18
L. monocytogenes	21	0	0	0	8.5	9.5	12.5	19
P. aeruginosa	23	0	0	0	10.5	11.5	15	23.5
P. vulgaris	26	0	0	0	0	10.5	12.5	17
S. aureus	25	0	0	0	8.5	9	12.5	21

Key: Concentrations are in µg/ml

Table 2: Zones of inhibition obtained from the synthesized AlloyNP-NL against pathogenic organisms using agar well diffusion method

Concentration	Ciprofloxacin (10 µg)	Water	10	20	40	60	80	100
	Zones of inhibition (mm)							
Escherichia coli	15.5	0	0	0	9	11.5	13.5	14
L. monocytogenes	21	0	0	0	7.5	10.5	13.5	14
P. aeruginosa	19	0	0	0	0	10.5	15.5	16.5
P. vulgaris	22.5	0	0	0	0	12.5	13.5	14
S. aureus	23	0	0	0	10.5	08	13.5	20

Key: Concentrations are in µg/ml

Medicinal plants are efficient remedies for a variety of disorders and conditions because they are easily available, cost effective, reliable, and have few to no adverse effects. Plants create bioactive or secondary chemicals as a defense strategy to ward off pests, attract pollinators, and aid in the survival of the species. There have been reports of medical benefits for *N. laevis*, including analgesic, anti-inflammatory, antioxidant, wound healing properties, antibacterial, and anti-fungal qualities (Akerele et al., 2011; Akande et al., 2020). The bark has traditionally been used to treat skin infections, Diarrhoea, tooth aches, stomach aches, fever, and other ailments are treated with a decoction of the bark. The present investigation revealed that the use of *N. laevis* in green synthesis facilitated the reduction of $HAuCl_4$ salt, thus, leading to the formation of

NP in just thirty minutes with the evidence of colour change. This supports the findings of Zangeneh and Zangeneh (2020) which showed that aqueous extract from *Hibiscus sabdariffa* flowers decreased $HAuCl_4 \cdot 3H_2O$ and produced spherical gold nanoparticles with a 15–45 nm particles size. To accomplish the green synthesis of AuNPs, *N. laevis* can be utilized as stabilizing and reducing agents and $HAuCl_4$ as the precursor. There have also been reports of the synthesis of AuNPs utilizing *Camellia sinensis* (green tea) extract as a reducing and stabilizing agent (Vilchis-Nestor et al., 2008).

This research showed that the gold and alloy nanoparticles have antibacterial activity against the test organisms which were able to inhibit all the organisms (*P. vulgaris, L. monocytogenes, P. aeruginosa, E. coli,* and *S. aureus*) at varying concentrations. From this study, it can be deduced that the antimicrobial activity of gold and alloy nanoparticles using *N. laevis* extract was high as compared to the control which showed no activity. The findings revealed that the alloy and gold nanoparticles exhibit potent antibacterial properties. This work is similar to that of Usman and Osuji (2007), who found that *N. leavis* extract had the broadest activity against the majority of the Gram negative pathogens they studied, including *Klebsiella* spp., *E. coli*, and *P. aeruginosa*. This further supports the results of Ayaz Ahmed et al. (2014), who found that gold nanoparticles made from the Indian plant *Salicornia brachiata* had strong antibacterial action against a number of pathogenic organisms, including *P. aeruginosa* and *E. coli* (Ayaz Ahmed et al. 2014). It was observed from this study that the higher the concentration, the more zones of inhibition obtained. This finding is consistent with the study by Fouda et al. (2022), which showed that the antibacterial efficacy of synthetic AuNP was contingent on dosage (dose-dependent). The findings of Muddapur et al. (2022) and Wani et al. (2013), which demonstrated that the anti-bacterial activity of biosynthesized NP depended on a number of variables, including concentration, size, and shape, are consistent with the findings of this study. The results of this study are in agreement with those of earlier reported studies (Inbaraj et al., 2020, Muniyappan et al., 2021). The main source of anti-bacterial activity is high surface to volume ratios, and the small size of nanoparticles facilitates their penetration of cell walls and membranes (Patil and Kim 2017; Wang et al., 2017). Using raw chemically produced AuNP, the dependence of antibacterial action on the size and concentration of AuNP was first confirmed and reported (Lavaee et al., 2021; Zhu et al., 2020). Numerous studies utilizing biosynthesized AuNP indicated that the stability, surface charge, and makeup of the AuNP envelope generated during the biological reduction process are the reasons for favorable antibacterial testing. These nanoparticles (gold and alloy) could be promising candidates for treating infections of those caused by the pathogenic strains.

4. Conclusion

The *N. laevis* mediated gold and alloy nanoparticles gotten from extract of exhibit significant and strong antibacterial properties against the pathogenic bacteria especially at higher concentrations which can be used as treating infections caused by these organisms. Higher concentrations are required for effective antibacterial activity, especially against multidrug resistant bacteria like *Pseudomonas aeruginosa* and *Proteus vulgaris*. Understanding the specific concentration thresholds for different bacteria is crucial for effective application. Further research into their mechanisms of action and potential clinical applications is warranted to fully explore their therapeutic potential.

Recommendations

1. Investigation into the mechanisms by which these gold and alloy nanoparticles *N. laevis* exert their antibacterial effects is necessary.
2. Additional studies could focus on optimizing nanoparticles synthesis and exploring their efficacy in clinical settings.

Authors Contribution

TOA and ADA conceptualized the experimental design and TOA, ERC, OTE, OOD performed the data analyses. ADA, TOA, OTE collected the samples. TOA, AFA, AAG, OOT wrote the manuscript. TOA, ERC and ADA performed the extraction and synthesize the nanoparticles. All authors contributed to the article and approved the final and submitted version.

References

Acharya B, Akansha R, Ashwani K, Shalini M, Vedpriya A, Vandana K, et al. 2023 Elucidating the Role of Plant Extracts Mediated Gold Nanoparticles as Smart Antimicrobials: Two-Way Attack, *J. Nanomaterials*, 4085090.

Aina AD, Owolo OD, Adeoye-Isijola MO, Aina FO, Omeiza F and Adewumi AG. 2018. Almond leaves for the one-pot Biofabrication of silver nanoparticles: Characterization and larvicidal application. *Int. J. Sci. Res. Pub*, **8 (11)**: 703-711.

Akande EB, Oladejo BO, Oladunmoye MK and Abodunrin TF. 2020. Antibacterial Effects of *Newbouldia laevis* {P. BEAUV} on the Bacteria Isolated from the Blood of Hepatitis C Virus Positive Individuals. *Asian Plant Res. J*, **4(1)**: 26-34.

Akerele JO, Ayinde BA and Ngiagah J. 2011. Phytochemical and antibacterial evaluations of the stem bark of *Newbouldia leavis* against isolates from infected wounds and eyes. *Trop J Pharm Res*, **10(2)**:211-218.

Allahverdiyev AM, Kon KV, Abamor ES, Bagirova M and Rafailovich M. 2011. Coping with antibiotic resistance: combining nanoparticles with antibiotics and other antimicrobial agents. *Expert Rev Anti Infect Ther*, **9(11)**: 1035-1052.

Arbonnier M. 2004 Trees, shrubs and lianas of West African dry zones. Cirad, Margraf, MNHN, 574 p.

Ayaz Ahmed KB, Subramanian S, Sivasubramanian A, Veerappan G and Veerappan A. 2014. Preparation of gold nanoparticles using Salicornia brachiata plant extract and evaluation of catalytic and antibacterial activity. *Spectrochim. Acta Part A Mol. Biomol. Spectrosc*, **130**: 54–58.

Bachheti RK, Fikadu, A, Bachheti A and Husen A. 2020. Biogenic fabrication of nanomaterials from flower-based chemical compounds, characterization and their various applications: a review. *Saudi J Biol Sci*, **27(10)**: 2551–2562.

Bale SI, Mukhtar MD and Rufa'i, FA. 2022. Bacteria Associated with Health-care Acquired infections from two Selected Hospitals in Kano, Nigeria. *Int. j. sci. res. biol. sci*, **9(4)**: 34-38.

Byrappa K, Ohara S and Adschiri T. 2008. Nanoparticles synthesis using supercritical fluid technology–towards biomedical application. *Adv. drug deliv. Rev*, **60(3):** 299-327.

Coyle MB. 2005. Manual of antimicrobial susceptibility testing. American Society for Microbiology (ASM) press, Washington, 39-62.

Dharman S, Maragathavalli G, Shanmugam R, Shanmugasundaram K. 2023. Curcumin mediated gold nanoparticles and analysis of its antioxidant, anti-inflammatory, antimicrobial activity against oral pathogens. *Pesqui Bras Odontopediatria Clín Integr*, **23:** e220068.

Fouda A, Eid AM, Guibal E, Hamza MF, Hassan SE-D and Alkhalifah DHM. 2022. Green Synthesis of Gold Nanoparticles by Aqueous Extract of *Zingiber officinale*: Characterization and Insight into Antimicrobial, Antioxidant, and In Vitro Cytotoxic Activities. *Appl. Sci*, ***12*:** 12879.

Gangwar RK, Tomar GB, Dhumale VA, Zinjarde S, Sharma RB and Datar S. 2013. Curcumin conjugated silica nanoparticles for improving bioavailability and its anticancer applications. *J Agric Food Chem*, **61(40)**: 9632-9637.

Ghasemi F and Jalal R. 2016. Antimicrobial action of zinc oxide nanoparticles in combination with ciprofloxacin and ceftazidime against multidrug-resistant *Acinetobacter baumannii*. *J Glob Antimicrob Resist*, **6:** 118–122.

He X and Lu H. 2014. Graphene-supported tunable extraordinary transmission. *Nanotechnology*, **25**: 325201. https://doi.org/10.1088/0957-4484/25/32/325201

Huang QH, Luo AH, Jiang LJ, Zhou Y, Yang YT, Liu Q and Zhang CF. 2019. Disinfection efficacy of green synthesized gold nanoparticles for medical disinfection applications. *Afr. Health Sci*, **19**: 1441–1448.

Inbaraj BS, Chen BY, Liao CW and Chen BH. 2020. Green synthesis, characterization and evaluation of catalytic and antibacterial activities of chitosan, glycol chitosan and poly (γ-glutamic acid) capped gold nanoparticles. *Int. J. Biol. Macromo,*. **161:**1484-1495.

Iwu MM. 2000. Handbook of African Medicinal Plants. London: CRC Press, Inc; p. 19.

Khanna P, Kaur A. and Goyal D. 2019. Algae-based metallic nanoparticles: synthesis, characterization and applications. *J Microbiol Methods*, **163**: 105656.

Kratošová G, Vávra I, Horska K, Životský O, Němcová Y, Bohunická M, Slabotinskú J, Rosenbergová K, Kadilak A and Schröfe A. 2013. Synthesis of metallic nanoparticles by diatoms and chrysophytes - prospects and applications. *Green Bio. Nano: Mec Appl*, 61-78. https://doi.org/10.1079/9781780642239.00

Lavaee F, Ranjbar Z, Modarezi F and Keshavarz F. 2021. The effect of gold nanoparticles with different sizes on *Streptococcus* species. *J. Dent.* **4:** 235–242.

Lee KX, Shameli K, Miyake M, Kuwano N, Khairudin NBBA, Mohamad SEB and Yew YP. 2016. Green synthesis of gold nanoparticles using aqueous extract of *Garcinia mangostana* fruit peels. *J. Nanomater*, **2016:** 8489094.

Li SQ, Al-Misned FA, El-Serehy HA and Yang, LL. 2021. Green synthesis of gold nanoparticles using aqueous extract of *Mentha Longifolia* leaf and investigation of its anti-human breast carcinoma properties in the in vitro condition. *Arab. J. Chem*, **14:** 102931.

Liaqat N, Jahan N, Rahman K, Anwar T. and Qureshi H. 2022. Green synthesized silver nanoparticles: optimization, characterization, antimicrobial activity and cytotoxicity study by hemolysis assay. *Front Chem*, **10:** 952006.

Makarov VV, Makarova SS, Love AJ, Sinitsyna OV, Dudnik AO, Yaminsky IV, Taliansky ME and Kalinina NO. 2014. Biosynthesis of stable iron oxide nanoparticles in aqueous extracts of Hordeum vulgare and Rumex acetosa plants. *Langmuir*, **30(20)**: 5982-8. doi: 10.1021/la5011924

Maliszewska I, Wanarska E, Thompson AC, Samuel IDW, Matczyszyn K. 2021. Biogenic gold nanoparticles decrease methylene blue photobleaching and enhance antimicrobial photodynamic therapy. *Molecules*, **26:** 623.

Mohl M, Dobo D, Kukovecz A, Konya Z, Kordas K, Wei J and Vajtai, R. 2011. Formation of CuPd and CuPt bimetallic nanotubes by galvanic replacement reaction. *J. Phys. Chem. C*, **115(19)**: 9403-9409.

Muddapur UM, Alshehri S, Ghoneim MM, Mahnashi MH, Alshahrani MA, Khan AA, Iqubal SMS, Bahafi A, More SS, Shaikh IA, Mannasaheb BA, Othman N, Maqbul MS, and Ahmad MZ.2022. Plant-based synthesis of gold nanoparticles and theranostic applications: A review. *Molecules*, **27(4):** 1391.

Muniyappan N, Pandeeswaran M and Amalraj A. 2021. Green synthesis of gold nanoparticles using Curcuma pseudomontana isolated curcumin: its characterization, antimicrobial, antioxidant and anti-inflammatory activities. *Environ Chem Ecotoxicol*, **3:** 117-124.

Obum-Nnadi CN, Okey-Ndeche FN, Nnagbo PA and Ohabughiro NB. 2020. Phytochemical and antibacterial activities of *Newbouldia laevis* leaves (ogirishi) on two drug resistant bacteria. *Int. J. Res. and Rev.* **7(5):** 59-66.

Omeje KO, Ezema BO, Ozioko JN, Omeje HC, Ogidigo JO, Okeke OR and Nnorom CO. 2020. Cholinesterases Inhibition and Antioxidant Potentials of *Newbouldia laevis* and *Ficus exasperata* Vahl Leaf Extract. *Archives*, **1:** 77-91

Oyewole TE, Thonda OA, Fagbemi KO and Amodu S. 2023. Comparative Study of Green Synthesis of Silver Nanoparticles Using Leaf Extracts of *Vitellaria Paradoxa* and Their Antioxidant Activities. *Cur. Trends Life Sci. Res*, **2(1):** 47-64.

Patil MP and Kim GD. 2017. Eco-friendly approach for nanoparticles synthesis and mechanism behind antibacterial activity of silver and anticancer activity of gold nanoparticles. *Appl. Microbiol. Biotechnol*, **101:** 79–92.

Riaz U, Anum W, Jatoi GH, Murtaza G, Qazi MA and Rehman M. 2023. Genetically modified organisms use in green synthesizes nanomaterials In: Ozturk, M., Roy, A., Bhat, R.A., Vardar

Sukan, F., Policarpo Tonelli, F.M. (eds.): Synthesis of Bionanomaterials for Biomedical Applications. Cambridge, *Elsevier*, pp. 151-163.

Sánchez-López E, Gomes D, Esteruelas G, Bonilla L, Lopez-Machado AL, Galindo R, Cano A, Espina M, Ettcheto M, Camins A, Silva AM, Durazzo A, Santini A, Garcia ML, Souto EB. 2020. Metal-based nanoparticles as antimicrobial agents: an overview. *Nanomaterials*, **10(2)**: 292.

Sathishkumar P, Gu FL, Zhan Q, Palvannan T and Yusof ARM. 2018. Flavonoids mediated 'green' nanomaterials: A novel nanomedicine system to treat various diseases. Current trends and future perspective. *Mater. Lett*, **210**: 26–30.

Singh J, Kaur G and Rawat M. A. 2016. Brief Review on Synthesis and Characterization of Copper Oxide Nanoparticles and its Applications. *J Bioelectron Nanotechnol*, **1(1)**: 9.

Singh, P.P. and Bhakat, C. 2012. Green Synthesis of Gold Nanoparticles and Silver Nanoparticles from Leaves and Bark of *Ficus carica* for Nanotechnological Applications. *Int. J. Sci. Res*, **2:** 1-4.

Stozhko NY, Bukharinova MA, Khamzina EI, Tarasov AV, Vidrevich MB and Brainina KZ. 2019. The effect of the antioxidant activity of plant extracts on the properties of gold nanoparticles. *Nanomaterials*, **9:** 1655.

Tao J, Fu Z, Dong C, Wang X, and Yang X. 2019. Green synthesis and characterization of monodisperse gold nanoparticles using aloe vera leaf extract. *Rare Metal Mat. Eng*, **48(11)**: 3470–3475

Thirumurugan A, Jiflin G, Rajagomathi G, Tomy N, Ramachandran S and Jaiganesh R. 2010. Biotechnological synthesis of gold nanoparticles of *Azadirachta indica* leaf extract". *Int J. Biol Tech*, **1**: 75-7.

Thonda OA, Okorie D, Ogidi CO, Aladejana OM, Olowookere BD and Olawoye AA. 2020. Antibacterial Efficacy of *Vernonia Amygdalina* Against Bacteria Strains Recovered from Hospital Fomites, Nigeria. *Curr Tr Biotech & Microbio.* **2(2)**: 381-388.

Thonda OA, Oluduro AO, Adewole OO and Obiajunwa PO. 2021. Phenotypic and genotypic characterization of plasmid-mediated AmpC beta-lactamases in enteric Gram-negative bacteria from patients with lower respiratory tract infections in a tertiary hospital, Southwest Nigeria. *Afr. J. Clin. Exp. Microbiol.* **22 (4):** 465–472.

Timoszyk A. 2018. A review of the biological synthesis of gold nanoparticles using fruit extracts: Scientific potential and application. *Bull. Mater. Sci*, **41:** 154–165.

Ugwoke HU, Ezema JN, Chinaka CB, Imanyikwa OE, Ukhureigbe OM, Ezugwu IA, Chukwuma ST and Eze EA. 2024. Evaluation of Antibacterial Effects of *Newbouldia laevis* and *Dracaena arborea* Methanol Extracts against Some Multidrug Resistant 'ESKAPE' Pathogens Isolated from Hospital Environments. *Trop J Nat Prod Res,* **8(7):** 7778-7785.

Usman H and Osuji JC. 2007. Phytochemical and in vitro antimicrobial assay of the leaf extract of *Newbouldia laevis. Afr J Tradit Complement Altern Med*, **4(4):** 476-80.

Varadavenkatesan T, Pai S, Vinayagam R and Selvaraj R. 2012. Characterization of silver nano-spheres synthesized using the extract of *Arachis hypogaea* nuts and their catalytic potential to degrade dyes. *Mater. Chem. Phys*, **272:** 125017.

Vilchis-Nestor AR, Sánchez-Mendieta V, Camacho-López MA, Gómez-Espinosa RM, Camacho-López MA and Arenas-Alatorre JA. 2008. Solventless synthesis and optical properties of Au and Ag nanoparticles using *Camellia sinensis* extract. *Mater. Lett*, **62:** 3103-3105.

Wang L, Hu C and Shao L. 2017. The antimicrobial activity of nanoparticles: Present situation and prospects for the future. *Int. J. Nanomed*, 1227–1249.

Wani IA and Ahmad T. 2013. Size and shape dependant antifungal activity of gold nanoparticles: A case study of Candida. *Colloids Surf. B-Biointerfaces*, **101:** 162–170.

Zangeneh MM and Zangeneh A. 2020. Novel green synthesis of *Hibiscus sabdariffa* flower extract conjugated gold nanoparticles with excellent anti-acute myeloid leukemia effect in comparison to daunorubicin in a leukemic rodent model. *Appl. Organomet. Chem*, **34(1):** 5271–5283.

Zhu S, Shen Y, Yu Y and Bai X. 2020. Synthesis of antibacterial gold nanoparticles with different particle sizes using chlorogenic acid. *R. Soc. Open Sci*, **7:** 191141–191151.

JJBS

Volume 18, Number 2,June 2025
ISSN 1995-6673
Pages 291 – 299
https://doi.org/10.54319/jjbs/180210

Jordan Journal of Biological Sciences

Biological Active Metabolite Compounds for Antibacterial Agent From Extremophile Microalgae

Mohd Asyraf Kassim[1,*], Tan Kean Meng[1], Mohamad Hafizi Abu Bakar[1] , Siti Nurfatimah Mohd Shahpudin[2], Chee-Yuan Gan [3], Nur Farah Atiqah binti Mohd Pazli[4], Rohazila Mohamad Hanafiah[4]

[1]*Bioprocess Technology Division, School of Industrial Technology, Universiti Sains Malaysia;* [2]*Integrative Medicine Cluster, Advanced Medical and Dental Institute, Universiti Sains Malaysia, Kepala Batas, Penang, Malaysia;* [3]*Analytical Biochemistry Research Centre (ABrC), Universiti Sains Malaysia, University Incubator Building, Sains@USM Campus, Lebuh Bukit Jalil, Bayan Lepas, Penang, 11900 Malaysia;* [4]*Department of Basic Sciences and Oral Biology, Faculty of Dentistry, Universiti Sains Islam Malaysia, Kuala Lumpur, Malaysia*

Received: January 27, 2024; Revised: October 19, 2024; Accepted: November 12, 2024

Abstract

The present investigation aimed to investigate and identify antimicrobial activity of four extremophile microalgae including *Tetraselmis suecica*, *Halochlorella rubescens*, *Cocomyxa dispar* and *Scendesmus parvus*. The comparative study of bioactive compounds in extraction yield, phytochemical screening and antimicrobial activities using disk diffusion method against pathogenic bacteria *Escherichia coli*, *Pseudomonas aeruginosa*, *Streptococcus* sp., and *Staphylococcus aureus* from two extraction solvent were evaluated. The study indicated that methanol extract gave higher extraction yield of all tested microalgae compared to those chloroform as solvent. Phytochemical screening analysis reveals the presence of flavonoids, alkaloids, tannins and saponin in methanol extract of *T. suecica*, *C.dispar* and *H. rubescens*. The study also showed that the microalgae crude extract exhibited effective inhibitory activity against all tested bacteria. The highest zone inhibitory of 11.33±1.23 mm and 11.67±0.37 mm was observed for *H. rubescens* chloroform extract and *S. parvus* methanol extract against *S. aureus*. The microalgal crude extracts were further chemically characterized by gas chromatography mass spectroscopy (GC−MS). GCMS profiling of both methanol and chloroform extract of all tested microalgal reveals the presence of different bioactive compound such as palmitic acid, octadecanoic acid, neophytadiene, phytol, loliolide and stigmasterol, with important antimicrobial properties. This finding indicates a promising antimicrobial activity of microalgal extract and can be possible to further develop for biologically active compound in various application such as aquaculture, nutraceutical, and food supplements.

Keywords: bioactive compound, phytochemical, antimicrobial, microalgae

1. Introduction

Microalgae is a unicellular photosynthetic microorganism and can be found in wide range of habitats including marine and fresh water environments (Mandal and Mallick 2014). Divers microalgae strains contain various metabolites such as lipid, carbohydrate, protein and minerals make its possibly potential source for various applications (Hachicha *et al.* 2022). Nutrient-rich microalgae biomass has been reported to have potential application as supplement for animal feed and health products (Agrawal and Verma 2022, Wang *et al.* 2021). Microalgae possess more advantages over other plant materials as such microorganisms are easy to cultivate, exhibit high growth rate, and are environmentally friendly and renewable. In addition, the microalgae-extracts from different microalgae strains consist of bioactive constituents that offer unlimited source of new bioactive compounds with different biological activities (Falaisae 2016., Hussein *et al.* 2020, Silva *et al*. 2021, Ghasemi *et al*. 2006).

Studies on screening and identification of metabolites from various microalgae strains found that bioactive compounds extracted such as fatty acids, acrylic acid, halogenated aliphatic compounds, terpenes, sulphur containing hetero cyclic compounds, carbohydrates and phenols demonstrated potential antimicrobial properties (Najdesnki *et al*. 2013, Toshkova-yotova *et al.* 2022, Kokou *et al*. 2012, Jun *et al*. 2018). These substances can inhibit the growth of microorganisms or eradicate them. In addition, the bioactive metabolites, such as phenolic compounds (e.g. simple phenols), phenolic acids (e.g. derivatives of benzoic acid and cinnamic acid), coumarins and flavonoids, from microalgae have also received much attention. These metabolites are known to have a wide range of pharmacological activities including, antimicrobial, antiviral, antifungi, anti-inflammatory, anti-oxidant and anticancer activities.

Isolation and characterization of bioactive secondary metabolites from various microalgae have been reported by many studies (Acurio *et al*. 2018, Makridis *et al*. 2006). The usage of extremophile microalgae in biotechnological applications like production of bioactive compounds has

* Corresponding author. e-mail: asyrafkassim@usm.my.

much greater potential. In general, production or accumulation of secondary bioactive metabolite is to aid cells in their interaction with the environment and in protection from predators as well as abiotic stress. Such microorganisms maintain their vitality by producing more stable materials in adapting to the changing environmental conditions. It is known that bioactive compound yield and its activity extracted from microalgae are significantly influenced by microalgae strain, cultivation condition, type of solvent and extraction method (Lomakool *et al*. 2021, Monteiro *et al*. 2020, Stirk *et al*. 2020). The accumulation of secondary bioactive metabolite can be influenced by several factors, and stress condition has been identified to be among the major factors that could affect the quality of the metabolites (Lafarga *et al*. 2021, Little *et al*. 2022). Microalgae that are able to grow in stress and extreme condition require the microalgae to maintain their metabolisms by adapting the changes which could require high energy consumption. This condition will eventually reduce photosynthesis activity, resulting in accumulation of intermediate compound such as secondary metabolite within the cell. A Study by Killic *et al.* (2018) on the biological and antimicrobial activity of *Dunaliella* sp. indicated that higher activity was observed from the microalgae extract cultivated under elevated NaCl concentration. Another study by Ameri *et al.* (2021) also found that changes of light exposure during cultivation condition could significantly affect the antimicrobial activity of *Chlorella* sp. extract. However, to the best of our knowledge, there are limited information of microalgae grown supplemented with elevated CO_2 conditions on their biological and antimicrobial activity. In addition, despite the many studies on the antimicrobial and antioxidant activity from different strains, no such investigation has been reported on the extremophile *Tetraselmis suecica*, *Halochlorella rubenses*, *Scenedesmus parvus* and *Cocomyxa dispar* strains. Thus, this study was designed to screen and evaluate ability of these locally isolated microalgae to produce antimicrobial and antioxidant compounds. The scientific novelty of this study lies in the identification of the extremophile microalgae strain that poses potential biological and antimicrobial activity which can be further developed for a new antimicrobial drug from renewable resources.

2. Materials And Methods

2.1. Microalgae strains

Four different extremophile microalgae, namely *Halochlorella rubescens*, *Tetraselmis suecica*, *Coccomyxa dispar* and *Scenedesmus parvus*, were used throughout the experiment. Microalgae *T. suecica* and *H. rubescens* were obtained from CSIRO Australia, while *C. dispar* and *S. parvus* were isolated from abandoned mining area at Tasik Katak (2°7'60" N · 103°51'0" E), Pulau Pinang Malaysia. The microalgae were grown in Bold Basal's Medium (BBM) medium that consisted of the following chemicals: 25 g/L sodium nitrate ($NaNO_3$), 7.5 g/L magnesium sulphate heptahydrate ($MgSO_4.7H_2O$), 2.5g/L sodium chloride (NaCl), 7.5 g/L dipotassium phosphate (K_2HPO_4), 17.5 g/L potassium dihydrogen phosphate (KH_2PO_4), 2.5 g/L calcium chloride dehydrate ($CaCl_2.2H_2O$), 8.82 g/L zinc sulphate heptahydrate ($ZnSO_4.7H_2O$), 1.44 g/L manganese chloride tetrahydrate ($MnCl_2.4H_2O$), 0.71 g/L molybdenum trioxide (MoO_3), 1.57 g/L copper sulphate pentahydrate ($CuSO_4.5H_2O$), 0.49 g/L cobalt nitrate hexahydrate ($Co(NO_3)_2.6H_2O$), 11.42 g/L boric acid (H_3BO_3), 50 g/L ethylenediaminetetraacetic acid (EDTA), 31 g/L potassium hydroxide (KOH), 4.98 g/L iron sulfate heptahydrate ($FeSO_4.7H_2O$) and 1 mL sulfuric acid (H_2SO_4). The cultivation process was conducted in two phases. Initially, the seed microalgae culture was grown in BBM medium at 32±3 °C, pH 7 and exposed to light intensity of 1500 lux for 14 days. The active microalgae culture was then centrifuged and standardized its optical density (OD_{680}) to 1.0. A total of 10% (v/v) of the standardized active microalgae seed culture was then added in the 1L Schott bottle, and the mixture was kept at 32 °C, pH 7 under light intensity of 1500 lux supplemented with 5% CO_2 intermittently for 14 days.

The growth of the microalgae was monitored every 24 hours. For this analysis, a total of 1 mL of the sample was withdrawn and was measured using spectrophotometer (Hach, DR-5000). The relationship with the microalgal cell concentration was determined by correlating the absorbance at 680 nm and dry cell weight (DCW). The microalgal DCW was calculated using the following equation (1-4):

$$\text{Biomass concentration}_{(H.rubescens)} = 0.549\,(OD_{680}) - 0.0046 \quad (1)$$

$$\text{Biomass concentration}_{(T.suecica)} = 0.524\,(OD_{680}) - 0.0129 \quad (2)$$

$$\text{Biomass concentration}_{(C.dispar)} = 0.2845\,(OD_{680}) + 0.0016 \quad (3)$$

$$\text{Biomass concentration}_{(S.parvus)} = 0.574\,(OD_{680}) - 0.00469 \quad (4)$$

After completed the cultivation period, the cell was harvested by centrifugation and kept for oven dried at 24 to 48 hours at 60°C. The dried microalgae biomass was then kept in tight container for further analysis.

2.2. Preparation of the microalgae crude extract

Approximately, 1000 mg of the dried microalgae samples were weighed, and then soaked in two different solvents namely methanol and chloroform. Each of the microalgae biomass was pre-treated using ultrasonication at 40 °C, 100 W and 40 kHz for 20 min and then kept for mixing for 72 h at room temperature. After the extraction process, the extracts were filtered, and the supernatant were collected, while the pellet fraction was re-extracted for three times to ensure the maximum metabolite recovery. The supernatant was then concentrated by evaporation to dryness at 40 °C using rotary evaporator prior to be used for the phytochemical screening. The yields of extracts were calculated by using the following formula (Norul Azilah *et al*. 2020):

$$Percentageyield = \frac{\text{weight of dry crude extract}}{\text{weight of dried microalgae}} \text{X}100$$

2.3. Phytochemical screening

The presence of secondary metabolites in the extract was investigated using qualitative phytochemical analysis. Its standard protocols were used to test for terpenoids, flavonoids, tannins, saponins, and sterols. Each test's aqueous extract was made by dissolving 40 mg of crude extract in 5 mL of solvent and filtering the mixture.

2.3.1. Tests for terpenoids

Determination of terpenoid in the microalgal crude extract was performed using Salkowski test (Das *et al*. 2014). In this analysis, a total volume of 2 mL of chloroform was added into the tube containing 2 mL of aqueous extract, and the sample was mildly shaken for 5 minutes. Then, 2 mL of concentrated sulfuric acid was added into the mixture to form a layer. The presence of reddish-brown color at the interface of the mixture indicates the terpenoids detected in the sample.

2.3.2. Test for flavonoids

Determination of flavonoids in the microalgal crude extract samples was performed using Alkaline reagent test (Munir *et al.* 2020). In this analysis, three to four drops of dilute sodium hydroxide (NaOH) solution were dropped to the tubes containing 2 mL of aqueous extract. Then, 2 mL of dilute acid was added to the tubes. The changes in the color and formation of a strong yellow color in the mixture indicates the presence of flavonoids in the extract.

2.3.3. Test for tannins

Determination of tannins in the microalgal extract was carried out via Lead acetate test as per described by Abdel-Karim *et al.* (2020). A total 3 mL of an aqueous extract was placed in a test tube, and then a few drops of $FeCl_3$ solution were added. The presence of greenish-black precipitate indicates the presence of tannins in the sample.

2.3.4. Test for saponins

Determination of saponins in the microalgal crude extract was performed via Foam test with slight modifications (Kancherla *et al*. 2019). Firstly, a total 50 mg of microalgal extract was mixed with 20 mg of sodium bicarbonate ($NaHCO_3$) diluted with distilled water and the sample was shaken vigorously until the formation of honeycomb-like froth. The formation of one centimetre layer of foam indicates the presence of saponins.

2.3.5. Test for sterols

Sterol in the extracted sample was determined by Salkowski reaction test as per described by Mojab *et al.* (2003). A total of 40 mg of extracted sample was dissolved in 2 mL of chloroform and filtered. Then, the filtrated sample was treated with 1mL of concentrated sulfuric acid (H_2SO_4). The presence of sterols in the microalgal extracted sampled was confirmed by the 2 phase formation with red color in the chloroform phase.

2.4. Antibacterial test

The antibacterial activity test of microalgal crude extract was performed by disc diffusion method (Mohamad-Hanafiah et al. 2015). The bacterial tests such as *Bacillus cereus, Staphylococcus aureus, Pseudomonas aeruginosa* and *Escherichia coli* were used in this study. Those bacteria were obtained from School of Industrial Technology, Universiti Sains Malaysia. The bacteria inoculum containing $1x10^8$ cell/mL was uniformly spread over the nutrient agar/Mueller-Hinton agar (MHA)/molten agar using sterilized cotton buds. For this experiment, the crude extract with 10 µg/ml was applied on the sterile disc and solvent was kept to evaporate prior to be placed on the inoculated plate. Similarly, commercial antibiotic such as Gentamycin (50 µg/disc) and Ampicillin (50 µg/disc) was used as positive control while solvent as negative control. All the plates were then incubated at 37 ± 2 °C for 24 hours, and the diameter of the minimum zone of inhibition was measured in mm. For each test, three replicates were performed.

2.5. Minimal inhibitory concentration (MIC)

In order to identify the optimum antimicrobial concentrations of microalgae extract against different bacteria, the minimal inhibitory concentration (MIC) was performed via two-fold serial dilution method in 96 well plates. In this analysis, the microalgal extracts were diluted in 1ml sterile deionised distilled water and a total of 100 µl was added in 96 well plates. Then, a total of 100 µl the standardized bacteria with concentration of 10^8 CFU/mL was added into the well to final volume 200 µL/well. Wells containing only sterile MHB were used as a negative control and gentamicin serves as a positive control. The plate was incubated at 37° C for 24 hours. MIC values were taken as the lowest concentration of extracts that produced no visible bacterial growth when compared with the control tubes after incubation period.

2.6. Gas chromatography – mass spectrometry (GC-MS)

The phytocomponent in the microalgal crude extract was determined using gas chromatography-mass spectrometer (GC/MS) (QP2010 Ultra Gas Chromatograph Mass Spectrometer (Shimadzu, Japan)) equipped with SUPELCOWAX^{TM} 10 Capillary GC (L × I.D. 30 m × 0.25 mm, df 0.25 µm) with direct capillary column bpx5. Helium gas was used as a carrier gas at a constant flow rate of 1 ml/min. For each injection, the solvent delay was 2 min, and 1 µL of diluted samples was injected automatically using an auto sampler in the split mode. The injector temperature was 290 °C. All the analysis was conducted at the following column temperature program: initial temperature of 50 °C holding for 1 min, and the increased by 2 °C/min to 180 °C withhold 3 min then to 280 °C by 2°C/min withhold 5 min and at 300 °C increased by 2°C/min held for 7 min. The GC-MS was operated in the electron ionization (EI) mass spectra, and the data were collected at 70 eV ionization voltages over the range of m/z 40-650 in full scan mode.

2.7. Statistical analysis

All results were expressed in triplicate to calculate the mean ± standard error. In order to be considered statistically significant, a value of $P < 0.05$ was performed using Minitab 16 software.

3. Results

3.1. Microalgae growth profile

The growth profile of four microalgae strain was monitored for 14 days of cultivation and the growth profiles are presented in Fig. 1. The study indicated that all the three microalgae strain exhibited different growth pattern, and *H. rubescens* exhibited highest biomass production of 0.81±0.02 g/L followed by *C. dispar* after 15 days of cultivation. On the other hand, the lowest microalgae biomass production of *T. suecica* was observed for 0.54±0.02 g/L. The maximum biomass concentration of *S. parvus* of 0.67±0.03 g/L was obtained for 15 days of incubation.

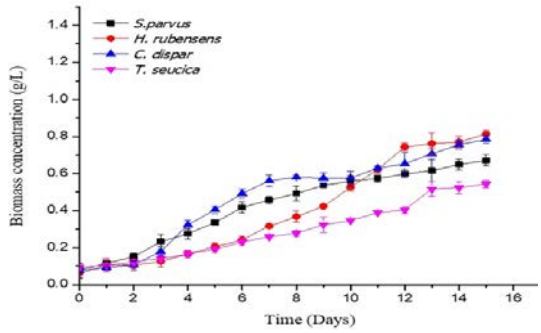

Figure 1. Growth profile of different microalgae cultivated at pH 7, light intensity 1500 lux, at 32±2.0℃ and supplemented with elevated CO_2 for 14 cultivation days.

3.2. Crude Extraction yield

Fig. 2 shows the crude extract yield obtained from different microalgae biomass using two different solvents. Overall, it was found that extraction using methanol gave better effect on extraction yield of all types of microalgae strain in comparison to extraction using chloroform. The highest crude extract yield was obtained from the extraction of *T. suecica* using methanol with 46.68% followed by extraction of *S. parvus* using similar solvent with yield of 31.90%. On the other hand, high extract yield for extraction using chloroform was observed for extraction using *C. dispar* biomass with yield of 15.12%. Only 3.54% of crude extract was successfully extracted from *S. parvus* using this solvent. It can be found that solvent and type of microalgae used for the extraction significantly affect the extraction yield.

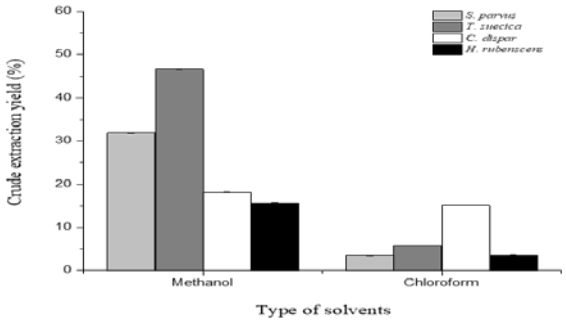

Figure 2. Crude extract yield (%) from different extremophile microalgae species extracted using methanol and chloroform

3.3. Phytochemicals screening

Primary screening of different phytochemicals bioactive compounds from *C. dispar*, *S. parvus* and *T. suecica* was conducted, and the results are presented in Table 1. The present study indicated that terpenoid is the only secondary metabolite that successfully recovered from all the microalgal biomass using different solvents. The study indicated that a higher number of bioactive compounds were successfully extracted from *C. dispar* and *T. suecica* using methanol as solvent. Flavanoids, terpenoids, saponin, tannins were present in methanol extract of *C. dispar*, whilst phytochemical compound, such as flavonoids, terpenoids, tannins, phenol and sterol were present in methanol extract of *T. suecica*. It was found that only terpenoids is present in the methanol extract of *Scenedesmus parvus*. Extraction using chloroform showed a fewer number of bioactive compound extracted from all the biomass tested. It was found that terpenoid, saponin and sterol were present in the chloroform extract of all microalgae biomass and flavonoids only present in the chloroform extract of *C. dispar*. In addition, flavonoids and terpenoids were present in both methanol and chloroform extract of *H. rubescens*. Compounds such as tannins and phenol were only detected in methanol extract; however, saponin and sterol were present in chloroform extract of *H. rubescens*. Phytochemicals extracted from these microalgal biomass are known to have medicinal importance.

Table 1. Screening of phytochemicals of chloroform and methanol as solvent extracts of different extremophile microalgae species.

Phytochemical Constituents	*C. dispar*		*S. parvus*		*T. suecica*		*H. rubescens*	
	ME	CE	ME	CE	ME	CE	ME	CE
Flavonoids	+	+	-	-	+	-	+	+
Terpenoids	+	+	+	+	+	+	+	+
Tannins	+	-	-	-	+	-	+	-
Saponin	+	+	-	+	-	+	-	+
Phenol	-	-	-	-	+	-	+	-
Sterol	-	+	-	+	+	+	-	+

Note: ME= Methanol extract, CE= Chloroform extract (+) positive reaction (-) negative reaction.

3.4. Antimicrobial activity

Antibacterial activities of crude extract obtained from four species of microalgae *Coccomyxa dispar*, *Tetraselmis suecica*, *H. rubescens* and *Scenedesmus parvus* against *Staphylococcus aureus*, *Streptococcus* sp, *Pseudomonas aeruginosa* and *Escherichia coli* were tested out using the disk diffusion method, and the results are shown in Table 2. This study indicated that methanol extract of *S. parvus* was able to inhibit Gram - negative and +positive bacteria. This extract effectively inhibited *E. coli*, *P. aeruginosa*, *Streptococcus* sp. and *S. aureus* with inhibition zone of 7.00±0.89, 7.67±0.52, 11.67±0.37 and 10.00±0.78 mm, respectively. On the other hand, chloroform extract of S. parvus was only able to inhibit *E. coli* with inhibition zone of 10.00±1.78 mm. Interestingly, methanol extract of H. rubescence only effectively inhibited gram negative bacteria *E. coli* and *P. aeruginosa* with inhibition zone of 8.33±0.68 and 7.33±0.52mm, respectively. There is a slight inhibition zone observed for this extract tested on S. aureus. However, the chloroform extract of *H. rubenscens* exhibited inhibition activity on *S. aureus* with inhibition zone of 11.33±1.23 mm. This study also indicated that the methanol extract of acidophilic *C. dispar* only showed a good bacteria inhibition activity for *P. aeruginosa* with 8.33±1.86 mm. However, chloroform extract of *C. dispar* biomass showed inhibition zone for E. coli and *Streptococcus* sp. bacteria with similar inhibition of 7.67±0.93 mm. However, methanol extract of microalgae gave high antibacterial activity against gram negative bacteria; however, the highest inhibition zone was obtained when the microalgae extracted were tested on gram positive bacteria. The highest inhibition zone was observed for chloroform and methanol extract of S. parvus against gram positive *S. aureus* with inhibition zone of 11.67±0.37mm. According to the Table 3, the methanol

extract of *S. parvus* also shows high inhibition activity on *Streptococcus* sp. with inhibition zone of 10.67±0.78 mm.

Table 2. Zone of inhibition (mm) exhibited by methanol and chloroform crude extracts of different microalgae species

Inhibition Zone diameter (mm)	*Escherichia coli*		*Pseudomonas aeruginosa*		*Streptococcus sp*		*Staphylococcus aureus*	
	ME	CE	ME	CE	ME	CE	ME	CE
H. rubescens	8.33±0.68	10.00±0.57	7.33±0.52	8.17±0.21	6.17±0.26	6.83±0.68	6.00±0.00	11.33±1.23
T. Suecica	7.67±1.36	10.00±0.37	6.17±0.26	6.33±0.26	6.5±0.45	6.67±0.52	6.5±0.00	7.00±0.89
C. dispar	7.00±0.89	9.5±0.23	8.33±1.86	7.67±0.93	6.67±0.03	7.67±0.52	7.67±0.52	8.33±0.52
S. parvus	7.00±0.89	10.00±1.78	7.67±0.52	7.67±0.52	10.67±0.78	8.00±0.78	11.67±0.37	10.66±0.72

* Gentamycin (30 µg/mL) *E. coli* = 14±0.00 mm, *P. aeruginosa*= 11±0.2 mm, *Streptococcus* sp.= 18±0.00 mm and *S. aureus* = 20±0.00 mm

Minimal inhibitory concentration of microalgae extract using different solvent system against gram positive and gram-negative bacteria is shown in Table 3. According to the analysis, difference in the activity of microalgae extract to inhibit bacteria growth is significantly influenced by the type of solvent, and extract concentration. The MIC value for gram-negative bacteria ranged between 0.98 mg/mL to 17.45 mg/mL. Analysis on *P. aeruginosa* using methanol extract of *C. dispar* showed the lowest MIC of 0.98 mg/mL observed for gram negative bacteria, whilst the highest MIC for gram positive bacteria was obtained for *P. suecica* tested with chloroform extract *C. dispar*. In contrast, the MIC value for gram positive bacteria ranged between 1 mg/mL to 34 mg/mL. It can be found that *Streptococcus* sp. exhibited highest MIC value for both methanol and chloroform extract of *T. suecica*. The study indicated that MIC value for chloroform extract of *T. suecica* on *S. aureus* gave lowest MIC value. This study indicated that MIC value for *S. aureus* obtained from this study is lower than those reported in the earliest report.

Table 3. Minimal inhibitory concentration (MIC) of microalgae extract of different solvent system against Gram-positive and Gram-negative bacteria

Inhibition Zone diameter (mm)	*Escherichia coli*		*Pseudomonas aeruginosa*		*Streptococcus sp*		*Staphylococcus aureus*	
	ME	CE	ME	CE	ME	CE	ME	CE
H. rubescens	4.03	1.48	8.03	1.48	16.05	11.85	2.00	1.48
T. Suecica	17.45	8.50	4.36	17.00	34.00	24.9	1.00	0.74
C. dispar	1.93	15.73	0.98	23.80	15.75	7.70	1.92	1.96
S. parvus	9.40	23.80	4.70	23.80	23.80	18.8	9.40	11.90

3.5. Compound identification using Gas Chromatography Mass Spectrometry

Extremophile microalgae have been reported to have capability to produce wide range of secondary metabolite compound which can be beneficial in pharmaceutical and medical therapy. Thus, further identification of bioactive compound from microalgae was conducted using gas-chromatography mass spectrometry (GC-MS). Several phytochemical compounds have been detected to be available in the microalgal crude extract (Table 4). A total of 50 and 30 phytochemicals compound peaks were detected from extraction of all microalgae sample using chloroform and methanol, respectively. The present study revealed that various phytochemical compounds such as fatty acid, fatty alcohol, alkane, alkene, phytosterol and phenol were identified present in the extracted fraction.

The obtained GC-MS results indicated that different extraction solvents could significantly affect the phytochemical composition extracted from microalgal biomass. The present study showed that palmitic acid, oleic acid, linoleic acid and pentadecanoic acid are among the dominant fatty acids present in the crude extract. It was found that palmitic acid has been identified in all extracted sample of all microalgal strain. In addition, it was also found that extractions using different solvents have affected the presence of alkane group in the extract. Several compounds such as pentadecane, hexadecane, octadecane, eicosane, tetracosane and tetracosane are among the compounds from alkane group have been identified presence in the chloroform extracted sample. It was found that pentadecane was detected in both chloroform and methanol extract of all microalgal samples. On the other hand, alkane such as tetrapentacontane, eicosane, tetracosane, octadecane, and hexadecane were only detected in the chloroform extracted sample. This present study also indicated that other phytosterol compounds such as phytol, tocopherol, stigmasterol, campesterol, cholesterol, sitosterol, liolide and squalene were also detected. Phytosterol compound such as Campesterol and Sitosterol only identified in chloroform extract of *T. suecica*. In addition, Squalene was only detected in chloroform extracted of *C. dispar* and *S. parvus*. This study also found that phytone and phytol were detected in all the microalgal biomass strains except for methanol extract of *T. suecica* and *S. parvus*. The presence of phytosterol and phytol in these extremophile microalgae shows their potential to be used in nutraceutical and pharmaceutical industries because they are precursors of some bioactive molecules.

Table 4. Phytochemical compounds detected in different microalgal crude extract extracted using methanol and chloroform

Classification	Compounds				*T. suecica*		*H. rubescens*		*C. dispar*		*S. parvus*	
		RT	Molecular weight	Formula	ME	CE	ME	CE	ME	CE	ME	CE
Fatty acid	Oleic acid (cis-9-0ctadecanoic acid)	78.861	296	$C_{18}H_{34}O_2$	1.49	-	0.13	9.34	0.96	2.92	-	0.44
	Linoleic acid (cis-9-12-octadecanoic acid)	78.221	294	$C_{18}H_{33}O_2$	1.68	-	3.68	-	0.38	21.08	-	-
	Palmitic acid (hexadecanoic acid)	71.413	256	$C_{17}H_{34}O_2$	1.55	5.33	16.76	9.34	11.98	0.46	3.71	18.04
	Eicosapentaenoic acid	66.297	316	$C_{21}H_{32}O_2$	-	-	0.28	0.07	3.01	-	-	-
	Tetradecynoic acid	12.869	238	$C_{15}H_{26}O_2$	-	-	0.44	-	0.48	-	-	-
	Octadecanoic acid	90.480	282	$C_{18}H_{34}O_2$	-	-	0.13	-	0.38	2.92	-	0.15
	Cis-9-hexadecenal	80.951	238	$C_{16}H_{30}O$	-	18.98	42.76	-	0.41	0.49	-	0.24
	Pentadecanoic acid	71.394	242	$C_{15}H_{30}O_2$	1.55	-		9.34	0.53	-	0.38	-
Fatty alcohol	Pentadecanol	55.071	228	$C_{15}H_{32}O$	-	-	-	0.15	-	-	-	0.17
	Hexadecanol	80.951	298	$C_{20}H_{42}O$	-	18.98	-	0.15	-	0.71	-	-
	Eicosanol	95.995	298	$C_{20}H_{42}O$	-	-	-	0.08	-	1.29	-	-
Alkane	Bromodocosane	136.195	446	$C_{22}H_{44}BrS_2$	-	-	-	0.17	-	-	-	-
	Tetrapentacontane	86.496	914	$C_{54}H_{11}O$	-	0.24	-	0.57	-	0.25	-	0.27
	Eicosane	55.054	282	$C_{20}H_{42}$	-	0.42	-	0.15	-	0.25	-	0.13
	Tetracosane	98.389	338	$C_{24}H_{50}$	-	0.28	-	0.19	-	0.16	-	0.39
	Octadecane	104.576	310	$C_{22}H_{46}$	-	0.91	-	0.16	-	0.49	-	0.28
	Pentadecane	66.263	268	$C_{16}H_{32}O_2$	-	0.57	16.67	0.16	-	11.08	3.71	18.04
	Hexadecane	133.364	420	$C_{20}H_{42}$	-	0.37	-	0.15	-	0.52	3.71	0.13
	Hexacosane	66.286	366	C26H54	-	0.57	-	0.15	-	-	-	-
	Neophytadiene	63.131	278	$C_{20}H_{38}$	-	2.85	0.22	8.69	1.87	11.88	-	1.64
	Tetracosane	87.913	338	$C_{24}H_{50}$		0.65		0.19		0.16		0.39
Phytolsterol	Phytol	96.456	296	$C_{20}H_{40}$	-	0.26	4.83	8.69	8.34	7.50	-	0.25
	Tocopherol	119.152	430	$C_{29}H_{50}O_2$	-	-	-	0.13	-	0.71	-	0.32
	Stigmasterol	127.488	412	$C_{31}H_{50}Br_2O_2$	-	-	-	0.76	-	-	-	0.32
	Cholesterol	125.402	400	$C_{28}H_{48}O$	-	-	-	0.51	-	0.46	-	1.49
	Sitosterol	123.003	400	$C_{29}H_{50}O$	-	5.36	-	-	-	-	-	-
	Loliolide	61.480	196	$C_{11}H_{16}O_3$	-	0.41	0.31	-	-	-	23.10	0.24
	Squalene			$C_{30}H_{50}$	-	-	-	-	-	0.68		0.32
Phenol	Phytone	63.730	268	$C_{18}H_{36}O$	-	3.48	-	0.91	0.58	0.66	-	0.20

4. Discussion

The bioactive compound extracted from different extremophile microalgae as antimicrobial agent was carried out against different pathogenic bacteria strain. This study indicated that all four tested microalgae strains were able to grow under high CO_2 concentration as carbon sources, which can be beneficial for CO_2 capture purpose. It is known that during cultivation process, microalgae when through photosynthesis process by utilizing CO_2 and sunlight to produce it biomass as well as main metabolite in its cell. In order to determine the effect of CO_2 on microalgae metabolite, further extraction of bioactive metabolites have been performed using methanol and chloroform as extraction solvent. It was found that different solvents used for extraction process significantly affect the percentage of crude extract from tested microalgae. Different solvents significantly affect the crude extract of different microalgae strains. This finding is in agreement with other studies on the bioactive compound extraction from different microalgae strains reported previously. A study by Fattah-Shaima *et al*. (2022) who compared methanol extraction yield of three microalgae biomass; *Chlorella sorokiniana* (UKM2), *Chlorella* sp. (UKM8) and *Scenedesmus* sp. (UKM9) indicated that different extraction yield was obtained from the extraction of type microalgae strains. The study found that the highest extraction yield of 29.5% was obtained from extraction of *Scenedesmus* sp. (UKM9). This study indicated that extraction efficiency is significantly influenced by the type of solvent used for the process. The differences of extraction yield obtained from different type of solvent could be explained by the solubility of microalgae metabolite into the solvent used. It is known that polar solvent could extract more metabolite and bioactive compound from the sample compared to non-polar solvent (Lezould *et al*. 2020, Jayakumar *et al*. 2020).

Indeed, methanol is a polar solvent with capability to extract more polar compounds from the biomass. Low extraction yield observed for all the microalgae biomass tested could be linked to the rapid volatility and low polarity which will only extract fatty acid from the biomass.

Further phytochemical screening was performed to identify the presence of metabolite compounds in crude extract from *C. dispar*, *S. parvus*, *T. suecica* and *H. rubescens* using a different solvent. It was found that a different solvent used during extraction process could significantly affect the recovery of metabolite compound such as flavonoids, terpenoids, saponin and tannins from microalgae. The presence of these compounds in the crude extract derived from microalgae is important to ensure its biological activity performance. For instance, flavonoid extracted from various plant materials has been reported to show biological activities such as antimicrobial against wide range of human pathogen and anti-inflammatory (Cushnie and Lamb 2005, Nguyen *et al*. 2015). Similarly, tannins derived from medicinal plants is known to have antimicrobial activities, antiviral and antitumor activities (Maisetta *et al*. 2019., Kaczmarek *et al*. 2020). In addition, terpenoids which are known to be the major secondary metabolites from plants have also been reported to have antimicrobial and anti-inflammatory activities (Wang *et al.* 2019).

Antimicrobial assay conducted from this study indicates that crude extract derived from microalgae exhibited different performance against *E.coli*, *Pseudomonas aeruginosa*, *Streptococcus* sp. and *Staphylococcus aureus*. Various studies on the antibacterial activity of microalgae extract against bacteria vary considerably (Matharasi *et al*. 2018). Generally, gram positive bacteria are more easily to be killed than those gram negative. The effectiveness of antibacterial activity against different bacteria strain is significantly influenced by their cell wall structure (Hidhayati *et al.* 2022). Gram positive bacteria have a thick monolayer cell wall; nevertheless, gram negative bacteria consist of thin with three-layer cell wall structure which makes these bacteria more resistant toward any antibacterial agents. In addition, the effectiveness of antibacterial activity of microalgae extract could also be attributed to the presence of biologically active compounds available in the extracted fraction (Toma and Aziz 2022).

GCMS analysis obtained indicated that several bioactive metabolite compounds were detected present in the crude extract. The presence of wide range fatty acid such as palmitic acid and metabolite in microalgal extract has exhibited potential to have great benefit on human health. Similar observation has been reported on the GC-MS profiling of *T. chuii*, *Nannochloropsis* and *Chlorella* sp. which found that the dominant fatty acid compound identified from both microalgae is palmitic acid (Fattah-Shaima *et al*. 2022, Gnanakani *et al.* 2019, El-Sayed *et al.* 2014). Several studies have reported that fatty acid from microalgae can act as antimicrobial, anti-inflammatory, anti-cancer and give positive impact on the cardiovascular disease (Cepas *et al.* 2021, Ruffell *et al.* 2016, Vilakazi *et al.* 2021). A study by Maligan *et al.* (2013) on antimicrobial activity of *T. suecica* indicated that antibacterial compounds such as fatty acid and ester have a significant role to inhibit the growth of bacteria. The long chain fatty acid has been found to exhibit the microbial lyse activity and disrupt bacterial cell wall (Willet *et al.* 1966, Yoon *et al.* 2018). The presence of other metabolites such a fatty alcohol, alkane, and phenol has also been reported to contribute to the inhibition effect of pathogenic bacteria. For instance, phytosterol is a natural steroid-alcohol compound that possesses anti-oxidant, anti-inflammatory and anti-atherogenicity activity (Le-Goff *et al.* 2019). Some phytosterols have also been reported to have anti-fungal, anti-bacterial, anti-inflammatory, anti-tumor, anti-oxidant, and anti-ulcerative properties (Danesi *et al.*2016).

5. Conclusion

This study evaluated and characterized the antibacterial activity of extremophile microalgae extract against *E. coli*, *P. aeruginosa*, *Streptococcus* sp. and *Staphylococcus aureus*. It can be concluded that the types of solvent and microalgae strain significantly affect the extraction yield. Higher extract yield was observed for extraction using methanol compared to chloroform. The study also indicated that methanol extract of *S. parvus* was able to effectively inhibit the growth of *P. aeruginosa*, *Streptococcus* sp. and *S. aureus*. GC-MS analysis indicated that there are various bioactive compounds present in the microalgae extract such as palmitic acid, lolinoide, phytol, phytone and stigmasterol known to have antibacterial activity. Based on this present study, extremophile microalgae such as *Scenedesmus parvus*, *Coccomyxa dispar* and *Halochlorella rubescens* have a great potential source of bioactive compound with pharmaceutical value from renewable resource. It is also indicated that these microalgae strains have economic value that can be further improved for agriculture and biomedical purposes. However, further investigation on bioactive metabolite accumulation improvement, purification, *in vitro* and *in vivo* study is needed to elucidate the compounds responsible for antibacterial activity against these bacteria.

Acknowledgments

The authors would like to thank the School of Industrial Technology, Universiti Sains Malaysia (USM) for the support to conduct this research.

References

Abdel-Karim OH., Gheda SF. Ismail GA and Abo-Shady AM. 2020. Phytochemical screening and antioxidant activity of *Chlorella vulgaris. Delta J Sci*., **41**: p. 81-91. http://doi.org/10.21608/DJS.2020.139231.

Acurio LP, Salazar DM., Valencia AF., Robalino DR., Barona AC., Alvarez FC and Rodriguez CA. 2018. Antimicrobial potential of *Chlorella* algae isolated from stacked waters of the Andean Region of Ecuador. *IOP Conf Ser Earth Environ Sci*., **151**. http://doi.org/10.1088/1755-1315/151/1/012040

Agrawal K. and Verma P. *Chapter 12* - An overview of various algal biomolecules and its applications, in *An Integration of Phycoremediation Processes in Wastewater Treatment*, M. Shah, et al., Editors, Elsevier. p. 249-270.

Ameri E, Shariati FP and Amrei HD. 2021. The effect of different light conditions on antimicrobial activity of the microalgae

Chlorella sp. ethanolic extract against *Streptococcus* mutans. *Gen Sci*., **30 (2)**: 532-537. doi: 10.37871/jbres1272.

Cepas V, Gutierrez-Del-Rio I, Lopez Y, Redondo-Blanco S, Gabasa Y, Iglesias MJ., Sooengas R, Fernandez-Lorenzo A, Lopez-Ibanez S, Villar CJ, Martins CB, Ferreira JD, Assuncao, MFG, Santos LMA, Morais J, Castelo-Branco R, Reis MA, Vasconcelos V, Lopz-Ortiz F, Lombo F et al. 2021. Microalgae and cyanobacteria strains as producers of lipids with antibacterial and antibiofilm activity. *Marine Drugs.*, 19, http://doi.org/10.3390/md19120675.

Cushnie, TPT and Lamb AJ. 2005. Antimicrobial activity of flavonoids. *Int J Antimicrob Agents.*, **26(5)**: p. 343-356.

Das BK, Al-Amin MM, Russel SM, Kabir S, Bhattacherjee, R and Hannan JMA. 2014. Phytochemical screening and evaluation of analgesic activity of *Oroxylum indicum.* Indian *J Pharma Sci*., **76 (6)**: 571-575.

Danesi F, Gomez-Caravaca AM, de Biase D, Verardo V and Bordoni A. 2016. New insight into the cholesterol-lowering effect of phytosterols in rat cardiomyocytes. *Food Res Int.*, **89**: p. 1056-1063. http://doi.org/10.1016/j.foodres.2016.06.028

El-Sayed HS, Ibrahim HAH., Beltagy EA and Khairy HM. 2014 Effects of short term feeding of some marine microalgae on the microbial profile associated with *Dicentrarchus labrax* post larvae. *Egypt J Aquat Res.*, **40(3)**: p. 251-260. doi.org/10.1016/j.ejar.2014.08.001

Falaise C, Francois C, Marie-Agnes T, Morga B, Haure J, Tremblay R, Turcotte F, Pasetto P, Gastineau R, Hardivillier Y, Leignel V and Jean-Luc M. 2016 Antimicrobial compounds from eukaryotic microalgae against human pathogens and diseases in aquaculture. *Marine Drugs.*, **14**, http://doi.org/10.3390/md14090159.

Fattah-Shaima AFS, Yasin NHM, Ibrahim N, Takriff MS, Gunasekaran D and Ismaeel MYY. 2021 Unveiling antimicrobial activity Of microalgae *Chlorella sorokiniana* (UKM2), *Chlorella sp.* (UKM8) and *Scenedesmus sp.* (UKM9). *Saudi J Biol Sci.*, **29**. http://doi.org/10.1016/j.sjbs.2021.09.069

Ghasemi Y, Moradian A, Mohagheghzadeh A, Shokravi S and Morowvat MS. 2007 Antifungal and antibacterial activity of the microalgae collected from paddy fields of Iran: Characterization of antimicrobial activity of *Chroococcus dispersus.* J Biol Sci., 7(6): p. 904-910.

Gnanakani P, Perumal S, Kilari K and Magharla D. 2019 Chemical composition, antioxidant, and cytotoxic potential of *Nannochloropsis* species extracts. *J Nat Sci Biol Med.*, **10:** p. 167. http://doi.org/10.4103/jnsbm.JNSBM_208_18

Hachicha R, Elleuch F, Hlima HB, Dubessay P, Baynast H, Delattre C, Pierre G, Hachicha R, Abdelkafi S, Michaud P and Fendri I. (2021) Biomolecules from microalgae and cyanobacteria: Applications and market survey. *Appl Sci.*, **12**, http://doi.org/10.3390/app12041924.

Hidhayati N, Agustini NWS., Apriastini M and Diaudin DPA. 2022. Bioactive compounds from microalgae *Spirulina platensis* as antibacterial candidates against pathogen bacteria. *Jurnal Kimia Sains dan Aplikasi.*; **25(2)**: http://doi.org/ 10.14710/jksa.25.2.41-48, 2022.

Hussein HA, Syamsumir DF, Radzi SAM, Fu-Siong JY, Zin NAM and Abdullah MA. 2020 Phytochemical screening, metabolite profiling and enhanced antimicrobial activities of microalgal crude extracts in co-application with silver nanoparticle. *Bioresour and Bioprocess.*, **7(1)**: p. 39. http://doi.org/10.1186/s40643-020-00322-w

Jayakumar C, Devi VM, and Sridar R. 2020 A study on the extraction of bioactive compounds from *Capparis zeylanica*. AIP *Conf Proc.*, **2225(1)**: p. 070002.

Jun JY. 2018. Antimicrobial and antibiofilm activities of sulfated polysaccharides from marine algae against dental plaque bacteria. *Mar Drugs*., **16**: http://doi.org/10.3390/md16090301.

Kaczmarek B. 2020. Tannic acid with antiviral and antibacterial activity as a promising component of biomaterials—A minireview. *Materials*., **13**: http://doi.org/10.3390/ma13143224.

Kancherla N, Dhakshinamoothi A, Chitra K and Komaram RB. 2019. Preliminary analysis of phytoconstituents and evaluation of anthelminthic property of *Cayratia auriculata* (In Vitro). *Maedica J Clin Med*., **14(4)**: 350-356.

Killic NK, Erdem K and Donmez G. 2018. Bioactive compounds produced by *Dunaliella* species, antimicrobial effects and optimization of the efficiency. *Turk J Fish & Aquat Sci*., **19(1)**: 923-933. http://doi.org/10.4194/1303-2712-v19_11_04

Kokou F, Makridis P and Divanach P. 2012. Antibacterial activity in microalgae cultures. *Aquac Res.*, **43**: p. 1520-1527. http://doi.org/10.1111/j.1365-2109.2011.02955.x

Lafarga T, Sanzhez-Zurano A, Morillas-Espana A and Acien-Fernandez FG. 2021. Extremophile microalgae as feedstock for high-value carotenoids: A review. *Int J Food Sci Technol*., **56(10):** p. 4934-4941. http://doi.org/10.1111/ijfs.15069

Le Goff M, Ferrec EL, Mayer C, Mimouni V, Lagadic-Gossmann D, Schoefs B and Ulmann L. 2019. Microalgal carotenoids and phytosterols regulate biochemical mechanisms involved in human health and disease prevention. *Biochimie*., **167**: p. 106-118. http://doi.org/10.1016/j.biochi.2019.09.012

Lezoul NEH, Belkadi M, Habibi F and Guillen F. 2020. Extraction processes with several solvents on total bioactive compounds in different organs of three medicinal plants. *Molecules.*, **25**: http://doi.org/10.3390/molecules25204672.

Little SM, 2021. Antibacterial compounds in green microalgae from extreme environments: a review. *Algae.*, **36(1)**: p. 61-72.

Lomakool S, Ruangsit K, Jeerapan I, Tragoolpua Y, Oumas C, Srinupan S, Pekkoh J and Duangjian K. 2021. Biological activities and phytochemicals profiling of different cyanobacterial and microalgal biomass. *Biomass Convers. Biorefin.*, **13**: 4195-4211. https://doi.org/10.1007/s13399-021-01974-0

Maisetta G, Batoni G, Caboni P, Esin S, Rinaldi AC and Zucca P. 2019. Tannin profile, antioxidant properties, and antimicrobial activity of extracts from two Mediterranean species of parasitic plant *Cytinus. BMC Complementary Altern Med.*, **19(1)**: p. 82. http://doi.org/10.1186/s12906-019-2487-7

Makridis P, Costa RA and Dinis MT. 2006. Microbial conditions and antimicrobial activity in cultures of two microalgae species, *Tetraselmis chuii* and *Chlorella minutissima*, and effect on bacterial load of enriched *Artemia metanauplii. Aquac.*, **255(1)**: p. 76-81. http://doi.org/10.1016/j.aquaculture.2005.12.010

Maligan J, Widayanti V and Zubaidah E. 2013. Production and identification of antimicrobial compounds from marine microalgae *Tetraselmis chuii* using ultrasound assisted extraction method. *Conference: Int Confer Food Eng Biotechnol*.

Mandal S, and Mallick N. 2014. *Microalgae.*, p. 171-184.

Matharasi A, Prabakaran G and Dineshkumar R. 2018. Phytochemical screening and antimicrobial activity of marine microalgae *Tetraselmis sp. Int J Pharma Biol Sci.*, **8(4)**: p. 85-90.

Mohamad-Hanafiah R, Noor WSAWM, Yaacob A, Said Z and Ibrahim N. 2015 Antibacterial and biofilm inhibition activities of *Melastoma malabathricum* stem bark extract against *Streptococcus mutans. Malays J Microbiol.*, **11**: p. 199-206. http://doi.org/10.21161/mjm.13314

Mojab F, Kamalinejad M, Ghaderi N and Vahidipour HR. 2003. Phytochemical screening of some species of Iranian plants. *Iran J Pharma Res.*, p. 77-82. http://doi.org/10.22037/ijpr.2010.16.

Monteiro M, Santos RA, Iglesias P, Couto A, Serra CR, Gouvinhas I, Barros A, Olivia-Teles A, Enes P and Diaz-Rosales P. 2020. Effect of extraction method and solvent system on phenolic content and antioxidants activity of selected macro- and microalgae extract. *J App Phycol*., 32: 349-362. https://doi.org/10.1007/s10811-019-01927-1.

Munir M, Khan AM, Qureshi R, Murtaza S and Munazir M. 2020. Preliminary phytochemical screening, proximate analysis, antioxidant and antibacterial activities of an algal species of hydrodictyon reticulatum. *J Bioresour Manage*., 7(4): p. 01-26.

Najdenski HM, Gigova LG, Iliev I, Pilarski PS, Lukavsky J, Tsvetkova IV, Ninova MS and Kussovski VK. 2013. Antibacterial and antifungal activities of selected microalgae and cyanobacteria. *Int J Food Sci Technol.*, 48(7): p. 1533-1540. http://doi.org/10.1111/ijfs.12122

Nguyen T, To DC, Tran MH, Lee JS, Lee JH, Kim JA, Woo MH and Min BS. 2015. Anti-inflammatory flavanoid isolated from *Passiflora foetida*. *Nat Prod Commun.*, 10(6): p. 929-931.

Ruffell SE, Müller KM and McConkey BJ. 2016. Comparative assessment of microalgal fatty acids as topical antibiotics. *J Appl Phycol.*, 28(3): p. 1695-1704. http://doi.org/10.1007/s10811-015-0692-4

Silva MGCD, Hort MA, Hadrich G, Bosco LD, Vaz GR, Silva MMA, Tavella RA, Badiale-Furlong E, Dora CL and Muccillo-Baisch AL. 2021. Anti-inflammatory and antioxidant effects of the microalga pediastrum boryanum in carrageenan-induced rat paw edema. *Braz Archof Biol Technol.*, 64. http://doi.org/10.1590/1678-4324-2021200748

Stirk WA, Balint P, Vambe M, Lovasz C, Molnar Z, Staden JV and Ordog V. 2020. Effect of cell disruption methods on the extraction of bioactive metabolites from microalgae biomass. *J Biotechnol.*, 307: 35-43. https://doi.org/10.1016/j.jbiotec.2019.10.012

Toma JJ and Aziz FH. 2022. Antibacterial activity of three algal genera against some pathogenic bacteria. *Baghdad Sci J.*, p. 32-40.

Toshkova-Yotova T, Georgieva A, Iliev I, Alexandrov S, Ivanova A, Pilarski P and Toshkova R. 2022. Antitumor and antimicrobial activity of fatty acids from green microalga *Coelastrella sp.* BGV. *S Afr J Bot.*, 151: p. 394-402. http://doi.org/10.1016/j.sajb.2022.04.003

Vilakazi H, Olasehinde TA and Olaniran AO. 2021. Chemical characterization, antiproliferative and antioxidant activities of polyunsaturated fatty acid-rich extracts from *Chlorella sp.* S14. *Molecules.*, 26. http://doi.org/10.3390/molecules26144109.

Wang CY, Chen YW and Hou CY. 2019. Antioxidant and antibacterial activity of seven predominant terpenoids. *Int J Food Prop.*, 22: p. 229-237. http://doi.org/10.1080/10942912.2019.1582541

Wang Y, Tibbetts SM and McGinn PJ. 2021. Microalgae as sources of high-quality protein for human food and protein supplements. *Foods.*, 10, DOI: 10.3390/foods10123002. http://doi.org/10.3390/foods10123002

Willett N and Morse G. 1966. Long chain fatty acid inhibition of growth of Streptococcus agalactiae in a chemically defined medium. *J Bacteriol.*, 91(6): p. 2245-2250. http://doi.org/10.1128/jb.91.6.2245-2250.1966

Yoon BK, Jackman JA, Valle-Gonzalez ER and Nam-Joon C. 2018. Antibacterial free fatty acids and monoglycerides: Biological activities, experimental testing, and therapeutic applications. *Int J Mol Sci.*, 19. http:// doi.org/10.3390/ijms19041114.

JJBS

Volume 18, Number 2,June 2025
ISSN 1995-6673
Pages 301 – 313
https://doi.org/10.54319/jjbs/180211

Jordan Journal of Biological Sciences

Attenuation of Quorum Sensing, Virulence Factors, and Biofilm Formation in *Pseudomonas aeruginosa* by *Psidium guajava* Leaf Extract

Haitham Qaralleh*

Department of Medical Laboratory Sciences, Mutah University, Mutah, Karak, Jordan

Received: September 11, 2024; Revised: October 4, 2024; Accepted: November 13, 2024

Abstract

This study was designed to assess the ability of the methanolic extract of *Psidium guajava* leaves to attenuate quorum sensing (QS), biofilm formation, and virulence factors of *Pseudomonas aeruginosa*. Liquid Chromatography - Mass spectrometry (LC-MS) was used to analyze the chemical composition. The effect on *P. aeruginosa* biofilm formation was evaluated using a crystal violet assay, light microscopy, and scanning electron microscopy. The effects on biofilm formation stages, including swarming motility, aggregation ability, surface hydrophobicity, and exopolysaccharide (EPS) production, were also investigated. Besides, the effect of *P. guajava* extract on different *P. aeruginosa* virulence factors, including violacein, pyocyanin, rhamnolipids, protease, and chitinase, was investigated. The mechanism of anti-QS action was evaluated by measuring the effect of the extract on the ability of *P. aeruginosa* to produce acyl-homoserine lactone and the analysis of QS-related gene expression via Real Time – Polymerase Chain Reaction (RT-PCR). LC-MS analysis revealed that quercetin (17.6%), avicularin (17.2%), and kaempferol (15.4%) were the most dominant compounds in the extract. The extract exhibited potent antibiofilm activity at concentrations of 0.37, 0.12, and 0.04 mg/mL, with up to 95% inhibition of biofilm formation. It also significantly interfered with key biofilm development stages, reducing swarming motility by 50% and EPS production by 72.2% at 0.37 mg/mL. The extract suppressed several virulence factors, including pyocyanin production (42.3% inhibition at 0.37 mg/mL), rhamnolipids (59.5% inhibition), and protease activity (49.7% inhibition). Furthermore, the extract reduced the production of acyl-homoserine lactone (AHL) by 29.5% and downregulated QS-related genes, particularly phzA1, indicating its ability to disrupt the QS system. These findings suggest that *P. guajava* methanolic extract holds promise as an anti-infective agent capable of attenuating biofilm formation and virulence factor production in *P. aeruginosa*.

Keywords: *P. guajava, P. aeruginosa*, Anti-infective, Quorum sensing, Biofilm, LC-MS

1. Introduction

Infections caused by *Pseudomonas aeruginosa* are among the most common hospital-acquired infections. *P. aeruginosa* infections can be mild and self-limited, but they may also be systemic, life-threatening infections, especially in those with impaired immune systems such as Acquired Immunodeficiency Syndrome (AIDS) and chemotherapeutic-treated patients (Qin et al. 2022). Moreover, *P. aeruginosa* ranks first in surgical wounds, burns, and diabetic ulcer infections (Bhardwaj et al. 2021). In cystic fibrosis patients, *P. aeruginosa* infection makes matters worse, leading to pulmonary failure and death (Rossi et al. 2021).

Several factors elect *P. aeruginosa* as one of the most common and dangerous pathogenic bacteria. Among these is its ability to resist antibiotics. Equally important is its ability to produce a broad range of virulence factors through an intrinsically interconnected, complex system called the quorum sensing (QS) system. In addition to its high virulence and drug resistance, *P. aeruginosa* tends to live in biofilm communities, making infections difficult to treat (Sahib et al. 2019; Alrawashdeh et al. 2019; Simanek and Paczkowski 2022).

Various approaches have been explored to overcome the challenges of infectious disease treatment, particularly antibiotic resistance. Some scientists are trying to modify the structure of currently used antibiotics, while others are trying to find new antibacterial agents from natural sources. To treat infectious diseases, an attractive approach is now being used to find new anti-infective agents. Anti-infective agents can attenuate virulence factors, biofilm formation, and the QS system of the causative agents (Pulingam et al. 2022; Hasan and Ahmed 2023; Qader and Ganjo 2024). These agents are usually applied at sub-inhibitory concentrations; hence, they exhibit no bacteriostatic or bactericidal activities. Rather, they suppress the QS system and allow the immune system to enhance their effect efficiently (Ma'aitah 2024). In addition, anti-QS agents at sub-inhibitory concentrations exhibited no or minimal toxicity (Haque et al. 2021).

P. aeruginosa, as a community in a biofilm, uses QS systems to achieve maximal effect of their pathogenicity

* Corresponding author. e-mail: haitham@mutah.edu.jo.

and to get through the immune system. The QS system controls the production of various virulence factors in *P. aeruginosa*. First, it starts to produce the chemical signals at a slow rate, which is called autoinducers (AIs) (Brindhadevi et al. 2020). As population density increases, the AI production reaches a threshold, which enables AIs to diffuse into the cytoplasm and complex with specific receptors. This interaction induces gene expression that results in the biosynthesis of virulence factors, which enhances biofilm formation (Vadakkan et al. 2023). It was established that bacteria in biofilms, such as in *P. aeruginosa*, have heightened sensitivity against antibiotics by up to a tenfold factor (Høiby et al. 2010). QS system inhibition could, therefore, reduce the biosynthesis of virulence factors and suppress biofilm formation.

The natural products of plants have been the source of novel biologically active agents (Najmi et al. 2022). Man, since ancient times, has utilized medicinal plants for treatment and relieving the symptoms of diseases. The use of these plants is still growing, specifically in developing countries (Khatib et al. 2021). Scientific testing of some of these traditional plants has provided strong evidence of their effectiveness and safety (Tran et al. 2020). Their traditional use in folk medicine, the successful development of some naturally-based drugs, and their multiple modes of action make them an attractive source for exploring new, promising drugs (Huang et al. 2022) (Bernstein et al. 2021).

Psidium guajava (local name: guava) is a plant tree from the Myetaceae family. Guava fruits are edible as row fruits or as juice. The leaves are known in traditional medicine to relieve respiratory tract symptoms such as flu, cough, and sore throat (Dange et al. 2020). *P. guajava* leaf extract has been found to exhibit antioxidant, antibacterial, anti-inflammatory, anti-allergy, anticough, antiplasmodial, antidiabetic, antinociceptive, antispasmodic, hepatoprotective, and cardioactive effects (Gutiérrez et al. 2008; Anand et al. 2016). However, *P. guajava* leaf extract possesses no or weak antibacterial activity against *P. aeruginosa* (Qaralleh et al. 2020). Thus, this study aimed to evaluate the ability of *P. guajava* methanolic extract to attenuate the quorum sensing system, inhibit biofilm formation, and suppress virulence factors in *P. aeruginosa*. Additionally, we analyzed the extract's chemical composition using LC-MS and examined its mode of action via RT-PCR.

2. Materials and method

2.1. Plant materials

Leaves of *Psidium guajava* were purchased from a traditional herbal market in Jordan. The voucher specimen (MU2023-011) was deposited in the department of biology, Mutah University, Karak, Jordan. The leaves were cleaned to remove dust and any extraneous plant material. The leaves were then processed into a fine powder. The extraction process was performed by soaking 250 g of powdered leaves in 500 mL of methanol and incubating them at room temperature for 24 hours. Then, the solvent was collected after filtration and evaporated using a rotary evaporator. The crude that was produced was collected and stored at 4°C.

2.2. Bacterial species

P. aeruginosa was provided by AlKarak Government Hospital, AlKarak, Jordan. The species was isolated from a urine sample and identified using standard methods, including culture on selective media, analysis of colony morphology, microscopic examination, and biochemical testing. Identification of species level and their antibiotic-resistant profile was made using Biomérieux VITEK®2. It was identified as Beta-Lactamase producing *P. aeruginosa*. *Chromobacterium violaceum* ATCC 12472 was purchased from American Type Culture Collection (ATCC).

Stock solutions of *P. guajava* extract were prepared in 10% DMSO. Bacterial cultures were standardized to 0.5 McFarland turbidity. For the treated samples, the desired final concentrations of the extract were achieved by diluting the stock solution in sterile broth and adding the adjusted bacterial culture. Untreated cultures were prepared using only broth media and the standardized bacterial suspension. In all experiments, a negative control was included, consisting of broth media, 10% DMSO, and the standardized bacterial culture.

2.3. The bacteriostatic effect on P. aeruginosa

The disc diffusion method was performed for preliminary antibacterial activity of methanolic extract *P. guajava* against *P. aeruginosa*. Muller Hinton Agar was prepared and inoculated with 100 µL of bacterial suspension at a concentration of 10^8 CFU/mL. A disc loaded with 1 mg/mL P. guajava methanolic extract was applied on the surface of prepared MHA. The inhibition zone diameter developed after 24h incubation at 37°C was measured in mm (Nigam et al. 2016).

A more precise evaluation of antibacterial activity was conducted using the microdilution method, which can provide a guide to determining the lowest inhibitory concentration (MIC) of *P. guajava* methanolic extract to prevent the complete visible growth of *P. aeruginosa* (Qaralleh et al. 2021). Briefly, several concentrations (4.8, 2.4, 1.2, 0.6, 0.3, and 0.015 mg/mL) of *P. guajava* methanolic extract were prepared in a 96-well plate. Then, 10 µL of bacterial suspension containing 10^4 CFU/mL was added to each well and incubated at 37°C for 24h. Then, the absorbance was measured using ELIZA reader (MCL-2100C, China) at 600 nm.

2.4. Biofilm inhibitory effect

The influence of the extract on *P. aeruginosa* as an anti-biofilm agent was assessed using the crystal violet assay according to (Qaralleh et al. 2020; Qaralleh 2023). A 96-well plate (Polystyrene) was prepared as described before for MIC. Its content was aspirated, washed, and replaced with crystal violet. Then, the dyed plate was incubated at a room temperature for 15 min. The plate contents were removed again, and a decolorization process was initiated by filling the well with 96% ethanol. The plate was incubated at room temperature for 15 min. Using a micropipette, the contents of the wells were transferred to a new 96-well plate, and the absorbance at 570 nm was measured. Untreated culture and culture treated with DMSO (10%) were used as controls. The percentage of inhibition in biofilm formation was calculated in reference to the untreated culture, and the lowest concentration

required to inhibit 50% of the biofilm was reported as MBIC50.

2.5. Effect on the viable cells of the biofilm

A 96-well plate was prepared and incubated as described in the MIC procedure (Gordya et al. 2017). The wells were emptied of their contents and washed adequately to remove free, nonattached cells. Then, 200 µL of a Triphenyltetrazolium chloride (TTC) (Santa Cruz Biotechnology, USA) solution (containing 0.2% glucose and 50 µL of 5 mg/mL TTC) was added to each well and incubated for 6 hours at 37°C with shaking at 150 rpm. The absorbance at 405 nm was measured, and the percentage of reduction in viable cells was calculated in reference to the standard control group.

2.6. Observation of the antibiofilm effect using Light Microscope (LM) and Scanning Electron Microscope (SEM)

A sterile cover slip was placed on the bottom surface of 24-well plates before adding untreated and treated *P. aeruginosa* cultures to the wells. The prepared plates were incubated without shaking for 48h at 37°C. Then, the glass slips were removed, washed, and stained with crystal violet for 1 min. Then, the slips were observed using a LM (NIKON, Japan). In parallel, another set of slips was similarly prepared for SEM observation. However, the slips were incubated in 5% glutaraldehyde for 24h and then dehydrated using a gradual increase in ethanol concentrations in water (10, 30, 50, 70, and 100%). The samples were subjected to critical point drying and finally observed using SEM (Thermo Scientific Phenom Desktop SEM, JU-24112022, Waltham, MA, USA).

2.7. Effect on biofilm stages

2.7.1. Swarming

A jelly-like swarming medium was prepared using 0.5% agar (Sagar et al. 2022). After autoclaving, the tested materials were mixed with the molted agar and poured into petri dishes. The prepared plates were left to solidify, and 1 µL of 24h old *P. aeruginosa* culture was inoculated at the center of the plate using a sterile calibratative loop. The inoculated plates were incubated for 48h, and the swarming area was measured in mm and compared with the typical swarming pattern of the normal untreated cells.

2.7.2. Aggregation

The effect on the aggregation ability of *P. aeruginosa* was evaluated according to (Shanks et al. 2008). In brief, the absorbance of 1 mL of the treated *P. aeruginosa* culture was measured at 600 nm to determine the initial absorbance (iAbs). The culture was then vortexed for 1 min and the post vortixing absorbance was measured again (sAbs). Untreated *P. aeruginosa* was used as a control. The percentage of aggregation for the untreated and treated cultures of *P. aeruginosa* was calculated according to the following formula:

Percentage of aggregation = [(sAbs – iAbs) / sAbs] * 100

2.7.3. Hydrophobicity

The effect on the surface hydrophobicity of *P. aeruginosa* was examined using n-hexadecane (Krishnan et al. 2012). In brief, the absorbance of 1 mL of the treated *P. aeruginosa* culture was measured at 600 nm to determine the initial absorbance (iAbs). This culture was then mixed with 1 mL n-hexadecane (Sigma Aldrich, USA). The mixture was subjected to vortexing (2 min) and left to fractionate. After 15 min., the second absorbance at 600 nm was measured (sAbs). The percentage of hydrophobicity was calculated using the following formula:

Percentage of hydrophobicity = [(sAbs – iAbs) / sAbs] * 100

2.7.4. EPS

Treated and untreated cultures of *P. aeruginosa* were centrifuged. After centrifugation, portions of the supernatant were mixed with cold ethanol in a 1:3 ratios. The solution was incubated at 4°C for 24h. Then, the centrifugation (10000 rpm for 15 min) was made, and to the collected pellets, distilled water (3 mL), 5% cold phenol (1 mL), and 98% sulfuric acid (5 mL) were supplemented. Absorbance at 490 nm (Shimadzu UV-1601, Japan) was reported, and the percentage of EPS was calculated in reference to the standard control group (Razack et al. 2011).

2.8. Effect on virulence factors

2.8.1. Pyocyanin

Pyocyanin was extracted from treated and untreated cultures of *P. aeruginosa* using chloroform (Hossain et al. 2017). 1 mL of the culture supernatant was mixed with an equal volume of chloroform. Chloroform containing pyocyanin was separated and added to 1.5 mL of 0.2N hydrochloric acid. The absorbance at 520 nm of the developed pink color solution was measured, and the percentage inhibition in pyocyanin production was calculated in reference to the untreated culture.

2.8.2. Rhamnolipids

Rhamnolipids were extracted from treated and untreated cultures of *P. aeruginosa* using diethyl ether (Luo et al. 2017). 1 mL of the culture supernatant was mixed with 3 mL of diethyl ether. Diethyl ether containing rhamnolipids was separated, concentrated using a rotary evaporator, and supplemented with 200 µL of water and 900 µL of 0.18% orcinol (w/v) in 53% (v/v) H_2SO_4. The solution was then heated at 24°C for 30 min and the absorbance at 421 nm was measured. The percentage of inhibition in rhamnolipid production was calculated in reference to the untreated culture.

2.8.3. LasA protease

LasA protease activity was measured using azocasein as a substrate (Andrejko et al. 2013). The reaction was prepared by mixing 1 mL of the culture supernatant with 0.1 mL of azocasein (Sigma Aldrich, USA) and 3 mL of 50 mM phosphate buffer (pH 7.5). The reaction was allowed to react for 1h, at 37°C, and 150 rpm. The reaction was terminated by adding 0.5 mL of trichloroacetic acid (TCA) (Thermo Fischer Scientific, China), followed by centrifugation at 10,000 rpm for 10 minutes. The absorbance of the collected supernatant was measured at 366 nm. The percentage of inhibition in LasA protease activity was calculated in reference to the untreated culture.

2.8.4. Chitinase

Chitinase activity was measured using chitin azure as a substrate (Hossain et al. 2017). The reaction was prepared

by mixing 0.5 mL of the culture supernatant with 4.5 mL of chitin azure (Bioscientific Carbosynth, UK) solution. The reaction was allowed to react for 24h, at 37°C. Then, it was subjected to centrifugation for 10 min and the absorbance of the collected supernatant was measured at 570 nm. The percentage of inhibition in chitinase activity was calculated in reference to the untreated culture.

2.9. Mechanism of quorum sensing

2.9.1. Effect on violacein production

The preliminary evaluation of *P. guajava* methanolic extract on violacein production by *C. violaceum* was made using the well diffusion method. MHA was inoculated with 100 µL of bacterial suspension containing 10^8 CFU/mL. A well of 6 mm was made in MHA and loaded with 100 µL of 1 mg/mL *P. guajava* methanolic extract. The development of the violacein inhibition zone after 24h of incubation at 37°C was measured in mm.

A more precise evaluation of the effect on violacein production was performed quantitatively (Gómez-Gómez et al. 2019). The violacein contents of a 1 mL supernatant from the untreated and treated cultures of *C. violaceum* were extracted using 1 mL DMSO for 30 min. Then, the mixture was centrifuged, and the absorbance at 575 nm for the supernatant was measured. The percentage of violacein inhibition was calculated in reference to the untreated group.

2.9.2. Acyl Homoserein Lactone (AHL) production

AHL was extracted from treated and untreated cultures of *P. aeruginosa* using ethyl acetate (Lee et al. 2017). 2 mL of the culture supernatant was mixed with 3 mL of ethyl acetate. At the end of the incubation (24h and 40°C), 40 µL of the ethyl acetate extract was supplemented with 50 µL from a solution that was prepared by mixing equal volumes of 2 M hydroxyl amine and 3.5 M NaOH, and 90 µL from a solution that was prepared by mixing equal volumes of 10% ferric chloride in 4% HCL and 95% ethanol. Next, absorbance at 520 nm was reported, and the percentage of AHL inhibition was calculated in reference to the standard control group.

2.9.3. Expression of Quorum sensing genes

The total RNA was extracted from the untreated and treated cultures of *P. aeruginosa* using a direct-zoltm RNA miniprep kit (Zymo Research Company, USA). The synthesis of the complementary cDNA was performed using the SensiFASTTM cDNA synthesis kit (Bioline Reagents, UK). The gene expression was prepared using the Bioline SensiFAST™ SYBR® No-ROX Kit (Bioline Reagents, UK), and the tested gene expressions were normalized to the expression of 16S rRNA as a housekeeping gene using the 2ΔCT formula. The primer sequences used in this test are presented in Table 1 (Banerjee et al. 2017).

Table 1. Sequences of primers of *PhazA1, apraA, PelA* and *Psl* genes.

Gene	Primer Sequence 5'-3'		References
16S rRNA	Forward	CAAAACTACTGAGCTAGAGTACG	(Lenz et al. 2008)
	Reverse	TAAGATCTCAAGGATCCCAACGGCT	
PelA	Forward	CCTTCAGCCATCCGTTCTTCT	(Li et al. 2019)
	Reverse	TCGCGTACGAAGTCGACCTT	
PslA	Forward	AAGATCAAGAAACGCGTGGAAT	(Irie et al. 2012)
	Reverse	TGTAGAGGTCGAACCACACCG	
PhazA	Forward	CGAACCACTTCTGGGTCGAGTGC	(Vandeputte et al. 2011)
	Reverse	GGGAATACCGTCACGTTTTATTTGC	
AprA	Forward	GGCAATCCTGGTACCTGATCAA	(Cabrol et al. 2003)
	Reverse	AGCGTCTGGCGCCCGTAGTT	

2.10. Chemical composition

The analysis of the chemical composition of *P. guajava* methanolic extracts was carried out using LC-MS (LC-8030, Shimadzu, Japan). The column used was XDB-C18 (150 mm length × 2.1 mm internal diameter, 3.5 µm film thick), and the mobile phase used was prepared using two solvents: A (0.1% formic acid in water) and B (0.1% formic acid in acetonitrile). A 50 µL of the sample was injected and eluted using a gradient mobile phase of 5% of A (5 min), 5-100% of B (15 min), and 100% of B (5 min) at a rate of 500 µL/min. 1 µl of the sample was injected using the Shimadzu CBM-20A system controller. Mass spectrometry was performed in positive ion mode using electrospray ionization (ESI-MS), scanning m/z from 100 to 1000. The ESI-MS was operated with a capillary voltage of 125 V, a skimmer voltage of 65 V, and nitrogen gas flow at 10 L/min at 45 psi. The capillary temperature was maintained at 350°C.

2.11. Statistical analysis

The significant difference between the treatment groups and the untreated standard group was assessed using one-way ANOVA and expressed as stars (*, **, or ***) corresponding to the P-values of $p < 0.05$, $p < 0.01$, and $p < 0.001$, respectively.

3. Results

3.1. Antibacterial activity

The inhibition zone observed for the methanolic extract of *P. guajava* against *P. aeruginosa* is 11.67 mm, and the MIC was found to be within the range of 1.1-3.3 mg/mL (Table 2). DMSO, the negative control, showed no antibacterial activity, while the positive control (tetracycline) showed an inhibition zone of 22.5 mm.

Table 2. Diameter of inhibition zone and MIC for the methanolic extract *P. guajava* leaf against *P. aeruginosa*

	Inhibition zones (mm)	MIC (mg/mL)
P. guajava methanolic extract (1 mg/disc)	11.67±0.3	1.1-3.3
Tetracycline (30 µg/disc)	22.5±0.3	-
DMSO	0.0	-

-: not determined

3.2. Antibiofilm

The impact of *P. guajava* extract on the formation of biofilm was investigated using a broad range of concentrations (10-0.0005 mg/mL) (Figure 1). Application of 10, 3.3, 1.1, and 0.37 mg/mL extracts completely (≥ 95%) prevented the formation of *P. aeruginosa* biofilm, while at lower concentrations (0.12–0.0005 mg/mL), the treatment led to a gradual decrease in inhibition. A significant ($P < 0.001$) percent of inhibition equal to 59.5% was reported at a treatment concentration of 0.12 mg/mL, while it dropped significantly to 37.0, 24.5, and 17.5% at 0.04, 0.014, and 0.005 mg/mL. As shown in Figure 1, the MBIC50 can be observed within the range of 0.12 and 0.04 mg/mL.

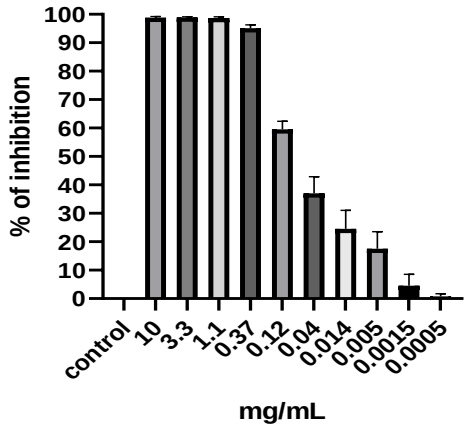

Figure 1. The effect of *P. guajava* methanolic extract on the ability of *P. aeruginosa* to form a biofilm, as indicated by the percentage inhibition. The percentage of inhibition for the untreated (control) culture was considered 0.

As previously mentioned, the MIC of *P. guajava* extract was within the range of 1.1 and 3.3 mg/mL. Consequently, the antibiofilm effect at ≥ 1.1 mg/mL appears to be due to the bacteriostatic action of the extract. Therefore, a TTC assay was performed to examine the effect of the extract on the viable cells within the biofilm matrix. The findings of the TTC assay (Figure 2) provide extra evidence that the inhibition of biofilm formation at concentrations of 10, 3.3, and 1.1 mg/mL is due to the bacteriostatic effect of *P. guajava* methanolic extract, as indicated by the significant reduction in the viable cell to less than 10%. However, the reduction in viable cells was non-significant for treatment concentrations equal to or less than 0.37 mg/mL, indicating that the inhibition of biofilm formation is not due to the bacteriostatic effect but rather to the antibiofilm action of the extract. Therefore, concentrations of 0.37, 0.12, and 0.04 mg/mL, which demonstrated the maximum antibiofilm effect without affecting cell viability, were selected for further investigation.

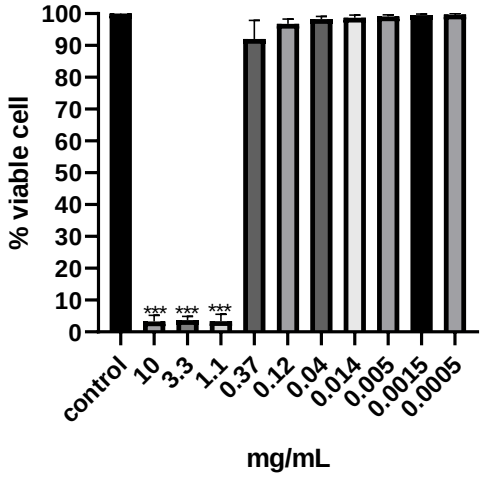

Figure 2. The effect of *P. guajava* methanolic extract on the percentage of viable cell. *, **, or *** corresponding to the P-values of $p < 0.05$, $p < 0.01$, and $p < 0.001$, respectively

3.3. Biofilm observation using LM and SEM

To confirm the effect of *P. guajava* methanolic extract on *P. aeruginosa* biofilm, the normal and treated biofilms were prepared and visualized using LM and SEM (Figure 3 and 4). SEM images clearly demonstrate the effect of the *P. guajava* extract on biofilm formation. As shown in the LM and SEM images (Figure 3 and 4), the images of untreated culture showed the ability of *P. aeruginosa* to form a normal biofilm that is composed of multilayered aggregated cells. The ability of the extract to prevent *P. aeruginosa* from building biofilm can be observed in Figure 3B-D, which showed the presence of no aggregated scattered cells. These signs appear to increase clearly as the concentrations of the treatment increase.

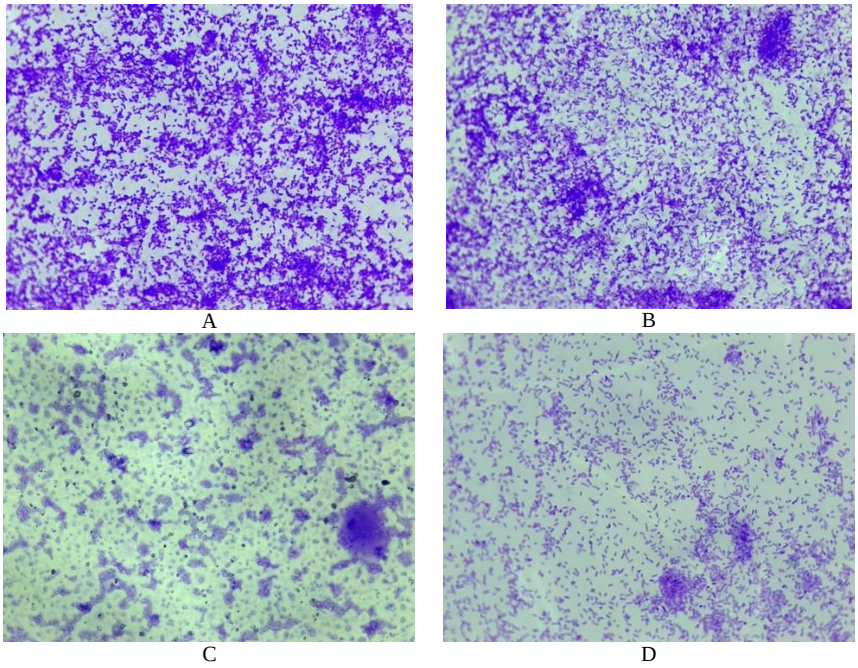

Figure 3. LM images (40X) of *P. aeruginosa* treated with 0 (A), 0.04 (B), 0.12 (C), and 0.37 mg/mL (D) *P. guajava* methanolic extract

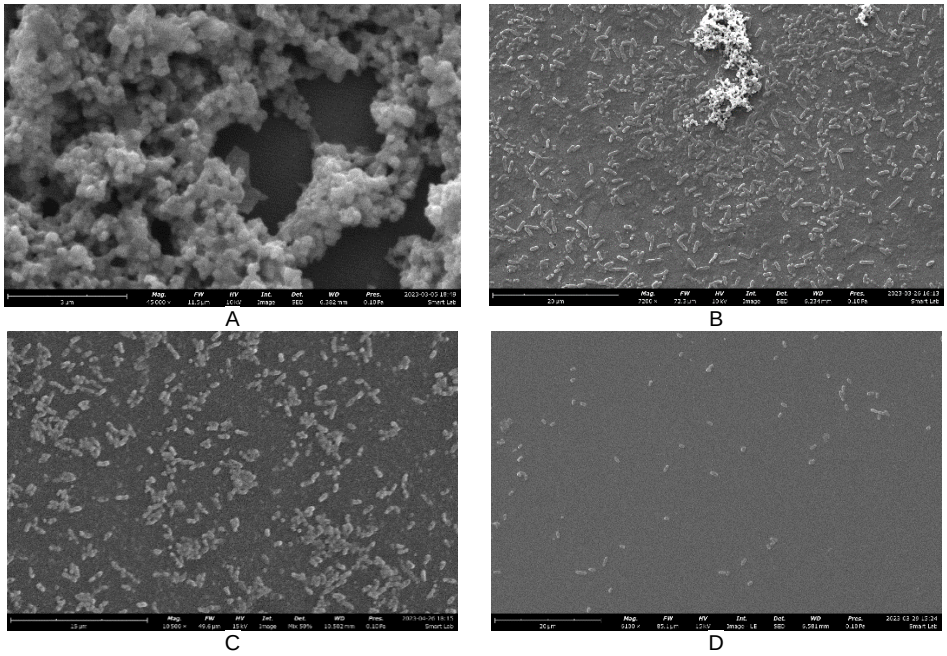

Figure 4. SEM images of *P. aeruginosa* treated with 0 (A), 0.04 (B), 0.12 (C), and 0.37 mg/mL (D) *P. guajava* methanolic extract

3.4. Effect on the biofilm development

The effect of *P. guajava* methanolic extract on swarming motility, aggregation ability, and surface hydrophobicity as significant factors in biofilm development has been evaluated.

3.4.1. Swarming motility

The ability of *P. aeruginosa* to swarm decreased in a dose-dependent manner as a result of the treatment with 0.37, 0.12, and 0.04 mg/mL *P. guajava* extract (Figure 5A). As the concentration of the extract increased, the zone of swarming (mm) decreased. However, the decrease was significant ($p < 0.01$) only at the treatment concentration of 0.37 mg/mL.

3.4.2. Aggregation

The results showed that *P. guajava* methanolic extract displayed a dose-dependent manner of inhibition in the aggregation (Figure 5B). At the treatment concentration of 0.37 mg/mL, the aggregation was significantly ($p < 0.05$) reduced from 28.0% to 10.0%. The aggregation at 0.12 mg/mL was notably reduced to 16.1%, but it was insignificant.

3.4.3. Hydrophobicity

As shown in Figure 5C, the reduction in hydrophobicity was significantly decreased from 62% to 26.3% when the treatment was made using 0.37 mg/mL. In contrast, the reduction due to the treatment with 0.12 or 0.04 mg/mL was insignificant.

3.4.4. EPS

As shown in Figure 5D, EPS production significantly decreased in a dose-dependent manner. At 0.37 and 0.12 mg/mL, EPS production decreased significantly to 72.2 and 88.7%, respectively. At a lower concentration (0.04 mg/mL), the reduction in EPS was insignificant.

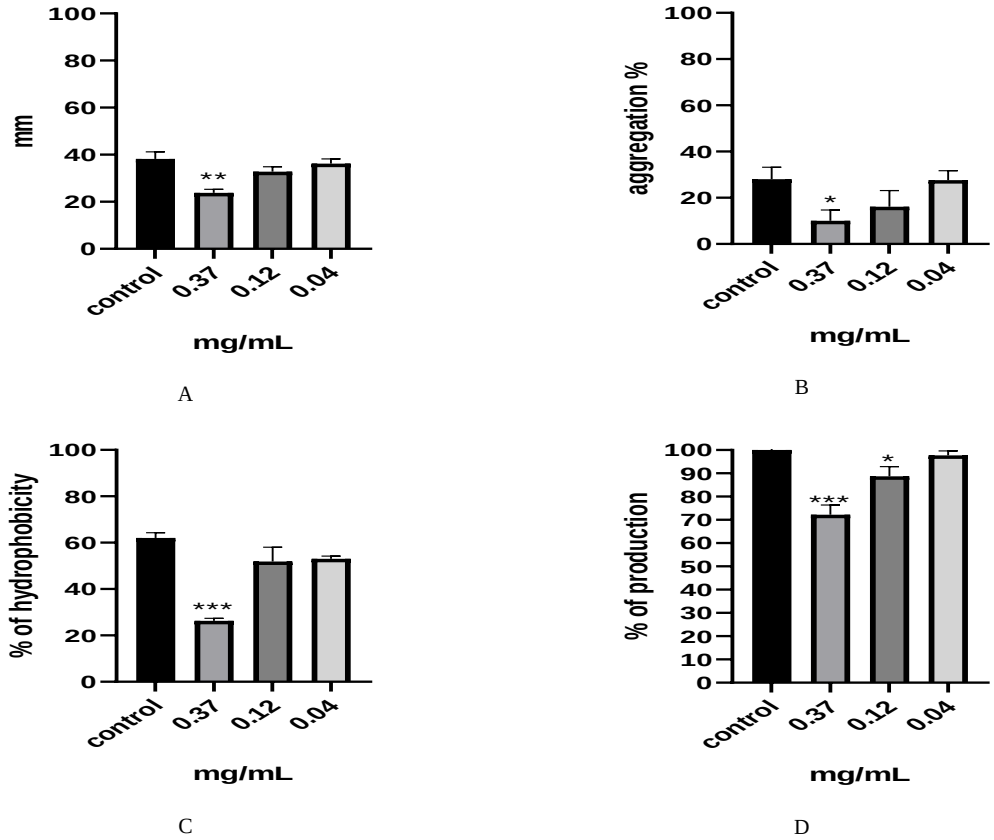

Figure 5. The effect of *P. guajava* methanolic extract on different stages in biofilm formation, including swarming motility (A), aggregation (B), hydrophobicity (C), and EPS production. *, **, or *** corresponding to the P-values of $p < 0.05$, $p < 0.01$, and $p < 0.001$, respectively

3.5. Effect on the virulence factors

3.5.1. Pyocyanin

The ability of *P. guajava* methanolic extract to suppress the production of pyocyanin pigment in *P. aeruginosa* was evaluated (Figure 6A). The treatment resulted in significant dose-dependent inhibition of pyocyanin production, with inhibition rates of 42.3% and 24.0% at concentrations of 0.37 and 0.12 mg/mL, respectively. The reduction at 0.04 mg/mL was insignificant.

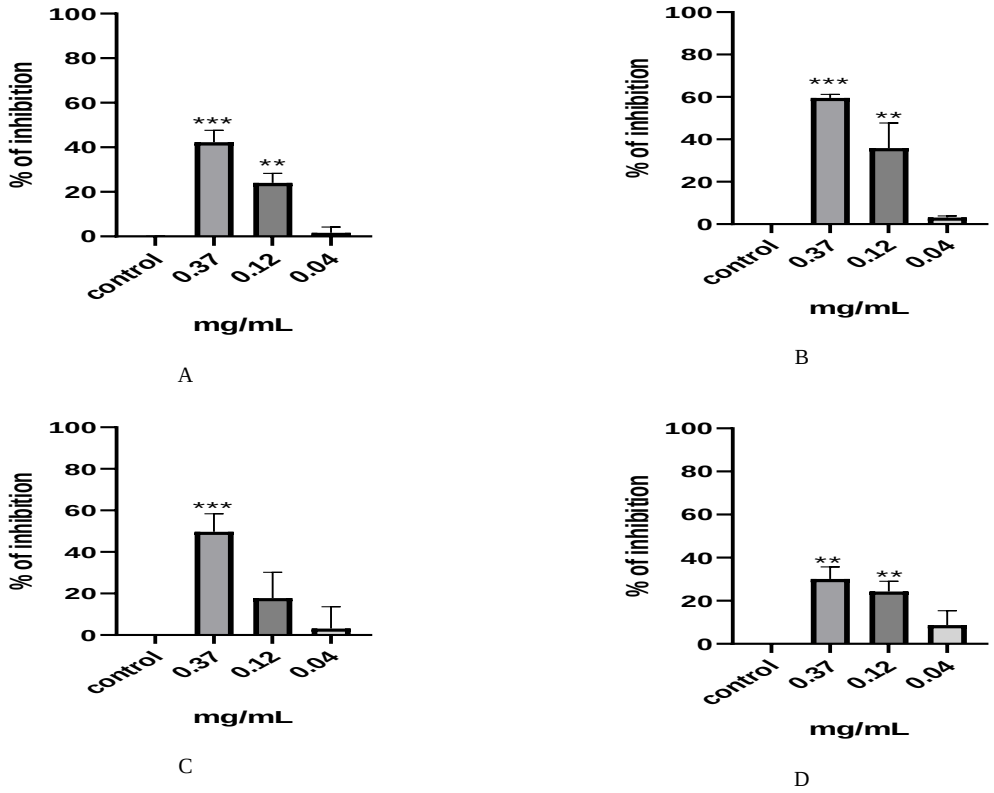

Figure 6. The effect of *P. guajava* methanolic extract on *P. aeruginosa* virulence factors, including pyocyanin (A), rhamnolipids (B), LasA protease (C), and chitinase (D). *, **, or *** corresponding to the P-values of $p < 0.05$, $p < 0.01$, and $p < 0.001$, respectively

3.5.2. Rhamnolipids

As shown in Figure 6B, the pattern of the inhibitory effect of *P. guajava* methanolic extract on rhamnolipid production appears to be similar to that of pyocyanin. A dose-dependent inhibitory effect was observed. The percentage of rhamnolipid inhibition was 59.5% and 35.9% at treatment concentrations of 0.37 and 0.12 mg/mL, respectively. No significant reduction was observed due to the treatment with 0.04 mg/mL.

3.5.3. LasA protease

As shown in Figure 6C, the inhibitory effect of *P. guajava* methanolic extract on the activity of LasA protease was displayed in a dose-dependent manner. However, the treatment at 0.37, 0.12, and 0.04 mg/mL led to a decrease in protease activity, as indicated by the percentage inhibition of 49.7, 17.8, and 3.1%, respectively. The statistically significant ($p < 0.001$) reduction was found only at 0.37 mg/mL.

3.5.4. Chitinase

Treating *P. guajava* methanolic extract resulted in a dose-dependent inhibitory effect on the chitinase activity (Figure 6D). Treating *P. aeruginosa* with the extract resulted in a significant ($p < 0.01$) reduction in the chitinase activity, with a percentage inhibition of 30.1 and 24.3% observed at 0.37 and 0.12 mg/mL, respectively. The percentage of inhibition was non-significant at 0.04 mg/mL.

3.6. Mechanism of action

3.6.1. Violacein

The effect of *P. guajava* methanolic extract on the production of violacein pigment by *C. violacium* was investigated to assess the effect of the extract on the QS system. A preliminary finding using the well diffusion method showed the ability of the extract to inhibit the QS system, as indicated by the development of a 13.5 mm non-pigmented zone around the well. Moreover, the quantitative analysis (Figure 7A) confirmed this finding and observed a significant ($p < 0.001$) reduction in violacein production. A percentage inhibition of 69.2 and 42.0% was observed when the extract was applied at 0.37 and 0.12 mg/mL, respectively.

3.6.2. AHL

The results showed that *P. guajava* extract causes a dose-dependent inhibition of AHL production (Figure 7B). The percent of AHL production was reduced significantly ($p < 0.001$) by 29.5% due to the treatment of 0.37 mg/mL extract. The reduction in AHL due to the treatment with the methanolic extract at lower concentrations (0.12 and 0.04 mg/mL) was insignificant.

3.6.3. The effect on PelA, PslA, PhzA1, and aprA genes

The effect of *P. guajava* methanolic extract on the mRNA expression of *PelA*, *PslA*, *PhzA1*, and *aprA* genes was evaluated using RT-PCR (Figure 7C). The results showed that the extract caused a significant reduction in the expression of these genes. Statically, the maximum reduction ($P < 0.01$) was observed in the expression of the *PhzA1* gene.

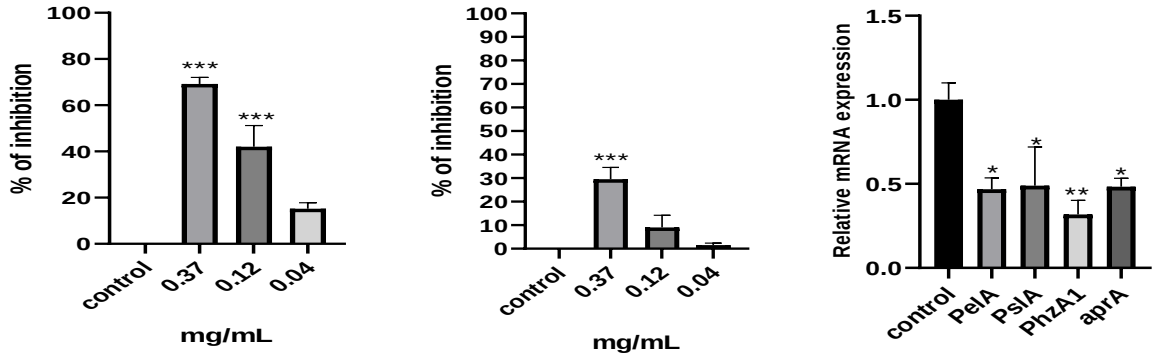

A B C

Figure 7. The effect of *P. guajava* methanolic extract on the ability of *C. violaceum* to produce violacein pigment (A), *P. aeruginosa* to produce AHL (B), on the mRNA expression of QS dependent genes (C). *, **, or *** corresponding to the P-values of $p < 0.05$, $p < 0.01$, and $p < 0.001$, respectively.

3.7. Chemical composition of P. guajava methanolic extract

The chemical composition of *P. guajava* methanolic extract was analyzed using LC-MS (Table 3). Flavonoids were identified as the most dominant components among a total of 22 compounds. The most dominant content identified was quercetin, representing 17.6% of the total content. Remarkably, the presence of 17.2% of avicularin and 15.4% of kaempferol as dominant components was also reported. These three main contents represent more than 50% of the total contents of the extract. Besides, the LC-MS analysis showed that chlorogenic acid (9.1%), kaempferol-3-glucoside (6.3%), lutein (6.1%), and beta-carotene (5.2%) were present in considerable amounts.

Table 3. Chemical composition of *P. guajava* methanolic leaf extract using LC-MS

	Chemical compound	**Classification**	**%**
1	Ellagic acid	Phenolic acid	0.2
2	Leucocyanidin	Leucoanthocyanidin (flavan-3,4-diols)	0.1
3	Querecetin	Flavonoid	17.6
4	Kaempferol-3-glucoside	Glycoside flavonoid	6.3
5	Avicularin	Flavonoid	17.2
6	Ferulic acid	Phenolic acid	7.3
7	Lutein	Carotenoid	6.1
8	Chlorogenic acid	Phenolic acid	9.1
9	Beta-Carotene	Carotenoid	5.2
10	Kaempferol	Flavonoid	15.4
11	Quercetin 3-beta-galactoside	Glycoside flavonoid	0.1
12	Gallic acid	Phenolic acid	2.2
13	Lycopene	Carotenoid	0.1
14	Guaijaverin	Flavonoid	2.2
15	Caffeic acid	Phenolic acid	1.3
16	Phytofluene	Carotenoid	1.3
17	Rubixanthin	Carotenoid	0.1
18	Oleanolic acid	Triterpene	0.1
19	Ursolic acid	Triterpene	0.1
20	Beta-Sitosterol	Triterpene	0.1
21	Uvaol	Triterpene	0.1
22	Protocatechuic acid	Phenolic acid	0.2

4. Discussion

Continuing to use antibiotics directly to kill or inhibit bacteria may become an ineffective therapy due to the ability of many pathogenic bacteria to produce biofilm. Therefore, the use of antibiotics to treat many infectious diseases has become impossible, and this may lead to many health problems that are dangerous to human life (Pulingam et al. 2022). With the diversity of strategies for producing new antibiotics or protocols to control infectious diseases, it is clear that finding a drug that can reduce bacteria's virulence factors is among the best-used strategies currently. This mechanism works by impairing the ability of bacteria to produce virulence and develop biofilms through QS disruption (Haque et al. 2021). Natural products with active ingredients can be excellent candidates to serve as a source for developing anti-QS agents. Thus, *P. guajava* has been selected for this study.

It was demonstrated that *P. guajava* exhibited weak antibacterial action both by using disc diffusion and a microdilution method. Thus, the findings are in agreement with the findings of (Cheruiyot et al. 2009; Qaralleh et al. 2020), which showed that this leaf methanolic extract obtained from the *P. guajava* leaf presents weak antibacterial action or its lack against *P. aeruginosa*.

The plant natural products were earlier reported as antibiofilm agents. *Tilia cordata* and *Nepeta curviflora* polar-essential oils extracts from *Thymbra capitata* were previously reported for their potent antibiofilm activity (Qaralleh 2019; Qaralleh et al. 2020; Qaralleh 2023). In this study, methanolic extract of *P. guajava* showed potent antibiofilm activity at 0.37, 0.12, and 0.04 mg/mL against *P. aeruginosa*. At these concentrations, there was no significant decrease in viable cells, which implicates the antibiofilm activity of the bioactive extract against *P. aeruginosa* as a mode of suppression of biofilm formation rather than through reductions in the number of viable cells. The methanolic extract of *P. guajava* was further confirmed to impede the development of the biofilm of *P. aeruginosa* by both light and scanning electron microscopy.

The transition of bacteria from a planktonic free-living lifestyle to one of living in communities and as a biofilm is an orderly process in a series of successive events. A conditioning film is formed that attracts other bacterial cells to the surface, where they attach and start to accumulate. The cells in the resultant community proliferate, and the biofilm matures. Some of these cells detach from the biofilm to colonize new surfaces during the dispersion phase where they express other biofilms. However, some of these cells in the dispersion phase could reattach themselves to other surfaces to form biofilms (Sauer et al. 2022). In this study, the effect of 0.37 mg/mL of *P. guajava* methanolic extract on different factors that affect biofilm development, including motility, hydrophobicity, aggregation, and EPS production, has been evaluated. Interestingly, *P. guajava* extract causes a significant reduction in these factors.

As shown in the results, the extract has a significant reduction effect on *P. aeruginosa* surface hydrophobicity, aggregation ability, and swarming motility. It is logical to assume that some components of the plant extract have affinity to bind with the adhesion sites, preventing adhesion and aggregation. The reduction in adhesion and aggregation may be due to the inhibition of bacterial motility. Agents that inhibit bacteria from swarming usually prevent the initial stage of biofilm formation (Shrout et al. 2006). In addition, perhaps one of the most important roles for the EPS is to stimulate adhesion and aggregation, and its role extends to maintaining the development of biofilm (Kassinger and van Hoek 2020). The use of the *P. guajava* extract led to the inhibition of these interfering factors, which in turn led to the prevention of the formation of biofilms. It is possible that the plant extract led to this result through several mechanisms.

P. guajava extract showed a profound effect on suppressing *P. aeruginosa* virulence factors. This suggests that it may interfere with the QS system. Suppression of the QS system results in decreasing AI production, decreasing virulence factor production, and hence attenuating pathogenicity (Ahmed et al. 2019). Protease and elastase, as secreted virulence factors, are concerned about adhesion and colonization. Furthermore, they act to cause tissue damage and facilitate invasiveness in the tissue host. With the help of the chitinase enzyme, they promote bacterial aggregation and infection. Pyocyanin is produced to function as a chelating agent to extract iron from transferrin (Andrejević et al. 2023). In biofilms, pyocyanin forms complexes with eDNA, increasing surface hydrophobicity and aggregation, thereby maintaining the integrity of the extracellular polymeric substance (EPS) and biofilm stability (Abdelaziz et al. 2023). Rhamnolipids are surfactant factors that mediate motility and biofilm initiation. Reports showed that reducing rhamnolipid production inhibits swarming motility, but when rhamnolipids are supplemented again, their function is restored and they facilitate motility (O'May and Tufenkji 2011). The significant suppression in the production of these factors suggests that *P. guajava* extract exhibits unique anti-QS activity that may disrupt the ability of *P. aeruginosa* to cause disease and impede the progression of the infection.

The sequence of events that make the free-living bacterial cells form a microcolony and reach a threshold level ends in the activation of the QS system and the production of AI. In this study, the results showed that the extract resulted in a significant reduction in AHL production. AHL is a type of AI that is produced due to the activation of the QS system (Ashraf et al. 2018). Therefore, a reduction in AHL may suggest that the extract may suppress the QS system. In *P. aeruginosa*, four QS systems are used: two are AHL-dependent, called the Las and Rhl systems, while the third system, the Pqs system, is quinolone-dependent, and the last one is the Iqs, carbaldehyde-dependent system. However, the Las system works as a master system that regulates all systems; the regulation of these systems is interconnected (Vetrivel et al. 2021). These QS systems regulate virulence factor production (Soukarieh et al. 2018). The Las system controls the production of alkaline protease, Psl EPS, Pel EPS, elastase A, and elastase B through the aprA, psl, pel, lasA, and lasB genes, respectively (Ueda and Wood 2009). All but aprA are also regulated by the Pqs system, which controls the production of rhamnolipids, pyocyanin, and lectin A and B (Lin et al. 2018; Turkina and Vikström 2019).

In the current investigation, the effect of the methanolic extract of *P. guajava* on the mRNA expression of the *psl*, *pel*, *aprA*, and *phzA1* genes was assessed. The production of pel and psl as part of the biofilm matrix is vital in mediating adhesion and organization as well as providing defense. While the *aprA* gene mediates alkaline protease production that denatures complementary and cytokine proteins, the *phzA1* gene controls the secretion of pyocyanin (Mellbye and Schuster 2014) (Pezzoni et al. 2020). When *P. aeruginosa* was treated with 0.37 mg/mL *P. guajava* extract, a significant reduction in *Pel*, *Psl*, *aprA*, and *phzA1* genes was observed. However, the most notable decrease was seen in the expression of the *phzA1* gene. In fact, *Pel*, *Psl*, and *aprA* are Las-dependent genes, while *phzA1* is a pqs-dependent gene. This may suggest that the extract may exert multiple effects through inhibition of the Las and pqs systems, or it may disrupt the interconnection and feedback mechanisms between these QS systems, such as those between the Las system and Rhl, Pqs and Iqs, the Pqs system and Rhl system, and the Iqs system and Pqs system (Pesci et al. 1997).

The inhibitory effect of *P. guajava* extract may be due to one of its active ingredients or a synergism between them. Vasavi and co-authors found that a flavonoid fraction of *P. guajava* significantly reduced biofilm formation, pyocyanin, protease, elastase, violacein production, and swarming motility in relevant strains of *P. aeruginosa* PAO1 and *C. violaceum* at low concentrations ranging from 25 to 400 µg/mL (Vasavi et al. 2014). Quercetin, the most dominant compound in the methanolic extract, has been found to reduce violacein production at 1.2 mg/mL (Vandeputte et al. 2011). At low concentrations (16 µg/mL), quercetin exhibited antibiofilm activity. It inhibited the production of pyocyanin, protease, and elastase and the expression of *lasI*, *lasR*, *rhlI*, and *rhlR* genes in *P. aeruginosa* (Ouyang et al. 2016). Other components, such as kaempferol, have been reported to have anti-QS activity against *E. coli* (Vikram et al. 2010).

In this study, the LC-MS analysis showed that the primary constituents of *P. guajava* methanolic extract are phenolics and flavonoids. The most abundant constituents were quercetin (17.6%), avicularin (17.2%), kaempferol (15.4%), chlorogenic acid (9.1%), kaempferol-3-glucoside (6.3%), lutein (6.1%), and beta-carotene (5.2%). Previous studies showed that the main constituents of *P. guajava* leaves are rutin, naringenin, gallic acid, catechins, epicatechins, kaempferol, quercetin, and guaijaverin (Sampath Kumar et al. 2021). However, the essential oil chemical analysis showed the presence of a significant amount of limonene (42.1%) and caryophyllene (21.3%) (Ogunwande et al. 2003), along with some other compounds, including α-pinene, β-pinene, isopropyl alcohol, menthol, terpenyl acetate, longicyclene, β-bisabolene, and oleanolic acid (Pino et al. 2001; Ogunwande et al. 2003; Begum et al. 2004; Naseer et al. 2018).

5. Conclusion

The methanolic extract of *P. guajava* has demonstrated significant potential in modulating key virulence factors of *P. aeruginosa* by disrupting its QS system. This study highlighted the extract's unique anti-QS properties, evidenced by its ability to selectively inhibit biofilm formation at sub-inhibitory concentrations without significantly affecting bacterial viability. Notably, the extract interfered with several biofilm formation stages, including swarming motility, aggregation, hydrophobicity, and exopolysaccharide (EPS) production, and suppressed important virulence factors such as pyocyanin, rhamnolipids, protease, and chitinase. These findings suggest that *P. guajava* methanolic extract acts through inhibition of the QS-regulated production of acyl-homoserine lactones (AHLs) and a reduction in the expression of QS-related genes (*pel*, *pslA*, *aprA*, and *phzA1*). Given the global rise in antibiotic resistance, the discovery of natural anti-QS agents like *P. guajava* extract provides a promising alternative therapeutic strategy. By targeting virulence mechanisms rather than bacterial viability, this extract reduces the selective pressure for resistance, which is critical in the fight against resistant pathogens. Future studies should focus on isolating the active compounds within the extract and further elucidating their specific mechanisms of action and potential therapeutic application.

6. Disclosure

The author reports no conflict of interests in this work.

References

Abdelaziz AA, Kamer AMA, Al-Monofy KB, Al-Madboly LA. 2023. Pseudomonas aeruginosa's greenish-blue pigment pyocyanin: its production and biological activities. *Microb Cell Fact* **22**(**1**): 110. https://doi.org/10.1186/s12934-023-02122-1

Ahmed SAKS, Rudden M, Smyth TJ, Dooley JSG, Marchant R, Banat IM. 2019. Natural quorum sensing inhibitors effectively downregulate gene expression of Pseudomonas aeruginosa virulence factors. *Appl Microbiol Biotechnol* **103**: 3521–3535. https://doi.org/10.1007/s00253-019-09618-0

ALrawashdeh I, Qaralleh H, Al-limoun M, Khleifat K. 2019. Antibactrial Activity of Asteriscus graveolens Methanolic Extract: Synergistic Effect with Fungal Mediated Nanoparticles against Some Enteric Bacterial Human Pathogens. *J Basic Appl Res Biomed* **5**(**2**): 89–98. https://doi.org/10.51152/jbarbiomed.v5i2.40

Anand V, Kumar V, Kumar S, Hedina A. 2016. Phytopharmacological overview of Psidium guajava Linn. *Pharmacogn J* **8**(**4**): 314–320. https://doi.org/10.5530/pj.2016.4.3

Andrejević T, Ašanin D, Pantović B, Stevanović N, Marković V, Djuran M, Glisic B. 2023. Metal complexes with valuable biomolecules produced by Pseudomonas aeruginosa: a review of coordination properties of pyocyanin, pyochelin and pyoverdines. *Dalt Trans* **52**(**14**): 4276–4289. https://doi.org/10.1039/D3DT00287J

Andrejko M, Zdybicka-Barabas A, Janczarek M, Cytryńska M. 2013. Three Pseudomonas aeruginosa strains with different protease profiles. *Acta Biochim Pol* **60**(**1**): 83–90

Ashraf MI, Ong S-K, Mujawar S, Pawar S, More P, Paul S, Lahiri C. 2018. A side-effect free method for identifying cancer drug targets. *Sci Rep* **8**(**1**): 6669. https://doi.org/10.1038/s41598-018-25042-2

Banerjee M, Moulick S, Bhattacharya KK, Parai D, Chattopadhyay S, Mukherjee SK. 2017. Attenuation of Pseudomonas aeruginosa quorum sensing, virulence and biofilm formation by extracts of Andrographis paniculata. *Microb Pathog* **113**: 85–93. https://doi.org/10.1016/j.micpath.2017.10.023

Begum S, Hassan SI, Ali SN, Siddiqui BS. 2004. Chemical constituents from the leaves of Psidium guajava. *Nat Prod Res* **18**(**2**): 135–140. https://doi.org/10.1080/14786410310001608019

Bernstein N, Akram M, Yaniv-Bachrach Z, Daniyal M. 2021. Is it safe to consume traditional medicinal plants during pregnancy? *Phyther Res* **35**(**4**): 1908–1924. https://doi.org/10.1002/ptr.6935

Bhardwaj S, Bhatia S, Singh S, Franco Jr F. 2021. Growing emergence of drug-resistant Pseudomonas aeruginosa and attenuation of its virulence using quorum sensing inhibitors: A critical review. *Iran J Basic Med Sci* **24**(**6**): 699–719. https://doi.org/10.22038/IJBMS.2021.49151.11254

Brindhadevi K, LewisOscar F, Mylonakis E, Shanmugam S, Verma TN, Pugazhendhi A. 2020. Biofilm and Quorum sensing mediated pathogenicity in Pseudomonas aeruginosa. *Process Biochem* **96**: 49–57. https://doi.org/10.1016/j.procbio.2020.06.001

Cabrol S, Olliver A, Pier GB, Andremont A, Ruimy R. 2003. Transcription of Quorum-Sensing System Genes inClinical and Environmental Isolates of Pseudomonasaeruginosa. *J Bacteriol* **185**(**24**): 7222–7230. https://doi.org/10.1128/jb.185.24.7222-7230.2003

Cheruiyot KR, Olila D, Kateregga J. 2009. In-vitro antibacterial activity of selected medicinal plants from Longisa region of Bomet district, Kenya. *Afr Health Sci* **9**(**S**): 42–46

Dange SS, Rao PS, Jadhav RS. 2020. Traditional uses of guava: a review. *World J Pharm Res* **9**(**5**): 452–464. https://doi.org/10.20959/wjpr20205-17297

Gómez-Gómez B, Arregui L, Serrano S, Santos A, Pérez-Corona T, Madrid Y. 2019. Selenium and tellurium-based nanoparticles as interfering factors in quorum sensing-regulated processes: Violacein production and bacterial biofilm formation. *Metallomics* **11**(**6**): 1104–1114. https://doi.org/10.1039/c9mt00044e

Gordya N, Yakovlev A, Kruglikova A, Tulin D, Potolitsina E, Suborova T, Bordo D, Rosano C, Chernysh S. 2017. Natural antimicrobial peptide complexes in the fighting of antibiotic resistant biofilms: Calliphora vicina medicinal maggots. *PLoS One* **12**(**3**): e0173559. https://doi.org/10.1371/journal.pone.0173559

Gutiérrez RMP, Mitchell S, Solis RV. 2008. Psidium guajava: a review of its traditional uses, phytochemistry and pharmacology. *J Ethnopharmacol* **117**(**1**): 1–27

Haque M, Islam S, Sheikh MA, Dhingra S, Uwambaye P, Labricciosa FM, Iskandar K, Charan J, Abukabda AB, Jahan D. 2021. Quorum sensing: a new prospect for the management of antimicrobial-resistant infectious diseases. *Expert Rev Anti Infect Ther* **19**(**5**): 571–586. https://doi.org/10.1080/14787210.2021.1843427

Hasan TI, Ahmed AA. 2023. Biogenic Silver Nanoparticles by Pseudomonas aeruginosa Reduce Expression of Biofilm and Quorum Signaling Genes in Multi-drug Resistant Acinetobacter baumannii. *Jordan J Biol Sci* **16**(**4**): 621–632. https://doi.org/10.54319/jjbs/160407

Høiby N, Bjarnsholt T, Givskov M, Molin S, Ciofu O. 2010. Antibiotic resistance of bacterial biofilms. *Int J Antimicrob Agents* **35**(**4**): 322–332. https://doi.org/10.1016/j.ijantimicag.2009.12.011

Hossain MA, Lee S-J, Park N-H, Mechesso AF, Birhanu BT, Kang J, Reza MA, Suh J-W, Park S-C. 2017. Impact of phenolic compounds in the acyl homoserine lactone-mediated quorum sensing regulatory pathways. *Sci Rep* **7**(**1**): 10618. https://doi.org/10.1038/s41598-017-10997-5

Huang P, Wan H, Shao C, Li C, Zhang L, He Y. 2022. Recent advances in Chinese herbal medicine for cerebral ischemic reperfusion injury. *Front Pharmacol* **12**: 688596. https://doi.org/10.3389/fphar.2021.688596

Irie Y, Borlee BR, O'Connor JR, Hill PJ, Harwood CS, Wozniak DJ, Parsek MR. 2012. Self-produced exopolysaccharide is a signal that stimulates biofilm formation in Pseudomonas aeruginosa. *Proc Natl Acad Sci* **109**(**50**): 20632–20636. https://doi.org/10.1073/pnas.1217993109

Kassinger SJ, van Hoek ML. 2020. Biofilm architecture: An emerging synthetic biology target. *Synth Syst Biotechnol* **5**(**1**): 1–10. https://doi.org/10.1016/j.synbio.2020.01.001

Khatib C, Nattouf A, Hasan Agha MI. 2021. Traditional medicines and their common uses in central region of Syria: Hama and Homs–an ethnomedicinal survey. *Pharm Biol* **59**(**1**): 776–786. https://doi.org/10.1080/13880209.2021.1936078

Krishnan T, Yin W-F, Chan K-G. 2012. Inhibition of quorum sensing-controlled virulence factor production in Pseudomonas aeruginosa PAO1 by Ayurveda spice clove (Syzygium aromaticum) bud extract. *Sensors* **12**(**4**): 4016–4030. https://doi.org/10.3390/s120404016

Lee J, Kim Y, Lee J. 2017. Carvacrol-rich oregano oil and thymol-rich thyme red oil inhibit biofilm formation and the virulence of uropathogenic Escherichia coli. *J Appl Microbiol* **123**(**6**): 1420–1428. https://doi.org/10.1111/jam.13602

Lenz AP, Williamson KS, Pitts B, Stewart PS, Franklin MJ. 2008. Localized gene expression in Pseudomonas aeruginosa biofilms. *Appl Environ Microbiol* **74**(**14**): 4463–4471. https://doi.org/10.1128/AEM.00710-08

Li R, Yuan X, Wei J, Zhang X, Cheng G, Wang ZA, Du Y. 2019. Synthesis and evaluation of a chitosan oligosaccharide-streptomycin conjugate against Pseudomonas aeruginosa biofilms. *Mar Drugs* **17**(**1**): 43. https://doi.org/10.3390/md17010043

Lin J, Cheng J, Wang Y, Shen X. 2018. The Pseudomonas quinolone signal (PQS): not just for quorum sensing anymore. *Front Cell Infect Microbiol* **8**: 230. https://doi.org/10.3389/fcimb.2018.00230

Luo J, Dong B, Wang K, Cai S, Liu T, Cheng X, Lei D, Chen Y, Li Y, Kong J. 2017. Baicalin inhibits biofilm formation, attenuates the quorum sensing-controlled virulence and enhances Pseudomonas aeruginosa clearance in a mouse peritoneal implant infection model. *PLoS One* **12**(**4**): e0176883. https://doi.org/10.1371/journal.pone.0176883

Ma'aitah S. 2024. Pseudomonas aeruginosa biofilm formation: Antibiofilm Strategies and conventional methods of evaluation. *J Basic Appl Res Biomed* **10**(**1**): 11–28. https://doi.org/10.51152/jbarbiomed.v10i1.234

Mellbye B, Schuster M. 2014. Physiological framework for the regulation of quorum sensing-dependent public goods in Pseudomonas aeruginosa. *J Bacteriol* **196**(**6**): 1155–1164. https://doi.org/10.1128/jb.01223-13

Najmi A, Javed SA, Al Bratty M, Alhazmi HA. 2022. Modern approaches in the discovery and development of plant-based natural products and their analogues as potential therapeutic agents. *Molecules* **27**(**2**): 349. https://doi.org/10.3390/molecules27020349

Naseer S, Hussain S, Naeem N, Pervaiz M, Rahman M. 2018. The phytochemistry and medicinal value of Psidium guajava (guava). *Clin phytoscience* **4**(**1**): 1–8. https://doi.org/10.1186/s40816-018-0093-8

Nigam P, Gidwani B, Kaur C, Dhongade H. 2016. Phytochemical Screening and Pharmacological Activity of Seed Extract and Seed Oil of Lagenaria siceraria. *J Basic Appl Res Biomed* **2**(**4**): 571–576

O'May C, Tufenkji N. 2011. The swarming motility of Pseudomonas aeruginosa is blocked by cranberry proanthocyanidins and other tannin-containing materials. *Appl Environ Microbiol* **77**(**9**): 3061–3067. https://doi.org/10.1128/AEM.02677-10

Ogunwande IA, Olawore NO, Adeleke KA, Ekundayo O, Koenig WA. 2003. Chemical composition of the leaf volatile oil of Psidium guajava L. growing in Nigeria. *Flavour Fragr J* **18**(**2**): 136–138. https://doi.org/10.1002/ffj.1175

Ouyang J, Sun F, Feng W, Sun Y, Qiu X, Xiong L, Liu Y, Chen Y. 2016. Quercetin is an effective inhibitor of quorum sensing,

biofilm formation and virulence factors in Pseudomonas aeruginosa. *J Appl Microbiol* **120**(**4**): 966–974. https://doi.org/10.1111/jam.13073

Pesci EC, Pearson JP, Seed PC, Iglewski BH. 1997. Regulation of las and rhl quorum sensing in Pseudomonas aeruginosa. *J Bacteriol* **179**(**10**): 3127–3132. https://doi.org/10.1128/jb.179.10.3127-3132.1997

Pezzoni M, Pizarro RA, Costa CS. 2020. Role of quorum sensing in UVA-induced biofilm formation in Pseudomonas aeruginosa. *Microbiology* **166**(**8**): 735–750. https://doi.org/10.1099/mic.0.000932

Pino JA, Agüero J, Marbot R, Fuentes V. 2001. Leaf oil of Psidium guajava L. from Cuba. *J Essent Oil Res* **13**(**1**): 61–62. https://doi.org/10.1080/10412905.2001.9699607

Pulingam T, Parumasivam T, Gazzali AM, Sulaiman AM, Chee JY, Lakshmanan M, Chin CF, Sudesh K. 2022. Antimicrobial resistance: Prevalence, economic burden, mechanisms of resistance and strategies to overcome. *Eur J Pharm Sci* **170**: 106103. https://doi.org/10.1016/j.ejps.2021.106103

Qader SS, Ganjo AR. 2024. Investigation of Quorum Sensing, Biofilm Production, and Detection of Virulence-associated Genes Among Clinical Isolates of Acinetobacter baumannii. *Jordan J Biol Sci* **17**(**2**): 301–306. https://doi.org/10.54319/jjbs/170210

Qaralleh H. 2023. Chemical Composition and Quorum Sensing Inhibitory Effect of Nepeta curviflora Methanolic Extract against ESBL Pseudomonas aeruginosa. *J Pharmacopuncture* **26**(**4**): 307–318. https://doi.org/10.3831/KPI.2023.26.4.307

Qaralleh H. 2019. Thymol rich thymbra capitata essential oil inhibits quorum sensing, virulence and biofilm formation of beta lactamase producing Pseudomonas aeruginosa. *Nat Prod Sci* **25**(**2**): 172–180. https://doi.org/10.20307/nps.2019.25.2.172

Qaralleh H, Al-Limoun M, Khlaifat A, Khleifat K, Al-Tawarah N, Hashem A-H, Alsharafa K. 2020. Antibacterial and Antibiofilm Activities of a Traditional Herbal Formula against Respiratory Infection Causing Bacteria. *Trop J Nat Prod Res* **4**(**9**): 527–534. https://doi.org/10.26538/tjnpr/v4i9.6

Qaralleh H, Khleifat KM, Khlaifat AM, Al-limoun M, Al-Tawarah NM, Alhroob AM, Alsaudi AB. 2021. Chemical Composition, Antioxidant and Inhibitory Effect of Cupressus sempervirens Essential Oils and Methanolic Extract on Beta-lactamase producing Isolates. *Res J Pharm Technol* **14**(**9**): 4673–4679. https://doi.org/10.52711/0974-360X.2021.00812

Qin S, Xiao W, Zhou C, Pu Q, Deng X, Lan L, Liang H, Song X, Wu M. 2022. Pseudomonas aeruginosa: Pathogenesis, virulence factors, antibiotic resistance, interaction with host, technology advances and emerging therapeutics. *Signal Transduct Target Ther* **7**: 199. https://doi.org/10.1038/s41392-022-01056-1

Razack SA, Vijayagopal V, Viruthagiri T. 2011. Production of Exopolysaccharides by P. aeruginosa, P. fluorescens and Bacillus sp. *IUP J Biotechnol* **5**(**4**): 14–19

Rossi E, La Rosa R, Bartell JA, Marvig RL, Haagensen JAJ, Sommer LM, Molin S, Johansen HK. 2021. Pseudomonas aeruginosa adaptation and evolution in patients with cystic fibrosis. *Nat Rev Microbiol* **19**(**5**): 331–342. https://doi.org/10.1038/s41579-020-00477-5

Sagar PK, Sharma P, Singh R. 2022. Inhibition of quorum sensing regulated virulence factors and biofilm formation by Eucalyptus globulus against multidrug-resistant Pseudomonas aeruginosa. *J Pharmacopuncture* **25**(**1**): 37–45. https://doi.org/10.3831/KPI.2022.25.1.37

Sahib A, Abbas S, Hasson K, Mahmoud M. 2019. Experience of Antibiotic Use and Resistance Among Pharmacy Students in the University of Kerbala. *J Basic Appl Res Biomed* **5**(**1**): 21–30

Sampath Kumar NS, Sarbon NM, Rana SS, Chintagunta AD, Prathibha S, Ingilala SK, Jeevan Kumar SP, Sai Anvesh B, Dirisala VR. 2021. Extraction of bioactive compounds from Psidium guajava leaves and its utilization in preparation of jellies. *AMB Express* **11**: 36. https://doi.org/10.1186/s13568-021-01194-9

Sauer K, Stoodley P, Goeres DM, Hall-Stoodley L, Burmølle M, Stewart PS, Bjarnsholt T. 2022. The biofilm life cycle: expanding the conceptual model of biofilm formation. *Nat Rev Microbiol* **20**(**10**): 608–620. https://doi.org/10.1038/s41579-022-00767-0

Shanks RMQ, Meehl MA, Brothers KM, Martinez RM, Donegan NP, Graber ML, Cheung AL, O'Toole GA. 2008. Genetic evidence for an alternative citrate-dependent biofilm formation pathway in Staphylococcus aureus that is dependent on fibronectin binding proteins and the GraRS two-component regulatory system. *Infect Immun* **76**(**6**): 2469–2477. https://doi.org/10.1128/iai.01370-07

Shrout JD, Chopp DL, Just CL, Hentzer M, Givskov M, Parsek MR. 2006. The impact of quorum sensing and swarming motility on Pseudomonas aeruginosa biofilm formation is nutritionally conditional. *Mol Microbiol* **62**(**5**): 1264–1277. https://doi.org/10.1111/j.1365-2958.2006.05421.x

Simanek KA, Paczkowski JE. 2022. Resistance is not futile: the role of quorum sensing plasticity in Pseudomonas aeruginosa infections and its link to intrinsic mechanisms of antibiotic resistance. *Microorganisms* **10**(**6**): 1247. https://doi.org/10.3390/microorganisms10061247

Soukarieh F, Williams P, Stocks MJ, Camara M. 2018. Pseudomonas aeruginosa quorum sensing systems as drug discovery targets: current position and future perspectives. *J Med Chem* **61**(**23**): 10385–10402. https://doi.org/10.1021/acs.jmedchem.8b00540

Tran N, Pham B, Le L. 2020. Bioactive compounds in anti-diabetic plants: From herbal medicine to modern drug discovery. *Biology (Basel)* **9**(**9**): 252. https://doi.org/10.3390/biology9090252

Turkina M V, Vikström E. 2019. Bacteria-host crosstalk: sensing of the quorum in the context of Pseudomonas aeruginosa infections. *J Innate Immun* **11**(**3**): 263–279. https://doi.org/10.1159/000494069

Ueda A, Wood TK. 2009. Connecting quorum sensing, c-di-GMP, pel polysaccharide, and biofilm formation in Pseudomonas aeruginosa through tyrosine phosphatase TpbA (PA3885). *PLoS Pathog* **5**(**6**): e1000483. https://doi.org/10.1371/journal.ppat.1000483

Vadakkan K, Ngangbam AK, Sathishkumar K, Rumjit NP, Cheruvathur MK. 2023. A review of chemical signaling pathways in the quorum sensing circuit of Pseudomonas aeruginosa. *Int J Biol Macromol* **254**: 127861. https://doi.org/10.1016/j.ijbiomac.2023.127861

Vandeputte OM, Kiendrebeogo M, Rasamiravaka T, Stevigny C, Duez P, Rajaonson S, Diallo B, Mol A, Baucher M, El Jaziri M. 2011. The flavanone naringenin reduces the production of quorum sensing-controlled virulence factors in Pseudomonas aeruginosa PAO1. *Microbiology* **157**(**7**): 2120–2132. https://doi.org/10.1099/mic.0.049338-0

Vasavi HS, Arun AB, Rekha P. 2014. Anti-quorum sensing activity of Psidium guajava L. flavonoids against Chromobacterium violaceum and Pseudomonas aeruginosa PAO1. *Microbiol Immunol* **58**(**5**): 286–293. https://doi.org/10.1111/1348-0421.12150

Vetrivel A, Ramasamy M, Vetrivel P, Natchimuthu S, Arunachalam S, Kim G-S, Murugesan R. 2021. Pseudomonas aeruginosa biofilm formation and its control. *Biologics* **1**(**3**): 312–336. https://doi.org/10.3390/biologics1030019

Vikram A, Jayaprakasha GK, Jesudhasan PR, Pillai SD, Patil BS. 2010. Suppression of bacterial cell–cell signalling, biofilm formation and type III secretion system by citrus flavonoids. *J Appl Microbiol* **109**(**2**): 515–527. https://doi.org/10.1111/j.1365-2672.2010.04677.

JJBS

Volume 18, Number 2,June 2025
ISSN 1995-6673
Pages 315 – 321
https://doi.org/10.54319/jjbs/180212

Jordan Journal of Biological Sciences

The Effect of *Memantine* and *Lactobacillus acidophilus* Supernatant on Apoptosis and Expression of Key Long non-coding RNAs in a Colon Cancer Cell Line

Paniz Erfanian Goli Zadeh Rauf Mohajer[1], Aras Rafiee[1,*], Soheila Zamanlui Benisi[2]

[1]*Department of Biology, CT.C., Islamic Azad University, Tehran, Iran;* [2] *Department of Biomedical Engineering, Central Tehran Branch, Islamic Azad University, Tehran, Iran*

Received: July 5, 2024; Revised: October 21, 2024; Accepted: November 26, 2024

Abstract

Alterations in the expression of long non-coding RNA (lncRNA) are linked to colon cancer progression. Recent studies suggest that *Memantine* (*ME*) and probiotics, such as *Lactobacillus acidophilus (LA)*, may have potential anti-cancer effects. This study investigates the impact of *Memantine*, *Lactobacillus acidophilus*, and their combination (*ME+LA*) on lncRNA expression, apoptosis, and the viability of HT-29 colon cancer cells. The MTT assay was used to evaluate cell viability and calculate IC50 using different concentrations of ME and *LA supernatant*. Expression levels of oncogenic lncRNAs (*SNHG16*, *NEAT1*, *CCAT2*, *MALAT1*, *H19*) were measured using Real-time PCR. Apoptosis and necrosis were analyzed via flow cytometry. The results demonstrated that higher concentrations of both *Memantine* and *LA supernatant* resulted in significantly reduced cell viability. Additionally, treatment with *ME* and *LA supernatant*, both individually and in combination, led to a reduction in the expression levels of oncogenic lncRNAs, induction of apoptosis and reducing cancer cell survival. The combination of *ME* and *LA* was found more effective. Therefore, combining *Memantine* and *LA supernatant* shows promise as a novel and effective treatment for colon cancer.

Keywords: Colon cancer, *Memantine*, *Lactobacillus acidophilus*, lncRNAs, Gene expression, Apoptosis

1. Introduction

Colon cancer is the third most prevalent cancer in the world to be diagnosed and presents a noteworthy health challenge, as indicated by the elevated incidence and mortality rates globally (Marcellinaro *et al.*, 2023). According to 2020 data, colon cancer affects 10% of the population and has a 9.4% death rate (Sung *et al.*, 2021). Despite multiple advancements in immunotherapy, chemotherapy, or radiotherapy, the adverse side effects of these therapies highlight the urgent need for innovative treatments. This necessity drives the exploration of novel and less invasive alternatives, such as probiotics and new drugs, which could potentially revolutionize colon cancer's preventive and therapeutic landscape.

Long non-coding RNAs (lncRNAs) have emerged as significant regulators in cancer biology, influencing gene expression and cellular behavior. Among these, several key lncRNAs, include Small Nucleolar R.N.A. Host Gene 16 (*SNHG16*), Nuclear Paraspeckle Assembly Transcript 1 (*NEAT1*), Colon Cancer-Associated Transcript 2 (*CCAT2*), Metastasis-Associated Lung Adenocarcinoma Transcript 1 (*MALAT1*), and H19. These lncRNAs are involved in various cellular processes, such as proliferation, apoptosis, and metastasis. For instance, *MALAT1*, known for its high conservation across mammals, regulates gene expression through its secondary structure and is associated with metastasis in multiple cancer types. Similarly, *NEAT1* plays a critical role in forming paraspeckles and is involved in the DNA damage response and cancer progression (Statello *et al.*, 2021). *CCAT2*, located upstream of the *MYC* gene, promotes tumor growth by regulating *MYC* expression (Ulitsky, 2016). *H19* functions as an oncogene in several cancers, including colon cancer, and regulates gene expression and cell growth (Ghafouri-Fard *et al.*, 2020). *SNHG16* has also been linked to poor prognosis in various cancers, contributing to tumorigenesis through its interaction with other molecular pathways (Chen *et al.*, 2020).

Recent studies suggest that the expression of lncRNAs can be influenced by dietary factors and the type of bacterial colonization in the colon. A study on patients with rectal cancer found that consumption of probiotics such as *L. acidophilus* was associated with improved expression of candidate lncRNAs (Khodaii *et al.*, 2022). Another research involving specific strains of *Bifidobacterium* and *Lactobacillus* has shown that they can

* Corresponding author.; e-mail: aras_rafiee@yahoo.com.

** **List of abbreviations:** CRC: colorectal cancer; LA: *Lactobacillus acidophilus*; Non-coding R.N.A.s (lncRNAs); *SNHG1:*Small Nucleolar R.N.A. Host Gene 16; *NEAT1:* Nuclear Paraspeckle Assembly Transcript 1; *CCAT2:* Colon Cancer-Associated Transcript 2; *MALAT1:* Metastasis-Associated Lung Adenocarcinoma Transcript 1

inhibit the growth of various types of cancer cells, including colorectal cancer cells (Śliżewska *et al.*, 2020). Probiotic metabolites, such as short-chain fatty acids (*SCFAs*), contribute to maintaining intestinal health, promoting apoptosis of cancer cells, and modulating immune responses (Kahouli *et al.*, 2013).

Similar to probiotics, *Memantine*, an *NMDA* receptor antagonist primarily used to treat Alzheimer's disease, has shown promising potential in cancer therapy (Maraka *et al.*, 2019). There are two types of glutamate receptors (GluRs): Metabotropic GluRs (mGluRs) and ionotropic GluRs (iGluRs). iGluRs form cation channels, allow Ca^{+2} and Na^{+} influx, and activate downstream apoptotic signaling pathways. One of the three iGluRs subcategories, N-methyl-Daspartate receptors (NMDARs), is particularly relevant to this research.

It has been demonstrated that NMDARs are more active in cancer cells than normal. NMDA receptors can activate cell growth cascades, such as the MAP kinase and ERK pathways, leading to the proliferation of non-neuronal cells including lung, colon, breast, bone, testis and pancreas (Yoon *et al.*, 2017). Therefore, NMDAR antagonists such as Memantine may possess anticancer properties (Gallo *et al.*, 2023; Shafiei-Irannejad *et al.*, 2021). Recent research indicates that *Memantine* can inhibit colorectal cancer, stop cancer cells from proliferating and cause them to undergo apoptosis (Mahboubi *et al.*, 2022). In a separate study, it was observed that the administration of Memantine increases the expression of Golgi glycoprotein 1 (GLG1). GLG1, in turn, reducing the bioavailability of fibroblast growth factor (FGF), a potent regulators of cell proliferation and differentiation during oncogenesis, by sequestering it intracellularly and extracellularly. Therefore, Memantine was found as a suppressor of malignant glioma and breast cancer cell growth by modulating the expression of GLG1, which functions as a traffic controller for FGF (Yamaguchi *et al.*, 2022). By disrupting cellular pathways that promote cancer cell survival, *Memantine* enhances the effectiveness of conventional therapies and offers a new avenue for targeted cancer treatment.

Considering the importance of developing effective treatments for colorectal cancer and the potential benefits of *Lactobacillus acidophilus (LA) supernatant* and *Memantine*, this study investigates their individual effects. Specifically, we assess the impact of *Memantine* and *LA supernatant* on apoptosis and the expression of five key lncRNAs (*SNHG16*, *NEAT1*, *CCAT2*, *MALAT1*, and *H19*) in colon cancer HT-29 cells. By examining these treatments, the study aims to provide insights into new therapeutic strategies for colorectal cancer.

2. Materials and Methods

2.1. Preparation of Memantine and LA supernatant

Memantine-coated tablets (5 mg) were purchased from Kimidaru Pharmaceutical Company (Iran). Two tablets (each, 5 mg) were crushed with a mortar, dissolved in 1 ml of DMEM solution, sterilized using a 0.2 nm filter, and stored in vials at 4℃ until use. Serial dilutions were then prepared to achieve various concentrations.

Lactobacillus acidophilus (ATCC 314) was procured from the Pasteur Institute. Bacterial cells were cultured on MRS agar. Then the colonies were inoculated into RPMI medium. The absorbance of the medium was monitored intermittently at 600 nm until reaching the optical density of 0.7 (equivalent to 0.5 MacFarland). The bacteria were then incubated for another 24 h at 37℃. After incubation, the culture was centrifuged at 3000 rpm for 15 minutes to isolate the supernatant. The supernatant metabolite was withdrawn with a syringe, passed through the 0.2 nm filter, freeze dried and finally stored in the refrigerator. At the time of use, 1 mg lyophilized powder was dissolved in 1 mL sterile DMEM.

HT-29 cells were treated with the IC50 values of both *LA* supernatant and memantine in Real-Time PCR and apoptosis assays.

2.2. Cell Line Preparation

The *HT-29* colon cancer cell line (IBRC C10071) was sourced from the National Center for Genetic and Biological Resources of Iran. These cells were maintained in DMEM culture medium.

HT-29 cells were maintained in *DMEM* supplemented with 20% *FBS* (Gibco, U.S.A.), 100 mg/ml streptomycin, 100 U/ml penicillin, and 2 mM L-glutamine at 37°C in a 5% CO2 incubator. The culture medium was refreshed every 24 to 48 hours. For cell passage, the medium was aspirated, and cells were detached by treating with 0.25% trypsin for 3-5 minutes. The trypsinization (Gibco, U.S.A.) process was halted by adding a medium containing serum. The cell suspension was then centrifuged at 1500 rpm for 5 minutes. The resulting pellet was resuspended in a fresh medium and transferred to new culture flask.

2.3. MTT Assay

HT-29 cells were seeded in 96-well plates and treated with different concentrations of *Memantine* (12.5, 25, 50, 100, 200 µg/ml) and *L. acidophilus (LA)* supernatant (250, 500, 1000, 2000, 4000 µg/ml). After 24 hours of incubation, MTT solution (5 mg/ml) was added to the cells, followed by an additional 3-hour incubation period. The medium was then discarded, and the resulting formazan crystals were dissolved in *DMSO*. Absorbance was measured at 570 nm using an *ELISA* reader. Cytotoxicity and cell viability were calculated using standard formulas. The IC50 values for *Memantine* and *L.A* supernatant were determined using the Pharm-PCS statistical package by analyzing the percentage of cytotoxicity.

2.4. Gene Expression Analysis by Real-Time PCR

We evaluated the impact of *L. acidophilus* supernatant on gene expression by real-time PCR. Briefly, 4×10^5 *HT-29* cells were seeded in 6-well plates containing 2ml of complete cell culture medium overnight. Then cells were treated with IC50 concentration of both memantine and *LA* supernatant (separately) for 24 hours. Negative controls received an equal volume of DMEM medium.

We followed the real-time procedures on the basis of MIQE guidelines (Bustin *et al.*, 2009). RNA extract from *HT-29* cells was performed using the RNX-Plus reagent (CinnaGen) following standard protocols. OD at A_{260}/A_{280} (purity) was investigated by a spectrophotometer. The RNA (OD ~ 1.9-2) was then used to synthesize cDNA with the miScript II RT kit without interruption (CinnaGen) (Table-1). 500 ng/20 µl RNA concentration was used for cDNA synthesis. cDNA was stored at 20℃.

The expression of target lncRNAs (*SNHG16*, *NEAT1*, *MALAT1*, *H19*, *CCAT2*) was quantified using SYBR Green-based Real-Time PCR with specific primers designed from the NCBI database and IDT online software. The mean Cq values of Gapdh and HPRT1 were used as the reference genes for normalization.

Table1. List of Genes and Primers:

Gene	Primer Sequence (5'-3')	Product Length (bp)	Melting Temperature (Tm)	Designed on exons
Gapdh	F: GTGGTCTCCTCTGACTTCAAC	96	57.97	7,8
	R: GGAAATGAGCTTGACAAAGTGG		58.09	
HPRT1	F: AAGGGTGTTTATTCCTCATGGAC	105	58.40	2,3
	R: AGCACACAGAGGGCTACAA		58.55	
SNHG16	F: CAGAATGCCATGGTTTCCCC	142	58.38	3,4
	R: TGGCAAGAGACTTCCTGAGG		59.12	
NEAT1	F: GTACGCGGGCAGACTAACAC	101	57.37	1-1
	R: TGCGTCTAGACACCACAACC		57.36	
MALAT1	F: AATGTTAAGAGAAGCCCAGGG	150	59.02	1 -1
	R: AAGGTCAAGAGAAGTGTCAGC		59.12	
H19	F: GGATCCAGTTAGAAAAAGCCCGGGCT	113	57.78	2,3
	R: ACGCGTGCTGTAACAGTGTTTATTGA		58.00	
CCAT2	F: CCACATCGCTCAGACACCAT	100	57.44	1-1
	R: ACCAGGCGCCCAATACG		57.58	

Primers were ordered from a commercial supplier (Sinaclon) and verified for specificity using NCBI BLAST and GeneRunner software.

2.5. Real-Time PCR Procedure:

We performed Real-time PCR reactions in a total volume of 25 µl. The reaction mixture included 12.5 µl of Master mix (Bioneer, Korea), 1 µl of forward primer (10 mM), 1 µl of reverse primer (10 mM), 1 µl of cDNA (0.1-1 µg), and 9.5 µl of DEPC-treated water. The reactions were performed using a Bioneer Exicycler 96. The thermal profile used for the real-time PCR reactions is detailed in Table 2. The qPCR data was analyzed by Livak method ($2^{-\Delta\Delta CT}$).

Table 2. Real-Time PCR Thermal Profile

Step	Function	Temperature (°C)	Time	Repeat
1	Initial Denature	95.0	15 minutes	1
2	Denature	95.0	20 seconds	40
3	Anneal	58.0	20 seconds	40
4	Extend	72.0	20 seconds	40
5	Melt Curve	55.0 to 94.0	1 second	1
6	End			

2.6. Apoptosis Analysis by Flow Cytometry

HT-29 cells were treated with the IC50 concentration of *Memantine* and *LA* supernatant to assess apoptosis. The cell staining was carried on with Annexin V-FITC and Propidium Iodide (PI) using the Annexin V-FITC kit (eBioscience, USA). The data were analyzed to determine the percentage of apoptotic cells, distinguishing between early apoptotic, late apoptotic, necrotic, and viable cells by Flow cytometry.

2.7. Statistical Analysis

Statistical analysis was conducted using REST 2009 and SPSS 16. Data analysis involved one-way ANOVA, with Tukey's HSD post-hoc test used to determine significant differences. Gene expression levels were evaluated using the CT method, and the results were visualized with GraphPad software. Data were presented as mean ± standard deviation (SD), with significance delimited at $P<0.05$.

3. Results

3.1. Cell Viability of the HT-29 Cell Line Under Various Treatments for 24 Hours

Figure 1 illustrates the results of the MTT assay conducted on HT-29 cells treated with *Memantine* and LA supernatant. Both *Memantine* and *Lactobacillus acidophilus (LA) supernatant* treatments significantly impacted the survival of cancer cells. *HT-29* cells were exposed to various concentrations of supernatant (250, 500, 1000, 2000, and 4000 µg/ml) and *Memantine* (12.5, 25, 50, 100, and 200 µg/ml). Cell viability was measured using the MTT assay over 24 hours. The results indicate that increasing concentrations of the *LA supernatant* led to a significant decrease in cell viability, with 44% of cancer cells eliminated at 4000 µg/ml after 24 hours ($P<0.001$) (Figure 1a). Concentrations of 1000 and 2000 µg/ml also significantly reduced cell viability ($P<0.05$, $P<0.01$), whereas 250 and 500 µg/ml did not have a significant effect. The IC50 value for *LA supernatant was* determined to be 5187.86 µg/ml, the concentration needed to achieve a 50% reduction in cell viability. Similarly, higher concentrations of *Memantine* significantly decreased cell viability, with 69% of cancer cells eliminated at 200 µg/ml after 24 hours ($P<0.001$) (Figure 1b). All concentrations of *Memantine* significantly reduced cell viability. The calculated IC50 value for *Memantine* was 35.21 µg/ml.

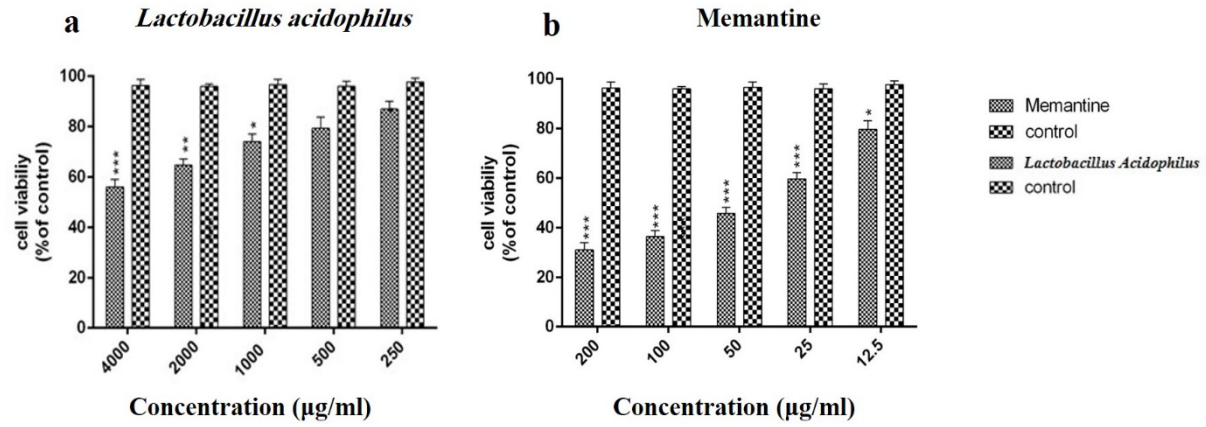

Figure 1. (a) Bar chart showing the cell viability of *HT-29* cells treated with *Lactobacillus acidophilus* supernatant. (b) Bar chart showing the cell viability of HT-29 cells treated with *Memantine*.

3.2. Expression of lncRNAs SNHG16, NEAT1, MALAT1, H19, and CCAT2 by Real-Time PCR

Prior to PCR, cDNA concentrations were measured and normalized using a NanoDrop spectrophotometer, with the reference genes. Figure 2 presents the comparative and average gene expression results for *HT-29* cells treated with *Memantine*, *Lactobacillus acidophilus*, and their combination. The relative gene expression of *SNHG16*, *NEAT1*, *MALAT1*, *H19*, and *CCAT2* in *HT-29* cells is illustrated under different treatments compared to the control. A significant reduction in gene expression was observed across all treatments compared to the control, with the most pronounced decrease noted in the combination treatment of *Memantine* and *LA supernatant.* Overall, these results indicate that treatment with *Memantine* and *LA supernatant*, both individually and particularly in combination, leads to a reduction of the oncogenic genes *SNHG16*, *NEAT1*, *MALAT1*, *H19*, and *CCAT2* in *HT-29* cancer cells.

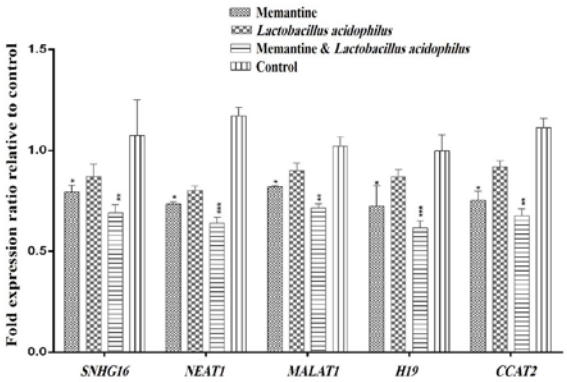

Figure 2. Relative fold expression levels of *SNHG16*, *NEAT1*, *MALAT1*, *H19*, and *CCAT2* genes in *HT-29* cells treated with IC50 concentrations of *Memantine*, *LA supernatant*, and their combination compared to control. Data are presented as mean ± SD based on three replicates. (* indicates P<0.05, ** indicates P<0.01, *** indicates P<0.001).

3.3. Flow Cytometry Analysis Using Annexin-V Kit

Figure 3 presents the flow cytometry results for apoptosis induction in control cells (panel b) and *HT-29* cells treated with the IC50 concentration of the *LA supernatant (*panel a). The results indicate that 98.4% of the control cells are viable, which is expected as they were not treated with the *LA* or *Memantine*. The percentage of early and late apoptosis was 1.41% and 0.13%, respectively, and a minimal 0.22% of the cells underwent necrosis due to the collection and preparation process, which is negligible compared to the healthy and viable cells.

The flow cytometry results demonstrated the effects of IC50 concentrations of *LA supernatant*, *Memantine* and their combination on *HT-29* cells. We found that combination treatment induced the highest levels of late apoptosis (28.20%), significantly higher than either treatment alone (*Memantine* at 11.32% and *LA supernatant at* 9.76%). Early apoptosis was also significantly elevated in cells treated with *Memantine* (15.60%) and the combination (5.14%) compared to the control (1.52%). While the necrosis rates remained relatively low and statistically insignificant across all groups, the combination treatment yet showed a slight increase (3.10%). We suggest a synergistic effect between *LA supernatant* and *Memantine*, enhancing apoptotic cell death while maintaining low necrosis levels, highlighting the potential for combined therapeutic strategies in targeting cancer cells.

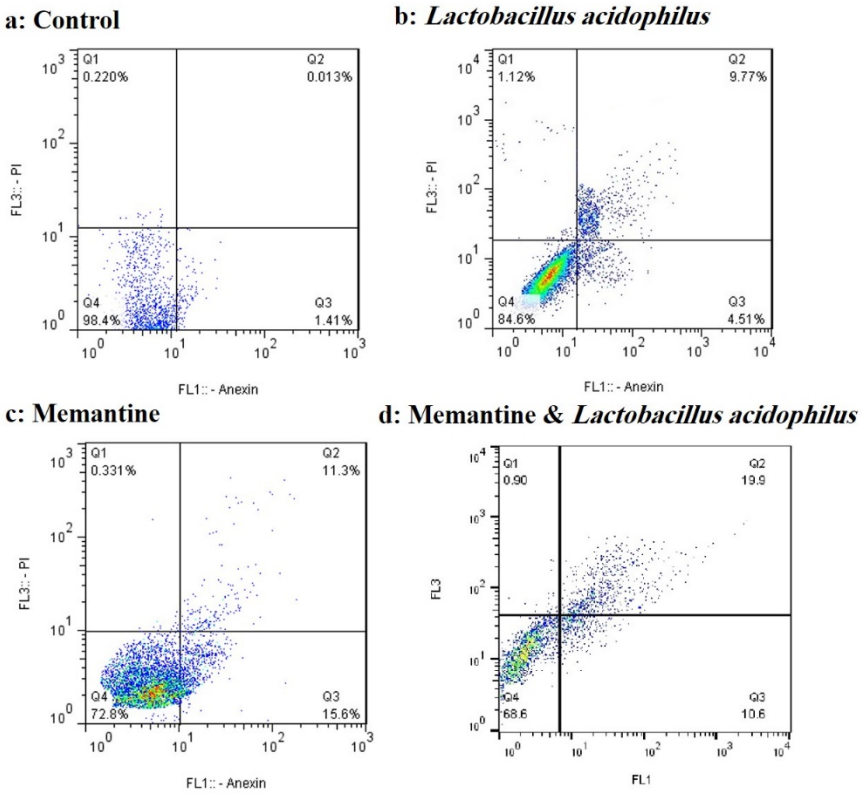

Figure 3. Flow cytometry analysis of apoptosis induction in *HT-29* cells. (a) Control cells without any treatment. (b) *HT-29* cells were treated with an IC50 concentration of the probiotic *Lactobacillus acidophilus (LA) aupernatant*. (c) *HT-29* cells were treated with an IC50 concentration of *Memantine*. (d) *HT-29* cells were treated with *Memantine* and *LA supernatant*.

4. Discussion

Colorectal cancer ranks among the most prevalent types of cancer, with its incidence rapidly increasing among both men and women in recent years. Each year, over 1 to 2 million new cases are diagnosed, and the disease is responsible for over 600,000 deaths. The prevalence is particularly higher among men and older adults (Rawla *et al.*, 2019). Early screening poses challenges, as over 80% of colorectal cancers derive from adenomatous polyps, but it can identify patients two to three years before symptoms appear.

Memantine, an *NMDA* receptor antagonist, has demonstrated potential anti-cancer effects by increasing mitochondrial complex 1 activity while reducing complex 5 activity. A study indicated that *Memantine* disrupts *glutamate* synthesis in prostate cancer cells, leading to cell death. *Memantine*'s effects on *NMDA* receptors, which play critical roles in various physiological processes due to their high calcium flow and magnesium block, suggest its potential in cancer therapy (Gulsah Albayrak *et al.*, 2021). *Lactobacilli* are catalase-negative, Gram-positive rods that ferment carbohydrates to produce lactic acid and exhibit immunomodulatory properties that benefit for maintaining microbial balance. However, some strains can transfer antibiotic-resistance genes, necessitating careful evaluation of their probiotic properties. Their benefits include antimicrobial activity, antibiotic resistance, acid and bile tolerance, and stability (Di Cerbo *et al.*, 2016).

This study assessed the cytotoxic effects of *Lactobacillus acidophilus supernatant* and *Memantine* using the MTT assay, revealing dose-dependent reductions in cancer cell viability. *Memantine* exhibited significantly greater cytotoxicity than the *LA supernatant*, with a 150-fold difference in IC50 values. Hence, memantine exhibits high cytotoxicity against cancer cells and can impede key metabolic pathways like glutamate synthesis in cancer cells while sparing normal cells. If its low toxicity effect on normal cells is confirmed, memantine could potentially be considered as a future option for cancer treatment, along with probiotics.

Previous studies have also indicated *Memantine*'s dose-dependent cytotoxic effects on various cancer cells (G Albayrak *et al.*, 2018).

We demonstrated that *Memantine* and *Lactobacillus acidophilus* significantly induced apoptosis in *HT-29* cells, with the combination treatment showing the highest levels of late apoptosis. Gene expression analysis indicated significant downregulation of oncogenic lncRNAs *SNHG16*, *NEAT1*, *MALAT1*, *H19*, and *CCAT2* following treatments, with the combination treatment yielding the most substantial reductions. These findings align with other studies that have reported the apoptotic and antiproliferative effects of *LA* and *Memantine* (Isazadeh *et al.*, 2020; Robinson *et al.*, 2020).

The observed effects may be due to *Memantine's* antagonistic effect on NMDA receptors, which disrupts intracellular calcium signaling and activates apoptotic pathways, particularly the mitochondrial (intrinsic) pathway. This calcium imbalance triggers *cytochrome c* release from mitochondria, subsequently activating *caspases* responsible for apoptosis (Calvo-Rodriguez *et al.*, 2020). On the other hand, *Lactobacillus acidophilus* has been found to modulate the gut microbiota and produce *SCFAs* metabolites with anti-inflammatory and

anti-cancer properties (Thananimit *et al.*, 2022). These metabolites can inhibit histone deacetylases (*HDACs*), resulting in histone hyperacetylation and increased tumor suppressor gene expression (Li *et al.*, 2022). Additionally, probiotics can bolster the host's immune response by promoting the production of anti-inflammatory cytokines, which may contribute to their anti-cancer properties (Wu *et al*., 2021).

The combination treatment appears to exert a synergistic effect, potentially through the simultaneous modulation of multiple pathways. The downregulation of oncogenic lncRNAs *SNHG16*, *NEAT1*, *MALAT1*, *H19*, and *CCAT2* suggests these treatments may interfere with the regulatory networks controlling gene expression and cellular proliferation. For instance, lncRNAs are famed for interaction with chromatin-modifying complexes and transcription factors, and their altered expression can lead to significant changes in the transcriptional landscape of cancer cells (Emam *et al.*, 2022; Segal and Dostie, 2023).

Furthermore, the apoptotic properties of the *LA supernatant* and *Memantine* were investigated using annexin flow cytometry. The results showed that both the *LA supernatant* and *Memantine* induced apoptosis, increasing early and late apoptosis in the treated cells. While there was no significant difference in the necrosis rates between cells treated with *LA supernatant* or *Memantine*, the apoptotic effects were noticeable. A study demonstrated that supernatants from *Lactobacillus acidophilus* and *casei* strains reduced cancer cell proliferation and increased apoptosis. Additionally, their supernatants could induce necrosis and reduce cell migration and invasion, which aligns with our apoptotic findings (Mirzadeh *et al.*, 2024). Another study examined the protective effects of oral *Lactobacillus casei BL23* in mice with induced CRC. The findings showed significant protection against CRC, reduced histological scores, and modulated immune response, as indicated by increased cytokine *IL-22* and caspase expression. This suggests the potential of *L. casei BL23* in developing probiotic-based strategies against CRC (Jacouton *et al.*, 2017).

In conclusion, we highlight the potential of *Memantine* and *Lactobacillus acidophilus supernatant* as effective agents for inducing apoptosis and reducing the viability of HT-29 colorectal cancer cells. The combined treatment significantly downregulated oncogenic lncRNAs, indicating a synergistic effect. These findings suggest that *Memantine* and *Lactobacillus acidophilus* could be promising candidates for colorectal cancer therapy. Take note of the following suggestions for future studies: 1- Explore the cytotoxic effects of *Lactobacillus acidophilus* and *Memantine* on other cancer cell lines and compare their effects on normal cell viability, 2- explore the impact on the expression of other lncRNAs involved in cancer, 3- assess the effects of different chemical drugs and probiotic supernatants on cancer cell lines, 4- investigate the role of different tumor microbiome in regulating cancer and develop microbiome-targeted therapies, and eventually 5- conduct further in vivo and clinical trial studies.

5. Conflict of Interest Statement

The authors declare no conflict of interests. The research was conducted independently without external funding or influence.

Acknowledgments

The authors would like to express their sincere gratitude to Pasteur Institute of Iran (IPI), Stem cell and Cell therapy research center for providing the necessary facilities and resources to conduct this research; special thanks go to Dr. Zahra Shahi, Dr. Farhad Riazi-Rad, Dr.Asal Katebi and Dr. for their invaluable guidance and support throughout the study. Additionally, appreciation is extended to all the staff members of the Microbiology Laboratory for their assistance and collaboration.

References

Albayrak G, Konac E, Dikmen AandBilen C. 2018. Memantine induces apoptosis and inhibits cell cycle progression in LNCaP prostate cancer cells. *Hum. Exp. Toxicol*., **37 (9)**: 953-958.

Albayrak G, Korkmaz FD, Bali EBandBagriacik EU. 2021. Antitumorigenic Effect of Memantine via Interfering Glutamate Metabolism in Mouse 4T1 Breast Tumor Model. *Anti-Cancer Agents Med. Chem*., **21 (12)**: 1575-1580.

Bustin SA, Benes V, Garson JA, Hellemans J, Huggett J, Kubista M, et al. 2009. T**he MIQE Guidelines: Minimum Information for Publication of Quantitative Real-Time PCR Experiments,** Oxford University Press.

Calvo-Rodriguez M, Kharitonova EKandBacskai BJ. 2020. Therapeutic strategies to target calcium dysregulation in Alzheimer's disease. *Cells*., **9 (11)**: 2513.

Chen L, Qiu C-H, Chen Y, Wang Y, Zhao J-JandZhang M. 2020. LncRNA SNHG16 drives proliferation, migration, and invasion of lung cancer cell through modulation of miR-520/VEGF axis. *Eur Rev Med Pharmacol Sci*., **24 (18)**: 9522-9531.

Di Cerbo A, Palmieri B, Aponte M, Morales-Medina JC, Iannitti T. 2016. Mechanisms and therapeutic effectiveness of lactobacilli. *J. Clin. Pathol*., **69 (3)**: 187-203.

Emam O, Wasfey EFandHamdy NM. 2022 .Notch-associated lncRNAs profiling circuiting epigenetic modification in colorectal cancer. *Cancer Cell Int.*, **22 (1)**: 316.

Gallo S, Vitacolonna AandCrepaldi T. 2023. NMDA receptor and its emerging role in cancer. *Int. J. Mol. Sc*., **24 (3)**: 2540.

Ghafouri-Fard S, Esmaeili MandTaheri M. 2020. H19 lncRNA: roles in tumorigenesis. *Biomed.*, **123**: 109774.

Isazadeh A, Hajazimian S, Shadman B, Safaei S, Bedoustani AB, Chavoshi R, et al. 2020. Anti-cancer Effects of Probiotic Lactobacillus acidophilus for Colorectal Cancer Cell Line Caco-2 through Apoptosis Induction. *Pharm. Res.*, **27 (2)**: 262-267.

Jacouton E, Chain F, Sokol H, Langella PandBermudez-Humaran LG. 2017. Probiotic strain Lactobacillus casei BL23 prevents colitis-associated colorectal cancer. *Front. immunol.*, **8**: 1553.

Kahouli I, Tomaro-Duchesneau CandPrakash S. 2013. Probiotics in colorectal cancer (CRC) with emphasis on mechanisms of action and current perspectives. *J.Med. Microbiol.*, **62 (8)**: 1107-1123.

Khodaii Z, Mehrabani Natanzi M, Khalighfard S, Ghandian Zanjan M, Gharghi M, Khori V, et al. 2022. Novel targets in rectal cancer by considering lncRNA–miRNA–mRNA network in response to Lactobacillus acidophilus consumption: a randomized clinical trial. *Sci. Rep.*, **12 (1)**: 9168.

Li P, Chen G, Zhang J, Pei C, Chen Y, Gong J, et al. 2022. Live *Lactobacillus acidophilus* alleviates ulcerative colitis via the SCFAs/mitophagy/NLRP3 inflammasome axis. *Food Funct.*, **13 (5)**: 2985-2997.

Mahboubi N, Shafiei-Irannejad V, Kahyaei_aghdam MandSoraya H. 2022. Memantine enhances the cisplatin-induced apoptosis in A2780 ovarian cancer cells via CyclinD1 and hTERT inhibition. *Process Biochem.*, **122**: 69-75.

Maraka S, Groves MD, Mammoser AG, Melguizo-Gavilanes I, Conrad CA, Tremont-Lukats IW, et al. 2019. Phase 1 lead-in to a phase 2 factorial study of temozolomide plus memantine, mefloquine, and metformin as postradiation adjuvant therapy for newly diagnosed glioblastoma. *Cancer Cell Int.*, **125 (3)**: 424-443.

Marcellinaro R, Spoletini D, Grieco M, Avella P, Cappuccio M, Troiano R, et al. 2023. Colorectal cancer: current updates and future perspectives. *J. Clin. Med.*, **13 (1)**: 40.

Mirzadeh MA, Eslami M, Ghanbari A, Zarbakhsh S, Yosefi SandPakdel A. 2024. Coadministration of doxorubicin with vitamin D3, *Lactobacillus acidophilu*s, and *Lactobacillus casei* in the 4T1 mouse model of breast cancer: anticancer and enteroprotective effects. *Med Oncol*., **41 (5)**: 111.

Rawla P, Sunkara TandBarsouk A. 2019. Epidemiology of colorectal cancer: incidence, mortality, survival, and risk factors. *Prz. Gastroenterol*., **14 (2)**: 89.

Robinson EK, Covarrubias SandCarpenter S. 2020. The how and why of lncRNA function: An innate immune perspective. *Biochim Biophys Acta Gene Regul Mech*., **1863 (4)**: 194419.

Segal DandDostie J. 2023. The talented LncRNAs: meshing into transcriptional regulatory networks in cancer. *Cancers (Basel)*., **15 (13)**: 3433.

Shafiei-Irannejad V, Abbaszadeh S, Janssen PMandSoraya H. 2021. Memantine and its benefits for cancer, cardiovascular and neurological disorders. *Eur. J. Pharmacol.*, **910**: 174455.

Śliżewska K, Markowiak-Kopeć PandŚliżewska W. 2020. The role of probiotics in cancer prevention. *Cancers.*, **13 (1)**: 20.

Statello L, Guo C-J, Chen L-LandHuarte M. 2021. Gene regulation by long non-coding RNAs and its biological functions. *Nat. Rev. Mol. Cell Biol.*, **22 (2)**: 96-118.

Sung H, Ferlay J, Siegel RL, Laversanne M, Soerjomataram I, Jemal A, et al. 2021. Global cancer statistics 2020: GLOBOCAN estimates of incidence and mortality worldwide for 36 cancers in 185 countries. *CA Cancer J Clin*., **71 (3)**: 209-249.

Thananimit S, Pahumunto NandTeanpaisan R. 2022. Characterization of short chain fatty acids produced by selected potential probiotic Lactobacillus strains. *J Biomolecules*., **12 (12)**: 1829.

Ulitsky I. 2016. Evolution to the rescue: using comparative genomics to understand long non-coding RNAs. *Nat. Rev. Genet.*, **17 (10)**: 601–614.

Wu Z, Pan D, Jiang M, Sang LandChang B. 2021. Selenium-enriched lactobacillus acidophilus ameliorates dextran sulfate sodium-induced chronic colitis in mice by regulating inflammatory cytokines and intestinal microbiota. *Front. Med.*, **8**：.716816

Yamaguchi F, Hayakawa S, Kawashima S, Asakura TandOishi Y. 2022. Antitumor effect of memantine is related to the formation of the splicing isoform of GLG1, a decoy FGF- binding protein. *Int. J. Cancer*., **61 (1)**: 1-11.

Yoon W-S, Yeom M-Y, Kang E-S, Chung Y-A, Chung D-SandJeun S-S. 2017. Memantine induces NMDAR1-mediated autophagic cell death in malignant glioma cells. *J Korean Neurosurg Soc.*, **60 (2)**: 130-137.

JJBS

Volume 18, Number 2,June 2025
ISSN 1995-6673
Pages 323 – 333
https://doi.org/10.54319/jjbs/180213

Jordan Journal of Biological Sciences

Characterization and In-vitro Evaluation of Positively Charged Oligopeptide as Gene Delivery Vehicle Candidate on BHK-21 Cells

Damai Ria Setyawati[1], Sjaikhurrizal El Muttaqien[1], Irvan Faizal[1], Efrida Martius[1], Indira Putri Negari[1], Asep Saepudin[2], Stefi Mitra Wahyuningsih[3], Neni Nurainy[4], Mulyoto Pangestu[5], and Tarwadi[1,6*]

[1] Research Centre for Vaccines and Drugs, National Research and Innovation Agency (BRIN), Puspiptek Area, Tangerang Selatan, Banten 15314, Indonesia; [2] Directorate for Facilitation, Monitoring Research, and Regional Innovation, National Research and Innovation Agency (BRIN), 12th Floor, Gedung BJ Habibie, Jl. M.H. Thamrin 8, Jakarta 10340, Indonesia; [3] Department of Biochemistry, Faculty of Mathematics and Natural Sciences, IPB University, Jl. Raya Dramaga, Babakan, Dramaga, Bogor, Jawa Barat 16680, Indonesia; [4] Research and Development Division, PT Bio Farma, Jl. Pasteur 28 Bandung, Jawa Barat 40161, Indonesia; [5] Department of Obstetrics and Gynaecology, Faculty of Medicine, Nursing and Health Sciences, Monash University, 246 Clayton Road, Clayton, Victoria 3168, Australia; [6] PT Indomabs Biosantika Utama, Gedung Technology Business and Innovation Centre (TBIC), Pengasinan, Gunung Sindur, Kabupaten Bogor, Jawa Barat 16340, Indonesia.

Received: June 1, 2024; Revised: November 11, 2024; Accepted: Dcember 5, 2024

Abstract

Peptide-based transfection agents have gathered significant interest and are being investigated globally as a possible gene delivery method. The preparation and in-vitro evaluation of oligopeptides composed of GRKKRRQRRR (TAT) and PKKKRKV (NLS) functionalized with the CKKHH sequence as a potential transfection agent is the main goal of this study. Solid-phase peptide synthesis was applied to generate the positively charged of the GRKKRRQRRR-PKKKRKV (OP-1, MW of ~ 2260 Da) and CKKKHH-YGRKKRRQRRR-PKKKRKV (OP-2, MW of ~ 3057 Da) sequences. The oligopeptide's capacity to condense DNA molecules was assessed using the ethidium bromide exclusion and DNA mobility retardation assays. Transmission electron microscopy (TEM) image examination and a particle size analyser were performed to further characterise the oligopeptide/DNA complexes. The MTT assay was used to determine the cytotoxicity, while transgene expression was carried out in BHK-21 cells using a gene encoding green fluorescence protein. Both oligopeptides of OP-1 and OP-02 were able to condense DNA molecules into compacted particles with a size range of 150–220 nm. The transfection agent based on TAT-NLS (OP-1) that functionalized with CKKHH (OP-2) was more efficient in condensing and compressing DNA molecules. Both oligopeptides were comparatively less hazardous to BHK-21 cells than those of poly-L-lysine (PLL), according to the MTT assay result. The oligopeptides' ability to promote GFP-encoding gene transgene expression further emphasises their effectiveness as potential transfection agent candidates. To further increase the positively charged oligopeptide efficacy, more development on the oligopeptide-based transfection agent needs to be explored.

Keywords: Cytotoxicity; DNA condensation; Gene delivery; Nanoparticle; Oligopeptide, Transfection agent.

1. Introduction

Among other qualities and abilities of biological advanced materials, their uniqueness in terms of physicochemical properties-such as their nanoparticle size, stability against enzymatic degradation, and low cytotoxicity-makes them appealing in medical research as drug candidates (Abd El Aty et al., 2023; Ibrahim & Abdel-Aziem, 2019) and gene delivery vehicles (Song et al., 2019; Supe et al., 2023). As transgene gene carriers, synthetic oligopeptide-based gene delivery systems can be designed for DNA condensing, endosomal escaping, and facilitating nuclear uptake to achieve optimum gene delivery (Danielsen & Hansen, 2018; Doh, 2015; Kichler et al., 2019; Koloskova et al., 2018). Oligopeptide-mediated gene transfer is an up-front, safe, and low-risk in immunogenicity for gene delivery vehicle that is attractive when contrasted with viral-based gene delivery carriers due to these attributes. In addition, the oligopeptide-based transfection systems also simultaneously display several features, including DNA condensation ability (Mann et al., 2014), endosomal escape capability (Moulay et al., 2017), facilitating nuclear localization (Yi et al., 2012), and receptor targeting (Todaro et al., 2023).

Amongst the oligopeptides used in gene delivery vehicles are well known as cell-penetrating peptides (CPPs) or protein transduction domains (PTDs). They consist of less than 30 amino acids with the ability to cross the biological membranes in an energy-dependent or energy-independent manner (Guidotti, Brambilla, & Rossi, 2017; Habault & Poyet, 2019). CPPs are probably the most

* Corresponding author. e-mail: tarw001@brin.go.id.

exploited oligopeptides for non-viral gene delivery vehicles due to their capability to interact with membrane cells and allow some modifications to enhance gene delivery efficiency (Danielsen & Hansen, 2018; Ho, White, & Pouton, 2018). Several CPPs and CPP-conjugated molecules are undergoing pre-clinical and clinical trials to treat inflammation-related disease, cancers, heart diseases, and age-related diseases (Guidotti, Brambilla, & Rossi, 2017; Habault & Poyet, 2019). Recently, CPPs have also been modified to target specific cells and organelle to reduce side effects as well as to improve cell uptake, achieving an optimal transgene expression (Cerrato & Langel, 2022; Szabó et al., 2022).

Li and co-workers revealed that the functionalization of TAT-NLS to build gene complexes and the introduction of oligohistidine (Hn) sequence into the transfection agent of short peptide sequence (REDV) might increase the endosomal escape rate and accelerate endothelization and angiogenesis (Li et al., 2018). Moreover, it was reported that conjugated the REDV-G-TAT-NLS with poly(lactide-co-glycolide)-g-polyethyleneimine and polyethyleneimine (PLGA-g-PEI) via a hetero-poly(ethylene glycol) spacer (OPSS-PEG-NHS) capable to increase internalization efficiency, endosomal/lysosomal escape, and nucleus location (Li et al., 2019). Guo and colleagues used the CAGW sequence in addition to the REDV motif to create a gene carrier that was conjugated with the PLGA-g-PEG and TAT-NLS sequences to improve endothelial cell internalisation and transfection efficiency (Duo et al., 2019). In addition, the human heterogenous nuclear ribonucleoprotein A1 (hnRNP A1) sequence of ^{263}FGNYNNQSSNF-GPMKGGNFGGRSSGPY^{289} has been investigated for sufficient nuclear import of gene delivery (Lu et al., 2021) or for sequence specific targeting of viral capsid as an alternative to using the classical NLS sequence of PKKKRKV (Chai et al., 2021).

In our previous research, we demonstrated that the CKKHH sequence plus lauryl or palmitoyl alkyl residues in a short linear lipopeptide can interact with importin-α as a potential gene carrier (Tarwadi et al., 2020). It was revealed that lipopeptides containing palmitoyl alkyl and the CKKHH peptide efficiently compacted DNA molecules and promoted greater transgenic expression than corresponding molecule containing CKHH sequence. In this study, to efficiently condense DNA into nanoparticles and promote transgene expression in BHK-21 cells, we have developed a transfection agent that is made up of CKKHH functionalized with TAT (GRKKRRQRRR) and NLS (PKKKRKV) peptide sequences. Moreover, we have also examined the transmission electron microscope (TEM) images and the cytotoxicity of the oligopeptide/DNA complexes.

2. Materials and Methods

2.1. Materials

All materials were obtained from Sigma Aldrich (Sydney, NSW, Australia) and were of molecular biology or analytical grade, unless otherwise stated. The suppliers of cell culture media of Dulbecco's Modified Eagle Medium (DMEM) and foetal calf serum (FCS) were GIBCO-BRL (Invitrogen Pty. Ltd., VIC, Australia). The Baby Hamster Kidney (BHK-21, ATCC CCL-10) cells were kindly donated by Tedjo Sasmono, PhD of the Eijkman Research Centre for Molecular Biology, Indonesia. The green fluorescent protein (GFP)-encoding plasmid pCSII-EF-AcGFP (9880 bp) was generously provided by the Laboratory of the Research Institute of Microbial Diseases via Prof Kurosu, Osaka University, Japan. We use PLL (Sydney, NSW, Australia) as positive control in this experiment because PLL is capable of condensing DNA effectively and has been used for transfection agent. In addition, PLL relatively has low cytotoxicity and highly positive charged that resembles the oligopeptide. These reasons made us choose PLL as the control.

2.2. Peptide synthesis

The oligopeptides of GRKKRRQRRR-PKKKRKV (OP-1) and CKKHH-YGRKKRRQRRR-PKKKRKV (OP-2) sequences were synthesized using an automated solid-phase synthesizer of a CEM Liberty Microwave peptide synthesizer (DKSH, Hallam, VIC, Australia) with 0.5 mmol of pre-loaded Tentagel S-RAM resin. The activating, coupling, de-protecting, washing, and final de-protecting of amino acids involved in the oligopeptide synthesis process were performed using the Liberty® software linked to the equipment as described previously (Zeng et al., 2016).

2.3. Plasmid DNA isolation

Following the supplier's instructions, the plasmid pCSII-EF-AcGFP, was extracted and kept in *E. coli* DH5α using the QIAGEN® QIAprep Maxi Kit (Qiagen Pty. Ltd., Vic, Australia). The amount and purity of the plasmid DNA were evaluated by spectrophotometric measurement at 260 and 280 nm and electrophoresis on a 1% agarose gel after a single digestion with *Bam*H1 (30 minutes, 90 volts) for the plasmid confirmation. The purified plasmid DNA was frozen at -20 °C and redissolved in Milli-Q water (MQW) for storage.

2.4. Charge and N/P ratio

Based on previous descriptions, the charge ratio (CR, +/-) reflects the number positively charged protonated nitrogen atoms of transfection agent per negatively charged nucleotide unit (Maiti et al., 2018; Tarwadi et al., 2008). For the purposes of the calculations, each nucleotide was given a mean mass of 330 Da. To achieve a charge ratio OP-1/DNA of 1.0, 522 ng of OP-1 (3/13 nmol, MW 2260) and 1000 ng of DNA plasmid (~ 3 nmol) were mixed. Since OP-1 has 13 positively charged amino acids that come from 6 (six) number of lysine (K) and 7 (seven) arginine (R) residues, every molecule of OP-1 generates 13 NH_3^+ groups in physiological pH (HGB pH 7.4). A similar calculation was performed for OP-2, as the oligopeptide OP-2 generates 15 NH_3^+ groups per molecule (8K and 7R). This resulted in a mixture of 1000 ng DNA and 611 ng OP-2 (MW 3057) to obtain a CR of 1.0. The nitrogen/phosphate (N/P) ratio was ascertained for the cationic polymer of PLL, which has a lysine unit (MW of 128), rather than the charge ratio.

2.5. DNA condensation assay

The transfection agent capacity of the oligopeptides or control PLL to condense DNA was assessed using the Ethidium bromide (EtBr) exclusion assay in 96-well black plates, as previously described (Tarwadi et al., 2020).

Briefly, 50 µL of HEPES Glucose Buffer (HGB,15 mM HEPES and 5.13% w/v glucose) pH 7.4 was used to dilute two micrograms (2 µg) of plasmid DNA, with an excess of EtBr (20 µL; 100 mg/mL). After that, the spectrophotometer was calibrated using this mixture to determine the fluorescence intensity, which was measured at λ-excitation = 485 nm and λ-emission = 590 nm. Serial mass ratios of 1, 2, 3, 4, 5, 10, and 20 were used to combine the plasmid DNA with OP-1, OP-2, or PLL. Into each well, MQW was added to obtain a total volume of 230 µL. After allowing the samples to stabilise for ~ 10 minutes at room temperature, 20 µL of EtBr solution (100 mg/mL) was added. Before measuring the fluorescence intensity in a plate reader (FluoSTAR OPTIMA, BMG Lab Tech, Sydney, NSW, Australia), the 96-well plate was orbitally shaken for 30 seconds. The relative fluorescence unit (RFU) of the sample and the reference solution, which is the solution without the transfection agent, were compared to ascertain the intensity of the sample's fluorescence.

2.6. 2.6 DNA mobility shift assay

The DNA mobility shift or DNA retardation experiment was used to determine the oligopeptide's affinity to DNA molecules, as previously described (Tarwadi et al., 2008). Briefly, 10 µL of HGB pH 7.4 was used to dissolve the DNA plasmid (1 µg) and the transfection agents of OP-1, OP-2, and PLL separately. The two solutions were then mixed to produce sample with charge ratios of 0.4, 0.8, 1.6, 3.2, 6.4, or 12.8. The mixture was then incubated for 30 minutes at room temperature, or 25 ^{o}C. After loading the complex samples (10 µL) with 2 µL of loading buffer, the samples were electrophoresed on a 1% agarose gel at 110 volts for 30 minutes, and the DNA bands were detected using a 320 nm transilluminator.

2.7. Complex stability from enzymatic degradation

To assess the transfection agent/DNA complexes' resistance to enzymatic degradation, the complexes were exposed to DNase I (Turbo DNase, Ambion, VIC, Australia). To put it briefly, 1 µg of DNA plasmid and the transfection agents for OP-1, OP-2, and PLL were dissolved in 10 µL of HGB pH 7.4. The charge ratios of 0.1, 0.4, 0.8, 1.6, 3.2, 6.4, or 12.8 were then achieved by mixing the DNA and transfection agent solutions. Prior to being subjected to a 30-minute run on a 1% agarose gel electrophoresis at 110 volts, the combined solutions were incubated for 15 minutes at 37 ^{o}C with 1 unit/µg DNA of DNase I. The presence of DNA bands on the agarose gel was then determined using transilluminations at 320 nm.

2.8. Particle size and zeta potential determination

The transfection agent/DNA complexes' mean particle size (nm) and zeta potential (□) values were determined using the Zetasizer Nano Series (Malvern Instruments, Worcestershire, UK). The mean particle sizes were measured using a 1.5 mL disposable cuvette, and the zeta potential values were determined using a folding capillary cell/Smoluchowski. Separately, 5 µg of plasmid DNA and the transfection agents of OP-1, OP-2, or PLL were dissolved in 500 µL of HGB pH 7.4. Two solutions were then combined to produce charge ratios of 1.0,2.0,3.0,4.0,5.0, and 10.0. Following the transfection agent/DNA complex formation, which took 20–30 minutes to develop, particle size and zeta potential values were assessed. To evaluate the stability of the particle size, the transfection agent/DNA particle sizes were monitored for 4 hours, 190 hours (8 days), 310 hours (13 days), and 480 hours (20 days). The complexes were maintained between point measurements at 4–8 ^{o}C in a refrigerator.

2.9. Transmission electron microscopy (TEM) analysis

A sample of the oligopeptide/DNA complex was dropped onto an EMR carbon-coated grid (EMS, Hatfield, UK), and it was then left to incubate for one to two minutes at room temperature. After two minutes of the grid being upside down on the UranyLess drop, any leftover solution was blotted out with filter paper. Subsequently, a sample containing a grid was left to dry for two hours at room temperature. Samples were examined using a Hitachi High Technology, Japan, HT7700-SS TEM device with an accelerating voltage range of 60–100 kV.

2.10. Cytotoxicity assay

The 3- (4 , 5-dimethyl-2-thiazolyl) – 2 , 5 - diphenyltetrazolium bromide (MTT) metabolic assay was used to assess the viability of the cells against the transfection agents in Baby Hamster Kidney (BHK-21) cells as previously described (Hidayat et al., 2023; Ibrahim & Abdel-Aziem, 2019). In brief, 5 x 10^4 cells/well were seeded in triplicate into a 96-well plate using DMEM supplemented with 10% foetal bovine serum (FBS) and 100 units/mL penicillin-streptomycin. The cells were cultured for 24 hours at 37 ^{o}C in an incubator with 5% CO_2. After the confluency of the cells was approximately 60%, 1.0 µg of DNA plasmid was complexed with the transfection agent in 25 µL HGB pH 7.4 at charge ratios of 1.0, 2.0, 4.0, 6.0, 8.0, 10.0, and 12.0. The complexes were then inserted into the cells, incubated for 24 hours. The culture media were changed with basal media containing 20 µL of MTT solution (5 mg/mL in PBS), then kept at 37 ^{o}C for a further 4 hours in 5% CO_2 incubator. To stop the process, 100 µL of sodium dodecyl sulphate (10% SDS) was applied to each well in the 96-well plate. Afterwards, the well plate was wrapped with aluminium foil and incubated for about 24 hours in a dark setting to dissolve formazan crystal formed. Using a plate reader equipment (Bio-Tek® Instrument, Vermont, USA) set at 570 nm, the absorbance density (OD) of dissolved formazan crystals were determined. Relative cell viability (%) was expressed as the percentage of treated cells relative to control cells.

2.11. Transfection study

A gene expressing green fluorescent protein (GFP) was used to evaluate the transfection investigation in Baby Hamster Kidney (BHK-21) cells in the 96-well plate. To summarise, 10,000 cells/well were seeded into DMEM media containing 10% FCS and 100 units/mL penicillin-streptomycin. The well plate was placed into humidified incubator and maintained at 37 ^{o}C with 5% CO_2. Once the cells had reached around 60% confluence, they were transfected with 100 µL of fresh basal culture media/well after a PBS wash. To generate a transfection agent/DNA mass ratio of 1.0, 2.0, 4.0, 6.0, 8.0, 10.0, or 12.0, the corresponding transfection agent solution was added dropwise into a microtube that contained 300 ng plasmid DNA (pCSII-EF-AcGFP) in 25 µL of HGB pH 7.4. The transfection agent/DNA solution was left to incubate at room temperature for 10-15 minutes before the complex was added to the cells. Subsequently, the cells were further

grown at 37 ^{o}C in a humidified incubator containing 5% CO_2. Finally, the expression of the green fluorescence protein was observed using an Axiovert 40 CFL fluorescent microscope (Carl Zeiss Microscopy GmbH, Germany) after 24-hours incubation.

3. Results

3.1. Design and synthesis of oligopeptides

The goal of the GRKKRRQRRR-PKKKRKV (OP-1) oligopeptide is to represent nuclear localisation sequence (NLS) and trans-activator transcription (TAT). The lengthier oligopeptide sequence made up of CKKHH-YGRKKRRQRRR-PKKKRKV (OP-2) was obtained by incorporating the peptide sequence of CKKHH into the oligopeptide of OP-1. However, we also include amino acid of tyrosine (Y) in the OP-2, simply to mimic an amino acid sequence trans activating transcription (TAT) of YGRKKRRQRRR. The sequence of TAT has been explored intensively in gene delivery as cellular uptake enhancer (Zhang et al., 2023; Zhang et al., 2014) and mediates in crossing the cell membranes (Kim, 2024; Yang & Hinner, 2015). However, the function of individual amino acid of tyrosine still needs to be further exploited.

The purpose of the oligopeptide-based transfection agent design is to bind, compress, and shield DNA molecules from enzyme destruction during gene transfer process. The cysteine (-C-) amino acid inclusion in the OP-2 molecules is intended to facilitate dimerization, enhance the oligopeptides' ability to condense DNA molecules effectively. To promote endosomal escape by the proton sponge effect at a low pH inside endosomal vesicles, two histidine (-H-H-) were also included (Arabzadeh et al., 2019). Before attaining successful transfection, it was anticipated that histidine residues, which supply weakly basic groups, would become protonated in the endosome and promote endosomal escape in a way similar to those of PEI (Belguise-Valladier & Behr, 2001). We utilized the CKKHH sequence as well as peptide sequences rich in lysine (K) and arginine (R) residues from the nuclear localisation sequence (PKKKRKV) and trans-activator of transcription (YGRKKRRQRRR-PKKKRKV) to facilitate and improve cellular and nuclear absorption (**Figure 1**).

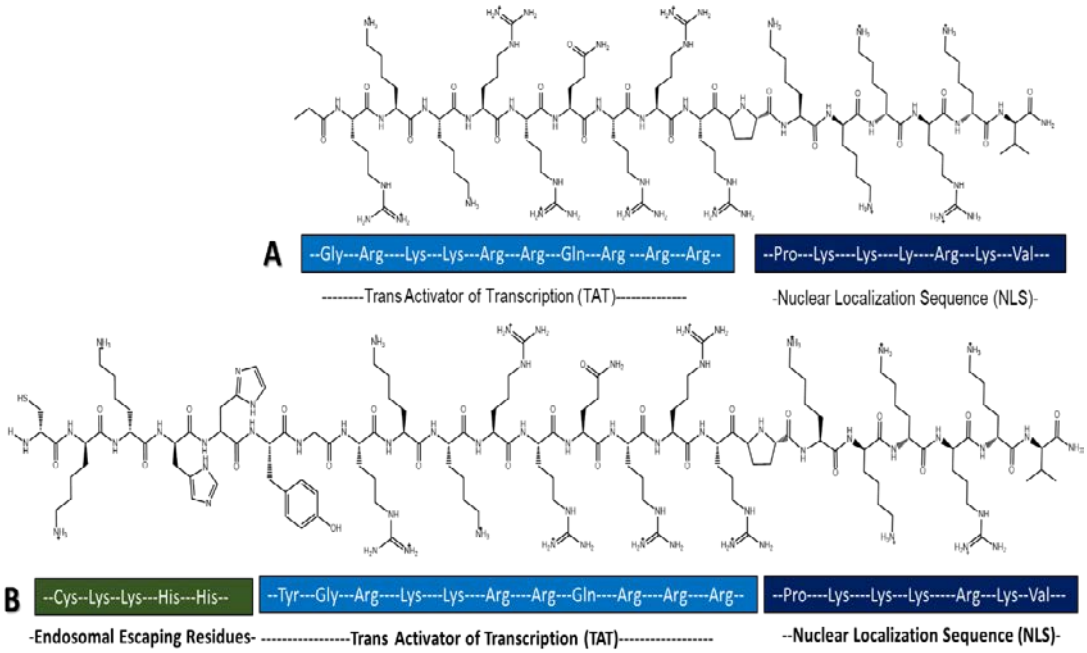

Figure 1. Representative molecular structures of positively charged oligopeptide-based transfection agents: (A). GRKKRRQRRR-PKKKRKV (OP-1) and (B). CKKHH-YGRKKRRQRRR-PKKKRKV (OP-2).

The purpose of the positively charged arginine (-R-) and lysine (-K-) residues inclusion was to facilitate transgene expression, create a compact particle, and provide ionic contact with negatively charged DNA. It has been previously observed that transfection agents' histidine-rich amphipathic peptides may facilitate the effective delivery of DNA molecules in mammalian cells (Kichler et al., 2013). The Fmoc solid-phase peptide synthesis (SPPS) method was used to synthesise the oligopeptides of OP-1 and OP-2, and LC-MS data was used to confirm their molecular structures (**Figure 2**). The molecular size of the oligopeptide of OP-1 was found to be ~ 2260 Da, which was calculated from the m/z values, as shown by the observed m/z peaks at 566.2 (4+), 754.6 (3+), and 1131.2 (2+). Concurrently, the OP-2's LC-MS spectra revealed m/z at 612.6 (5+), 765.4 (4+), and 1020.1 (3+), which supported the molecular size of ~ 3057 Da.

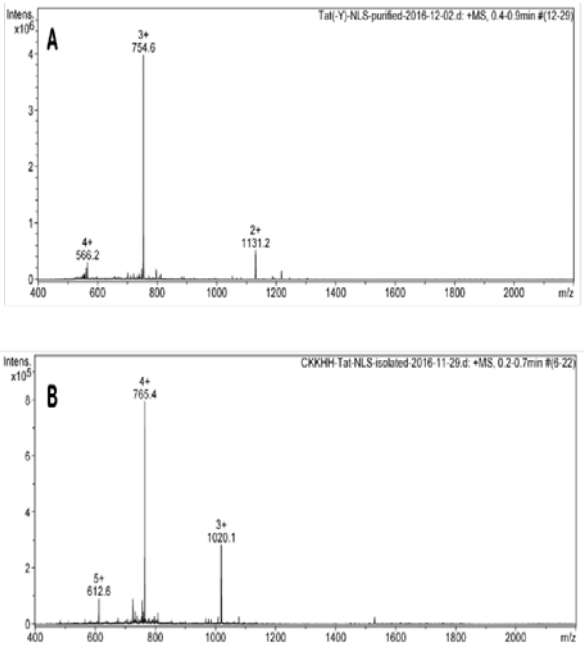

Figure 2. Liquid chromatography-mass spectroscopy (LC-MS) spectra of (A) OP-1 that has specific signals at m/z: 566.2 (4+), 754.6 (3+), and 1131.2 (2+), (B). OP-2 that has specific signals at m/z: 612.6 (5+), 765.4 (4+), and 1020.1 (3+).

3.2. Physicochemical characterization

The EtBr exclusion experiment was used to test the oligopeptides' ability to condense DNA molecules. EtBr creates fluorescence after intercalating between DNA strands with ease. When a transfection agent attaches or condenses DNA molecules, some EtBr will be omitted or excluded from the DNA molecules, resulting in a reduced intensity of fluorescence (Blessing, Remy, & Behr, 1998; Chen et al., 2016). The fluorescence intensity of the oligopeptide/DNA diminishes as the concentration of the transfection agent increases (Figure 3).

Figure 3. The binding studies of oligopeptides and the PLL (as the control) with DNA molecules were performed by EtBr exclusion assay at charge ratio 0-10. The samples' fluorescence intensity was measured at 485 nm for excitation and 590 nm for emission. The data are displayed as mean ± SD (n=3).

At a charge ratio of 5.0, the fluorescence intensities of the DNA molecules condensed by OP-1 and OP-2 oligopeptides were approximately 50%; however, at charge ratio of 10, their fluorescence intensities decreased up to ~45% and ~40%, respectively. The data shows that a longer amino acid sequence of OP-2 (which consists of 23 amino acids) condenses DNA more efficiently than OP-1 (which consists of 17 amino acids). Both oligopeptides, along with the control PLL, displayed similar physicochemical characteristics in condensing DNA molecules. Fascinatingly, when the ratio of the transfection agents to DNA molecules increased from 10 to 20, the fluorescence intensities remained almost constant. This suggests that EtBr still has access to intercalate between the double strands of DNA molecules to produce fluorescence even though the transfection agent's concentration increased two-fold from the charge ratio of 10 to 20. The ability of the oligopeptide to condense and protect DNA molecules were further evaluated by agarose gel electrophoresis experiments. Based on the DNA mobility shift assay, the oligopeptides of OP-1 (13+) and OP-2 (15+) were considered strong DNA condensers, as there were no DNA bands observed at a low charge ratio of 0.4 (Figures 4A and 4B).

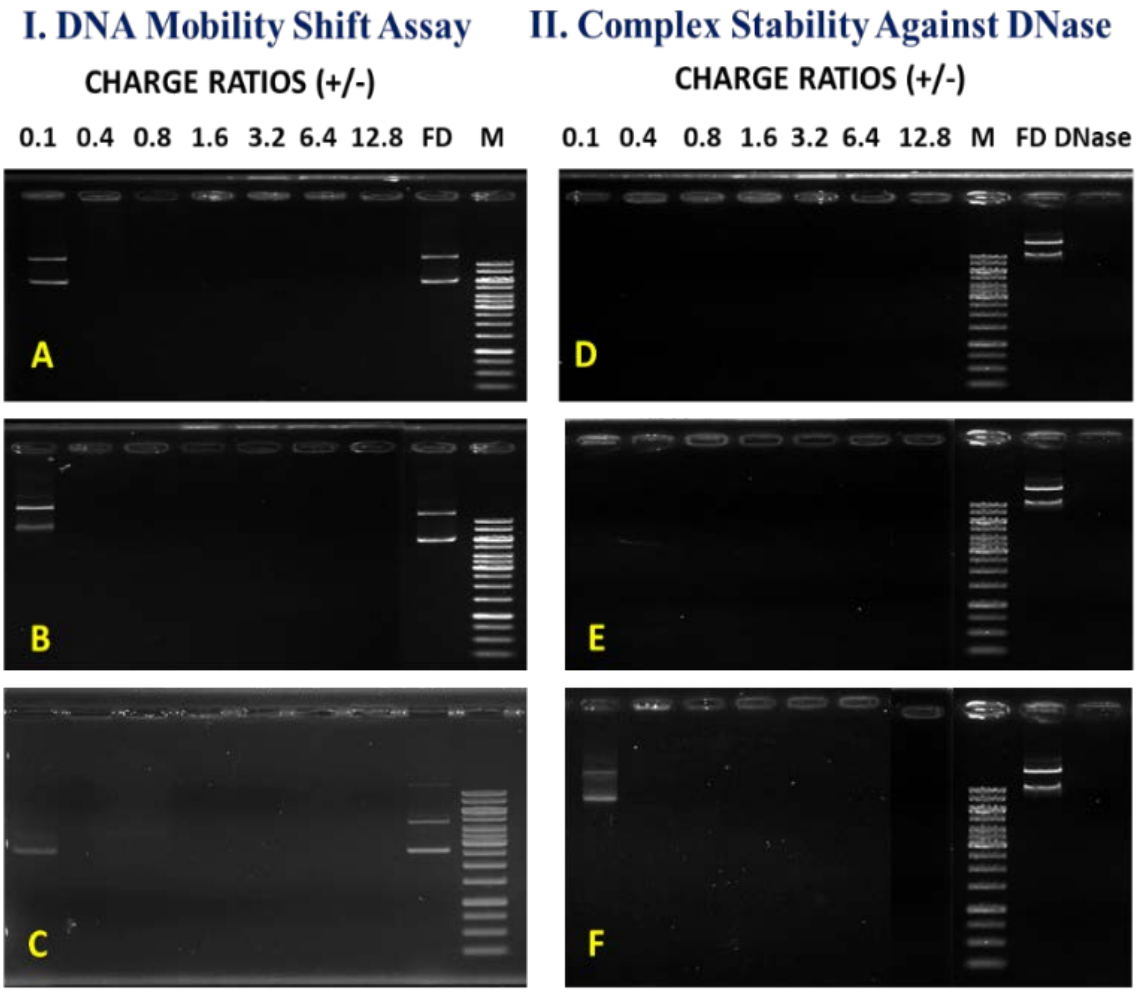

Figure 4. Gel mobility shift assays (I) and complex stability against DNase (II) of the oligopeptide/DNA performed in agarose gel electrophoresis: A/D. OP-1, B/E. OP-2, and C/F. PLL. M: DNA marker, 1 kb ladder, FD: free DNA molecules without transfection agent. DNase: DNA + DNase without transfection agent. PLL was used as the control.

The capability of the oligopeptides to condense DNA molecules was comparable to that of the cationic polymer PLL. The DNA bands were clearly detected on agarose gel from un-complexed, free DNA plasmid (lane FD) as shown (Figures 4A-4C). However, as the DNA molecules were complexed by both OP-1 and OP-2 or PLL, the DNA molecules were retarded in the agarose gel wells. This indicates that oligopeptides are very efficient in condensing DNA molecules, comparable to the control of cationic polymer PLL. The oligopeptide of OP-1 and OP-2 were further evaluated by incubating the oligopeptide/DNA complexes in the presence of DNase. In the absence of oligopeptide, the free DNA plasmid (lane DNase) was fully degraded as observed (Figures 4D-4F). The ability of the oligopeptides to protect DNA molecules from DNase degradation was also similar to that of the PLL. The smeared DNA bands were un-detected in agarose gels as the DNA molecules were protected by the oligopeptide and the control PLL. The complex of the oligopeptide/DNA was further evaluated by measuring their particle sizes and zeta potential values (Figure 5).

The complex particle sizes of the OP-1 and OP-2 with DNA molecules were comparable to the PLL/DNA complexes, approximately 110-200 nm. However, based on Wilcoxon signed-rank test analysis, there was a statistically different (p<0.05) of the complex particle size between PLL, OP-1, and OP2 (Figure 5A). As the charge ratio of the oligopeptide to DNA increases, the zeta potential (ζ) value also increases. Theoretically, as the charge ratio increases, the positive value will continue to rise. We discovered that when the oligopeptide/DNA charge ratio was 3.0, the zeta potential value was nearly negative and there was not statistically different amongst the transfection agent of OP-1, OP-2 and PLL (Figure 5B). Interestingly, the particle size of the PLL or OP-1/DNA at charge ratio of 1.5 that were incubated for up to 480 hours (20 days), remained nearly unchanged, suggesting that there was no evidence of PLL/DNA or OP-1/DNA aggregation (Figure 5C). Compared to the complexes of PLL/DNA and OP-1/DNA, OP-2/DNA behaved differently as the particle size dropped from ~150 nm to ~100 nm as it was incubated up to 20-days (480 hours).

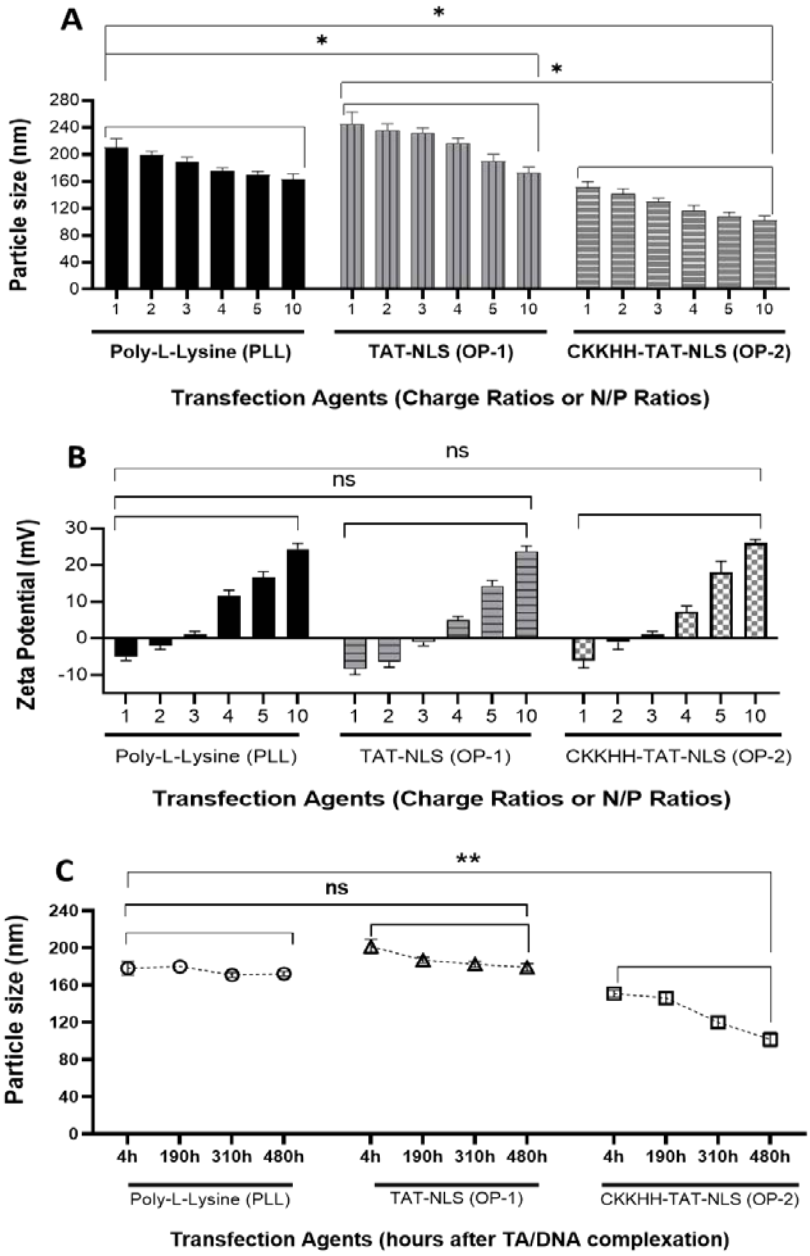

Figure 5. Particle size (nm), zeta potential value, and oligopeptide/DNA complex stability in HGB pH 7.4: (A) particle size of transfection agent/DNA at charge (N/P) ratios of 1.0-10.0, (B) zeta potential values of transfection agent/DNA at charge ratios of 1.0-10.0, and (C) particle size stability of the transfection agent/DNA up to 480 hours after the complex formation at a charge ratio of 1.5. Data are triplicates, expressed as mean ± SD and subjected to Wilcoxon signed-rank test analysis.

Transmission electron microscopy (TEM) image analysis was used to further characterise the particle size and morphology of the oligopeptide/DNA complexes (Figure 6). The complexes of OP-1/DNA and OP-2/DNA at charge ratio 4.0 resulted in compacted particles with diameters of 100-150 nm (Figures 6D-6E).

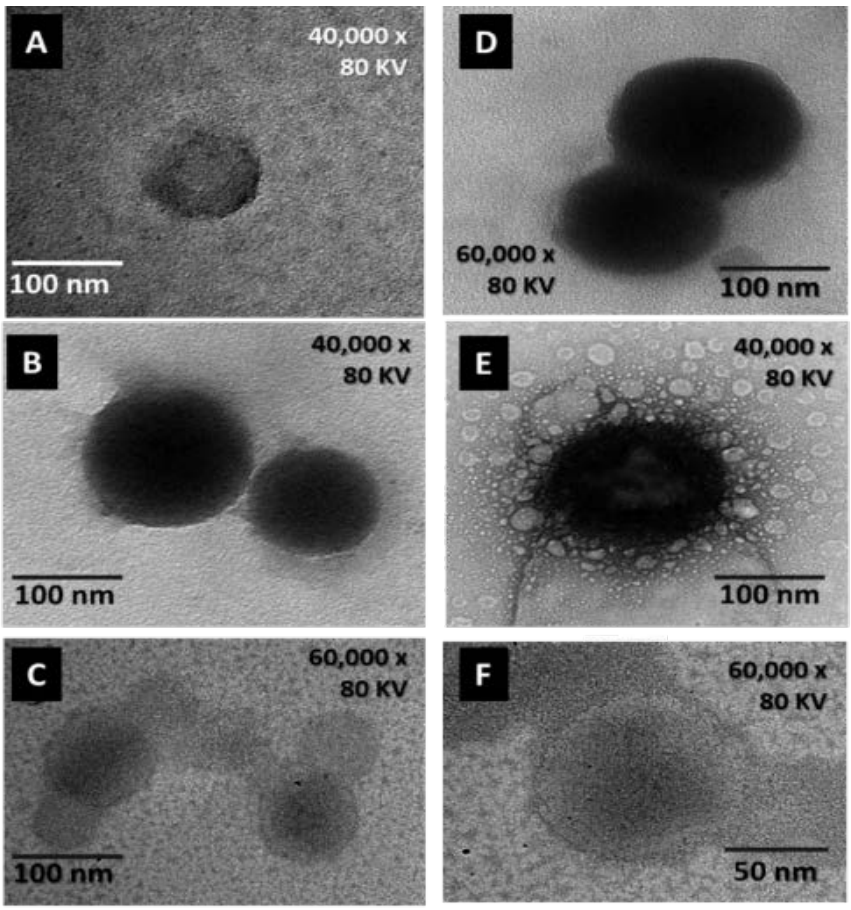

Figure 6. TEM images of the oligopeptide-based transfection agent and the oligopeptide/DNA complexes in HGB pH 7.4 at a charge ratio 4.0. (A) OP-1, (B) OP-2, (C) PLL, (D) OP-1/DNA, (E) OP-2/DNA, and (F) PLL/DNA. PLL was used as the control.

The individual nanoparticle was clearly observed, and no aggregation was detected as the oligopeptide was diluted in HGB pH 7.4 or complexed with DNA molecules. Based on TEM analysis, the oligopeptide/DNA complex particle size was comparable to PLL/DNA (100-150 nm).

3.3. Biological activity evaluation

Following a 24-hour growth period, the MTT assay was used to assess the viability of the oligopeptide/DNA complexes on BHK-21 cells at charge ratios of 1, 2, 4, 8. 16, and 32. These charge ratio values are equivalent with sample concentration of 10, 20, 40, 80, 160, and 320 µg/mL or ppm. The findings showed that the charge ratio of the oligopeptide/DNA has a significant impact on the BHK-21 cell viability (Figure 7). The oligopeptides are less toxic compared to BHK-21 cells compared to PLL based on the Wilcoxon signed-rank test analysis (p<0.01). Furthermore, it was evident that when BHK-21 cells were treated with PLL at charge (N/P) ratios > 8.0 or above 80 ppm, over 40% of the cells were inhibited; in contrast, only around 20% of the cells were inhibited by OP-1 and OP-2 at the same concentration.

Figure 7. Cytotoxicity assay of the OP-1, OP-2, and PLL at charge ratio 1.0-32.0 in HGB pH 7.4 on BHK-21 cells. PLL was used as the control. Data are displayed as mean ± SD (n=3) and subjected to Wilcoxon signed-rank test analysis.

The oligopeptides were further evaluated to transfect BHK-21 cells (**Figure 8**). The GFP-expressing cells were detected at the oligopeptide/DNA charge ratios of 2.0, 4.0, and 6.0. However, when the charge ratio increased further beyond 6.0, the GFP-expressing cells were hardly detectable. Although the GFP-expressing cells mediated by the oligopeptides are relatively higher than those mediated by PLL, the transfection enhancement was not significantly improved. It might be due to the presence of

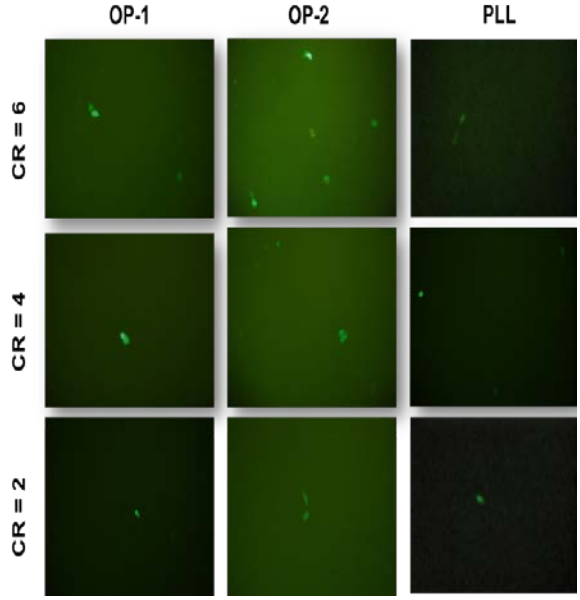

Figure 8. GFP expression of 24-hours post transfection in BHK-21 cells with plasmid DNA encoding GFP gene condensed with OP-1, OP-2, and PLL at charge ratios of 2.0, 4.0, and 6.0. PLL was used as the control.

4. Discussion

We have successfully demonstrated that the oligopeptides of GRKKRRQRRR-PKKKRKV (OP-1) and CKKKHH-YGRKKRRQRRR-PKKKRKV (OP-2) with molecular sizes of ~ 2260 Da and ~3057 Da, respectively (Figures 1 and 2). This means, the molecular weight of the OP-1 can be calculated as follows: = (566.2 x 4)-4 = 2260.8 Da, or (754.6 x 3)-3=2260.8 Da, or (1131.2 x 2)-2 = 2260, 4 Da. Similarly, based on LC-MS data, the molecular weight of the OP-2 was calculated as follows: = (612.6 x 5)-5 = 3058 Da, or (765.4 x 4)-4=3057.6 Da, or (1020.1 x 3)-3 = 3057.3 Da. Both oligopeptides were capable of condensing and protecting DNA molecules efficiently (Figures 3) and forming nanoparticle sizes of 100-220 nm as revealed by TEM image analysis (Figure 6). Moreover, by visualizing the DNase-treated samples from agarose gel electrophoresis, we have demonstrated that our oligopeptides were able to protect DNA molecules from enzymatic degradation (Figure 4). Instead of visualizing DNA bands on agarose gel, He *et al*. quantified the effectiveness of the DNA protection by measuring the optical density (OD260) after incubating the samples in the DNase solution (He et al., 2013). Meanwhile, Fihurka and co-workers have employed the EtBr exclusion assay to determine the undigested DNA of the samples after incubation with DNase solution (Fihurka, Sanchez-Ramos, & Sava, 2018). They found that as the transfection agent 13 or 15 positively charged amino acids (OP-1 or OP-2) which provide very strong ionic interaction between the oligopeptides and the DNA molecules. As the charge ratio of the oligopeptide and DNA increases, the complexes of oligopeptide/DNA are more compacted than those of low charge ratio. This compacted oligopeptide/DNA complex limited the release of the DNA molecule from the complex to be further transcribed into functional mRNA and, as a result, decreased the number of GFP-expressing cells. condensed DNA molecules efficiently to form compacted nanoparticles, the release of DNA from transfection agents was very slow. This implies that a very strong interaction between the transfection agent and the DNA molecules might result in unfavorable conditions.

The physicochemical characteristics of the oligopeptides in condensing, binding, and protecting DNA molecules as well as the particle size were comparable to PLL. Interestingly, we found that our oligopeptides that compose of CKKHH, TAT, and NLS (OP-2) are capable of condensing DNA molecules more effectively than the conjugated TAT-NLS compound only (OP-1) as more compacted particle size was achieved (Figure 5A). Previously, it was reported that the conjugate TAT-NLS condensed DNA molecules at N/P ratios of 5.0 (Yi et al., 2012) or mass ratio 2.0-3.0 (Li et al., 2018). In our research, the DNA molecules were condensed effectively even at a very low mass ratio of 0.4 (Figure 4). The presence of 13 or 15 positive charges from lysine and arginine in the OP-1 or OP-2 provides very strong ionic interaction between the oligopeptides and the negative charges of the DNA molecules. This interaction creates compact nanoparticles of the oligopeptides composed of TAT and NLS sequences as revealed by particle size and TEM analysis of the oligopeptide/DNA complex. Both oligopeptides are effective at condensing DNA into nanoparticle sizes of approximately 200 nm. OP-2 has more capability to condense DNA molecular effectively as shown in Figure 3 and Figure 5, where DNA condensation and DNA complex formation facilitated by OP-2 was tighter and smaller compared to OP-1. These physicochemical characteristics of OP-2 might come from longer amino acid sequence (23 > 17 amino acids), higher positively charge (15 > 13 charges), and inclusion of cysteine residue (-C-). Longer amino acid sequence and higher positively charges of the oligopeptide enhance ionic interaction between positively charged oligopeptide and the negatively charged DNA molecules. Meanwhile, cysteine has been reported capable of promoting complexation by the formation of disulfide bonds (Dauty et al., 2001; Tarwadi, 2018) that might enhance the compactness of the oligopeptide/DNA particles.

Homogenous particle and complex stability of the oligopeptide/DNA are beneficial for the transgene expression since they are influence cellular uptake and cytoplasmic delivery (Sang et al., 2015). However, for transgene expression to occur, DNA molecules are expected to be released safely from the carrier prior to gene transcription. Therefore, it should be kept in mind that the interaction between the gene of interests and the carriers must be flexible enough, protected from enzymatic degradation, and capable of penetrating nucleus membrane before resulting transgene expression. Two (2) histidine residues in the CKKHH sequence of OP-2 were expected to enhance transgene expression as the histidine capable of

facilitating endosomal escape. Our Findings in transfection study on BHK-21 cells have showed that there was only a minor transfection enhancement as the number of GFP-expressing cells slightly increased as cells were treated with OP-2 compared to the control PLL (Figure 8). It is interesting to note that although both oligopeptides are capable of condensing and protecting DNA molecules from enzymatic degradation during cellular transport (Figure 4), the transgene expression facilitated by the oligopeptides was still moderate. We speculate this phenomenon might be due to very tight ionic interaction between the oligopeptides and DNA molecules that made it difficult for RNA Polymerase to initiate transcription process and hampered gene expression. Nevertheless, our oligopeptides are relatively non-toxic as the viability of BHK-21 cells was ~ 80% compared to control, although cells were treated with oligopeptides at a charge ratio of 12.0 that gives a chance to interfere and damage the cell membranes. To achieve safe and efficient non-viral gene delivery vehicles, these transfection agents composing of CKKHH, TAT, and NLS could be further explored by formulating the oligopeptides with lipids or other components.

5. Conclusion

We have successfully demonstrated that inclusion of CKKHH functionalized positively charged amino acid of lysine and arginine in TAT and NLS sequence is capable of condensing and compacting DNA molecules to form nanoparticle sizes (100-220 nm) as revealed by DNA condensation, DNA shift mobility, particle size and TEM image analysis. Based on MTT assays, both oligopeptide sequences of GRKKRRQRRR-PKKKRKV (OP-1) and CKKKHH-YGRKKRRQRRR-PKKKRKV (OP-2) with molecular sizes of ~ 2260 Da and ~3057 Da, respectively, have low cytotoxicity in BHK-21 cells. However, a very strong ionic interaction between DNA molecules and the oligopeptide hampered DNA molecules released from the complexes and in turn limited the transgene expression. Therefore, further exploration to optimize the oligopeptide sequence or modulate the ionic interaction of the positively charged amino acids and the negatively charged DNA molecules is needed by formulating the oligopeptide with lipids or other compounds to increase transfection agent efficiency.

Conflict of Interest

All authors declare that there is no conflict of interests.

Author Contribution

Damai Ria Setyawati: data curation and analysis; Sjaikhurrizal El Muttaqien: data analysis and manuscript correction, Irvan Faizal: data analysis and manuscript correction, Asep Saepudin: data curation and analysis, Efrida Martius: data analysis and manuscript preparation, Indira Putri Negari: data analysis and manuscript preparation, Stefi Mitra Wahyuningsih: data curation and analysis; Neni Nurainy: data curation and review; Mulyoto Pangestu: formal analysis and review; Tarwadi: conceptualization, data curation, formal analysis, writing original draft, supervision, editing, and final revision.

Acknowledgement

We thank the National Research and Innovation Agency (BRIN) under the funding scheme of Research and Innovation for Advanced Indonesia (RIIM-3) of Fiscal Year 2023 through decree No. **12/II.7/HK/2023** from the Deputy for Research Facilitation and Innovation-National Research and Innovation Agency (BRIN). We also thank Professor David Jackson for the oligopeptide synthesis in the Peter Doherty Institute -The University of Melbourne-Australia.

References

Abd El Aty, A. A., Alshammari, S. O., Alharbi, R. M., & Soliman, A. A. 2023. Astragalus sarcocolla Gum-mediated a Novel Green-synthesis of Biologically Active Silver-Nanoparticles with Effective Anticancer and Antimicrobial activities. *Jordan J Biol Sci*., **16(1)**.

Arabzadeh, S., Amiri Tehranizadeh, Z., Moalemzadeh Haghighi, H., Charbgoo, F., Ramezani, M., & Soltani, F. 2019. Design, Synthesis, and In Vitro Evaluation of Low Molecular Weight Protamine (LMWP)-Based Amphiphilic Conjugates as Gene Delivery Carriers. *AAPS Pharm Sci Tech.*., **0(3):** 111.

Blessing, T., Remy, J. S., & Behr, J. P. 1998. Monomolecular collapse of plasmid DNA into stable virus-like particles. *Proc Natl Acad Sci USA.*, **95(4):** 1427-1431.

Cerrato, C. P., & Langel, Ü. 2022. An update on cell-penetrating peptides with intracellular organelle targeting. *Expert Opinion on Drug Delivery*, **19(2):** 133-146.

Chai, K., Wang, Z., Pan, Q., Tan, J., Qiao, W., & Liang, C. 2021. Effect of Different Nuclear Localization Signals on the Subcellular Localization and Anti-HIV-1 Function of the MxB Protein [Original Research]. *Front. Microbiol.*, **12**.

Chen, W., Li, H., Liu, Z., & Yuan, W. 2016. Lipopolyplex for Therapeutic Gene Delivery and Its Application for the Treatment of Parkinson's Disease. *Front Aging Neurosci.*, **8 (68)**.

Danielsen, E. M., & Hansen, G. H. 2018. Impact of cell-penetrating peptides (CPPs) melittin and Hiv-1 Tat on the enterocyte brush border using a mucosal explant system. *Biochim Biophys Acta Biomembr*., **1860(8):** 1589-1599.

Dauty, E., Remy, J. S., Blessing, T., & Behr, J. P. 2001. Dimerizable cationic detergents with a low cmc condense plasmid DNA into nanometric particles and transfect cells in culture. *J Am Chem Soc.*, **123(38):** 9227-9234.

Doh, K. O. 2015. Validation of Heterodimeric TAT-NLS Peptide as a Gene Delivery Enhancer. *J Microbiol Biotechnol.*, **25(6):** 788-794.

Duo, X., Bai, L., Wang, J., Ji, H., Guo, J., Ren, X., Shi, C., Xia, S., Zhang, W., & Feng, Y. 2019. CAGW and TAT-NLS peptides functionalized multitargeting gene delivery system with high transfection efficiency. *Polym Adv Technol.*, **30(10):** 2567-2576.

Fihurka, O., Sanchez-Ramos, J., & Sava, V. 2018. Optimizing Nanoparticle Design for Gene Therapy: Protection of Oligonucleotides from Degradation Without Impeding Release of Cargo. *Nanomed Nanosci Res.*, **2(6)**.

Guidotti, G., Brambilla, L., & Rossi, D. 2017. Cell-Penetrating Peptides: From Basic Research to Clinics. *Trends Pharmacol Sci.*, **38(4):** 406-424.

Habault, J., & Poyet, J. L. 2019. Recent Advances in Cell Penetrating Peptide-Based Anticancer Therapies. *Molecules*, **24(5).**

He, S. N., Li, Y. L., Yan, J. J., Zhang, W., Du, Y. Z., Yu, H. Y., Hu, F. Q., & Yuan, H. 2013. Ternary nanoparticles composed of cationic solid lipid nanoparticles, protamine, and DNA for gene delivery. *Int J Nanomedicine*, **8:** 2859-2869.

Hidayat, T. A., Maharani, R., Chaerunisaa, Y. A., Masduki, F. F., Aditama, R., Setiawan, H., & Tarwadi, T. 2023. Synthesis, Characterization, and In vitro Evaluation of Short Cationic Peptides for Gene Delivery Vehicle Candidate. *Curr. Bioact. Compd.*, **19:** 1-11.

Ho, J. K., White, P. J., & Pouton, C. W. 2018. Self-Crosslinking Lipopeptide/DNA/PEGylated Particles: A New Platform for DNA Vaccination Designed for Assembly in Aqueous Solution. *Mol Ther Nucleic Acids*, **12:** 504-517.

Ibrahim, F. M., & Abdel-Aziem, S. H. 2019. Assessment of Satureja Montana L. and Mentha piperita L. antioxidant activity, cytotoxicity and pattern of apoptotic gene expression in hepatoma cells. *Jordan J Biol Sci.*, **12(3)**.

Kichler, A., Mason, A. J., Marquette, A., & Bechinger, B. 2013. Histidine-rich cationic amphipathic peptides for plasmid DNA and siRNA delivery. *Methods Mol Biol.*, 948: 85-103.

Kichler, A., Mason, A. J., Marquette, A., & Bechinger, B. 2019. Histidine-Rich Cationic Cell-Penetrating Peptides for Plasmid DNA and siRNA Delivery. *Methods Mol Biol*., **1943:** 39-59.

Kim, J. W. 2024. Transcription factors crossing the cell membrane. *Nat Rev Mol Cell Biol*. **25(2):** 86-86.

Koloskova, O. O., Gileva, A. M., Drozdova, M. G., Grechihina, M. V., Suzina, N. E., Budanova, U. A., Sebyakin, Y. L., Kudlay, D. A., Shilovskiy, I. P., Sapozhnikov, A. M., Kovalenko, E. I., Markvicheva, E. A., & Khaitov, M. R. 2018. Effect of lipopeptide structure on gene delivery system properties: Evaluation in 2D and 3D in vitro models. *Colloids Surf B Biointerfaces*, **167:** 328-336.

Li, Q., Hao, X., Wang, H., Guo, J., Ren, X.-k., Xia, S., Zhang, W., & Feng, Y. 2019. Multifunctional REDV-G-TAT-G-NLS-Cys peptide sequence conjugated gene carriers to enhance gene transfection efficiency in endothelial cells. *Colloids and Surfaces B: Biointerfaces*, **184:**110510.

Li, Q., Hao, X., Zaidi, S. S. A., Guo, J., Ren, X., Shi, C., Zhang, W., & Feng, Y. 2018. Oligohistidine and targeting peptide functionalized TAT-NLS for enhancing cellular uptake and promoting angiogenesis in vivo. *J. Nanobiotechnology*, **16(1):** 29.

Lu, J., Wu, T., Zhang, B., Liu, S., Song, W., Qiao, J., & Ruan, H. 2021. Types of nuclear localization signals and mechanisms of protein import into the nucleus. *Cell Commun Signal.*, **19(1):** 60.

Maiti, B., Kamra, M., Karande, A. A., & Bhattacharya, S. 2018. Transfection efficiencies of α-tocopherylated cationic gemini lipids with hydroxyethyl bearing headgroups under high serum conditions [10.1039/C7OB02835K]. *Org Biomol Chem.*, **16(11):** 1983-1993.

Mann, A., Shukla, V., Khanduri, R., Dabral, S., Singh, H., & Ganguli, M. 2014. Linear short histidine and cysteine modified arginine peptides constitute a potential class of DNA delivery agents. *Mol Pharm*., **11(3):** 683-696.

Moulay, G., Leborgne, C., Mason, A. J., Aisenbrey, C., Kichler, A., & Bechinger, B. 2017. Histidine-rich designer peptides of the LAH4 family promote cell delivery of a multitude of cargo. *J Pept Sci*., **23(4):** 320-328.

Sang, Y., Xie, K., Mu, Y., Lei, Y., Zhang, B., Xiong, S., Chen, Y., & Qi, N. 2015. Salt ions and related parameters affect PEI-DNA particle size and transfection efficiency in Chinese hamster ovary cells. *Cytotechnology*, **67(1):** 67-74.

Song, X., Yan, G., Quan, S., Jin, E., Quan, J., & Jin, G. 2019. MRI-visible liposome-polyethylenimine complexes for DNA delivery: preparation and evaluation. *Biosci Biotechnol Biochem.*, **83(4):** 622-632.

Supe, S., Upadhya, A., Tripathi, S., Dighe, V., & Singh, K. 2023. Liposome-polyethylenimine complexes for the effective delivery of HuR siRNA in the treatment of diabetic retinopathy. *Drug Deliv Transl Res.*, **13(6):** 1675-1698.

Szabó, I., Yousef, M. a., Soltész, D., Bató, C., Mező, G., & Bánóczi, Z. 2022. Redesigning of Cell-Penetrating Peptides to Improve Their Efficacy as a Drug Delivery System. *Pharmaceutics*, **14(5):** 907.

Tarwadi, Jazayeri, J. A., Prankerd, R. J., & Pouton, C. W. 2008. Preparation and in vitro evaluation of novel lipopeptide transfection agents for efficient gene delivery. *Bioconjug Chem*., **19(4):** 940-950.

Tarwadi, S. P., Heni Rachmawati, Rahmana Emran Kartasasmita, Sukmadjaja Asyarie, Jalal A. Jazayeri, and Colin W. Pouton. 2018. Nanoparticle evaluation of synthetic Palmitoyl-CKKHH as transfection reagent for non-viral gene delivery vehicle. *IJERA*, **8(1):** 40-48.

Tarwadi, T., Jazayeri, J. A., Pambudi, S., Arbianto, A. D., Rachmawati, H., Kartasasmita, R. E., & Asyarie, S. 2020. In-silico Molecular Interaction of Short Synthetic Lipopeptide/Importin-alpha and In-vitro Evaluation of Transgene Expression Mediated by Liposome- Based Gene Carrier. *Curr Gene Ther.*, **20(5):** 383-394.

Todaro, B., Ottalagana, E., Luin, S., & Santi, M. 2023. Targeting Peptides: The New Generation of Targeted Drug Delivery Systems. *Pharmaceutics*, **15(6):** 1648.

Yang, N. J., & Hinner, M. J. 2015. Getting across the cell membrane: an overview for small molecules, peptides, and proteins. *Methods Mol Biol*., **1266:** 29-53.

Yi, W. J., Yang, J., Li, C., Wang, H. Y., Liu, C. W., Tao, L., Cheng, S. X., Zhuo, R. X., & Zhang, X. Z. 2012. Enhanced nuclear import and transfection efficiency of TAT peptide-based gene delivery systems modified by additional nuclear localization signals. *Bioconjug Chem.*, **23(1):** 125-134.

Zeng, W., Horrocks, K. J., Tan, A. C. L., & Jackson, D. C. 2016. Chemical Synthesis of Monomeric, Dimeric and Tetrameric Forms of the Ectodomain of Influenza Matrix 2 Protein. *European J Org Chem.*, **2016(5):** 1054-1059.

Zhang, H., Zhang, Y., Zhang, C., Yu, H., Ma, Y., Li, Z., & Shi, N. 2023. Recent Advances of Cell-Penetrating Peptides and Their Application as Vectors for Delivery of Peptide and Protein-Based Cargo Molecules. *Pharmaceutics*, **15(8):** 2093.

Zhang, P., Lock, L. L., Cheetham, A. G., & Cui, H. 2014. Enhanced Cellular Entry and Efficacy of Tat Conjugates by Rational Design of the Auxiliary Segment. *Mol Pharm.*, **11(3):** 964-973.

JJBS

Volume 18, Number 2,June 2025
ISSN 1995-6673
Pages 335 – 341
https://doi.org/10.54319/jjbs/180214

Jordan Journal of Biological Sciences

First Application of *FLORICAULA* second intron (*FLint2*) as a Phylogenetic Marker in Bananas (Musaceae)

Lia Hapsari[1,*], Apriyono Rahadiantoro[1], Didik Wahyudi[2], Sundari Sundari[3], Rodiyati Azrianingsih[4]

[1]*Research Center for Applied Botany, National Research and Innovation Agency, Cibinong 16911, Indonesia;* [2]*Department of Biology, Faculty of Science and Technology, State Islamic University of Maulana Malik Ibrahim, Malang, 65144, Indonesia;* [3]*Department of Biology Education, Faculty of Teacher Training and Education, University of Khairun, Ternate 97719, Indonesia;* [4]*Department of Biology, Faculty of Mathematics and Natural Sciences, University of Brawijaya, Malang 65145, Indonesia*

Received: June 1, 2024; Revised: November 11, 2024; Accepted: December 5, 2024

Abstract

The utility of potential low-copy genes as molecular markers is becoming more practical for phylogenetic study because they often outperform the multi-copy genes. The application of a low-copy gene, *FLORICAULA* second intron (*FLint2*), that contributes to early flowering as a phylogenetic marker in bananas (Musaceae), has never been reported. Yet, inflorescence remains a dominant distinguishing characteristic in bananas and its closely related species. Hence, this study aimed to determine the potential phylogenetic utility of *FLint2* compared with *Internal Transcribed Spacer* (*ITS*) as a multicopy gene in bananas and closely related species. Results showed that *FLint2* was easily amplified under optimized PCR conditions. The *FLint2* amplicons were found to be medium length (450-500 bp) in bananas and significantly differ from its closely related species of Heliconiaceae and Strelitziaceae (1200-1300 bp). The sequences were GC-rich and highly variable at 89.11%. Individual maximum-likelihood phylogenetic trees of both markers were mostly congruent. The *FLint2* provides an alternative internal topology within bananas and is better at separating the cultivar genome groups, although weak in bootstrap support. The combined sequences improved the tree topology and strong-supported clades. In conclusion, *FLint2* was proven to have high potential phylogenetic utility to intraspecific and genomic levels in bananas and it is also suggested to be suitable for use in closely related species within the Zingiberales order.

Keywords: *FLORICAULA*, *LEAFY*, phylogeny, polymorphism, Musaceae, Zingiberales

1. Introduction

The tropical fruit of bananas (Musaceae) is a globally important cash crop and nutritious food source. More than 1,000 cultivated varieties (cultivars) were recorded, mainly produced and consumed for local home consumption, and a few of them contributed to international trade (Pareek, 2016). Most of today's cultivated bananas presumably come from diploid wild species of *Musa acuminata* (genome A) and *Musa balbisiana* (genome B). Hybridizations that occur among and within those species were generated progenies with various levels of ploidy and genome groups such as AA, AB, BB (diploids); AAA, AAB, ABB (triploids); and AAAA, AAAB, AABB (tetraploids) (De Jesus *et al*., 2013). Furthermore, sterility, parthenocarpy, and human selection have complicated the domestication of bananas (De Langhe *et al*., 2009). Hence, evolutionary study through phylogenetic analysis of *Musa* genetic resources is significant as the basis information for further banana breeding programs.

In plants, molecular markers are mainly derived from nuclear and plastid genomes. The nuclear ribosomal *Internal Transcribed Spacer* (*ITS*) is a multi-copy gene that has been popularly used as a molecular marker in land plants with high resolving power and more informative results than plastid markers such as *trn*L, *mat*K, *rbc*L, *atp*B-*rbc*L, *rps16*, *rpo*C, and others (Ranibala *et al*., 2018; Ha *et al*., 2022; Amer *let al*., 2022; Salih, 2023). The *ITS* has high phylogenetic utility as an intron (non-coding region) because evolution may occur more neutrally. However, multiple divergent *ITS* sequence types and paralogues were detected due to the complex and several phylogenetic scenarios of rRNA loci in hybrids, particularly in allopolyploid bananas. It promotes bad signaling and has a negative effect on phylogenetic inference. Therefore, plasmid cloning is necessary before sequencing (Hřibová *et al*., 2011; Hapsari *et al*., 2018).

The utility of potential low-copy genes as molecular markers is becoming more practical for phylogenetic study because they often outperform the multi-copy genes. The *FLORICAULA*, or *LEAFY*, is one of the low-copy nuclear genes, comprising three exons and two introns. It is one of the main regulatory genes that contributed to controlling the change from vegetative to generative phase, initiating and developing flowers (Yang *et al*., 2017). Particularly, the second intron of the *FLORICAULA* gene (*FLint2*) is considered a recommended marker for phylogenetic

* Corresponding author. e-mail: liah001@brin.go.id.

studies at lower taxonomic levels of flowering plants (Angiosperms) (Grob *et al*., 2004). Several studies have utilized *FLint2* for phylogenetic analyses of various plant species, including *Amorphophallus* (Nikmah *et al*., 2016), orchids (Schlüter *et al*., 2007), papaya (Yu *et al*., 2005), *Brassica* (Pankin *et al*., 2008), *Citrus* (Yingzhi *et al*., 2007), and *Cinnamomum* (Huang *et al*., 2016).

Until today, the phylogenetic study using *FLint2* in bananas has not been investigated. Meanwhile, inflorescence remains a dominant distinguishing characteristic in bananas (Jaitrong and Manthey, 2018; Inta *et al*., 2023) and its closely related species such as the bird of paradise plants (Iles *et al*., 2017; Kholqiyah *et al*., 2024) and gingers (Kress *et al*., 2002; Záveská *et al*., 2016), *Canna* (Sultana *et al*., 2019), and others. This makes *FLint2* allegedly suitable for phylogenetic studies. Both *FLint2* and *ITS* are introns (untranslated gene regions of genomic DNA that are spliced out in the formation of mature RNA molecules) and present in the nuclear genome (Creer *et al*., 2007); thus, a phylogenetic study for the combination sequences is possible. Hence, the purpose of this study was to provide a new opportunity for the potential utility of a low-copy *FLint2* gene in comparison with a multi-copy *ITS* gene as a molecular marker to study the phylogenetic study at the lower taxonomic level of bananas. The finding of this study may become the basis reference of molecular evidence to support further breeding programs and proposing a genetic conservation strategy in bananas, and possibly in its closely related species within the Zingiberales order.

2. Materials and Methods

2.1. Plant Materials

Nine living plant accessions of bananas (*Musa* spp., Musaceae) from East Java, Indonesia, were used as the study material's ingroup. It comprised five cultivars representing four genome groups and four wild species representing their two putative ancestral parents. Two closely related species from the order of Zingiberales, namely Heliconiaceae and Strelitziaceae, were used as the outgroup (Table 1, Figure 1).

Table 1. Plant study material of bananas and closely related species

Code	Species name	Local name	Genome group	Family
M1	*Musa balbisiana*	Pisang Klutuk Ijo	BBw	Musaceae
M2	*Musa balbisiana*	Pisang Klutuk Wulung	BBw	Musaceae
M3	*Musa acuminata* var. *rutilifes*	Pisang Cici	AAw	Musaceae
M4	*Musa acuminata* var. *alasensis*	Pisang Monyet	AAw	Musaceae
M5	*Musa acuminata*	Pisang Gading	AAcv	Musaceae
M6	*Musa acuminata*	Pisang Nangka	AAA/AAB	Musaceae
M7	*Musa x paradisiaca*	Pisang Ongkap	AAB	Musaceae
M8	*Musa x paradisiaca*	Pisang Saba Landa	ABB	Musaceae
M9	*Musa x paradisiaca*	Pisang Ebung	ABB	Musaceae
H1	*Heliconia wagneriana*	Pisang Hias	-	Heliconiaceae
S1	*Ravenala madagascariensis*	Pisang Kipas	-	Strelitziaceae

Figure 1. Inflorescence morphology of bananas and closely related species.

2.2. DNA Isolation, PCR and sequencing

Whole genome DNA was isolated from fresh young leaves using an isolation kit (Promega), following the manufacturer's protocol for plants. PCR was performed using a thermocycler (Bio-rad) with primer pair, i.e., *FLint2*F1 5'-CTTCCACCTCTACGACCAGTG-3' and *FLint2*R1 5'-TCTTGGGCTTGTTGATGTAGC-3' (Grob *et al*., 2014). PCR reactions comprised 30 cycles with an initial denaturation at 94°C for 4 minutes, followed by denaturation at 94°C for 30 seconds, annealing at 62°C for 30 seconds, extension at 72°C for 30 seconds and final

extension at 72°C for 7 minutes (Nikmah *et al*., 2016). The amplifications were evaluated by electrophoresis 1.5% agarose gel. The PCR products were directly sequenced with ABI Sequencer (Applied Biosystems) at 1stBASE Lab. Sdn Bhd (Malaysia). The *FLint2* sequences from this study have been deposited for open access to the NCBI GenBank with accession numbers OL690520 to OL690530 (Table 1).

2.3. Data analysis molecular polymorphism and phylogenetic tree reconstruction

Raw sequences were evaluated using Seqscanner v.10. Polymorphism and phylogenetic analyses were carried out on separate *FLint2*, and *ITS*, and combined sequences. The *ITS* sequences of the same samples from previous studies (Hapsari *et al*., 2018) were retrieved from the NCBI GenBank for further comparison phylogenetic study (Table 2). Multiple sequence alignments were conducted in ClustalW (Thompson *et al*., 1994). DNA polymorphisms were analyzed with DnaSP 6.12.03 (Librado and Rozas, 2009). Phylogenetic tree reconstructions were performed in MEGA X by Kimura 2 model maximum likelihood, and 1000 bootstraps (Kumar *et al*., 2018). Bootstrap supports were categorized as strong (>85%), moderate (70-85%), weak (50-69%), and very weak (<50%) (Kress *et al*., 2002). Visual comparisons of tree topologies were performed to determine the congruence of phylogenetic signal and combinability of *FLint2* and *ITS* datasets.

3. Results

3.1. FLint2 amplicons

The *Flint2* amplification successfully yielded a single band at an annealing time of 62 °C. The *FLint2* amplicon length in bananas was approximately 450-500 bp, which is significantly different from the outgroup Heliconiaceae and Strelitziaceae (1200-1300 bp) (Figure 2). Furthermore, direct sequencing on *FLint2* amplicons of 9 banana samples yielded raw nucleotides with a length of 520-534 bp, as for *H. wagneriana* at 1,300 bp and *R. madagascariensis* at 1,291 bp. In comparison, *ITS* amplicons in bananas were longer, around 643-651 bp, yet shorter in *H. wagneriana* and *R. madagascariensis*, i.e., 569 bp and 602 bp, respectively. Meanwhile, the GC content of *Flint2* sequences in bananas was high, 56.40-60.30%, but lower in *H. wagneriana* (44.10%) and *R. madagascariensis* (43.20%). Nonetheless, the GC content of *ITS* was higher than *FLint2* (Table 2).

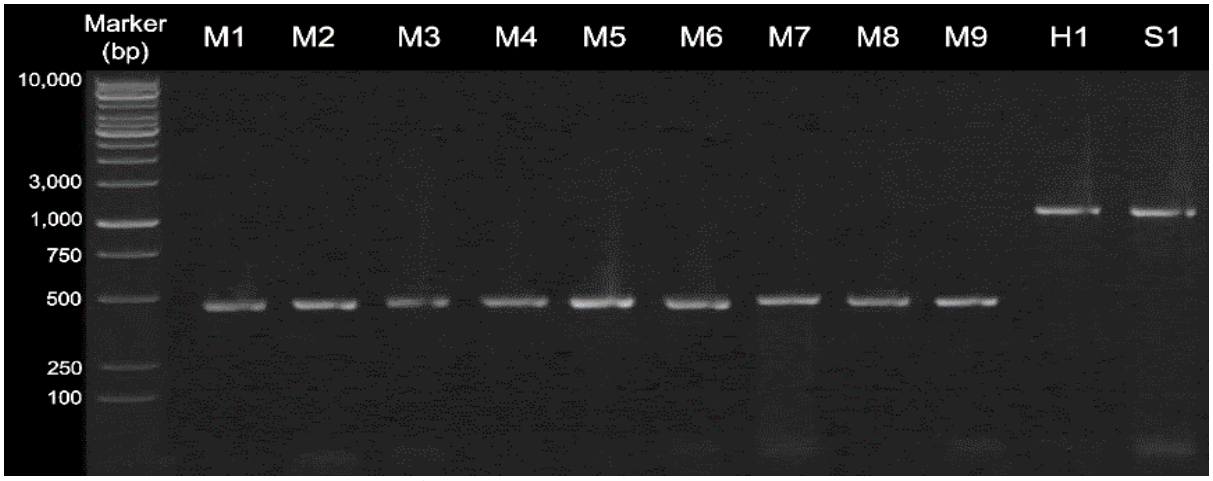

Figure 2. Electrophoregram *FLint2* amplicons of bananas and closely related species.

Table 2. Statistic sequences of *FLint2* and *ITS* in bananas and closely related species

Code	Operational Taxonomic Unit	NCBI acc. number		Seq. length (bp)		GC (%)	
		FLint2	*ITS*	*Flint2*	*ITS*	*Flint2*	*ITS*
M1	*M. balbisiana* Klutuk Ijo	OL690520	KT696444	532	650	58.9	63.7
M2	*M. balbisiana* Klutuk Wulung	OL690521	KT696445	524	651	58.4	63.6
M3	*M. acuminata* var. *rutilifes*	OL690522	KT696459	533	648	59.5	62.9
M4	*M. acuminata* var. *alasensis*	OL690523	KT696462	525	647	58.7	60.7
M5	Pisang Gading (AAcv)	OL690524	KT696473	534	650	59.3	62.0
M6	Pisang Nangka (AAA/AAB)	OL690525	KT696477	526	648	56.4	62.7
M7	Pisang Ongkap (AAB)	OL690526	KT696457	532	650	60.3	62.9
M8	Pisang Saba Landa (ABB)	OL690527	KT696449	520	643	59.5	63.6
M9	Pisang Ebung (ABB)	OL690528	KT696452	520	649	57.7	63.1
H1	Pisang Hias	OL690529	KY215128	1300	569	44.1	70.3
S1	Pisang Kipas	OL690530	FJ428107	1291	602	43.2	73.2

3.2. DNA polymorphisms of FLint2 compared to ITS

The comparison of DNA polymorphism analyses of *FLint2* compared to *ITS* and the combined sequences of both regions in bananas and closely related species are presented in Table 3. The results showed that *FLint2* was highly polymorphic at 89.11%, with a total number of mutations reaching up to 906 events. Further, the mutation events consisted of 44 singleton variables (19 variants, 18 three variants, 7 four variants) and 414 informative parsimonies (105 two variants, 202 three variants, and 107 four variants). The *FLint2* and *ITS* regions were high in

GC content, with *FLint2* having 57.20% GC and *ITS* having 65.10% GC. The *ITS* region was much more conserved (polymorphic 36.90%, monomorphic 63.10%) than *FLint2*. Meanwhile, the combined sequences yielded moderate variations (40.33%) yet relatively conserved (59.67%) ones.

Table 3. Comparison of polymorphisms data of *FLint2*, *ITS* and combined sequences in bananas

Polymorphisms	***FLint2***	***ITS***	**Combined sequences**
Number of all aligned sites	1308	1179	2496
Number of sites with alignment gaps	794	599	1400
Number of sites in the final dataset	514	580	1096
Number of polymorphic sites	458 (89.11%)	214 (36.90%)	442 (40.33%)
Number of monomorphic sites	56 (10.89%)	366 (63.10%)	654 (59.67%)
G+C content	57.20%	65.10%	61.30%
Total number of mutations (Eta)	906	251	506
Number of parsimony informative sites	414	113	311
Number of singleton sites	44	101	131
Haplotype (gene) diversity (Hd±SD)	1.000± 0.039	0.982±0.046	0.982±0.046
Nucleotide diversity (π±SD)	0.480±0.076	0.113±0.029	0.131±0.039
Genetic similarities (%)	38.16-99.82	64.45-100	57.21-100
Number of haplotypes	11	10	10
Number of haplogroups	0	1 (M1+M2)	1 (M1+M2)
Number of clades in all taxa	3	3	3
Number of subclades in Musaceae	4	4	5
Number of clades and subclades in Musaceae with ≥70% BS	2	5	6

Remarks: G=Guanine, C=Cytosine, BS=Bootstrap Support, SD=Standard Deviation, BS=Bootstrap

Due to the high DNA polymorphisms of *FLint2*, haplotype analysis resulted in haplotype gene diversity at maximum level (1.000±0.039) with high nucleotide diversity (0.480±0.076). Further, it was separated into 11 haplotypes with none of the haplogroups. The bananas and closely related species examined had a high genetic variation of *FLint2*, with similarities ranging from 38.16% to 99.82% (Table 3). Meanwhile, the *ITS* and the combined sequences resulted in lower haplotype and nucleotide diversity but were still categorized as high (Hd>0.5; π>0.5%). They resulted in 10 haplotypes with one haplogroup, *i.e*. Pisang Klutuk Wulung and Pisang Klutuk Ijo (*M. balbisiana*), with 100% genetic similarity (Table 2).

3.3. Phylogenetic trees of FLint2, ITS and combined sequences

Individual phylogenetic reconstruction in bananas using *FLint2* and *ITS* resulted in phylogenetic trees, which are primarily congruent. It comprised two main clades in which the Heliconiaceae and Strelitziaceae were separated from Musaceae and served as an outgroup with a strong bootstrap support. Specific to the Musaceae only (ingroup), the phylogenetic tree of *Flint2* was clustered into three clades. The *FLint2* tree demonstrated an alternative internal topology among and within the genome group of bananas but supported by weak to moderate bootstraps. Banana cultivars with two or more A genomes (AAw, AAcv, AAA, and AAB) were clustered in clade 1. Two wild bananas, *M. balbisiana* (BBw), were separated in clade 2, and banana cultivars with ABB genome were separated in clade 3 (Figure 3).

Meanwhile, the *ITS* phylogenetic tree resulted in only two clades. The first clade is similar to *Flint2* and was comprised of banana genome groups AAw, AAcv, AAA, and AAB. The second clade consists of wild *M. balbisiana* and ABB as sisters supported by strong bootstraps (Figure 4). Likewise, the combined analysis of *FLint2* and *ITS* shows an improvement in tree topology and increases the number of clades with solid bootstrap compared to individual analysis. The tree topology of combined sequences was much more congruent with *ITS* than *FLint2* (Table 3, Figure 5).

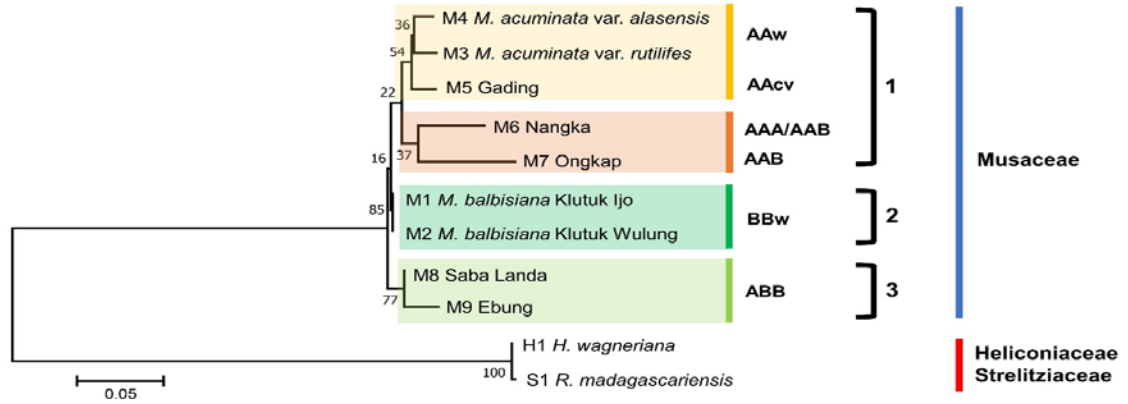

Figure 3. Maximum likelihood phylogenetic tree of *FLint2*

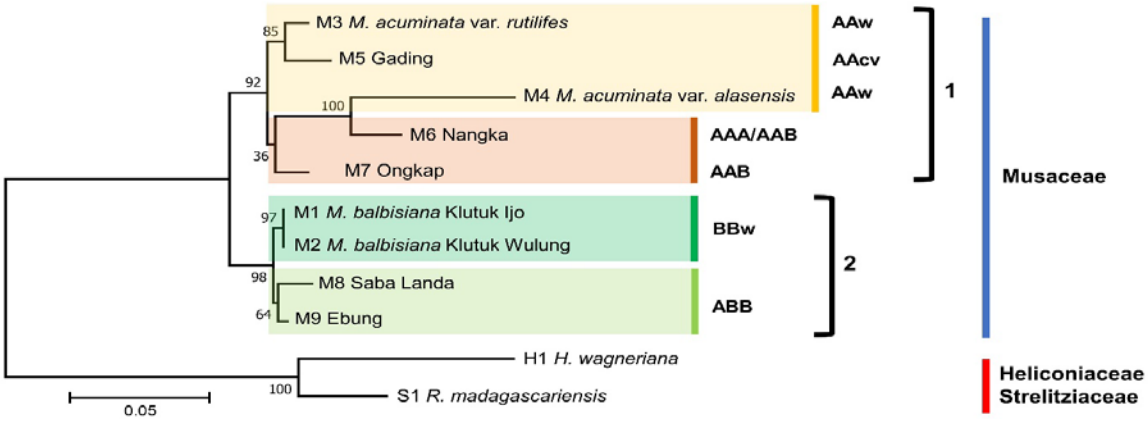

Figure 4. Maximum likelihood phylogenetic tree of *ITS*

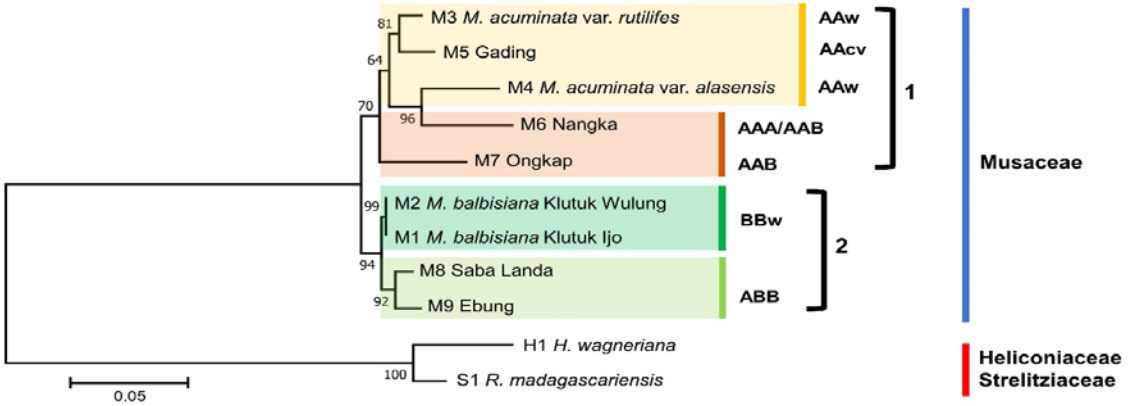

Figure 5. Maximum likelihood phylogenetic tree of combined *FLint2* and *ITS*

4. Discussion

The *FLint2* primers were found to be easily amplified to the whole genome DNA of bananas and closely related species under optimized PCR conditions. The amplifications successfully yielded single bands (Figure 2), thus allowing direct sequencing. In this current study, the *FLint2* primers in bananas need high annealing temperatures to produce single bands at 62 °C; meanwhile, *ITS* needs a low annealing temperature at 53 ºC (Hapsari *et al*., 2018). The *FLint2* primers were known to be strongly temperature-dependent (Nikmah *et al*., 2016). At lower annealing temperatures, the templates resulted in multiple bands, possibly due to nonspecific priming (Ruiz-Villalba *et al*., 2017).

Interestingly, the *FLint2* amplicon length in bananas significantly differs compared to Heliconiaceae and Strelitziaceae. The amplicon's length gaps were about 600-700 bp. Heliconiaceae was found to have the same amplicon size as Strelitziaceae (Figure 2). These results are supported by a previous report by Pankin *et al*. (2008), which stated that *FLint2* was considered highly varied in size, even between genera under the same family. In comparison, *ITS* amplicons in bananas were longer than *Flint2* in wild species and cultivars yet shorter in *H. wagneriana* and *R. madagascariensis* (Table 2). In general, there is no significant difference in the length of the *ITS* amplicon in Angiospermae, which is around 600-700 bp (CBOL, 2009; Hřibová *et al*., 2011).

Furthermore, the *FLint2* sequences in bananas from this study were considered medium in size and sufficient for phylogenetic analysis. BLAST NCBI analysis has

confirmed the generated sequences homologous to partial cds *Floricaula/Leafy* of some species from the Zingiberales order, such as *Curcuma* spp. with a similarity of 91.84%-97.62%, *Globba* sp. with a similarity of 93.33%-95.84% and *Zingiber* spp. with similarity of 91.11%-93.33% (Záveská *et al*., 2016).

Both *FLint2* and *ITS* regions are introns with high GC content. A higher GC content level indicates a higher mutation and recombination events become mutation hotspots (Amit *et al*., 2012; Kiktev *et al*., 2018). Interestingly, comparative DNA polymorphism analysis showed that *FLint2* has higher polymorphism and mutation occurrence than *ITS* and thus will provide better phylogenetic information (Kress *et al*., 2002). Furthermore, haplotype analysis of *FLint2* also resulted in higher haplotype gene diversity than *ITS*. A haplotype is a specific allele or a cluster of DNA sequences of closely linked genes on a chromosome passed down from a common ancestral (Garg *et al*., 2021).

This study found that *FLint2* sequences in bananas and closely related species were highly variable and informative; therefore, they were powerful in differentiation at lower taxonomic levels. This finding is also supported by the fact that the Zingiberales order is classified as a group of highly diverse species, varieties, hybrids, and cultivars, which are distinguished mainly based on morphology, including the flowering organ, which is important for taxonomic differentiation (Kress *et al*., 2002; Iles *et al*., 2017).

Particularly in bananas, about 13 out of 15 distinguishing morphological characters among genome groups are dominated by inflorescence characteristics, including peduncle texture, pedicel length, ovules arrangement, bract curling behavior, bract shape and color, and male flower shape and color (Jaitrong and Manthey, 2018; Gusmiati *et al*., 2018; Inta *et al*., 2023) (Figure 1). Therefore, polymorphisms in *Flint2* sequences that contributed to early flowering allegedly may affect the inflorescence phenotype characteristics of the individual. Polymorphisms commonly occur in nature and are often associated with biodiversity, genetic variation, and adaptation processes (Chung *et al*., 2023).

Maximum likelihood is an accurate method commonly used for phylogenetic analysis. This method searches for the best tree topology with the highest probability or likelihood of character state changes from a precise evolutionary model (Lin *et al*., 2013). The phylogenetic trees of individual and combined sequences resulted in phylogenetic trees which are mostly congruent. It comprised two main clades in which the Heliconiaceae and Strelitziaceae were separated from Musaceae and served as an outgroup with a strong bootstrap support. An outgroup clade provides a time arrow for the historical sequence polarization of all subsequent evolutionary events (Graham *et al*., 2002). Hence, this study supports that Heliconiaceae and Strelitziaceae were primitive relatives of bananas.

Specific to the Musaceae only (ingroup), the phylogenetic tree of *Flint2* was clustered into three clades; meanwhile, in *ITS* and combined sequences, it was separated into two clades. However, the taxon members of the clade were quite similar (Figures 3, 4, 5). Although supported by weak to moderate bootstraps, the *FLint2* phylogenetic tree demonstrated an alternative internal topology and is better at separating the cultivar genome groups. Furthermore, the combined analysis of *FLint2* and *ITS* shows an improvement in tree topology and increases the number of clades with strong bootstrap compared to individual analysis (Table 3, Figure 5). In addition, the phylogenetic trees from this study supported the banana cultivar domestication theory (De Langhe *et al*., 2009) that diploid AAcv first came from intersubspecific hybridization of wild *M. acuminata* (AAw); then, triploid AAA appeared, followed by AAB, and next ABB from hybridization of edible AAcv with wild *M. balbisiana* (BBw). However, due to continuous evolution resulting from genetic variation and mutations, the AAcv and AAA genome groups cannot be separated (Hariyanto *et al*., 2021).

5. Conclusion

The present study is the first report of the application of *Flint2* as a phylogenetic marker in bananas (Musaceae). The finding of this study indicates that *FLint2* has a high potential phylogenetic utility at lower taxonomic levels to intraspecific and genomic levels in bananas. *FLint*2 was easy to amplify and yielded a single product suitable for direct sequencing. It resulted in medium-sized amplicons in bananas but larger in their closely related species of different genera. The *FLint2* sequences were highly variable and informative; therefore, they were powerful enough to differentiate at lower taxonomic levels. The phylogenetic analysis of *FLint2* provides an alternative internal topology within bananas and is better at separating the cultivar genome groups; it also well supports the banana domestication theory. Further research suggests that studies at the intra and interspecific levels of the closely related species in the Zingiberales order should be done using this *FLint2* marker by involving more taxonomically diverse samples.

Acknowledgments

Acknowledgment is conveyed to Purwodadi Botanic Garden (National Research and Innovation Agency Republic of Indonesia) for the plant study materials. Appreciation is also given to the Department of Biology (University of Brawijaya) for the laboratory of molecular genetics. Sincere thanks are dedicated to the Plant Taxonomy working group colleagues for the meaningful discussions. All authors (L.H., A.R., D.W., S.S., R.A.) declared that L.H. is the main author of this manuscript.

References

Amer WM, Shoulkamy MA, Abd El-Baset HD and Faried AM. 2022. Infraspecific identity of the wild *Brassica nigra* (L.) Koch. using morphological, cytogenetics, and molecular (nuclear and chloroplast) approaches. *Jordan J Biol Sci*., **15(3):** 489-500.

Amit M, Donyo M, Hollander D, Goren A, Kim E, Gelfman S, Lev-Maor G, Burstein D, Schwartz S, Postolsky B, Pupko T and Ast G. 2012. Differential GC content between exons and introns establishes distinct strategies of splice-site recognition. *Cell Rep*., **1(5):** 543-556.

CBOL Plant Working Group. 2009. A DNA barcode for land plants. *Proc Natl Acad Sci USA.*, **106(31):** 12794-12797.

Chung MY, Merilä J, Li J, Mao K, Lopez-Pujol J, Tsumura Y and Chung MG. 2023. Neutral and adaptive genetic diversity in plants: An overview. *Front Ecol Evol*., **11**: 1-14.

Creer S. 2007. Choosing and using introns in molecular phylogenetics. *Evol Bioinform*., **3**: pp. 99-108.

De Jesus ON, de Oliveira e Silva E, Amorim EP, Ferreira CF, de Campos JMS, de Gaspari Silva G and Figueira A. 2013. Genetic diversity and population structure of *Musa* accessions in *ex-situ* conservation. *BMC Plant Biol.*, **13**: 41.

De Langhe E, Vrydaghs L, de Maret P, Perrier X and Denham T. 2009. Why bananas matter: An introduction to the history of banana domestication. *Ethnobot Res Appl*., **7**: 165-177.

Garg S. 2021. Computational methods for chromosome-scale haplotype reconstruction. *Genome Biol.,* **101**: pp. 1–24.

Graham SW, Olmstead RG and Barrett SC. 2002. Rooting phylogenetic trees with distant outgroups: a case study from the commelinoid monocots. *Mol Biol Evol*., **19(10):** 1769-1781.

Grob GBJ, Gravendeel B and Eurlings MCM. 2004. Potential phylogenetic utility of the nuclear *FLORICAULA/LEAFY* second intron: comparison with three chloroplast DNA regions in *Amorphophallus* (Araceae). *Mol Phyl Evol*., **30(1):** 13-23.

Gusmiati LH, Hapsari L and Wahyudi D. 2018. Morphological diversity and clustering of 10 cooking bananas (*Musa* cv. Group ABB) collection of Purwodadi Botanic Garden–LIPI. *Floribunda*, **5(8):** 299-314.

Ha DC, Cao PB, Nguyen VD and Le CT. 2022. Molecular phylogeny and deep origins of the hybrid Mokara Dear Heart (Orchidaceae). *Jordan J Biol Sci*., **15(5):** 805-811.

Hapsari L, Azrianingsih R and Arumingtyas EL. 2018. Genetic variability and relationship of banana cultivars (*Musa* L.) from East Java, Indonesia based on the *Internal Transcribed Spacer* region nrDNA sequences. *J Trop Biol Conserv*., **15**: 101-120.

Hariyanto S, Ainiyah RK, Utami ESW and Hapsari L. 2021. Genetic diversity and network within dessert bananas (*Musa acuminata* cv. AA andAAA) inferred by newly designed *matK* marker. *Int J Conserv Sci*., **12(2):** 585-598.

Hřibová E, Jćížková J, Christelová P, Taudin S, de Langhe E and Doleżel J. 2011. The *ITS1-5.8S-ITS2* sequence region in the Musaceae: structure, diversity, and use in molecular phylogeny. *PLoS ONE*, **6**: e17863.

Huang JF, Li L, Conran JG and Li J. 2016. Phylogenetic utility of *LEAFY* gene in *Cinnamomum* (Lauraceae): Gene duplication and polymerase chain reaction-mediated recombination. *J Syst Evol*., **54(3):** 238–249.

Iles WJD, Lagomarsino L, Benson-martin G and Driscoll H. 2017. The phylogeny of *Heliconia* (Heliconiaceae) and the evolution of floral presentation. *Mol Phyl Evol*., **117**: 150-167.

Inta W, Traiperm P, Ruchisansakun S, Janssens SB, Viboonjun U and Swangpol SC. 2023. Evolution and classification of Musaceae based on male floral morphology. *Plants*, **12(8):** 1602.

Jaitrong S and Manthey JA. 2018. Male bud characteristics of diploid, triploid, and tetraploid bananas. *Act Hort*., 1210: pp. 171–176.

Kholqiyah SF, Wahyudi D and Hapsari L. 2024. Genetic diversity and relationship among and within the bird of paradise plants of Strelitziaceae and Heliconiaceae. *Jordan J Biol Sci*., **17(1):** 163-171.

Kiktev DA, Sheng Z, Lobachev KS and Petes TD. 2018. GC content elevates mutation and recombination rates in the yeast *Saccharomyces cerevisiae*. *Proc Natl Acad Sci USA*., **115(30):** E7109-E7118.

Kress WJ, Prince LM and Williams KJ. 2002. The phylogeny and a new classification of the gingers (Zingiberaceae): Evidence from molecular data. *Am J Bot*., **89(10):** 1682–1696.

Kumar S, Stecher G, Li M, Knyaz C and Tamura K. 2018. MEGA X: Molecular Evolutionary Genetics Analysis across computing platforms. *Mol Biol Evol*., **35(6):** 1547-1549.

Librado P and Rozas J. 2009. DnaSP v5: a software for comprehensive analysis of DNA polymorphism data. *Bioinformatic*s, **25(11):** 1451-1452.

Lin Y, Hu F, Tang J and Moret BM. 2013. Maximum likelihood phylogenetic reconstruction from high-resolution whole-genome data and a tree of 68 eukaryotes. *Pac Symp Biocomp*., 285-296.

Nikmah IA, Azrianingsih R and Wahyudi D. 2016. Genetic diversity of porang populations (*Amorphophallus muelleri* Blume) in Central Java and West Java based on *LEAFY* second intron marker. *J Trop Life Sci*., 6(1): 23-27.

Pankin AA, Vorobiev VA and Khavkin EE. 2008. Polymorphism of intron 2 of the *FLORICAULA/LEAFY* gene in *Brassica* plants. *Russ J Plant Phyiol*., **55**: 565-570.

Pareek S. 2016. Nutritional and biochemical composition of banana (*Musa* spp.) cultivars. In: Simmonds MSJ and Preedy VR. Nutritional composition of fruit cultivars, Academic Press, Massachusetts, USA. p. 49–81.

Ranibala G, Singh SS, Singh WR and Khan ML. 2018. Molecular identification and phylogeny of *Musa* species from North-Eastern India by *Internal Transcribed Spacer* 2 of nuclear DNA. *Bionature*, **38(4):** 266-276.

Ruiz-Villalba A, Van Pelt-verkuil E, Gunst QD and Ruijter JM. 2017. Biomolecular detection and quantification amplification of nonspecific products in quantitative polymerase chain reactions (qPCR). *Biomol Detect Quant*., **14**: 7-18.

Salih RHM. 2023. Comparative analysis of Cichorieae tribe (Asteraceae) chloroplast genomes: insight to structure, repetitive DNA, and phylogeny. *Jordan J Biol Sci*., **16(3):** 477-502.

Schlüter PM, Kohl G, Stuessy TF and Paulus HF. 2007. A screen of low-copy nuclear genes reveals the *LFY* gene as phylogenetically informative in closely related species of orchids (*Ophrys*). *Taxon*, **56(2):** 493-504.

Sultana N, Akhi SS, Hassan MA and Rahman MO. 2019. Morphological and anatomical investigation among six variants of *Canna indica* L. *Bangladesh J Plant Taxon.*, **26(2):** 219-230.

Thompson JD, Higgins DG, and Gibson TJ. 1994. CLUSTAL W: improving the sensitivity of progressive multiple sequence alignment through sequence weighting, position-specific gap penalties and weight matrix choice. *Nucleic Acids Res.,* **22(22):** 4673-80.

Yang T, Du M, Guo Y and Liu X. 2017. Two *LEAFY* homologs *ILFY1* and *ILFY2* control reproductive and vegetative developments in *Isoetes* L. *Sci Rep*., **7(1):** 225.

Yingzhi L, Yunjiang C, Nengguo T and Xiuxin D. 2007. Phylogenetic analysis of mandarin landraces, wild mandarins, and related species in China using nuclear *LEAFY* second intron and plastid *trnL-trnF* sequence. *J am Soc Hort Sci*., **132(6):** 796-806.

Yu Q, Moore PH, Albert HH, Roader AHK and Ming R. 2005. Cloning and characterization of a *FLORICAULA/LEAFY* ortholog, *PFL*, in polygamous papaya. *Cell Res*., **15(8)**: 576–584.

Záveská E, Fér T, Šída O, Marhold K and Leong-Škorničková J. 2016. Hybridization among distantly related species: Examples from the polyploid genus *Curcuma* (Zingiberaceae). *Mol Phyl Evol*., **100**: 303-321.

JJBS

Volume 18, Number 2,June 2025
ISSN 1995-6673
Pages 343 – 355
https://doi.org/10.54319/jjbs/180215

Jordan Journal of Biological Sciences

Morphological Characterization and Taxonomic Assessment of *Micromeria* Bentham from Jordan: Key Species and Their Taxonomic Significance

Bilal Azmi Ayasrah[1,*], Sawsan Atallah Oran[2], and Khaldoun Al-Hadid[2]

[1]*Fieldfare Ecology Company;* [2] *Department of Biological Sciences, School of Science, The University of Jordan*

Received: August 24, 2024; Revised: November 30, 2024; Accepted: December 30, 2024

Abstract

This study investigates the taxonomic status of the genus *Micromeria* in Jordan, focusing on the morphological features variation within five species: *M. nervosa, M. fruticosa, M. myrtifolia, M. sinaica,* and *M. danaensis.* Key morphological features, such as leaf shape, stem indumentum, floral structure, and nutlet texture, were used to distinguish these species. The study found that these features provide reliable characters for species identification, with no evidence of *M. graceca* in Jordan.

A key for identifying the species is provided, contributing to the systematic understanding of *Micromeria* in the region. These findings have important implications for species identification and conservation efforts in Jordan

Keywords: *Micromeria,* Systematics, Lamiaceae, Plant Taxonomy, Jordan

1. Introduction

Jordan, located in the Eastern Mediterranean, with a total area of 89,287 km² and acts as a bridge between the Mediterranean region and Arabia peninsula. Its climatic zones support distinct biogeographical regions, namely the Mediterranean, Irano-Turanian, Saharo-Arabian, and the Sudanian (sub-Tropical) regions , which collectively host 13 major vegetation types (Al-Eisawi 1996). This diversity has resulted in over 2,500 plant species, belonging to 142 families and 868 genera (Al-Eisawi, 2013). Despite this richness, taxonomic uncertainties persist for several taxa, including those in the genus *Micromeria*

The genus *Micromeria* (Lamiaceae) comprises approximately 69 species, native to regions ranging from the Mediterranean Basin to southern Africa and parts of Asia (Kew, 2021).

Micromeria species are known for their ecological adaptability and medicinal properties, with several species traditionally used in herbal medicine. In Jordan, six species are recorded: *M. danaensis, M. fruticosa, M. graeca, M. myrtifolia, M. nervosa, and M. sinaica* (Al-Eisawi, 2013). Of these, *M. danaensis* is endemic to Jordan and restricted to the Dana Biosphere Reserve, contributing to its designation as a Key Biodiversity Area (KBA, 2017). Additionally, *M. nervosa* and *M. myrtifolia* have shown antiproliferative potential against cancer cell lines (Oran *et al*., 2022).

Historically, the taxonomy of *Micromeria* has been complex. Initially described by Bentham (1834) as part of *Satureja*, the genus was later divided into distinct genera based on morphological and ecological traits (Boissier, 1879; Feinbrun-Dotan, 1978). Earlier works in the Middle East region, such as those by (Post and Dinsmore, 1933) and (Feinbrun-Dotan, 1978), highlighted inconsistencies in species identification and descriptions.

Morphological features remain a primary tool in plant taxonomy despite advancements in molecular and genetic methods (Stuessy, 2009; Duminil & Di Michele, 2009). These traits are particularly valuable for distinguishing closely related species in *Micromeria*. However, the absence of a comprehensive taxonomic key for *Micromeria* in Jordan has hindered efforts to resolve ambiguities and assess recently discovered taxa like *M. danaensis*.

This study provides a systematic study for the genus in Jordan and establish an updated taxonomic key that will assess the identifying of *Micromeria* taxa in Jordan based on their morphometric features.

This study provides a systematic revision of the genus *Micromeria* in Jordan. By integrating morphological, ecological, and taxonomic analyses, we aim to develop an updated taxonomic key to facilitate species identification and contribute to the understanding of *Micromeria* species diversity and distribution of Jordan.

2. Materials and Methods

A total of 30 *Micromeria* specimens representing the whole plant, including all plant parts, were collected during seven field trips conducted from March to May 2021. The specimens were pressed and dried, and then were poisoned chemically using a mixture of 150 g mercuric chloride (HgCl) and 350 g ammonium chloride (NH4Cl) dissolved in as little water as possible, and 10 L

* Corresponding author. e-mail: bilalayasrah@fieldfareecology.com.

of 96% ethanol. After processing, the specimens were identified, labeled, and mounted. Voucher specimens of each species were deposited at the herbarium of the Royal Society for the Conservation of Nature (RSCN). Additionally, 37 *Micromeria* specimens deposited at two herbaria in Jordan, were consulted and examined in detail: the Biological Sciences Department herbarium at the University of Jordan (AMM) and the herbarium of the Royal Society for the Conservation of Nature (RSCN) (Table 1).

Table 1. Specimen details and collection sites of *Micromeria* species in Jordan.

Species	No. of field specimens	A voucher number	Date of collection	Locality	No. of herbarium specimens	A voucher number
M. nervosa	11	33856	8. March. 2021	Jarash – Sakeb	14	18
		33857	9. March. 2021	Ajloun – Ajloun Forest reserve		31
		33858	9. March. 2021	Ajloun – Ajloun Forest reserve		67
		33859	1. April. 2021	Irbid – Yarmouk Forest reserve		73
		33860	26. April. 2021	Tafilah – Dana Biosphere reserve		107
		33861	26. April. 2021	Tafilah – Dana Biosphere reserve		125
						139
						183
						232
						545
						1973
						18655
						35339
						35881
M. myrtifolia	9	33862	8. March. 2021	Jarash – Sakeb	9	93
		33863	9. March. 2021	Ajloun – Ajloun Forest reserve		140
		33864	1. April. 2021	Irbid – Yarmouk Forest reserve		5844
		33865	1. April. 2021	Irbid – Yarmouk Forest reserve		6272
		33866	26. April. 2021	Tafilah – Dana Biosphere reserve		7477
						7748
						31397
						32850
						35617
						5950
M. sinaica	4	33867	26. April. 2021	Tafilah – Dana Biosphere reserve	8	7237
		33868	16. May. 2021	Tafilah – Dana Biosphere reserve		7700
		33869	16. May. 2021	Tafilah – Dana Biosphere reserve		11249
						30337
						31169
						31397
						38136
						38579
M. fruticosa	4	33870	24. April. 2021	Irbid- Judayta	4	10133
		33871	24. April. 2021	Irbid- Judayta		
		33872	29. April. 2021	Ajloun- Alhashmeh		
		33873	29. April. 2021	Ajloun- Alhashmeh		
M. danaensis	2	33874	26. April. 2021	Tafilah – Dana Biosphere reserve	2	236
		33875		Tafilah – Dana Biosphere reserve		
M. graceca	0		-	-	0	0

The morphological features studied for all collected taxa of *Micromeria* included plant length; stem indumentum and color; leaf type, width, length, shape, margin, petiole, apex, marginal vein, and indumentum; floral leaf shape, length, and indumentum; inflorescence type, number of flowers, peduncle, and pedicel; calyx shape, teeth, and indumentum; corolla color and indumentum; nutlet shape and surface texture. In each sample of the specimens studied, at least 4 readings were taken for each morphological character. Characters, such as hair type and the presence or absence of glands, were studied using a stereomicroscope at different magnifications (10x, 20x, and 40x). All measurements were taken using a Vernier caliper for accuracy.

3. Results

Five different *Micromeria* species were identified in Jordan. These are *M. nervosa* (Desf.) Benth., *M. fruticosa* (L.) Druce, *M. myrtifolia* Boiss. and Hohen, *M. sinaica* Benth. and *M. danaensis* Danin. Three species were distributed within the Mediterranean region; *M. fruticosa*, *M. danaensis*, and *M. nervosa*. The *M. myrtifolia* was distributed within the Mediterranean and Irano _Turanian region. The fifth species, *M. sinaica*, was distributed within the Saharo _Arabian region _Desert plant (Fig. 1).

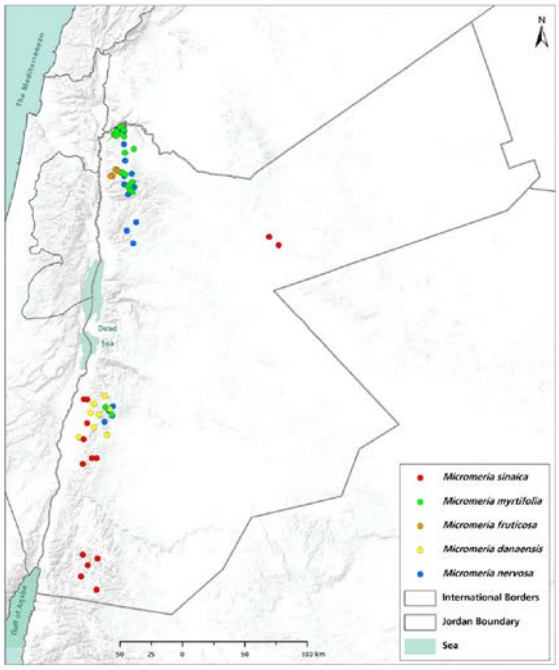

Figure 1. A Map of the Localities of the studied *Micromeria* specimens (Fresh and Herbarium specimens).

The morphological results of similarities and differences were summarized for each species in Table 2. The study species were described as follows:

3.1. Micromeria fruticosa

Description: Chamaephyte, 25_50 cm, divaricately branched, yellowish when dry (see Fig. 2- A&B). Stems erect, long _ paniculate, covered with densely puperulent hairs (see Fig. 3- E), glandular.

Leaves: Petiolate, entire, or crenate, 0.5 _ 2 cm x 0.5 _ 1 cm, ovate, obtuse to subacute, with thin margins, glandular and covered with short hairs (see Fig. 4- A&B). floral leaves lanceolate, shorter than calyx.

Verticillasters: Lax, many flowered (4_7), long pedunculate cymes (2_4 cm), without Pedicle, glandular and covered with short hairs (see Fig 5-A).

Calyx: Cupuliform, pedunculate, glandular, and covered with short hairs (tomentose), teeth short and equal (see Fig. 6-A).

Corolla: White, tube exserted, 2_labiate, hairy, lower lip somewhat longer than the upper.

Nutlet: Oblong (spheroidal), hairy and shiny (see Fig. 7-A).

Flowering time: February _ June.

Habitat: Mediterranean region and among rocks

Distribution: Irbid, Um Qais, Alsholah, Ajloun mountains.

Specimens examined.

Irbid, Alal,7 km North of Irbid towards the borders with Syria, waste places & uncultivated segments & roadsides; 10. May. 1983; D. Al-Eisawi. Irbid, Alsholah; 15. May. 1987; D. Al-Eisawi. Nablus; September. 1991; D. Al-Eisawi. Ajloun, Ishtafena, 25. April.1999; D. Al-Eisawi. Irbid, Judayta; 13. April. 2021; B. Ayasrah. Irbid, Judayta, along the road to Irbid; 24. April. 2021; B. Ayasrah. Ajloun, Alhashmeh; 29. April. 2021; B. Ayasrah.

3.2. M. danaensis

Description: Chamaephyte, 5_10 cm, many stemmed from base (see Fig. 2- I&J). Stems erect, short paniculate, covered with densely puberulent hairs (see Fig. 3-D), glandular.

Leaves: Sessile, entire, 0.2 _ 0.4 x 0.1 _ 0.2 cm, oblong to lanceolate, acuminate, with thick margins, somewhat revolute, glandular, and covered with short hairs (see Fig. 4- I&J). floral leaves linear, shorter than calyx, as long as Pedicle.

Verticillasters: Lax, few flowered (1_2) (-4), cymes short pedunculate (0.2 _ 0.4 cm), flowers pedicellate, half as long as calyx, glandular and covered with short hairs (see Fig. 5-E).

Calyx: Tubular, covered with short hairs, glandular, teeth erect, short and equal (see Fig. 6-E).

Corolla: Cream-colored, lilac spotted, tube exserted, 2_labiate, hairy.

Nutlet: Ovoid(elliptical), minutely puperulous on the upper surface (see Fig. 7-E).

Flowering time: March_ May.

Habitat: Mediterranean region; crevices of smooth_faced white sandstone outcrops.

Distribution: Dana Biosphere Reserve.

Specimens examined:

Dana reserve; 5. April. 1997; RSCN. Team. Dana reserve, Wadi Araba; 11. April. 1997; RSCN. Team. Dana reserve, Wadi Barra, 2Km SE of the visitor center; 14. May. 1996; RSCN. Team. Tafila, Dana Biosphere Reserve, Al-Barrah, East Southeastern side of the reserve; 5. April. 2021; B. Ayasrah. Tafila, Dana Biosphere Reserve, Khunaq Al-Arz, Middle North of the reserve, near Ain Lahtha; 6. April. 2021; B. Ayasrah.

3.3. M. nervosa

Description: Chamaephyte, 15_25 (-45) cm, many stemmed from base (see Fig. 2- C&D). Stems are mostly purplish, simple, or sparingly branched, covered with long hooked hairs (see Fig. 3-C), glandular.

Leaves: Petiolate, entire, 0.6 _ 0.9 x 0.4 _ 0.6 cm, ovate, acuminate, with thick margins, somewhat revolute, glandular, and covered with long hairs (see Fig. 4- E&F). Floral leaves linear, as long as verticillaster.

Verticillasters: Long hairy, many flowered (7_10), pedunculate (1cm), forming spike -like inflorescences, glandular, flowers Pedicellate (see Fig. 5-C).

Calyx: Tubular, longer than pedicle, glandular and covered with long hairs as long as or exceeding in length of the calyx_ tube, teeth not equal, lower teeth longer than upper as long as calyx (see Fig. 6-C).

Corolla: Purplish_ pink, tube sub-included, 2_labiate, hairy.

Nutlet: Oblong, smooth (see Fig 7-C).

Flowering time: March_ May.

Habitat: Mediterranean region and among rocks

Distribution: Ajloun mountains, Jarash, Amman, Salt, Dana and Petra.

Specimens examined:

Al-Aloak; 14. April. 1983; S. Abdulhadi. Ajloun, Qalaet elrabath; 17. May. 1972; D. Al-Eisawi. King Talal Dam; 14. April. 1983; R. H. Jayyosi. King Talal Dam, along the road to Jarash; 14. April. 1983; N. Al-Najjar. Wadi Um Rakham between Mersa Matruh and Agiba; 21. March. 1975; T. Hadidi. Salt, Sbahi; 12. April. 1984; S. Alkhateeb. Amman, Naour, 200 the main road; 22. April. 1993; H. Alkhatib & M. Abu- Hammour. Salt- Near Zai National Park; 12. April. 1984; W. Jabri. Salt, Sbahi; 22. April. 1993; Y. Al- Mograbe. Salt. Rabad Fortress, near Ajlun; 23. May. 1974; W. Jallad, L. Boulos & J. Lahham. Jarash, Way of Ras Dabboos, 15 km south of Jarash; 16. April. 1997; T. Rawashdeh. Jarash, Zarqa eiver, 500 m N. of the river, degraded deciduous oak forest; 29. April. 1999; D. Al-Eisawi & J. Zaidan. 12 Km north Irbid, 3 Km north Sal; 26. April. 1975; W. Jallad, L. boulos & J. lahham. 15 Km north of Suweilih, along the road of Jarash; 29. March. 1984; M. Alhabash. Jarash; 17. April. 1986; D. Al-Eisawi. Jordan vally, 2-3 Km E. of Abu Obaidah, along the road to Khirbit Alwahadneh; 28. March. 1996; D. Al-Eisawi, K. Arid & I. Aziz. Amman, 13 Km west of Amman, along the road from Naur to Ghor, near Children Wood; 9. March. 1978; D. Al-Eisawi. Al-Salt, Al- wasia; 28. April. 1999; M. Abu- Hammor. Jarash, King Talal Dam; 29. March. 1984; L. Boulos & S. Darras. Ajloun, Wahadneh, 12 Km at the crossing point with Halawa; 28. March. 1996; D. Al-Eisawi. Al- Salt, Subehi; 22. April. 1993; M. Kamel & S. Abu- Romman. Tafila, Dana Biosphere Reserve, Middle of the reserve; 4. April. 2016; S, Khatatbeh, B, Ayasrah, & M. Zoubi. Jarash, Dibeen Forest Reserve, 23. March. 2019; B. Ayasrah. Dibeen Forest Reserve, Wadi alsoan; 14. April. 2019; B. Ayasrah. Ajloun, Ajloun Forest Reserve, Building of the reserve; 8. April. 2018; S, Khatatbeh & B, Ayasrah. Irbid, Yarmouk Forest Reserve, Wadi Ain Arkeh; 22. March .2017; A. Sabbarenie, S. Khatatbeh, B. Ayasrah & S. Malkawy.

3.4. M. myrtifolia

Description: Chamaephyte, 15_40 cm, many stemmed from base (see Fig. 2- E&F). Stems erect or ascending, generally simple, covered with short, hooked hairs (see Fig. 3-A), glandular.

Leaves: Sessile, somewhat short petiolate, entire, 1 _ 1.5 x 0.5 _ 0.8 cm, elliptic, acute to acuminate, with thick margins, glandular and covered with short hairs (see Fig. 4- C&D). Basal leaves ovate, petiolate. Floral leaves linear, shorter than verticillaster. Verticillasters: Short hairy, many flowered (4_7), very dense, pedunculate (1 cm), sometimes part of the stems bearing few flowered sessile, Thyrse (compound dichasium arranged as raceme), glandular, flowers Pedicellate (see Fig. 5-D).

Calyx: Tubular, longer than pedicle, glandular and covered with short hairs, teeth not equal, upper teeth longer than lower (see Fig. 6-D).

Corolla: Purplish_ pink, densely hairy, tube sub-included, 2_labiate.

Nutlet: Ovoid or elliptical, smooth (see Fig. 7-D).

Flowering time: March_ August.

Habitat: Mediterranean region and Irano -Turanian region.

Distribution: Irbid, Ajloun, Jarash, Amman, Salt, Dana, Petra and shoubak

Specimens examined:

Amman, near Naour, Children Forest, along the road to Ghor; 8. May. 1981; A. Khlilieh & D. Al-Eisawi. Dibben National Park; 31. December.2003; M. Mahklouf & D. Al-Eisawi. 3-4 Km west Rum Rest House, 18 Km from the main road to Aqaba; 23. March. 1975; L. Boulos, W. Jalld, J. Lahham, M.A. Abu Hamaidan. Dana Reserve, Wadi Finan; 28. April. 1994; D. Al-Eisawi. Dibbin National Park; 14. December. 1973; L. Boulos & R. Hauke. Petra; 15. March. 1974; L. Boulos, D. Al-Eisawi & W. Jallad. Wadi Yutum, Upper stream, 15 Km north of Aqaba; 21. March. 1975; L. Boulos, W. Jallad, J. Lahham, & M.A.Abu Hmaidan. Irbid, Yarmouk Forest Reserve; 18. March. 2017; Sabbarenie, S. Khatatbeh, B. Ayasrah & S. Malkawy. Jarash, Dibeen Forest Reserve; 13. March. 2018; B. Ayasrah. Tafila, Dana Biosphere Reserve, East-South of the reserve, Wadi Dana; 7. May. 2016; S. Khatatbeh & B. Ayasrah. Jarash, Sakeb; 1. April. 2021: B. Ayasrah.

3.5. M. sinaica

Chamaephyte, 10_35 cm, many stemmed from base (see Fig. 2- G&H). Stems erect, virgate, simple or sparsely branched, covered with short, hooked hairs (see Fig. 3-B), glandular.

Leaves: Sessile, entire, .02_ 0.5 x 0.1_0.4 cm, ovate, obtuse, with thick margins, somewhat revolute, glandular, and covered with short hairs (see Fig. 4- G&H). Floral leaves lanceolate, as long as verticillaster.

Verticillasters: Lax, short hairy, many flowered (7_10), sessile, forming spike _ like inflorescences, glandular, flowers pedicellate (see Fig. 5-B).

Calyx: Tubular, as long as pedicel, glandular and covered with short hairs, teeth not equal, upper teeth longer than lower (see Fig. 6-B).

Corolla: Purplish_ pink, short hairy, tube exserted, 2_labiate.

Nutlet: Ovoid or elliptical, minutely puberulous on the upper surface and have two curves (see Fig. 7-B).

Flowering time: March_ May.

Habitat: Saharo _Arabian region _ —arid rocky desert habitat.

Distribution: Dana, Wadi Arabah, Rum and Petra

Specimens examined:

Four Km south Rum Rest House, along the road to Rum Police Station; 23. March. 1975; L. Boulos, W. Jalld, J. Lahham, M.A. Abu Hamaidan. Ishtafena to Deir Abu Said; 11. May. 1996; S. Khaleel & V. Slageren. Tafila, 23 Km S. of Tafila, Khonaq Al- Arz, 1 Km W. of Ain Lahtha; 1. May. 1997; D. Al-Eisawi. Tafila, S. end of Tafila, along the road to Shoubak; 11. April. 1979; D. Al-Eisawi. Wadi Dana, Wadi el Jaifeh; 27. April. 1999; RSCN. Team. Wadi Dana, Wadi Al Rommanah; 11. May. 1999; RSCN. Team. Wadi Dana, Wadi Al Rommanah; 4. May. 1999; RSCN. Team. Wadi Dana, Wadi Fatmeh; 26. April. 1994; RSCN. Team. Wadi Dana, Wadi Al Barrah; 16. May. 1994; RSCN. Team. Tafieleh, Dana Biosphere Reserve, East of the reserve, Al Barrah area, wadi Al Qaraya; 17. AUG. 2016; S. Khatatbeh & B. Ayasrah. Tafila, Dana Biosphere Reserve, Wadi Feynan, Southern side of the reserve; 16.

May. 2016; S. Khatatbeh & B. Ayasrah. Tafila, Dana Biosphere Reserve, East of the reserve, Rumannah camp, Daghla area; 26. April. 2016; S. Khatatbeh, M. Zoubi & B. Ayasrah.

Table 2. Morphological characters examined for the five sampled species of *Micromeria* from Jordan.

Taxon		*M. myrtifolia*	*M. sinaica*	*M. nervosa*	*M. fruticosa*	*M. danaensis*
Morphological characters						
Height (cm)		15_40 cm	10_35 cm	15_25 cm	25_50 cm	5_10 cm
Stems	Type of Hairs	Short hooked hairs	Short hooked hairs	long hooked hairs	puperulent hairs	puperulent hairs
	Indumentums	yellow gland	yellow gland	yellow gland	yellow gland	yellow gland
	Color	Green	Green	Red_Green	Green and yellow when dry	Green
Verticillasters	Type	Thyrse (compound dichasium arranged as raceme)	Spike like	Spike like	Cymes long pedunculate	
	Number of flowers	Many flowered (4_7) very dense	many more than 7 flowered,	many more than 7 flowered	Many flowered (4_7)	few flowered (1_2) (_4)
	Peduncle	Pedunculate (1 cm), sometimes part of the stems bearing dense flowered sessile	Sessile (0)	Pedunculate (1 cm)	Pedunculate (2_4 cm)	Pedunculate (1 cm)
	Pedicle	short (2mm)	short (2mm)	short 4 mm	0	short (2mm)
	Indumentums Hairs	short hairs	short hairs	Long hair	short hairs	short hairs
	gland	Glandular	Glandular	Glandular	glandular	glandular
Calyx	Shape	Tubular	Tubular	Tubular	Cupuliform	tubular
	Teeth	Not equal (upper teeth longer than lower)	Not equal (upper teeth longer than lower)	Not equal (lower teeth longer than upper as long as calyx)	Short and equal	Short and equal
	Indumentums	glandular and covered with short hairs	glandular and covered with short hairs	glandular and covered with long hairs	glandular and covered with short hairs	Glandular and covered with puberulent hairs
	Long	longer than pedicle	as long as pedicel	longer than pedicle	Long	longer than pedicle
Corolla	Type	Tube, 2_labiate, subincluded	Tube, 2_labiate, exserted	Tube, 2_labiate, subincluded	Tube, 2_labiate, exserted	Tube, 2_labiate, exserted
	Color	Pink	Pink	purplish- pink	White	cream-coloured
	Indumentums	Hairy	Hairy	Hairy	Hairy	Hairy
Leaves	Shape	Elliptic	Ovoid	Ovate	Ovate	oblong to lanceolate
	Long	1 cm	0.2 _ 0.5 cm	0.6 _ 0.9 cm	0.5 _ 2 cm	0.2 _ 0.4 cm
	Width	0.5 cm	0.1 _ 0.4 cm	0.4 _ 0.6 cm	0.5 _ 1 cm	0.1 _ 0.2 cm
	Apex	acute to acuminate	Obtuse	Acuminate	obtuse to subacute	acuminate
	Margin	Entire	Entire	Entire	entire sometimes crenate	entire
	Petiole	Sessile	Sessile	Petiolate	Petiolate	sessile
	marginal vein	Thick	Thick	Thick	Thin	thick
	Indumentums	Glandular and Short hairs	Glandular and Short hairs	Glandular and long hair	Glandular and short hair	Glandular and short hair
Nutlet	Shape	ovoid(elliptical)	Ovoid (elliptical)	Oblong	Oblong (spheroidal)	Ovoid (elliptical)
	Surface Texture	Smooth	minutely puberulous on the upper surface and have tow curves	Smooth	hairy and shiny	minutely puberulous on the upper surface

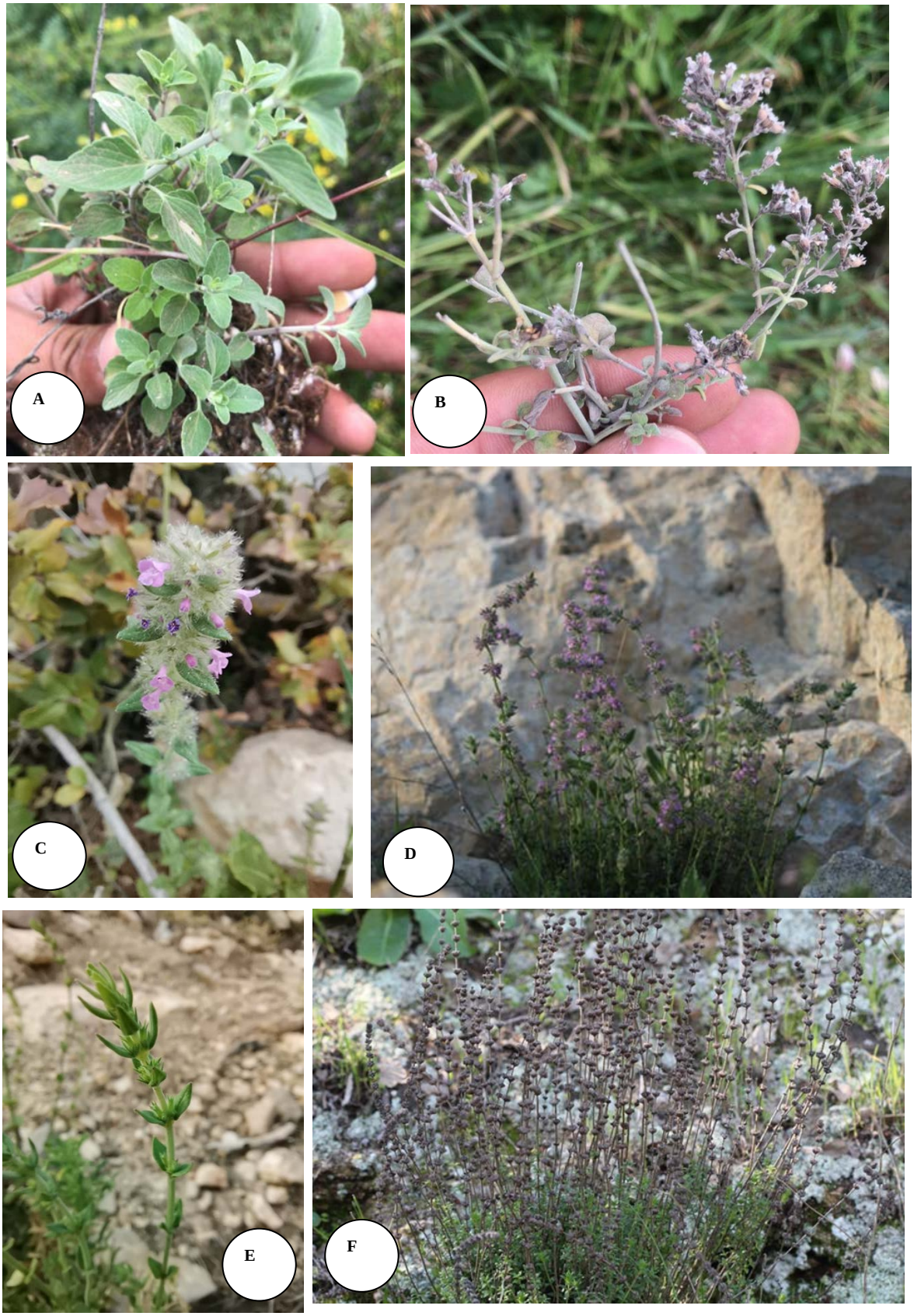

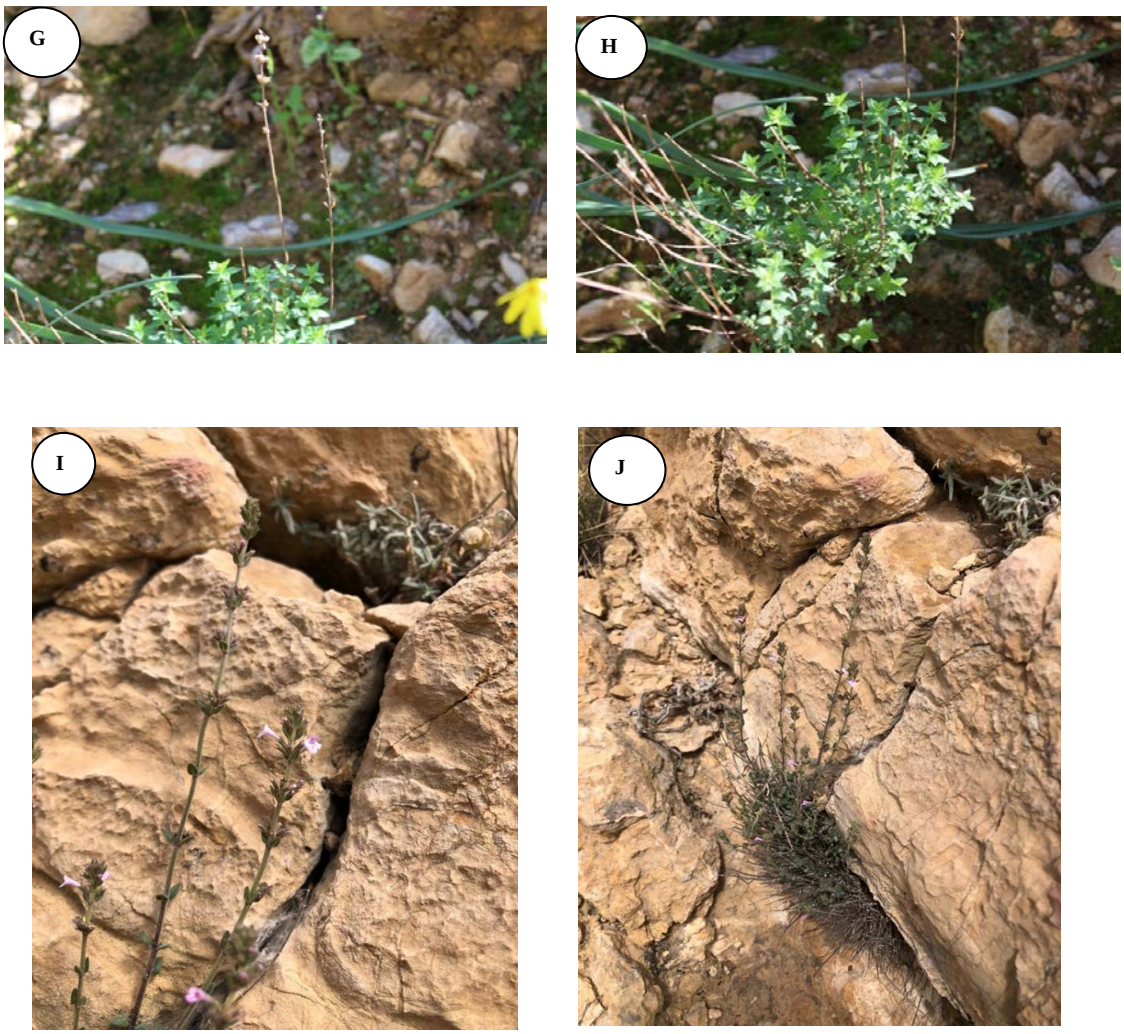

Figure 2: Wild accessions of *Micromeria* species in their natural habitats in Jordan. A&B. *M. fruticosa*, C&D. *M. nervosa*, E&F. *M. myrtifolia*, G&H. *M. sinaica*, and I&J. *M. danaensis*.

Figure 3. Types of the hairs on the stems for the five *Micromeria* species. *A. M. myrtifolia*; stem covered with short, hooked hairs (40x); *B. M. sinaica*; stem covered with short, hooked hairs (40x). *C, M. nervosa*; stem covered with long, hooked hairs (40x); *D. M. danainses*; stem covered with puberulent hairs (40x). *E. M. fruticose*; stem covered with puberulent hairs (40x).

Figure 4. Upper and lower leaves of the five *Micromeria* species. A. the upper leaves of *M. fruticosa* (20x), B. the lower leaves of *M. fruticosa* (20x), C. the upper leaves of *M. myrtifolia* (20x), D. the lower leaves of *M. myrtifolia* (20x), E. the upper leaves of *M. nervosa* (20x), F. the lower leaves of *M. nervosa* (20x), G. the upper leaves of *M. sinaica* (40x), H. the lower leaves of *M. sinaica* (40x), I. the upper leaves of *M. danaensis* (40x), and J. the lower leaves of *M. danaensis* (40x).

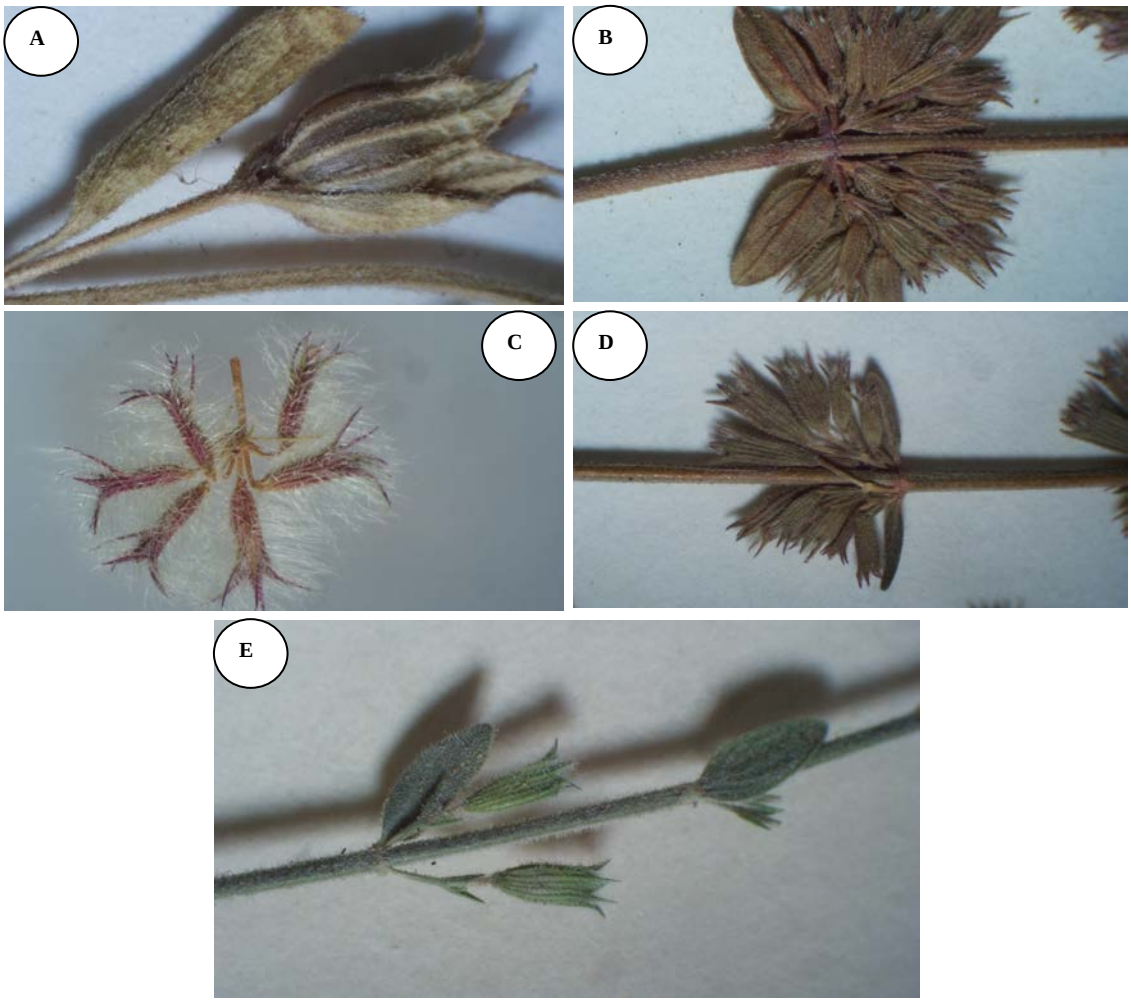

Figure 5. Verticillasters for the five *Micromeria* species under compound microscope (20x). A. *M. fruticosa*, B. *M. sinaica*, C. *M. nervosa*, D. *M. myrtifolia*, and E. *M. danaensis.*

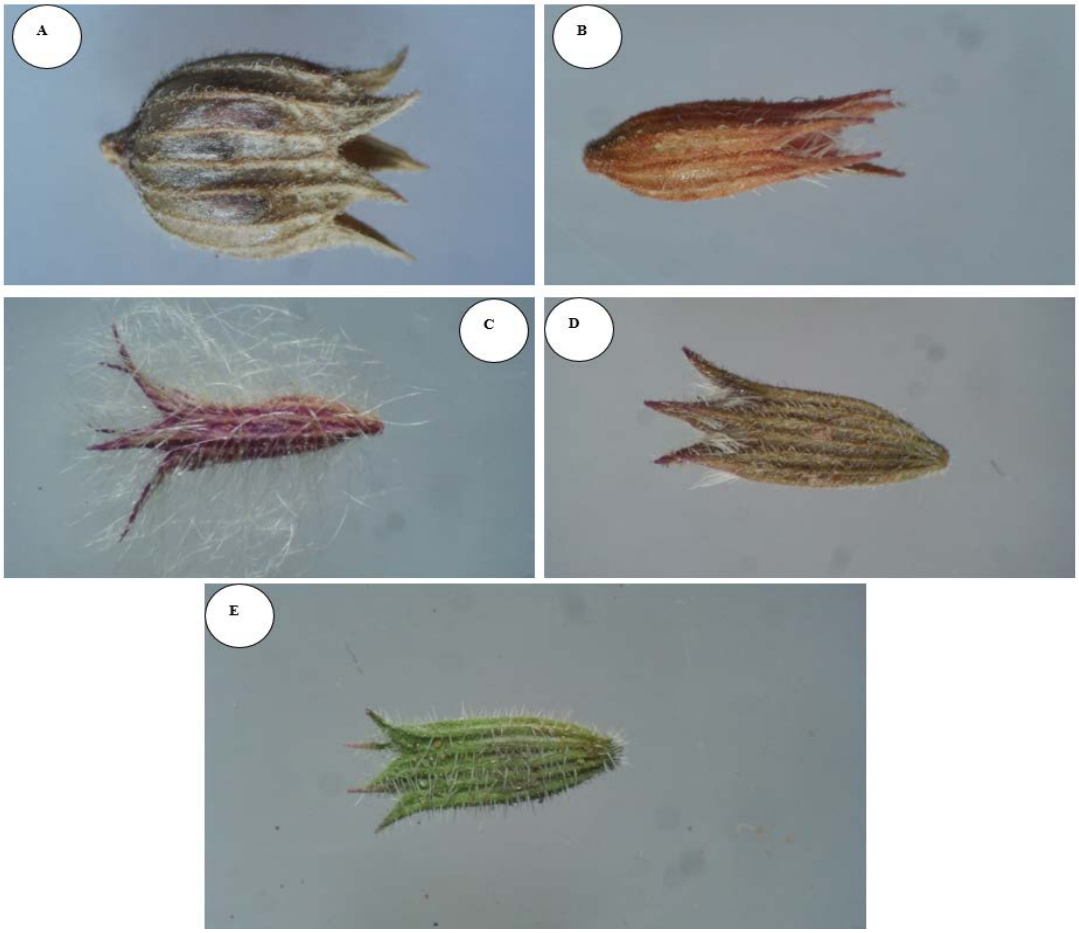

Figure 6. Calyx for the five *Micromeria* species under compound microscope (40X). A. *M. fruticosa*, B. *M. sinaica*, C. *M. nervosa*, D. *M. myrtifolia*, and E. *M. danaensis*.

Figure 7. Nutlets for the five *Micromeria* species under compound microscope (40X); A. *M. fruticosa*, B. *M. sinaica*, C. *M. nervosa*, D. *M. myrtifolia*, and E. *M. danaensis*.

The sixth species of *Micromeria*, which is *M. graceca* was not found in any field trip, and no voucher specimen of this species was found in the herbarium of the Biological Sciences Department, School of Science, at the University of Jordan, and in the herbarium of the Royal Society for the Conservation of Nature (RSCN).

A new key for the species of *Micromeria* in Jordan was constructed to illustrate the variations among closely related species, as following:

1. 1. Corolla white to cream- colored; stem covered with puberulent hairs……...2
2. _ Corolla purplish to pink; stem covered with hooked hairs……...……...3
3. 2. Verticillasters many flowered (4_7); cymes long pedunculate (2_4 cm). calyx; cupuliform.; leaves; ovate, petiolate……*M. fruticosa*
4. _ Verticillasters few flowered (1_2) (-4); cymes short pedunculate less than 1 cm; calyx; tubular; leaves; oblong to lanceolate, sessile……*M. danaensis*
5. 3. Hairs of calyx very long, as long as or exceeding in length of the calyx- tube; calyx teeth as long as calyx.……*M. nervosa*
6. 3- Hairs of calyx shorter than above; calyx teeth less than half as long as calyx tube
7. 4. Verticillasters very dense; Pedunculate (1 cm), part of the stems bearing dense flowered sessile. Calyx longer than pedicle…… *M. myrtifolia*

4. Verticillasters sparse; nearly sessile. Calyx as long as pedicle.……...…*M. sinaica*

4. Discussion

The genus *Micromeria* has been extensively studied taxonomically, with varying perspectives on its classification. Bentham (1829) first described *Micromeria* as a distinct genus, and later (Bentham 1848), he considered it a single distinct genus. However, Killick (1961) considered *Micromeria* as part of *Satureja* complex. Some taxonomists have divided this complex into several genera, *Satureja* L., *Clinopodium* L., *Calamintha* Mill., *Acinos* Mill. and *Micromeria* Benth. (Bentham 1848, Boissier 1879, Ball, *et al*. 1972, Davis 1982, Doroszenko 1986). While other taxonomists consolidated the group to a single genus *Clinopodium* (Kuntze 1891) or *Satureja* s.l. (Briquet 1896, and Brenan 1955, Greuter 1986). More recently, taxonomists have considered *Micromeria* as a distinct genus (Doroszenko 1986, Morales Valverde 1993,), while Harley *et al*. (2004) suggested four sections (*Micromeria*, *Pineolentia*, *Cymularia*, and *Pseudomelissa*) for *Satureja* complex.

This study focused on the morphological features of five *Micromeria* species in Jordan and have provided systematic evidence for distinguishing between these species. As a result of the morphometric variations observed, five species of *Micromeria* in Jordan are identified: *M. nervosa* (Desf.) Benth., *M. fruticosa* (L.) Druce, *M. myrtifolia* Boiss. & Hohen, *M. sinaica* Benth. and *M. danaensis* Danin. Key morphological features, such as differences in leaf shape, stem indumentum, floral structure, and nutlet texture, were instrumental in differentiating these species.

Boulos (2002) in his book “Flora of Egypt” reported and described five species of the genus *Micromeria*; *M. serbaliana, M. sinaica, M. imbricata, M. nervosa* and *M. mertifolia*. Three of these species; *M. sinaica, M. nervosa* and *M. mertifolia* were recorded in Jordan. Additionally, Chaudhry (2001) reported two species in his book Flora of the kingdom of Saudi Arabia: *M. abyssinica* and *M. imbericata*, and none of them recorded in Jordan. Although Al-Eisawi mentioned the presence of *M. graceca* in his 2013 publication (Al-Eisawi, 2013), this species was not found in any of the field trips, or herbariums. Referring to Al-Eisawi (pers. Comm.), his expectation of the presence of this species was based on the records from neighboring regions, such as Egypt and Palestine, in habitats that are similar to Jordan. However, there is still no evidence of the presence of this species in Jordan.

The findings of this study contribute to the broader understanding of *Micromeria* taxonomy in Jordan and neighboring regions. The observed morphological traits align with earlier taxonomic classifications in the region but also highlight areas requiring further investigation. For instance, the absence of *M. graceca* raises questions about its actual range. Future research, incorporating genetic analyses and additional sampling in underexplored areas, could provide deeper insights into the taxonomic relationships and potential undiscovered species within the genus.

5. Conclusion

This study provides a detailed morphometric character of five *Micromeria* species in Jordan: *M. nervosa, M. fruticosa, M. myrtifolia, M. sinaica, and M. danaensis*. Key morphological features, such as leaf shape, stem indumentum, floral structure, and nutlet texture, were critical in differentiating these species. The study confirmed the absence of *M. graceca* in Jordan, despite its prior mention in neighboring regions. The findings underscore the importance of morphometric features in species identification and contribute to distinguish the taxonomic framework for *Micromeria* in the region.

The results have significant implications for the conservation of *Micromeria* species in Jordan. By providing clear diagnostic features for species identification, the study helps in monitoring and conserving these species, which are vital to the region's biodiversity. Given the potential for undiscovered *Micromeria* species in Jordan, as seen in neighboring areas such as *M. imbricata* in northern Saudi Arabia (Chaudhry, 2001; Ryding, 2007), *M. serbaliana* in Sinai (Boulos, 2002), and *Micromeria juliana* in Syria (Post & Dinsmore 1933), all in habitats similar to those found in Jordan. This observation opens the way for further research to explore and identify more *Micromeria* species that may potentially exist in Jordan.

Future research should also integrate molecular techniques alongside morphometric data to better resolve taxonomic ambiguities and phylogenetic relationships within the genus. Expanding sampling efforts to include other regions in the Mediterranean and Saharo-Arabian zones, where *Micromeria* species may overlap, could provide valuable insights into species distribution and evolutionary patterns. Additionally, investigating the ecological factors influencing species distribution will be essential for a comprehensive understanding of the genus and its conservation needs.

Acknowledgement

We express our gratitude to the Deanship of Scientific Research at the University of Jordan for their financial support. Additionally, we extend our thanks to the Royal Society for the Conservation of Nature (RSCN) and all the staff members. I would like to express my appreciation to Dr. Nashat A. Hamidan, who was consistently supportive throughout the entire project and provided valuable recommendations. Many thanks to Qamar Al Mimi for assisting us in preparing the map.

Conflict of Interest

The authors declare that they have no conflicts of interest to disclose.

Reference

Al-Eisawi, D. 1996. **Vegetation of Jordan**: UNESCO, Regional Office for Science and Technology for the Arab States.

Al-Eisawi, D. M. 1998. **Field guide to wildflowers of Jordan and neighbouring countries**.

Al-Eisawi, D. M. H. 2013. **Flora of Jordan Checklist, Revised.** ***Book Flora of Jordan Checklist****, Revised (Editor ed.^ eds.). City: The University of Jordan Press, Amman, Jordan*.

Ball, P. W., Getliffe, F. M., Tutin, T. G., Heywood, V. H., Burges, N. A., Moore, D. M., ... & Webb, D. A. 1972. Satureja, Acinos, Clinopodium, Calamintha. **Flora Europaea**, 3: 163-167.

Bentham, G. 1834. ***Scutellaria*** **and** ***Perilomia*** **in** ***Labiatarum*** **Genera and Species** 416-446. *London: Ridgeway*.

BOISSIER, P. 1879. **Flora Orientalis. Genève**, Basel, Lyon: Georg, 4: 150–162.

Boulos, L. 2002. **Flora of Egypt (*Verbinaceae*-Compositae)**. Al-Hadara Publishing, Cairo, Egypt, 373. 3: 14-16.

Brenan, J.P., 1955. Notes on Mimosoideae: I. *Kew Bulletin*, *10*(2), pp.161-192

Briquet, J. 1896. **Stachydoideae-melissinae**. Die Natürlichen Pflanzenfamilien, 4, 292-306.

Chaudhary, S. A. 2001. **Flora of the Kingdom of Saudi Arabia (vascular plants)**. *National Agriculture and Water Research Center, National Herbarium, Ministry of Agriculture and Water, Riyadh*.

Feinbrun-Dotan, N. 1978. **Flora Palestina**. Israel Academy of Sciences and Humanities, Jerusalem, Israel, 3: 148-150.

Greuter, W., Burdet, H.M. and Long, G., 1986. **Med-Checklist 4 Conservatoire et Jardin botaniques de la Ville de Genève. Genéve**, 3, pp.366-380.

Davis, P. H., Mill, R. R., & Tan, K. 1988. **Flora of Turkey and the East Aegean Islands**; Edinburgh Univ. Pres: Edinburgh, UK, 7: 335-345.

Doroszenko, A.M., 1986. **Taxonomic studies on the *Satureja* complex (Labiatae)**. KB thesis scanning project 2015.

Duminil, J. and Di Michele, M., 2009. Plant species delimitation: a comparison of morphological and molecular markers. *Plant Biosyst*, *143*(3), pp.528-542.

Harley, R.M., Atkins, S., Budantsev, A.L., Cantino, P.D., Conn, B.J., Grayer, R., Harley, M.M., De Kok, R.D., Krestovskaja, T.D., Morales, R. and Paton, A.J., 2004. **Labiatae. In Flowering plants**· Dicotyledons: Lamiales (except Acanthaceae including Avicenniaceae) (pp. 167-275). Berlin, Heidelberg: Springer Berlin Heidelberg.

KBA, Key Biodiversity Areas factsheet 2017: Dana (8198), Jordan Middle East. (online) Available at: https://www.keybiodiversityareas.org/site/factsheet/8198

Kew, R. B. G., 2021. Plants of the World Online. [Online] Available at: https://powo.science.kew.org/ [Accessed December 2021].

Killick, D.J.B., 1961. South African species of Satureia. *Bothalia*, *7*(3), pp.435-437

Morales Valverde R. (1992) Synopsis of the Genus *Micromeria*. Lamiales Newsletter, 1: 20.

Oran, S. A., Yousef, I., & Jaffal, S. M. 2022. Evaluation of the antiproliferative effect of selected plant extracts on colon and skin cancer cell lines. *J. Appl. Pharm. Sci.*, **12(11)**, 091-096.

Post, G.E. and Dinsmore, J.E., 1933. ***Origanum*** **L.** ***Flora of Syria, Palestine and Sinai***, *2*, pp.332-335

Ryding, O. 2007. Revision of the *Micromeria* (Labiatae) in tropical to southern Africa and on the Arabian Peninsula. *Bo. J. Linn. Soc*., **155(3)**, 427-446.

Stuessy, T. F. 2009. **Plant taxonomy: the systematic evaluation of comparative data**. Columbia University Press.

JJBS

Volume 18, Number 2,June 2025
ISSN 1995-6673
Pages 357 – 365
https://doi.org/10.54319/jjbs/180216

Jordan Journal of Biological Sciences

Exploring The Potential of *Momordica charantia L*. as a Natural Therapeutic Agent for Osteoarthritis: In-Silico Analysis of ADAMTS-5 and Binding Potential Assessment

Olabode Oluwadare Akintoye[1,2]; Ayodeji Johnson Ajibare[1,*]; Blessing Tolulope Owolabi[3] Olayinka Alfred Taylor [4] ; Kehinde Samuel Olaniyi[2]

[1]*Physiology Department, College of Medicine, Lead City University, Ibadan, Oyo State, Nigeria;* [2]*Cardio/Endo-metabolic and Epigenetic Research Unit, Department of Physiology, College of Medicine and Health Sciences, Afe Babalola University, Ado-Ekiti, 360101, Nigeria.;* [3]*University Hospital Coventry and Warwickshire NHS Trust, United Kingdom ;* [4]*Physiology Department, Ekiti State University College of Medicine, Ado Ekiti, Nigeria.*

Received: June 7, 2024; Revised: December 18, 2024; Accepted: December 30, 2024

Abstract

Osteoarthritis (OA) is a prevalent global health issue, with its incidence increasing steadily due to aging populations and unhealthy lifestyles. This study explored the potential of *Momordica charantia L*, a plant known for its potent antioxidant, anti-inflammatory, and anti-degenerative properties, as a therapeutic agent for osteoarthritis. An *in-silico* analysis was conducted to investigate the phylogeny, antigenicity, and structural insights of a Disintegrin and Metalloproteinase with ThromboSpondin motifs 5 (ADAMTS-5), a key enzyme involved in OA progression and the binding potential of *Momordica charantia L* on ADAMTS-5. Techniques in structural bioinformatics and theoretical chemistry were used to discover novel inhibitors of ADAMTS-5 by utilizing molecular docking and molecular mechanics generalized Born surface area (MM-GBSA). This novel technique facilitated the discovery of new molecules that hold potential as inhibitors of ADAMTS-5, thereby providing an alternative avenue for osteoarthritis treatment. Given the pressing need for safe and effective OA treatments, this study offers a promising therapeutic approach and highlights the importance of further research.

Keyword: Osteoarthritis; Aggrecan; ADAMTS-5; Molecular docking; ADMETox; Disease-modifying Osteoarthritis Drugs (DMOADs)

1. Introduction

Osteoarthritis (OA) is a disabling, progressive, and painful joint disease that ranks prominently among global public health priorities (Chow & Chin, 2020). It is one of the most common diseases that affect millions of people globally, with older people above fifty years being the most affected (Pegreffi *et al.,* 2023). OA is defined as wearing joint cartilage and subchondral bone, causing intense pain, stiffness, and reduced motion and flexibility, significantly affecting daily functioning and quality of life (Grässel *et al.,* 2021). The global rates of OA have been rising steadily due to increased lifespans and a higher prevalence of risky dieting and non-physical activities (Scheuing *et al.,* 2023). Despite negatively impacting millions worldwide, OA is a burden due to treatment costs and lost productivity (Fang & Zhao, 2021; Liu *et al.,* 2024). The pathogenesis of OA involves several biological processes related to the disease that may occur in parallel or sequentially. Since aggrecan is an important cartilage structural protein, degraded aggrecan is likely to impact the stability of joints. Other alterations in the properties of aggrecan are important in understanding OA through the accelerated breakdown of the cartilage matrix (Peng *et al.,* 2021).

One more enzyme, identified as ADAMTS-5 (A disintegrin-like and metalloproteinase with thrombospondin motifs-5), participates in the aggrecan breakdown within the cartilage. This enzyme is recognized as the most potent aggrecanase affecting human cartilage. Notably, ADAMTS-5 is primarily linked with the deterioration of the N-terminal IGD segment of aggrecan, as documented by Santamaria and de Groot in 2020, also Kemberi *et al* in 2023. This cleavage produces aggrecan residuals, which are more susceptible to other proteases, and this enhances the release of aggrecan and the weakening of the extracellular matrix, ultimately contributing to the development of OA (Yamamoto *et al.,* 2021; Li *et al.,* 2022). The breakdown of aggrecan and other extracellular matrix (ECM) proteins has a notable effect on the chondrocyte signaling cascade and various metabolic processes within cartilage. This process alters the production of ECM proteins and diminishes the creation of anabolic signals typically responsible for maintaining healthy cartilage, as evidenced by (Chery *et al.,*2020; Peng *et al.,* 2021). The degradation of aggrecan and other ECM proteins can lead to changes in the signaling cascade of chondrocytes and metabolic

* Corresponding author. e-mail: ajibare.ayodeji@lcu.edu.ng .

processes, ultimately affecting the maintenance and repair of cartilage. This has implications for cartilage's overall health and function, particularly in conditions such as osteoarthritis (Peng *et al.,* 2021). These changes also affect the mechanical properties of cartilage and weaken them, thereby making them more vulnerable to mechanical stress and other related factors that contribute to cartilage degeneration. It has been shown that aggrecan degradation is one of the key factors in the pathogenesis of OA, which directly affects joint tissue remodeling and breakdown of the extracellular matrix and contributes to increased production of inflammatory cytokines in chondrocytes of osteoarthritic joints (Liu *et al.,* 2022).

The approach targeting ADAMTS-5 is a potential solution for formulating a new class of DMOADs (Oo *et al.*,2021; Kim *et al.,* 2022; Lin *et al.,* 2023). Currently, no approved DMOADs are available in the market, but few inhibitors specifically targeting ADAMTS-5 have given promising outcomes, reducing aggrecan breakdown and delaying OA progression in different animal models (Brebion *et al.,* 2021; Latourte & Richette, 2022). Hence, the attempt at targeting ADAMTS-5 presents a potential way to treat OA; the design of effective ADAMTS-5 inhibitors appears as a major advancement toward forming DMOADs for this painful disease.

Bitter gourd is a monoecious plant called '*Momordica charantia L*' and falls under the family Cucurbitaceae, which has proven to have enormous nutritive and medicinal importance (Waqas Mazhar *et al.,* 2024). Previous works have also demonstrated that *Momordica charantia L* possesses strong antioxidant activity, anti-inflammatory ability, anticancer propensity, and anti-degenerative effect, suggesting it might be used to cure OA (Shal *et al.,* 2018). Experimental research has also shown promising results on different models of why the compound could slow cartilage degeneration and reduce the inflammation seen in OA.

Momordica charantia contains a diverse array of active ingredients, including alkaloids, flavonoids, terpenoids, and phenolic compounds, which have been identified as potential therapeutic agents (de Oliveira *et al.,* 2018; Gayathry & John, 2022). These compounds exhibit anti-inflammatory and antioxidant properties, suggesting that their mechanisms of action involve the modulation of signaling pathways related to oxidative stress and inflammation. Given the increasing prevalence of OA and its substantial economic burden, identifying novel therapeutic avenues for safe and effective treatments is paramount (Cai *et al.,* 2021).

This study contributes a novel dimension to the existing knowledge of OA biology by providing a comparative analysis of ADAMTS-5. Through in-silico analysis, the phylogeny, antigenicity, and structural insights of ADAMTS-5 were explored, offering valuable insights into the molecular characterization of this enzyme. Furthermore, the binding potential of *Momordica charantia L* on ADAMTS-5 was investigated using a computational approach. This investigation explores the potential of natural products, such as *Momordica charantia L*, in inhibiting ADAMTS-5 activity and reducing inflammation, offering a valuable avenue for treating OA.

2. Materials and Methods

2.1. Computational Investigation

The computational investigation used the Schrödinger Suite software (Maestro 12.8) (https://www.schrodinger.com).

2.2. Target Preparation

The three-dimensional crystal structure of ADAMTS-5 complexed with the inhibitor GLPG1972 (PDB ID: 6YJM) was selected from the RCSB Protein Data Bank. This structure has a resolution below 2.3Å, an R-value free of 0.256, an R-value Work of 0.212, and an R-value observed of 0.215 (https://www.rcsb.org). Maestro's Schrödinger Suite's Protein Preparation Wizard tool (https://www.schrodinger.com) was employed to import and prepare the protein structure (Ruswanto *et al.,* 2024). The preparation process encompassed several steps: assigning bond orders, adding hydrogens, creating zero-order metal bonds, generating disulfide bonds, removing water molecules, and generating het states using Epik at pH levels ranging from 7.0 to 9.0. PROPKA pH 7.0 (https://propka.readthedocs.io) was utilized to refine the protein by optimizing hydrogen bond assignments. After removing water molecules located further than 3.0 Å from het groups, restrained minimization was done using the OPLS4 force field to minimize the protein. The Ramachandran Plot was generated and saved to validate the protein structure.

2.3. Ligand Preparation

118 compounds associated with *Momordica charantia L* were gathered from the PubChem database. To predict their inhibitory potential, these compounds underwent molecular docking with the active site of ADAMTS-5. The structures of these compounds, obtained in SDF format, were imported into the LigPrep tool in the Maestro Schrödinger panel. The OPLS4 force field (https://www.schrodinger.com/platform/products/opls4) was employed to perform energy minimization, ensuring the generation of a maximum of one stereoisomer per ligand.

2.4. Active Site Prediction

The active site of the ADAMTS-5 protein (PDB ID: 6YJM) was predicted for ligand binding using the Receptor Grid Generation tool. This tool created a three-dimensional cubic grid box around the binding site, encompassing all the amino acid residues in the active site region (Ruswanto *et al.,* 2024). The grid was generated by selecting the co-crystallized ligand present at the active site of ADAMTS-5. The calculated three-dimensional coordinates of the generated grid were 77.81 Å, 26.87 Å, and -29.61 Å. Predicting the active site of a protein is a crucial step in structure-based drug design and virtual screening. Grid-based methods are commonly used to represent the binding site and efficiently sample the conformational space of potential ligands. The grid allows for rapid evaluation of different ligand poses and facilitates the identification of favorable interactions between the ligand and receptor (Tung *et al.,* 2023).

2.5. Molecular Docking

Molecular docking was performed using the ligand docking tool in Maestro version 12.8. The process began

with High-Throughput Virtual Screening (HTVS), which rapidly identified potential ligands by treating both the ligand and target as rigid entities. This was followed by Super Precision (SP) docking, which employed increased sampling precision to refine ligand binding evaluation. Extra Precision (XP) docking was conducted with a rigid body, utilizing a more refined scoring function and exhaustive conformational exploration. Finally, XP docking with Flexible Docking was performed to simulate better realistic ligand-target interactions and account for potential conformational changes in target proteins. The binding free energy of all the docked complexes was determined using MM-GBSA, a tool compatible with Prime in Schrödinger Maestro 12. 8. This was done through thermodynamics calculations within the program to establish the extent of interaction between the molecules (Srinivasa *et al*., 2024).

2.6. Drug-likeness, Pharmacokinetic, and Toxicity Prediction

The investigated ligands ' pharmacokinetic aspects and possible toxicity were analyzed using the SwissADME and Pro-Tox II online tools to determine the drug-likeness. This assessment entailed the general evaluation of the ADMET properties, which are significant measures that indicate the nature of a compound and its functionality within the human body. ADMET comprises parameters such as Absorption, Distribution, Metabolism, Excretion, and toxicity that define any compound's suitability for the likely use of a drug (Diningrat *et al.*, 2023). Besides the ADMET evaluation, other significant molecular descriptors such as the molecular weight (MW), the number of HBA (hydrogen bond acceptors), the number of HBD (hydrogen bond donors), and the TPSA (topological polar surface area) were calculated for the considered compounds. These descriptors were measured based on the Lipinski rule of 5.

2.7. Quantitative Structure-Activity Relationship (QSAR) Model.

Data concerning the activity of ADAMTS-5 inhibitors was sourced from the CHEMBL database. To initiate the process of QSAR and search for antagonists, the protein's FASTA sequence extracted from the PDB under the accession code 6YJM (https://www.rcsb.org/structure/6YJM), was employed to query the CHEMBL database (https://www.ebi.ac.uk/chembl/). The list of inhibitors was transformed into an ".SDF" format through the use of DataWarrior software, after which the ligands were prepared and used for QSAR creation with the AutoQSAR module. Among the generated models, the best model was determined based on ranking, leading to the selection of the KPLS_MOLPRINT2D_7 model. This model was utilized to predict the bioactivity of the top compounds highlighted in the research.

3. Results and Discussion

Osteoarthritis is among the most prevalent forms of arthritis, characterizing joint pain in millions of people worldwide and the elderly population. It is now prevalent all over the globe due to aspects like population ageing and others, including obesity and a sedentary lifestyle (Hawker, 2019; Allen *et al.*, 2022). Aggrecan degradation contributes to the emergence of discomfort, rigidity, and limited movement, resulting in disability and reduced economic productivity globally. Aggrecan plays a pivotal role as a primary proteoglycan in cartilage tissue, vital for maintaining joint integrity. The involvement of ADAMTS-5 in aggrecan degradation is associated with the progression of OA. Therefore, discovering compounds capable of inhibiting ADAMTS-5 represents a potential approach to managing OA (Hawker, 2019).

Table 1. Docking and MMGBSA scores of the lead compounds from *Momordica charantia L* docked against ADAMTS-5 active site.

COMPOUND NAME	DOCKING SCORE (Kcal/mol)	MM/GBSA (ΔGbind)
Isoquercitrin	-11.659	-51.54
Chlorogenic acid	-11.648	-53.77
Quercitrin	-11.172	-68.96
Epicatechin	-10.443	-54.61
Catechin	-10.349	-54.24
Naringenin-7-O-glucoside	-10.188	-59.78
Luteolin-7-O-glucoside	-9.863	-57.61

In this study, a computational method was used to look for possible lead compounds from MC that can antagonise the activity of the ADAMTS-5 enzyme. Schrodinger Maestro 12. 8 was used to perform molecular docking on 118 compounds against the binding pocket of ADAMTS-5 enzyme (PDB ID: 6YJM). Firstly, the compounds were sorted according to the docking score and then further evaluated according to their MMGBSA score and ADMETox features. These findings indicated that the selected hit compounds were well positioned into the active site of the ADAMTS-5.

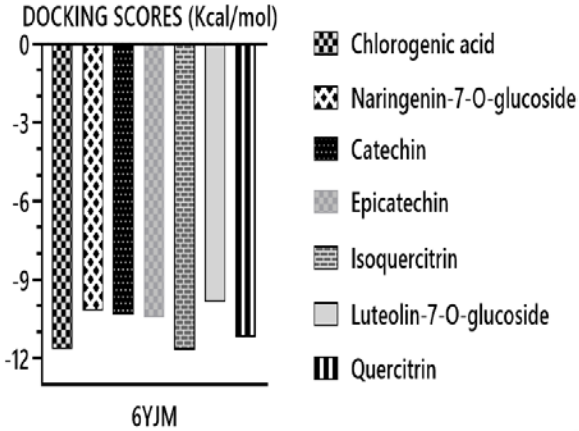

Figure 1: Chart showing the docking scores of the lead compounds from *Momordica charantia L* docked against ADAMTS-5 active site.

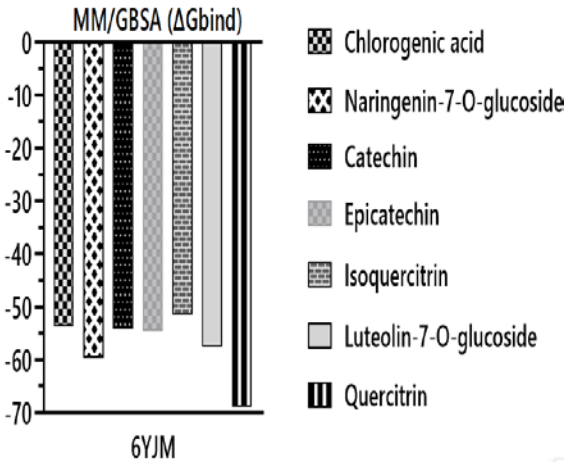

Figure 2: Chart showing the MMGBSA scores of the lead compounds from *Momordica charantia L* docked against ADAMTS-5 active site.

From Isoquercitrin to Luteolin-7-O-glucoside, the compounds displayed a pronounced binding affinity with the ADAMTS-5 active site, with negative binding energies indicating a high level of affinity. The lead compounds listed in Table 1 exhibited primary amino acid interactions with crucial hydrophobic amino acid residues such as PHE 406, ILE 442, LEU 443, LEU 379, and MET 381(Figure 3), which are essential for ADAMTS-5's binding site and catalytic activity. These docked molecules also form hydrogen bonds with GLH 411, GLY 380, LEU 379, and THR 378 within the ADAMTS-5 binding pocket, thereby effectively saturating its active region. The best bioactive molecule Isoquercitrin, which has a maximum binding energy of -11.659Kcal/mol, forms a hydrogen bond with the residues GLH 411, GLY 380, LEU 379, THR 378 and ASP 377 and interact with the hydrophobic amino residues PHE 406, LEU 438, ILE 442, LEU 443, ILE 446, LEU 379 and MET 381(Figure 3; Table 2).

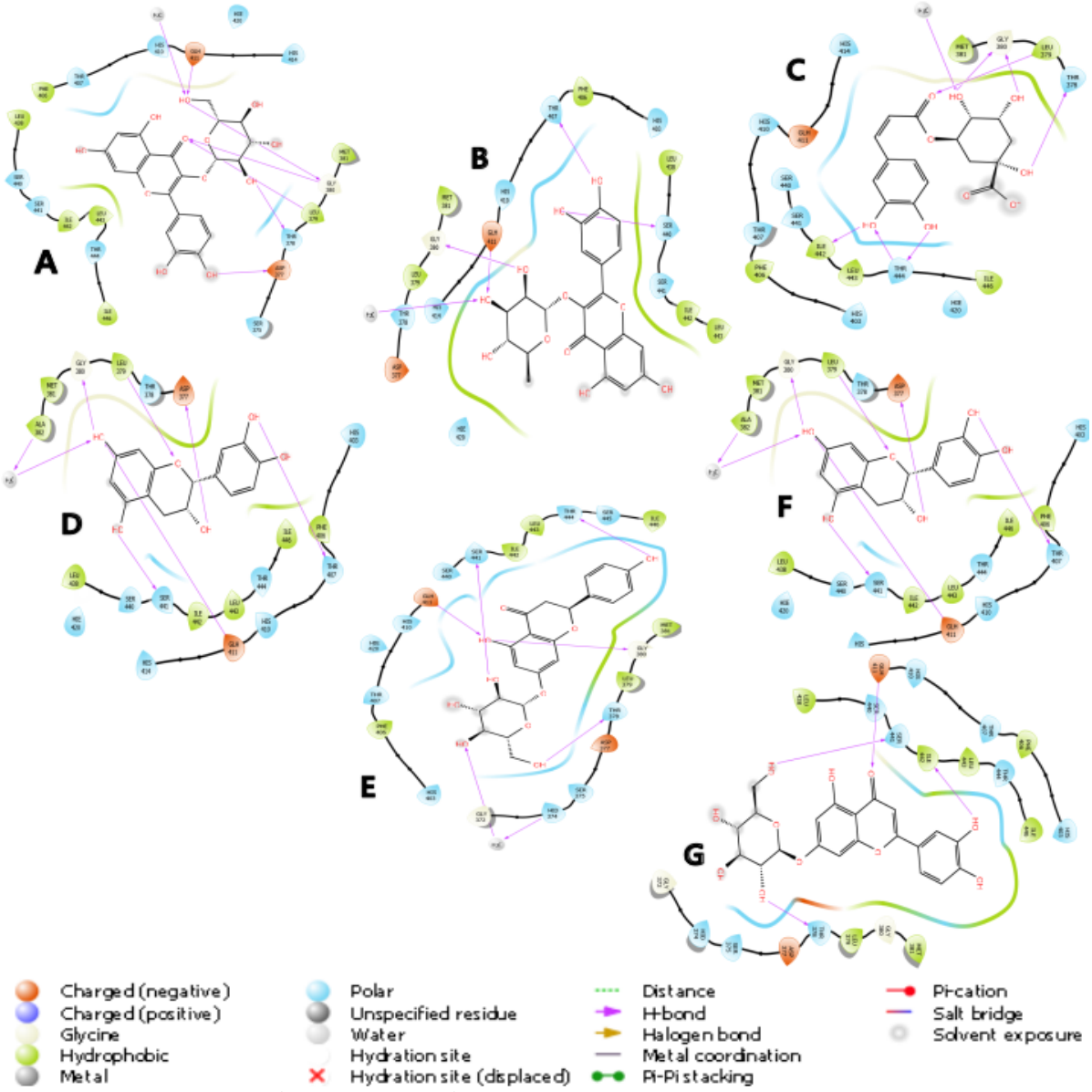

Figure 3: 2D-molecular interaction of the lead compounds from *Momordica charantia L* docked against ADAMTS-5 active site: **(A)** Isoquercitrin **(B)** Quercitrin **(C)** Chlorogenic acid **(D)** Epicatechin **(E)** Naringenin-7-O-glucoside **(F)** Catechin **(G)** Luteolin-7-O-glucoside

With binding energies of -11.648Kcal/mol, Chlorogenic acid is thought to form hydrogen bonds with the aliphatic amino acids GLY 380, LEU 379, THR 378, ILE 442 and THR 444 and interact with the key amino acids MET 381, LEU 379, PHE 406, ILE 442, LEU 443 and ILE 446. Quercitrin completely occupied the ADAMTS-5 binding site, displaying a binding energy of -11.172Kcal/mol while interacting with the hydrophobic amino acids MET 381, LEU 379, LEU 443, ILE 442, LEU 438, and PHE 406, alongside amino acid residues GLY 380, GLH 411, SER 440, and THR 407 via hydrogen bonds.

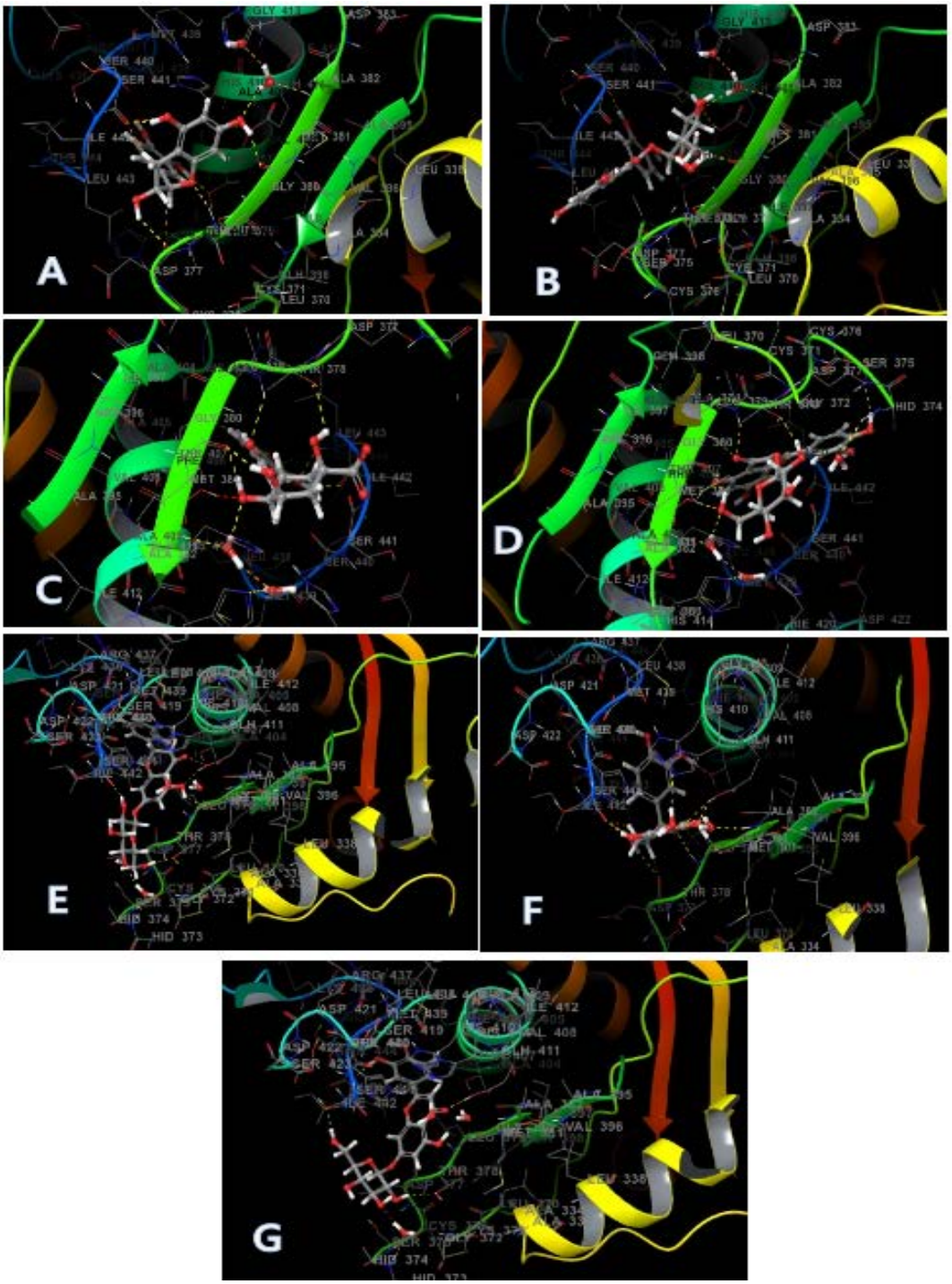

Figure 4: 3D-molecular interaction of the lead compounds from *Momordica charantia L* docked against ADAMTS-5 active site: **(A)** Isoquercitrin **(B)** Quercitrin **(C)** Chlorogenic acid **(D)** Epicatechin **(E)** Naringenin-7-O-glucoside **(F)** Catechin **(G)** Luteolin-7-O-glucoside

While establishing a hydrogen bonding connection with the amino acid GLY 380, LEU 379, ASP 377, GLH 411 and THR 407, Epicatechin and Catechin had binding energies of -10.443Kcal/mol and -10.349Kcal/mol respectively, with both interacting with the hydrophobic amino acids ALA 382, MET 381, LEU 379, PHE 406, ILE 446, LEU 443, ILE 442 and LEU 438 residues. Naringenin-7-O-glucoside, with binding eniergies of -10.188Kcal/mol interacts with key residues ILE 446, LEU 443, ILE 442, PHE 406, MET 381and LEU 379 through

amino acid interactions, while also forming hydrogen bonds with THR 444, SER 441, GLY 380, THR 378 and HID 374 residues. Luteolin-7-O-glucoside, having binding energies of -9.863Kcal/mol, forms hydrogen bonds with the residues ILE 442, SER 441, GLH 411 and THR 378 and interacts with the hydrophobic amino residues as Isoquercitrin (PHE 406, LEU 438, ILE 442, LEU 443, ILE 446, LEU 379 and MET 381). These findings indicate that these compounds have strong potential to bind the ADAMTS-5 enzyme in the treatment of various arthritis, particularly osteoarthritis.

Table 2: Hydrogen Bonds and Hydrophobic interactions of the lead compounds from *Momordica charantia L* docked against ADAMTS-5 active site

COMPOUNDS	H-BOND	Hydrophobic interacting amino acids	Other Interactions
Isoquercitrin	GLH 411, GLY 380, LEU 379, THR 378, ASP 377	PHE 406, LEU 438, ILE 442, LEU 443, ILE 446, LEU 379, MET 381	None
Chlorogenic acid	GLY 380, LEU 379, THR 378, ILE 442, THR 444	MET 381, LEU 379, PHE 406, ILE 442, LEU 443, ILE 446	None
Quercitrin	GLY 380, GLH 411, SER 440, THR 407	MET 381, LEU 379, LEU 443, ILE 442, LEU 438, PHE 406	None
Epicatechin	GLY 380, LEU 379, ASP 377, GLH 411, THR 407	ALA 382, MET 381, LEU 379, LEU 438, ILE 442, LEU 443, ILE 446, PHE 406	None
Catechin	GLY 380, LEU 379, ASP 377, THR 407, GLH 411, SER 441	ALA 382, MET 381, LEU 379, PHE 406, ILE 446, LEU 443, ILE 442, LEU 438	None
Naringenin-7-O-glucoside	THR 444, SER 441, GLY 380, THR 378, HID 374	ILE 446, LEU 443, ILE 442, PHE 406, MET 381, LEU 379	None
Luteolin-7-O-glucoside	ILE 442, SER 441, GLH 411, THR 378	ILE 446, PHE 406, LEU 443, ILE 442, LEU 438, MET 381, LEU 379	None

The binding affinities of ADAMTS-5 lead compounds were further evaluated using the MMGBSA and Schrodinger program. This method involves calculating the free energy change of binding for the ligands in their binding pose. Isoquercitrin, Chlorogenic acid, Quercitrin, Epicatechin, Catechin, Naringenin-7-O-glucoside and Luteolin-7-O-glucoside had binding free energies of -51.54ΔGbind, -53.77ΔGbind, -68.96ΔGbind, -54.61ΔGbind, -54.24ΔGbind, -59.78ΔGbind and -57.61ΔGbind respectively (Table 1; Figure 2).

Table 3: Pharmacokinetics profile of lead compounds of *Momordica charantia L* docked against ADAMTS-5 active site

MODEL	QPlogHERG	QPlogBB	QplogKhsa
Isoquercitrin	-5.085	-3.468	-0.885
Chlorogenic acid	-3.298	-3.328	-0.917
Quercitrin	-5.22	-3.29	-0.661
Epicatechin	-4.41	-1.88	-0.442
Catechin	-4.302	-1.853	-0.441
Naringenin-7-O-glucoside	-5.786	-3.239	-0.719
Luteolin-7-O-glucoside	-5.819	-3.952	-0.808

QPlogHERG: IC50 value for blockage Human Ether-a-go-go-Related Gene (hERG) K+ channels (below − 5)

QPlogBB: Brain/blood partition coefficient (− 3.0 to 1.2)

QplogKhsa: Binding to human serum albumin (− 1.5 to + 1.5)

It is imperative to comprehend the pharmacokinetics of phytochemicals for their use as new agents for drug administration (Rai *et al.*, 2023; Rathaur and SR, 2019). To predict the pharmacokinetic properties of the lead compounds, the QikProp activity available in the Maestro software was used. This included the determination of compounds' affinity to human serum albumin (QPlogkhsa), the blood-brain barrier penetration (QPPlogBB), and finally the 50% inhibitory concentration concerning Human Ether-a-go-go-Related Gene (hERG) K+ channels (QPlogHERG). As shown in Table 3, all designed lead compounds targeting the ADAMTS-5 enzyme are within the QPlogKHSA range of 0-0.5, suggesting their promising drug candidacy. This range of values signals that the compounds may have favourable pharmacokinetic characteristics; longer circulation within the body, improved distribution in the tissues, and slower clearance rates which could benefit their therapeutic outcomes. As demonstrated in Table 3, none of the HERG values recorded for all the compounds selected for the study were above 10µM, proving that these are good compounds to work with for drug discovery and development from the perspective of cardiac safety. Indeed, this discovery is very important to note because substances with low degrees of HERG inhibition can help to prioritize promising drug candidates with better cardiovascular characteristics. As seen earlier, all the lead compounds were found to possess reasonable log bb/p values that fall in between the expected range.

Table 4: In-silico drug likeness prediction of the lead compounds from *Momordica charantia L* docked against ADAMTS-5 active site

COMPOUNDS	MW	HBA	HBD	TPSA	ILOGP	LOGKP	ROV
Isoquercitrin	464.40	12	8	210.51	0.94	-8.88	2
Chlorogenic acid	354.31	9	6	164.75	0.87	-8.76	1
Quercitrin	448.38	11	7	190.28	1.60	-8.42	2
Epicatechin	290.27	5	5	110.38	1.47	-4.594	0
Catechin	290.27	6	5	110.38	1.33	-7.82	0
Naringenin-7-O-glucoside	434.39	10	6	166.14	2.35	-8.49	1
Luteolin-7-O-glucoside	448.38	11	7	190.28	1.76	-8.00	2

Table 5: The bio-availability and pharmacokinetic properties (ADMETox) of the lead compounds from *Momordica charantia L* docked against ADAMTS-5 active site

Models	Isoquercitrin	Chlorogenic acid	Quercitrin	Epicatechin	Catechin	Naringenin-7-O-glucoside	Luteolin-7-O-glucoside
BBB	Does not cross	Does not cross	Does not cross	Does not cross	Does not cross	Does not cross	Does not cross
GI absorption	Low	Low	Low	High	High	Low	Low
CYP2C9 Inhibitor	No	No	No	No	No	No	No
CYP2C19 Inhibitor	No	No	No	No	No	No	No
CYP1A2 Inhibitor	No	No	No	No	No	No	No
CYP3A4 Inhibitor	No	No	No	No	No	No	No
CYP2D6 Inhibitor	No	No	No	No	No	No	No
P-gp Substrate	Yes	No	No	Yes	Yes	Yes	Yes
Carcinogenicity	No	No	Yes	No	No	No	No
Hepatotoxicity	No	No	No	No	No	No	No
Mutagenicity	No	No	No	No	No	No	No
Cytotoxicity	No	No	No	No	No	No	No

The drug discovery and development process requires a thorough evaluation of the suitability of potential compounds (Adelusi *et al.*, 2022). One well-established method for assessing this suitability is the Lipinski rule of five (RO5), which takes into account various factors including molecular weight, lipophilicity, hydrogen bond donors, and the number of rotatable bonds (Daoud *et al.*, 2023). As per the Lipinski Rule of Five, a drug is deemed to exhibit favourable oral bioavailability if its molecular weight is under 500, its log P value is less than 5, it possesses fewer than 5 hydrogen bond donors, and has fewer than 10 hydrogen bond acceptors (Chen *et al.*, 2020; Olugbogi *et al.*, 2024). This evaluation is instrumental in determining the potential of a molecule to be developed into an oral drug with minimal adverse effects.

The results of the drug-likeness property analysis are presented in Table 4. All investigated compounds conform to Lipinski's ROV computations. Table 5 shows the result obtained from the ADMETox software, suggesting that none of the ligand molecules selected can pass through the blood-brain barrier. According to the results, the bioavailability level of Epicatechin and Catechin possesses a positive alert of human intestinal absorption in the human body, and all the selected ligand molecules are potential inhibitors of the CYP1A2, CYP2C19, CYP2C9, CYP2D6, and CYP3A4 metabolic enzymes. It can be postulated that Chlorogenic acid and Quercitrin are not effluxed through P-glycoprotein and are therefore not substrates. Moreover, not all the chosen ligand molecules showed any signs of carcinogen, mutagen, hepatotoxic or cytotoxic nature apart from quercetin, which proved to be a carcinogen.

3.1. Auto-QSAR Model

The Quantitative Structure-Activity Relationship (QSAR) methodology is a computational and statistical modelling approach to predict biological activity (or physicochemical properties) of chemical compounds from their molecular structure. It calculates a quantitative correlation between molecular structural features and observed biologic or chemical activities. QSAR has become a popular method in drug discovery, toxicology and environmental chemistry to design new compounds with specific properties or predict a compound's activity for compounds that have not been tested (Samuel *et al.*, 2023).

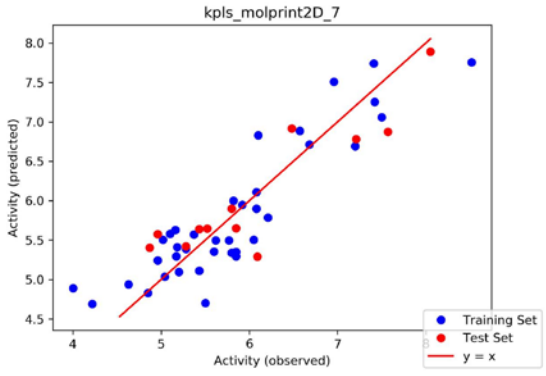

The developed QSAR model correctly clones the biological activities of the leading compounds and juxtaposes them to the standard ADAMTS-5 inhibition. The AutoQSAR module was used in constructing the QSAR model. The best model (KPLS_MOLPRINT2D_7)

for predicting the pIC50 values of the top compounds has an R-squared value of 0.8097, a Q-squared value of 0.8033 and the root mean square error (RMSE) stands at 0.4391, with a standard deviation (S.D) of 0.4200. Thus, our result is suggestive of the positive therapeutic potential of phytochemical compounds of *Momordica charantia L* on inhibition of ADAMTS-5 when compared to the standard ADAMTS-5 inhibitors.

3.2. LIMITATION

while this study provides a strong foundation for further investigation of *Momordica charantia L.* compounds as potential ADAMTS-5 inhibitors, it should be viewed as a starting point rather than a definitive assessment. The findings warrant experimental validation, cell-based studies, and eventually, animal models of osteoarthritis to elucidate these compounds' therapeutic potential fully.

4. Conclusion

The utilization of *Momordica charantia* leaf in this study has shown great potential as a potential drug for treating osteoarthritis. This plant possesses various beneficial properties, including strong antioxidant, anti-inflammatory, anticancer, and antidegenerative effects. These results have significant implications for the exploration of new therapeutic options for osteoarthritis treatment. Taken together, this study will inspire further research interest among scientists, leading to advancements in developing novel treatments for this debilitating condition.

5. Conflict of interests

The authors declare no conflict of interests.

Author Contribution

Akintoye Olabode Oluwadare, Ajibare Ayodeji Johnson and Olaniyi Kehinde Samuel conceptualised and designed the study.

Akintoye Olabode Oluwadare and Owolabi Blessing Tolulope provided the initial draft.

Akintoye Olabode Oluwadare, Ajibare Ayodeji Johnson, Owolabi Blessing conducted the whole experiment tasks and tests.

Akintoye Olabode Oluwadare, Taylor Olayinka Alfred, Ajibare Ayodeji Johnson, and Owolabi Blessing Tolulope contributed to data collection, formal analysis and statistical analysis.

All authors read and approved the final draft of the manuscript.

References

Adelusi, T. I., Oyedele, A. Q. K., Boyenle, I. D., Ogunlana, A. T., Adeyemi, R. O., Ukachi, C. D., ... & Abdul-Hammed, M. 2022. Molecular modeling in drug discovery. ***Informatics Med. Unlock.***, 29, 100880.

Allen, K. D., Thoma, L. M., & Golightly, Y. M. 2022. Epidemiology of osteoarthritis. ***Osteoarthr. Cartil.,*** 30(2), 184–195.

Brebion, F., Gosmini, R., Deprez, P., Varin, M., Peixoto, C., Alvey, L., ... & Amantini, D. 2021. Discovery of GLPG1972/S201086, a potent, selective, and orally bioavailable ADAMTS-5 inhibitor for the treatment of osteoarthritis. ***J. Med. Chem.,*** 64(6), 2937–2952.

Cai, X., Yuan, S., Zeng, Y., Wang, C., Yu, N., & Ding, C. 2021. New trends in pharmacological treatments for osteoarthritis. ***Front. Pharmacol.,*** 12, 645842.

Chen, X., Li, H., Tian, L., Li, Q., Luo, J., & Zhang, Y. 2020. Analysis of the physicochemical properties of acaricides based on Lipinski's rule of five. ***J. Comput. Biol.,*** 27(9), 1397–1406.

Chery, D. R., Han, B., Li, Q., Zhou, Y., Heo, S. J., Kwok, B., ... & Han, L. 2020. Early changes in cartilage pericellular matrix micromechanobiology portend the onset of post-traumatic osteoarthritis**.** ***Acta Biomater.,*** 111, 267–278.

Chow, Y. Y., & Chin, K. Y. 2020. The role of inflammation in the pathogenesis of osteoarthritis**.** ***Mediators Inflamm.,*** 2020.

Daoud, S., Alabed, S.J., Bardaweel, S.K. Mutasem O.T (2023). Discovery of potent maternal embryonic leucine zipper kinase (MELK) inhibitors of novel chemotypes using structure-based pharmacophores. ***Med. Chem. Res.,*** 32, 2574–2586.https://doi.org/10.1007/s00044-023-03160-5

de Oliveira, M. S., da Costa, W. A., Bezerra, F. W. F., AraÃºjo, M. E., Ferreira, G. C., & de Carvalho Junior, R. N. 2018. Phytochemical profile and biological activities of Momordica charantia L.(Cucurbitaceae): A review. ***Afr. J. Biotechnol.,*** 17(27), 829–846.

Diningrat, D. S., Sari, A. N., & Harahap, N. S. (2023). Potential of Bioactive Compounds from Jamblang (Syzygium Cumini) and Hanjeli (Coix lacryma-jobi L.) Essential Oils as SARS-COV-2 Antivirus Targeting NSP5 and ACE2 Receptors. ***Jordan J. Biol. Sci.,*** 16(4).

Fang, T., Zhou, X., Jin, M., Nie, J., & Li, X. 2021. Molecular mechanisms of mechanical load-induced osteoarthritis. ***Int. Orthop.,*** 45, 1125–1136.

Gayathry, K. S., & John, J. A. 2022. A comprehensive review on bitter gourd (Momordica charantia L.) as a gold mine of functional bioactive components for therapeutic foods. ***Food Prod. Process. Nutr.,*** 4(1), 1–14.

Grässel, S., Zaucke, F., & Madry, H. 2021. Osteoarthritis: novel molecular mechanisms increase our understanding of the disease pathology. ***J. Clin. Med.,*** 10(9), 1938..

Hawker, G. A. 2019. Osteoarthritis is a serious disease. ***Clin. Exp. Rheumatol.,*** 37(Suppl 120), 3–6.

Kemberi, M.; Salmasi, Y.; Santamaria, S. 2023. The Role of ADAMTS Proteoglycanases in Thoracic Aortic Disease. ***Int. J. Mol. Sci.,*** 24, 12135. https://doi.org/10.3390/ ijms241512135

Kim, H., Seo, J., Lee, Y., Park, K., Perry, T. A., Arden, N. K., & Choi, H. 2022. The current state of the osteoarthritis drug development pipeline: a comprehensive narrative review of the present challenges and future opportunities. ***Ther. Adv. Musculoskelet. Dis.,*** 14, 1759720X221085952..

Latourte, A., & Richette, P. 2022. Inhibition of ADAMTS-5: the right target for osteoarthritis?**.** ***Osteoarthr. Cartil.,*** 30(2), 175–177.

Li, T., Peng, J., Li, Q., Shu, Y., Zhu, P., & Hao, L. 2022. The mechanism and role of ADAMTS protein family in osteoarthritis. ***Biomolecules,*** 12(7), 959.

Lin, J., Jia, S., Zhang, W., Nian, M., Liu, P., Yang, L., ... & Zhang, X. 2023. Recent advances in small-molecule inhibitors for the treatment of osteoarthritis. ***J. Clin. Med***., 12(5), 1986.

Liu, S., Deng, Z., Chen, K., Jian, S., Zhou, F., Yang, Y.,& Zhu, W. 2022. Cartilage tissue engineering: From proinflammatory and anti-inflammatory cytokines to osteoarthritis treatments. ***Mol. Med. Rep***., 25(3), 1–15

Liu H, Wu X, Liu R, Wang W, Zhang D, Jiang Q, 2024. Cartilage-on-a-chip with magneto-mechanical transformation for osteoarthritis recruitment**,** ***Bioact. Mater***., 33, 61–68. ISSN 2452-199X,https://doi.org/10.1016/j.bioactmat.2023.10.030.

Muhammad Waqas Mazhar, Muhammad Ishtiaq, Mehwish Maqbool, Eman A. Mahmoud, Fazal Ullah & Hosam O. Elansary (2024) Optimizing bitter gourd (Momordica charantia L.) performance: exploring the impact of varied seed priming durations and zinc oxide nanoparticle concentrations on germination, growth, phytochemical attributes, and agronomic outcomes, ***Coqent Food Agric***., 10(1), 2313052.DOI: 10.1080/23311932.2024.2313052

Olugbogi, E. A., et al. (2024). Unlocking Neurodegeneration: Scaffold-Derived Blockers of MAO-B and AChE inspired by *Bryophyllum pinnatum*: A Structural Exploration**.** Preprint.

Oo, W. M., Little, C., Duong, V., & Hunter, D. J. (2021). The development of disease-modifying therapies for osteoarthritis (DMOADs): the evidence to date. ***Drug Des. Devel. Ther,*** 15, 2921–2945.

Peng, Z., et al. **(**2021). The regulation of cartilage extracellular matrix homeostasis in joint cartilage degeneration and regeneration. ***Biomaterials***, 268**,** 120555.

Pegreffi, F., et al. (2023). Prevalence of Sarcopenia in Knee Osteoarthritis: A Systematic Review and Meta-Analysis. ***J. Clin. Med.***, 12(4), 1532. https://doi.org/10.3390/jcm12041532

Rai, M., et al. (2023). Herbal concoction unveiled a computational analysis of phytochemicals' pharmacokinetic and toxicological profiles using novel approach methodologies (NAMs). **Curr. Res. Toxicol.**, 5, 100118.

Rathaur, P., & SR, K. J. (2019). Metabolism and pharmacokinetics of phytochemicals in the human body. ***Curr. Drug Metab.*** 20(14), 1085–1102.

Ruswanto, R., et al. (2024). Potential Active Compounds of Propolis as Breast Anticancer Candidates: In Silico Study. ***Jordan J. Biol. Sci.***, 17**(**1).

Belfield, S. J., et al. (2023). A review of quantitative structure-activity relationship modelling approaches to predict the toxicity of mixtures. ***Comput. Toxicol.***, 25, 100251. https://doi.org/10.1016/j.comtox.2022.100251

Santamaria, S., & de Groot, R. (2020). ADAMTS proteases in cardiovascular physiology and disease. ***Open Biol.***, 10(12), 200333.

Scheuing, W. J., et al. (2023). The burden of osteoarthritis: Is it a rising problem? ***Best Pract. Res. Clin. Rheumatol.*** 101836.

Shal, B., et al. (2018). Anti-neuroinflammatory potential of natural products in attenuation of Alzheimer's disease. ***Front. Pharmacol.***, 9**,** 548.

Shultz, M. D. (2018). Two decades under the influence of the rule of five and the changing properties of approved oral drugs: miniperspective. ***J. Med. Chem.***, 62(4), 1701–1714.

Srinivasa, M. G., et al. (2024). Novel Thiazolidinedione Linked 1,3,4-Oxadiazole Derivatives as AXL Inhibitors Targeting Breast Cancer: In-Silico Design, ADMET Screening, and MM-GBSA Binding Free Energy. ***Jordan J. Biol. Sci.***, 17(1).

Tung, K. C. C., et al. (2023). Molecular Simulations of *Moringa oleifera* Phytochemicals as Potential Antagonists of the Proinflammatory NF-κB p50 Transcription Factor. ***Jordan J. Biol. Sci.***, 16(3).

Yamamoto, K., et al. (2021). Targeting dysregulation of metalloproteinase activity in osteoarthritis. ***Calcif. Tissue Int.***, 109, 277–290.

JJBS

Volume 18, Number 2,June 2025
ISSN 1995-6673
Pages 367 – 381
https://doi.org/10.54319/jjbs/180217

Jordan Journal of Biological Sciences

Antimicrobial Potential of Biosurfactants from Microbial Sources: A Bibliometric Analysis

Achmad Rifky Alfian[1], Novita Yustinadiar[2], Abdul Rahman Siregar[2], FurzaniPa'ee[3], Ekachai Taowkrue[4], Neng Tanty Sofyana[5], Wahyu Aristyaning Putri[2,*]

[1]International Islamic School Amanatul Ummah, Mojokerto, Indonesia; [2]Department of Tropical Biology, Faculty of Biology, Universitas Gadjah Mada, Yogyakarta, Indonesia; [3]Advanced Herbal and Ethnomedical Research (AdHerb) Research Group, Faculty of Applied Sciences and Technology, Universiti Tun Hussein Onn Malaysia, Johor, Malaysia; [4]Research, Innovation and Partnerships Office, King Mongkut's University of Technology Thonburi, Bangkok, Thailand; [5]Marine Science Department, Faculty of Fishery and Marine Science, Universitas Padjadjaran, Bandung, Indonesia

Received: June 24, 2024; Revised: December 10, 2024; Accepted: December 30, 2024

Abstract

Background. Biosurfactants exhibit exceptional biological activities against pathogenic microorganisms, gaining significant attention for their potential in combating antimicrobial drug resistance. These molecules have been globally studied and widely published in reputable international journals. This study aims to provide a comprehensive bibliometric analysis of the global research profile, utilization, and advancements of biosurfactants as antimicrobial agents over the past three decades.

Methods. Publication data on biosurfactants as antimicrobial agents were obtained from the Scopus database (1991–2023) and analyzed bibliometrically through VOSviewer.

Results. A total of 908 publications, with an annual average of 28 articles, including notable contributions in *Frontiers in Microbiology*, with 43 documents are obtained in this study. Publication trends have shown consistent growth since 2000, peaking in 2022. India emerged as the most prolific contributor, followed by Ulster University as the leading institution and Banat, I.M. as the most productive author. Popular research themes include biosurfactants, antimicrobial activity, and anti-infective agents.

Conclusion. This research offers a brief overview of the utilization of biosurfactants as antimicrobial agents research at a worldwide level from 1991 through 2023. This analysis highlights research trends and provides a foundation for future studies in this field.

Keywords: Antimicrobial agent, Biosurfactant, Bibliometric, VOSviewer

1. Introduction

Antimicrobial resistance stands as one of the greatest challenges rapidly facing modern medicine and public health globally (Rzycki *et al*., 2024). The World Health Organization (WHO) has highlighted that antimicrobials, including antibiotic resistance, pose a major concern to the public health, with the potential to contribute ineffective drugs to treat bacteria to antibiotics due to prolonged and improper antimicrobial use (Rzycki *et al*., 2024; Antimicrobial Resistance Collaborators, 2022; Prastiyanto *et al*., 2024). To solve this urgent problem, researchers and other groups are actively coordinating action plans to develop novel antibiotics and antimicrobial agents. A thorough study and screening process are critical to precisely characterize compounds and define possible targets for tackling antimicrobial resistance and other human diseases.

Natural products (NPs), such as medicinal plants (Anand *et al*., 2019; Manan *et al*., 2022), fungi (Jakubczyk and Dussart, 2020), and endophytic plants have the ability to compete with other microorganisms and are abundant source of antimicrobial compounds. These compounds have unique features when compared to synthetic compounds in terms of structural complexity and enormous scaffold diversity (Atanasov e*t al*., 2021). The phenolic compound of *Ruta chalepensis* L. leaf extract has antimicrobial activity against bacteria, such as *Bacillus cereus, Pseudomonas aeruginosa, Staphylococcus aureus,* and fungi like *Candida albicans* (Al-Ghamdi *et al*., 2020). Plants and fungi-based pharmaceuticals have been used in the reduction of human disease for over 5000 years (Hu *et al*., 2019). The endophytic thermophilic fungus *Gymnascella thermotolerans*-GTE-21 on *Euphorbia geniculata* have antimicrobial activity against human pathogenic microbial *Staphylococcus epidermidis* and *Candida ciferrii* (El-Zayat *et al*., 2024). This highlights that natural products are a promising source of antimicrobials, particularly biosurfactants derived from bacteria, fungi, or plants (Figure 1) (Ceresa et al. 2021, Kumar et al. 2021, Sarubbo et al. 2022).

* Corresponding author. e-mail: wahyuaristyaningputri@ugm.ac.id.

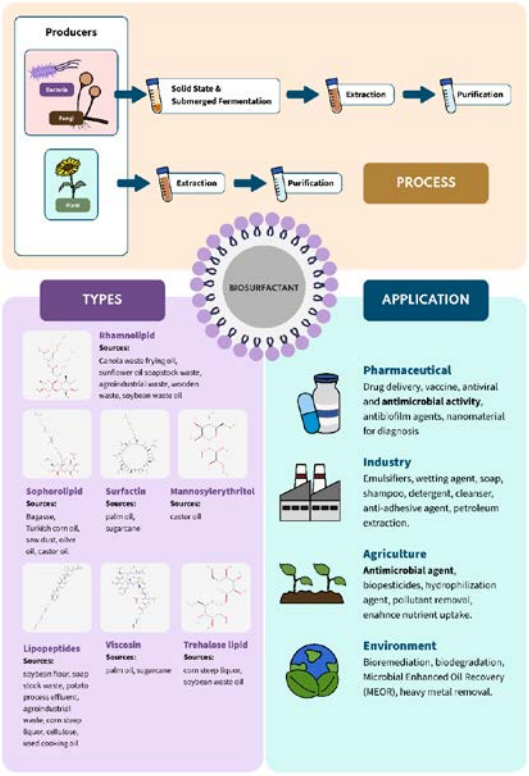

Figure 1. Production, Types, and Application of Biosurfactants.

Biosurfactants belong to surface-active compounds that consist of hydrophobic and hydrophilic moieties of biological origin to encourage the presence of interfaces with different polarities between fluids (Eras-Munoz *et al*., 2022). Biosurfactants possess several benefits compared with chemical surfactants, including being non-toxic, biodegradable, not accumulating in the environment, and stable under several environmental conditions (Alfian *et al*., 2022); thereby providing various future applications, including industrial sectors. These surface-active compounds possess promising biological features against pathogenic microbes in the host organisms, including anti-biofilm (Ali *et al*., 2022; Adnan *et al*., 2023; Kaur and Kaur, 2019), anti-adhesive (Mouafo *et al*., 2023; Firdose *et al*., 2023), and anti-microbial activities (Akgul *et al*., 2019; Adnan *et al*., 2023; Adu *et al*., 2022; AA *et al*., 2020).

Studies in biosurfactants used for treating pathogenic agents in plants and humans are increasing gradually. Low molecular weight groups, like glycolipids and lipopeptides, have been authorized for biological qualities based on their molecular. Glycolipids have been effective therapeutic agents in combating various diseases (Shu *et al*., 2021), including antiadhesive (Kadhum and Haydar, 2020), and antimicrobial properties, such as antifungal (Ayed *et al*., 2023), antibacterial (de Freitas *et al*., 2019; da Fontoura *et al*., 2020), and antiviral effects (Tsuji *et al*., 2023). Nevertheless, lipopeptides showed biocontrol agents against plant pathogens (Huang *et al*., 2022; Ghazala *et al*., 2022; Abdallah *et al*, 2018), antimicrobial impact in food (Ali *et al*., 2022), biofilm inhibition (Englerova *et al*., 2021; Ceresa *et al*., 2021), and antimicrobial (Chauhan *et al*., 2022). Biosurfactants like rhamnolipid produced by *Pseudomonas aeruginosa* ST5 and surfactin from *Bacillus amyloliquefaciens* ST34 have demonstrated efficacy against antibiotic-resistant *Escherichia coli* and *Staphylococcus aureus* (Ndlovu et al., 2017). Similarly, Sambanthamoorthy et al. (2014) reported that biosurfactants from *Lactobacillus jensenii* and *Lactobacillus rhamnosus* exhibit potent antimicrobial and anti-adhesive activities against multidrug-resistant (MDR) strains, including *Acinetobacter baumannii*, *Escherichia coli*, and methicillin-resistant *Staphylococcus aureus* (MRSA).

The aims of this study was to carry out a bibliometric analysis of the biosurfactants related-research, especially of antimicrobial activities. Bibliometric analysis has been widely used in several research worldwide, such as snake venom, Indonesian biodiversity through DNA barcoding, prevalence of chikungunya cases, prevalence of monkeypox cases, organoid in regenerative medicine also global trends in non-alcoholic fatty acid liver (Sofyantoro *et al*., 2022a; Priyono *et al*., 2023; Sofyantoro *et al*., 2023; Sofyantoro *et al*., 2022b; Setiawan *et al*., 2024; Putri *et al*., 2023). Regarding current bibliometric studies, there is only one that evaluates the output of renewable source production of biosurfactants quantitively and qualitatively (Nunes *et al*., 2022), and no bibliometric studies of biosurfactants as antimicrobial agents. Therefore, evaluation the worldwide research profile of literature on antimicrobial agents of biosurfactants is critical. In order to provide a comprehensive profile of biosurfactants as antimicrobial agents literature for the last three decades, this study mapped collaboration worldwide, evaluated the eminent institutions performance and authors, investigated the output of reputable journals, analyzed the highly cited articles, as well as highlighted arising research topics. The current study findings may present a visual summary of research advancements in this field and assess future research implications.

2. Materials and Methods

This study used data from the Scopus database, selected for its broad journal coverage, which supports both keyword searches and citation analysis. Scopus also indexes journals from other databases (Falagas *et al*., 2008). On February 20, 2024, a bibliometric filter was generated and run using the key terms (TITLE-ABS-KEY (biosurfactant) AND TITLE-ABS-KEY (antimicrobial) OR TITLE-ABS-KEY (antibiotic)) AND (EXCLUDE (PUBYEAR , 2024)) in the title and abstract parts to identify biosurfactants as antimicrobial-related publications from the Scopus database. Type of documents, including key terms, journal titles, publication year, countries, institutions, and citations, were extracted. The data were analyzed with VOSviewer to evaluate global profiles, international and author collaborations and to map prevalent keywords over the past three decades (McAllister *et al*., 2022).

3. Results

3.1. Publication profile of biosurfactant as antimicrobial-related research from 1991 to 2023

Between 1991 and 2023, 908 documents were published worldwide, generating in an average of 28 papers a year related to biosurfactants as anti-microbial

agents. Since the 2000s, there has been a steady growth in the amount of research on biosurfactants as antimicrobial agents; the highest number of publications was published in 2022 (112 documents). The highest number published were research articles (n = 679), reviews (n = 142), book chapters (n = 55), and conference papers (n = 14), respectively. English was written in many of the documents (n = 893), followed by Chinese (n = 4), and French (n = 3). Since 1991, the number of documents about biosurfactants as antimicrobial agent has been steadily rising, with the maximum productivity recorded in 2022 (n = 113) (Figure 2).

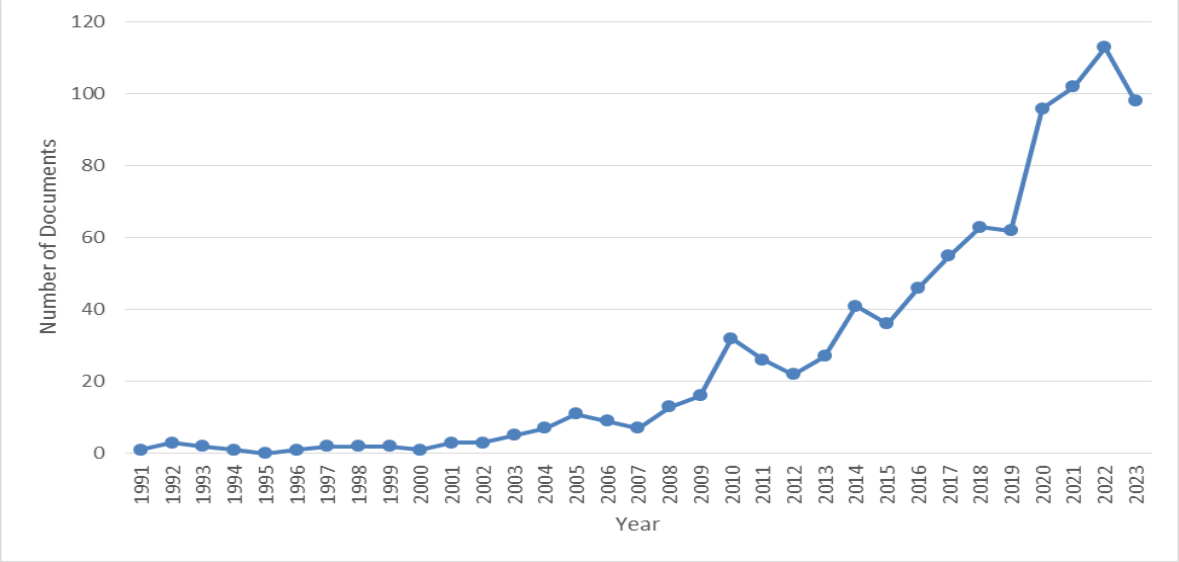

Figure 2. Publication profile of biosurfactant as antimicrobial-related research from 1991 to 2023. 908 documents were obtained from the Scopus database.

3.2. Collaboration and contribution countries of biosurfactant as antimicrobial-related research during the years 1991-2023

Between 1991-2023, 79 countries contributed to the literature on biosurfactants as antimicrobial agents. The publication shares of the top ten most prolific countries ranged from 26.9% for India to 3.1% for South Korea. Table 1 presents the top ten countries globally related to their relative contribution to the total number of publications. With 245 (26.9%) documents published, India was the top prolific country, followed by Brazil (n = 84, 9.2%), China (n = 72, 7.9%), the United States (n = 64, 7.0%), and the United Kingdom (n = 58, 6.3%) (Table 1). Figure 3a reveals the formation of nine distinct clusters visualized using VOSviewer, each represented by a different color: green (Italy, Canada, Belgium), purple (Brazil, Portugal), red (Germany, Poland, India), dark blue (France, Mexico, Nigeria), yellow (India, Saudi Arabia, Egypt), light blue (Thailand), and orange (Spain, Tunisia). Meanwhile, Figure 3b maps countries based on publication year, with a color gradient from purple to yellow indicating older to more recent publications. The earliest publication year is 2014, while the most recent one is 2020.

Table 1. Collaboration and contribution of the Top Ten Countries for Biosurfactant Research Publications on Antimicrobial Agents Worldwide.

SCR[a]	Country	Number of Documents (%)
1	India	245 (26.9%)
2	Brazil	84 (9.2%)
3	China	72 (7.9%)
4	United States	64 (7.0%)
5	United Kingdom	58 (6.3%)
6	Spain	43 (4.7%)
7	France	34 (3.7%)
8	Germany	31 (3.3%)
9	Italy	30 (3.2%)
10	South Korea	29 (3.1%)

[a]SCR: standard competition ranking.

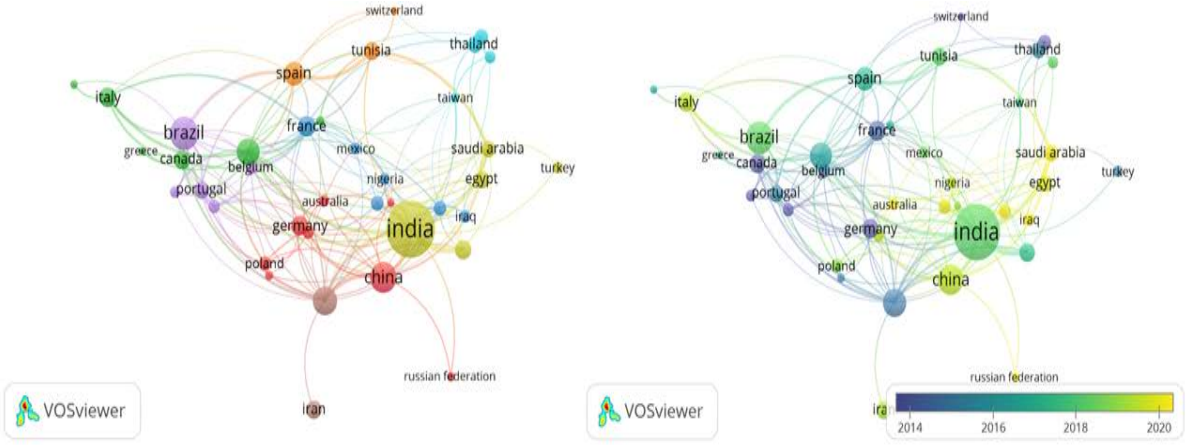

(a) **(b)**

Figure 3. Mapping the collaboration among countries: The number of collaborations with other countries is reflected in the size of the circle. Visualizations in (a) network and (b) overlay. The size of the circles corresponds to the frequency of appearances. The degree of relationship is indicated by the length of the links. The different colors reveal distinct clusters. The color gradient, from purple to yellow, indicates the timeline from older to more recent publications

3.3. The highest journals of biosurfactant as antimicrobial-related research during the years 1991-2023

Table 2 displays the top fourteen journals with the most documents globally, with 195 (21.47%) documents. Frontiers in Microbiology (n = 43), Colloids and Surfaces B Biointerfaces (n = 15), and Applied Microbiology and Biotechnology (n = 15) were the most published journals on the study of biosurfactants as antimicrobial agents.

.

Table 2. The highest journals in the field of biosurfactant research related to antimicrobials.

SCR	Journal	No. of Documents	SJR	H-index
1	“Frontiers in Microbiology”	43 (4.73%)	1.19	233
2	“Applied Microbiology and Biotechnology”	15 (1.65%)	0.968	267
3	“Colloids and Surfaces B Biointerfaces”	15 (1.65%)	0.868	198
4	“Bioresource Technology”	13 (1.43%)	2.473	364
5	“International Journal of Molecular Sciences”	13 (1.43%)	1.154	269
6	“World Journal of Microbiology and Biotechnology”	12 (1.32%)	0.726	115
7	“Applied Biochemistry and Biotechnology”	12 (1.32%)	0.514	135
8	“Pharmaceutics”	11 (1.21%)	0.795	106
9	“Antibiotics”	11 (1.21%)	0.792	77
10	“Scientific Reports”	10 (1.10%)	0.973	315
11	“Process Biochemistry”	10 (1.10%)	0.676	182
12	“Journal of Applied Microbiology”	10 (1.10%)	0.774	185
13	“Current Microbiology”	10 (1.10%)	0.526	108
14	“Biocatalysis And Agricultural Biotechnology”	10 (1.10%)	0.655	70

SCR: standard competition ranking.

3.4. The highest cited article of biosurfactant as antimicrobial-related research during the years 1991-2023

The article titled “Natural functions of lipopeptides from *Bacillus* and *Pseudomonas*: More than surfactants and antibiotics” was the most cited article on biosurfactants as antimicrobial-related research in FEMS Microbiology Reviews (Table 3). The second-highest cited article “Biosurfactant: Potential applications in medicine” published in Journal of Antimicrobial Chemotherapy was co-authored by Banat, I.M who is the first of the top ten authors (Table 5).

Table 3. The most cited articles on biosurfactant as antimicrobial-related research

SCR	Authors	Article title	Journal	Year	Citation
1	Raajimakers *et al*., 2010	"Natural functions of lipopeptides from Bacillus and Pseudomonas: More than surfactants and antibiotics"	FEMS Microbiology Reviews, 34(6), pp. 1037–1062	2010	779
2	Rodrigues *et al*., 2006	"Biosurfactants: Potential applications in medicine"	Journal of Antimicrobial Chemotherapy, 57(4), pp. 609–618	2006	724
3	Abdel-Mawgoud *et al*., 2010	"Rhamnolipids: Diversity of structures, microbial origins and roles"	Applied Microbiology and Biotechnology, 86(5), pp. 1323–1336	2010	656
4	Singh *et al*., 2007	"Surfactants in microbiology and biotechnology: Part 2. Application aspects"	Biotechnology Advances, 25(1), pp. 99–121	2007	595
5	Galie *et al*., 2018	"Biofilms in the food industry: Health aspects and control methods"	Frontiers in Microbiology, 9(MAY), 898	2018	551
6	Singh and Cameotra, 2004	"Potential applications of microbial surfactants in biomedical sciences"	Trends in Biotechnology, 22(3), pp. 142–146	2004	493
7	Reid *et al*., 2011	"Microbiota restoration: Natural and supplemented recovery of human microbial communities"	Nature Reviews Microbiology, 9(1), pp. 27–38	2011	423
8	Thomas *et al*., 2013	"Current developments in solid-state fermentation"	Biochemical Engineering Journal, 81, pp. 146–161	2013	412
9	Elshikh *et al*., 2016	"Resazurin-based 96-well plate microdilution method for the determination of minimum inhibitory concentration of biosurfactants"	Biotechnology Letters, 38(6), pp. 1015–1019	2016	399
10	Van Hamme *et al*., 2006	"Physiological aspects. Part 1 in a series of papers devoted to surfactants in microbiology and biotechnology"	Biotechnology Advances, 24(6), pp. 604–620	2006	390

SCR: standard competition ranking.

3.5. The most productive institutions of biosurfactant as antimicrobial-related research during the years 1991-2023

Table 4 displays the top 10 productive affiliations worldwide in the field of biosurfactants as antimicrobial agents from 1991 to 2023, with a total of 133 (14.64%) documents. Ulster University is the most prolific contributor with 25 (2.73%) biosurfactants as antimicrobial-related documents. Second through fifth on the list were the Universidade de São Paulo (n = 23, 2.51%), Universidade do Minho (18, 1.98%), Universidade de Vigo (n = 16, 1.75%), University of Sfax (n = 13, 1.42%), respectively.

Table 4. The most productive organization in publications related to antimicrobial agents of biosurfactants.

SJR	Affiliation	Country	Number of documents (%)
1	Ulster University	Northern Ireland	25 (2.73%)
2	Universidade de São Paulo	Brazil	23 (2.51%)
3	Universidade do Minho	Portugal	18 (1.98%)
4	Universidade de Vigo	Spain	16 (1.75%)
5	University of Sfax	Tunisia	13 (1.42%)
6	Savitribai Phule Pune University	India	12 (1.31%)
7	Universitat de Barcelona	Spain	11 (1.20%)
8	Universidade Catolica de Pernambuco	Brazil	11 (1.20%)
9	Prince of Songkla University	Thailand	11 (1.20%)
10	Ministry of Education of the People's Republic of China	China	10 (1.09%)

SCR: standard competition ranking.

3.6. The top authors contributed of biosurfactant as antimicrobial-related research during the years 1991-2023

Table 5 displays the top 10 authors worldwide who commit to the field of biosurfactants as antimicrobial agents from 1991 to 2023 according to the amount of document publications. Banat, I.M. is the first of the top ten authors with 24 documents of biosurfactant as microbial-related publication and Vecino, X. is the lowest author with 9 documents.

Table 5. The top ten authors contributed to antimicrobial agents of biosurfactants.

SCR	Authors	No of document	H-index
1	Banat, I.M.	24	80
2	Moldes, A.B.	13	41
3	Cruz, J.M.	12	45
4	Sarubbo, L.A.	12	51
5	Saimmai, A.	11	14
6	Rodríguez-López, L.	11	19
7	Nitschke, M.	11	30
8	Rodrigues, L.R.	10	66
9	Maneerat, S.	10	25
10	Vecino, X.	9	28

SCR: standard competition ranking.

Figure 4 maps the occurrence of terms extracted from 908 documents about biosurfactants as antimicrobial agents indexed by Scopus. Of the 8603 terms that were retrieved, 81 were determined in more than 50 occurrences, leading to the formation of 5 distinct clusters: red, purple, blue, yellow, and green. (Figure 4a). Terms like antibiofilm activity, antibiotic agent, antibiotic resistance, biosurfactant, bacterial strain, *Candida albicans*, biofilm, *Escherichia coli*, human, hydrophobicity, *Pseudomonas aeruginosa*, *Staphylococcus aureus*, 16s RNA, quorum sensing are present in cluster 1 (red color); cluster 2 (green color): animal, anti-bacterial agents, antiinfective agent, chemistry, drug effect, genetics, Isolation and purification, metabolism, microbial sensitivity test, surface-active agents; cluster 3 (blue color): bacteria, biomolecules, bioremediation, emulsification, emulsion, Fourier transform infrared spectroscopy, surface tension; cluster 4 (yellow color): antifungal activity, *Bacillus subtilis*, biosynthesis, fungi, lipopeptide, surfactin; cluster 5 (purple color): antimicrobial activity, glycolipid, lipid, rhamnolipid. In Figure 4b, the extracted terms are categorized by VOSviewer into a color gradient that represents old to recent publishing years, ranging from blue to yellow. Several key terms including antibiotic agent, biosynthesis, bacterial strain, lipopeptide, surfactin, lipid, surface-active agents, surface tension, and *Bacillus subtilis* were deciphered upon in the early years of biosurfactant research as it pertained to antimicrobials. Meanwhile, some keywords like animal, chemistry, drug effect, anti-infective agent, antibiofilm activity, antibiotic resistance, biofilm, Fourier transform infrared spectroscopy, and 16s RNA are the topics that have appeared in recent years.

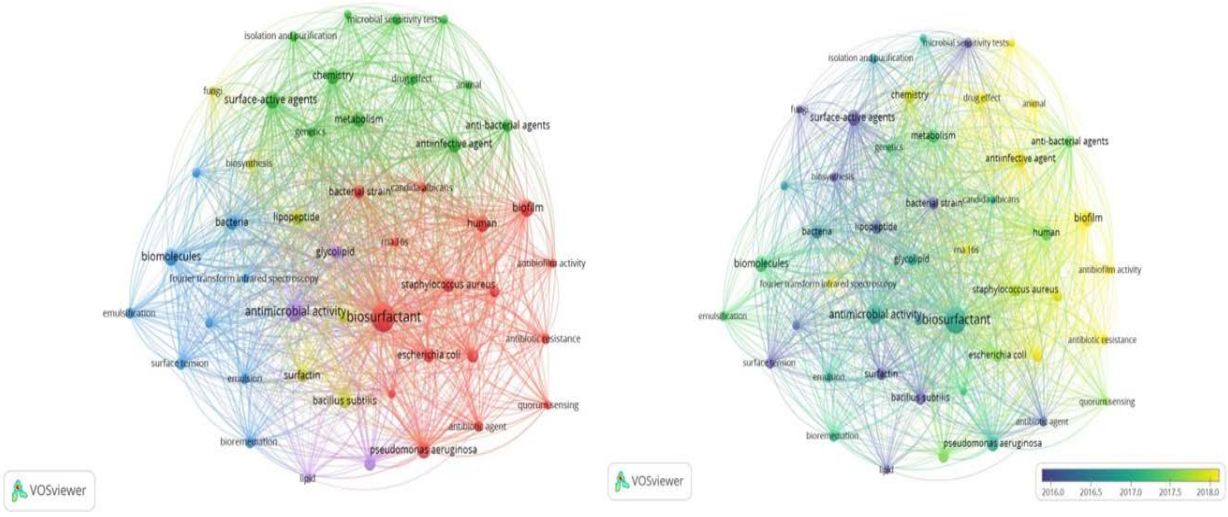

(a) **(b)**

Figure 4. Mapping of occurrence terms retrieved from titles and abstracts in biosurfactant as antimicrobial-related research articles conducted by VOSviewer. Visualizations in (a) network and (b) overlay. The circles' sizes correspond to the frequency of appearances. The degree of relationship is indicated by the length of the link. The different colors reveal distinct clusters. The color gradient, from purple to yellow, indicates the timeline from older to more recent publications

4. Discussion

Biosurfactants can be classified as either low-molecular-weight or high–molecular–weight biosurfactants (Kubicki *et al*., 2019). Lipopolysaccharides, lipoproteins, and a combination of these types belong to high-molecular-weight biosurfactants (Kubicki *et al*., 2019), while low-molecular-weight biosurfactants include fatty acids, phospholipids, glycolipids, polyketideglycosides, lipopeptides, and spiculisporic acid (Vieira *et al*., 2021). Moldes et al. (2021) reported glycolipopeptides and glycopeptides as the least studied microbial biosurfactants. Both glycopeptides and glycolipopeptides have been investigated and reviewed for their antimicrobial ability (Butler *et al*., 2014; Vecino *et*

al., 2018; Acharya *et al*., 2022). Glycolipids and lipopeptides are the most investigated biosurfactant classes for antimicrobial properties as shown in Supplementary 1 and Supplementary 2.

Polymyxins biosurfactants from bacteria were first reported in 1947 as one of the earliest classes of antibiotic, and in 1949, polymyxin E from *Paenibacillus polymyxa* was produced (Ledger *et al*., 2022). However, several adverse effects, including neuromuscular blockade, nephrotoxicity, and neurotoxicity as well as the availability of less toxic antimicrobials, caused it to lose popularity (Grill and Maganti, 2011). Glycopeptides as antibiotics from actinomycetes were discovered and reported in 1954 and introduced clinically in 1958 (Hutchings *et al*., 2019). Iturin as an interesting lipopeptide for antimicrobial and antifungal activity (Yaraguppi *et al*., 2023). Furthermore, a review article titled "Natural functions of lipopeptides from *Bacillus* and *Pseudomonas*: More than surfactants and antibiotics" published in FEMS Microbiology Reviews (Raajimakers *et al*., 2010) was the most cited article on biosurfactants as antimicrobial-related research, indicating that lipopeptide has gained attention in this study.

Based on our findings, India is the most prolific country in terms of antimicrobial properties of biosurfactants research. Biosurfactant research is gradually increasing together with a remarkable market surge in growth for biosurfactant demand in India (TechSci Research, 2023). This trend is especially apparent in personal care products that use antimicrobial natural ingredients. Starting in 2016, the number of published documents significantly increased, and the highest number was in 2022, indicating the field of antimicrobial properties of biosurfactants had high research productivity in recent years. In the research progress of antimicrobial properties of biosurfactant, Saudi Arabia, Egypt, and Iraq contributed as collaboration countries besides developed countries. This result differs from the institution's productivity in publications related to antimicrobial agents of biosurfactants. Ulster University from Northern Ireland has the most number of documents on antimicrobial properties of biosurfactant-related research.

Frontiers in Microbiology was listed as the most prominent journal with many documents discussing the antimicrobial properties of biosurfactants in this study. The first publication from *Frontiers in Microbiology* obtained in this study was published in 2014 titled "Analysis of biosurfactants from industrially viable *Pseudomonas* strain isolated from crude oil suggests how rhamnolipids congeners affect emulsification property and antimicrobial activity" by Das and colleagues from China (Das *et al*., 2014). *Frontiers in Microbiology* journal contributed 4.73% (n = 43) of the total publications retrieved from the Scopus database. Interestingly, although the oldest article related to antimicrobial properties of biosurfactants in *Colloids and Surfaces B Biointerfaces* journal was published in 1996 (Araki *et al*., 1996), this journal was identified as having the third-highest number of published documents 1.65% (n = 15).

The highest citations of research articles in Table 3 emphasize the most significant studies in biosurfactants as research with an antimicrobial focus. They can be used as references in finding present trends and prospects. According to the cluster formed (Figure 4), the red color (cluster 1) indicated the biological activity of biosurfactant and pathogen-caused infection. The green color (cluster 2) indicated the relationship between biosurfactant properties within organisms and their drug combination. The blue color (cluster 3) showed the characterization of biosurfactants, followed by the yellow color showed certain biosurfactants (lipopeptide and surfactin) with their antifungal activity. The purple color showed the major biosurfactants studied, such as glycolipid and rhamnolipid with their antimicrobial activity. As shown in Figure 4, biosurfactant research starting in 2017 has the emerging trend research in several keywords, such as animal, chemistry, drug effect, anti-infective agent, antibiofilm activity, antibiotic resistance, biofilm, Fourier transform infrared spectroscopy, and rna 16s.

Antimicrobial resistance like antibiotic resistance in 2019 caused 1.27 million deaths globally (Antimicrobial Resistance Collaborators, 2022). Exploration of natural compounds particularly biosurfactants for tackling human disease due to antimicrobial resistance is interesting among researchers worldwide. Several studies have demonstrated the biological activity of biosurfactants in vivo or cell line animals like mice (Huang *et al*., 2018; Tsuji *et al*., 2023), human cells (Vazquez *et al*., 2018), mouse fibroblast and mouse macrophage cell lines (Farias *et al*., 2019), chorioallantoic membrane (Rodriguez-Lopez *et al*., 2019), and *Aedes aegypti* larvae (de Andrade Teixeira Fernandes *et al*., 2020). Biosurfactants are capable of degrading microbial cell membranes. These molecules, composed of a hydrophilic head and a hydrophobic tail, interact with bacterial membrane lipids, leading to cellular damage. The mechanism begins with biosurfactants binding to lipopolysaccharides and peptidoglycan in the bacterial membrane, followed by their accumulation on the membrane surface. Furthermore, biosurfactants disrupt membrane proteins, triggering membrane disintegration and ultimately causing bacterial cell lysis (Lourenco *et al*., 2024; Adu *et al*., 2020).

Biofilm formation enhances antimicrobial resistance by increasing bacterial metabolism and strengthening defenses against antimicrobial agents (Uruen *et al*., 2020; Zhao *et al*., 2023). Many studies informed the antibiofilm potential of biosurfactants on the host or medical devices (Supplementary 3). Biosurfactants form micelles that interact with bacterial membranes, modifying the hydrophobic layer to inhibit biofilm formation and adhesion. They also alter surface tension and membrane permeability, causing membrane leakage (Jimoh *et al*., 2023). Moreover, the established combination formula of biosurfactant to combat antibiotic resistance and multidrug-resistant (MDR) strains has also been reported including nanoparticle-promising technology (Supplementary 4) (Falakaflaki *et al*., 2022; Diaz De Rienzo *et al*., 2016; Arif *et al*., 2021; Amirinejad *et al*., 2023; Sharaf *et al*., 2022; Giordani *et al*., 2019; Lin *et al*., 2023). Combining natural and synthesized compounds, this technology possesses a synergetic action against antimicrobial resistance compared to biosurfactants or drugs alone. Additionally, this strategy developed widespread biosurfactant applications related to the keyword "drug effect" on the host.

Several methods exist to investigate biosurfactant composition (Barale *et al*., 2022; Gharaei *et al*., 2022; Sen *et al*., 2017), such as Thin Layer Chromatography (TLC),

nuclear magnetic resonance (NMR), high-performance liquid chromatography (HPLC), gas chromatography-mass spectrometry (GC-MS), liquid chromatography-mass spectrometry (LC-MS), and Fourier transform infrared spectroscopy (FTIR). In this study, FTIR is the prominent compositional analysis to determine the functional groups of biosurfactant compounds (Arif *et al*., 2021; Nataraj *et al*., 2021; AA *et al*., 2020; Alfian *et al*., 2022; Athira *et al*., 2021; Challaraj Emmanuel *et al*., 2019;). On the other hand, the established technique for identifying biosurfactant-producing bacterial strains was 16S rRNA gene sequence analysis (Saleh *et al*., 2019; Rani *et al*., 2020; Englerova *et al*., 2021; Elkhawaga *et al*., 2018; Cheffi *et al*., 2021; Reddy *et al*., 2018; Buonocore *et al*., 2020; Challaraj Emmanuel *et al*., 2019) besides biosurfactant-producing yeast strains using rDNA regions (the D1/D2 LSU domains and ITS) (Sen *et al*., 2017). Interestingly, Villela *et al*., (2023) carried out whole-genome gene markers not just the 16S rRNA gene to identify strains. The result showed identified strains differed from the original paper.

5. Future Perspective

Biosurfactants have recently drawn the attention of the research area on drug-delivery systems, pharmaceuticals, and especially antimicrobial resistance. Firstly, further exploration of the functional roles of biosurfactants could enhance our understanding of their impacts on tackling human diseases. Moreover, the exploration of biosurfactants is boundless from direct producers like bacteria, plants, and fungi, yet it can be produced by producers associated with animals and sponges. On the other hand, the adverse effect due to the interaction of the properties should be emphasized especially for differences in application effects. The challenges regarding the cost and effectiveness of biosurfactant applications are important to be resolved.

6. Conclusion

A total of 908 documents have been published over three decades, with an average of 28 publications per year. Most publications were reported in 2022. India emerged as the leading country in publication volume, while Ulster University ranked as the top institution. Banat, I.M. was identified as the most prolific author. Prominent keywords in this research include biosurfactants, antimicrobial activity, and anti-infective agents. In summary, the data provided in this study illustrates the advancements made in the scope of biosurfactants research focusing on their antimicrobial properties from 1991 to 2023, and it may help provide insights for future research.

7. Limitations of Study

A limitation of this study is that it primarily focuses on data from Scopus databases, which may not include all consistent publications. Additionally, the selection of keywords and filters could unintentionally narrow the scope, possibly skewing results toward particular research areas or geographic regions. Another limitation is the potential impact of publication bias, where studies with more favorable or significant results are more likely to be published, potentially leading to an overestimation of the antimicrobial potential of biosurfactants. Lastly, the timing of publications could influence trends observed in the analysis, with surges in publication frequency possibly reflecting external factors such as increased funding or interest rather than true advancements in the field.

Acknowledgements

We thank to Universitas Gadjah Mada, International Islamic School Amanatul Ummah, Universiti Tun Hussein Onn Malaysia, King Mongkut's University of Technology Thonburi, and Universitas Padjajaran.

References

A A, E.K R and Mathew J. 2020. Characterization of biosurfactant produced by the endophyte *Burkholderia* sp. WYAT7 and evaluation of its antibacterial and antibiofilm potentials. *J Biotechnol*., **313**: 1-10.

Abdallah DB, Tounsi S, Gharsallah H, Hammami A and Frikha-Gargouri O. 2018. Lipopeptides from *Bacillus amyloliquefaciens* strain 32a as promising biocontrol compounds against the plant pathogen *Agrobacterium tumefaciens*. *Environ Sci Pollut Res*., **25(36)**: 36518-29.

Abdel-Mawgoud AM, Lépine F and Déziel E. 2010. Rhamnolipids: Diversity of structures, microbial origins and roles. *Appl Microbiol Biotechnol*., **86(5)**: 1323-36.

Acharya Y, Bhattacharyya S, Dhanda G and Haldar J. 2022. Emerging roles of glycopeptide antibiotics: Moving beyond gram-positive bacteria. *ACS Infect Dis*., **8(1)**: 1-28.

Adnan M, Siddiqui AJ, Noumi E, Ashraf SA, Awadelkareem AM, Hadi S, Snoussi M, Badraoui R, Bardacki F, Sachidanandan M and Patel M. 2023. Biosurfactant derived from probiotic *Lactobacillus acidophilus* exhibits broad-spectrum antibiofilm activity and inhibits the quorum sensing-regulated virulence. *Biomol Biomed*., **23(6)**: 1051-68.

Adu SA, Naughton PJ, Marchant R and Banat IM. 2020. Microbial biosurfactants in cosmetic and personal skincare pharmaceutical formulations. *Pharmaceutics*., **12(11)**:1099.

Akgul O, Erginkaya Z, Konuray G and Turhan EU. 2019. Antibacterial and anti-adhesive properties of biosurfactants produced by yeasts from food waste. *Fresenius Environ Bull*., **28(5)**: 4283-92.

Alfian AR, Watchaputi K, Sooklim C and Soontorngun N. 2022. Production of new antimicrobial palm oil-derived sophorolipids by the yeast *Starmerella riodocensis* sp. nov. against *Candida albicans* hyphal and biofilm formation. *Microb Cell Fact*., **21(1)**: 163.

Al-Ghamdi AY, Fadlelmula AA and Abdalla MOM. 2020. Total phenolic content, antioxidant and antimicrobial activity of *Ruta chalepensis* L. leaf extract in Al-Baha Area, Saudi Arabia. *Jordan J Biol Sci*., **13(6)**: 675-680.

Ali N, Pang Z, Wang F, Xu B and El-Seedi HR. 2022. Lipopeptide Biosurfactants from *Bacillus* spp.: Types, production, biological activities, and applications in food. *J Food Qual*., **2022(1)**: 1-19.

Ali SAM, Sayyed RZ, Mir MI, Khan MY, Hameeda B, Alkhanani MF, Haque S, Al Tawaha ARM and Poczai P. 2022. Induction of systemic resistance in maize and antibiofilm activity of surfactin from *Bacillus velezensis* MS20. *Front Microbiol*, **13**: 879739.

Amer MA, Wasfi R and Hamed SM. 2023. Biosurfactant from *Nile Papyrus* endophyte with potential antibiofilm activity against global clones of *Acinetobacter baumannii*. *Front Cell Infect Microbiol*., **13**: 1210195.

Amirinejad N, Shahriary P and Hassanshahian M. 2023. Investigation of the synergistic effect of glycolipid biosurfactant produced by *Shewanella algae* with some antibiotics against planktonic and biofilm forms of MRSA and antibiotic resistant *Acinetobacter baumannii*. *World J Microbiol Biotechnol*., **39(2)**: 45.

Anand U, Jacobo-Herrera N, Altemimi A and Lakhssassi N. 2019. A comprehensive review on medicinal plants as antimicrobial therapeutics: potential avenues of biocompatible drug discovery. *Metabolites*., **9(11)**: 258.

Ankulkar R and Chavan M. 2019. Characterisation and application studies of sophorolipid biosurfactant by *Candida tropicalis* RA1. *J Pure Appl Microbiol*., **13(3)**: 1653-65.

Antimicrobial Resistance Collaborators. 2022. Global burden of bacterial antimicrobial resistance in 2019: A systematic analysis. *Lancet*., **399(10325)**: 629-55.

Antolak H, Mizerska U, Berłowska J, Otlewska A and Kręgiel D. 2018. Quillaja saponaria saponins with potential to enhance the effectiveness of disinfection processes in the beverage industry. *Applied Sciences*., **8(3)**: 368.

Araki YI, Lee S, Sugihara G, Furuichi M, Yamashita S and Ohseto F. 1996. New cationic surfactants derived from bile acids: Synthesis and thermodynamic and biophysicochemical properties such as membrane perturbation and protein solubilizing abilities. *Colloids Surf B Biointerfaces*., **8(1-2)**: 81-92.

Argentin MN, Martins LF, Sousa MP and Bossolan NRS. 2023. Biosurfactant from a thermo-halophilic strain of *Bacillus alveayuensis* isolated from a Brazilian oil reservoir: Production, chemical characterization, antimicrobial activity, and efficiency in wettability reversal and oil removal from oil-soaked sand. *Geoenergy Sci Eng*., **231**: 212324.

Arif M, Sharaf M, Khan S, Chi Z and Liu CG. 2021. Chitosan-based nanoparticles as delivery-carrier for promising antimicrobial glycolipid biosurfactant to improve the eradication rate of *Helicobacter pylori* biofilm. *J Biomater Sci Polym Ed*., **32(6)**: 813-32.

Atanasov AG, Zotchev SB, Dirsch VM, International Natural Product Sciences T and Supuran CT. 2021. Natural products in drug discovery: advances and opportunities. *Nat Rev Drug Discov*., **20(3)**: 200-16.

Athira K, Gurrala L and Kumar DVR. 2021. Biosurfactant-mediated biosynthesis of CuO nanoparticles and their antimicrobial activity. *Appl Nanosci (Switzerland)*., **11(4)**: 1447-57.

Ayed A, Essid R, Mankai H, Echmar A, Fares N, Hammami M, Sewald N, Limam F, Tabbene O. 2023. Synergistic antifungal activity and potential mechanism of action of a glycolipid-like compound produced by *Streptomyces blastmyceticus* S108 against *Candida* clinical isolates. *J Appl Microbiol*., **134(11)**: lxad246.

Barale SS, Ghane SG and Sonawane KD. 2022. Purification and characterization of antibacterial surfactin isoforms produced by *Bacillus velezensis* SK. *AMB Express*., **12(1)**: 7.

Bezerra KGO, Silva IGS, Almeida FCG, Rufino RD and Sarubbo LA. 2021. Plant-derived biosurfactants: Extraction, characteristics and properties for application in cosmetics. *Biocatal Agric Biotechnol*., **34**: 102036.

Buonocore C, Tedesco P, Vitale GA, Esposito FP, Giugliano R, Monti MC, D'Auria MV and de Pascale D. 2020. Characterization of a new mixture of mono-rhamnolipids produced by *Pseudomonas gessardii* isolated from edmonson point (antarctica). *Mar Drugs*., **18(5)**: 269.

Butler MS, Hansford KA, Blaskovich MA, Halai R and Cooper MA. 2014. Glycopeptide antibiotics: Back to the future. *J Antibiot (Tokyo)*., **67(9)**: 631-44.

Ceresa C, Rinaldi M, Tessarolo F, Maniglio D, Fedeli E, Tambone E, Caciagli P, Banat IM, De Rienzo MAD and Fracchia L. 2021. Inhibitory effects of lipopeptides and glycolipids on C. *albicans–Staphylococcus* spp. dual-species biofilms. *Front Microbiol*., **11**: 545654.

Ceresa, Chiara, Letizia Fracchia, Emanuele Fedeli, Chiara Porta, and Ibrahim M. Banat. 2021. Recent advances in biomedical, therapeutic and pharmaceutical applications of microbial surfactants. Pharmaceutics., 13(4): 466.

Challaraj Emmanuel ES, Sree Priya S and George S. 2019. Isolation of biosurfactant from *Lactobacillus* sp. and study of its inhibitory properties against E.*coli* Biofilm. *J Pure Appl Microbiol*., **13(1)**: 403-11.

Chauhan V, Dhiman VK and Kanwar SS. 2022. Purification and characterization of a novel bacterial Lipopeptide(s) biosurfactant and determining its antimicrobial and cytotoxic properties. *Process Biochem*., **120**:114-25.

Cheffi M, Maalej A, Mahmoudi A, Hentati D, Marques AM, Sayadi S and Chamkha M. 2021. Lipopeptides production by a newly *Halomonas venusta* strain: Characterization and biotechnological properties. *Bioorg Chem*., **109**: 104724.

Clements T, Ndlovu T and Khan W. 2019. Broad-spectrum antimicrobial activity of secondary metabolites produced by *Serratia marcescens* strains. *Microbiol Res*., **229**: 126329.

da Fontoura ICC, Saikawa GIA, Silveira VAI, Pan NC, Amador IR, Baldo C, de Rocha SPD and Celligoi MAPC. 2020. Antibacterial activity of sophorolipids from *Candida bombicola* against human pathogens. *Braz Arch Biol Technol*., **63**: e20180568.

Da Silva GO, Farias BCS, Da Silva RB, Teixeira EH, Cordeiro RDA, Hissa DC and Melo VMM. 2021. Effects of lipopeptide biosurfactants on clinical strains of *Malassezia furfur* growth and biofilm formation. *Med Mycol*., **59(12)**: 1191-201.

Das P, Yang XP and Ma LZ. 2014. Analysis of biosurfactants from industrially viable *Pseudomonas* strain isolated from crude oil suggests how rhamnolipids congeners affect emulsification property and antimicrobial activity. *Front Microbiol*., **5**: 696.

de Andrade Teixeira Fernandes N, de Souza AC, Simões LA, Ferreira dos Reis GM, Souza KT, Schwan RF and Dias DR. 2020. Eco-friendly biosurfactant from *Wickerhamomyces anomalus* CCMA 0358 as larvicidal and antimicrobial. *Microbiol Res*., **241**: 126571.

de Freitas Ferreira J, Vieira EA and Nitschke M. 2019. The antibacterial activity of rhamnolipid biosurfactant is pH dependent. *Food Res Int*., **116**: 737-44.

de Souza Freitas F, Coelho de Assis Lage T, Ayupe BAL, de Paula Siqueira T, de Barros M and Tótola MR. 2020. *Bacillus subtilis* TR47II as a source of bioactive lipopeptides against gram-negative pathogens causing nosocomial infections. *Biotech*., **10(11)**: 474.

Diaz De Rienzo MA, Stevenson PS, Marchant R and Banat IM. 2016. Effect of biosurfactants on *Pseudomonas aeruginosa* and *Staphylococcus aureus* biofilms in a BioFlux channel. *Appl Microbiol Biotechnol*., **100(13)**: 5773-9.

Dong S, Yang X, Zhao L, Zhang F, Hou Z and Xue P. 2020. Antibacterial activity and mechanism of action saponins from *Chenopodium quinoa* Willd. husks against foodborne pathogenic bacteria. *Ind Crops Prod*., **149**: 112350.

Elkhawaga MA. 2018. Optimization and characterization of biosurfactant from *Streptomyces griseoplanus* NRRL-ISP5009 (MS1). *J Appl Microbiol*., **124(3)**: 691-707.

Elshikh M, Ahmed S, Funston S, Dunlop P, McGaw M, Marchant R and Banat IM. 2016. Resazurin-based 96-well plate microdilution method for the determination of minimum inhibitory concentration of biosurfactants. *Biotechnol Lett*., **38(6)**: 1015-9.

El-Zayat SA, Kamel NM, Abdel-Motaal FF, El-Sayed MA, Abdelrahman M, Abou-Ellail M, Mohamed AEH and Darwish DB. 2024. *Gymnascella thermotolerans*-GTE-21, an endophytic Fungus in *Euphorbia geniculata* as a Versatile Producer of Bioactive Metabolites. *Jordan J Biol Sci*., **17(1)**: 363-374.

Englerová K, Bedlovičová Z, Nemcová R, Király J, Mad'ar M, Hajdučková V, Stykova E, Mucha R and Reiffova K. 2021. *Bacillus amyloliquefaciens* - derived lipopeptide biosurfactants inhibit biofilm formation and expression of biofilm-related genes of *Staphylococcus aureus*. *Antibiotics*., **10(10)**: 1252.

Eras-Munoz E, Farre A, Sanchez A, Font X and Gea T. 2022. Microbial biosurfactants: a review of recent environmental applications. *Bioengineered*., **13(5)**: 12365-91.

Falagas ME, Pitsouni EI, Malietzis GA and Pappas G. 2008. Comparison of PubMed, Scopus, Web of Science, and Google Scholar: Strengths and weaknesses. *FASEB J*., **22(2)**: 338-342.

Falakaflaki M, Varshosaz J and Mirian M. 2022. Local delivery of usnic acid loaded rhamnolipid vesicles by gelatin /tragacanth gum/montmorillonite/vanillin cryogel scaffold for expression of osteogenic biomarkers and antimicrobial activity. *J Drug Deliv Sci Technol*., **69**: 103147.

Farias JM, Stamford TCM, Resende AHM, Aguiar JS, Rufino RD, Luna JM and Sarubbo LA. 2019. Mouthwash containing a biosurfactant and chitosan: An eco-sustainable option for the control of cariogenic microorganisms. *Int J Biol Macromol*., **129**: 853-60.

Firdose A, Chong NHH, Ramli R and Aqma WS. 2023. Antimicrobial, antiadhesive, and antibiofilm actions of rhamnolipids on ESKAPE pathogens. *Lett Appl Microbiol*., **76(2)**: ovad013.

Galié S, García-Gutiérrez C, Miguélez EM, Villar CJ and Lombó F. 2018. Biofilms in the food industry: Health aspects and control methods. *Front Microbiol*., **9**: 898.

Gharaei S, Ohadi M, Hassanshahian M, Porsheikhali S and Forootanfar H. 2022. Isolation, optimization, and structural characterization of glycolipid biosurfactant produced by marine isolate *Shewanella algae* B12 and evaluation of its antimicrobial and anti-biofilm activity. *Appl Biochem Biotechnol*., **194(4)**: 1755-74.

Ghazala I, Charfeddine S, Charfeddine M, Gargouri-Bouzid R, Ellouz-Chaabouni S and Haddar A. 2022. Antimicrobial and antioxidant activities of *Bacillus mojavensis* I4 lipopeptides and their potential application against the potato dry rot causative *Fusarium solani*. *Arch Microbiol*., **204(8)**: 484.

Giordani B, Costantini PE, Fedi S, Cappelletti M, Abruzzo A, Parolin C, Foschi C, Frisco G, Calonghi N, Cerchiara T, Bugucci F, Luppi B and Vitali B. 2019. Liposomes containing biosurfactants isolated from *Lactobacillus gasseri* exert antibiofilm activity against methicillin resistant *Staphylococcus aureus* strains. *Eur J Pharm Biopharm*., **139**: 246-52.

Grill MF and Maganti RK. 2011. Neurotoxic effects associated with antibiotic use: management considerations. *Br J Clin Oharmacol*., **72(3)**: 381–393.

Haba E, Pinazo A, Jauregui O, Espuny MJ, Infante MR and Manresa A. 2003. Physicochemical characterization and antimicrobial properties of rhamnolipids produced by *Pseudomonas aeruginosa* 47T2 NCBIM 40044. *Biotechnol Bioeng*., **81(3)**: 316-22.

Haddaji N, Bahloul B, Bahia W, Bechambi O and Mahdhi A. 2023. Development of nanotechnology-based drug delivery systems for controlling clinical multidrug-resistant *Staphylococcus aureus* and *Escherichia coli* Associated with aerobic vaginitis. *Pharmaceutics*., **15(8)**: 2133.

Henkel M and Hausmann R. 2019. Chapter 2 - Diversity and Classification of Microbial Surfactants. In: Hayes DG, Solaiman DKY and Ashby RD (Eds). **Biobased Surfactants (Second Edition).** AOCS Press, pp. 41-63.

Hu H, Shen X, Liao B, Luo L, Xu J and Chen S. 2019. Herbgenomics: A stepping stone for research into herbal medicine. *Sci China Life Sci*., **62(7)**: 913-20.

Huang W, Lang Y, Hakeem A, Lei Y, Gan L and Yang X. 2018. Surfactin-based nanoparticles loaded with doxorubicin to overcome multidrug resistance in cancers. *Int J Nanomed*., **13**: 1723-36.

Huang Y, Zhang X, Xu H, Zhang F, Zhang X, Yan Y, He L and Liu J. 2022. Isolation of lipopeptide antibiotics from *Bacillus siamensis*: a potential biocontrol agent for *Fusarium graminearum*. *Can J Microbiol*., **68(6)**: 403-11.

Hutchings MI, Truman AW and Wilkinson B. 2019. Antibiotics: past, present and future. *Current Opinion in Microbiology*., **51**:72-80.

Iswanti W, Ekawidyani KR, Asmarinah, Budijanto S and Abdullah M. 2024. The Effect of Anthocyanins Black Rice Bran Extract (ABRiBE) on Colorectal Cancer Cell Proliferation and ABCA1 Gene Expression in the HT-29 CeLL Line. *Jordan J Biol Sci*., **17(1):** 197-205**.**

Jakubczyk D and Dussart F. 2020. Selected fungal natural products with antimicrobial properties. *Molecules*., **25(4)**: 911.

Janek T, Krasowska A, Czyznikowska Z and Łukaszewicz M. 2018. Trehalose lipid biosurfactant reduces adhesion of microbial pathogens to polystyrene and silicone surfaces: An experimental and computational approach. *Front Microbiol*., **9**: 2441.

Jimoh AA, Booysen E, Van Zyl L and Trindade M. 2023. Do biosurfactants as anti-biofilm agents have a future in industrial water systems?. *Front Bioeng Biotechnol*., **11**: 1244595.

Kaur S and Kaur R. 2019. Biosurfactant from *Lactobacillus* sp. as an antibiofilm agent. *Biotechnologia*., **100(3)**: 335-43.

Kiran GS, Priyadharsini S, Sajayan A, Priyadharsini GB, Poulose N and Selvin J. 2017. Production of lipopeptide biosurfactant by a marine *Nesterenkonia* sp. and its application in food industry. *Front Microbiol*., **8**: 1138.

Kubicki S, Bollinger A, Katzke N, Jaeger KE, Loeschcke A, Thies S. 2019. Marine biosurfactants: biosynthesis, structural diversity, and biotechnological applications. *Mar Drugs*., **17(7)**: 408.

Kulakovskaia EV, Kulakovskaia TV, Golubev VI, Shashkov AS, Grachev AA and Nifant'ev NE. 2007. Fungicidal activity of cellobiose lipids from cultural fluid of yeast *Cryptococcus humicola* and *Pseudozyma fusiformata*. *Bioorg Khim*., **33(1)**: 167-71.

Kumar, Ajay, Sandeep Kumar Singh, Chandra Kant, Hariom Verma, Dharmendra Kumar, Prem Pratap Singh, Arpan Modi et al. 2021. Microbial biosurfactant: a new frontier for sustainable agriculture and pharmaceutical industries. Antioxidants., 10(9): 1472.

Lin S, Li X, Zhang Y, Zhang W, Shu G, Li H, Xu F, Lin J and Fu H. 2023. Rhamnolipid micelles assist azithromycin in efficiently disrupting *Staphylococcus aureus* biofilms and impeding their re-formation. *Int J Nanomed*., **18**: 7403-15.

Liu X, Shu Q, Chen Q, Pang X, Wu Y, Zhou W, Wu Y, Niu J and Zhang X. 2020. Antibacterial efficacy and mechanism of mannosylerythritol lipids-A on listeria monocytogenes. *Molecules*., **25(20)**: 4857.

Lourenco M, Duarte N and Ribeiro IAC. 2024. Exploring biosurfactants as antimicrobial approaches. *Pharmaceuticals*., **17(9)**:1239.

Manan NA, Jusoh I and Pa'ee F. 2022. Antifungal activities of *Neobalanocarpus heimii* (Cengal) heartwood extracts on *Trametes versicolor* and *Coniophora puteana*. *Journal of Tropical Biodiversity and Biotechnology*., **7(3):** jtbb69942.

McAllister JT, Lennertz L and Atencio Mojica Z. 2022. Mapping a discipline: A guide to using vosviewer for bibliometric and visual analysis. *Science & Technology Libraries.*, **41(3)**: 319-48.

Mohamed EH, Abdel-Hafez SM, Soliman MM, Alotaibi SH, Alkhedaide A and Mostafa MA. 2020. Characterization and identification of methicillin-resistant *Staphylococcus aureus* (MRSA) producing biofilm: Impacts of garlic extract and *Lactobacillus* Biosurfactants. *Biomed Pharmacol J*., **13(3)**:1103-12.

Moldes AB, Rodriguez-Lopez L, Rincon-Fontan M, Lopez-Prieto A, Vecino X and Cruz JM. 2021. Synthetic and bio-derived surfactants versus microbial biosurfactants in the cosmetic industry: An overview. *Int J Mol Sci*., **22(5)**: 2371.

Morais IMC, Cordeiro AL, Teixeira GS, Domingues VS, Nardi RMD, Monteiro AS, Alves RJ, Siqueira EP and Santos VL. 2017. Biological and physicochemical properties of biosurfactants produced by *Lactobacillus jensenii* P6A and *Lactobacillus gasseri* P65. *Microb Cell Fact*., **16(1)**: 155.

Mouafo HT, Sokamte AT, Manet L, Mbarga AJM, Nadezdha S, Devappa S and Mbawala A. 2023. Biofilm inhibition, antibacterial and antiadhesive properties of a novel biosurfactant from *Lactobacillus paracasei* N2 against multi-antibiotics-resistant pathogens isolated from braised fish. *Fermentation*., **9(7)**: 646.

Nataraj BH, Ramesh C and Mallappa RH. 2021. Functional group characterization of lactic bacterial biosurfactants and evaluation of antagonistic actions against clinical isolates of methicillin-resistant *Staphylococcus aureus. Lett Appl Microbiol*., **73(3)**: 372-82.

Ndlovu T, Rautenbach M, Vosloo JA, Khan S and Khan W. 2017. Characterisation and antimicrobial activity of biosurfactant extracts produced by *Bacillus amyloliquefaciens* and *Pseudomonas aeruginosa* isolated from a wastewater treatment plant. *AMB Express*., **7**:108.

Nunes H, Vieira IMM, Santos BLP, Silva DP and Ruzene DS. 2022. Biosurfactants produced from corncob: A bibliometric perspective of a renewable and promising substrate. *Prep Biochem Biotechnol*., **52(2)**: 123-34.

Ohadi M, Forootanfar H, Dehghannoudeh G, Eslaminejad T, Ameri A, Shakibaie M and Adeli-Sardou M. 2020. Antimicrobial, anti-biofilm, and anti-proliferative activities of lipopeptide biosurfactant produced by *Acinetobacter junii* B6. *Microb Pathog*., **138**: 103806.

Prastiyanto ME, Iswara A, Khairunnisa A, Sofyantoro F, Siregar AR, Mafiroh WU, Setiawan J, Nadifah F, Wibowo AT and Putri WA. 2024. Prevalence and antimicrobial resistance profiles of multidrug-resistant bacterial isolates from urinary tract infections in Indonesian patients: A cross-sectional study. *Clinical Infection in Practice*., **22**: 100359.

Priyono DS, Sofyantoro F, Putri WA, Septriani NI, Rabbani A and Arisuryanti T. 2023. A bibliometric analysis of Indonesian biodiversity identification through DNA barcoding research from 2004-2021. *Nat Life Sci Commun.*, **22(1)**: e2023006.

Putri WA, Setiawan J, Sofyantoro F, Priyono DS, Septriani NI, Mafiroh WU, Yano Y and Wasityastuti W. 2023. Global research trends in non-alcoholic fatty liver disease. *Bratisl Med J*., **124(8)**: 590-598.

Quinn GA, Maloy AP, McClean S, Carney B and Slater JW. 2012. Lipopeptide biosurfactants from *Paenibacillus polymyxa* inhibit single and mixed species biofilms. *Biofouling*., **28(10)**: 1151-66.

Raaijmakers JM, de Bruijn I, Nybroe O and Ongena M. 2010. Natural functions of lipopeptides from *Bacillus* and *Pseudomonas*: More than surfactants and antibiotics. *FEMS Microbiol Rev*., **34(6)**: 1037-62.

Rani M, Weadge JT and Jabaji S. 2020. Isolation and characterization of biosurfactant-producing bacteria from oil well batteries with antimicrobial activities against food-borne and plant pathogens. Front Microbiol., **11**: 64.

Reddy GS, Srinivasulu K, Mahendran B and Reddy RS. 2018. Biochemical characterization of anti-microbial activity and purification of glycolipids produced by dodecanoic acid-undecyl ester. *Res J Pharm Technol*., **11(9)**: 4066-73.

Reid G, Younes JA, Van Der Mei HC, Gloor GB, Knight R and Busscher HJ. 2011. Microbiota restoration: Natural and supplemented recovery of human microbial communities. *Nat Rev Microbiol*., **9(1)**: 27-38.

Resende AHM, Farias JM, Silva DDB, Rufino RD, Luna JM, Stamford TCM and Sarubbo LA. 2019. Application of biosurfactants and chitosan in toothpaste formulation. *Colloids Surf B Biointerfaces*., **181**:77-84.

Risdian C, Mozef T and Wink J. 2019. Biosynthesis of polyketides in *Streptomyces*. *Microorg*., **7(5)**: 124.

Rodrigues L, Banat IM, Teixeira J and Oliveira R. 2006. Biosurfactants: Potential applications in medicine. *J Antimicrob Chemother.*, **57(4)**: 609-18.

Rodríguez-López L, Rincón-Fontán M, Vecino X, Cruz JM and Moldes AB. 2019. Preservative and irritant capacity of biosurfactants from different sources: A comparative study. *J Pharm Sci*., **108(7)**: 2296-304.

Rzycki M, Gladysiewicz-Kudrawiec M and Kraszewski S. 2024. Molecular guidelines for promising antimicrobial agents. *Sci Rep*., **14(1)**: 4641.

Sabarinathan D, Vanaraj S, Sathiskumar S, Poorna Chandrika S, Sivarasan G, Arumugam SS, Preethi K, Li H and Chen Q. 2021. Characterization and application of rhamnolipid from *Pseudomonas plecoglossicida* BP03. *Lett Appl Microbiol*., **72(3)**: 251-62.

Saleh D, Jarry J, Rani M, Aliferis KA, Seguin P and Jabaji SH. 2019. Diversity, distribution and multi-functional attributes of bacterial communities associated with the rhizosphere and endosphere of timothy (*Phleum pratense* L.). *J Appl Microbiol*., **127(3)**: 794-811.

Sambanthamoorthy K, Feng X, Patel R, Patel S and Paranavitana C. 2014. Antimicrobial and antibiofilm potential of biosurfactants isolated from lactobacilli against multi-drug-resistant pathogens. *BMC Microbiol.*, **14**: 197.

Sarethy IP, Bhatia N and Maheshwari N. 2015. Antibacterial activity of plant biosurfactant extract from *Sapindus mukorossi* and in silico evaluation of its bioactivity. *Int J Pharmcy Pharm Sci*., **7(10)**: 419-21.

Sarubbo, Leonie A., C. Silva Maria da Gloria, Italo José B. Durval, Káren Gercyane O. Bezerra, Beatriz G. Ribeiro, Ivison A. Silva, Matthew S. Twigg, and Ibrahim M. Banat. 2022. Biosurfactants: Production, properties, applications, trends, and general perspectives. Biochemical Engineering Journal., 181: 108377.

Sen S, Borah SN, Bora A and Deka S. 2017. Production, characterization, and antifungal activity of a biosurfactant produced by *Rhodotorula babjevae* YS3. *Microb Cell Fact*., **16(1)**: 95.

Setiawan J, Rizal DM, Sofyantoro F, Priyono DS, Septriani NI, Mafiroh WU, Takenori K, Takashi M and Putri WA. 2024. Bibliometric analysis of organoid in regenerative medicine-related research worldwide over two decades (2002-2022). *Regen Med*., **19(3)**: 119-133.

Sharaf M, Sewid AH, Hamouda HI, Elharrif MG, El-Demerdash AS, Alharthi A, Hashim N, Hamad AA, Selim S, Alkhalifah DHM, Hozzein WN, Abdalla M and Saber T. 2022. Rhamnolipid-coated iron oxide nanoparticles as a novel multitarget candidate against major foodborne E. *coli* serotypes and methicillin-resistant S. *aureus*. *Microbiol Spectr*., **10(4)**: e0025022.

Shu Q, Lou H, Wei T, Liu X and Chen Q. 2021. Contributions of glycolipid biosurfactants and glycolipid-modified materials to antimicrobial strategy: A review. *Pharmaceutics*., **13(2)**: 1-22.

Shu Q, Wei T, Lu H, Niu Y and Chen Q. 2020. Mannosylerythritol lipids: dual inhibitory modes against *Staphylococcus aureus* through membrane-mediated apoptosis and biofilm disruption. *Appl Microbiol Biotechnol*., **104(11)**: 5053-64.

Singh A, Van Hamme JD and Ward OP. 2007. Surfactants in microbiology and biotechnology: Part 2. Application aspects. *Biotechnol Adv*., **25(1)**: 99-121.

Singh P and Cameotra SS. 2004. Potential applications of microbial surfactants in biomedical sciences. *Trends Biotechnol*., **22(3)**: 142-6.

Sofyantoro F, Frediansyah A, Priyono DS, Putri WA, Septriani NI, Wijayanti N, Ramadaningrum WA, Turkistani SA, Garout M, Aljedah M, Al Shammari BR and Alwashmi ASS. 2023. Growth in chikungunya virus-related research in ASEAN and South Asian countries from 1967 to 2022 following disease emergence: a bibliometric and graphical analysis. *Global Health*., **19(1)**: 9.

Sofyantoro F, Kusuma HI, Vento S, Rademaker M and Frediansyah A. 2022. Global research profile on monkeypox-related literature (1962-2022): A bibliometric analysis. *Narra J*., **2(3)**: e96.

Sofyantoro F, Yudha DS, Lischer K, Nuringtyas TR, Putri WA, Kusuma WA, Purwestri YA and Swasono RT. 2022. Bibliometric analysis of literature in snake venom-related research worldwide (1933-2022). *Animals*., **12(16)**: 2058.

TechSci Research. 2023. India biosurfactants market by type (glycolipids, alkyl polyglucosides, methyl ethyl sulfonates, sucrose esters, others), by application (personal care, food processing, oil field, chemicals, textiles, others), by region, competition, forecast and opprtunities 2019-2029. Available from: https://www.techsciresearch.com/report/india-biosurfactants-market/1786.html.

Thomas L, Larroche C and Pandey A. 2013. Current developments in solid-state fermentation. *Biochem Eng* J., **81**: 146-61.

Tsuji M, Nair MS, Masuda K, Castagna C, Chong Z, Darling TL, Seehra K, Hwang Y, Ribeiro AL, Ferreira GM, Corredor L, Coelho-Dos-Reis JGA, Tsuji Y, Mori M, Boon ACM, Diamond MS, Huang Y and Ho DD. 2023. An immunostimulatory glycolipid that blocks SARS-CoV-2, RSV, and influenza infections in vivo. *Nat Commun.*, **14(1)**: 3959.

Uruén C, Chopo-Escuin G, Tommassen J, Mainar-Jaime RC and Arenas J. 2020. Biofilms as promoters of bacterial antibiotic resistance and tolerance. *Antibiotics (Basel).*, **10(1)**.

Van Hamme JD, Singh A and Ward OP. 2006. Physiological aspects. Part 1 in a series of papers devoted to surfactants in microbiology and biotechnology. *Biotechnol Adv*., **24(6)**: 604-20.

Vazquez L, Teixeira da Silva Ferreira A, Cavalcante FS, Garcia IJP, dos Santos KRN, Barbosa LADO, Almeida MDS, Mignaco JA and Fontes CFL. 2018. Properties of novel surfactin-derived biosurfactants obtained through solid-phase synthesis. *J Pept Sci*., **24(11)**: e3129.

Vecino X, Rodríguez-López L, Ferreira D, Cruz JM, Moldes AB and Rodrigues LR. 2018. Bioactivity of glycolipopeptide cell-bound biosurfactants against skin pathogens. *Int J Biol Macromol*., **109**: 971-9.

Vieira IMM, Santos BLP, Ruzene DS and Silva DP. 2021. An overview of current research a developments in biosurfactants. *J Ind Eng Chem*., **100**: 1-18.

Villela H, Modolon F, Schultz J, Delgadillo-Ordoñez N, Carvalho S, Soriano AU and Peixoto RS. 2023. Genome analysis of a coral-associated bacterial consortium highlights complementary hydrocarbon degradation ability and other beneficial mechanisms for the host. *Sci Rep*., **13(12273)**: 1-14.

Wang Y, Zhang C, Liang J, Wu L, Gao W and Jiang J. 2020. Iturin a extracted from *Bacillus subtilis* WL-2 affects phytophthora infestans via cell structure disruption, oxidative stress, and energy supply dysfunction. *Front Microbiol.*, **11**: 536083.

Yaraguppi DA, Bagewadi ZK, Patil NR and Mantri N. 2023. Iturin: A promising cyclic lipopeptide with diverse applications. *Biomolecules*., **13(10)**: 1515.

Zhao A, Sun J and Liu Y. 2023. Understanding bacterial biofilms: from definition to treatment strategies. *Front Cell Infect Microbiol*., **13**: 1137947.

Supplementary 1. Antimicrobial activities of biosurfactants produced by microorganisms.

Producer microorganism	Biosurfactant class	Biosurfactant type	Antimicrobial activity	Reference
Bacillus amyloliquefaciens	Lipopeptides		*Agrobacterium tumefaciens*	Abdallah *et al*., 2018
Bacillus alveayuensis		Mixture of surfactins, iturins, and fengycins	*Desulfovibrio marinus*	Argentin *et al*., 2023
Bacillus subtilis		Iturin A	*Phytophthora infestans*	Wang *et al*., 2020
Serratia marcescens		Serrawettin	*Pseudomonas aeruginosa*, methicillin-resistant *Staphylococcus aureus*, *Cryptococcus neoformans*	Clements *et al*., 2019
Pseudomonas aeruginosa	Glycolipids	Rhamnolipids	Bacteria: *Serratia marcescens*, *Enterobacter aerogenes*, *Klebsiella pneumoniae*, *Staphylococcus aureus*, *Staphylococcus epidermidis*, *Bacillus subtilis*, and phytopathogenic fungal species: *Chaetonium globosum*, *Penicillium funiculosum*, *Gliocadium virens* and *Fusarium solani*	Haba *et al*., 2003
Candida tropicalis		Sophorolipids	*Escherichia coli*, *Listeria monocytogenes* and *Staphylococcus aureus*	Ankulkar *et al*., 2019
Rhodococcus fascians		Trehalose lipid	*Vibrio harveyi* and *Proteus vulgaris*	Janek *et al*., 2018
Pseudozyma aphidis		Mannosylerythritol lipids-A	*Listeria monocytogenes*	Liu *et al*., 2020
Cryptococcus humicola and *Pseudozyma fusiformata*		Cellobiose lipids	pathogenic *Cryptococcus* and *Candida* species	Kulakovskaia *et al*., 2007
Streptomyces	Polyketides		Pathogenic fungi, various bacteria	Risdian *et al*., 2019

Supplementary 2. Antimicrobial activities of biosurfactants produced by plants.

Producer plants	Biosurfactant class	Biosurfactant type	Antimicrobial activity	Reference
Chenopodium quinoa	Saponins			Bezerra *et al*., 2021
Glycine max	Saponins			Bezerra *et al*., 2021
Malphiguia ermaginata	Saponins			Bezerra *et al*., 2021
Quillaja saponaria	Saponins		*Asaia spp.* biofilm	Antolak *et al*., 2018
Chenopodium quinoa Wild.	Saponins		*Staphylococcus aureus*, *Staphylococcus epidermidis*, *B. aureus*, *S. enteritidis*, *P. aeruginosa*, *L. ivanovii*	Dong *et al*., 2020
Sapindus mukorossi fruits	Saponins	Sapindoside B, Sapinmusaponin A, Sapinmusaponin F, Sapinmusaponin N	*B. subtilis*, *B. linens*, *M. luteus*, *S. epidermidis*, *E. coli*, *P. fluorescens*	Sarethy *et al*., 2015

Supplementary 3. Antibiofilm properties of biosurfactants

Producer microorganism	Biosurfactant class	Biosurfactant type	Antibiofilm activity	Reference
Endophyte *Burkholderia* sp.	Glycolipid		*Staphylococcus aureus*	AA *et al*., 2020
Paenibacillus polymyxa	Lipopeptide	Polymyxin D1 Surfactins	*Bacillus subtilis, Micrococcus luteus, Pseudomonas aeruginosa, S. aureus, Streptococcus bovis*.	Quinn *et al*., 2012
Nesterenkonia sp.	Lipopeptide		*Staphylococcus aureus*	Kiran *et al*., 2017
Lactobacillus jensenii P_{6A} and *Lactobacillus gasseri* P_{65}	Unclassified		*Staphylococcus saprophyticus, Enterobacter aerogenes* and *Klebsiella pneumoniae*	Morais *et al*., 2017
Bacillus subtilis	Lipopeptide		*Achromobacter xylosoxidans, Alcaligenes faecalis, Pseudomonas alcaligenes*	de Souza Freitas *et al*., 2020
Acinetobacter junii	Lipopeptide		*Proteus mirabilis, S. aureus, Pseudomonas aeruginosa*	Ohadi *et al*., 2020
Pseudozyma aphidis	Glycolipid	Mannosylerythritol lipids	*S. aureus*	Shu *et al*., 2020
Bacillus velezensis	Lipopeptide	Surfactin	*P. aeruginosa, E. coli, K. pneumoniae, S. aureus*	Ali *et al*., 2022
Shewanella algae	Glycolipid		*Bacillus cereus, Streptococcus pneumoniae, Pseudomonas aeruginosa, Escherichia coli, K. pneumoniae, Acinetobacter sp.*	Gharaei *et al*., 2022
Lactobacillus acidophilus	Unclassified		*Chromobacterium violaceum, Serratia marcescens, Pseudomonas aeruginosa*	Adnan *et al*., 2023
Bacillus subtilis B. vallismortis	Lipopeptides	Iturin Fengycin Surfactin	*Malassezia furfur*	Da Silva *et al*., 2021
Pseudomonas plecoglossicida	Glycolipid	Rhamnolipid	*S. aureus, B. subtilis, Aeromonas hydrophila*	Sabarinathan *et al*., 2021
Bacillus amyloliquefaciens	Unclassified		*Acinetobacter baumannii*	Amer *et al*., 2023
P. aeruginosa	Glycolipid	Rhamnolipid	*Baumannii, Enterococcus faecium*	Firdose *et al*., 2023
Lactobacillus paracasei		glycolipoprotein	*E. coli, S. aureus, Salmonella enteritidis, P. aeruginosa, Yersinia enterolitica, Proteus mirabilis, K. pneumoniae*	Mouafo *et al*., 2023

Supplementary 4. Development of Biosurfactant formulation strategy

Formulation strategy	Antimicrobial activity	Reference
Liposomes containing biosurfactants	*S. aureus*	Giordani *et al*., 2019
Toothpaste with biosurfactant and chitosan or sodium fluoride	*Streptococcus mutans*	Resende *et al*., 2019
Garlic extract with biosurfactant	*S. aureus*	Mohamed *et al*., 2020
Chitosan-based nanoparticle	*Helicobacter pylori*	Arif *et al*., 2021
Lipopeptides and glycolipids combination	*albicans*	Ceresa *et al*., 2021
	Staphylococcus spp.	
Usnic acid-loaded Rhamnolipid vesicle	*S. aureus*	Falakaflaki *et al*., 2022
Rhamnolipid-coated iron oxide nanoparticles	*coli*	Sharaf *et al*., 2022
	S. aureus	
Glycolipid and antibiotics combination	*S. aureus*	Amirinejad *et al*., 2023
	A. baumannii	
Biosurfactant nanoemulsion	*E. coli*	Haddaji *et al*., 2023
	S. aureus	

Subscription

Jordan Journal of Biological Sciences

An International Peer – Reviewed Research Journal

Published by the Deanship of Scientific Research, The Hashemite University, Zarqa, Jordan

Name: ..... الاسم:

Specialty: ..... التخصص:

Address: ..... العنوان:

P.O. Box: ..... صندوق البريد:

City &Postal Code:..... المدينة: الرمز البريدي:

Country: ..... الدولة:

Phone: ..... رقم الهاتف

Fax No.: ..... رقم الفاكس:

E-mail: ..... البريد الإلكتروني:

Method of payment: ..... طريقة الدفع:

Amount Enclosed: ..... المبلغ المرفق:

Signature: ..... التوقيع:

Cheque should be paid to Deanship of Research and Graduate Studies – The Hashemite University.

I would like to subscribe to the Journal

For

- ☐ One year
- ☐ Two years
- ☐ Three years

One Year Subscription Rates

	Inside Jordan	Outside Jordan
Individuals	JD10	$70
Students	JD5	$35
Institutions	JD 20	$90

Correspondence

Subscriptions and sales:

The Hashemite University
P.O. Box 330127-Zarqa 13115 – Jordan
Telephone: 00 962 5 3903333
Fax no. : 0096253903349
E. mail: jjbs@hu.edu.jo

المجلة الأردنية للعلوم الحياتية
Jordan Journal of Biological Sciences (JJBS)

http://jjbs.hu.edu.jo

المجلة الأردنية للعلوم الحياتية: مجلة علمية عالمية محكمة ومفهرسة ومصنفة، تصدرعن الجامعة الهاشمية وبدعم من صندوق دعم البحث العلمي والإبتكار – وزراة التعليم العالي والبحث العلمي.

ترسل البحوث الى العنوان التالي:

رئيس تحرير المجلة الأردنية للعلوم الحياتية
الجامعة الهاشمية
ص.ب , 330127 , الزرقاء, 13115 , الأردن
هاتف: 0096253903333
E-mail: jjbs@hu.edu.jo, Website: www.jjbs.hu.edu.jo

المملكة الأردنية الهاشمية

المجلة الأردنية

للعلوم الحياتية

مجلة علمية عالمية محكمة

تصدر بدعم من صندوق دعم البحث العلمي و الابتكار

http://jjbs.hu.edu.jo/